

主論文

**Heteroatom-Embedding Annulative  $\pi$ -Extension Reaction**

ヘテロ原子を組み込む縮環  $\pi$  拡張反応の開発

**Kou Kawahara**

川原 巧

Department of Chemistry, School of Science,  
Nagoya University

**2023**

## Preface

The studies presented in this thesis have been carried out under the direction of Professor Kenichiro Itami at Department of Chemistry, Graduate School of Science, Nagoya University between April 2017 and March 2023.

First and foremost, I would like to express my heartfelt and utmost gratitude to Professor Kenichiro Itami for providing and arranging the opportunity to work together, valuable suggestions and encouragement throughout this work. I would like to express my sincerest appreciation to Associate Professor Hideto Ito for his kind guidance, technical assistance, helpful discussions and constant enthusiasm during the course of this study. I also show my significant acknowledgement to Associate Professor Yasutomo Segawa (Institute for Molecular Science), Team Leader Shinya Hagihara (RIKEN), Associate Professor Kei Murakami (Kwansei Gakuin University), Designated Associate Professor Akiko Yagi, Assistant Professor Kazuma Amaike and Research Associate Takehisa Maekawa for their insightful comments, constructive discussions, and much encouragements for pushing the study forward.

I cannot express much thanks enough to Dr. Wataru Matsuoka, Ms. Honami Katsuragawa, Ms. Kanna Fujishiro and Mr. Kanami Nakata for all experimental supports and beneficial suggestions. This thesis cannot exist without their contribution.

I must make special mention of Mr. Hiroyuki Kitano and Dr. Shuya Yamada for personal encouragement. Their existence had a great influence on my character as an organic chemist.

I appreciate to Mr. Yugo Aoki, Ms. Ayaka Ueda, Ms. Rika Kato (Monica), Mr. Shusei Fujiki, Mr. Satoshi Matsubara and Ms. Sakura Miyauchi. With their support and encouragement, I was able to get through the tough days of research.

My especial appreciation goes to Ms. Rika Kato, Ms. Yui Ueyama, Ms. Nanako Kato, Ms. Hideyo Kinoshita, Ms. Hanae Yoshida, Ms. Yoko Shirotani, Ms. Yume Saito, Ms. Yuko Otsubo, Ms. Yumi Muroi, and Ms. Yurie Shouiriki for their kind support and great hospitality throughout my long-term laboratory life.

I am deeply grateful to Professor Susumu Saito and Professor Shigehiro Yamaguchi for their helpful guidance and encouragement. I am also deeply grateful to Professor Atsushi Wakamiya (Kyoto University, ICR) and Assistant Professor Tomoya Nakamura (Kyoto University, ICR) for their helpful guidance and advises on some measurements.

I sincerely thank to

Dr. Asraa Ziadi	Dr. Guillaume Povie	Dr. Tomohiro Fukushima
Mr. Motonobu Kuwayama	Dr. Nobuhiko Mitoma	Dr. Hirotohi Sakamoto
Dr. Levine David Robert	Dr. Gregory Perry	Dr. Yuanming Li
Dr. Chaolumen	Dr. Takayuki Nakamuro	Dr. Maciej Krzeszewski
Dr. Kwan Yin Cheung	Dr. Iain Stepek	Dr. Hiroki Sato
Dr. Greco Gonzalez Miera	Dr. Majji Shankar	Dr. Nicola Stephanie Skoulding
Dr. Louis Evans	Dr. Atsushi Usami	Dr. Hayato Yamada
Dr. Shuhei Kusano	Mr. Sho Ishida	Mr. Motoaki Usui
Mr. Genki Mori	Dr. Hidefumi Nakatsuji	Mr. Keita Seda
Mr. Shunsuke Ishida	Mr. Yuichi Nakashige	Dr. Yutaro Saito
Dr. Shin Suzuki	Dr. Ryosuke Takise	Dr. Masahiko Yoshimura
Dr. Tsuyoshi Ohshima	Dr. Kenta Kato	Ms. Mari Shibata
Dr. Shun Yamashita	Ms. Masako Fushimi	Dr. Ryotaro Yamada
Ms. Eri Suzuki	Mr. Kazushi Kumazawa	Mr. Yoshito Koga
Mr. Jumpei Suzuki	Ms. Wakana Hayashi	Dr. Yip Shu Jan
Mr. Kazuya Kawai	Dr. Yota Sakakibara	Dr. Michihisa Toya
Mr. Taito Hiraga	Ms. Ayana Mashimo	Ms. Letitia Sarah
Mr. Ryo Okude	Ms. Mizuho Uryu	Mr. Hiroki Shudo
Ms. Mai Nagase	Mr. Bumpei Maeda	Ms. Eri Makino
Ms. Kaho Matsushima	Mr. Duong Nguyen Dinh	Ms. Jung Jaehyun
Mr. Keigo Yamada	Mr. Hisayasu Ishibashi	Mr. Ryo Akagami
Ms. Erika Kato	Mr. Hideya Kono	Mr. Kaito Maekawa
Mr. Kosuke Watanabe	Mr. Bui Son Quy	Ms. Kyoka Ohashi
Mr. Yoshifumi Toyama	Mr. Takaku Yoshihara	Mr. Tomoki Kato
Mr. Ryuto Kojo	Mr. Nguyen Bach Xuan	Mr. Daiki Imoto
Mr. Nobushige Kai	Mr. Satoshi Hattori	Ms. Miu Fukatsu

Mr. Takato Mori	Mr. An Quang Nguyen	Ms. Yuri Arachi
Ms. Miyuka Ogawa	Ms. Nanase Chihara	Mr. Tomoya Nakagomi
Mr. Kumpei Hasebe	Mr. Hagumi Hasebe	Mr. Yuma Takeda
Mr. Nghia Minh Le	Ms. Sojung Kim	Mr. Ryan Fan
Dr. Phillip Steib	Mr. Matthew Robinson	Dr. Phillippa Cooper
Mr. Jake Wilson	Mr. Julian Fliege	Ms. Katherine Lynn Bay
Ms. Kaylin Nicole Flesch	Ms. Samantha Phan	Mr. Dominik Zetschok
Mr. Robin Warstat	Ms. Katja Schlegel	Mr. Konstantin Günther
Mr. Manuel Rondelli	Mr. Stephan Schmidt	Mr. Luca Hagemeyer

and all alumni of Itami group.

I appreciate the Japan Society for the Promotion of Science (JSPS) for the research fellowship for young scientists (DC1). I also thank to the Graduate Program of Transformative Chem-Bio Research (GTR), Dr. Yuta Morinaka as the GTR mentor, for their financial support.

Finally, I would like to express my deepest gratitude to my family, Mr. Tomonori Kawahara, Ms. Mika Kawahara for their constant assistance and encouragement.

Kou Kawahara

Department of Chemistry  
Graduate School of Science  
Nagoya University

2023



## Contents

<b>List of Abbreviations</b>	1
<b>General Introduction</b>	2
<b>Chapter 1</b>	
Synthesis of Nitrogen-Containing Polyaromatics by Aza-Annulative $\pi$ -Extension of Unfunctionalized Aromatics	26
<b>Chapter 2</b>	
Rapid Access to Polycyclic Thiopyrylium Compounds from Unfunctionalized Aromatics by Thia-APEX Reaction	86
<b>Chapter 3</b>	
Rapid Access to Polycyclic Thianthrenes from Unfunctionalized Aromatics by Thia-APEX Reaction	182
<b>Conclusion of this thesis</b>	228
<b>List of Publications</b>	230

## List of Abbreviations

Å	ångström unit	<i>m</i>	meta
Abs	absorption	min	minute(s)
Ac	acetyl	Me	methyl
APCI	atmospheric pressure chemical ionization	MO	molecular orbital
aq	aqueous solution	Ms	methanesulfonyl
Ar	aryl	(HR)MS	(high resolution) mass spectroscopy
Bn	benzyl	MW	microwave
Boc	<i>tert</i> -butoxycarbonyl	<sup>t</sup> Bu	1-butyl
Bpin	(pinacolato)boryl	NIR	near infrared
cat	catalyst/catalytic	NMR	nuclear magnetic resonance
Cp*	pentamethyl- cyclopentadienyl	<i>o</i>	ortho
Cy	cyclohexyl	ORTEP	Oak Ridge Thermal Ellipsoid Program
δ	chemical shift (NMR)	<i>p</i>	para
DART	direct analysis in real time	PAC	polycyclic aromatic compound
DDQ	2,3-dichloro-5,6-dicyano- <i>p</i> - benzoquinone	PAH	polycyclic aromatic hydrocarbon
DFT	density functional theory	Ph	phenyl
DG	directing group	Piv	pivaloyl
DMF	<i>N,N</i> -dimethylformamide	ppm	parts per million
DMSO	dimethyl sulfoxide	R	an organic group
eq / equiv	equivalent(s)	r.t.	room temperature
ESI	electrospray ionization	S <sub>E</sub> Ar	electrophilic aromatic Substitution
Et	ethyl	S <sub>N</sub> Ar	nucleophilic aromatic substitution
FL	fluorescence	<sup>t</sup> Bu	1,1-dimethyl-1-ethyl
GPC	gel permeation chromatography	TD-DFT	time-dependent density functional theory
h	hour(s)	Tf	trifluoromethanesulfonyl
HFIP	1,1,1,3,3,3-hexa- fluoropropan-2-ol	THF	tetrahydrofuran
HOMO	highest occupied molecular orbital	TMEDA	<i>N,N,N',N'</i> -tetramethyl- ethylenediamine
<i>hν</i>	photoirradiation	tol	tolyl
IEF-PCM	integral equation formalism- polarizable continuum model	Ts	<i>para</i> -toluenesulfonyl
<sup>t</sup> Pr	1-methyl-1-ethyl	UV	ultraviolet
IRF	instrument response function	vis	visible
<i>J</i>	coupling constant (NMR)	wt%	percentage by weight
LG	leaving group		
LUMO	lowest unoccupied molecular orbital		

## General Introduction

### 1. Introduction

#### 1-1. Heteroatom-Embedded Polycyclic Aromatic Compounds

Recently, heteroatom-embedded polycyclic aromatic compounds (hetero-PACs) have gathered great attention in various areas of science and technologies such as organic electronics and chemical biology.<sup>[1]</sup> Hetero-PACs have fused  $\pi$ -conjugated structures consisted of multiple aromatic rings and heteroatoms such as boron, nitrogen, oxygen, phosphorous, and sulfur. Depending on the pattern of ring-fusion, the nature of aromatic system, and the kind of embedded heteroatoms, hetero-PACs show diverse optoelectronic properties.<sup>[2]</sup> Figure 1 describes representative examples of hetero-PACs that were employed in photochemical, electrochemical and biological applications. For example, azabenzochrysene derivatives and tetrapyrrophenazine (TPP) including pyridine rings have studied as key materials for organic light-emitting diodes (OLEDs) and organic field-effect transistors (OFETs).<sup>[2c,2d]</sup> Dictyodendrin A is a polycyclic aromatic natural product containing pyrrole moieties, displaying telomerase inhibiting activity.<sup>[2e]</sup> 2,8-Dimethylanthra[2,3-*b*:7,6-*b'*]dithiophene (DMADT) has been used as a *p*-type semiconductor.<sup>[2j]</sup> Thioxanthylum (TXT) derivatives including six-membered sulfur-embedded rings are one of the organophotoredox catalysts to realize milder chemical reactions.<sup>[2k]</sup> Benzo[5,6][1,4]dithiino[2,3-*a*]thianthrene-6,7-di-carbonitrile (bTEoCN) is a room-temperature-phosphorescence (RTP) material which is realized by the 1,4-dithiin moieties, two sulfur atom-containing six-membered rings.<sup>[2l]</sup> Furan-fused aromatic compound DPNDF3 has properties as a *p*-type semiconductor as same as DMADT. However, the furan moieties having a weaker aromaticity than thiophene realize the unique properties different from thiophene analogues.<sup>[2m]</sup> Oxygen-containing cationic six-membered aromatic ring are called pyrylium. Pyrylium-fused aromatic compounds such as *O*-doped ePHAC is utilized as a molecular probe for tracking mitochondria.<sup>[2n]</sup> These molecules are only a handful examples of reported functional hetero-PACs. Enriching structural patterns of hetero-PACs will undoubtedly lead to a discovery of novel functions and applications. Therefore, syntheses of such hetero-PACs in a regioselective, step- and atom-economical fashion are very important issues in this field.

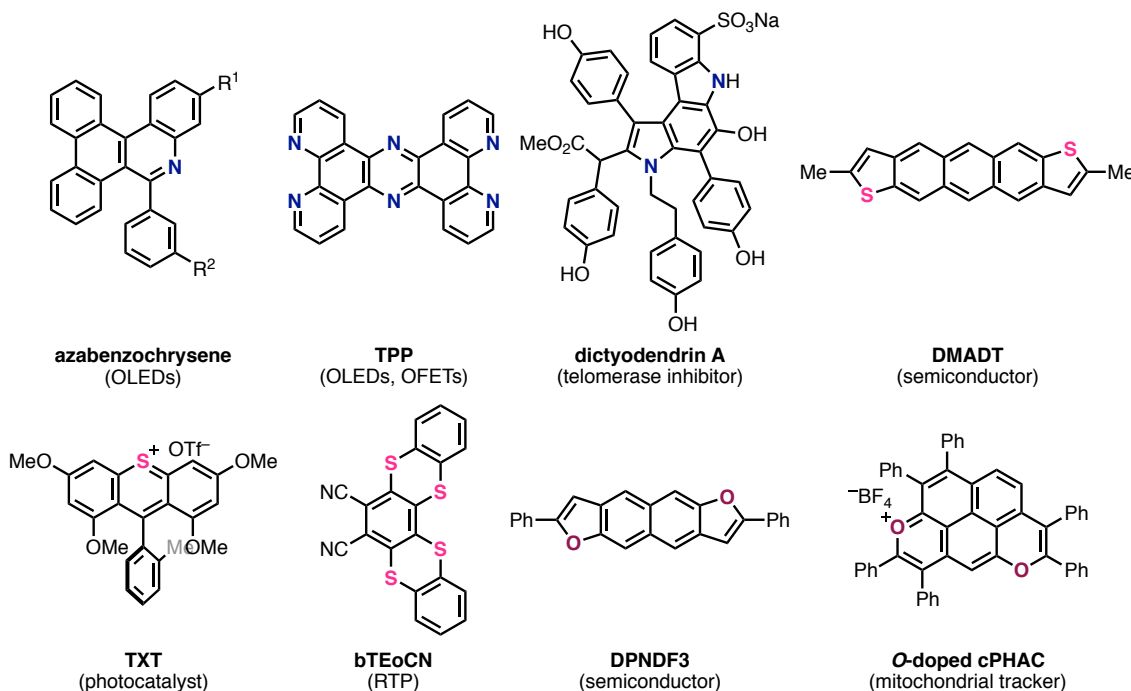
#### 1-2. Organic synthesis of hetero-PACs

To obtain hetero-PACs, a stepwise preparation is widely adopted as a general and conventional synthetic strategy (Figure 2).<sup>[1a,1b]</sup> In this strategy, functionalizations such as halogenation, metalation and/or introduction of heteroatom are first needed for unfunctionalized starting materials. After that, the functionalized aromatics participate in the intermolecular C–heteroatom

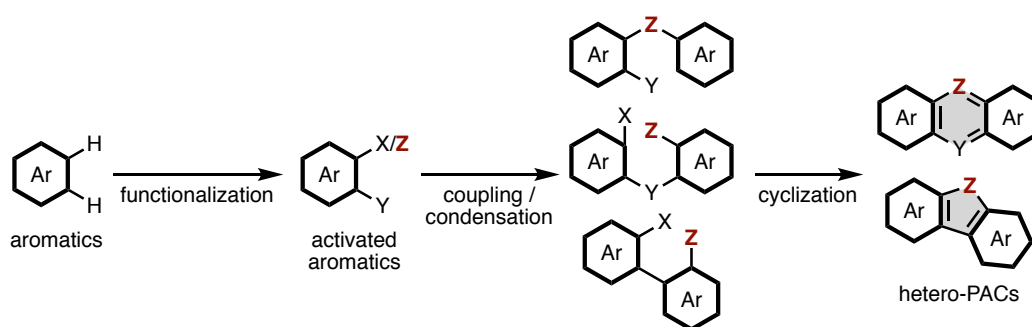


(C–Z) bond formation via metal-promoted cross-coupling reaction, intermolecular aromatic electrophilic/nucleophilic substitution and condensation. Finally, cyclization via intramolecular C–C or C–Z bond formation with/without post-aromatization affords hetero-PACs.

Heteroatom-embedded polycyclic aromatic compounds (hetero-PACs)



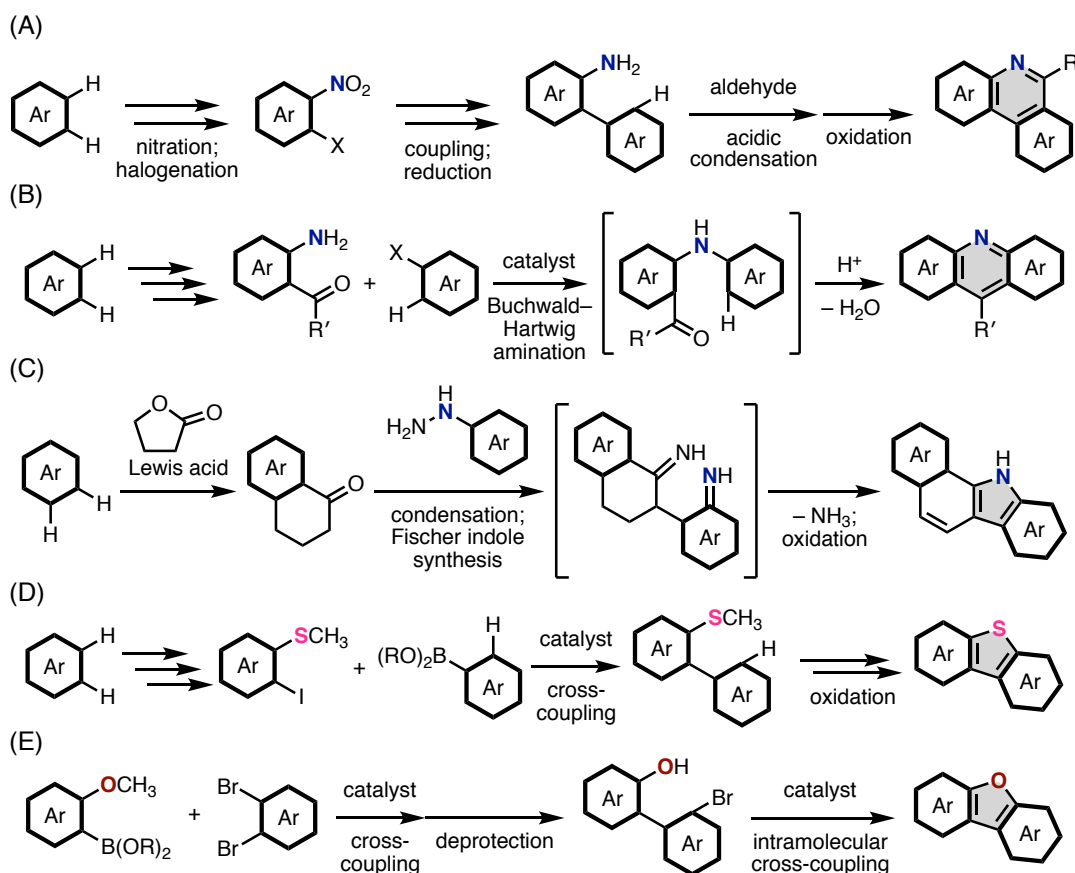
**Figure 1.** Representative hetero-PACs as functional molecules.



**Figure 2.** Schematic illustrations on a general synthetic approach to hetero-PACs.

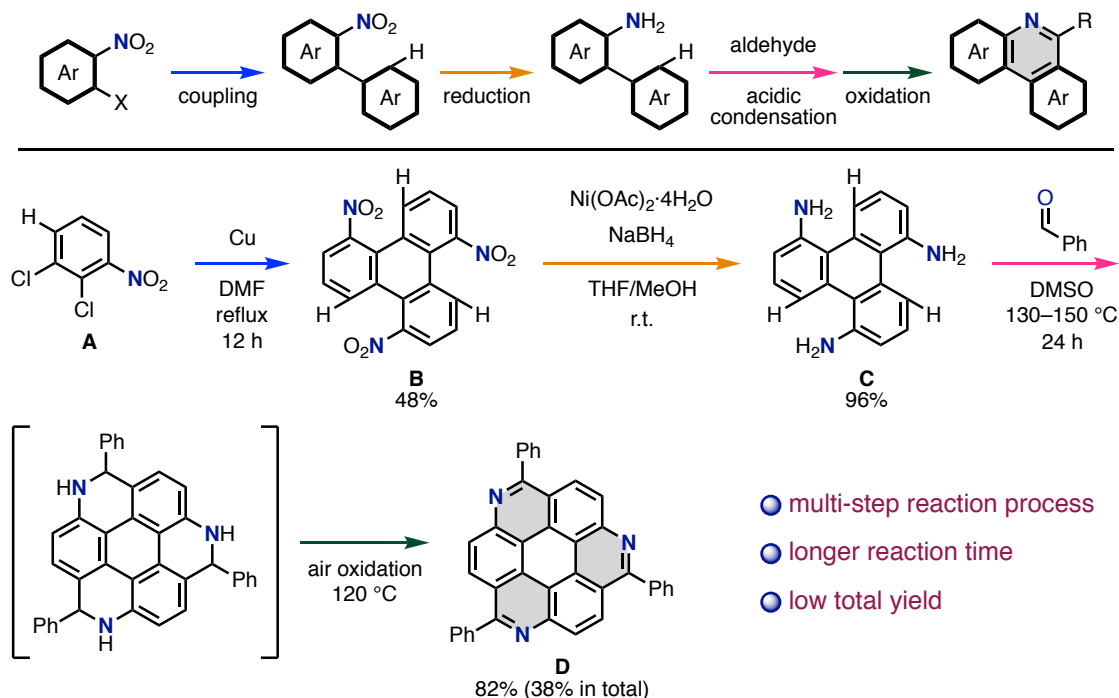
Figure 3 describes representative synthetic approaches to hetero-PACs. For constructing pyridine-fused PACs, the combination of cross-coupling reaction, condensation, and amination of aromatic compounds is often employed, as shown in Figure 3A.<sup>[3]</sup> For instance, arylated anilines prepared via multi-step halogenation, nitration and coupling reaction are condensed with aldehyde under acidic conditions. After that, the resulting condensed product affords a  $\pi$ -extended pyridine ring via oxidative cyclization.<sup>[3a–d]</sup> Besides, Buchwald–Hartwig amination using transition metal

catalysts is often utilized for the construction of an *ortho*-acyldiarylamine structure, which can be further transformed to an acridine structure through dehydrative cyclization (Figure 3B).<sup>[3e-i]</sup> With regard to the syntheses of pyrylium- and thiopyrylium-fused PACs, the similar methods to  $\pi$ -extended pyridine synthesis have been commonly employed.<sup>[4]</sup> In regards to construction of five-membered heteroaromatics (*e. g.*, pyrrole, thiophene and furan), metal-catalyzed cross-coupling reactions involving in Ar–heteroatom and Ar–Ar bonds formation<sup>[5]</sup> and classical condensation reactions<sup>[6]</sup> are regarded as effective synthetic methods. In particular, Fischer indole synthesis using aryl hydrazines and ketones is a fundamental reaction for constructing pyrrole-fused PACs (Figure 3C).<sup>[6]</sup> Thiophene rings can be constructed from biarylyl thioether intermediates by C–S bond formation using oxidants such as H<sub>2</sub>O<sub>2</sub> and CF<sub>3</sub>CO<sub>3</sub>H (Figure 4D).<sup>[7]</sup> Moreover, thiophene/furan rings are constructed by transition metal-catalyzed intramolecular C–X/C–S or C–X/C–O bond formations (X = halogen) (Figure 4E).<sup>[5,8]</sup> In summary, there are various established synthetic methods for constructing heteroarene cores in hetero-PACs.<sup>[9]</sup> However, most of them are based on the transformation of functionalized aromatics having heteroatoms, carbonyls group and halogen atoms.



**Figure 3.** Representative synthetic approaches for hetero-PACs.

Figure 4 describes an actual synthetic example of a triazacoronene derivative as one of representative nitrogen-containing PACs.<sup>[3b]</sup> In this synthesis, 2,3-dichloronitrobenzene (**A**) was trimerized by copper-mediated Ullmann coupling to give trinitrotriphenylene **B**. Next, trinitrotriphenylene **B** is reduced using  $\text{Ni}(\text{OAc})_2$  and  $\text{NaBH}_4$  to give triaminotriphenylene **C**. In the final step, condensation of triaminotriphenylene **C** with benzaldehyde followed by oxidation under air afforded the target triazacoronene **D**. Thus, hetero-PAC **D** was obtained in 38% overall yield from starting nitrobenzene **A**. As shown here, increase of reaction steps results in dramatic increase of total experimental time and required cost with decrease of the total yield of target compounds. In addition, the availability of functionalized PAHs is even lower than that of simple aromatics. The limited access to large and functionalized aromatics stems from the lack of regioselective and regio-divergent functionalization methods of PAHs. In other words, a potential structural and functional diversity of obtainable hetero-PACs is undoubtedly narrowed and limited. These general synthetic problems are unfavorable for rapid discovery, application and supply of novel functional hetero-PACs. Therefore, the development of new synthetic methods for realizing more efficient preparations of hetero-PACs are highly important in the field of not only organic synthesis but also materials science.

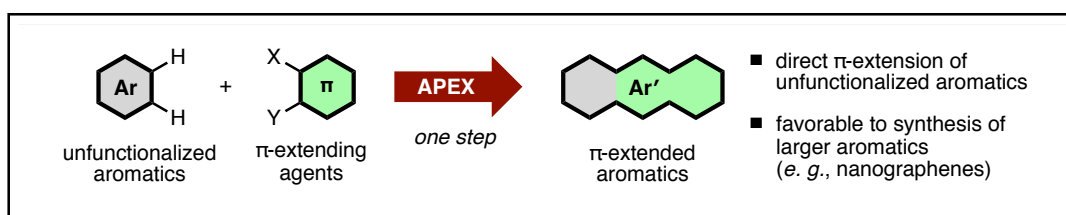


**Figure 4.** Synthesis of a triazacoronene derivative.

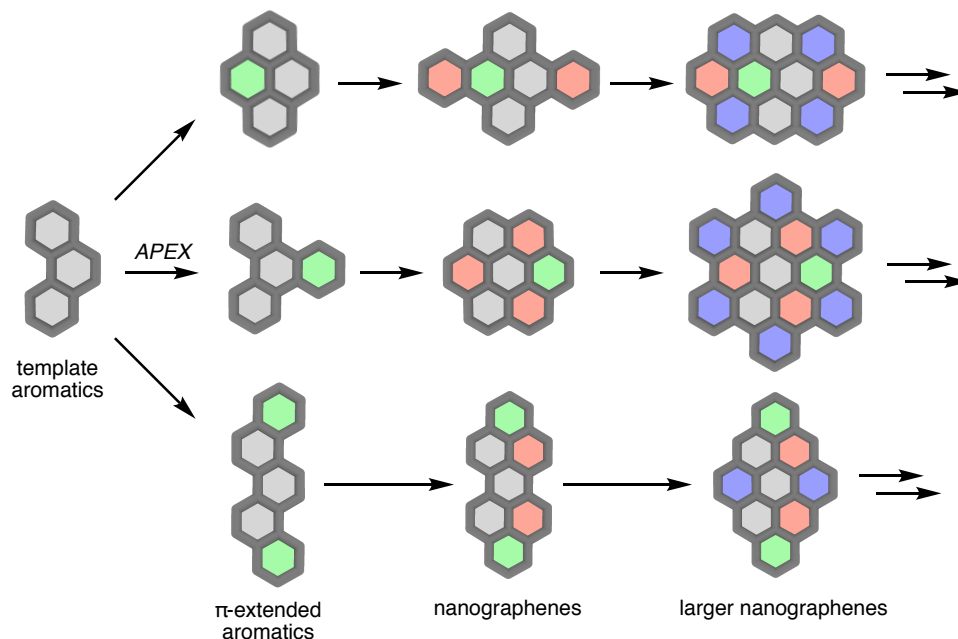
## 2. One-step/one-pot synthesis of hetero-PACs

### 2-1. Annulative $\pi$ -extension (APEX) reaction

One of intuitive solutions for the synthetic problem of hetero-PACs is a one-step synthesis from easily available aromatics with a suitable  $\pi$ -extending agent. One-step synthesis of hetero-PACs can greatly diminish operation time and costs required for reaction and purification. Besides, the total yields of target hetero-PACs can be potentially improved than those in the multi-step reactions. In this regard, an insight on annulative  $\pi$ -extension (APEX) developed by Itami and Ito would be convenient for efficient synthesis of hetero-PACs.<sup>[10,11]</sup> APEX is defined as a one-step  $\pi$ -extension reaction or reaction sequences enabling the direct construction of one or more fused aromatic rings onto unfunctionalized aromatics.<sup>[10]</sup> Thus, APEX reaction has been recognized a powerful synthetic tool for rapid access to larger  $\pi$ -extended aromatics such as polycyclic aromatic hydrocarbons (PAHs) and nanographenes. In addition, utilizing the feature of direct C–H functionalization in APEX, the products obtained by APEX reactions can further participate the successive APEX reactions, realizing a diversity-oriented synthesis of nanographenes.

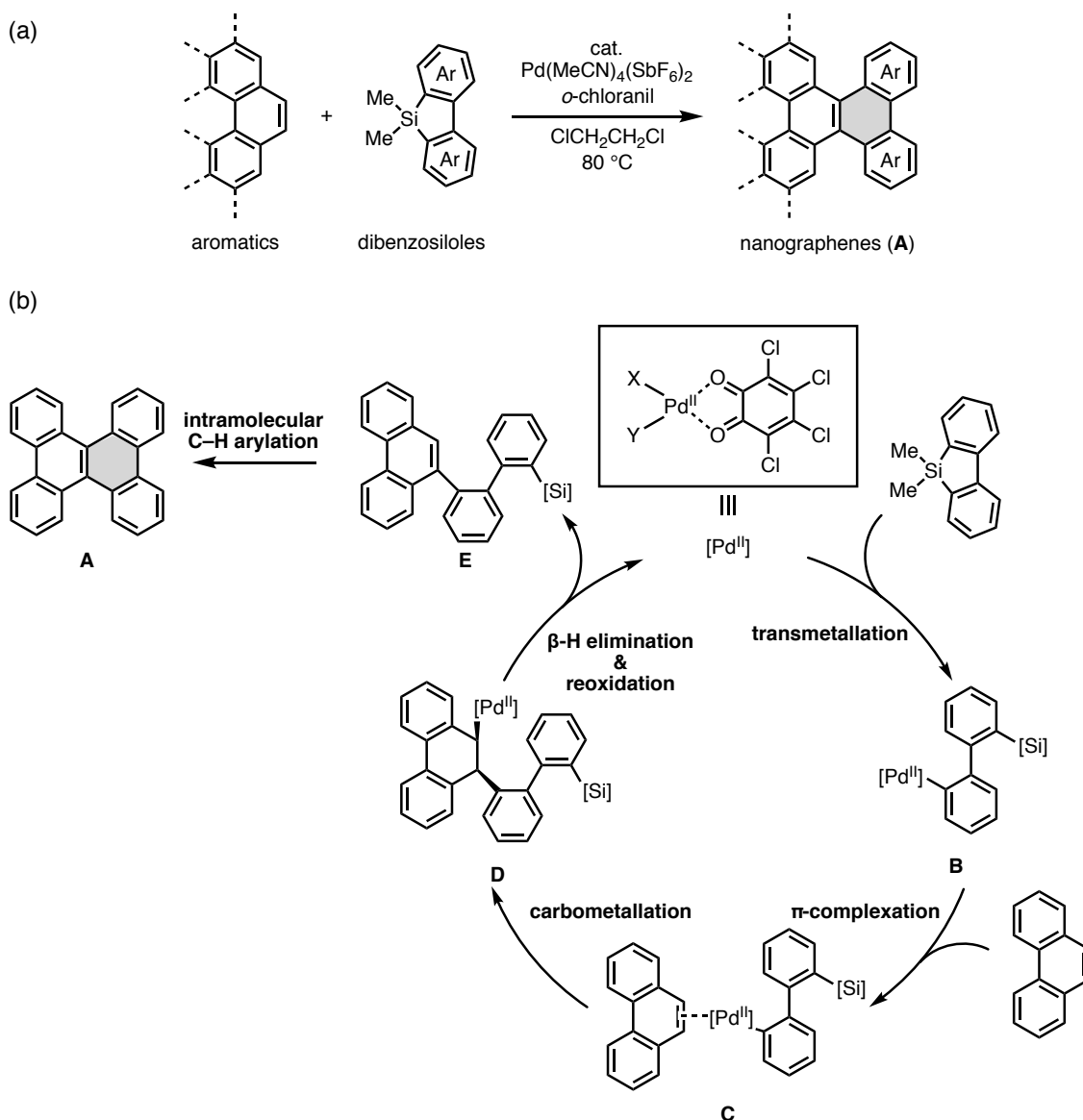


Synthesis of diverse aromatics using APEX reactions



**Figure 5.** Schematic illustrations of a concept of APEX reaction.

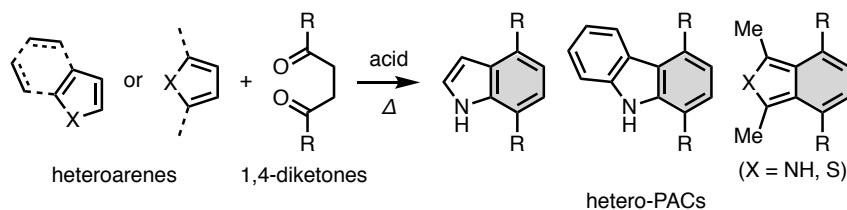
As one of representative APEX reactions, a palladium-catalyzed APEX reaction using dibenzosilole derivatives as  $\pi$ -extending agents was reported by Itami and Ito in 2015 (Figure 6a).<sup>[11b]</sup> In this reaction, direct transformation of unfunctionalized PAHs (*e. g.*, phenanthrenes, pyrenes) to nanographenes **A** were achieved with exclusive *K*-region (a convex armchair-edge) selectivity. The key of APEX reaction is the use of cationic Pd(II) species Pd(MeCN)<sub>4</sub>(SbF<sub>6</sub>)<sub>2</sub> as a catalyst and *o*-chloranil as an oxidant.<sup>[12]</sup> As shown in Figure 6b, a cationic aryl-palladium(II)/*o*-chloranil species **B** is considered to be formed by transmetalation from the palladium(II)/*o*-chloranil complex and the dibenzosilole. Furthermore, this highly electrophilic Pd(II) species can be coordinated at unfunctionalized *K*-region (C9,C10-positions of phenanthrene, a  $\pi$ -complex **C**), then carbometallation affords an alkyl palladium intermediate **D**. Finally, the direct C–H arylation is completed via  $\beta$ -hydrogen elimination, and repeating the same arylation process intramolecularly affords the annulatively  $\pi$ -extended product **A**. After the first definition of APEX, various catalytic and stoichiometric APEX reactions have been developed so far.<sup>[10,11,13]</sup>



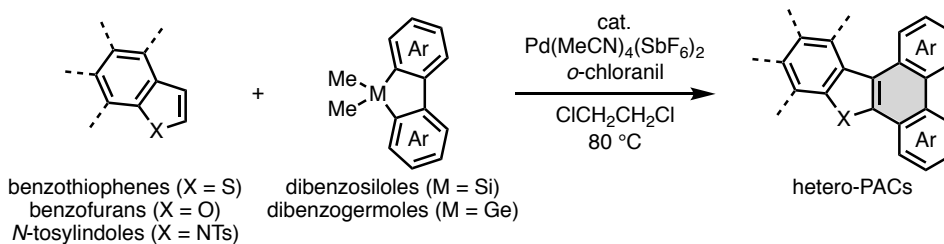
**Figure 6.** Pd-catalyzed APEX reactions using dibenzosiloles and *o*-chloranil.

Not only PAHs but also hetero-PACs can be obtained by APEX reactions.<sup>[10,11,13]</sup> Utilizing APEX reactions with heteroarenes such as pyrroles, indoles, (benzo)thiophenes, and (benzo)furans, various hetero-PACs can also be obtained. For example, 1,4-diketone compounds are often chosen as  $\pi$ -extending agents with acids for APEX reaction involving in pyrrole-to-indole/isoindole and indole-to-carbazole type transformations (Figure 7A).<sup>[13d,13e]</sup> As alternative synthetic methods,  $\pi$ -extended heteroarenes can be synthesized by Pd-catalyzed APEX reactions using dibenzosiloles/germoles as  $\pi$ -extending agent, which enables to construct highly fused structures containing heteroles (Figure 7B).<sup>[11c,11e]</sup>

(A) APEX reaction of heteroarenes using 1,4-diketone compounds

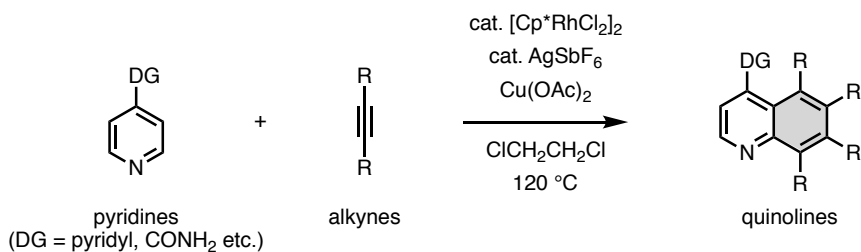
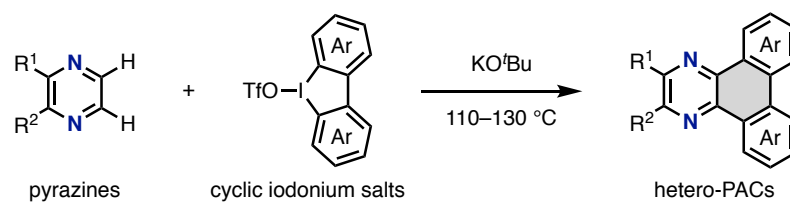


(B) APEX reaction of heteroarenes using dibenzosiloles/germoles

**Figure 7.** Synthesis of heterole-embedded hetero-PACs by APEX reactions of heteroles.

Electron-deficient heteroarenes such as pyridines and pyrazines are not applicable to the reaction systems of APEX reactions in Figure 7. There are quite few examples of APEX reaction of pyridine derivatives. One of them is realized by Rh-catalyzed C–H activation of pyridine bearing pyridyl or benzamide directing groups with alkynes as  $\pi$ -extending agents (Figure 8A).<sup>[13m]</sup> As another example, APEX reaction of pyrazine derivatives have been achieved by KO<sup>t</sup>Bu-mediated double arylation with cyclic iodonium salts.<sup>[13n]</sup> Compared with the abundant examples of APEX reaction of heteroles, the APEX of azines and other six-membered heteroaromatics seems to be more difficult due to the electron-deficient nature. Therefore, APEX reactions using azine type substrates have been still under developing.

(A) Rh-catalyzed APEX reaction using pyridine substrates

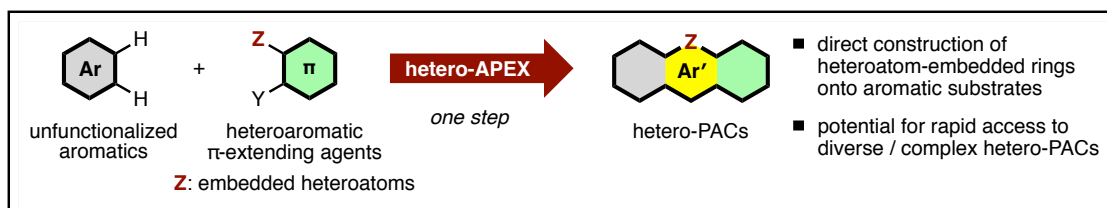
(B) KO<sup>t</sup>Bu-mediated APEX reaction using pyrazine substrates**Figure 8.** APEX reactions of azine substrates.

## 2-2. Heteroatom-embedding annulative $\pi$ -extension (hetero-APEX) reaction

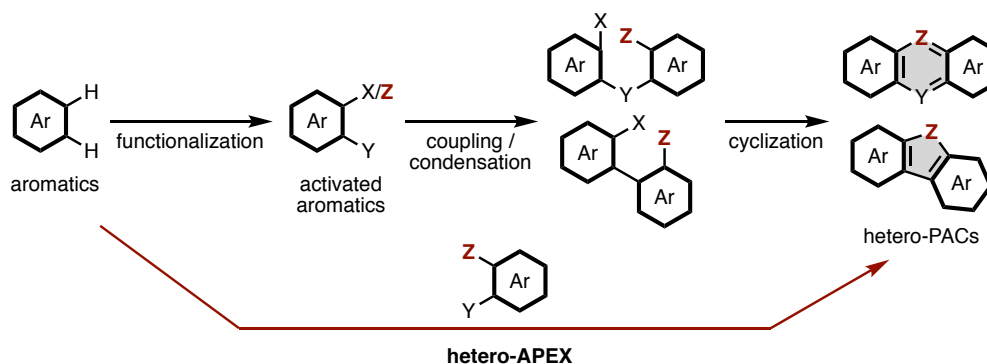
As mentioned above, APEX reaction is a useful method for rapid synthesis of nanographenes and hetero-PACs. However, synthesis of hetero-PACs by APEX reaction requires beforehand prepared heteroarenes. This means that potential problems of prefunctionalizations for the synthesis of hetero-PACs have not been solved by the current APEX reactions. Moreover, almost all the APEX reactions in the hetero-PAC synthesis can construct one and more new aromatic hydrocarbon structures to one heterole core so that the provided hetero-PACs contain only one heterole core. The APEX reaction of hexagonal heteroarenes such as pyridines and pyrazines may be established as an alternative synthetic strategy to hetero-PACs. However, it remains undeveloped due to the lack of reactivity without directing groups. In other words, the present APEX reactions are not suitable for constructing hetero-PACs with structural diversity.

Taking into account of these backgrounds in hetero-PACs and APEX, the author conceived a new synthetic concept of heteroatom-embedding annulative  $\pi$ -extension (hetero-APEX) for a rapid synthesis of hetero-PACs from unfunctionalized aromatics. As same as APEX reaction, hetero-APEX reaction achieves one-step  $\pi$ -extension of unfunctionalized aromatics through formal C–H functionalizations with suitable  $\pi$ -extending agents with/without catalysts. Unlike APEX reaction, hetero-APEX reaction can construct one or more fused heteroaromatics including hexagonal and non-hexagonal rings (Figure 9). Furthermore, depending on the kind of heteroatoms on the  $\pi$ -extending agents, diverse hetero-PACs containing different heteroaromatics can be easily prepared. In this regard, hetero-APEX reactions will dramatically expand structural diversity compared with conventional stepwise synthesis and even previous APEX reactions. For instance, with  $\pi$ -extending agents embedding nitrogen, oxygen, sulfur, boron and phosphorus atoms, hetero-APEX reactions that can construct new pyridine, pyrrole, pyrylium, furan, thiopyrylium, thiophene, borole, phosphabenzene, phosphole rings are realized; herein these reactions are defined as aza-APEX, oxa-APEX, thia-APEX, bora-APEX and phospho-APEX, respectively. Utilizing these hetero-APEX reactions in a highly regioselective manner, not only a synthesis of variety of hetero-PACs but also a diversity-oriented synthesis as well as a late-stage/successive  $\pi$ -extension will be potentially possible. Furthermore, creation of novel heteroaromatics having unique structures, properties and functions can be promoted by hetero-APEX. Consequently, it is highly anticipated that synthetic chemistry and functional organic chemistry as well as materials science will be further developed upon exploring hetero-APEX chemistry.

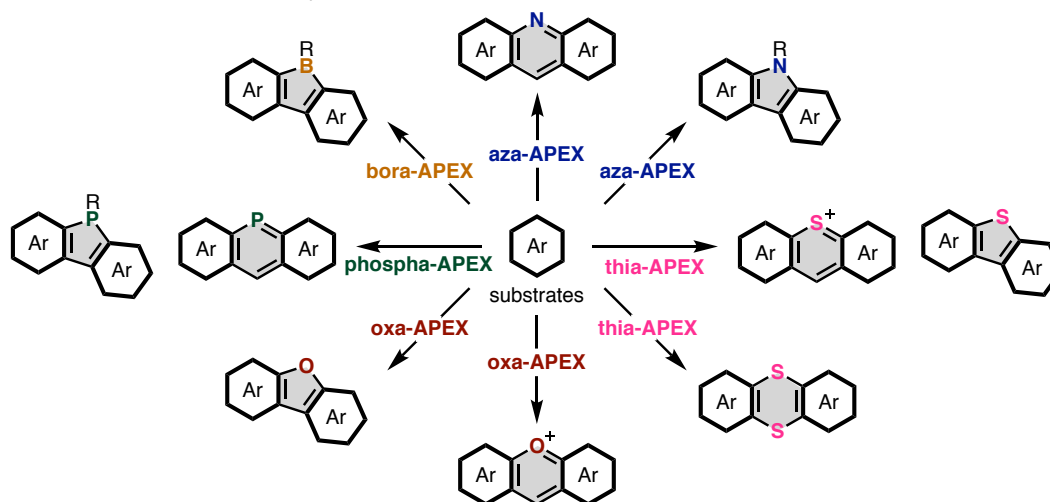




Shortening reaction process



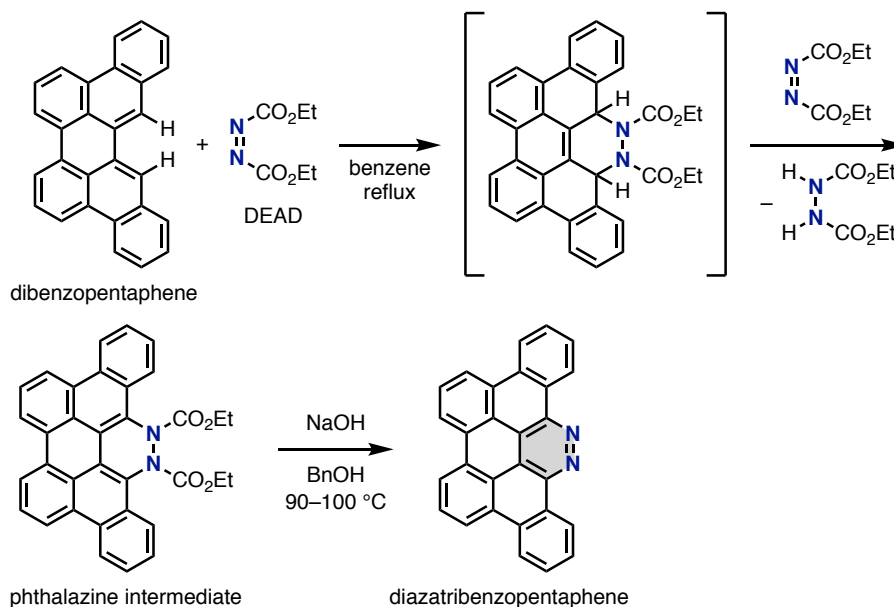
Various hetero-APEX reactions for rapid creation of novel hetero-PACs



**Figure 9.** Concept of hetero-APEX reaction, synthetic advantages over conventional methods and applications to synthesize hetero-PACs.

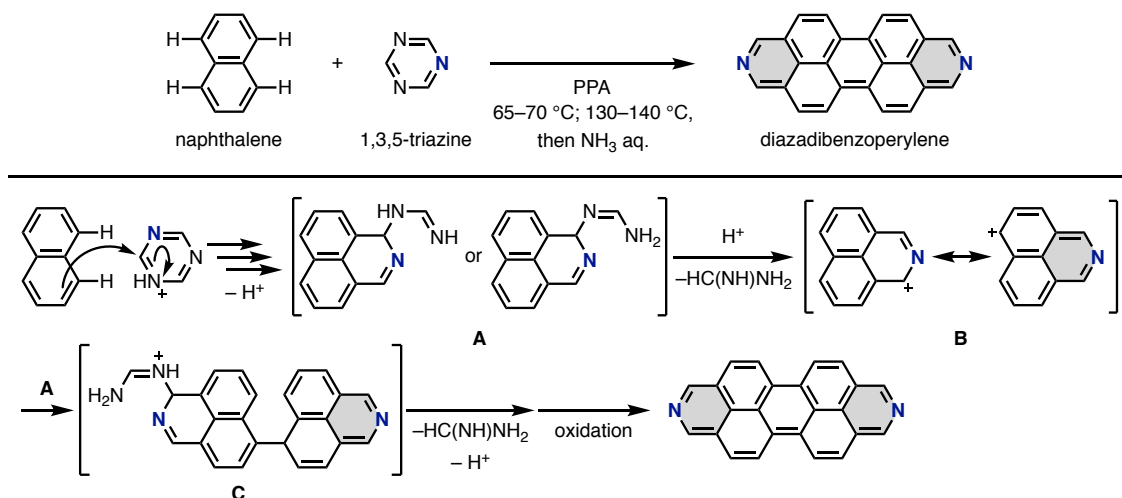
The hetero-APEX is a new synthetic concept when the author defined and started to investigate in 2017. However, there are some preliminary reported reactions that are related or categorized to hetero-APEX reaction. As an early example of formal aza-APEX reaction, a two-step synthesis of diazatribenzopentaphene using unfunctionalized dibenzopentaphene with diethyl azodicarboxylate (DEAD) was reported by Tokita and co-workers in 1982 (Figure 10).<sup>[14]</sup> Under the reflux reaction conditions in benzene, dibenzopentaphene and DEAD affords a Diels–Alder reaction-type cycloadduct which

was auto-oxidized to a phthalazine intermediate. This intermediate was then aromatized to diazatribenzopentaphene by sodium hydroxide in benzyl alcohol. As a whole, this reaction sequence can be regarded as a formal aza-APEX reaction involving in diazabenzoannulation.



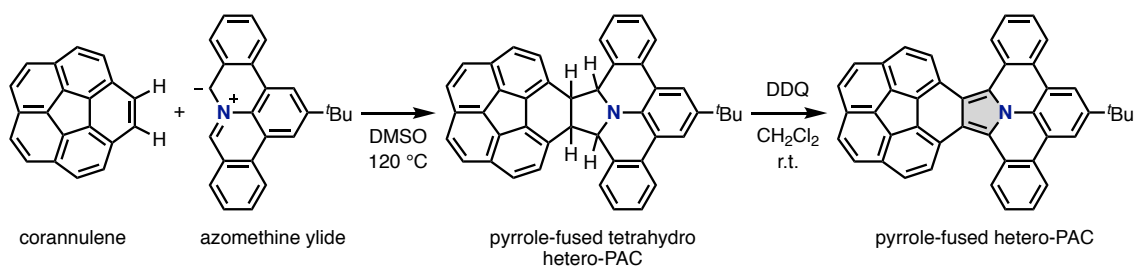
**Figure 10.** Diels–Alder-type formal aza-APEX reaction.

As another example of aza-APEX, one-step synthesis of diazadibenzoperylene using 1,3,5-triazine and naphthalene was reported by Aksenov in 2009 (Figure 11).<sup>[15]</sup> 1,3,5-Triazine becomes electrophilic under acidic conditions with polyphosphoric acid (PPA). The protonated 1,3,5-triazine was first reacted with naphthalene in an aromatic nucleophilic substitution ( $S_NAr$ ) fashion accompanied by cleavage of triazine ring. Thus, various intermediates including neutral intermediate **A** were converged to azaphenalenylium ion intermediate **B**, which is thought to react with another intermediate **A** to form biaryl intermediate **C**. Finally, biaryl intermediate **C** was converted to diazadibenzoperylene via sequences of cyclization and oxidative aromatization. This reaction is fascinating because small pristine naphthalene can be expanded to larger nitrogen-embedded hetero-PACs with simple reagents and reaction conditions, albeit only one synthetic example with low yield of product.



**Figure 11.** Aza-APEX dimerization of naphthalene using 1,3,5-triazine.

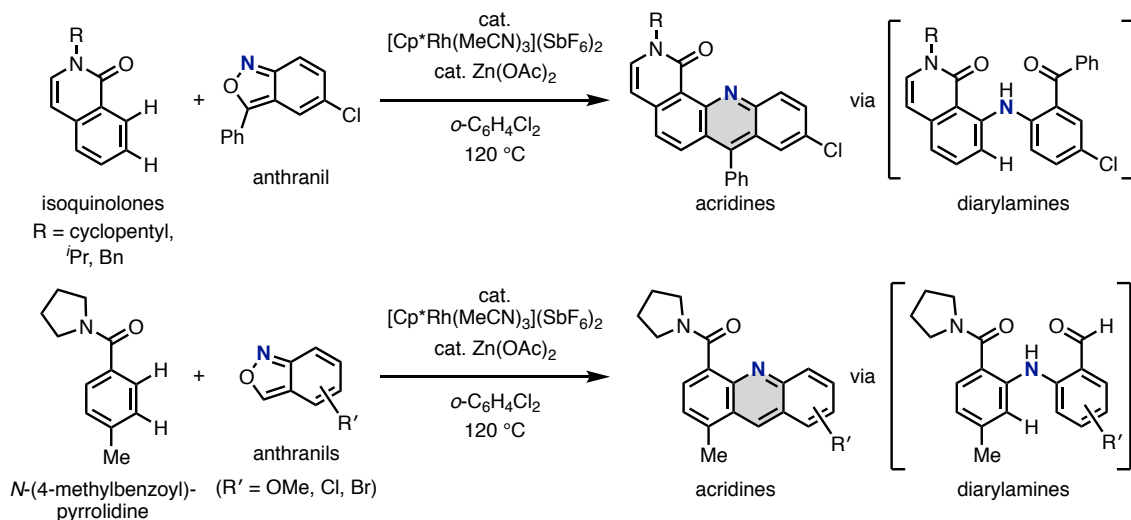
Later, some groups reported one-pot or one-step  $\pi$ -extension reactions of unfunctionalized aromatics which can be classified as hetero-APEX or formal hetero-APEX. For example, in 2017, Nozaki, Ito and co-workers achieved synthesis of pyrrole-fused hetero-PAC using polycyclic azomethine ylide as a  $\pi$ -extending agent (Figure 12).<sup>[16]</sup> This polycyclic azomethine ylide worked as a 1,3-dipole reagent, which directly participated in a [3+2] cycloaddition reaction with pristine corannulene under heating conditions. Through a successive oxidation by DDQ, the fully aromatized polycyclic pyrrole structure was successfully synthesized. The overall synthetic protocol is stepwise and the reaction can be classified as a formal aza-APEX reaction. However, this report provides an important insight that the azomethine ylide can directly react at a peripheral region of PAH.



**Figure 12.** Formal aza-APEX reaction using azomethine ylide.

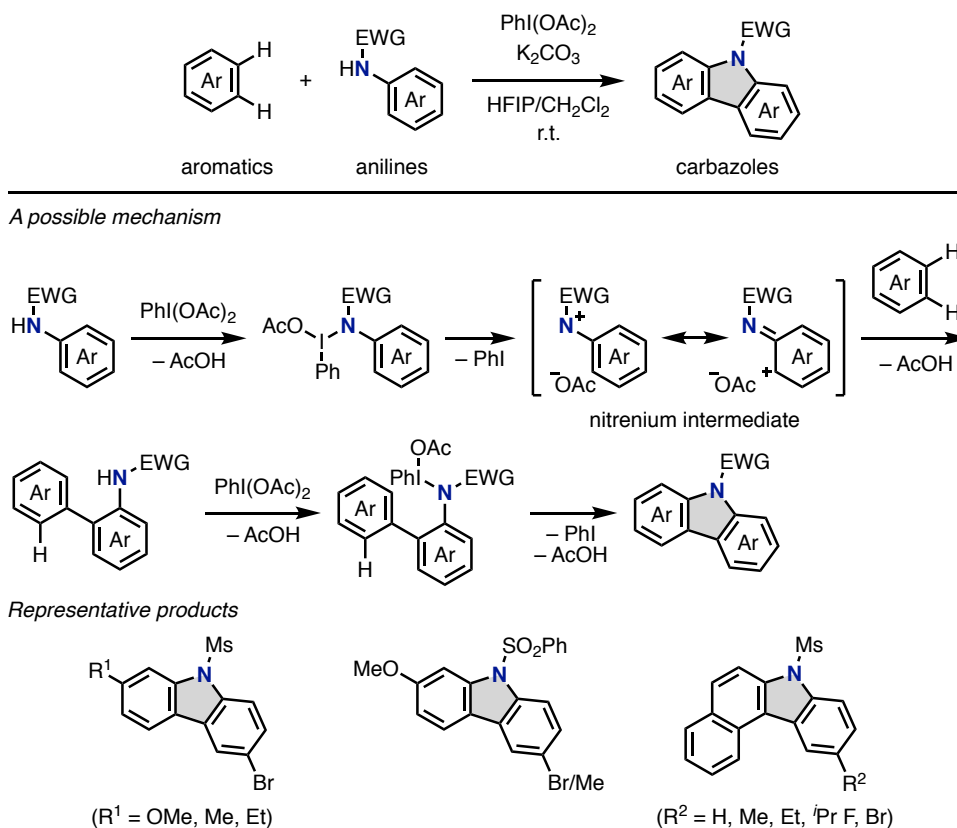
One-step aza-APEX reaction by C–H activation was developed by Wang, Li and co-workers in 2017 (Figure 13).<sup>[17]</sup> The aza-APEX reaction of isoquinolones proceeded in the presence of anthranils, a cationic rhodium complex and zinc (II) acetate as catalysts to afford acridine derivatives in one step. In this reaction, the amide groups of

isoquinolones work as directive groups for C–H activation by rhodium. In addition, the C–N bond formations are considered to give diarylamine intermediates at first which participates in the following intramolecular dehydrative cyclization. The same type aza-APEX reaction was demonstrated in the reaction of *N*-(4-methylbenzoyl)-pyrrolidine, providing acridine derivatives having an amide group. Compared with the conventional stepwise synthesis of acridine derivatives via the similar diarylamine intermediates (Figure 3), there is an advantage in terms of step-economy. However, there are some critical limitations on a substrate scope. One is that the starting aromatics need amide directing groups, and these are always included in the products. The other limitation would be a narrow substrate scope regarding both starting aromatics and anthranils. In other words, a directing group-free APEX reaction will be ideally desired in the future.



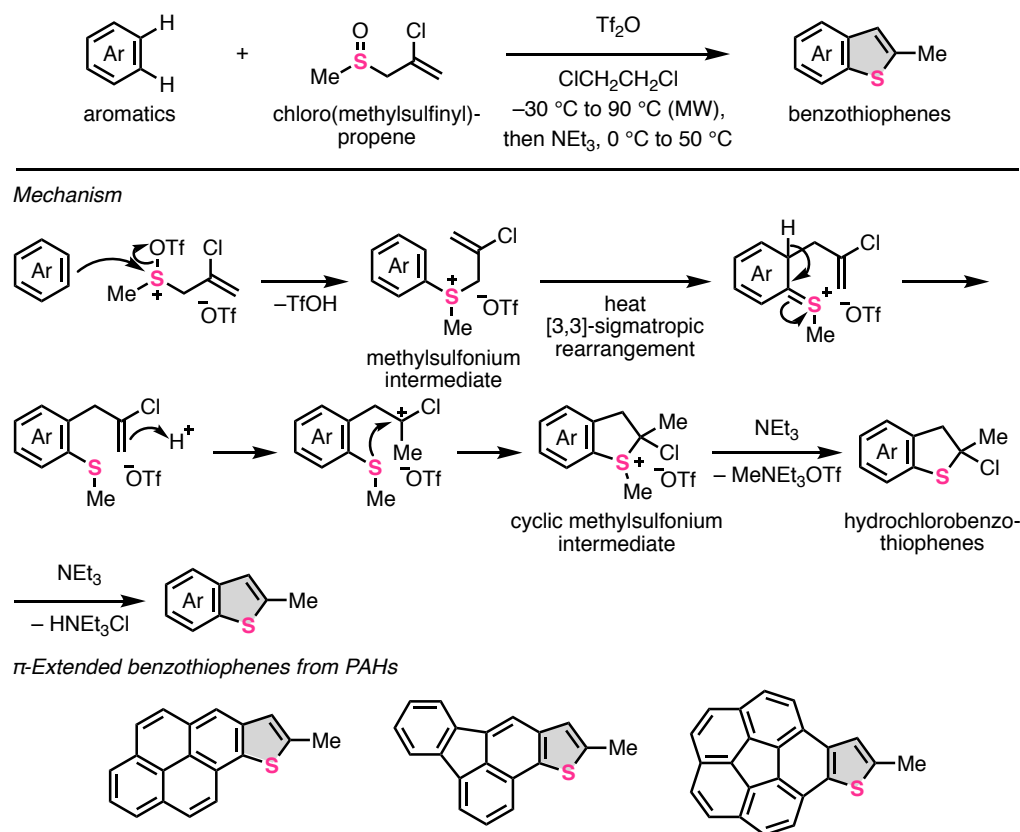
**Figure 13.** Directing group-assisted and rhodium-catalyzed APEX reactions of isoquinolones and pyrrolidine derivatives with anthranils as  $\pi$ -extending agents.

Moreover, synthesis of carbazoles by aza-APEX reaction was developed by Mal and co-workers in 2017 (Figure 14).<sup>[18]</sup> One-step synthesis of carbazole derivatives from aromatics such as toluene, anisole, and naphthalene was achieved with aniline derivatives bearing electron-withdrawing (EWG) groups. The aniline derivative was activated by iodobenzene diacetate to be transformed to a nitrenium intermediate, which is an electrophilic activated species. Then aromatic nucleophilic substitution occurred between the unfunctionalized aromatic substrate the cationic intermediates to afford an *ortho*-aminobiaryl intermediate. This intermediate can be further cyclized upon oxidation of nitrogen atom by iodobenzene diacetate. With this aza-APEX reaction, various carbazole derivatives such as benzocarbazoles and precursors of some carbazole alkaloids were easily synthesized.



**Figure 14.** Aza-APEX reactions using anilines and iodobenzene diacetate.

Procter and co-workers achieved a thia-APEX reaction to construct thiophene rings onto various unfunctionalized aromatics in 2019 (Figure 15).<sup>[19]</sup> In this reaction system, chloro(methylsulfinyl)-propane activated by  $\text{Tf}_2\text{O}$  directly reacted with unfunctionalized aromatic substrates to afford a methylsulfonium intermediate. Then, this intermediate underwent [3,3]-sigmatropic rearrangement and rearomatization, followed by intramolecular nucleophilic addition by the sulfur atom to form a cyclic methylsulfonium intermediate. The cyclic methylsulfonium intermediate was transformed to the corresponding benzothiophene derivatives by a base such as triethylamine. Furthermore, this thia-APEX reaction system was applicable to unfunctionalized polycyclic aromatic hydrocarbons (PAHs) such as pyrene, fluoranthene and corannulene. Using such PAHs as substrates, several hetero-PACs having 2-methylthiophene ring were afforded.

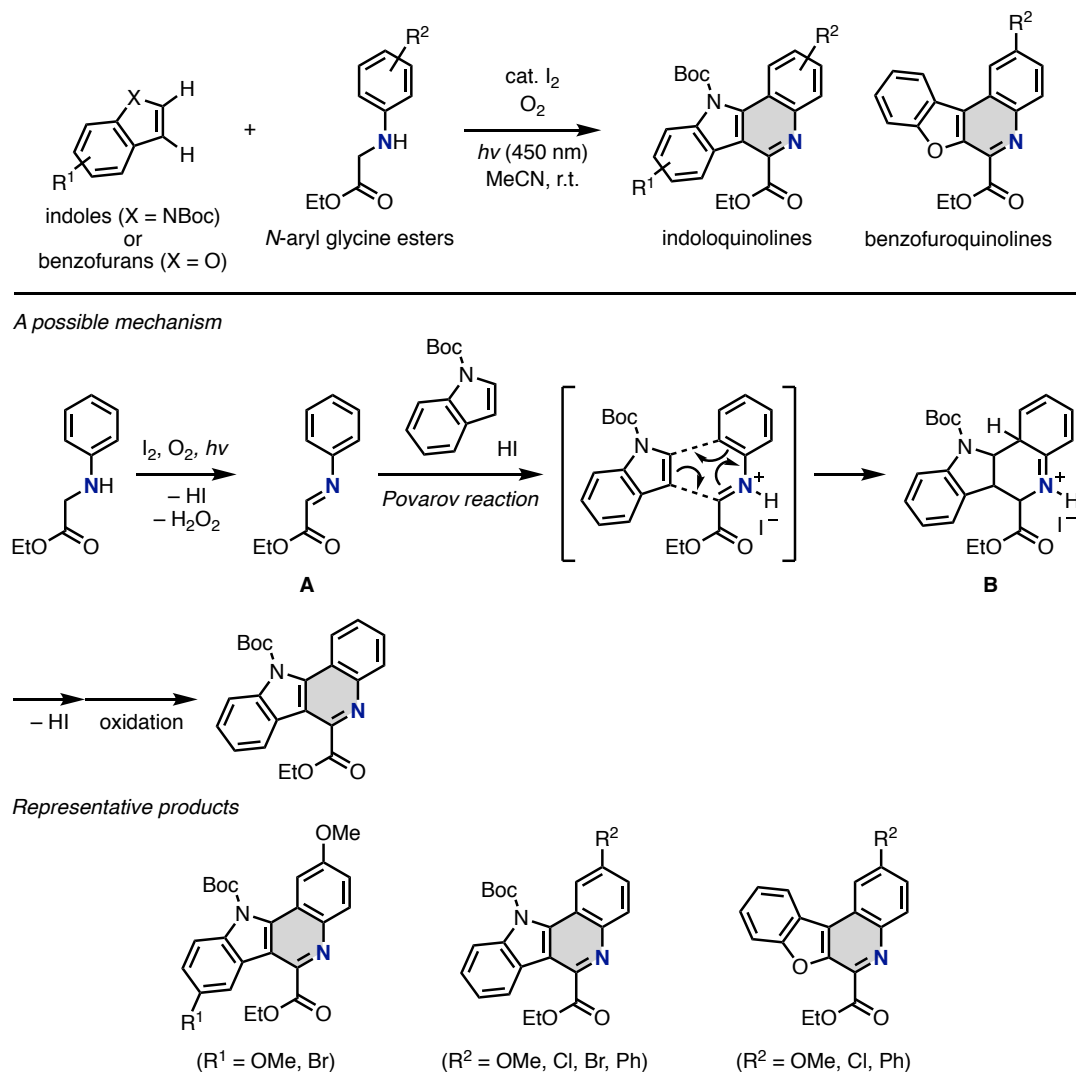


**Figure 15.** Thia-APEX of unfunctionalized aromatics by chloro(methylsulfinyl)propene as a  $\pi$ -extending agent.

In 2020, Brasholz and co-workers developed an aza-APEX reaction for synthesis of indoloquinoline and benzofuroquinoline derivatives by iodine-mediated photoredox reaction (Figure 16).<sup>[20]</sup> Utilizing *N*-aryl glycine esters with catalytic amounts of iodine under oxygen atmosphere with irradiation of 450 nm light, aza-APEX reactions of indole and benzofuran derivatives proceeded in a fashion of quinolino-annulation. In Figure 16, a possible mechanism of this reaction using *N*-Boc indole as a substrate is described. At first, the *N*-aryl glycine ester is oxidized to imine intermediate **A** by iodine and oxygen along with releasing hydrogen iodide and hydrogen peroxide. Intermediate **A** is also known as a key intermediate in Povarov reaction which constructs a pyridine structure upon reacting with alkene.<sup>[21]</sup> In this aza-APEX system, *in situ*-generated intermediate **A** directly constructed tetrahydropyridine rings onto indoles with an exclusive regioselectivity, leading to the formation of intermediate **B**. Finally, intermediate **B** is oxidatively aromatized to form the corresponding indoloquinoline products. Interestingly, the regiochemistry of benzofuroquinolines afforded from benzofurans is different from indoloquinolines, while the detailed mechanism and reason are not clarified in the

Brasholz's report. Moreover, this reaction is applicable to other substituted indoles/benzofurans and *N*-aryl glycine esters, whereas some heteroles such as benzothiophene cannot be used in this reaction.

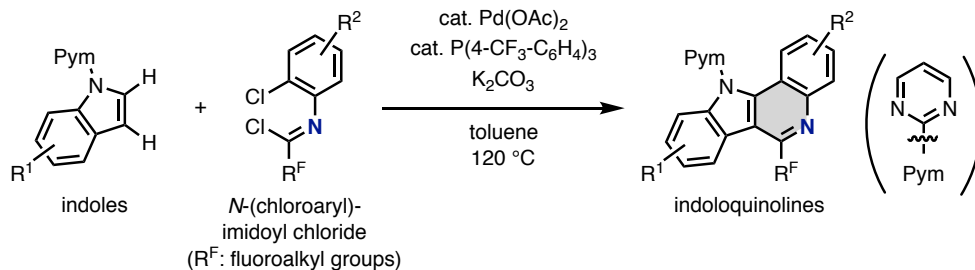
+



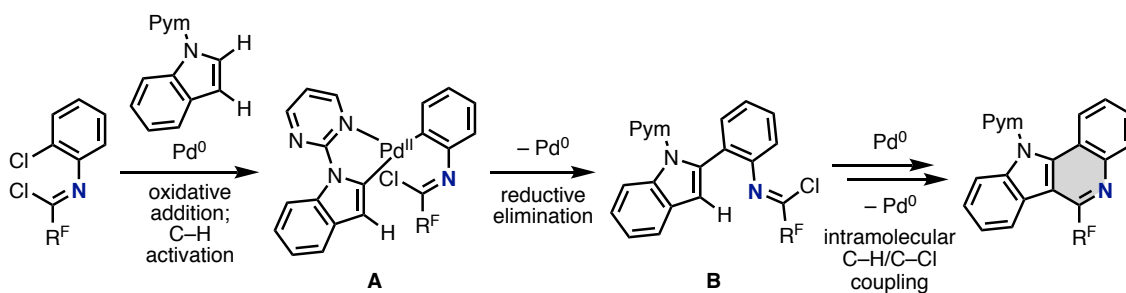
**Figure 16.** Povarov reaction-type aza-APEX reaction of indoles and benzofurans with *N*-aryl glycine esters by a photoredox catalytic system with iodine/O<sub>2</sub>.

A similar quinolino-annulation type aza-APEX reaction of indole derivatives was developed by Chen and Zhu in 2020. In this report, a *N*-pyrimidyl group was utilized as a directing group for palladium-catalyzed annulative double C–H activation of indoles (Figure 17).<sup>[22]</sup> With *N*-(chloroaryl)imidoyl chlorides including perfluoroalkyl groups, the one-step annulation was realized through a catalytic direct C–H arylation and C–H acylation with excellent regioselectivity. As one of possible reaction mechanisms, the formation of Pd-complex **A** and arylated indole intermediate **B** are expected. Moreover,

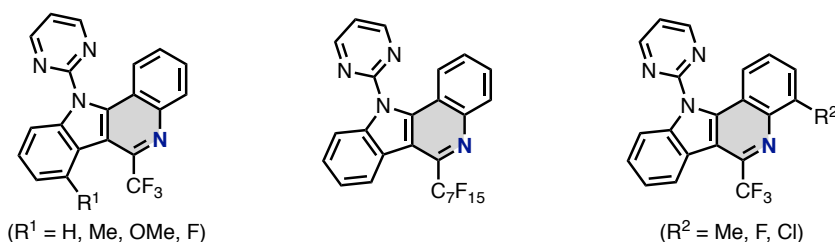
indoloquinoline can be formed through an intramolecular C–H/C–Cl coupling. Both the fluoroalkyl groups and the pyrimidyl (Pym) group must be contained in the skeleton of products so that the scope of substrate seems to be narrow and specific. However, regioselective and one-step quinolino-annulations is attractive from a viewpoint of step-economy and easy and rapid preparation of polycyclic heteroaromatic skeleton.



A possible mechanism



Representative products



**Figure 17.** Pyrimidyl group-directed and palladium-catalyzed aza-APEX reaction of indole derivatives using *N*-(chloroaryl)imidoyl chlorides as  $\pi$ -extending agents.

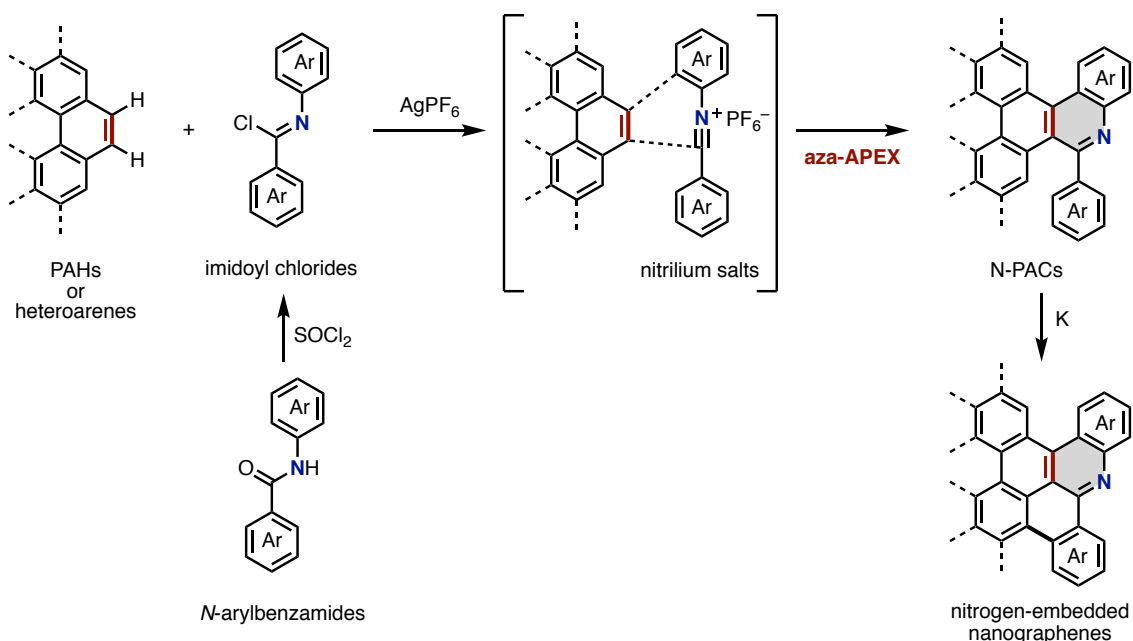
### 3. Overview of Thesis

As described in the previous sections, the concept of hetero-APEX and such reactions are undoubtedly important for realizing an efficient preparation of hetero-PACs. Besides, late-stage functionalization by hetero-APEX is also expected, which has a potential to contribute to a future development of novel functional materials, synthetic organic chemistry, functional organic chemistry as well as materials science. Before the author's unofficial definition of the concept of hetero-APEX in early 2017, there are only quite a few examples that can be categorized to hetero-APEX or formal hetero-APEX as exemplified in Figures 10, 11 and 14.<sup>[14,15,18]</sup> It should also be noted that several recent



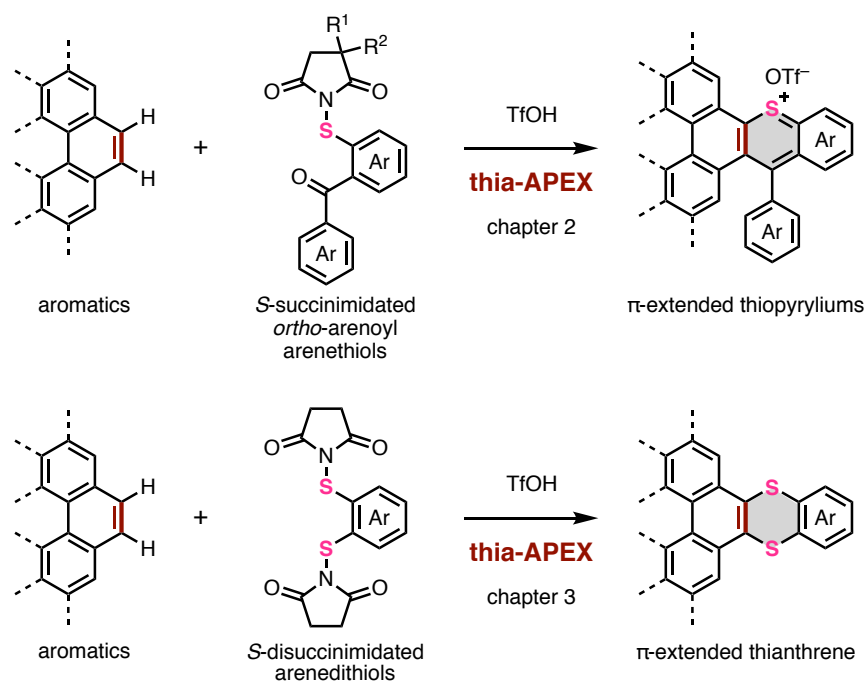
examples of one-step aza-/thia-APEX reactions have been reported by Procter, Brasholz, and Chen and Zhu in 2019–2020.<sup>[19,20,22]</sup> They appeared at almost the same time as the author's official definition of hetero-/aza-APEX in the paper on aza-APEX reaction<sup>[23]</sup> described in Chapter 1. After this official definition, some aza-APEX reactions were reported in 2021.<sup>[24]</sup> Even until the time when the author summarized this Ph.D. thesis on December 2022, the total number of reports on hetero-APEX reaction is still quite a few.<sup>[14–20,22–24]</sup> The chemistry of hetero-APEX includes various synthetic limitations such as the narrow scope of substrates, hetero-APEX and constructable hetero-PAC skeletons. For example, the substrates for hetero-APEX reactions often require electron-rich heterole moieties and appropriate directing groups, whereas pristine PAHs are still difficult to be used as substrates. Therefore, the development of new hetero-APEX reactions and new design of  $\pi$ -extending agents are still essential to expand the hetero-APEX chemistry as well as the synthetic chemistry of hetero-PACs. With these backgrounds, in early 2017, the author had begun to develop new synthetic methodologies for hetero-PACs by exploring novel hetero-APEX reactions. In this thesis, the development of three kinds of novel hetero-APEX reactions are described.

Chapter 1 describes the development of a novel aza-APEX reaction of functionalized PAHs and heteroarenes realized by diarylimidoyl chlorides as  $\pi$ -extending agents (Figure 18).<sup>[23]</sup> *In situ*-generated highly electrophilic diaryl nitrilium hexafluorophosphates from aryl imidoyl chlorides and AgPF<sub>6</sub> efficiently coupled with unfunctionalized substrates through a formal [4+2] cycloaddition and rearomatization. As a result, nitrogen-containing PACs (N-PACs) composed of polycyclic quinoline structures were synthesized in one step from various unfunctionalized aromatics. One of advantages in this reaction is a high synthetic utility and variety of simple *N*-arylbenzamides as precursors of imidoyl chlorides, and synthesis of various N-PACs was possible even with unreactive PAHs under simple reaction conditions. The detailed scope on substrates, reaction mechanism computed by the density functional theory (DFT) method as well as applications to the synthesis of nitrogen-embedded nanographenes are demonstrated.



**Figure 18.** Chapter 1: aza-APEX reaction of PAHs/heteroarenes with diaryimidoyl chlorides affording quinoline-fused N-PACs

In Chapters 2 and 3, novel thia-APEX reactions affording sulfur-containing PACs (S-PACs) are described (Figure 19). In Chapter 2, a new thia-APEX reaction by one-step  $\pi$ -extension with *S*-succinimidated *ortho*-arenoyl arenethiols was newly developed. In this thia-APEX reaction, various  $\pi$ -extended thiopyrylium salts as S-PACs, sulfur analogues of cationic six-membered pyrylium ring, having characteristic absorption/emission properties were obtained from easily available aromatic compounds in one step. The key of successful reaction is a double nucleophilic activation of *S*-succinimide and *ortho*-arenoyl groups by TfOH, resulting in the sequence of annulative  $\text{S}_{\text{E}}\text{Ar}$  reaction and successive dehydroxylative aromatization in one step. Furthermore, the detailed scope of substrates and the discussions on the photophysical properties of  $\pi$ -extended thiopyrylium salts are described. In Chapter 3, the author optimized the structure of  $\pi$ -extending agents to realize another thia-APEX reaction affording S-PACs including thianthrene structures ( $\pi$ -extended thianthrenes). Utilizing *S*-disuccinimidated arenedithiols with TfOH, a one-step synthesis of  $\pi$ -extended thianthrenes from commercially available unfunctionalized aromatic compounds was achieved. In addition, reaction features, a substrate scope, and photophysical properties of new  $\pi$ -extended thianthrenes are described in detail.



**Figure 19.** Thia-APEX reaction for one-step synthesis of S-PACs containing thiopyrylium rings (Chapter 2), and thia-APEX reaction for one-step synthesis of S-PACs containing thianthrene cores (Chapter 3).

## References

- [1] (a) Stępień, M.; Gonka, E.; Żyła, M.; Sprutta, N. *Chem. Rev.* **2017**, *117*, 3479. (b) Borissov, A.; Maurya, Y. K.; Moshniaha, L.; Wong, W.-S.; Żyła-Karwowska, M.; Stępień, M. *Chem. Rev.* **2022**, *122*, 565. (c) Li, H.; Shi, W.; Song, J.; Jang, H.-J.; Dailey, J.; Yu, J.; Katz, H. E. *Chem. Rev.* **2019**, *119*, 3. (d) Karak, P.; Rana, S. S.; Choudhury, J. *Chem. Commun.* **2022**, *58*, 133. (e) Wang, C.; Dong, H.; Hu, W.; Liu, Y.; Zhu, D. *Chem. Rev.* **2012**, *112*, 2208. (f) Janosik, T.; Rannug, A.; Rannug, U.; Wahlström, N.; Slatt, J.; Bergman, J. *Chem. Rev.* **2018**, *118*, 9058. (g) Hirai, M.; Tanaka, N.; Sakai, M.; Yamaguchi, S. *Chem. Rev.* **2019**, *119*, 8291. (h) Dhbaibi, K.; Favereau, L.; Crassous, J. *Chem. Rev.* **2019**, *119*, 884. (i) Wöhrle, T.; Wurzbach, I.; Kirres, J.; Kostidou, A.; Kapernaum, N.; Litterscheidt, J.; Haenle, J. C.; Staffeld, P.; Baro, A.; Giesselmann, F.; Laschat, S. *Chem. Rev.* **2016**, *116*, 1139. (j) Cai, Z.; Awais, M. A.; Zhang, N.; Yu, L. *Chem* **2018**, *4*, 2538. (k) Anthony, J. E. *Chem. Rev.* **2006**, *106*, 5028.
- [2] (a) Terrones, H.; Lv, R.; Terrones, M.; Dresselhaus, M. S. *Rep. Prog. Phys.* **2012**, *75*, 062501. (b) Szűcs, R.; Bouit, P.-A.; Nyulászi, L.; Hissler, M. *ChemPhysChem* **2017**, *18*, 2618. (c) Jeong, E.-J.; Kim, Y.-K.; Park, J.-H.; Lee, E.-Y.; Hwang, S.-H. Condensed Cyclic Compounds and Organic Light-Emitting Devices Including the Same. US 20150349275 A1, Dec. 3, 2015. (d) Nakayama, K.; Hashimoto, Y.; Sasabe, H.; Pu, Y.-J.; Yokoyama, M.; Kido, J. *Jpn. J. Appl. Phys.* **2010**, *49*, 01AB11. (e) Yamaguchi, A. D.; Chepiga, K. M.; Yamaguchi, J.; Itami, K.; Davies, H. M. L. *J. Am. Chem. Soc.* **2015**, *137*, 644. (f) Ma, Y.; Sun, Y.; Liu, Y.; Gao, J.; Chen, S.; Sun, X.; Qiu, W.; Yu, G.; Cui, G.; Hu, W.; Zhu, D. *J. Mater. Chem.* **2005**, *15*, 4894. (g) Bazzini, C.; Brovelli, S.; Caronna, T.; Gambarotti, C.; Giannone, M.; Macchi, P.; Meinardi, F.; Mele, A.; Panzeri, W.; Recupero, F.; Sironi, A.; Tubino, R. *Eur. J. Org. Chem.* **2005**, *2005*, 1247. (h) Xiao, L.; Lan, H.; Kido, J. *Chem. Lett.* **2007**, *36*, 802. (i) Cheng, C.-H.; Wu, J.-L.; Liao, C.-Y. Green Phosphorescent Iridium Complexes, Fabrication Method Thereof and Organic Light-Emitting Diodes Comprising the Same. US 20148753756 B2, Jun. 17, 2014. (j) Mamada, M.; Minamiki, T.; Katagiri, H.; Tokito S. *Org. Lett.* **2012**, *14*, 4062. (k) Tanaka, K.; Iwama, Y.; Kishimoto, M.; Ohtsuka, N.; Hoshino, Y.; Honda, K. *Org. Lett.* **2020**, *22*, 5207. (l) Li, M.; Xie, W.; Cai, X.; Peng, X.; Liu, K.; Gu, Q.; Zhou, J.; Qiu, W.; Chen, Z.; Gan, Y.; Su, S.-J. *Angew. Chem., Int. Ed.* **2022**, *61*, e202209343. (m) Tsuji, H.; Nakamura, E. *Acc. Chem. Res.* **2017**, *50*, 396. (n) Chen, X.; Yan, L.; Liu, Y.; Yang, Y.; You, J. *Chem. Commun.* **2020**, *56*, 15080.
- [3] (a) Marco-Contelles, J.; Pérez-Mayoral, E.; Samadi, A.; Carreiras, M. d. C.; Soriano, E. *Chem. Rev.* **2009**, *109*, 2652. (b) Sun, Y.-X.; Wang, X.-G.; Shen, G.-D.; Yang, T.; Yang, Y.-H.; Li, J.; Yang, M.-Y.; Sun, H.-M.; Wei, J.-F. *Adv. Synth. Catal.* **2020**, *362*, 1651. (c) Goujon, A.; Rocard, L.; Cauchy, T.; Hudhomme, P. *J. Org. Chem.* **2020**, *85*, 7218. (d) Streckowski, L.; Czarny, A.; Lee, H. *J. Fluor. Chem.* **2000**, *104*, 281. (e) Tselikhovsky, D.; Buchwald, S. L. *J. Am. Chem. Soc.*

- 2010**, 132, 14048. (f) Ye, X.; Xu, B.; Sun, J.; Dai, L.; Shao, Y.; Zhang, Y.; Chen, J. *J. Org. Chem.* **2020**, 85, 13004. (g) Wang, T.-J.; Chen, W.-W.; Lia, Y.; Xu, M.-H. *Org. Biomol. Chem.* **2015**, 13, 6580. (h) Pang, X.; Lou, Z.; Li, M.; Wen, L.; Chen, C. *Eur. J. Org. Chem.* **2015**, 3361. (i) Guo, H.-M.; Mao, R.-Z.; Wang, Q.-T.; Niu, H.-Y.; Xie, M.-S.; Qu, G.-R. *Org. Lett.* **2013**, 15, 5460.
- [4] Examples of construction of pyrylium/thiopyrylium structures: (a) Kharchenko, V. G.; Kleimenova, V. I.; Yakoreva, A. R. *Chem. Heterocycl. Compd.* **1970**, 6, 834. (b) Berényi, S.; Tóth, M.; Gyulai, S.; Szilágyi, L. *Heterocycles* **2002**, 57, 135. (c) Wu, D.; Pisula, W.; Haberecht, M. C.; Feng, X.; Müllen, K. *Org. Lett.* **2009**, 11, 5686. (d) Nagahora, N.; Kushida, T.; Shioji, K.; Okuma, K. *Organometallics* **2019**, 38, 1800. (e) Tanaka, K.; Kishimoto, M.; Sukekawa, M.; Hoshino, Y.; Honda, K. *Tetrahedron Lett.* **2018**, 59, 3361. (f) Shen, G.-B.; Xia, K.; Li, X.-T.; Li, J.-L.; Fu, Y.-H.; Yuan, L.; Zhu, X.-Q. *J. Phys. Chem. A* **2016**, 120, 1779. (g) Shenbor, M. I.; Azarov, A. S. *Khim. Getero. Soedin.* **1979**, 29. (h) Rao, K. P.; Kusamoto, T.; Toshimitsu, F.; Inayoshi, K.; Kume, S.; Sakamoto, R.; Nishihara, H. *J. Am. Chem. Soc.* **2010**, 132, 12472. (i) Wehrmann, C. M.; Charlton, R. T.; Chen, M. S. *J. Am. Chem. Soc.* **2019**, 141, 3240. (j) Spiliopoulos, I. K.; Mikroyannidis, J. A. *Macromolecules* **2002**, 35, 7254.
- [5] Lv, B.; Xiao, J.; Zhou, J.; Zhang, X.; Duan, J.; Su, W.; Zhao, J. *ACS Appl. Mater. Interfaces* **2016**, 8, 18998.
- [6] Saint-Ruf, G.; Buu-Hoï, N. P.; Jacquignon, P. *J. Chem. Soc.* **1958**, 0, 1773–1776.
- [7] Zhang, S.; Qiao, X.; Chen, Y.; Wang, Y.; Edkins, R. M.; Liu, Z.; Li, H.; Fang, Q. *Org. Lett.* **2014**, 16, 342.
- [8] (a) Mackey, K.; Jones, D. J.; Pardo, L. M.; McGlacken, G. P. *Eur. J. Org. Chem.* **2021**, 495. (b) Đorđević, L.; Milano, D.; Demitri, N.; Bonifazi, D. *Org. Lett.* **2020**, 22, 4283.
- [9] Other examples of constructing heteroaromatic rings: (a) Waley, M. W.; Gorindachari, T. R. *Org. React.* **1951**, 6, 74. (b) Imran, M.; Wehrmann, C. M.; Chen, M. S. *J. Am. Chem. Soc.* **2020**, 142, 38. (c) Grebies, S.; Ito, M.; Sakai, M.; Osaki, H.; Kim, J. H.; Gensch, T.; Daniliuc, C.; Ando, N.; Yamaguchi, S.; Glorius, F. *Chem. Eur. J.* **2021**, 27, 2753. (d) Larock, R. C.; Yum, E. K.; Refvik, M. D. *J. Org. Chem.* **1998**, 63, 7652. (e) Masuya, Y.; Tobisu, M.; Chatani, N. *Org. Lett.* **2016**, 18, 4312. (f) Zeng, W.; Wu, W.; Jiang, H.; Huang, L.; Sun, Y.; Chen, Z.; Li, X. *Chem. Commun.* **2013**, 49, 6611. (g) Wang, S.; Lv, B.; Cui, Q.; Ma, X.; Ba, X.; Xiao, J. *Chem. Eur. J.* **2015**, 21, 14791. (h) Yue, D.; Larock, R. C. *J. Org. Chem.* **2002**, 67, 1905. (i) Meng, L.; Fujikawa, T.; Kuwayama, M.; Segawa, Y.; Itami, K. *J. Am. Chem. Soc.* **2016**, 138, 10351. (j) Song, T.; Han, Y.; Jin, P.; Li, X.; Song, Y.; Xiao, J. *J. Mater. Chem. C* **2019**, 7, 6344. (k) Miletić, T.; Fermi, A.; Orfanos, I.; Avramopoulos, A.; De Leo, F.; Demitri, N.; Bergamini, G.; Ceroni, P.; Papadopoulos, M. G.; Couris, S.; Bonifazi, D. *Chem. Eur. J.* **2017**, 23, 2363. (l) Saha, M.; Bao, Y.-H.; Zhou, C. A. *Chem. Lett.* **2018**, 47, 1383. (m) Ma, Y.; Shi, Z.; Zhang, A.; Li, J.; Wei, X.; Jiang, T.; Li, Y.; Wang, X. *Dyes Pigm.* **2016**, 135, 41.

- [10] (a) Ito, H.; Ozaki, K.; Itami, K. *Angew. Chem., Int. Ed.* **2017**, *56*, 11144. (b) Ito, H.; Segawa, Y.; Murakami, K.; Itami, K. *J. Am. Chem. Soc.* **2019**, *141*, 3.
- [11] Representative examples of APEX reaction of PAH and heteroaromatics: (a) Ozaki, K.; Zhang, H.; Ito, H.; Lei, A.; Itami, K. *Chem. Sci.* **2013**, *4*, 3416. (b) Ozaki, K.; Kawasumi, K.; Shibata, M.; Ito, H.; Itami, K. *Nat. Commun.* **2015**, *6*, 6251. (c) Ozaki, K.; Matsuoka, W.; Ito, H.; Itami, K. *Org. Lett.* **2017**, *19*, 1930. (d) Matsuoka, W.; Ito, H.; Itami, K. *Angew. Chem., Int. Ed.* **2017**, *56*, 12224. (e) Kitano, H.; Matsuoka, W.; Ito, H.; Itami, K. *Chem. Sci.* **2018**, *9*, 7556. (f) Nakamuro, T.; Kumazawa, K.; Ito, H.; Itami, K. **2019**, *30*, 423. (g) Matsuoka, W.; Ito, H.; Sarlah, D.; Itami, K. *Nat. Commun.* **2021**, *12*, 3940.
- [12] Shibata, M.; Ito, H.; Itami, K. *J. Am. Chem. Soc.* **2018**, *140*, 2196.
- [13] Examples of APEX reactions reported by other groups: (a) Schuler, B.; Collazos, S.; Gross, L.; Meyer, G.; Pérez, D.; Guitián, E.; Peña, D. *Angew. Chem., Int. Ed.* **2014**, *53*, 9004. (b) Sakakibara, T.; Tanaka, Y.; Yamaki, S. *Chem. Lett.* **1986**, *15*, 797. (c) Pham, V. M.; Cramer, N. *Angew. Chem., Int. Ed.* **2014**, *53*, 3484. (d) Abid, M.; Spaeth, A.; Török, B. *Adv. Synth. Catal.* **2006**, *348*, 2191. (e) Dann, O.; Kokorudz, M.; Gropper, R. *Chem. Ber.* **1954**, *87*, 140. (f) Tang, R.-Y.; Li, J.-H. *Chem. Eur. J.* **2010**, *16*, 4733. (g) Clement, J. A.; Sivasakthikumar, R.; Mohanakrishnan, A. K.; Sundaramoorthy, S.; Velmurugan, D. *Eur. J. Org. Chem.* **2011**, 569. (h) Deb, M. L.; Baruah, B.; Bhuyan, P. J. *Synthesis* **2008**, No.2, 286. (i) Alonso, M. Á.; López-Alvarado, P.; Avendaño, C.; Menéndez, J. C. *Tetrahedron* **2003**, *59*, 2821. (j) Laha, J. K.; Dayal, N. *Org. Lett.* **2015**, *17*, 4742. (k) Matsuda, Y.; Naoe, S.; Oishi, S.; Fujii, N.; Ohno, H. *Chem. Eur. J.* **2015**, *21*, 1463. (l) Yamashita, M.; Horiguchi, H.; Hirano, K.; Satoh, T.; Miura, M. *J. Org. Chem.* **2009**, *74*, 7481. (m) Song, G.; Gong, X.; Li, X. *J. Org. Chem.* **2011**, *76*, 7583. (n) Lee, J. B.; Kim, G. H.; Jeon, J. H.; Jeong, S. Y.; Lee, S.; Park, J.; Lee, D.; Kwon, Y.; Seo, J. K.; Chun, J.-H.; Kang, S. J.; Choe, W.; Rohde, J.-U.; Hong, S. Y. *Nat. Commun.* **2022**, *13*, 2421.
- [14] Hiruta, K.; Kitahara, K.; Nishi, H.; Tokita, S. *Synthesis* **1982**, 1982, 229.
- [15] Aksenov, A. V.; Aksenov, N. A.; Lyakhovnenko, A. S.; Aksenova, I. V. *Synthesis* **2009**, No.20, 3439.
- [16] (a) Tokimaru, Y.; Ito, S.; Nozaki, K. *Angew. Chem., Int. Ed.* **2018**, *57*, 9818. (b) Tokimaru, Y.; Ito, S.; Nozaki, K. *Angew. Chem., Int. Ed.* **2017**, *56*, 15560.
- [17] Wang, M.; Kong, L.; Wang, F.; Li, X. *Adv. Synth. Catal.* **2017**, *359*, 4411.
- [18] Maiti, S.; Achar, T. K.; Mal, P. *Org. Lett.* **2017**, *19*, 2006.
- [19] Yan, J.; Pulis, A. P.; Perry, G. J. P.; Procter, D. J. *Angew. Chem., Int. Ed.* **2019**, *58*, 15675.
- [20] Schendera, E.; Unkel, L.-N.; Quyen, P. P. H.; Salkewitz, G.; Hoffmann, F.; Villinger, A.; Brasholz, M. *Chem. Eur. J.* **2020**, *26*, 269.
- [21] Kouznetsov, V. V. *Tetrahedron* **2009**, *65*, 2721.
- [22] Chen, C.; Wang, Y.; Shi, X.; Sun, W.; Zhao, J.; Zhu, Y.-P.; Liu, L.; Zhu, B. *Org. Lett.* **2020**,

22, 4097.

[23] Kawahara, K. P.; Matsuoka, W.; Ito, H.; Itami, K. *Angew. Chem., Int. Ed.* **2020**, *59*, 6383.

[24] Bashir, M. A.; Zhang, Y.; Yu, H.; Wang, B.; Zhao, W.; Zhong, F. *Green Chem.* **2021**, *23*, 5031.

## Synthesis of Nitrogen-Containing Polyaromatics by Aza-Annulative $\pi$ -Extension of Unfunctionalized Aromatics

### Abstract

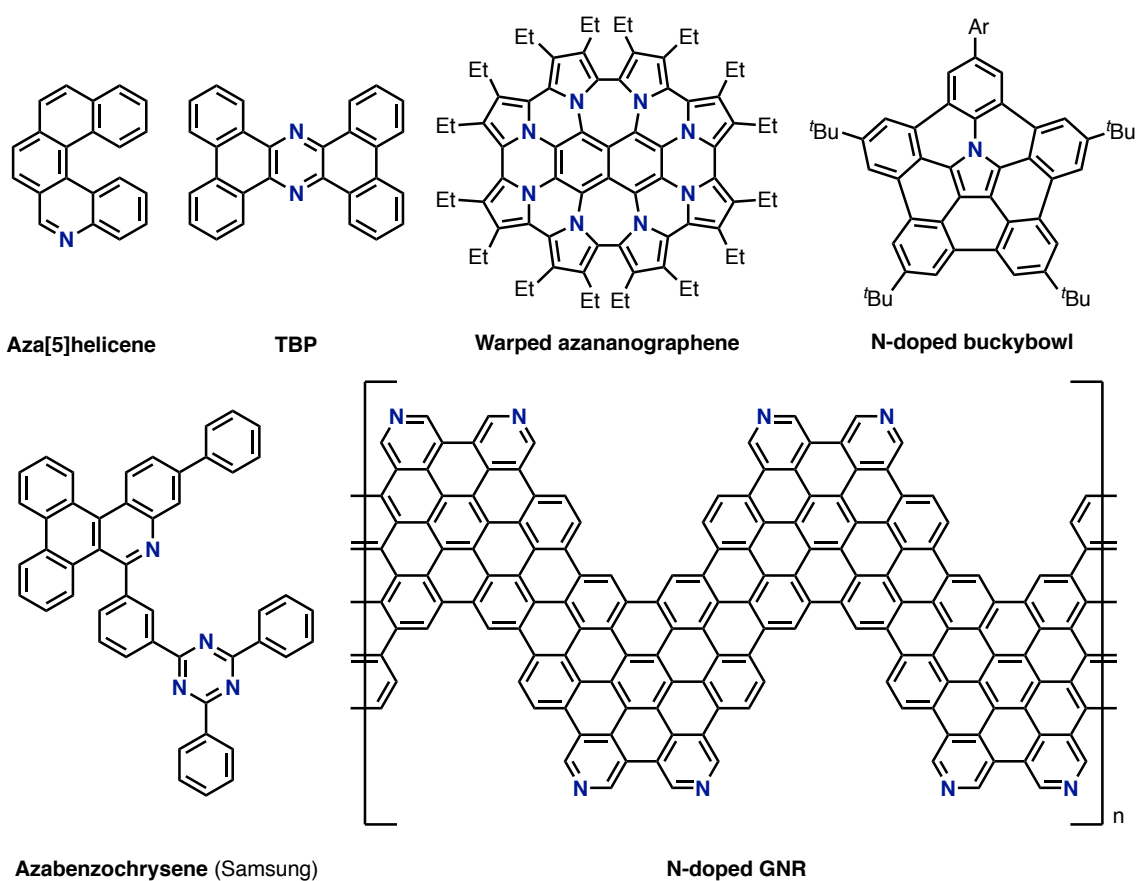
In this chapter, development of a new nitrogen-embedding annulative  $\pi$ -extension (aza-APEX) reaction that allows a rapid access to a range of nitrogen-containing polycyclic aromatic compounds (N-PACs) from readily available unfunctionalized aromatics and arylimidoyl chlorides are described. In the presence of  $\text{AgPF}_6$ , unfunctionalized arenes were coupled with arylimidoyl chlorides in a regioselective fashion, and subsequent oxidative treatment with *p*-chloranil affords structurally diverse N-PACs containing quinoline cores in 11–84% yields. DFT calculations reveal that the aza-APEX reaction proceeds through the formal [4+2] cycloaddition of the arene and an *in-situ* generated diarylnitrilium salt followed by sequential aromatization with relatively low activation energies. Transformation of N-PACs to nitrogen-doped nanographenes and their photophysical properties are also described.



## 1. Introduction

### 1-1. Nitrogen-embedded polycyclic aromatic compounds

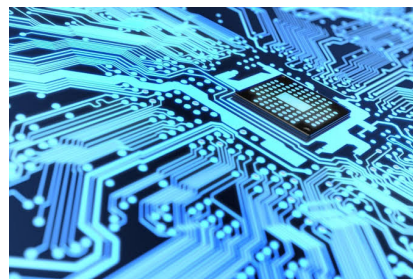
Nitrogen-embedded polycyclic aromatic compounds (N-PACs) have recently received a considerable amount of attention in synthetic chemistry and materials science.<sup>[1]</sup> Their electronic structures and properties such as HOMO–LUMO gaps, absorption/emission properties, redox potentials, basicity, coordinating behavior to metal, and supramolecular behavior depend heavily on the structures of N-PACs.<sup>[2]</sup> For instance, N-PACs containing pyridine rings as electron-deficient moieties show the potentials as electron-injecting materials. With pyrrole structures which are electron-rich than pyridines in general, N-PACs can show the ability of hole mobility. Some N-PACs react with metal salts such as iridium to form novel metal complexes showing phosphorescence emission from triplet excitation state. Besides, organic devices such as flexible thin film displays, organic light-emitting diodes (OLED), and organic field effect transistors (OFET) based on the photochemical properties of N-PACs are desired. Furthermore, if properly  $\pi$ -extended, N-PACs can enter the realm of nitrogen-doped nanographenes that are emerging class of materials in molecular electronics and devices.<sup>[3,4]</sup> Figure 1 shows some representative examples of functional N-PACs having unique photophysical and electronic properties. For instance, aza[5]helicene shows a long triplet lifetime enough to emit phosphorescent light.<sup>[1c]</sup> Tetrabenzophenazine (TBP) has low-lying energies of HOMO and LUMO, low film crystallinity, and high electron mobility.<sup>[1d]</sup> Warped azananographene consisted of naphthalene core and pyrrole moieties reported by Uno and co-workers shows unique UV/Vis absorption and aromaticity at the dication state.<sup>[3d]</sup> Nitrogen-doped buckybowls reported by Shinokubo and co-workers has attracted a great attention for its warped  $\pi$ -system, anisotropic  $\pi$  donors, and host–guest behavior with fullerene.<sup>[3f]</sup> Nitrogen-containing azabenzochrysene analogues have been developed as candidates of an electron transport layer (ETL) by Samsung.<sup>[4]</sup> Nitrogen-doped graphene nanoribbons (N-doped GNRs) are expected to have lower HOMO and LUMO than those of corresponding pristine GNRs.<sup>[3c]</sup> Therefore the construction of nitrogen-containing aromatic systems in a desired fashion is particularly important for controlling electronic properties and applications to electronic devices.



*Applications for EL device*



**thin film display**

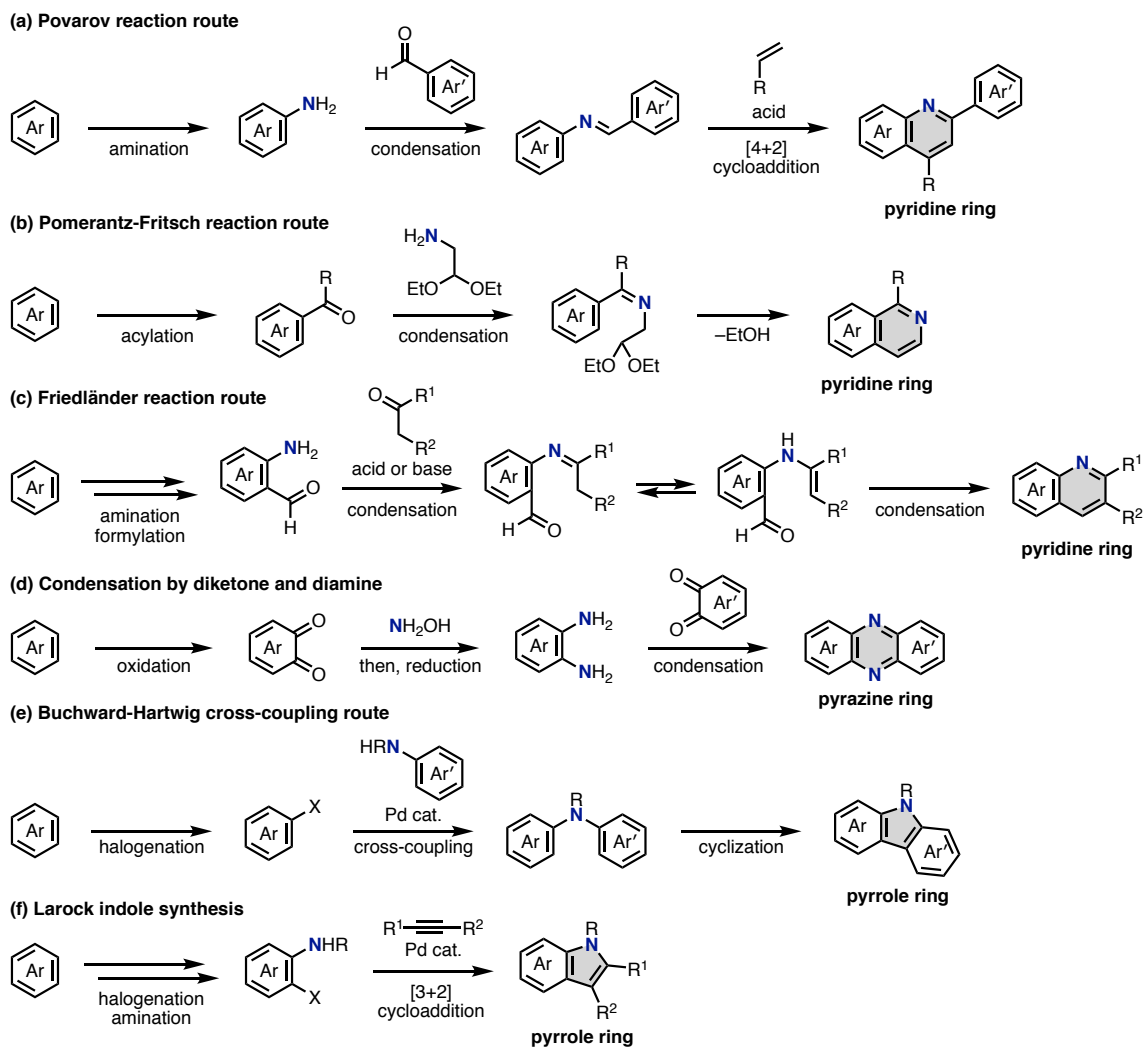


**OLED / OFET**

**Figure 1.** Representative examples of nitrogen-containing polycyclic aromatic compounds and their applications.

## 1-2. Conventional synthetic methods for N-PACs

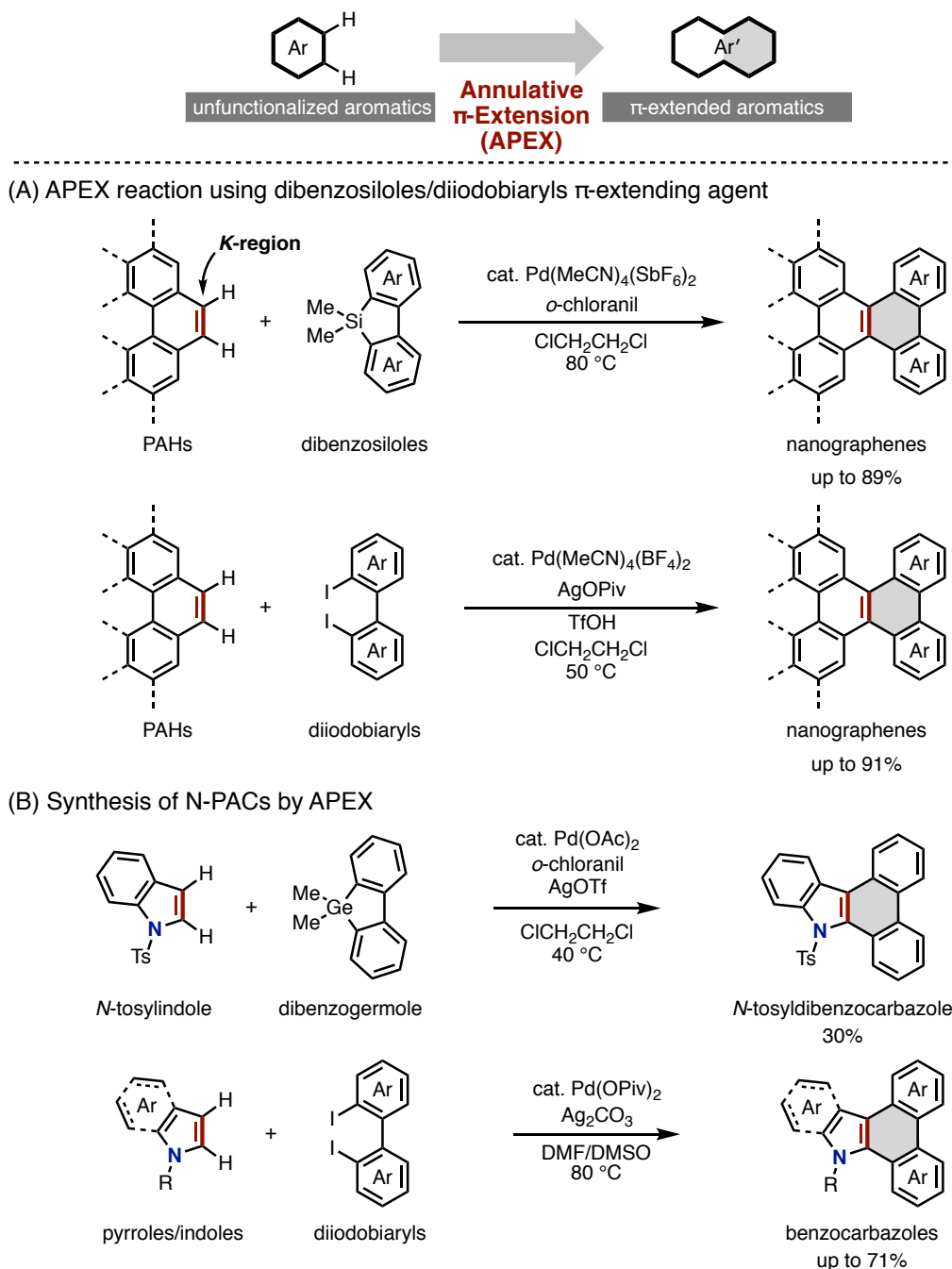
In response to high demands of N-PACs as mentioned in the previous section, there is a huge demand for the efficient and precise synthetic method to obtain N-PACs. The typical synthetic strategies for constructing nitrogen-doped aromatics rely on multi-step reactions.<sup>[2g,5,6]</sup> For example, as shown in Figure 2a–2d, condensations of (aromatic)aldehydes/ketones with (aromatic)amines and subsequent cyclization are the most versatile ways for obtaining N-PACs having pyrrole, pyridine, pyrazine and quinoline substructures. In particular, [4+2] cycloaddition between olefins and imines prepared from aldehydes and amines can construct pyridine ring (*i.e.*, Povarov reaction, Figure 2a).<sup>[6a,b]</sup> Even when condensing (aromatic)aldehydes and aminoacetaldehyde acetals, pyridine rings can be constructed (*i.e.*, Pomerantz–Fritsch reaction, Figure 2b).<sup>[6c,d]</sup> Moreover, pyridines are obtained by the condensations of 2-aminobenzaldehydes and ketones under acidic or basic conditions (*i.e.*, Friedländer reaction, Figure 2c).<sup>[6e]</sup> By condensing aromatic diamines and diketones such as phenanthrene-1,9-dione, pyrazine structures are formed (Figure 2d).<sup>[1d,6f]</sup> Furthermore, transition metal-catalyzed cross-coupling reactions such as Buchwald–Hartwig coupling and the Larock indole synthesis provide alternative synthetic routes to N-PACs from simple halogenated aromatics and (aromatic)amines, or halogenated aromatic amines. In particular, after the synthesis of diaryl amines by palladium-catalyzed arylation to halogenated arenes, a pyrrole ring can be afforded by subsequent photocyclization reactions (Figure 2e).<sup>[6g,h]</sup> On the other hand, pyrroles are also obtained even when alkynes are coupled with 2-haloanilines through palladium catalysis (Figure 2f).<sup>[6i,j]</sup> In any cases, preparations of functionalized starting materials are necessary, thus resulting in the stepwise protocols for obtaining N-PACs.



**Figure 2.** Representative synthetic routes to N-PACs via multi-step functionalizations and cyclizations.

### 1-3. APEX strategy for synthesis of N-PACs

Toward achieving more rapid and efficient access to fused aromatics such as N-PACs and nitrogen-doped nanographenes, the one-step  $\pi$ -extension of unfunctionalized (hetero)aromatics is considered as a prominent and ideal way. In this regard, Itami and Ito have established a novel synthetic concept, annulative  $\pi$ -extension (APEX) for the synthesis of  $\pi$ -extended (hetero)aromatics and polycyclic aromatic hydrocarbons (PAHs) (Figure 3).<sup>[7,8]</sup> For instance, they reported Pd-catalyzed one-step  $\pi$ -extension reaction of unfunctionalized PAHs with dibenzosiloles as  $\pi$ -extending agents (Figure 3A, above).<sup>[8a,b]</sup> This reaction regioselectively proceeds on *K*-region, the most olefinic sites on PAHs, affording various  $\pi$ -extended PAHs and nanographenes in one step. In addition, Itami and Ito improved the scope of substrates of APEX reaction utilizing diiodobiaryls with a AgOPiv/TfOH-mediated Pd-catalyzed reaction system (Figure 3A, below).<sup>[8h]</sup> In these APEX reaction systems, N-PACs can be synthesized from electron-rich heteroaromatics such as pyrroles and indoles are available as substrates. For example, *N*-tosylindole is transformed to *N*-tosyldibenzocarbazole in 30% yield by APEX reaction using dibenzogermole with Pd(OAc)<sub>2</sub> catalyst, *o*-chloranil, and AgOTf (Figure 3B, above).<sup>[8f]</sup> Moreover, utilizing Pd(OPiv)<sub>2</sub> catalyst, Ag<sub>2</sub>CO<sub>3</sub>, diiodobiaryls as  $\pi$ -extending agents, and DMF/DMSO solvent, more diverse benzocarbazoles are obtained in higher yield from pyrroles/indoles, in one step (Figure 3B, below).<sup>[8i]</sup> These examples indicate a potential of APEX for the rapid synthesis of N-PACs. However, the heteroaromatic moieties in N-PACs are derived from the pyrroles/indoles as starting materials, which means pre-construction/pre-embedding of appropriate heteroaromatic rings in advance are essential. In other words, a post-construction of heteroaromatic rings is impossible by the previous APEX reactions. Furthermore, the previous APEX reactions are only applicable to electron-rich five-membered ring heteroaromatics (heteroles), so that electron-deficient N-PACs such as pyridine-fused ones are difficult to be synthesized. To extend the chemistry of APEX as well as developing the synthetic chemistry of N-PACs, a new synthetic strategy such as a post-construction of various heteroaromatic rings is highly required.



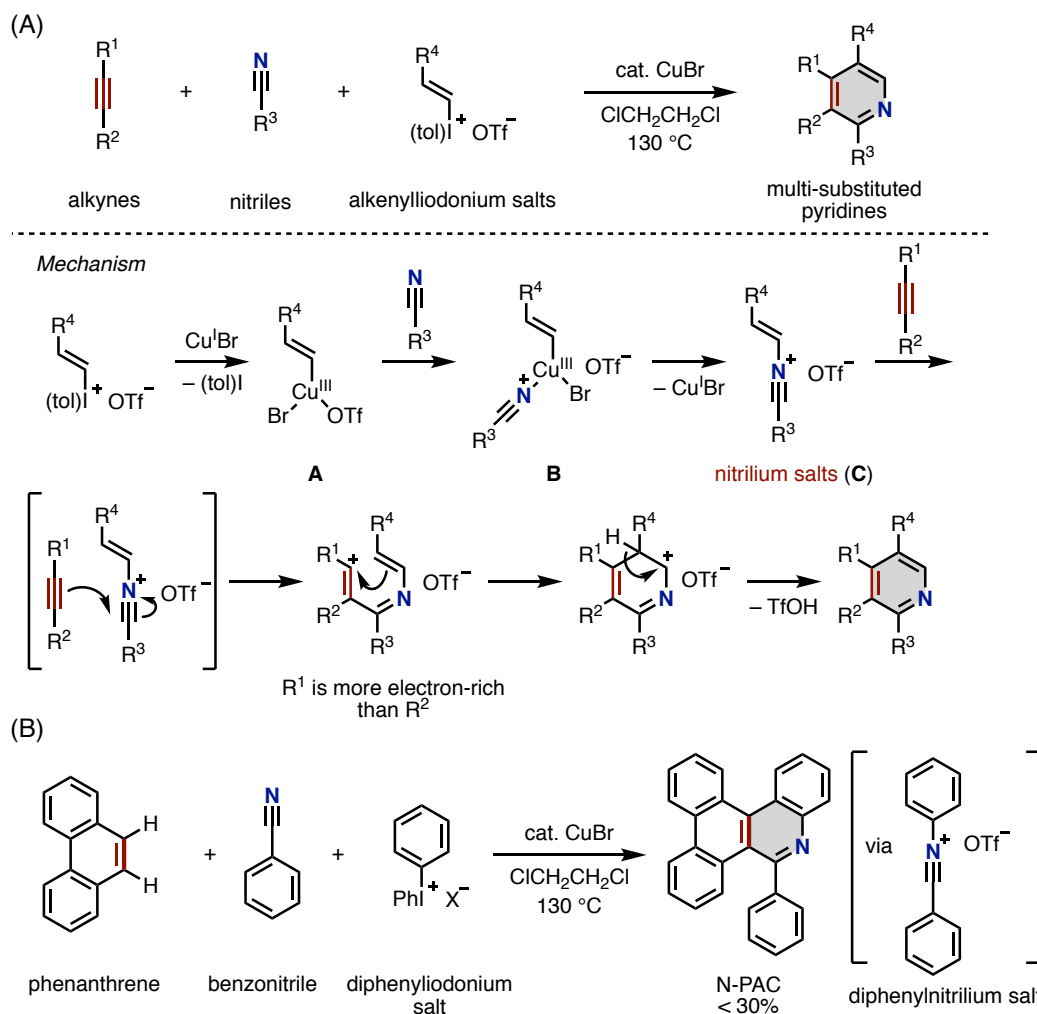
**Figure 3.** Concept of APEX and APEX reactions of unfunctionalized aromatics and heteroaromatics such as PAHs (A), indoles and pyrroles (B).

#### 1-4. Direct construction of pyridine ring by aza-APEX

With these backgrounds, the author was interested in a one-step  $\pi$ -extension of unfunctionalized (hetero)aromatics to achieve a rapid access to pyridine-fused N-PACs which are difficult to be synthesized in neither one-pot nor one-step. If one could develop an APEX reaction constructing new pyridine-fused structure, *i.e.*, “aza-APEX”,<sup>[9]</sup> the accessibility and utilization of emerging pyridine-fused

N-PACs and nitrogen-doped nanographenes will be significantly enhanced. To date, Aksenov and Blasholz reported an aza-APEX reaction that constructs new pyridine rings onto unfunctionalized aromatic templates as described in General Introduction of this thesis (pages 13 and 17, Figures 11 and 16).<sup>[9b,h]</sup> However as of 2017 when the author started researches on hetero-APEX reactions, any aza-APEX reaction constructing pyridine skeletons onto more diverse aromatic substrates such as PAHs has yet to be achieved. Hence, those aza-APEX reactions were only applied to limited aromatics.<sup>[9]</sup>

To realize aza-APEX for constructing pyridine structure, the author envisioned an aza-APEX using nitrilium salts as a nitrogen-containing reactive intermediate. Nitrilium salt is known as a reactive intermediate in a number of classical organic reactions such as Beckmann rearrangement,<sup>[10]</sup> Ritter reaction<sup>[11]</sup> and so on. In 2013–2017, Chen and co-workers achieved pyridine synthesis from alkynes and *in situ*-generated alkenylnitrilium salts by copper bromide, nitriles, and alkenyliodonium salts (Figure 4A).<sup>[12]</sup> In this reaction, alkenylnitrilium salts **C** seem to be generated via (1) the oxidative addition of alkenyliodonium salts to copper(I) bromide, (2) the ligand exchange of thus-formed alkenylcopper(III) complex **A** with nitriles and (3) the reductive elimination from intermediate **B**. Then, the formal [4+2] cycloaddition between alkynes and alkenylnitrilium salts **C** occurs to afford multi-substituted pyridines. Inspired by this report, the author expected that diarylnitrilium salt can directly react with phenanthrene under the Chen's reaction conditions. Thus, the author preliminary examined the reaction of phenanthrene with copper(I) bromide, benzonitrile and diphenyliodonium salt which can afford diphenylnitrilium salt *in situ* (Figure 4B).<sup>[13]</sup> After screening several conditions, a target N-PAC was obtained in up to 30% yield, which served as proof of concept and indicated a potential of nitrilium salts as  $\pi$ -extending agents for realizing a novel aza-APEX reaction. However, the low yield of APEX product, the moderate conversion of phenanthrene, and the side-production of a quinazoline derivative forced the author to explore other suitable  $\pi$ -extending agents as well as reaction conditions.



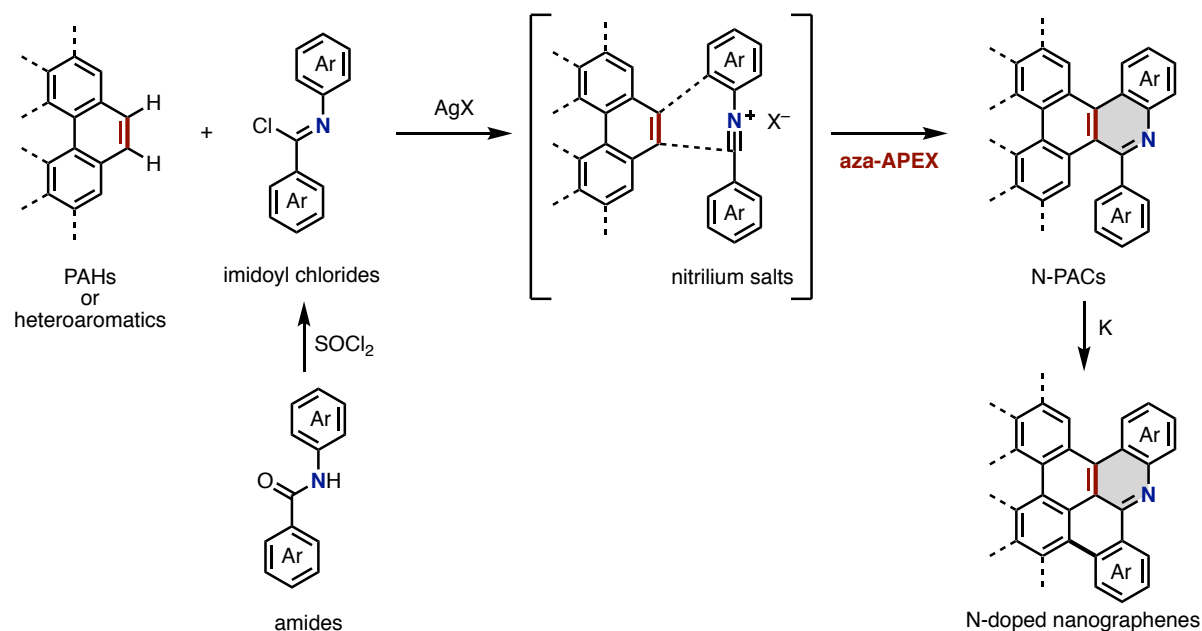
**Figure 4.** [4+2] Cycloaddition between alkyne and alkenylnitrilium salt. (A) Chen's pyridine synthesis using alkynes, nitriles and alkenyliodonium salts. (B) Author's preliminary experiments for development of aza-APEX reaction of phenanthrene using benzonitrile and diphenyliodonium salts.

### 1-5. This work

After an extensive screening of  $\pi$ -extending agents, additives and reaction conditions, the author finally discovered a more efficient aza-APEX reaction than the reaction with copper(I) bromide/benzonitrile/diphenyl iodonium salts. Herein, the author reports a new aza-APEX reaction of unfunctionalized PAHs and heteroaromatics using diarylimidoyl chlorides as precursors of diarylnitrilium intermediates. Diarylimidoyl chlorides can be readily prepared from the corresponding *N*-aryl benzamides, and thus-formed diarylnitrilium salts by the reaction with silver salts enabled a formal [4+2] cycloaddition with unfunctionalized aromatics to afford structurally and electronically diverse N-PACs upon treating the reaction crude mixtures with *p*-chloranil. In this chapter, detailed aza-APEX reaction conditions, a substrate scope, computational studies on reaction mechanism, and applications to synthesis



of nitrogen-doped nanographenes are described.

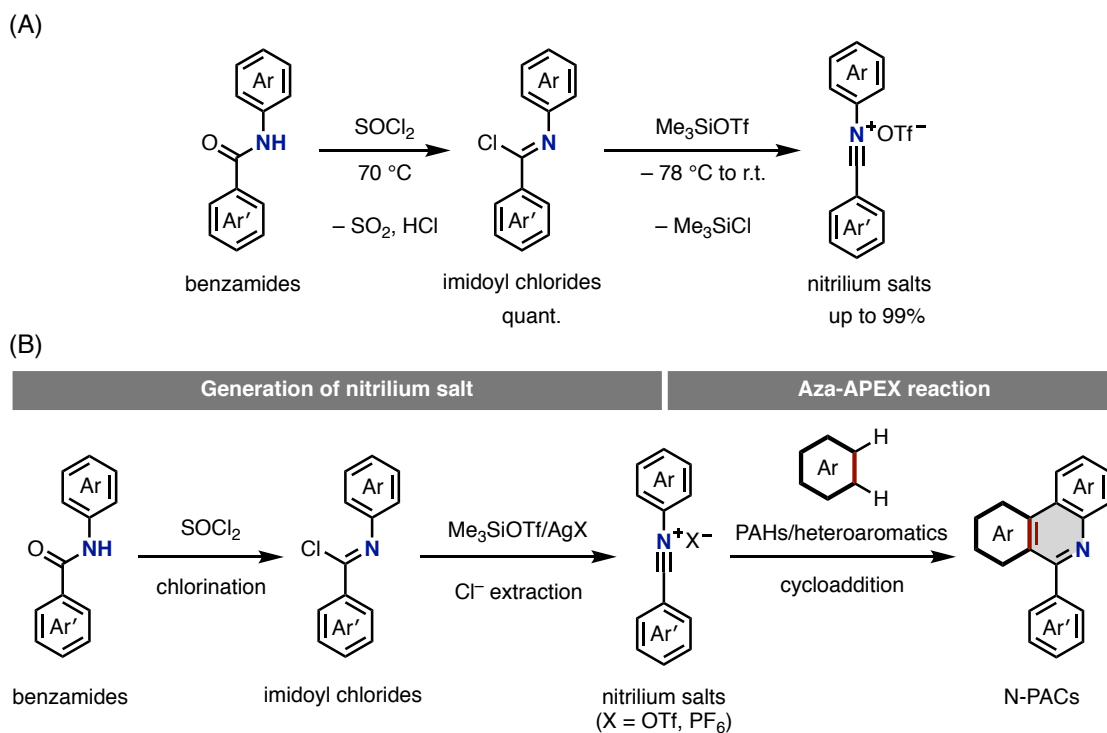


**Figure 5.** Aza-APEX reaction and synthesis of N-PACs and N-doped nanographenes.

## 2. Results and discussion

### 2-1. Optimization of reaction conditions for aza-APEX reaction

For maximizing an efficiency of aza-APEX reaction using nitrilium salts as  $\pi$ -extending agents, various methods for generating nitrilium salts were taken into account.<sup>[10,11]</sup> Among these, the author focused on the dechlorination of imidoyl chloride using trimethylsilyl triflate (Me<sub>3</sub>SiOTf) reported by Slootweg and Lammertsma (Figure 6A).<sup>[14]</sup> This method seems to be highly efficient because imidoyl chlorides are easily and quantitatively prepared from the corresponding *N*-arylbenzamide derivatives with thionyl chloride at 70 °C. According to this report, the author proposed that an aza-APEX reaction can be achieved through the following reaction steps: (1) preparation of diarylimidoyl chlorides from benzanilides, (2) generation of nitrilium salts by elimination of chloro group with Me<sub>3</sub>SiOTf, and (3) formal [4+2] cycloaddition between nitrilium salts and aromatic templates such as unfunctionalized PAHs and heteroaromatics followed by aromatization (Figure 6B). In addition, the use of silver salts such as AgOTf and AgPF<sub>6</sub> was also considered as an alternative activation way instead of using Me<sub>3</sub>SiOTf.

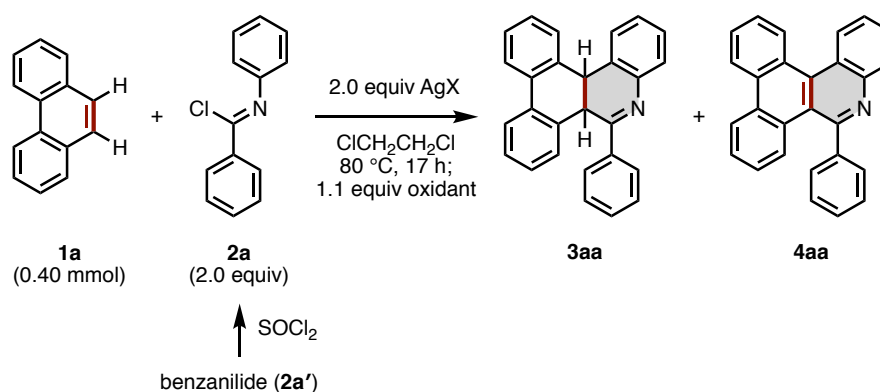


**Figure 6.** (A) Reported preparation method of nitrilium salts by Slootweg and Lammertsma. (B) Considered generation methods of nitrilium salts from benzamides, and working hypothesis for achieving the aza-APEX reaction using nitrilium salts as the  $\pi$ -extending agents (this work).

Based on the hypothesis in Figure 6B, the aza-APEX reactions were examined by treating phenanthrene (**1a**) (0.40 mmol, 1.0 equiv) with imidoyl chloride **2a** (2.0 equiv) prepared from benzanilide (**2a'**), and silver salts (2.0 equiv) in 1,2-dichloroethane at 80 °C for 17 h (Table 1). When the reaction was carried out with AgPF<sub>6</sub>, the aza-APEX reaction proceeded to afford desired 5-phenyldibenzo[*i,k*]phenanthridine (**4aa**) in 14% yield (entry 1), while the dihydro compound **3aa** was also obtained as the main product in 68% yield. The identification of structure of **4aa** and the regioselectivity of the aza-APEX reaction were elucidated by <sup>1</sup>H/<sup>13</sup>C NMR spectroscopies, and X-ray crystallographic analysis revealing that the  $\pi$ -extension occurred at the C9–C10 (*i.e.*, *K*-region) position selectively. When additional oxidants (1.1 equiv) such as *p*-chloranil, *o*-chloranil, *p*-benzoquinone, or 2,3-dichloro-5,6-dicyano-*p*-benzoquinone (DDQ) were added after the reactions, **4aa** was obtained as the main product in 65–77% yield (entries 2–5). In these reactions, **3aa** was hardly produced (<3% yield). As the result, *p*-chloranil was chosen as an oxidant in terms of exclusive formation of **4aa** with high yield. Moreover, the effects of counter anion of silver salts were also examined (entries 6–12). When employing AgCl and AgNO<sub>3</sub>, **4aa** was not formed at all (entries 6 and 7). The use of AgBF<sub>4</sub>, AgSbF<sub>6</sub>, and AgNTf<sub>2</sub> was found to be ineffective because yields of **4aa** were decreased to 32–42% yield (entries 8–10). When AgOTf or Me<sub>3</sub>SiOTf was used, yields were dramatically dropped (entries 11 and 12). Therefore, AgPF<sub>6</sub>

was found to be a suitable silver salt for the present aza-APEX reaction.

**Table 1.** Optimization of reaction conditions for aza-APEX reaction of phenanthrene (**1a**) with imidoyl chloride **2a**.



entry	X	oxidant	yield of <b>3aa</b> <sup>a</sup>	yield of <b>4aa</b> <sup>a</sup>
1	PF <sub>6</sub>	none	68%	14%
2	PF <sub>6</sub>	<i>p</i> -chloranil	N.D.	73%
3	PF <sub>6</sub>	DDQ	3%	77%
4	PF <sub>6</sub>	<i>o</i> -chloranil	N.D.	65%
5	PF <sub>6</sub>	<i>p</i> -benzoquinone	N.D.	70%
6	Cl	<i>p</i> -chloranil	N.D.	N.D.
7	NO <sub>3</sub>	<i>p</i> -chloranil	N.D.	N.D.
8	BF <sub>4</sub>	<i>p</i> -chloranil	N.D.	32%
9	SbF <sub>6</sub>	<i>p</i> -chloranil	N.D.	32%
10	NTf <sub>2</sub>	<i>p</i> -chloranil	N.D.	42%
11	OTf	<i>p</i> -chloranil	N.D.	5%
12 <sup>b</sup>	OTf	<i>p</i> -chloranil	N.D.	7%

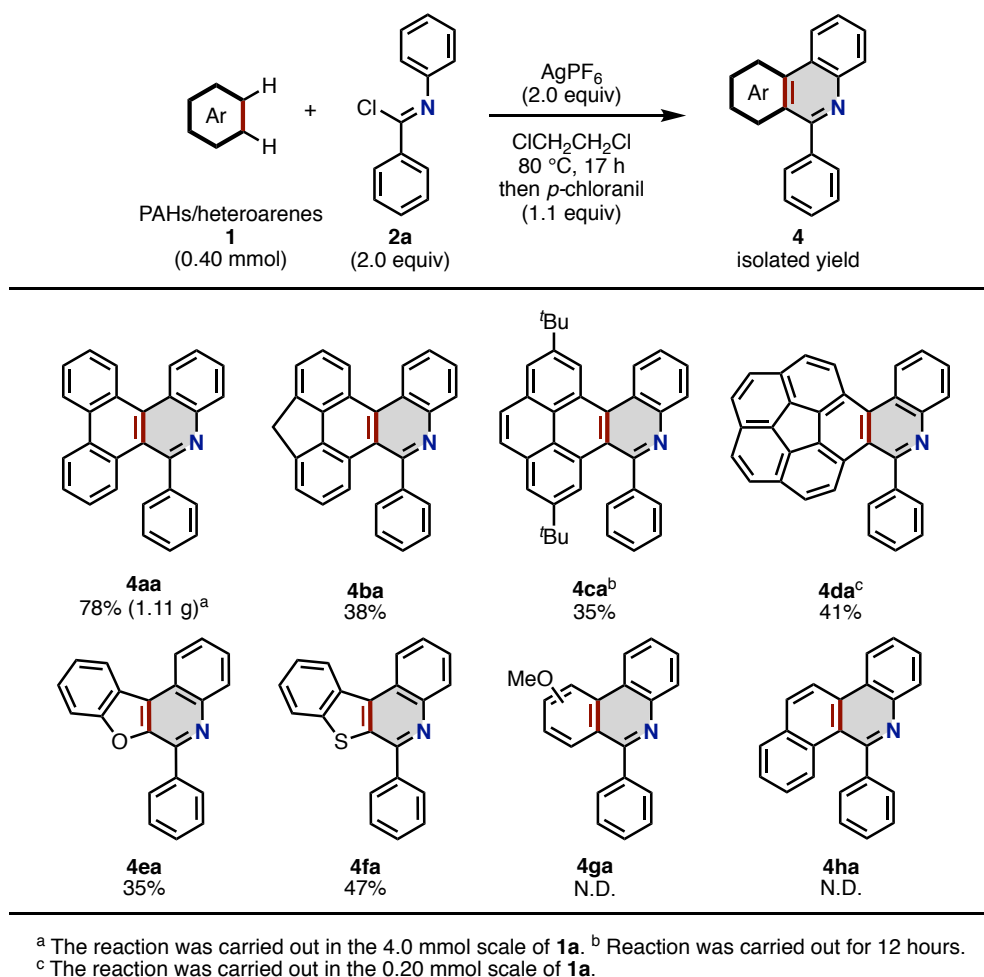
<sup>a</sup> NMR yiled. Dibromomethane was used as the internal standard.

<sup>b</sup> Me<sub>3</sub>SiOTf was employed as OTf anion source.

## 2-2. Scope of substrates

To assess the generality and applicability of the present aza-APEX reaction, the author explored the substrate scope of unfunctionalized PAHs/heteroaromatics **1** and diarylcarbimidoyl chlorides **2** (Figure 7). The optimized reaction conditions showed high generality toward the aza-APEX of **1a** with **2a** even on a gram-scale reaction, and the product **4aa** was isolated in 78% yield (1.11 g). When structural analogs of phenanthrene such as methylene-bridged phenanthrene **1b**, 2,9-di-*tert*-butylpyrene (**1c**) and corannulene (**1d**) were used, and the corresponding N-PACs **4ba**, **4ca** and **4da** were obtained in 38–41% yields. Furthermore, benzo[*b*]furan (**1e**) and benzo[*b*]thiophene (**1f**) were also reacted with **2a** to give

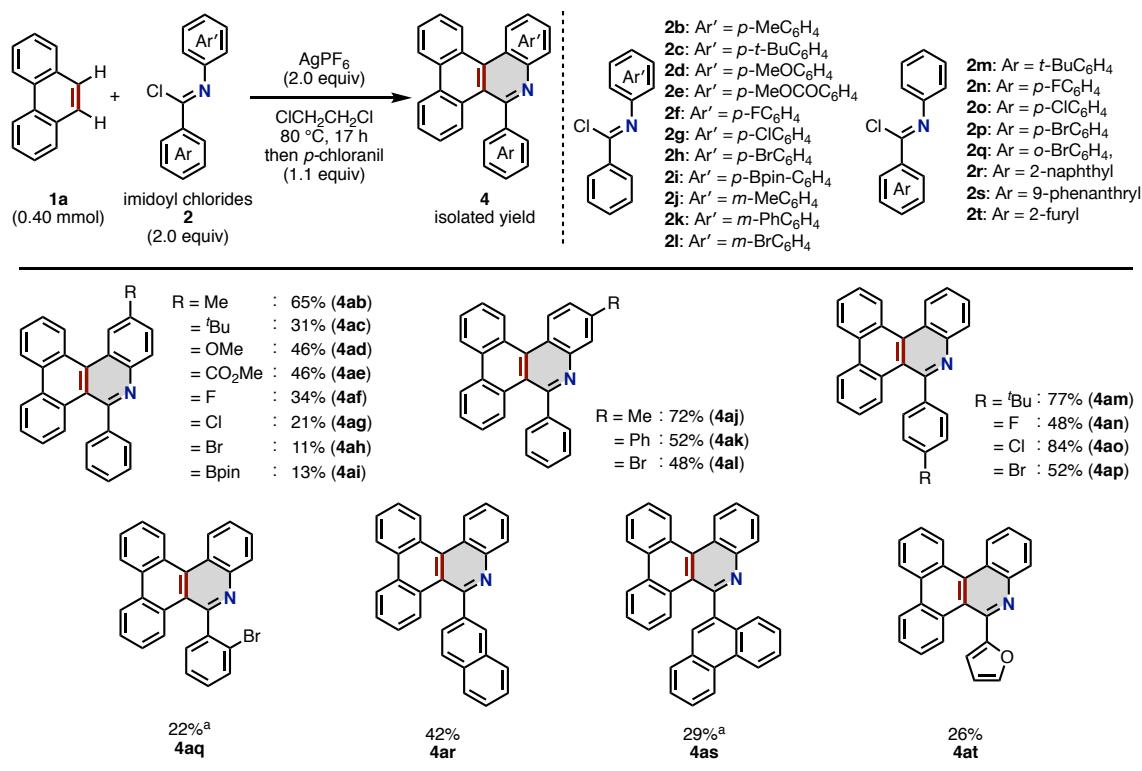
benzofuroisoquinoline **4ea** and benzothienoisoquinoline **4fa** in 35–47% yields. The reactions using other aromatic compounds such as anisole and naphthalene did not give the corresponding cyclized products **3** nor **4** at all.



**Figure 7.** Substrate scope of PAHs/heteroaremetics.

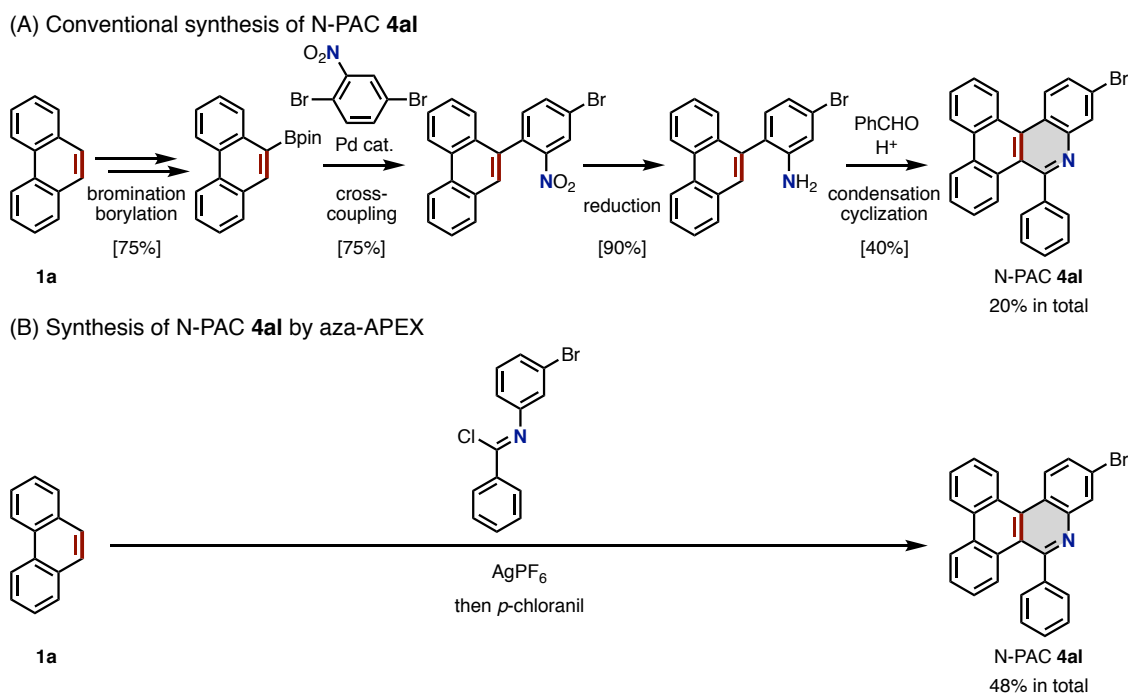
For exploring the scope of  $\pi$ -extending agents, the author tested aza-APEX reactions of **1a** with various imidoyl chlorides **2** which were derived from the corresponding amides (Figure 8). *Para*-substituents (R) on *N*-aryl groups (Ar) in **2** were tolerated when R was Me, <sup>t</sup>Bu, CO<sub>2</sub>Me and OMe groups, producing **4ab**, **4ac**, **4ad** and **4ae** in 46–65% yields. The *para*-fluoro, -chloro, -bromo, and Bpin groups showed lower tolerances (11–34% yields), probably due to electronic effects, but it was very useful to obtain the otherwise difficult-to-synthesize products **4af**, **4ag**, **4ah**, and **4ai** having transformable substituents. In the case of reactions with **2j** and **2k** having *meta*-methyl and phenyl groups, only products **4aj** and **4ak** were obtained in 52–72% yields as single regioisomers. These were probably formed by avoiding steric repulsion in the cyclization step. The use of **2l**, having a *N*-*meta*-bromophenyl group, did not markedly drop the reactivity and produced bromodibenzo[*i,k*]phenanthridine **4al** in 48% yield.

Regarding the variability of *N*-aryl groups (**Ar'**) on the benzimide moiety, *para*-<sup>t</sup>Bu, fluoro, chloro, bromo, 2-naphthyl, 9-phenanthryl, and 2-furyl groups afforded corresponding 5-aryldibenzo[*i,k*]phenanthridines (**4am**, **4an**, **4ao**, **4ap**, **4ar**, **4as**, and **4at**) in 26–84% yields, whilst an *ortho*-bromophenyl group decreased the yield of product **4aq** (22% yield).



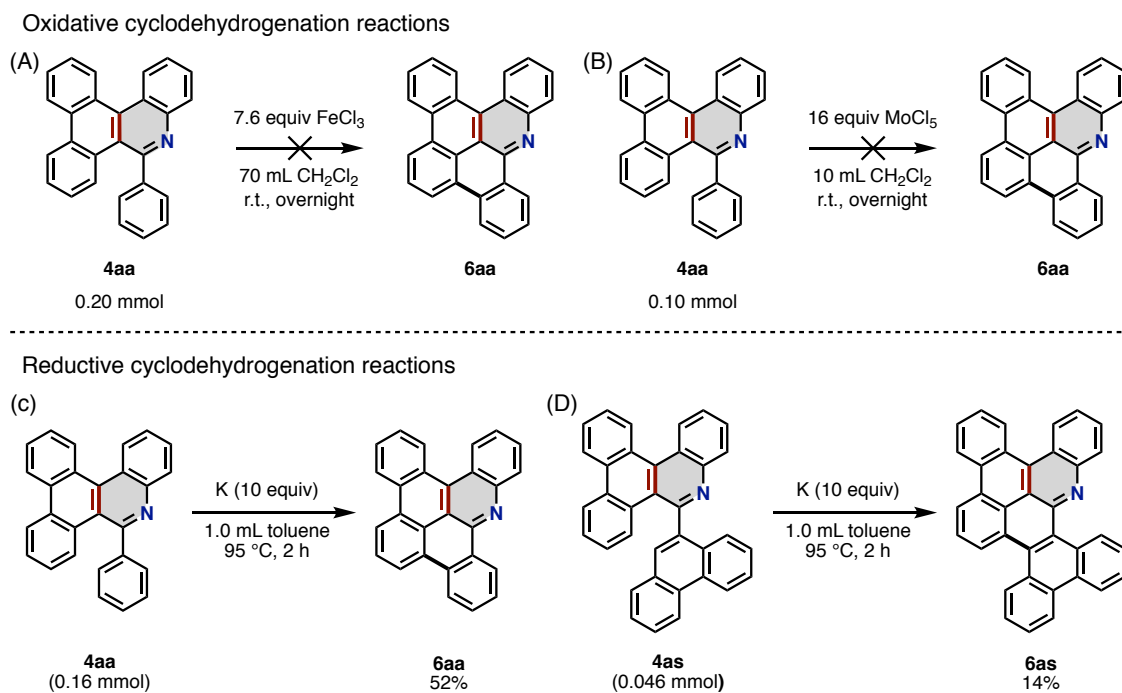
**Figure 8.** Substrate scope of imidoyl chlorides.

To further showcase the utility of present aza-APEX reaction, the author compared with a representative example of synthesizing N-PACs (Figure 9).<sup>[15]</sup> In the recent example by Samsung Display Co., Ltd. showed in the patent that N-PAC **4al** can be synthesized from phenanthrene by stepwise protocols performing bromination, borylation, coupling reaction with bromoarenes, reduction, condensation, and cyclization, thus resulting in the low reaction efficiency and the total yield (20%). Compared with this report, the present aza-APEX reaction can provide an alternative or a further efficient one-step synthetic strategy for N-PACs starting from simple and readily available unfunctionalized PAHs.



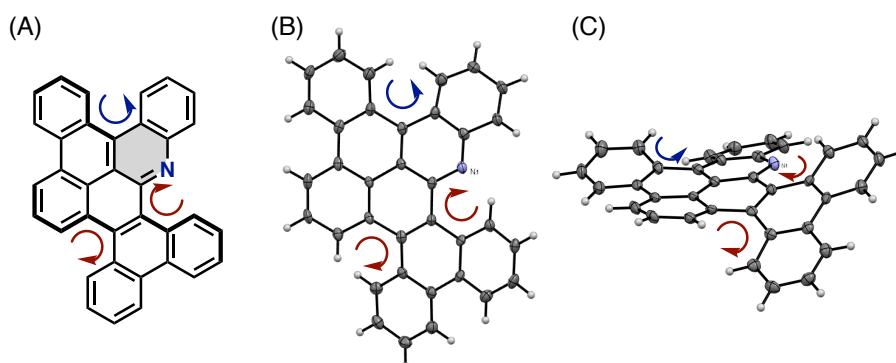
### 2-3. Synthesis of nitrogen-doped nanographenes

The structural characteristics of 5-aryl pendants in aza-APEX products were expected to be utilized for synthesis of functional nanocarbons such as nitrogen-doped nanographenes with further  $\pi$ -extensions. Thus, dehydrogenative cyclization of aza-APEX products was conducted by the oxidative cyclodehydrogenation so called Scholl reaction that is commonly used for the synthesis of PAHs and nanographenes.<sup>[16]</sup> When the reaction mixture containing **4aa** (0.20 mmol),  $\text{FeCl}_3$  (7.6 equiv) and dichloromethane (70 mL) was stirred at room temperature overnight, the desired nitrogen-doped nanographene **6aa** (Figure 10A) was not obtained at all, while **4aa** was fully consumed after the reaction. Moreover, almost the same result was obtained even when the reaction was carried out with  $\text{MoCl}_5$  (16 equiv) (Figure 10B). This can be due to a more electron-deficient nature of **4aa** than other general PAHs, which would make the oxidation more difficult. Therefore, the author decided to use the radical anion coupling reactions with metal.<sup>[17]</sup> By following the literatures, intramolecular radical anion coupling by potassium in toluene of **4aa** was conducted, and **6aa** was obtained in 52% yield (Figure 10C). Furthermore, aza-nanographene **6as** was also obtained from **4as** in 14% yield under the same reaction conditions (Figure 10D).

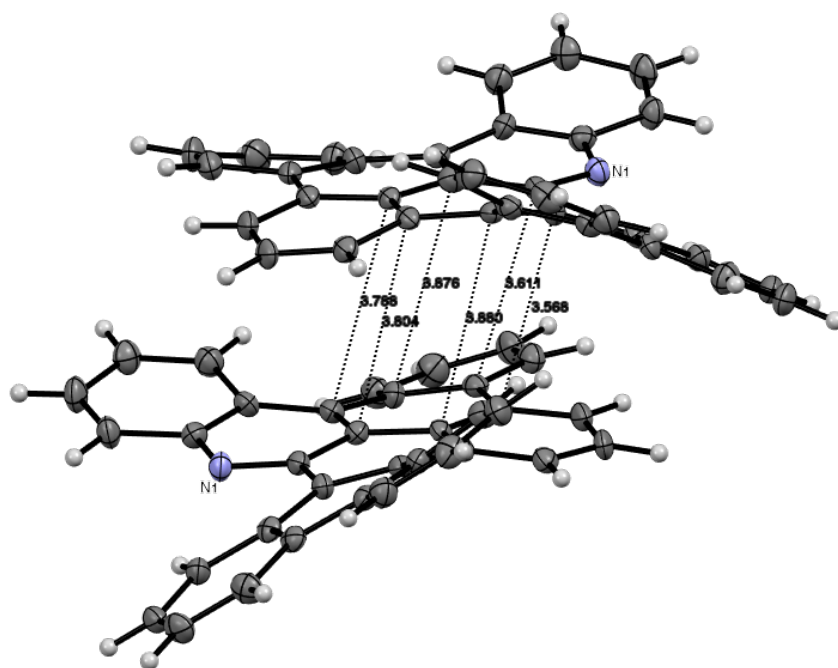


**Figure 10.** (A) Oxidative cyclodehydrogenation of **4aa** with  $\text{FeCl}_3$ . (B) Oxidative cyclodehydrogenation of **4aa** with  $\text{MoCl}_5$ . (C) Radical anion coupling of **4aa** with potassium. (D) Radical anion coupling of **4as** with potassium.

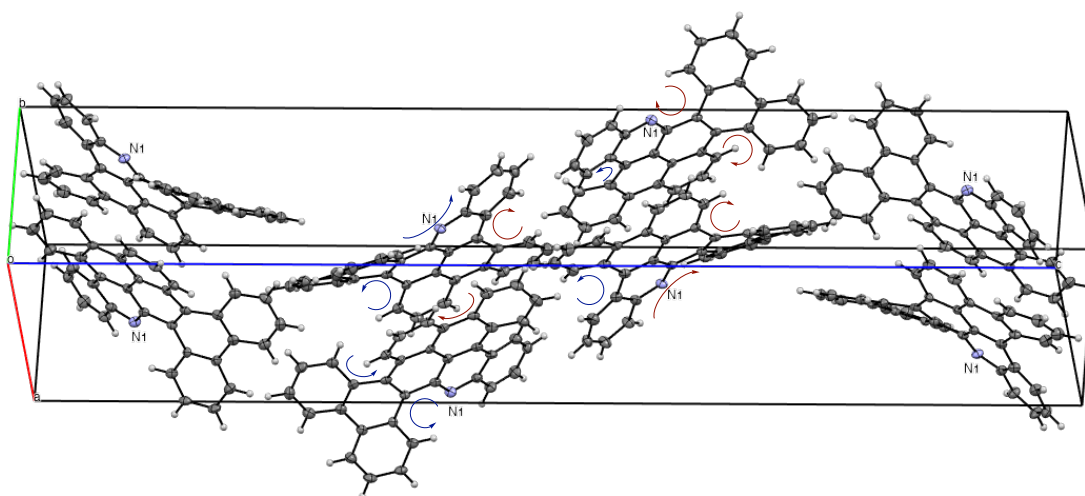
The solid-state structure of **6as** was confirmed by X-ray crystallographic analyses using a single crystal of **6as** obtained by the recrystallization from pentane and chloroform. As a result, it was found that **6as** includes three helical moieties derived from [4]helicene structures and form a twisted structure as a whole molecule (Figures 11A–11C). In the packing structure (Figure 12), **6as** forms homochiral dimeric  $\pi$ - $\pi$  stacking structures whose stacking distances are ranging between 3.6–3.9 Å.<sup>[18]</sup> In the packing structure of **6as**, racemic dimers are aligning in a *c* axis. In conclusion, it was revealed that **6as** was found to have a planarized but twisted structure inducing unique packing structure in a solid state (Figure 13).



**Figure 11.** (A) Chemical structure of **6as**. ORTEP drawings with a 50% thermal ellipsoidal obtained by X-ray crystallographic analysis in (B) top-view and (C) side view. Red and blue arrows show the helicity of each [4]helicene moiety.



**Figure 12.** Stacking structure of two neighboring molecules in a single crystalline of **6as**. Distances between selected carbon atoms are given in Å unit.



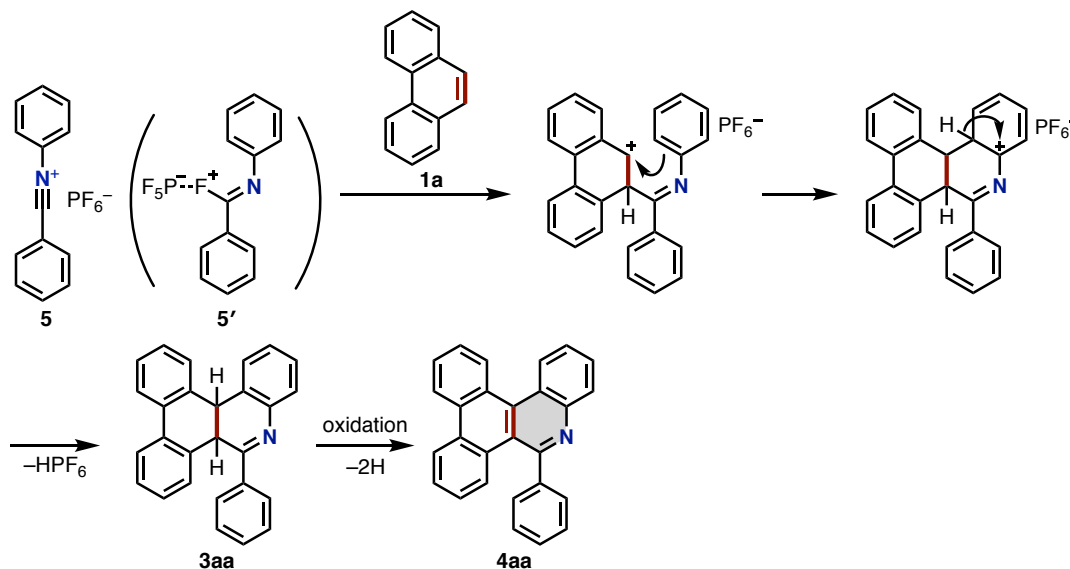
**Figure 13.** Packing structure of **6as**. Red and blue arrows show the helicity of each [4]helicene moiety.

#### 2-4. Computational study on reaction mechanism and regioselectivity

Based on the pyridine synthesis and its reaction mechanism reported by Chen and co-workers (Figure 4),<sup>[12a,b]</sup> the author assumed that the aza-APEX reaction of phenanthrene (**1a**) with imidoyl chloride **2a** would be triggered by the formation of *N*-phenyl benzonitrilium hexafluorophosphate (**5**) or its equivalent imidoyl fluoride-PF<sub>5</sub> complex **5'** and the subsequent electrophilic aromatic substitution (S<sub>E</sub>Ar) reaction



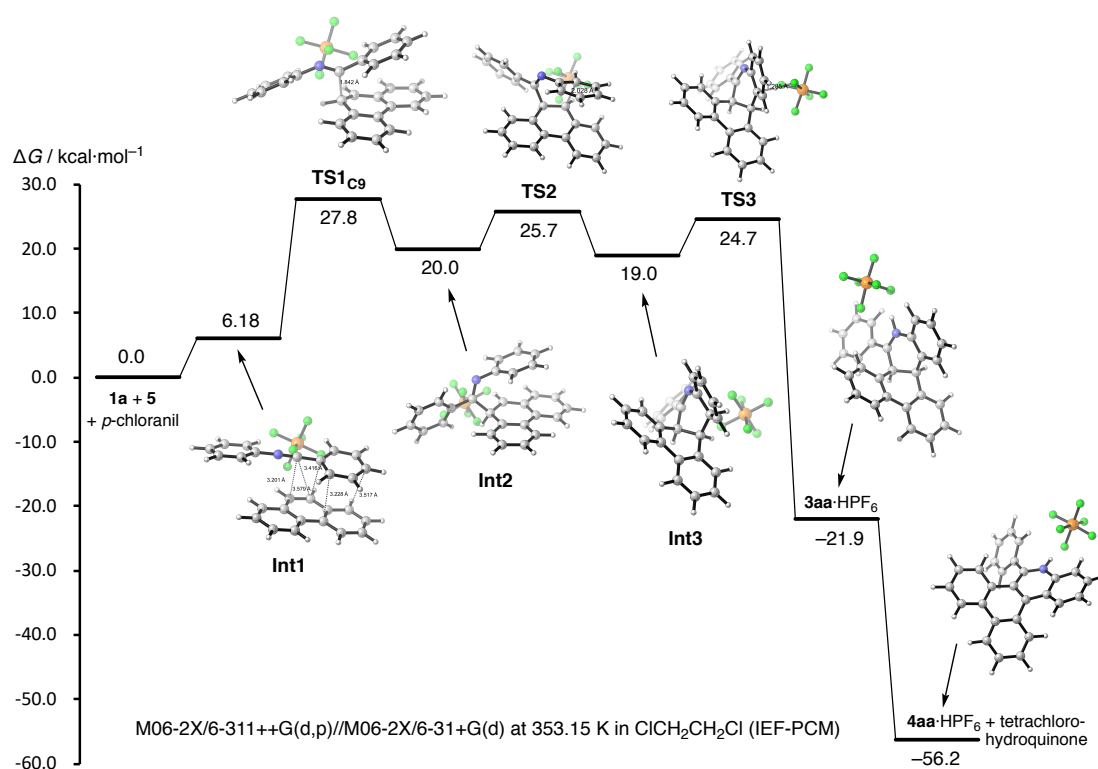
with **1a** (Figure 14). After the C–C bond formation between *K*-region on **1a** and a highly electrophilic carbon atom on **5/5'**, the intramolecular  $S_{\text{E}}\text{Ar}$  can occur to afford first product **3aa** which was certainly observed in the reaction without oxidant. Then, the aromatization of **3aa** is expected to proceed affording final product **4aa** by being accelerated by oxidant.



**Figure 14.** A proposed mechanism of aza-APEX reaction using **1a** and **2a**.

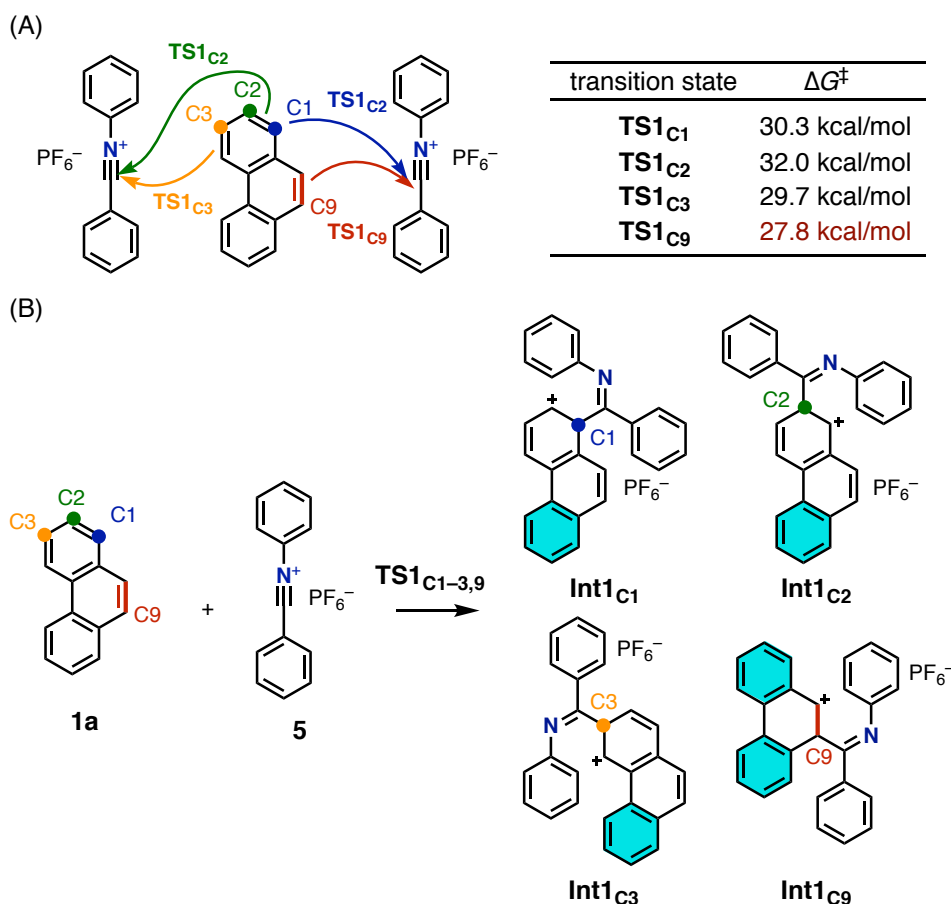
To verify the proposed mechanism in Figure 14, DFT calculations with the M06-2X/6-31+G(d) level of theory were performed for optimization of each stable intermediates and transition state. In addition, the M06-2X/6-311++G(d,p) level of theory with Truhlar's quasi-harmonic correction<sup>[19]</sup> was applied to each intermediate and transition state to obtain further accurate energies. First of all, preliminary calculations with the M06-2X/6-31+G(d) level of theory revealed that diarylnitrilium salt **5** preferably forms in gas phase rather than imidoyl fluoride-PF<sub>5</sub> **5'**: (**5** was more stable by 20.9 kcal/mol than **5'**: see Table S6 for detail). As the result of calculations, it was found that the aza-APEX reaction likely proceeds through a formal [4+2] cycloaddition of **1a** with nitrilium salt **5**. After the complexation affording **Int1**, the electrophilic addition of an electron-deficient *sp*-carbon on **5** to the C9-position (*K*-region) of **1a** occurs forming dihydrophenanthrenium intermediate **Int2** through a transition state **TS1**<sub>C9</sub> with the activation energy ( $\Delta G^\ddagger$ ) of 27.8 kcal/mol. The  $S_{\text{E}}\text{Ar}$  between a benzylic cation and an *ortho*-carbon atom on the *N*-phenyl group then takes place rather than re-aromatization by deprotonation. Through a transition state **TS2** with a 25.7 kcal/mol activation barrier from **Int1**, an arenium ion intermediate **Int3** having *cis*-dihydrophenanthrene structure is formed. Subsequent abstraction of a proton assisted by a PF<sub>6</sub><sup>-</sup> ion along with re-aromatization are shown to be kinetically and thermodynamically favorable, affording complex **3aa**·HPF<sub>6</sub> through **TS3** ( $\Delta G^\ddagger = 24.7$  kcal/mol from **1a** + **5**). Finally, oxidation of **3aa**·HPF<sub>6</sub> with *p*-chloranil gives much more stable product **4aa**·HPF<sub>6</sub> along with tetrachlorohydroquinone as a co-

product.



**Figure 14.** Energy diagram of calculated reaction pathway in the aza-APEX reaction of **1a** with **5**. *p*-Chloranil molecules were omitted in the structures of each intermediate and transition state for clarity.

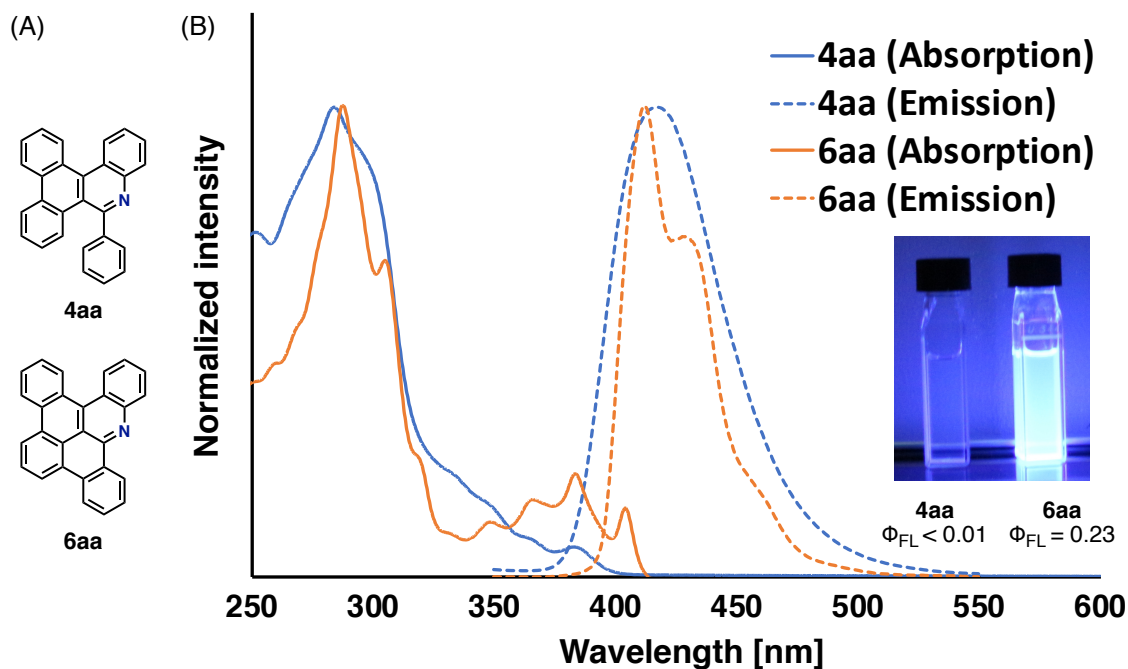
The author further estimated the predominant selectivity within the *K*-region of **1a** in the present aza-APEX reaction (Figure 15). When the transition states of addition reaction by nitrilium salt **5** to C1, C2, and C3 position on **1a** (**TS1<sub>C1</sub>**, **TS1<sub>C2</sub>**, and **TS1<sub>C3</sub>**) were calculated, activation energies in the electrophilic addition step were calculated as 30.3, 32.0 and 29.7 kcal/mol, respectively, which are higher (by more than 2 kcal/mol) than that in the addition to *K*-region (Figure 15A). This can be due to the higher instability of the less aromatic resonance stabilization on of phenanthrene rings in the transition states **TS1<sub>C1</sub>**, **TS1<sub>C2</sub>**, **TS1<sub>C3</sub>**, and corresponding intermediates **Int1<sub>C1</sub>**, **Int1<sub>C2</sub>**, and **Int1<sub>C3</sub>**, while two aromatic sextets are retained in the phenanthrene part in the more stable **TS1<sub>C9</sub>**/**Int1<sub>C9</sub>** (Figure 15B, blue-colored benzene rings). In conclusion, the calculations fully support an assumed mechanism and the origin of regioselectivity of aza-APEX reaction.



**Figure 15.** (A) Activation energies in the transition states of electrophilic addition (**TS1<sub>C1</sub>**, **TS1<sub>C2</sub>**, **TS1<sub>C3</sub>** and **TS1<sub>C9</sub>**) at each carbon atom on **1a**. (B) Pictorial comparison of aromatic nature of phenanthrene rings in each transition state/intermediate.

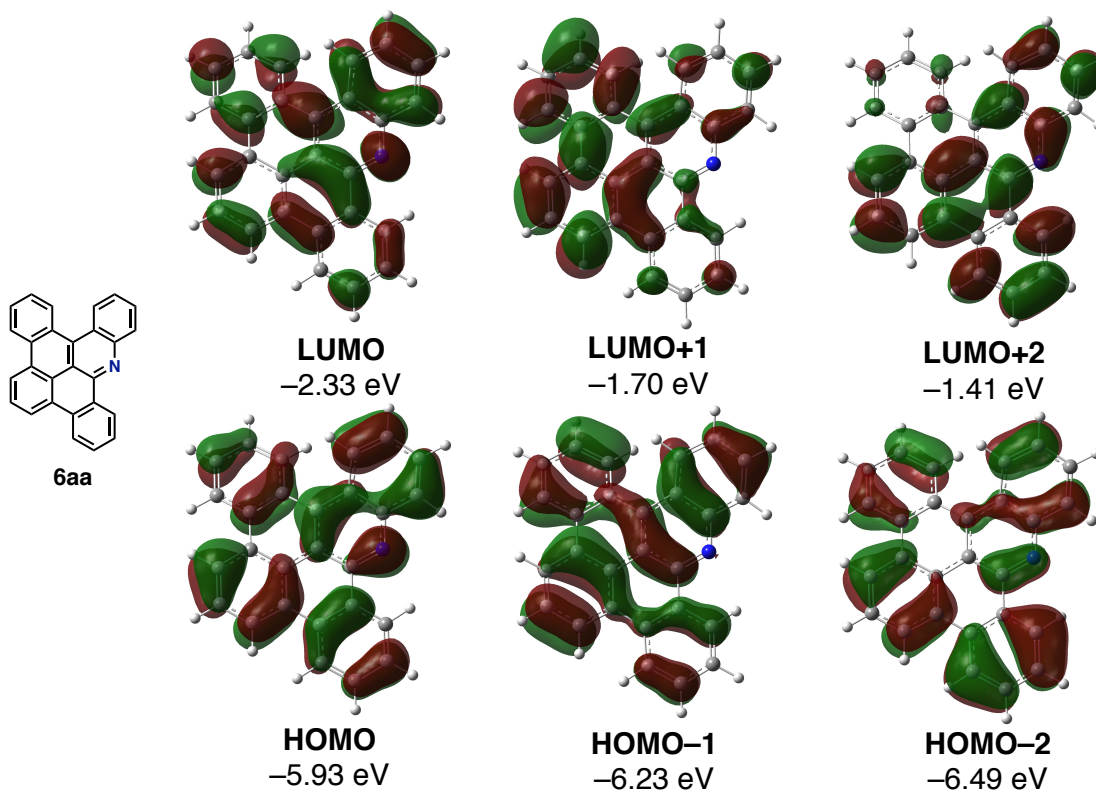
## 2-5. Photophysical properties of N-PACs and nitrogen-doped nanographenes

The photophysical properties of N-PACs (**4aa** and **4as**) and nitrogen-doped nanographenes (**6aa** and **6as**) were investigated by measuring UV-vis absorption and emission spectra. The absorption and emission spectra of **4aa** and **6aa** are described in Figure 16. Both **4aa** and **6aa** showed maximum absorption around 280–290 nm. Moreover, **6aa** showed longer absorption peaks at 350–420 nm, while **4aa** showed only a very weak absorption in the same region. When measuring emission spectra, both **4aa** and **6aa** showed the peak tops at 410–420 nm. However, **6aa** gave more narrow-shaped spectra than that of **4aa**. Furthermore, the fluorescence quantum yield ( $\Phi_{\text{FL}}$ ) of **6aa** was measured as 0.23, whose value is much higher than that of **4aa** ( $\Phi_{\text{FL}} < 0.01$ ) (Figure 16).

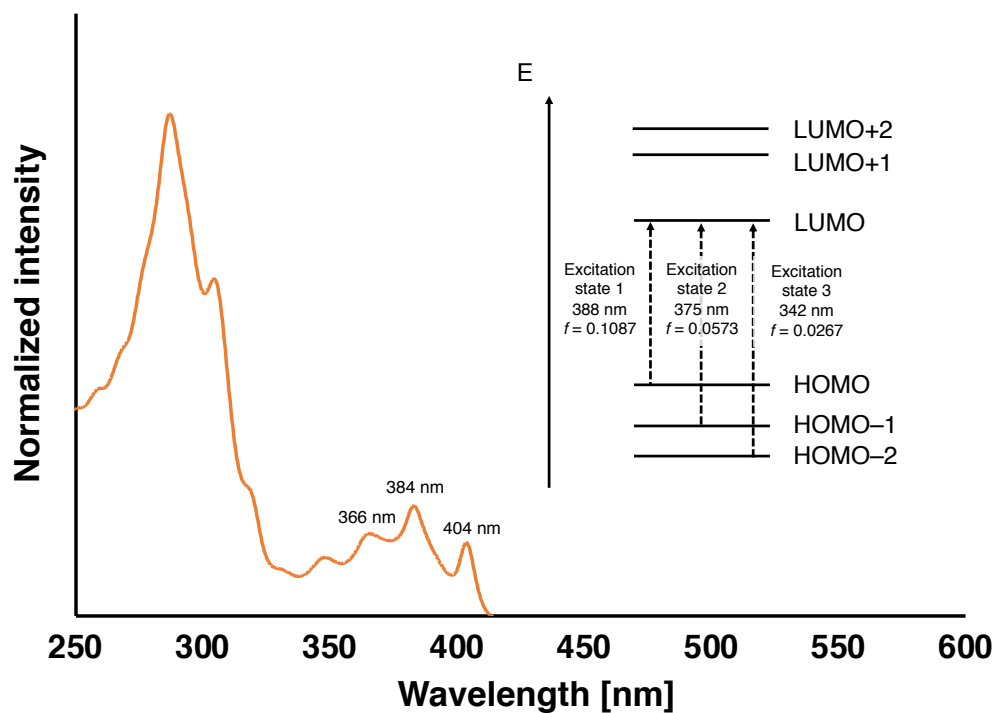


**Figure 16.** (A) Chemical structures of **4aa** and **6aa**. (B) UV-vis absorption and emission spectra, and  $\Phi_{FL}$  of **4aa** and **6aa** in dichloromethane. 287 nm light was used for excitation.

Further investigations on the photophysical properties of **6aa** were conducted by using the DFT calculation with the B3LYP/6-311++G(d,p) level of theory (Figure 17). As the result, the energy levels of HOMO, LUMO, HOMO-1, HOMO-2, LUMO+1, and LUMO+2 were calculated as -5.93, -2.33, -6.23, -6.49, -1.70, and -1.41 eV, respectively. HOMO and LUMO were found to be delocalized over the molecule, which indicates the effective  $\pi$ -extension from uncyclized compound **4aa**. In addition, according to TD-DFT calculation with the same level, the absorption wavelength (energy) of an energetically lowest HOMO→LUMO excitation was calculated as 388 nm (3.20 eV) with 0.1087 of oscillation strength ( $f$ ) (Figure 18). This calculated excitation wavelength well matched to the observed longest absorption peak at 404 nm. In addition, the other calculated excitation wavelengths of HOMO-1→LUMO (375 nm), HOMO-2→LUMO (342 nm) are considered to correspond to peaks at 384 nm and 366 nm, respectively.



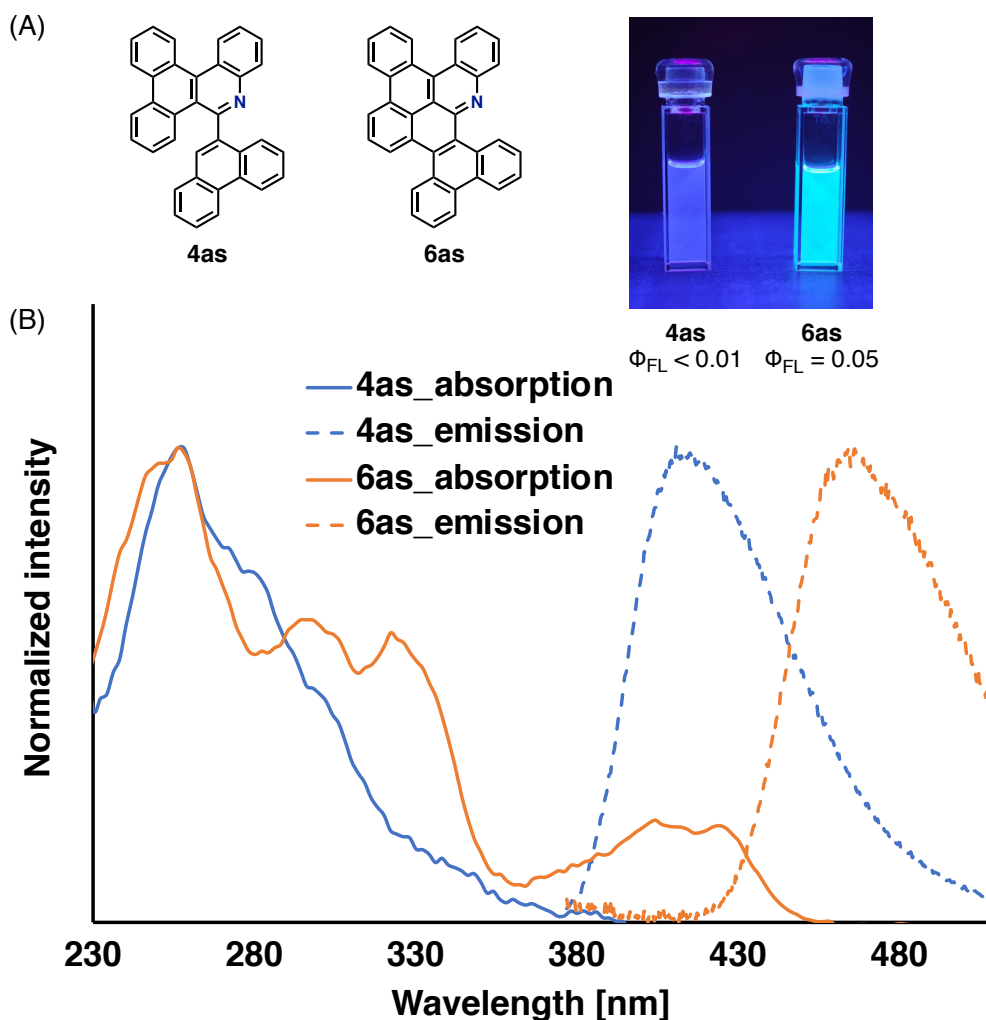
**Figure 17.** Frontier MOs and energy levels of **6aa** calculated by DFT/B3LYP/6-311++G(d,p) level of theory (isovalue = 0.02).



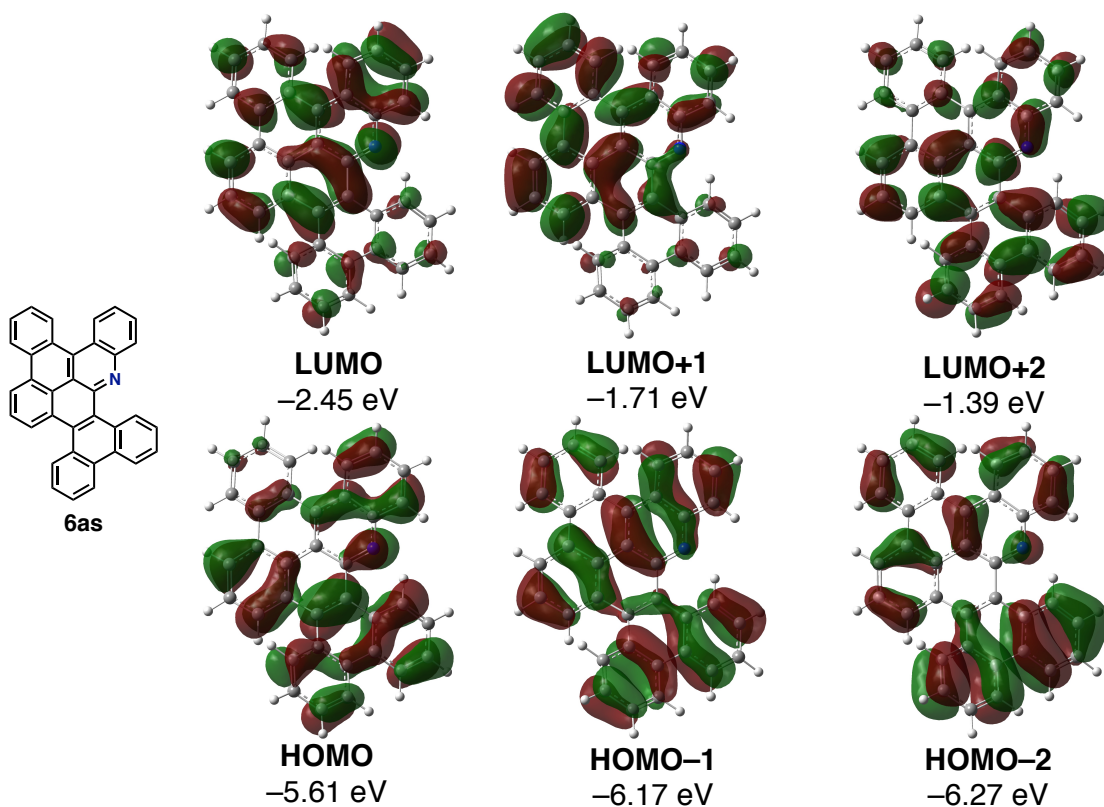
**Figure 18.** Comparison of UV-vis absorption spectrum of **6aa** and calculated excitation wavelengths by TD-DFT.

The absorption and emission spectra of **4as** and **6as** are shown in Figure 19. Both **4as** and **6as** showed absorption maxima around 260 nm. Moreover, **6as** showed longer absorptions at 360–460 nm, while **4as** showed only very weak absorptions around 380–400 nm. In emission spectra, **4as** showed the emission maximum peak around 412 nm. Besides, **6as** showed a remarkable red-shift of emission spectra to show a peak top at 464 nm. Furthermore,  $\Phi_{\text{FL}}$  of **6as** was measured as 0.05, whose value is lower than  $\Phi_{\text{FL}}$  of **6aa** (0.23) but even higher than that of **4as** ( $<0.01$ ).

Furthermore, the computational investigation on the photophysical properties of **6as** was conducted using DFT calculations with the B3LYP/6-311++G(d,p) level of theory (Figure 20). As a result, the energy levels of HOMO, LUMO, HOMO–1, HOMO–2, LUMO+1, and LUMO+2 were calculated as –5.61, –2.45, –6.17, –6.27, –1.71, and –1.39 eV, respectively. In addition, the HOMO and LUMO were found to be delocalized over the molecule as same as the case of **4as**.

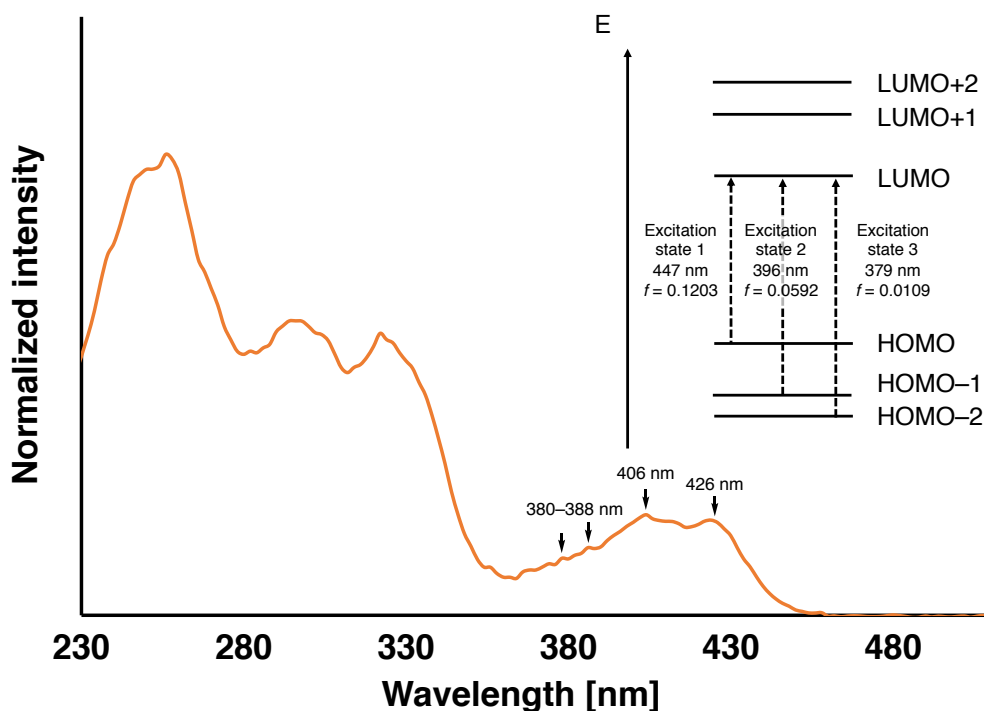


**Figure 19.** (a) Chemical structures of **4as** and **6as**, and  $\Phi_{\text{FL}}$ . (b) UV-vis absorption and emission spectra of **4as** and **6as** in dichloromethane. 260 nm light was used for excitation.



**Figure 20.** The detail of DFT calculations of **6as**: the frontier MOs and energy levels (isovalue = 0.02).

Moreover, according to the TD-DFT calculation with the same level, the excitation wavelength (energy) of an energetically lowest HOMO→LUMO transition was calculated as 447 nm (2.78 eV) with 0.1203 of  $f$  (Figure 21). This calculated excitation wavelength was found to be well matched to an observed longest absorption peak at 426 nm. In addition, the other calculated excitation HOMO-1→LUMO (396 nm,  $f = 0.0592$ ) and HOMO-2→LUMO (379 nm,  $f = 0.0109$ ) are considered to correspond to the observed broad peaks around 370–410 nm.

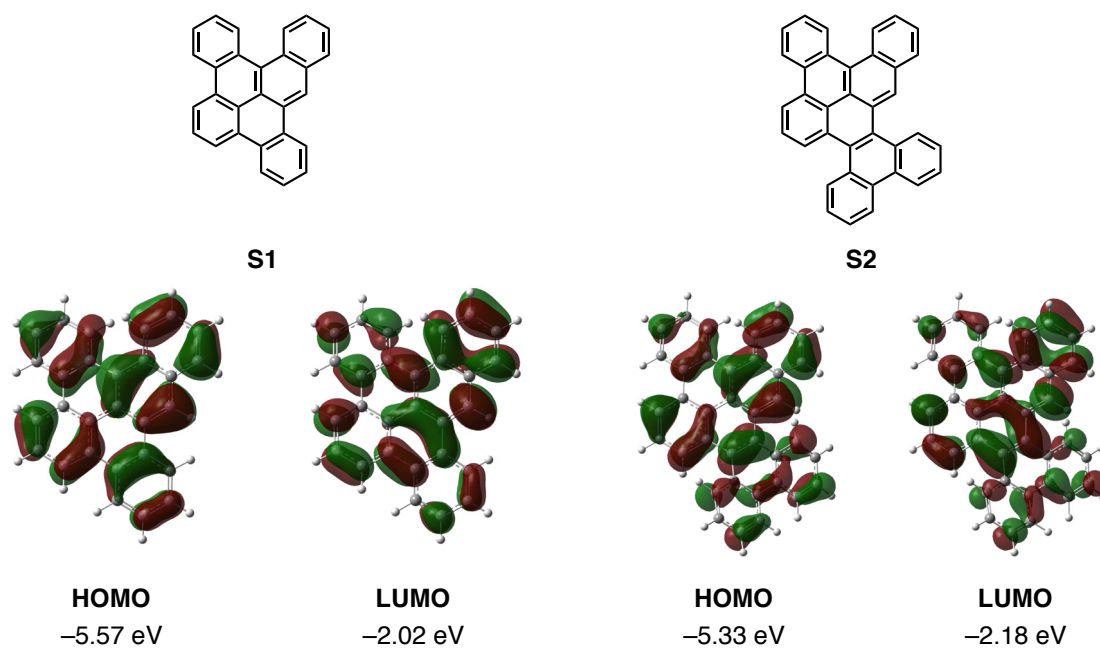


**Figure 21.** Comparison of UV-vis spectra of **6as** and calculated excitation wavelengths by TD-DFT.

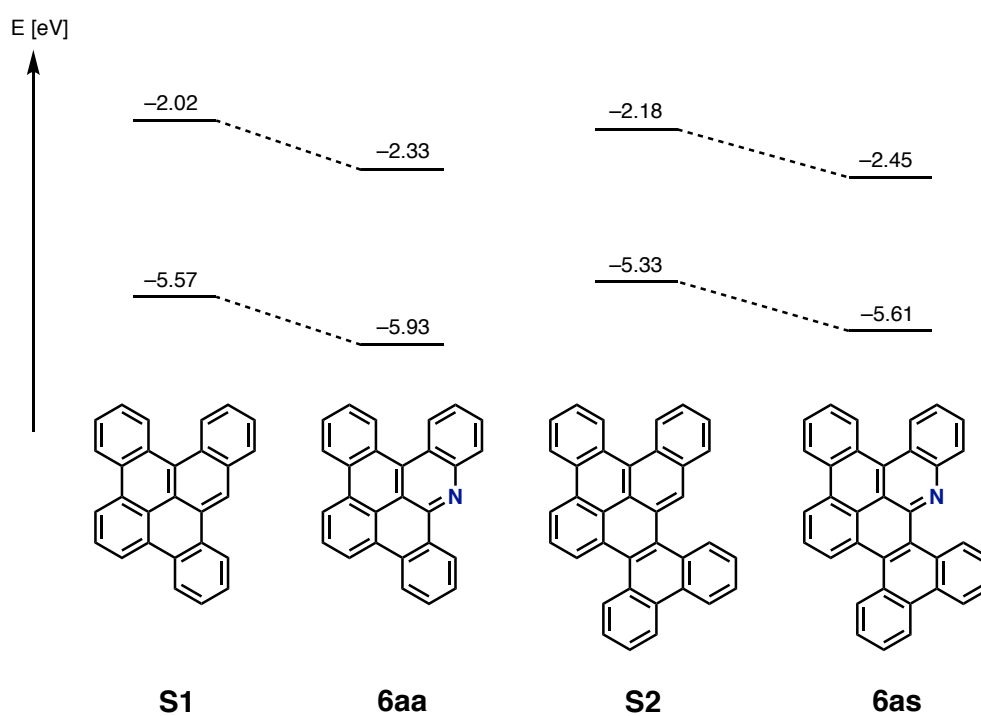
## 2-6. Effect of nitrogen-doping

Finally, the author investigated the effect of nitrogen-doping in compound **6aa** and **6as** by DFT calculations (Figure 22). Using the B3LYP/6-311++G(d,p) level of theory, the frontier MOs of all-hydrocarbon analogs **S1** and **S2** which are corresponding to **6aa** and **6as** were calculated. As a result, (HOMO, LUMO) of **S1** and **S2** was calculated to be (−5.57, −2.20 eV) and (−5.33 eV, −2.18 eV), respectively. Compared to the hydrocarbon analogs **S1** and **S2** (Figure 11), **6aa** and **6as** possess lower lying (by ~0.3 eV) HOMO and LUMO than those of **S1** and **S2** without significant changes of HOMO–LUMO gap energy (**S1**: 3.55 eV, **6aa**: 3.60 eV, **S2**: 3.14 eV, **6as**: 3.17 eV) (Figure 23). These results imply that the introduction of one nitrogen atom into nanographene represents an effective strategy for increasing electron-accepting ability without changing a HOMO–LUMO gap, which will provide an opportunity for applications in electron-transporting materials





**Figure 22.** Frontier MOs of hydrocarbon analogs of **6aa** and **6as** (isovalue = 0.02).



**Figure 23.** The effect of nitrogen-doping on nanographene structures.

### 3. Conclusion

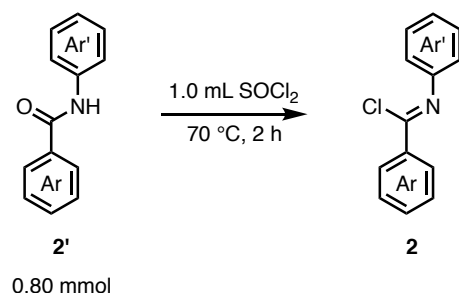
A novel synthetic method for N-PACs, the aza-APEX reactions of unfunctionalized aromatics with imidoyl chlorides as  $\pi$ -extending agents with  $\text{AgPF}_6$  as an activating additive, has been established. Due to the abundance of diarylcarbimidoyl chlorides which are easily prepared from commercially available benzanilide analogs, a broad range of 5-aryldibenzo[*i,k*]phenanthridine derivatives were successfully obtained with *K*-region selectivity. Moreover, aza-APEX reactions using heteroaromatics or structural analogs of phenanthrene such as corannulene, a pyrene derivative was also found to proceed well, affording various N-PACs. Finally, synthesis of nitrogen-doped nanographenes was achieved by further  $\pi$ -extension of aza-APEX products under conditions of radical anion coupling. In addition, using DFT calculations, it was revealed that aza-APEX reaction of phenanthrene proceeds as  $\text{S}_{\text{E}}\text{Ar}$ -type [4+2] cycloaddition reaction. In addition, the regioselectivity onto *K*-region was supported by the lower activation energy of  $\text{TS1}_{\text{C9}}$  than those of other electrophilic addition reactions of nitrilium salt at C1–3 positions. Furthermore, UV-vis absorption spectra and emission spectra on nitrogen-doped nanographenes obtained via aza-APEX reactions were measured. As a result, synthesis of novel nitrogen-doped nanographenes with unique emission was found to proceed. Experimental UV-vis absorption spectra of the nanographenes were found to be consistent to the result of TD-DFT calculation, so that the MO of nitrogen-doped nanographenes were experimentally and theoretically revealed. Finally, DFT calculations revealed that nitrogen-doping onto nanographene structures constructed by aza-APEX reactions can make the energy level of LUMO lower to increase electron-acceptability of nanographenes. In conclusion, the author believes that the newly developed aza-APEX reaction will open an alternative avenue to the rapid access to various difficult-to-synthesize N-PACs having designed functions and properties.

## 4. Experimental section

### 4-1. General

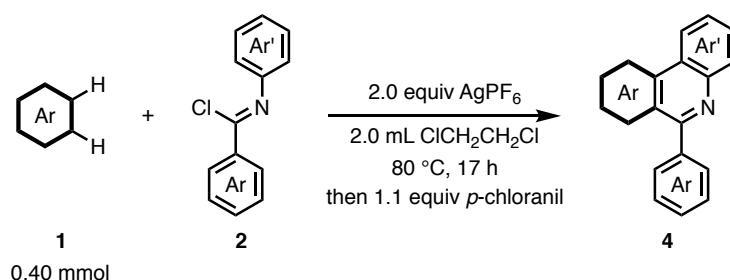
Unless otherwise noted, all materials including dry solvents were obtained from commercial suppliers and used without further purification. Thionyl chloride was purchased from Wako. AgOTf, AgPF<sub>6</sub>, AgNTf<sub>2</sub>, and *o*-chloranil were purchased from TCI. AgNO<sub>3</sub> and AgCl were purchased from Nacalai Tesque. AgBF<sub>4</sub>, AgSbF<sub>6</sub>, Me<sub>3</sub>SiOTf, FeCl<sub>3</sub>, and MoCl<sub>5</sub> were purchased from Aldrich. *p*-Chloranil, *p*-benzoquinone, and DDQ were purchased from Wako. PAHs and heteroaromatics were purchased from TCI. Di-*tert*-butylpyrene (**1c**) was synthesized by referring a literature.<sup>[20]</sup> Benzanilide (**2a'**) derivatives were purchased from TCI. The other benzamide derivatives (**2b'** - **2t'**) were synthesized from corresponding aniline derivatives and aroyl chlorides according to procedures reported in a literature.<sup>[11]</sup> Unless otherwise noted, all reactions were performed with dry solvents under an atmosphere of nitrogen in oven-dried glassware with standard vacuum-line techniques. All work-up and purification procedures were carried out with reagent-grade solvents in air. Analytical thin-layer chromatography (TLC) was performed using E. Merck silica gel 60 F254 precoated plates (0.25 mm). The developed chromatogram was analyzed by UV lamp (254 nm and 365 nm). Flash column chromatography was performed with KANTO Silica Gel 60N (spherical, neutral, 40-100 μm) or Biotage Isolera<sup>®</sup> equipped with Biotage SNAP Cartridge KP-Sil columns. Preparative thin-layer chromatography (PTLC) was performed using Wako-gel<sup>®</sup> B5-F silica coated plates (0.75 mm) prepared in our laboratory, or Gel Permeation Chromatography (GPC) was performed with a JAI LC-9260 II NEXT instrument equipped with JAIGEL-1H/JAIGEL-2H columns using chloroform as an eluent. The developed chromatogram was analyzed by UV lamp (254 nm and 365 nm). High-resolution mass spectra (HRMS) were obtained from a Bruker Compact (APCI). Nuclear magnetic resonance (NMR) spectra were recorded on a JEOL ECS-600 (<sup>1</sup>H 600 MHz, <sup>13</sup>C 150 MHz,) spectrometer and a JEOL ECA 600II with Ultra COOLTM probe (<sup>1</sup>H 600 MHz, <sup>13</sup>C 150 MHz). Chemical shifts for <sup>1</sup>H NMR are expressed in parts per million (ppm) relative to tetramethylsilane (δ 0.00 ppm) or CD<sub>2</sub>Cl<sub>2</sub> (δ 5.32 ppm). Chemical shifts for <sup>13</sup>C NMR are expressed in ppm relative to CDCl<sub>3</sub> (δ 77.16 ppm) or CD<sub>2</sub>Cl<sub>2</sub> (δ 54.00 ppm) or Cl<sub>2</sub>CDCDCl<sub>2</sub> (δ 73.78 ppm). Chemical shifts for <sup>19</sup>F NMR are expressed in ppm relative to hexafluorobenzene as an internal standard (δ -162.00 ppm). Data are reported as follows: chemical shift, multiplicity (s = singlet, d = doublet, dd = doublet of doublets, ddd = doublet of doublet of doublets, t = triplet, td = triplet of doublets, q = quartet, m = multiplet), coupling constant (Hz), and integration.

## 4-2. General procedure

General procedure A: preparation of imidoyl chlorides<sup>[14]</sup>

To a J-Young tube containing a magnetic stirrer bar were added benzamide derivatives **2'** (0.80 mmol), thionyl chloride (1.0 mL, 34 equiv) under a stream of nitrogen. After stirring at 70 °C for 2 h, thionyl chloride in the reaction mixture was removed by a vacuum pump to afford the corresponding imidoyl chlorides **2** as oil or solid in a quantitative yield which was directly used in the next step without further purifications.

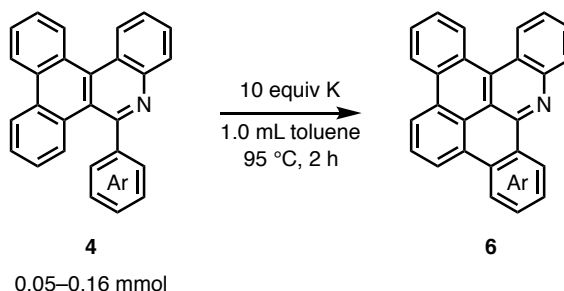
## General procedure B: synthesis of N-PACs by aza-APEX reaction of PAHs/heteroarenes with imidoyl chlorides



A J-Young tube containing imidoyl chlorides **2** was vacuumed through a manifold under reduced pressure, capped with a Teflon<sup>®</sup> cock, and placed in a glovebox. Then AgPF<sub>6</sub> (0.80 mmol, 2.0 equiv stored in a glovebox) was added to the J-Young tube under an argon atmosphere, and the tube was brought out to furnish a manifold and silicon septum under a nitrogen atmosphere. PAHs/heteroarenes **1** (0.40 mmol, 1.0 equiv) and 1,2-dichloroethane (2.0 mL) were added to a tube under a stream of nitrogen, and a silicon septum was replaced with a Teflon<sup>®</sup> cock again. After stirring at 80 °C for 17 h, the reaction mixture was cooled to room temperature, and then *p*-chloranil (0.44 mmol, 1.1 equiv) was added under air. After stirring at room temperature for 3 h, saturated NaHCO<sub>3</sub> aq. was added to the reaction mixture for neutralization. Then, the mixture was passed through a short pad of Celite<sup>®</sup>, and organic phase was washed three times with chloroform. Extracted organic layers were combined, dried with Na<sub>2</sub>SO<sub>4</sub>, filtered and concentrated under reduced pressure to afford the crude product which was purified by PTLC or flush

column chromatography on silica gel (eluent: hexane/chloroform = 1:1 to 1:2) to yield N-PAC **4** as a colored solid.

**Procedure C: synthesis of aza-nanographenes **6** by radical anion coupling of N-PACs **4** with potassium<sup>[17]</sup>**



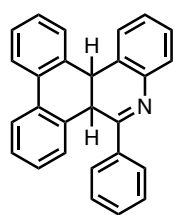
To a J-Young tube containing a magnetic stirrer bar were added N-PACs **4** (0.05–0.16 mmol, 1.0 equiv) under a stream of nitrogen. Then, toluene (1.0 mL) and potassium (0.5–1.6 mmol, 10 equiv) were added in a globe box filled with argon. After stirring at 95 °C for 2 h, the reaction mixture was cooled to room temperature. Then, water was added to quench the reaction after careful addition of *tert*-amyl alcohol under a stream of nitrogen. Then, organic phase was extracted three times with dichloromethane. The combined organic layers were dried with Na<sub>2</sub>SO<sub>4</sub>, filtered and concentrated under reduced pressure to obtain the crude product which was further purified by PTLC on silica gel (eluent: hexane/chloroform = 2:1) to yield corresponding aza-nanographene **6** as colored solid.

### 4-3. Compound data of aza-APEX products

#### 5-Phenyl-4b,10b-dihydrodibenzo[*i,k*]phenanthridine (**3aa**)

Yield: 68% determined using <sup>1</sup>H NMR and CH<sub>2</sub>Br<sub>2</sub>, pale yellow solid.

(Note: **3aa** is gradually transformed to **4aa** under air). While obtained <sup>1</sup>H NMR spectra indicated the presence of single diastereomer and it can be roughly assigned as a *cis*-isomer by judging from the coupling constants between benzylic protons ( $J = 6.0$  to  $6.6$  Hz), detail structural analyses such as X-ray crystallography could not be conducted due to the instability of **4aa** under air.



<sup>1</sup>H NMR (600 MHz, CDCl<sub>3</sub>) δ 8.18–8.21 (m, 2H), 7.88 (d,  $J = 7.8$  Hz, 1H), 7.67 (d,  $J = 7.8$  Hz, 1H), 7.46–7.52 (m, 4H), 7.39–7.43 (m, 3H), 7.19 (t,  $J = 7.2$  Hz, 1H), 7.15 (t,  $J = 7.8$  Hz, 1H), 7.00 (t,  $J = 7.5$  Hz, 1H), 6.96 (d,  $J = 7.2$  Hz, 1H), 6.93 (t,  $J = 7.5$  Hz, 1H), 6.65 (d,  $J = 7.8$  Hz, 1H), 4.62 (d,  $J = 6.6$  Hz, 1H), 4.23 (d,  $J = 6.0$  Hz, 1H).

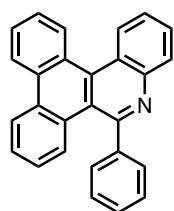
<sup>13</sup>C NMR (150 MHz, CDCl<sub>3</sub>) δ 167.31, 144.81, 139.20, 134.78, 133.86, 132.76, 131.07, 130.65, 128.97, 128.48, 128.08, 128.04, 128.00, 127.80, 127.73, 127.43, 127.32, 127.16, 126.69, 126.09,

124.75, 123.69, 40.01, 38.19. One  $sp^2$  carbon peak is overlapped.

HRMS (APCI<sup>+</sup>)  $m/z$  calcd for  $C_{27}H_{19}N$   $[M+H]^+$ : 358.1590, found: 358.1587.

#### 5-Phenyldibenzo[*i,k*]phenanthridine (4aa)

Yield: 114.2 mg, 80% (1.11 g, 78% in 4.0-mmol scale), yellow solid.



<sup>1</sup>H NMR (600 MHz, CDCl<sub>3</sub>) δ 8.88 (d,  $J$  = 7.8 Hz, 1H), 8.75 (d,  $J$  = 8.4 Hz, 1H), 8.72 (d,  $J$  = 8.4 Hz, 1H), 8.59 (d,  $J$  = 8.4 Hz, 1H), 8.29 (d,  $J$  = 7.8 Hz, 1H), 7.82 (t,  $J$  = 6.9 Hz, 1H), 7.72–7.79 (m, 5H), 7.63 (ddd,  $J$  = 8.4, 7.2, 1.2 Hz, 1H), 7.53 (ddd,  $J$  = 8.4, 7.2, 1.2 Hz, 1H), 7.43–7.47 (m, 3H), 7.20 (ddd,  $J$  = 8.1, 6.8, 1.4 Hz, 1H).

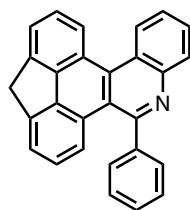
<sup>13</sup>C NMR (150 MHz, CDCl<sub>3</sub>) δ 157.80, 146.12, 143.86, 135.86, 132.72, 130.70, 130.04,

129.97, 129.47, 129.41, 129.22, 129.03, 128.87, 128.83, 128.18, 127.39, 127.21, 127.12, 126.47, 126.22, 123.96, 123.43, 123.33, 121.72. One  $sp^2$  carbon peak is overlapped.

HRMS (APCI<sup>+</sup>)  $m/z$  calcd for  $C_{27}H_{17}N$   $[M+H]^+$ : 356.1434, found: 356.1445.

#### 6-Phenyl-10H-fluoreno[4,5-*ijk*]phenanthridine (4ba)

Yield: 56.5 mg, 38%, pale white solid.



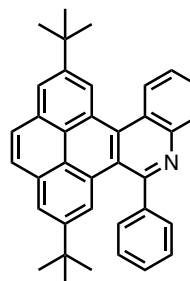
<sup>1</sup>H NMR (600 MHz, CD<sub>2</sub>Cl<sub>2</sub>) δ 9.24 (d,  $J$  = 8.4 Hz, 1H), 8.96 (d,  $J$  = 8.4 Hz, 1H), 8.28 (dd,  $J$  = 8.4, 1.2 Hz, 1H), 7.93 (d,  $J$  = 6.6 Hz, 1H), 7.82–7.88 (m, 2H), 7.76 (ddd,  $J$  = 8.4, 6.9, 1.5 Hz, 1H), 7.67 (d,  $J$  = 7.2 Hz, 1H), 7.62–7.64 (m, 2H), 7.53–7.59 (m, 3H), 7.26 (dd,  $J$  = 8.4, 7.2 Hz, 1H), 7.14 (d,  $J$  = 8.4 Hz, 1H), 4.40 (s, 2H).

<sup>13</sup>C NMR (150 MHz, CDCl<sub>3</sub>) δ 160.07, 145.75, 144.40, 142.01, 141.17, 140.04, 138.47,

135.60, 129.97, 129.50, 129.15, 128.95, 128.74, 127.69, 127.02, 126.82, 126.70, 125.94, 125.74, 125.53, 125.02, 124.03, 122.73, 122.35, 37.34. One  $sp^2$  carbon peak is overlapped.

HRMS (APCI<sup>+</sup>)  $m/z$  calcd for  $C_{28}H_{17}N$   $[M+H]^+$ : 368.1434, found: 368.1421.

#### 8,13-Di-*tert*-butyl-6-phenylphenanthro[4,5-*ijk*]phenanthridine (4ca)



Yield: 48.7 mg, 25% (68.6 mg, 35% in 12 h reaction.), yellow oil.

<sup>1</sup>H NMR (600 MHz, CDCl<sub>3</sub>) δ 9.22 (d,  $J$  = 1.8 Hz, 1H), 8.93 (d,  $J$  = 8.4 Hz, 1H), 8.36 (d,  $J$  = 8.4 Hz, 1H), 8.31 (d,  $J$  = 1.8 Hz, 1H), 8.22 (d,  $J$  = 1.8 Hz, 1H), 8.00–8.06 (m, 3H), 7.79 (ddd,  $J$  = 8.1, 6.9, 1.2 Hz, 1H), 7.72–7.75 (m, 2H), 7.67 (ddd,  $J$  = 8.1, 6.9, 1.2 Hz, 1H), 7.42–7.49 (m, 3H), 1.64 (s, 9H), 1.15 (s, 9H).

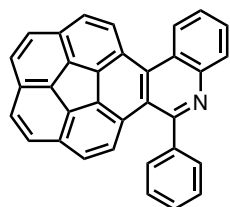
<sup>13</sup>C NMR (150 MHz, CDCl<sub>3</sub>) δ 158.74, 148.58, 147.74, 146.16, 144.81, 136.70,

131.06, 130.68, 129.92, 129.67, 129.24, 128.82, 128.61, 127.93, 127.77, 127.16, 127.08, 126.92, 126.45, 125.72, 125.26, 124.28, 124.23, 122.99, 122.73, 122.58, 35.60, 34.97, 32.00, 31.41. One  $sp^2$  carbon peak is overlapped.

HRMS (APCI<sup>+</sup>)  $m/z$  calcd for C<sub>37</sub>H<sub>33</sub>N [M+H]<sup>+</sup>: 492.2686, found: 492.2670.

### 12-Phenylbenzo[6,7]fluorantheno[1,10-*ijk*]phenanthridine (4da)

Yield: 35.3 mg (Note: 0.20 mmol scale), 41%, yellow solid.

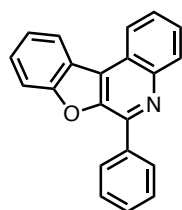


<sup>1</sup>H NMR (600 MHz, CDCl<sub>3</sub>) δ 9.40 (dd,  $J = 8.1, 0.9$  Hz, 1H), 8.70 (d,  $J = 9.0$  Hz, 1H), 8.36 (dd,  $J = 8.1, 0.9$  Hz, 1H), 7.91–7.94 (m, 3H), 7.87 (ddd,  $J = 8.1, 6.9, 1.2$  Hz, 1H), 7.79–7.84 (m, 3H), 7.77 (d,  $J = 8.4$  Hz, 1H), 7.73 (d,  $J = 8.4$  Hz, 1H), 7.61–7.66 (m, 3H), 7.45 (d,  $J = 9.0$  Hz, 1H), 6.94 (d,  $J = 9.0$  Hz, 1H).

<sup>13</sup>C NMR (150 MHz, CDCl<sub>3</sub>) δ 160.06, 145.86, 143.84, 138.36, 138.13, 137.42, 136.07, 134.70, 134.47, 131.73, 131.13, 131.08, 130.47, 129.67, 129.51, 129.16, 128.96, 128.90, 128.55, 128.46, 128.34, 128.04, 127.85, 127.41, 127.26, 127.15, 127.04, 127.00, 125.18, 125.02. One sp<sup>2</sup> carbon peak is overlapped.

HRMS (APCI<sup>+</sup>)  $m/z$  calcd for C<sub>33</sub>H<sub>17</sub>N [M+H]<sup>+</sup>: 428.1434, found: 428.1450.

### 6-Phenylbenzofuro[2,3-*c*]quinoline (4ea)



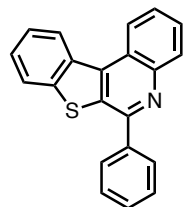
Yield: 41.4 mg, 35%, white solid. The structure was distinguished by comparing with NMR spectra of 6-phenylbenzofuro[3,2-*c*]quinoline as a corresponding isomer.<sup>[22]</sup>

<sup>1</sup>H NMR (600 MHz, CDCl<sub>3</sub>) δ 8.61 (dd,  $J = 7.8, 1.2$  Hz, 1H), 8.55–8.57 (m, 2H), 8.49 (d,  $J = 8.4$  Hz, 1H), 8.38 (dd,  $J = 8.4, 1.2$  Hz, 1H), 7.83 (d,  $J = 7.8$  Hz, 1H), 7.73–7.80 (m, 2H), 7.62–7.69 (m, 3H), 7.54–7.56 (m, 2H).

<sup>13</sup>C NMR (150 MHz, CDCl<sub>3</sub>) δ 156.38, 148.34, 145.66, 144.79, 136.55, 130.84, 129.98, 129.44, 128.85, 128.77, 127.79, 127.35, 125.71, 124.06, 124.02, 123.54, 123.34, 123.27, 113.00.

HRMS (APCI<sup>+</sup>)  $m/z$  calcd for C<sub>21</sub>H<sub>13</sub>NO [M+H]<sup>+</sup>: 296.1070, found: 296.1080.

### 6-Phenylbenzo[4,5]thieno[2,3-*c*]quinoline (4fa)



Yield: 59.0 mg, 47%, off-white solid. The structure was distinguished by comparing with NMR spectra of 6-phenylbenzo[4,5]thieno[3,2-*c*]quinoline as a corresponding isomer.<sup>[23]</sup>

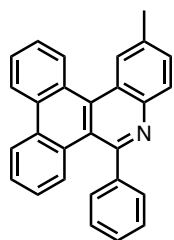
<sup>1</sup>H NMR (600 MHz, CDCl<sub>3</sub>) δ 8.97 (d,  $J = 7.8$  Hz, 1H), 8.93 (d,  $J = 8.4$  Hz, 1H), 8.39 (dd,  $J = 8.1, 1.5$  Hz, 1H), 8.09–8.12 (m, 2H), 8.02 (d,  $J = 7.8$  Hz, 1H), 7.75–7.81 (m, 2H), 7.54–7.68 (m, 5H).

<sup>13</sup>C NMR (150 MHz, CDCl<sub>3</sub>) δ 154.76, 146.27, 141.69, 140.13, 136.80, 135.71, 132.91, 131.16, 129.78, 128.97, 128.81, 128.08, 127.58, 127.37, 126.08, 125.46, 124.70, 123.51, 122.88.

HRMS (APCI<sup>+</sup>)  $m/z$  calcd for C<sub>21</sub>H<sub>13</sub>NS [M+H]<sup>+</sup>: 312.0841, found: 312.0841.

**9-Methyl-5-phenyldibenzo[*i,k*]phenanthridine (4ab)**

Yield: 96.9 mg, 65%, yellow solid.

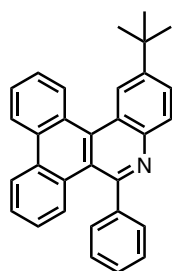


$^1\text{H NMR}$  (600 MHz,  $\text{CDCl}_3$ )  $\delta$  8.89 (d,  $J = 7.8$  Hz, 1H), 8.71 (d,  $J = 8.4$  Hz, 1H), 8.58 (d,  $J = 8.4$  Hz, 1H), 8.53 (s, 1H), 8.19 (d,  $J = 8.4$  Hz, 1H), 7.82 (ddd,  $J = 8.4, 7.1, 1.4$  Hz, 1H), 7.71–7.78 (m, 4H), 7.59 (dd,  $J = 8.4, 1.2$  Hz, 1H), 7.52 (ddd,  $J = 8.4, 7.1, 1.4$  Hz, 1H), 7.42–7.46 (m, 3H), 7.19 (ddd,  $J = 8.4, 7.1, 1.4$  Hz, 1H), 2.62 (s, 3H).

$^{13}\text{C NMR}$  (150 MHz,  $\text{CDCl}_3$ )  $\delta$  156.93, 144.61, 143.91, 136.31, 135.44, 132.64, 130.75, 130.63, 130.02, 129.87, 129.48, 129.22, 128.98, 128.69, 128.32, 127.09, 127.03, 126.53, 126.15, 123.94, 123.37, 123.28, 121.86, 22.28. Two  $\text{sp}^2$  carbon peaks are overlapped.

HRMS (APCI<sup>+</sup>)  $m/z$  calcd for  $\text{C}_{28}\text{H}_{19}\text{N}$  [ $\text{M}+\text{H}$ ]<sup>+</sup>: 370.1590, found: 370.1587.**9-(*tert*-Butyl)-5-phenyldibenzo[*i,k*]phenanthridine (4ac)**

Yield: 51.0 mg, 31%, yellow solid (Note: GPC (eluent: chloroform) after PTLC was required for purification).

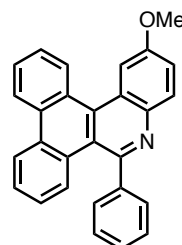


$^1\text{H NMR}$  (600 MHz,  $\text{CDCl}_3$ )  $\delta$  8.86 (d,  $J = 8.4$  Hz, 1H), 8.69–8.72 (m, 2H), 8.56 (d,  $J = 8.4$  Hz, 1H), 8.24 (d,  $J = 8.4$  Hz, 1H), 7.84 (dd,  $J = 8.7, 2.1$  Hz, 1H), 7.80 (t,  $J = 7.8$  Hz, 1H), 7.71–7.76 (m, 4H), 7.50 (t,  $J = 8.1$  Hz, 1H), 7.42–7.45 (m, 3H), 7.17 (t,  $J = 8.4$  Hz, 1H), 1.47 (s, 9H).

$^{13}\text{C NMR}$  (150 MHz,  $\text{CDCl}_3$ )  $\delta$  157.24, 149.20, 144.52, 143.97, 135.96, 132.73, 130.59, 130.02, 129.75, 129.50, 129.18, 128.98, 128.94, 128.73, 128.66, 128.37, 127.33, 127.05, 126.96, 126.15, 123.99, 123.27, 123.00, 122.94, 121.88, 35.36, 31.56.

HRMS (APCI<sup>+</sup>)  $m/z$  calcd for  $\text{C}_{31}\text{H}_{25}\text{N}$  [ $\text{M}+\text{H}$ ]<sup>+</sup>: 412.2060, found: 412.2065.**9-Methoxy-5-phenyldibenzo[*i,k*]phenanthridine (4ad)**

Yield: 71.0 mg, 46%, pale yellow solid.



$^1\text{H NMR}$  (600 MHz,  $\text{CDCl}_3$ )  $\delta$  8.96 (d,  $J = 8.4$  Hz, 1H), 8.72 (d,  $J = 7.2$  Hz, 1H), 8.58 (d,  $J = 8.4$  Hz, 1H), 8.21 (d,  $J = 9.6$  Hz, 1H), 8.16 (d,  $J = 2.4$ , 1H), 7.77–7.83 (m, 2H), 7.70–7.74 (m, 3H), 7.53 (ddd,  $J = 8.4, 7.2, 1.2$  Hz, 1H), 7.41–7.46 (m, 4H), 7.19 (ddd,  $J = 8.4, 7.1, 1.4$  Hz, 1H), 3.99 (s, 3H).

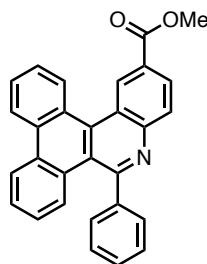
$^{13}\text{C NMR}$  (150 MHz,  $\text{CDCl}_3$ )  $\delta$  158.13, 155.60, 143.88, 141.83, 135.09, 132.55, 130.94, 130.67, 129.97, 129.47, 129.29, 128.99, 128.69, 128.59, 128.46, 127.21, 127.00, 126.19, 124.30, 124.07, 123.28, 122.38, 119.64, 107.46, 55.85. One  $\text{sp}^2$  carbon peak is overlapped.

HRMS (APCI<sup>+</sup>)  $m/z$  calcd for  $\text{C}_{28}\text{H}_{19}\text{NO}$  [ $\text{M}+\text{H}$ ]<sup>+</sup>: 386.1539, found: 386.1523.



**Methyl 5-phenyldibenzo[*i,k*]phenanthridine-9-carboxylate (4ae)**

Yield: 72.9 mg, 46%, pale yellow solid.



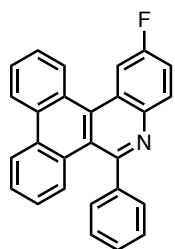
$^1\text{H NMR}$  (600 MHz,  $\text{CDCl}_3$ )  $\delta$  9.45 (sd,  $J = 1.8$  Hz, 1H), 8.80 (d,  $J = 7.2$  Hz, 1H), 8.71 (d,  $J = 7.2$  Hz, 1H), 8.57 (d,  $J = 7.2$  Hz, 1H), 8.33 (dd,  $J = 8.7, 1.5$  Hz, 1H), 8.29 (d,  $J = 8.4$  Hz, 1H), 7.84 (ddd,  $J = 8.4, 7.1, 1.4$  Hz, 1H), 7.72–7.80 (m, 4H), 7.54 (ddd,  $J = 8.1, 6.9, 1.2$  Hz, 1H), 7.43–7.48 (m, 3H), 7.20 (ddd,  $J = 8.4, 7.2, 1.2$  Hz, 1H), 4.01 (s, 3H).

$^{13}\text{C NMR}$  (150 MHz,  $\text{CDCl}_3$ )  $\delta$  167.18, 159.74, 148.00, 143.38, 136.54, 132.86, 130.86, 130.49, 130.05, 129.92, 129.47, 129.26, 129.23, 129.15, 129.04, 128.62, 127.71, 127.60, 127.57, 126.31, 124.01, 123.39, 122.71, 122.16, 52.56. Two  $\text{sp}^2$  carbon peaks are overlapped.

HRMS (APCI $^+$ )  $m/z$  calcd for  $\text{C}_{29}\text{H}_{19}\text{NO}_2$   $[\text{M}+\text{H}]^+$ : 414.1489, found: 414.1480.

**9-Fluoro-5-phenyldibenzo[*i,k*]phenanthridine (4af)**

Yield: 50.5 mg, 34%, yellow solid.



$^1\text{H NMR}$  (600 MHz,  $\text{CDCl}_3$ )  $\delta$  8.84 (d,  $J = 7.8$  Hz, 1H), 8.73 (d,  $J = 7.2$  Hz, 1H), 8.59 (d,  $J = 8.4$  Hz, 1H), 8.41 (dd,  $J = 11.1, 2.7$  Hz, 1H), 8.28 (dd,  $J = 9.0, 6.0$ , 1H), 7.84 (ddd,  $J = 8.4, 7.1, 1.4$  Hz, 1H), 7.75–7.81 (m, 2H), 7.71–7.74 (m, 2H), 7.50–7.57 (m, 2H), 7.44–7.47 (m, 3H), 7.21 (ddd,  $J = 8.4, 7.1, 1.4$  Hz, 1H).

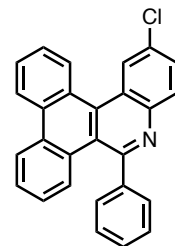
$^{13}\text{C NMR}$  (150 MHz,  $\text{CDCl}_3$ )  $\delta$  161.05 (d,  $^1J_{\text{C-F}} = 246.2$  Hz), 157.24, 143.67, 143.02, 135.25 (d,  $^4J_{\text{C-F}} = 4.2$  Hz), 132.62, 131.75 (d,  $^3J_{\text{C-F}} = 8.7$  Hz), 130.88, 129.94, 129.28, 129.20, 129.14, 129.06, 129.04, 128.91, 127.98, 127.55, 127.39, 126.30, 124.16 (d,  $^3J_{\text{C-F}} = 8.6$  Hz), 124.07, 123.37, 122.45, 118.24 (d,  $^2J_{\text{C-F}} = 24.6$  Hz), 111.58 (d,  $^2J_{\text{C-F}} = 24.5$  Hz). Two  $\text{sp}^2$  carbon peaks are overlapped.

$^{19}\text{F NMR}$  (560 MHz,  $\text{C}_6\text{F}_6$ )  $\delta$  -113.90.

HRMS (APCI $^+$ )  $m/z$  calcd for  $\text{C}_{27}\text{H}_{16}\text{FN}$   $[\text{M}+\text{H}]^+$ : 374.1340, found: 374.1349.

**9-Chloro-5-phenyldibenzo[*i,k*]phenanthridine (4ag)**

Yield: 32.8 mg, 21%, off-white solid.



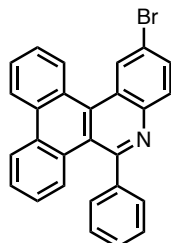
$^1\text{H NMR}$  (600 MHz,  $\text{CDCl}_3$ )  $\delta$  8.81 (d,  $J = 8.4$  Hz, 1H), 8.72–8.74 (m, 2H), 8.59 (d,  $J = 7.8$  Hz, 1H), 8.22 (d,  $J = 9.0$  Hz, 1H), 7.85 (ddd,  $J = 8.4, 7.1, 1.4$  Hz, 1H), 7.79 (ddd,  $J = 8.4, 7.2, 1.2$  Hz, 2H), 7.71–7.74 (m, 2H), 7.70 (dd,  $J = 8.4, 2.4$  Hz, 1H), 7.56 (ddd,  $J = 8.1, 6.9, 1.2$  Hz, 1H), 7.44–7.47 (m, 3H), 7.21 (ddd,  $J = 8.4, 7.1, 1.4$  Hz, 1H).

$^{13}\text{C NMR}$  (150 MHz,  $\text{CDCl}_3$ )  $\delta$  158.02, 144.41, 143.53, 134.91, 132.71, 132.30, 130.96, 130.87, 129.96, 129.44, 129.42, 129.22, 129.13, 129.05, 129.02, 127.76, 127.59, 127.48, 126.33, 126.32, 124.18, 124.06, 123.37, 122.41. One  $\text{sp}^2$  carbon peak is overlapped.

HRMS (APCI<sup>+</sup>)  $m/z$  calcd for C<sub>27</sub>H<sub>16</sub>NCl [M+H]<sup>+</sup>: 390.1044, found: 390.1050.

### 9-Bromo-5-phenyldibenzo[*i,k*]phenanthridine (4ah)

Yield: 19.7 mg, 11%, off-white solid.



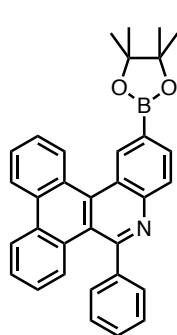
<sup>1</sup>H NMR (600 MHz, CDCl<sub>3</sub>) δ 8.86 (d,  $J = 2.4$  Hz, 1H), 8.77 (d,  $J = 8.4$  Hz, 1H), 8.69 (d,  $J = 8.4$  Hz, 1H), 8.56 (d,  $J = 7.8$  Hz, 1H), 8.13 (d,  $J = 9.0$  Hz, 1H), 7.75–7.84 (m, 4H), 7.70–7.73 (m, 2H), 7.53 (ddd,  $J = 8.4, 7.2, 1.2$  Hz, 1H), 7.42–7.46 (m, 3H), 7.19 (ddd,  $J = 8.4, 7.2, 1.2$  Hz, 1H).

<sup>13</sup>C NMR (150 MHz, CDCl<sub>3</sub>) δ 158.10, 144.62, 143.51, 134.76, 132.70, 132.07, 131.08, 130.86, 129.95, 129.47, 129.42, 129.20, 129.13, 129.04, 127.70, 127.59, 127.50, 126.31, 124.65, 124.06, 123.36, 122.33, 120.40. Two sp<sup>2</sup> carbon peaks are overlapped.

HRMS (APCI<sup>+</sup>)  $m/z$  calcd for C<sub>27</sub>H<sub>16</sub>NBr [M+H]<sup>+</sup>: 434.5039, found: 434.0531.

### 5-Phenyl-9-(4,4,5,5-tetramethyl-1,3,2-dioxaborolan-2-yl)dibenzo[*i,k*]phenanthridine (4ai)

Yield: 24.4 mg, 13%, brown oil (Note: Isolation of this compound required GPC (eluent: chloroform) after PTLC. Moreover, this compound showed  $R_f \cong 0$  (eluent: hexane/chloroform = 1:1) while other N-PACs showed  $R_f = 0.1$ – $0.2$  (eluent: hexane/chloroform = 1:1)).



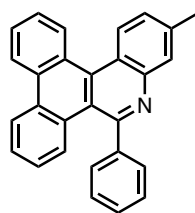
<sup>1</sup>H NMR (600 MHz, CDCl<sub>3</sub>) δ 9.21 (s, 1H), 8.91 (dd,  $J = 8.4, 1.2$  Hz, 1H), 8.72 (d,  $J = 7.8$  Hz, 1H), 8.58 (d,  $J = 7.8$  Hz, 1H), 8.26 (d,  $J = 9.0$  Hz, 1H), 8.13 (dd,  $J = 8.4, 1.2$  Hz, 1H), 7.79–7.86 (m, 2H), 7.73–7.78 (m, 3H), 7.53 (t,  $J = 7.8$  Hz, 1H), 7.43–7.46 (m, 3H), 7.19 (ddd,  $J = 8.4, 7.2, 1.2$  Hz, 1H), 1.39 (s, 12H).

<sup>13</sup>C NMR (150 MHz, CDCl<sub>3</sub>) δ 158.57, 147.70, 143.76, 136.39, 135.24, 134.05, 132.76, 130.70, 130.37, 130.10, 129.36, 129.18, 128.97, 128.92, 128.87, 128.41, 128.22, 127.35, 127.17, 126.17, 123.87, 123.31, 122.82, 121.61, 84.20, 25.10. One sp<sup>2</sup> carbon peak is overlapped.

HRMS (APCI<sup>+</sup>)  $m/z$  calcd for C<sub>33</sub>H<sub>28</sub>BNO<sub>2</sub> [M+H]<sup>+</sup>: 482.2286, found: 482.2282.

### 8-Methyl-5-phenyldibenzo[*i,k*]phenanthridine (4aj)

Yield: 106.8 mg, 72%, pale yellow solid.



<sup>1</sup>H NMR (600 MHz, CDCl<sub>3</sub>) δ 8.86 (d,  $J = 7.8$  Hz, 1H), 8.71 (d,  $J = 7.8$  Hz, 1H), 8.63 (d,  $J = 8.4$  Hz, 1H), 8.57 (d,  $J = 8.4$  Hz, 1H), 8.08 (s, 1H), 7.81 (t,  $J = 7.5$  Hz, 1H), 7.71–7.77 (m, 4H), 7.51 (t,  $J = 7.2$  Hz, 1H), 7.43–7.47 (m, 4H), 7.18 (ddd,  $J = 8.4, 7.2, 1.2$  Hz, 1H), 2.62 (s, 3H).

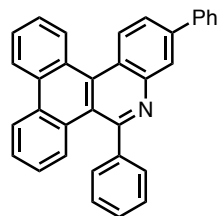
<sup>13</sup>C NMR (150 MHz, CDCl<sub>3</sub>) δ 157.69, 146.29, 143.92, 139.00, 135.84, 132.63,

130.45, 130.00, 129.87, 129.47, 129.11, 128.95, 128.73, 128.71, 128.43, 128.20, 127.06, 126.97, 126.92, 126.11, 123.86, 123.24, 121.28, 121.20, 21.68. One  $sp^2$  carbon peak is overlapped.

HRMS (APCI<sup>+</sup>)  $m/z$  calcd for  $C_{28}H_{19}N$   $[M+H]^+$ : 370.1590, found: 370.1597.

#### 5,8-Diphenyldibenzo[*i,k*]phenanthridine (4ak)

Yield: 89.0 mg, 52%, white solid.



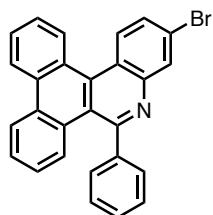
<sup>1</sup>H NMR (600 MHz, CDCl<sub>3</sub>) δ 8.84 (d,  $J$  = 8.4 Hz, 1H), 8.73 (d,  $J$  = 8.4 Hz, 1H), 8.67 (d,  $J$  = 8.4 Hz, 1H), 8.54 (d,  $J$  = 8.4 Hz, 1H), 8.52 (d,  $J$  = 1.8 Hz, 1H), 7.86 (dd,  $J$  = 8.7, 2.1 Hz, 1H), 7.83 (d,  $J$  = 7.8 Hz, 2H), 7.69–7.80 (m, 5H), 7.48–7.53 (m, 3H), 7.43–7.46 (m, 3H), 7.41 (t,  $J$  = 7.5 Hz, 1H), 7.17 (t,  $J$  = 7.8 Hz, 1H).

<sup>13</sup>C NMR (150 MHz, CDCl<sub>3</sub>) δ 158.15, 146.37, 143.79, 141.13, 140.12, 135.66, 132.62, 130.59, 129.94, 129.75, 129.31, 129.11, 128.97, 128.82, 128.79, 128.04, 127.93, 127.78, 127.40, 127.12, 127.05, 126.95, 126.14, 125.54, 123.87, 123.26, 122.43, 121.66. Three  $sp^2$  carbon peaks are overlapped.

HRMS (APCI<sup>+</sup>)  $m/z$  calcd for  $C_{33}H_{21}N$   $[M+H]^+$ : 432.1747, found: 432.1747

#### 8-Bromo-5-phenyldibenzo[*i,k*]phenanthridine (4al)

Yield: 83.3 mg, 48%, white solid.



<sup>1</sup>H NMR (600 MHz, CDCl<sub>3</sub>) δ 8.76 (d,  $J$  = 8.4 Hz, 1H), 8.72 (d,  $J$  = 7.8 Hz, 1H), 8.58 (d,  $J$  = 8.4 Hz, 2H), 8.46 (d,  $J$  = 2.4 Hz, 1H), 7.83 (t,  $J$  = 7.8 Hz, 1H), 7.68–7.78 (m, 5H), 7.55 (t,  $J$  = 7.5 Hz, 1H), 7.43–7.47 (m, 3H), 7.20 (t,  $J$  = 7.8 Hz, 1H).

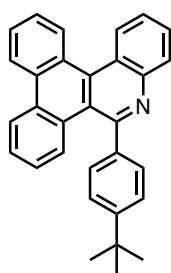
<sup>13</sup>C NMR (150 MHz, CDCl<sub>3</sub>) δ 158.71, 146.77, 143.41, 135.73, 132.76, 131.68, 130.69, 129.98, 129.62, 129.57, 129.16, 129.13, 129.08, 129.01, 128.74, 127.72,

127.45, 127.27, 126.32, 124.02, 123.35, 122.64, 122.11, 121.88. One  $sp^2$  carbon peak is overlapped.

HRMS (APCI<sup>+</sup>)  $m/z$  calcd for  $C_{27}H_{16}NBr$   $[M+H]^+$ : 434.0539, found: 434.0543.

#### 5-(4-(*tert*-Butyl)phenyl)dibenzo[*i,k*]phenanthridine (4am)

Yield: 126.3 mg, 77%, pale yellow solid.



<sup>1</sup>H NMR (600 MHz, CDCl<sub>3</sub>) δ 8.87 (d,  $J$  = 7.8 Hz, 1H), 8.73 (t,  $J$  = 7.8 Hz, 2H), 8.58 (d,  $J$  = 7.8 Hz, 1H), 8.28 (d,  $J$  = 7.2 Hz, 1H), 7.86 (d,  $J$  = 7.8 Hz, 1H), 7.82 (ddd,  $J$  = 8.1, 7.1, 1.1 Hz, 1H), 7.72–7.76 (m, 2H), 7.66 (dt,  $J$  = 8.4, 2.0 Hz, 2H), 7.61 (ddd,  $J$  = 8.4, 7.1, 1.4 Hz, 1H), 7.53 (ddd,  $J$  = 8.1, 6.9, 1.2 Hz, 1H), 7.46 (dt,  $J$  = 9.0, 1.8 Hz, 2H), 7.21 (ddd,  $J$  = 8.4, 7.2, 1.2 Hz, 1H), 1.37 (s, 9H).

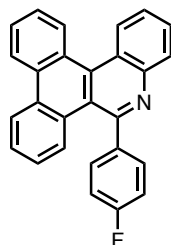
<sup>13</sup>C NMR (150 MHz, CDCl<sub>3</sub>) δ 157.82, 151.92, 146.17, 141.00, 135.71, 132.69, 130.62, 129.94, 129.59, 129.53, 129.43, 129.16, 128.77, 128.73, 128.19, 127.34, 127.12, 127.04, 126.28, 126.16,

125.95 123.92, 123.36, 123.25, 121.75, 34.88, 31.49.

HRMS (APCI<sup>+</sup>) *m/z* calcd for C<sub>31</sub>H<sub>25</sub>N [M+H]<sup>+</sup>: 412.2060, found: 412.2054.

#### 5-(4-Fluorophenyl)dibenzo[*i,k*]phenanthridine (4an)

Yield: 71.4 mg, 48%, pale white solid.



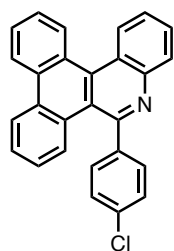
<sup>1</sup>H NMR (600 MHz, CDCl<sub>3</sub>) δ 8.86 (d, *J* = 8.4 Hz, 1H), 8.73 (d, *J* = 8.4 Hz, 1H), 8.71 (d, *J* = 8.4 Hz, 1H), 8.58 (d, *J* = 8.4 Hz, 1H), 8.27 (d, *J* = 8.2 Hz, 1H), 7.82 (t, *J* = 7.8 Hz, 1H), 7.72–7.76 (m, 5H), 7.62 (t, *J* = 7.8 Hz, 1H), 7.54 (t, *J* = 7.5 Hz, 1H), 7.22 (t, *J* = 7.8 Hz, 1H), 7.14 (t, *J* = 9.0 Hz, 2H).

<sup>13</sup>C NMR (150 MHz, CDCl<sub>3</sub>) δ 163.37 (d, <sup>1</sup>*J*<sub>C-F</sub> = 250.7 Hz), 156.53, 146.03, 139.89 (d, <sup>4</sup>*J*<sub>C-F</sub> = 3.0 Hz), 136.01, 132.68, 131.91 (d, <sup>3</sup>*J*<sub>C-F</sub> = 8.6 Hz), 130.72, 129.93, 129.35, 129.20, 129.00, 128.95, 128.92, 128.10, 127.38, 127.29, 127.18, 126.56, 126.27, 123.94, 123.44, 123.40, 121.51, 116.01 (d, <sup>2</sup>*J*<sub>C-F</sub> = 21.6 Hz).

<sup>19</sup>F NMR (560 MHz, C<sub>6</sub>F<sub>6</sub>) δ -113.20.

HRMS (APCI<sup>+</sup>) *m/z* calcd for C<sub>27</sub>H<sub>16</sub>FN [M+H]<sup>+</sup>: 374.1340, found: 374.1335.

#### 5-(4-Chlorophenyl)dibenzo[*i,k*]phenanthridine (4ao)



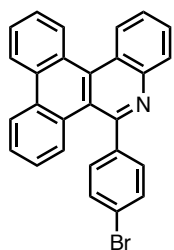
130.2 mg, 84%, off-white solid.

<sup>1</sup>H NMR (600 MHz, CD<sub>2</sub>Cl<sub>2</sub>) δ 8.84 (d, *J* = 8.4 Hz, 1H), 8.72 (t, *J* = 9.0 Hz, 2H), 8.58 (d, *J* = 7.8 Hz, 1H), 8.21 (dd, *J* = 8.4, 1.2 Hz, 1H), 7.82 (ddd, *J* = 8.4, 7.1, 1.4 Hz, 1H), 7.72–7.78 (m, 3H), 7.68 (dt, *J* = 8.4, 2.3 Hz, 2H), 7.64 (ddd, *J* = 8.4, 6.9, 1.5 Hz, 1H), 7.54 (ddd, *J* = 8.4, 7.1, 1.4 Hz, 1H), 7.42 (dt, *J* = 8.4, 2.3 Hz, 2H), 7.23 (ddd, *J* = 8.4, 7.1, 1.4 Hz, 1H).

<sup>13</sup>C NMR (150 MHz, CDCl<sub>3</sub>) δ 156.29, 145.99, 142.18, 135.95, 134.92, 132.60, 131.40, 130.64, 129.85, 129.35, 129.17, 129.05, 128.97, 128.92, 128.90, 128.01, 127.33, 127.29, 127.13, 126.61, 126.28, 123.90, 123.40, 123.35, 121.36.

HRMS (APCI<sup>+</sup>) *m/z* calcd for C<sub>27</sub>H<sub>16</sub>NCl [M+H]<sup>+</sup>: 390.1044, found: 390.1042.

#### 5-(4-Bromophenyl)dibenzo[*i,k*]phenanthridine (4ap)



Yield: 90.3 mg, 52%, off-white solid.

<sup>1</sup>H NMR (600 MHz, CD<sub>2</sub>Cl<sub>2</sub>) δ 8.86 (d, *J* = 8.4 Hz, 1H), 8.74 (t, *J* = 9.6 Hz, 2H), 8.60 (d, *J* = 8.4 Hz, 1H), 8.22 (d, *J* = 8.1 Hz, 1H), 7.83 (t, *J* = 7.7 Hz, 1H), 7.73–7.79 (m, 3H), 7.61–7.67 (m, 3H), 7.54–7.60 (m, 3H), 7.25 (t, *J* = 7.8 Hz, 1H).

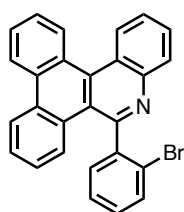
<sup>13</sup>C NMR (150 MHz, CDCl<sub>3</sub>) δ 156.37, 146.03, 142.66, 136.01, 132.65, 132.13, 131.70,

130.67, 129.90, 129.38, 129.10, 128.99, 128.96, 128.94, 128.05, 127.36, 127.33, 127.17, 126.66, 126.34, 123.94, 123.44, 123.38, 123.26, 121.35.

HRMS (APCI<sup>+</sup>) *m/z* calcd for C<sub>27</sub>H<sub>16</sub>NBr [M+H]<sup>+</sup>: 434.0539, found: 434.0532.

#### 5-(2-Bromophenyl)dibenzo[*i,k*]phenanthridine (4aq)

A J-Young tube containing imidoyl chloride prepared from 2-bromo-*N*-phenylbenzamide was vacuumed through a manifold under reduced pressure, capped with a Teflon<sup>®</sup> cock. Then AgPF<sub>6</sub> (0.80 mmol, 2.0 equiv), phenanthrene (0.40 mmol, 1.0 equiv) and 1,2-dichlorobenzene (2.0 mL) were added to a tube under a stream of nitrogen, and a silicon septum was replaced with a Teflon<sup>®</sup> cock again. After stirring at 150 °C for 17 h, the reaction mixture was cooled to room temperature, and then to the J-Young tube were added *p*-chloranil (0.44 mmol, 1.1 equiv) in open air. After stirring at r.t. for 3 h, saturated NaHCO<sub>3</sub> aq. was added for neutralization of obtained reaction mixture. Then, the mixture was passed through a short pad of Celite<sup>®</sup>, and organic phase was extracted three times with chloroform. Extracted organic phase was dried with Na<sub>2</sub>SO<sub>4</sub>. After the organic solvent was removed under reduced pressure, 1,2-dichlorobenzene was removed by flush column chromatography. Then, the residue was purified by PTLC or flush column chromatography to yield N-PAC (eluent: hexane/chloroform = 1:1 to 1:2) to yield 5-(2-bromophenyl)dibenzo[*i,k*]phenanthridine (38.2 mg, 22%) as yellow solid.

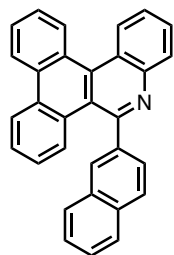


<sup>1</sup>H NMR (600 MHz, CD<sub>2</sub>Cl<sub>2</sub>) δ 8.90 (d, *J* = 8.4 Hz, 1H), 8.81 (d, *J* = 8.4 Hz, 1H), 8.75 (d, *J* = 8.4 Hz, 1H), 8.65 (d, *J* = 8.4 Hz, 1H), 8.24 (d, 8.4 Hz, 1H), 7.78–7.85 (m, 2H), 7.65–7.77 (m, 5H), 7.58 (t, *J* = 7.8 Hz, 1H), 7.52 (t, *J* = 7.5 Hz, 1H), 7.38 (ddd, *J* = 8.4, 7.4, 1.1 Hz, 1H), 7.24 (t, *J* = 8.1 Hz, 1H).

<sup>13</sup>C NMR (150 MHz, CDCl<sub>3</sub>) δ 156.49, 145.80, 144.78, 135.30, 133.89, 132.71, 131.86, 130.61, 130.15, 130.04, 129.37, 129.27, 128.96, 128.86, 128.36, 128.21, 127.63, 127.40, 127.03, 126.94, 126.82, 123.94, 123.58, 123.40, 122.88, 122.65. One sp<sup>2</sup> carbon peak is overlapped.

HRMS (APCI<sup>+</sup>) *m/z* calcd for C<sub>27</sub>H<sub>16</sub>NBr [M+H]<sup>+</sup>: 434.0539, found: 434.0554.

#### 5-(Naphthalen-2-yl)dibenzo[*i,k*]phenanthridine (4ar)



Yield: 68.8 mg, 42%, yellow solid.

<sup>1</sup>H NMR (600 MHz, CDCl<sub>3</sub>) δ 8.90 (d, *J* = 7.8 Hz, 1H), 8.77 (d, *J* = 8.4 Hz, 1H), 8.74 (d, *J* = 8.4 Hz, 1H), 8.60 (d, *J* = 8.4 Hz, 1H), 8.42 (s, 1H), 8.33 (dd, *J* = 8.1, 0.9 Hz, 1H), 7.74–7.94 (m, 7H), 7.71 (dd, *J* = 8.7, 1.5 Hz, 1H), 7.65 (ddd, *J* = 8.4, 6.9, 1.5 Hz, 1H), 7.49–7.55 (m, 3H), 7.10 (ddd, *J* = 8.4, 7.1, 1.4 Hz, 1H).

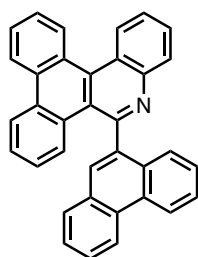
<sup>13</sup>C NMR (150 MHz, CDCl<sub>3</sub>) δ 157.56, 146.23, 141.37, 135.97, 133.91, 133.56, 132.76, 130.66, 129.99, 129.45, 129.38, 129.21, 128.93, 128.91, 128.88, 128.46, 128.20, 128.05, 127.89, 127.42,

127.27, 127.13, 126.70, 126.53, 126.38, 126.34, 123.97, 123.46, 123.33, 121.81. One  $sp^2$  carbon peak is overlapped.

HRMS (APCI<sup>+</sup>)  $m/z$  calcd for  $C_{31}H_{19}N$   $[M+H]^+$ : 406.1590, found: 406.1573.

#### 5-(Phenanthren-9-yl)dibenzo[*i,k*]phenanthridine (4as)

A J-Young tube containing imidoyl chloride prepared from *N*-phenylphenanthrene-9-carboxamide was vacuumed through a manifold under reduced pressure, capped with a Teflon<sup>®</sup> cock. Then  $AgPF_6$  (0.80 mmol, 2.0 equiv), phenanthrene (0.40 mmol, 1.0 equiv) and 1,2-dichlorobenzene (2.0 mL) were added to a tube under a stream of nitrogen, and a silicon septum was replaced with a Teflon<sup>®</sup> cock again. After stirring at 150 °C for 17 h, the reaction mixture was cooled to room temperature, and then to the J-Young tube were added *p*-chloranil (0.44 mmol, 1.1 equiv) in open air. After stirring at r.t. for 3 h, saturated  $NaHCO_3$  aq. was added for neutralization of obtained reaction mixture. Then, the mixture was passed through a short pad of Celite<sup>®</sup>, and organic phase was extracted three times with chloroform. Extracted organic phase was dried with  $Na_2SO_4$ . After the organic solvent was removed under reduced pressure, 1,2-dichlorobenzene was removed by flush column chromatography. Then, the residue was purified by PTLC or flush column chromatography to yield N-PAC (eluent: hexane/chloroform = 1:1 to 1:2) to yield 5-(phenanthren-9-yl)dibenzo[*i,k*]phenanthridine (53.1 mg, 29%) as yellow solid.



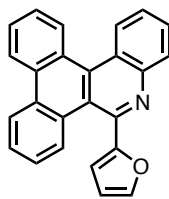
<sup>1</sup>H NMR (600 MHz,  $CDCl_3$ )  $\delta$  8.93 (d,  $J = 8.4$  Hz, 1H), 8.79–8.84 (m, 2H), 8.75 (d,  $J = 8.4$  Hz, 1H), 8.69 (d,  $J = 7.8$  Hz, 1H), 8.52 (d,  $J = 8.4$  Hz, 1H), 8.32 (dd,  $J = 8.4, 0.6$  Hz, 1H), 8.01 (d,  $J = 8.4$  Hz, 1H), 7.78–7.83 (m, 3H), 7.77 (s, 1H), 7.72–7.76 (m, 2H), 7.64–7.70 (m, 3H), 7.53 (ddd,  $J = 8.1, 7.1, 1.1$  Hz, 1H), 7.43 (ddd,  $J = 8.4, 7.1, 1.4$  Hz, 1H), 7.36 (ddd,  $J = 8.1, 7.1, 1.1$  Hz, 1H), 6.87 (ddd,  $J = 8.4, 7.2, 1.2$  Hz, 1H).

<sup>13</sup>C NMR (150 MHz,  $CDCl_3$ )  $\delta$  157.06, 145.97, 140.38, 135.55, 132.80, 131.84, 131.43, 130.72, 130.70, 130.52, 130.24, 129.44, 129.39, 129.24, 129.08, 128.97, 128.92, 128.12, 127.97, 127.67, 127.24, 127.21, 127.15, 127.03, 126.99, 126.86, 126.72, 123.96, 123.54, 123.48, 123.20, 123.18, 122.73. Two  $sp^2$  carbon peaks are overlapped.

HRMS (APCI<sup>+</sup>)  $m/z$  calcd for  $C_{35}H_{21}N$   $[M+H]^+$ : 456.1747, found: 456.1736.

#### 5-(Furan-2-yl)dibenzo[*i,k*]phenanthridine (4at)

Yield: 36.5 mg, 26%, brown oil (Note: Purification of this compound required GPC (eluent: chloroform) after PTLC).

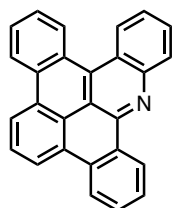


$^1\text{H}$  NMR (600 MHz,  $\text{CDCl}_3$ )  $\delta$  8.82 (d,  $J = 7.8$  Hz, 1H), 8.71 (t,  $J = 9.6$  Hz, 2H), 8.60 (d,  $J = 7.8$  Hz, 1H), 8.27 (d,  $J = 8.4$  Hz, 1H), 7.80 (t,  $J = 7.5$  Hz, 1H), 7.69–7.77 (m, 2H), 7.56–7.64 (m, 3H), 7.48–7.50 (m, 1H), 7.38 (t,  $J = 7.8$  Hz, 1H), 7.18 (d,  $J = 3.0$  Hz, 1H), 6.65 (dd,  $J = 3.3, 1.5$  Hz, 1H).

$^{13}\text{C}$  NMR (150 MHz,  $\text{CDCl}_3$ )  $\delta$  155.60, 146.85, 146.30, 143.50, 135.91, 132.84, 130.52, 129.87, 129.39, 129.14, 128.96, 128.90, 128.00, 127.45, 127.41, 127.29, 127.11, 126.74, 126.71, 124.04, 123.84, 123.32, 121.57, 112.24, 111.37.

HRMS (APCI<sup>+</sup>)  $m/z$  calcd for  $\text{C}_{25}\text{H}_{15}\text{NO}$   $[\text{M}+\text{H}]^+$ : 346.1226, found: 346.1222.

### Benzo[*c*]phenanthro[9,10,1-*mna*]acridine (6aa)



Yield: 29.4 mg, 52%, yellow solid.

$^1\text{H}$  NMR (600 MHz,  $\text{CDCl}_3$ )  $\delta$  9.68–9.71 (m, 1H), 9.16 (d,  $J = 8.4$  Hz, 1H), 9.13 (d,  $J = 7.8$  Hz, 1H), 8.98 (d,  $J = 7.8$  Hz, 1H), 8.97 (d,  $J = 8.4$  Hz, 1H), 8.92 (d,  $J = 8.4$  Hz, 1H), 8.74 (dd,  $J = 7.8, 2.4$  Hz, 1H), 8.60 (dd,  $J = 8.4, 1.2$  Hz, 1H), 8.12 (t,  $J = 8.1$  Hz, 1H), 7.94 (ddd,  $J = 8.4, 6.9, 1.5$  Hz, 1H), 7.90 (ddd,  $J = 8.4, 7.1, 1.4$  Hz, 1H), 7.80–7.87

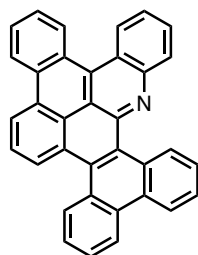
(m, 3H), 7.78 (ddd,  $J = 8.7, 7.1, 1.7$  Hz, 1H).

$^{13}\text{C}$  NMR (150 MHz,  $\text{Cl}_2\text{CDCDCl}_2$ )  $\delta$  147.14, 146.70, 132.42, 132.30, 132.00, 130.89, 130.06, 129.95, 129.86, 129.31, 128.80, 128.64, 128.01, 127.91, 127.26, 127.10, 126.87, 126.21, 125.87, 123.88, 123.03, 122.86, 122.51, 122.42, 121.84, 117.20. One  $\text{sp}^2$  carbon peak is overlapped.

HRMS (APCI<sup>+</sup>)  $m/z$  calcd for  $\text{C}_{27}\text{H}_{15}\text{N}$   $[\text{M}+\text{H}]^+$ : 354.1277, found: 354.1283.

### Diphenanthro[9,10-*c*:9',10',1'-*mna*]acridine (6as)

Yield: 3.0 mg, 14%, yellow solid.



$^1\text{H}$  NMR (600 MHz,  $\text{CD}_2\text{Cl}_2$ )  $\delta$  10.67 (dd,  $J = 8.7, 1.5$  Hz, 1H), 9.18 (d,  $J = 8.4$  Hz, 2H), 8.99 (d,  $J = 7.8$  Hz, 2H), 8.90 (d,  $J = 7.8$  Hz, 1H), 8.81–8.84 (m, 2H), 8.74 (dd,  $J = 8.4, 0.6$  Hz, 1H), 8.63 (dd,  $J = 8.1, 1.5$  Hz, 1H), 8.08 (t,  $J = 7.8$  Hz, 1H), 7.99 (ddd,  $J = 8.1, 6.9, 1.2$  Hz, 1H), 7.93 (ddd,  $J = 8.1, 6.9, 1.2$  Hz, 1H), 7.77–7.86 (m, 5H), 7.68 (ddd,  $J = 8.1, 7.1, 1.1$  Hz, 1H).

$^{13}\text{C}$  NMR (150 MHz,  $\text{CD}_2\text{Cl}_2$ )  $\delta$  148.84, 147.32, 133.29, 133.03, 132.90, 132.70, 131.69, 130.84, 130.77, 130.71, 130.28, 129.86, 129.56, 129.40, 129.34, 129.15, 128.86, 128.60, 128.16, 127.72, 127.65, 127.58, 127.42, 126.88, 126.85, 126.62, 126.49, 124.44, 124.19, 123.64, 123.30, 122.05, 121.79, 118.72. One  $\text{sp}^2$  carbon peak is overlapped.

HRMS (APCI<sup>+</sup>)  $m/z$  calcd for  $\text{C}_{35}\text{H}_{19}\text{N}$   $[\text{M}+\text{H}]^+$ : 454.1590, found: 454.1587.

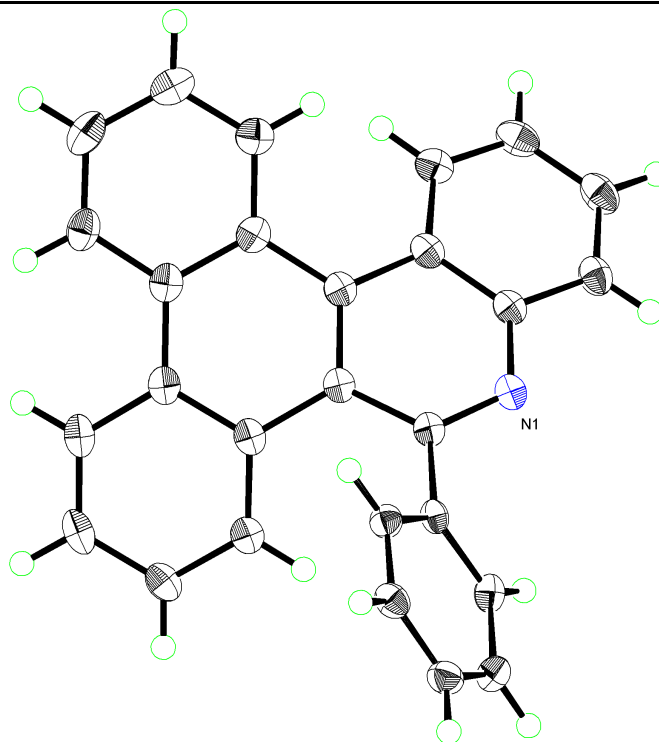
#### 4-4. X-ray Crystal Structure Analysis

Details of the crystal data and a summary of the intensity data collection parameters for **4aa**, **4da** dimer, and **6as** are listed in Table S1–S3 and Figure S1–S3. A suitable crystal, obtained by crystallization from pentane/chloroform solution, was mounted with mineral oil on glass fiber and transferred to the goniometer of a Rigaku PILATUS diffractometer. Graphite-monochromated Mo K $\alpha$  radiation was used. The structures were solved by direct methods with (SIR-97)<sup>[24]</sup> and refined by full-matrix least-squares techniques against *F*<sup>2</sup> (SHELXL- 2014/7)<sup>[25]</sup> by using Yadokari-XG<sup>[26]</sup> or Olex2<sup>[27]</sup> software package. The intensities were corrected for Lorentz and polarization effects. The non-hydrogen atoms were refined anisotropically. Hydrogen atoms were placed using AFIX instructions.



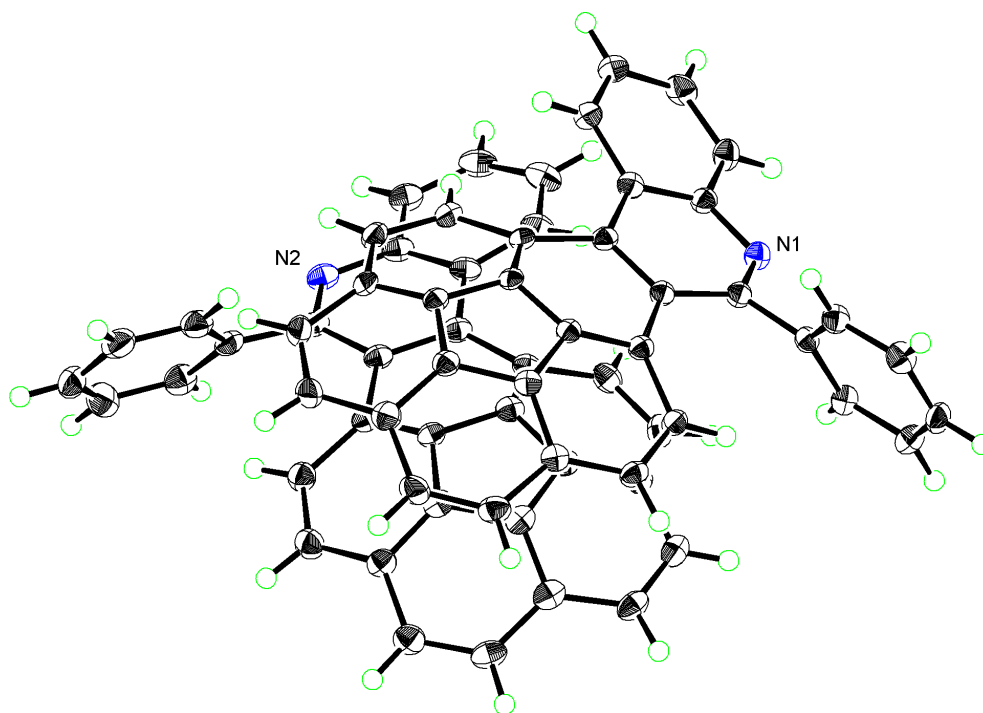
**Table S1.** Crystallographic data and structure refinement details for **4aa**.

CCDC deposition No.	1960273
formula	C <sub>27</sub> H <sub>17</sub> N
fw	355.42
<i>T</i> (K)	123(2) K
$\lambda$ (Å)	0.71073 Å
cryst syst	Monoclinic
space group	<i>I</i> 2/ <i>a</i>
<i>a</i> (Å)	20.4777(11)
<i>b</i> (Å)	9.9150(5)
<i>c</i> (Å)	17.5698(10)
$\alpha$ (deg)	90
$\beta$ (deg)	93.490(5)
$\gamma$ (deg)	90
<i>V</i> (Å <sup>3</sup> )	3560.7(3)
<i>Z</i>	8
<i>D</i> <sub>calc</sub> (g / cm <sup>3</sup> )	1.326
$\mu$ (mm <sup>-1</sup> )	0.077
F(000)	1488.0
cryst size (mm)	0.15 × 0.15 × 0.15
$\theta$ range (deg)	1.993 – 24.997
reflns collected	11038
indep reflns/ <i>R</i> <sub>int</sub>	3137/0.0417
params	253
GOF on <i>F</i> <sup>2</sup>	1.076
<i>R</i> <sub>1</sub> , <i>wR</i> <sub>2</sub> [ <i>I</i> > 2 $\sigma$ ( <i>I</i> )]	0.0376, 0.0906
<i>R</i> <sub>1</sub> , <i>wR</i> <sub>2</sub> (all data)	0.0460, 0.0954

**Figure S1.** Crystallographic image of **4aa**.

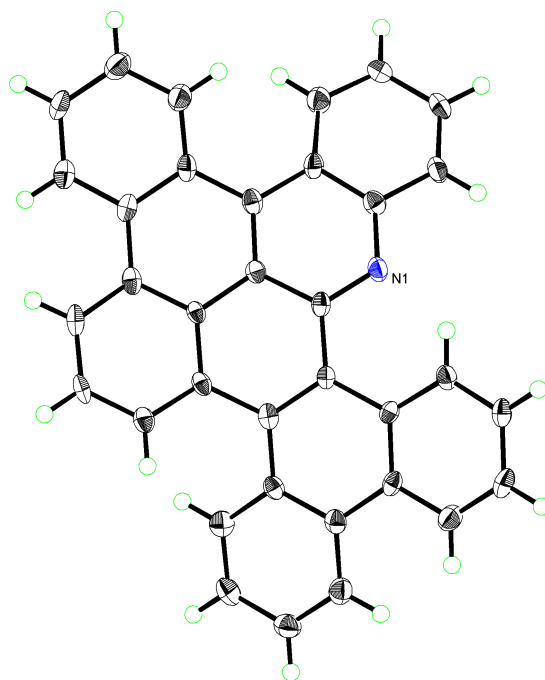
**Table S2.** Crystallographic data and structure refinement details for **4da** dimer.

CCDC deposition No.	1960274
formula	C <sub>66</sub> H <sub>34</sub> N <sub>2</sub>
fw	854.95
<i>T</i> (K)	123(2) K
$\lambda$ (Å)	0.71073 Å
cryst syst	Triclinic
space group	<i>P</i> -1
<i>a</i> (Å)	12.4034(6)
<i>b</i> (Å)	13.7035(7)
<i>c</i> (Å)	15.2489(8)
$\alpha$ (deg)	97.625(4)
$\beta$ (deg)	113.937(5)
$\gamma$ (deg)	112.875(5)
<i>V</i> (Å <sup>3</sup> )	2048.7(2)
<i>Z</i>	2
<i>D</i> <sub>calc</sub> (g / cm <sup>3</sup> )	1.386
$\mu$ (mm <sup>-1</sup> )	0.080
F(000)	888
cryst size (mm)	0.10 × 0.10 × 0.10
$\theta$ range (deg)	1.718 – 24.998
reflns collected	25818
indep reflns/ <i>R</i> <sub>int</sub>	7206/0.0785
params	613
GOF on <i>F</i> <sup>2</sup>	1.052
<i>R</i> <sub>1</sub> , <i>wR</i> <sub>2</sub> [ <i>I</i> > 2 $\sigma$ ( <i>I</i> )]	0.0467, 0.1140
<i>R</i> <sub>1</sub> , <i>wR</i> <sub>2</sub> (all data)	0.0679, 0.1251

**Figure S2.** Crystallographic image of **4da** dimer.

**Table S3.** Crystallographic data and structure refinement details for **6as**.

CCDC deposition No.	1960275
formula	C <sub>35</sub> H <sub>19</sub> N
fw	453.51
<i>T</i> (K)	123(2) K
□ (Å)	0.71073 Å
cryst syst	Orthorhombic
space group	<i>Pbca</i>
<i>a</i> (Å)	11.6206(13)
<i>b</i> (Å)	7.9880(7)
<i>c</i> (Å)	46.137(8)
α (deg)	90
β (deg)	90
γ (deg)	90
<i>V</i> (Å <sup>3</sup> )	4282.7(9)
<i>Z</i>	8
<i>D</i> <sub>calc</sub> (g / cm <sup>3</sup> )	1.407
μ (mm <sup>-1</sup> )	0.081
F(000)	1888.0
cryst size (mm)	0.15 × 0.10 × 0.050
θ range (deg)	1.766 – 24.999
reflns collected	18756
indep reflns/ <i>R</i> <sub>int</sub>	3777/0.1848
params	325
GOF on <i>F</i> <sup>2</sup>	0.999
<i>R</i> <sub>1</sub> , <i>wR</i> <sub>2</sub> [ <i>I</i> > 2σ( <i>I</i> )]	0.0797, 0.1959
<i>R</i> <sub>1</sub> , <i>wR</i> <sub>2</sub> (all data)	0.1401, 0.2390

**Figure S3.** Crystallographic image of **6as**.

#### 4-5. DFT calculation

The Gaussian 16 program, revision C.01,<sup>[28]</sup> with the M06-2X<sup>[29]</sup> density function was used for investigation on reaction mechanism (Figure 2). According to the literature,<sup>[30]</sup> geometry optimizations and harmonic vibration frequency calculations of the all local minima (with no imaginary frequency) and transition states (with one imaginary frequency) were conducted using the 6-31+G(d) level of theory in the gas phase at 353.15 K and 1 atm without any symmetry assumptions, and those accurate energies were estimated by the single-point calculations of optimized geometries with the 6-311++G(d,p) level of theory at 353.15 K in 1,2-dichloroethane (IEF-PCM<sup>[31]</sup>). All calculated Gibbs energies were corrected by Truhlar's quasi-harmonic correction<sup>[19]</sup> by setting all positive frequency below 100 cm<sup>-1</sup> to a value of 100 cm<sup>-1</sup> using 0.967 of scaling factor to vibration frequencies.<sup>[19]</sup> We used the GoodVibes program ver. 2.0.2<sup>[32]</sup> for the calculations of Truhlar's quasi-harmonic correction.<sup>[19]</sup>

For calculation of photophysical properties of **6aa** and **6as**, and the B3LYP<sup>[33]</sup>/6-311++G(d,p) level of basis set was used for optimizations of structures, frequency calculations and TD-DFT calculations without any symmetry assumptions. Zero-point energy, enthalpy, and Gibbs free energy at 298.15 K and 1 atm were estimated from the gas-phase unless otherwise noted. Harmonic vibration frequency calculations at the same level were performed to verify all stationary points as local minima with no imaginary frequency. Visualization of the results was performed by use of GaussView 6.1 software.<sup>[34]</sup> and CYLview 1.0b.<sup>[35]</sup>

**Table S4.** TD-DFT (B3LYP/6-311++G(d,p)) vertical one-electron excitations (4 states) calculated for the conformation of optimized **6aa**.

Exited state	Energy / eV	Wavelength / nm	Oscillator strength ( <i>f</i> )	Description
1	3.1984	387.65	0.1087	HOMO -> LUMO
2	3.3098	374.60	0.0573	HOMO-1 -> LUMO
3	3.6218	342.30	0.0267	HOMO-2 -> LUMO
4	3.8208	324.50	0.0394	HOMO-3 -> LUMO

**Table S5.** TD-DFT (B3LYP/6-311++G(d,p)) vertical one-electron excitations (4 states) calculated for the conformation of optimized **6as**.

Exited state	Energy / eV	Wavelength / nm	Oscillator strength ( <i>f</i> )	Description
1	2.7762	446.60	0.1203	HOMO -> LUMO
2	3.1308	396.02	0.0592	HOMO-1 -> LUMO
3	3.2681	379.38	0.0109	HOMO-2 -> LUMO
4	3.4853	355.74	0.0869	HOMO-3 -> LUMO

**Table S6.** Uncorrected (315.15 K, 1atm, dichloroethane) and thermal-corrected (315.15 K, 1atm) energies

and Truhlar's quasi-harmonic-corrected energies of stationary points (Hartree).<sup>a</sup>

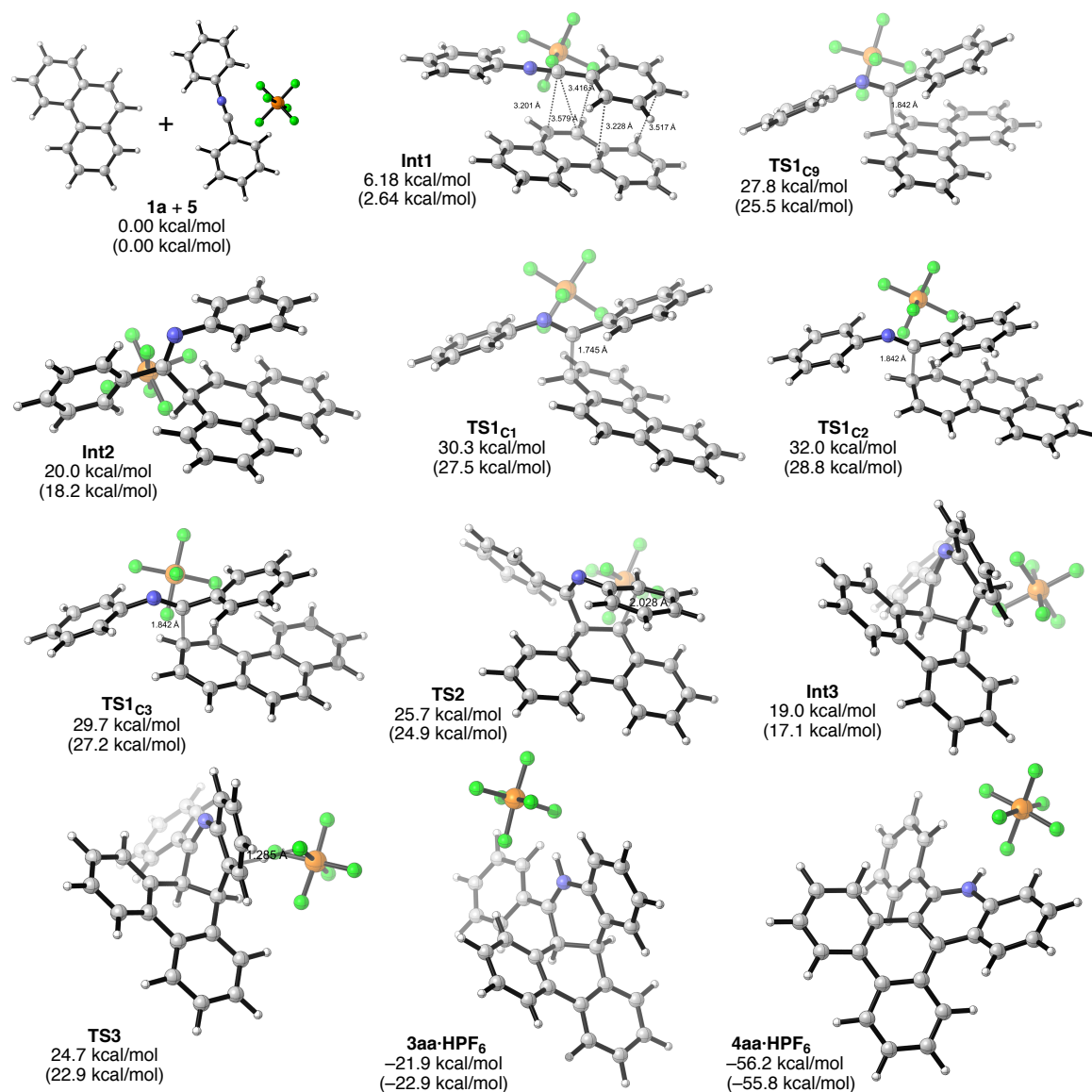
Structure	$E$	$ZPE$	$H$	$G$	$qh-G$
<b>1a</b>	-539.441498	0.189952	-539.236626	-539.295434	-539.295336
<b>PF<sub>6</sub><sup>-</sup></b>	-940.758015	0.018828	-940.729717	-940.772959	-940.772959
<b>HPF<sub>6</sub></b>	-941.129102	0.027406	-941.089607	-941.143267	-941.143167
<b>diphenylnitrilium</b>	-555.844845	0.187766	-555.640300	-555.707192	-555.703114
<b>5</b>	-1496.621615	0.208054	-1496.386244	-1496.477391	-1496.471298
<b>5'</b>	-1496.587469	0.208108	-1496.351682	-1496.447860	-1496.438018
<b><i>p</i>-chloranil</b>	-2219.793141	0.046547	-2219.730727	-2219.795911	-2219.794094
<b>tetrachlorohydroquinone</b>	-2221.039888	0.069114	-2220.953996	-2221.019220	-2221.018794
<b>Int1</b>	-2036.082855	0.398828	-2035.640378	-2035.768617	-2035.756792
<b>TS1<sub>C9</sub></b>	-2036.049438	0.398504	-2035.608667	-2035.732160	-2035.722377
<b>Int2</b>	-2036.064307	0.400553	-2035.621756	-2035.743835	-2035.734793
<b>TS1<sub>C1</sub></b>	-2036.045460	0.398401	-2035.604712	-2035.728980	-2035.718358
<b>TS1<sub>C2</sub></b>	-2036.042731	0.398299	-2035.602072	-2035.726988	-2035.715610
<b>TS1<sub>C3</sub></b>	-2036.046403	0.398412	-2035.605703	-2035.729441	-2035.719230
<b>TS2</b>	-2036.057392	0.401431	-2035.615197	-2035.733065	-2035.725700
<b>Int3</b>	-2036.068608	0.402095	-2035.625320	-2035.745547	-2035.736309
<b>TS3</b>	-2036.055834	0.397564	-2035.617724	-2035.736273	-2035.727334
<b>3aa</b>	-1094.922540	0.371650	-1094.521173	-1094.613311	-1094.609729
<b>3aa·HPF<sub>6</sub></b>	-2036.136853	0.404999	-2035.691175	-2035.809388	-2035.801483
<b>4aa·HPF<sub>6</sub></b>	-2034.945038	0.382695	-2034.522308	-2034.638410	-2034.631499

- a)  $E$ : electronic energy in dichloroethane (IEF-PCM) at 353.15 K and 1 atm calculated by M06-2X/6-311++G(d,p);  $ZPE$ : zero-point energy calculated by M06-2X/6-31+G(d);  $H$  (enthalpy) =  $E + TCE$ : sum of electronic energy ( $E$ ) and thermal correction to enthalpy ( $TCE$ , M06-2X/6-31+G(d));  $G$  (free energy) =  $E + TCF$ : sum of electronic energy ( $E$ ) and thermal corrections to free energies ( $TCF$ , M06-2X/6-31+G(d));  $qh-G$  (free energy with Truhlar's quasiharmonic approximation). A 0.967 of scaling factor was used for vibration frequencies.

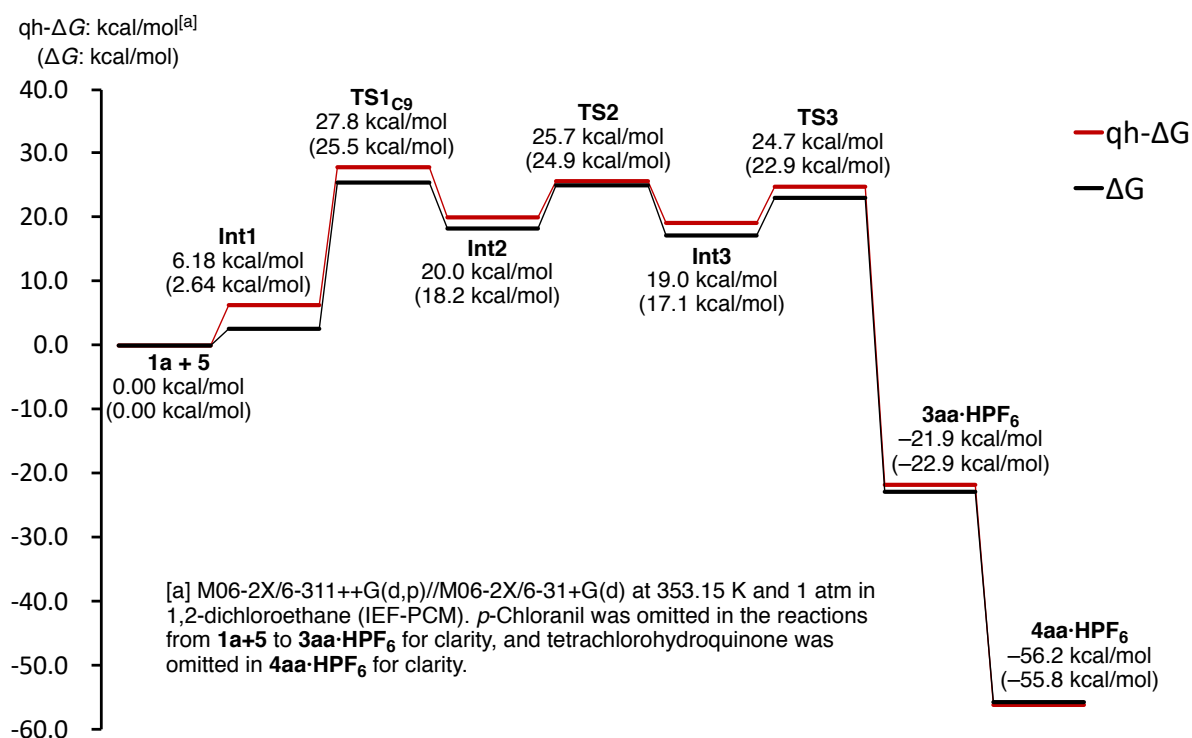
**Table S7.** Uncorrected and thermal-corrected (298.15 K, 1 atm) energies of stationary points (Hartree) calculated by B3LYP/6-311++G(d,p).<sup>a</sup>

structure	$E$	$E + ZPE$	$H$	$G$
<b>6aa</b>	-1092.985548	-1092.650943	-1092.631831	-1092.696415
<b>6as</b>	-1400.319407	-1399.891592	-1399.867061	-1399.943405
<b>S1</b>	-1384.270185	-1383.830269	-1383.805683	-1383.881840
<b>S2</b>	-1076.934734	-1076.588520	-1076.569201	-1076.634154

- b)  $E$ : electronic energy;  $ZPE$ : zero-point energy;  $H$ : sum of electronic and thermal correction to enthalpies;  $G$ : sum of electronic and thermal correction to free energies.



**Figure S4.** Optimized structure of local minima and transition states with free energies. Truhlar's quasi-harmonic corrected free energies ( $qh-\Delta G$ ) are shown in parenthesis, and *p*-chloranil and tetrachlorohydroquinone are omitted for clarity.



**Figure S5.** Energy diagrams of calculated reaction pathway in the aza-APEX reaction of **1a** with **5**.

**Table S8.** Cartesian coordinates of optimized structures.

<b>phenanthrene (1a)</b>				F	-0.2238840	-0.0986820	0.8170140
C	-3.5541070	-0.2965390	0.0000000	F	2.1920090	2.1574500	-0.8692340
C	-2.8315620	0.8767460	-0.0000040	F	0.0268160	1.7395170	-1.1145410
C	-1.4189460	0.8615120	-0.0000030	F	-0.4633110	2.8049470	0.7745410
C	-0.7289320	-0.3770280	0.0000010	F	1.5121170	1.8842960	1.2278300
C	-1.4947770	-1.5645280	0.0000060	F	1.0939920	4.0261500	-0.2833920
C	-2.8745090	-1.5284870	0.0000050	N	-0.1943730	-2.1357920	-0.2241090
C	-0.6773670	2.0939600	-0.0000030	C	2.0430120	-1.2086450	-0.6280160
C	0.7289320	-0.3770280	0.0000000	C	1.2123210	-2.2110210	-0.1166710
C	1.4189460	0.8615120	0.0000010	C	1.7758080	-3.3572980	0.4490650
C	0.6773660	2.0939600	0.0000000	C	3.1600110	-3.4762590	0.5425330
C	2.8315620	0.8767460	0.0000020	C	3.9898840	-2.4708280	0.0473120
C	3.5541070	-0.2965390	0.0000010	C	3.4256020	-1.3415920	-0.5455140
C	2.8745090	-1.5284870	-0.0000030	C	-0.8385410	-1.1394050	0.1833250
C	1.4947770	-1.5645280	-0.0000040	C	-2.2943010	-0.9497100	0.0719300
H	3.3412970	1.8373690	0.0000040	C	-2.9005870	0.2192040	0.5407690
H	-1.2322850	3.0289300	-0.0000060	C	-3.0665060	-1.9569090	-0.5188350
H	-4.6397100	-0.2726720	-0.0000010	C	-4.2796310	0.3760850	0.4191430
H	-3.3412970	1.8373690	-0.0000070	C	-4.4410650	-1.7930380	-0.6350560
H	-1.0007710	-2.5300010	0.0000120	C	-5.0496840	-0.6265140	-0.1662750
H	-3.4370350	-2.4574460	0.0000100	H	1.6021530	-0.3416570	-1.1100530
H	1.2322850	3.0289300	0.0000010	H	1.1186150	-4.1395950	0.8163740
H	4.6397100	-0.2726720	0.0000020	H	3.5914380	-4.3637920	0.9961580
H	3.4370350	-2.4574460	-0.0000070	H	5.0688590	-2.5706720	0.1146500
H	1.0007710	-2.5300010	-0.0000080	H	4.0604960	-0.5566300	-0.9462250
<b>imidoyl fluoride (5')</b>				H	-2.2980750	0.9990810	0.9939250
P	0.8699340	2.5041330	-0.0454600	H	-2.5733280	-2.8544100	-0.8783550
				H	-4.7509330	1.2840380	0.7825670

H	-5.0407190	-2.5744440	-1.0917600
H	-6.1244940	-0.5008890	-0.2588480

**PF<sub>6</sub><sup>-</sup>**

P	-0.7046220	-0.1071030	0.0000000
F	-0.7046220	-1.7378850	0.0000000
F	-0.7046220	-0.1071030	1.6307820
F	0.9261600	-0.1071030	0.0000000
F	-0.7046220	1.5236790	0.0000000
F	-0.7046220	-0.1071030	-1.6307820
F	-2.3354040	-0.1071030	0.0000000

**diphenylnitrilium**

N	-0.5868300	0.0002800	-0.0001600
C	4.0550260	-1.1249090	0.4640010
C	2.6681110	-1.1369310	0.4689700
C	1.9851840	0.0001130	-0.0000630
C	2.6683330	1.1370490	-0.4690360
C	4.0552460	1.1248070	-0.4639420
C	4.7421530	-0.0001050	0.0000610
C	0.5669700	0.0002280	-0.0001300
C	-1.9798700	0.0001260	-0.0000630
C	-2.6479300	0.4703170	1.1333350
C	-2.6479830	-0.4702040	-1.1333720
C	-4.0371620	0.4651090	1.1212120
C	-4.0372140	-0.4652700	-1.1210710
C	-4.7270690	-0.0001500	0.0001160
H	4.6020740	-1.9906830	0.8210860
H	2.1169490	-2.0011390	0.8254350
H	2.1173390	2.0013450	-0.8255500
H	4.6024630	1.9904950	-0.8209770
H	5.8277620	-0.0001910	0.0001100
H	-2.0884760	0.8266730	1.9919850
H	-2.0885700	-0.8264460	-1.9920960
H	-4.5812840	0.8246190	1.9879080
H	-4.5813770	-0.8248880	-1.9876970
H	-5.8123230	-0.0002590	0.0001860

**diphenylnitrilium·PF<sub>6</sub> (5)**

C	0.84564500	-0.92587100	-0.09325800
N	1.81355600	-0.31296000	0.01471500
C	-0.30378400	-1.76477700	-0.06390200
C	-0.68593600	-2.27814500	1.18828400
C	-1.00174800	-2.07943200	-1.23934900
C	-1.78932000	-3.11502400	1.25976300
H	-0.12609200	-2.01767200	2.08118500
C	-2.09959100	-2.92584600	-1.13982300
H	-0.69541900	-1.65828800	-2.18955900
C	-2.49275600	-3.43736200	0.09657900
H	-2.10150900	-3.51476900	2.21877800
H	-2.65525100	-3.17598700	-2.03724000
H	-3.35706000	-4.09185800	0.15762900
C	3.00772800	0.39848600	0.04038700
C	3.75909700	0.48089800	-1.13264200
C	3.40743200	0.98909900	1.23978800
C	4.95695600	1.18418700	-1.08471700
H	3.38225000	0.03324900	-2.04533700
C	4.60896100	1.68641900	1.26073900

H	2.78373400	0.90597500	2.12372500
C	5.38102000	1.78235700	0.10212900
H	5.55372400	1.27423400	-1.98613100
H	4.93889600	2.15850500	2.18018800
H	6.31616100	2.33320300	0.12369800
P	0.40418500	0.81602300	-3.14278000
F	1.53341000	1.69784000	-2.36870900
F	-0.41957500	2.13399800	-3.53279700
F	1.25904400	0.87143700	-4.50351000
F	-0.70916400	-0.14103600	-3.83786700
F	1.23656200	-0.55907900	-2.69510300
F	-0.42154700	0.69856200	-1.72056200

**p-chloranil**

Cl	-2.7113110	-1.6060710	-0.0002370
Cl	-2.7114120	1.6060510	0.0000270
Cl	2.7113130	1.6060460	-0.0001440
Cl	2.7114140	-1.6060290	-0.0000650
O	-0.0001150	-2.6578510	0.0004560
O	0.0001160	2.6578580	0.0002470
C	-1.2818640	0.6719630	0.0000440
C	0.0000280	1.4533140	0.0000760
C	1.2818280	0.6718730	-0.0000180
C	1.2818520	-0.6719610	0.0000180
C	-0.0000210	-1.4533150	0.0001670
C	-1.2818410	-0.6718750	-0.0000390

**tetrachlorohydroquinone**

Cl	2.6625410	-1.6241340	0.0000970
Cl	2.7008730	1.5544460	-0.0002080
Cl	-2.6624860	1.6242610	-0.0002500
Cl	-2.7007250	-1.5546420	0.0001140
O	0.0210900	-2.7585490	-0.0002880
O	-0.0213900	2.7586250	0.0003880
C	1.2069050	0.6754470	0.0001060
C	0.0167600	1.4103590	0.0003430
C	-1.1981790	0.7191920	0.0001370
C	-1.2070200	-0.6753580	0.0000560
C	-0.0166540	-1.4103080	-0.0001040
C	1.1980890	-0.7193270	0.0000130
H	-0.8826520	-3.1136370	0.0002600
H	0.8821890	3.1141840	-0.0001680

**HPF<sub>6</sub>**

P	-0.3138600	-0.0000060	-0.0005050
F	-1.8549690	-0.0103030	-0.1525490
F	-0.0523260	1.5597520	-0.0749490
F	0.1682560	-0.0843730	-1.5155050
F	2.1472280	0.0113030	0.1619220
F	-0.1150360	0.0872650	1.5605420
F	-0.0492150	-1.5579790	0.0991720
H	2.5124610	-0.0508980	-0.7001320

**Int1**

P	2.0725220	-2.6922040	-0.4894100
F	3.5792350	-2.0789570	-0.4803400
F	2.5832650	-4.0628990	-1.1393970
F	2.2832730	-3.2684520	1.0141090



F	0.5294280	-3.2276980	-0.4604470
F	1.5470280	-1.2627480	0.1886190
F	1.8089800	-2.0377650	-1.9521990
N	1.2595660	1.1526450	1.3696300
C	-0.3642570	4.1489760	-0.9618790
C	0.0954570	2.8904450	-1.2864020
C	-0.7694040	1.7707830	-1.2756080
C	-2.1395240	1.9480700	-0.9471830
C	-2.5837120	3.2504980	-0.6205560
C	-1.7187980	4.3271380	-0.6214650
C	-3.0209140	0.7871460	-0.9419200
C	-2.4686340	-0.4933560	-1.2047580
C	-1.0711840	-0.6291750	-1.5165100
C	-3.2994570	-1.6360260	-1.1582760
C	-4.6443150	-1.5239320	-0.8774090
C	-5.1999620	-0.2533970	-0.6350840
C	-4.4042270	0.8747530	-0.6664570
C	0.3350480	0.4974650	1.5761050
C	-0.8376030	-0.2426430	1.8692420
C	-2.0224160	0.4733160	2.1114440
C	-0.7973280	-1.6478240	1.8734470
C	-3.1875170	-0.2370850	2.3608520
C	-1.9794370	-2.3316070	2.1184040
C	-3.1647840	-1.6326820	2.3559080
C	2.3997600	1.8434190	0.9760840
C	3.4048530	1.1429510	0.3057770
C	2.4748730	3.2118140	1.2439590
C	4.5226020	1.8616490	-0.1094740
C	3.6007400	3.9033390	0.8162350
C	4.6212720	3.2301240	0.1402200
C	-0.2620120	0.4573050	-1.5679600
H	-2.8497500	-2.6074500	-1.3505740
H	0.3120470	4.9993220	-0.9757220
H	1.1382690	2.7373810	-1.5587840
H	-3.6236960	3.4202940	-0.3615790
H	-2.0892050	5.3161760	-0.3678870
H	-0.6636250	-1.6203510	-1.6958290
H	-5.2748360	-2.4080260	-0.8512630
H	-6.2624690	-0.1569600	-0.4298460
H	-4.8638460	1.8405360	-0.4826740
H	-2.0230500	1.5589610	2.0747330
H	0.1262440	-2.1738350	1.6616160
H	-4.1171020	0.2955210	2.5305990
H	-1.9734880	-3.4164040	2.1053370
H	-4.0863120	-2.1812400	2.5273760
H	3.3031040	0.0782000	0.1165410
H	1.6589500	3.7107100	1.7566700
H	5.3160100	1.3397770	-0.6342680
H	3.6809870	4.9683110	1.0086320
H	5.4977720	3.7774680	-0.1924690
H	0.7936170	0.3340530	-1.8003780

**TS1c9**

P	2.9822910	-1.9228480	-0.1162990
F	2.7436660	-1.0559970	-1.4968210
F	3.8891060	-2.9762020	-0.9159110
F	4.2566650	-0.9986240	0.2329270
F	3.1370430	-2.7434600	1.2581340

F	1.9983030	-0.8332520	0.6560890
F	1.6265750	-2.7857960	-0.4791000
N	0.6977250	1.7270830	1.3049970
C	-3.1410140	3.5281660	-0.8626600
C	-1.8883360	2.9413960	-0.8738590
C	-1.7589860	1.5466850	-0.9691470
C	-2.9046550	0.7287210	-1.0380290
C	-4.1707270	1.3476120	-1.0299720
C	-4.2877650	2.7226560	-0.9412670
C	-2.7375800	-0.7229760	-1.1172060
C	-1.4325390	-1.2740770	-1.3058860
C	-0.3022570	-0.4332790	-1.2720480
C	-1.2506380	-2.6737650	-1.4561200
C	-2.3327780	-3.5211970	-1.3798640
C	-3.6118260	-2.9844590	-1.1474250
C	-3.8137310	-1.6180900	-1.0236550
C	-0.1111650	0.9059690	0.8935320
C	-1.0456060	0.0231310	1.6172030
C	-2.2260900	0.5791390	2.1201480
C	-0.7823390	-1.3434400	1.7523840
C	-3.1485080	-0.2379600	2.7674660
C	-1.7115390	-2.1493330	2.4057230
C	-2.8930360	-1.6022150	2.9058780
C	1.6040430	2.5963710	0.6872670
C	2.6426910	2.0982550	-0.1078770
C	1.4682140	3.9694100	0.9222620
C	3.5302640	2.9995260	-0.6917100
C	2.3541890	4.8534790	0.3166480
C	3.3867840	4.3712860	-0.4906510
C	-0.4239970	0.9279950	-0.9215650
H	-0.2402990	-3.0511030	-1.5834450
H	-3.2371290	4.6077810	-0.8009260
H	-0.9889490	3.5512320	-0.8132960
H	-5.0715270	0.7482160	-1.1036930
H	-5.2722950	3.1801870	-0.9400860
H	0.6879390	-0.8561420	-1.4271680
H	-2.2000750	-4.5936080	-1.4764020
H	-4.4638990	-3.6531340	-1.0622230
H	-4.8173090	-1.2526290	-0.8382620
H	-2.4196640	1.6416850	1.9932590
H	0.1381840	-1.7620420	1.3553590
H	-4.0647110	0.1915910	3.1611570
H	-1.5066110	-3.2092850	2.5198340
H	-3.6139980	-2.2393190	3.4099270
H	2.7625700	1.0280820	-0.2404630
H	0.6735850	4.3218980	1.5733700
H	4.3411770	2.6147580	-1.3022440
H	2.2468780	5.9205430	0.4866100
H	4.0843580	5.0645980	-0.9502910
H	0.4146730	1.5657560	-1.2067900

**TS1c1**

P	3.6162160	-1.6656650	-0.3492700
F	3.5173540	-0.5767140	-1.5805060
F	4.5815810	-2.5991130	-1.2267870
F	4.8635390	-0.8534800	0.2649650
F	3.6257590	-2.7084370	0.8800010
F	2.5784670	-0.6911320	0.5036720

F	2.2932140	-2.4241260	-0.9711500	N	1.7674930	1.7758200	1.0815490
N	0.8666540	1.5265170	1.3452880	C	-2.3430800	0.7582610	-1.1185590
C	-3.7288660	2.1336780	-0.3476460	C	-1.4626740	-0.3558750	-1.2484830
C	-2.3734290	2.1174870	-0.4896470	C	-0.0843780	-0.1431620	-1.2803500
C	-1.7105800	0.9187960	-0.8740460	C	-1.9733690	-1.7003320	-1.2791440
C	-2.4433120	-0.2589440	-1.1188090	C	-3.3024530	-1.9231460	-1.1422900
C	0.3879260	-0.2623960	-1.4751350	C	0.7143920	1.2557640	0.7475580
C	0.1548930	0.6562510	0.8649090	C	-0.4585120	0.8415560	1.5400660
C	-0.5675120	-0.4627230	1.4983650	C	-1.2868830	1.8445670	2.0539000
C	-1.7626050	-0.1728750	2.1690900	C	-0.7609890	-0.5078700	1.7417640
C	-0.0886080	-1.7721290	1.4205860	C	-2.4332480	1.4963470	2.7617490
C	-2.4836010	-1.2019720	2.7627170	C	-1.9078170	-0.8440880	2.4570540
C	-0.8172350	-2.7936140	2.0307720	C	-2.7479040	0.1511870	2.9551580
C	-2.0110060	-2.5141860	2.6913070	C	2.8873780	2.2335150	0.3759710
C	1.5825160	2.5974670	0.7996270	C	3.8432680	1.3174150	-0.0773810
C	2.6628220	2.3594770	-0.0580100	C	3.0394660	3.6078690	0.1683630
C	1.2115980	3.8978300	1.1578670	C	4.9483310	1.8007520	-0.7734790
C	3.3534570	3.4518070	-0.5781830	C	4.1497300	4.0680870	-0.5331010
C	1.9060160	4.9742540	0.6163620	C	5.1047840	3.1671960	-1.0055350
C	2.9772380	4.7540890	-0.2514750	C	0.4558880	1.1531560	-1.0733140
C	-0.2597960	0.8756240	-0.9163370	C	-3.7526110	0.5100140	-0.9383570
C	-3.8849370	-0.2548580	-0.9435030	C	-4.2207550	-0.8335780	-0.9534830
C	-4.5165700	0.9563200	-0.5571680	C	-4.6880600	1.5507020	-0.7150120
C	-5.9192250	0.9920100	-0.3774220	C	-6.0252030	1.2768160	-0.5336880
C	-4.6912520	-1.4012920	-1.1251190	C	-6.4865750	-0.0546480	-0.5652950
C	-6.6808610	-0.1384530	-0.5651360	C	-5.5979060	-1.0872750	-0.7689940
C	-6.0564190	-1.3445320	-0.9398050	C	-1.7956610	2.0782710	-1.1842400
C	-1.7232990	-1.4077670	-1.5352390	C	-0.4476080	2.2784500	-1.2002560
C	-0.3483840	-1.4127310	-1.7325320	H	-1.2591650	-2.5139420	-1.3710580
H	-4.2400310	3.0512170	-0.0661550	H	0.5913610	-0.9869330	-1.3769170
H	-1.7799750	3.0123590	-0.3151240	H	-3.6985140	-2.9350140	-1.1478080
H	1.4621630	-0.2475710	-1.6359210	H	-1.0328710	2.8887040	1.8908130
H	-2.1195150	0.8525140	2.2196490	H	-0.1098120	-1.2799330	1.3416960
H	0.8425470	-1.9854070	0.9048900	H	-3.0795860	2.2733940	3.1582870
H	-3.4100940	-0.9799610	3.2834100	H	-2.1433980	-1.8915980	2.6167230
H	-0.4394990	-3.8102820	1.9861360	H	-3.6471030	-0.1210020	3.5000320
H	-2.5728720	-3.3171840	3.1593750	H	3.7123090	0.2564690	0.1131630
H	2.9642250	1.3406670	-0.2832890	H	2.2962940	4.2954140	0.5621290
H	0.3910500	4.0465360	1.8536010	H	5.6898630	1.0948310	-1.1343000
H	4.1957920	3.2730720	-1.2391890	H	4.2713880	5.1334370	-0.7039720
H	1.6176850	5.9867120	0.8821880	H	5.9722370	3.5309860	-1.5473570
H	3.5243400	5.5970230	-0.6620630	H	1.4961120	1.2918150	-1.3704960
H	0.2450410	1.8343540	-1.0515760	H	-4.3544640	2.5812960	-0.6676180
H	-6.3845770	1.9303410	-0.0863510	H	-6.7253540	2.0881180	-0.3609010
H	-4.2441920	-2.3478420	-1.4077310	H	-7.5423980	-0.2644870	-0.4232160
H	-7.7567020	-0.1049270	-0.4249170	H	-5.9447330	-2.1170700	-0.7869980
H	-6.6545750	-2.2390290	-1.0840050	H	-2.4584010	2.9351960	-1.2203750
H	-2.2646200	-2.3284740	-1.7285420	H	-0.0313760	3.2821560	-1.2272370
H	0.1609510	-2.3074340	-2.0724450				

**TSI<sub>c2</sub>**

P	2.4183200	-2.5739050	0.0357410
F	2.4733250	-1.9128680	-1.4639610
F	2.8009000	-4.0121080	-0.5600700
F	3.9708640	-2.1856060	0.2601180
F	2.3037320	-3.1611910	1.5301860
F	1.9861290	-1.0755710	0.6094610
F	0.8144980	-2.8752920	-0.1996560

**TSI<sub>c3</sub>**

P	-1.6383910	2.8077090	0.0591750
F	-1.5831430	1.9694410	-1.3507410
F	-1.7067110	4.1930220	-0.7440780
F	-3.2509050	2.6678610	0.0701490
F	-1.6547340	3.5634640	1.4775460
F	-1.5256200	1.3507520	0.8475500
F	0.0093370	2.8603330	0.0514390
N	-2.0442010	-1.5873120	1.1295350

C	1.9944220	-1.9902210	-1.3554890
C	1.8450520	-0.5948230	-1.0916780
C	0.5556490	-0.0853700	-0.9615270
C	-0.8992460	-1.2736130	0.8387420
C	0.3323110	-1.2512730	1.6507020
C	0.9328670	-2.4712760	1.9649990
C	0.9164000	-0.0401810	2.0369110
C	2.1389860	-2.4814260	2.6652080
C	2.1125550	-0.0647280	2.7453120
C	2.7289520	-1.2802660	3.0507040
C	-3.2214790	-1.6965960	0.3747480
C	-3.8787200	-0.5447490	-0.0685350
C	-3.7351900	-2.9715280	0.1163390
C	-5.0461510	-0.6887100	-0.8147480
C	-4.8996490	-3.0932380	-0.6351360
C	-5.5558710	-1.9538690	-1.1038900
C	-0.5873040	-0.9341220	-0.9446160
C	0.8435960	-2.8207550	-1.5082270
C	-0.4115760	-2.3143630	-1.3498910
C	4.3042400	-0.3528740	-1.0670970
C	3.0258820	0.2458620	-0.9387460
C	5.4683590	0.4310440	-0.9088800
C	5.3701890	1.7755230	-0.6235220
C	4.1008870	2.3683930	-0.4873990
C	2.9479810	1.6219390	-0.6396170
C	3.3000490	-2.5450200	-1.4848850
C	4.4022990	-1.7548690	-1.3465960
H	0.3843370	0.9718440	-0.7914090
H	0.4614430	-3.4003640	1.6563070
H	0.4360510	0.9004630	1.7806000
H	2.6136510	-3.4276970	2.9061620
H	2.5682470	0.8716750	3.0520720
H	3.6697190	-1.2887790	3.5931090
H	-3.4834220	0.4374000	0.1707970
H	-3.2222160	-3.8451650	0.5085160
H	-5.5544210	0.2034920	-1.1671110
H	-5.2999460	-4.0802750	-0.8463970
H	-6.4675960	-2.0537020	-1.6846300
H	-1.5372240	-0.4396880	-1.1584000
H	0.9922140	-3.8664210	-1.7643220
H	-1.2925310	-2.9410280	-1.4631380
H	6.4404150	-0.0443650	-1.0139400
H	6.2660580	2.3764760	-0.5019530
H	4.0203440	3.4266880	-0.2587440
H	1.9869770	2.1115560	-0.5189960
H	3.4007570	-3.6063860	-1.6931220
H	5.3954790	-2.1873830	-1.4456770

**Int2**

C	0.78190100	1.21675900	3.60066600
C	0.95024500	1.00448200	2.24040700
C	-0.14919500	0.99147600	1.37192400
C	-1.44162900	1.23463200	1.88637400
C	-1.59155800	1.43251200	3.27213800
C	-0.49936600	1.41876300	4.12177700
C	-2.59801300	1.29017700	0.98473100
C	-2.42518900	0.97839300	-0.39509800
C	-1.16445400	0.62908100	-0.89000100

C	-3.51445500	1.03059900	-1.30386900
H	-3.32174800	0.79705900	-2.34837600
C	-4.76424300	1.40506200	-0.86223700
C	-4.93512200	1.72245600	0.49517300
C	-3.88222000	1.66647600	1.40028200
H	1.64668000	1.21984000	4.25695800
H	1.94780300	0.84235300	1.84326500
H	-2.57689900	1.59328600	3.69478900
H	-0.64054300	1.57105900	5.18720200
H	-1.05559500	0.45834300	-1.95399800
H	-5.60125000	1.46575500	-1.54940700
H	-5.91509800	2.02872700	0.85073400
H	-4.07267700	1.94130100	2.43082500
C	1.01394400	-0.50581200	-0.30109100
N	0.55594200	-1.68902700	-0.29522200
C	2.47422800	-0.26239000	-0.38333800
C	2.98912700	0.86241800	-1.03495600
C	3.34648400	-1.20037900	0.18353700
C	4.36782800	1.04482100	-1.11590300
H	2.33340100	1.56597900	-1.54056100
C	4.72075900	-1.00211900	0.11785500
H	2.93102300	-2.07635700	0.67298700
C	5.23337800	0.12206500	-0.53251100
H	4.75935000	1.90328900	-1.65232400
H	5.39318300	-1.72641500	0.56784200
H	6.30744600	0.27161400	-0.59277100
C	-0.82326200	-1.90033900	-0.26484400
C	-1.51494100	-1.99538800	0.95447400
C	-1.51514800	-2.04478500	-1.48306800
C	-2.89598200	-2.13383500	0.94429100
H	-0.96111800	-1.91931100	1.88627400
C	-2.89565600	-2.22384600	-1.47473800
H	-0.95215500	-1.99795500	-2.41190400
C	-3.59142900	-2.23930300	-0.26772400
H	-3.43924200	-2.16560300	1.88452200
H	-3.42723400	-2.32585500	-2.41622400
H	-4.67142900	-2.35303300	-0.26278000
C	0.06396700	0.71768700	-0.09922900
H	0.57935500	1.57256100	-0.57469100
P	0.45137300	1.39471900	-4.00968000
F	0.23691900	2.31764700	-2.65093200
F	0.08461700	2.65744100	-4.92920600
F	2.01815100	1.78403100	-4.00560200
F	0.63743700	0.44206100	-5.28771000
F	0.77579300	0.11935200	-3.00569900
F	-1.14228600	0.98205200	-3.91973300

**TS2**

C	0.76403000	1.20046800	3.60385200
C	0.91617100	1.07465900	2.22956700
C	-0.19497300	0.99455400	1.38012000
C	-1.48690900	1.10149100	1.92742200
C	-1.62372200	1.19204900	3.32296700
C	-0.51682300	1.23273300	4.15642800
C	-2.66162800	1.19741300	1.03740700
C	-2.50776200	0.96446000	-0.34127400
C	-1.23772200	0.51659000	-0.89393700
C	-3.57594600	1.19099200	-1.22698600

H	-3.41131700	1.03410200	-2.29124400	C	-4.20919100	2.68762500	-1.30643300
C	-4.80337400	1.62051600	-0.75684600	C	-4.56025000	2.99586700	0.00764700
C	-4.97255700	1.82647900	0.61802300	C	-3.78918300	2.52509900	1.06669900
C	-3.91803600	1.62832100	1.49710000	H	0.47934600	-0.09599000	4.79736100
H	1.64083300	1.26087900	4.24106800	H	1.35372400	0.07751000	2.49326700
H	1.91683100	1.03350400	1.80947700	H	-3.34488900	1.30191300	3.44784100
H	-2.61237700	1.22841200	3.76741200	H	-1.89290100	0.50044400	5.26794600
H	-0.65079000	1.30230900	5.23156900	H	-0.72894300	0.80146100	-1.76968500
H	-1.12150500	0.71204400	-1.95330500	H	-4.80353800	3.06108700	-2.13471400
H	-5.62082300	1.80769200	-1.44572800	H	-5.42834600	3.61640700	0.20881500
H	-5.92905800	2.17015000	1.00088300	H	-4.05504100	2.80338700	2.08225300
H	-4.06926000	1.85135400	2.54711300	C	1.14740000	-0.04833500	-0.07414000
C	1.03047800	-0.40803700	-0.22101900	N	0.86199000	-1.31406100	-0.01132800
N	0.56391900	-1.58233600	-0.03993400	C	2.48255800	0.38747700	-0.45877900
C	2.47770900	-0.16655700	-0.35645000	C	2.98895900	1.62270200	-0.02860600
C	2.95920100	0.93458500	-1.07243200	C	3.24659400	-0.43425900	-1.30244300
C	3.37585500	-1.07437900	0.22128500	C	4.26181600	2.02130100	-0.41806600
C	4.33223100	1.12142400	-1.20916000	H	2.39968000	2.26087800	0.62524400
H	2.27654100	1.60788400	-1.58228000	C	4.50151300	-0.01238600	-1.71751800
C	4.74435600	-0.86935000	0.09951800	H	2.81782900	-1.36355200	-1.66534700
H	2.98550100	-1.92766500	0.76815800	C	5.01183400	1.20770600	-1.26901900
C	5.22385400	0.22941200	-0.61729100	H	4.66310500	2.96919300	-0.07384500
H	4.69925400	1.95752000	-1.79567600	H	5.07448600	-0.62551500	-2.40530000
H	5.43856500	-1.56754800	0.55731900	H	5.99560400	1.53317600	-1.59469500
H	6.29396400	0.38264400	-0.72203700	C	-0.41155600	-1.70180500	0.06992500
C	-0.78149300	-1.76853000	-0.10568800	C	-0.76881700	-2.80799900	0.87711400
C	-1.56286000	-2.18280800	0.99620900	C	-1.43188900	-0.96803000	-0.71745100
C	-1.40964900	-1.45141100	-1.35057100	C	-2.09279600	-3.12518200	1.02417500
C	-2.92124000	-2.31928200	0.82442500	H	0.01501400	-3.33915000	1.40576000
H	-1.08261400	-2.35012800	1.95483300	C	-2.83293500	-1.36605700	-0.45043000
C	-2.79222300	-1.76744300	-1.52449800	H	-1.24674000	-1.29915000	-1.76691100
H	-0.77027400	-1.37380100	-2.22609700	C	-3.14098600	-2.40572800	0.35758500
C	-3.54148700	-2.14690200	-0.44659200	H	-2.36583600	-3.94890400	1.67900200
H	-3.53767000	-2.59396200	1.67599700	H	-3.60941900	-0.82844400	-0.98803900
H	-3.23355000	-1.65452600	-2.51019900	H	-4.17100100	-2.71133100	0.50540100
H	-4.60488600	-2.33814200	-0.54837400	C	0.02321600	0.92401800	0.23426000
C	0.02310900	0.75965800	-0.11304400	H	0.34510900	1.94763300	0.01613900
H	0.47156300	1.64374400	-0.58598800	P	0.54294900	-0.65203900	-4.06541700
P	0.53512800	0.96541900	-4.10895700	F	0.94584900	0.57818400	-3.04987100
F	0.30057000	2.08154200	-2.91511500	F	0.43794700	0.38362600	-5.28882200
F	0.16718300	2.06123800	-5.21986300	F	2.10793400	-0.92406900	-4.35181400
F	2.09874500	1.35856200	-4.15180200	F	0.10731400	-1.88166000	-5.00683200
F	0.73990300	-0.17802800	-5.21789700	F	0.61136600	-1.67429000	-2.76832900
F	0.85544200	-0.13963200	-2.91428800	F	-1.04377600	-0.38007200	-3.68471800
F	-1.05721100	0.55023900	-3.96998000				

### Int3

C	-0.16576600	0.26132000	4.00055300
C	0.32568900	0.36658300	2.70226000
C	-0.48874000	0.81994600	1.66270600
C	-1.81920600	1.19625100	1.93003300
C	-2.30760300	1.06068100	3.23585400
C	-1.49194600	0.59984500	4.26373200
C	-2.66215600	1.72810100	0.83181000
C	-2.30814500	1.43596800	-0.49431700
C	-1.09681900	0.58238200	-0.76884800
C	-3.07818200	1.91260000	-1.55460800
H	-2.78103500	1.67221300	-2.57345700

### TS3

C	-0.04666000	0.44729500	3.96419400
C	0.42592500	0.48425400	2.65371300
C	-0.38607700	0.93879800	1.61448100
C	-1.69887300	1.36997000	1.88836800
C	-2.16706900	1.30613200	3.20600500
C	-1.34983300	0.85470000	4.23791600
C	-2.55104900	1.86395800	0.77866200
C	-2.23830200	1.49115500	-0.54002700
C	-1.03402900	0.61636900	-0.78996900
C	-3.03738800	1.91368500	-1.60173600
H	-2.77919700	1.60622500	-2.61230700
C	-4.15057800	2.71881700	-1.36622900

C	-4.45507100	3.11252600	-0.06415600
C	-3.65870500	2.69205300	0.99744000
H	0.59673800	0.08924400	4.76207300
H	1.43734300	0.14487100	2.44040600
H	-3.19107100	1.59217800	3.42672300
H	-1.73538400	0.81166300	5.25210600
H	-0.68563600	0.77978600	-1.81272800
H	-4.76694000	3.04773100	-2.19731700
H	-5.30792600	3.75736900	0.12584600
H	-3.89072600	3.03214100	2.00236500
C	1.26374600	0.05612900	-0.09828900
N	1.07984800	-1.21708800	-0.21562000
C	2.63074500	0.58425200	-0.24439000
C	3.00379600	1.79637300	0.35181200
C	3.57311400	-0.14509800	-0.98377700
C	4.30795700	2.26505200	0.22468200
H	2.28472700	2.36470600	0.93700800
C	4.86770500	0.33802200	-1.12647400
H	3.26346900	-1.07338800	-1.45343900
C	5.23788600	1.53982100	-0.51932600
H	4.59618500	3.19743800	0.70016900
H	5.58950100	-0.21859000	-1.71608300
H	6.25142400	1.91379300	-0.63098700
C	-0.21728200	-1.68544100	-0.14927000
C	-0.43893800	-2.99899300	0.27953000
C	-1.32730000	-0.88432200	-0.59791800
C	-1.73415900	-3.48232300	0.38129700
H	0.41920900	-3.60498100	0.54973100
C	-2.65140500	-1.40027400	-0.39120300
H	-1.33103400	-1.42651500	-1.76262900
C	-2.84824800	-2.69032700	0.04900600
H	-1.89213800	-4.50098100	0.72453800
H	-3.49094700	-0.77402400	-0.68238000
H	-3.85146000	-3.09171800	0.13867500
C	0.10064500	0.99608700	0.17365100
H	0.39899100	2.02247300	-0.06868800
P	-0.51039500	-1.21357300	-4.23680600
F	0.53401500	-0.72819600	-3.07946400
F	0.24537600	-0.37945200	-5.36283800
F	0.36956800	-2.52970100	-4.47444500
F	-1.63841400	-1.74475600	-5.23934300
F	-1.33480600	-2.07503800	-2.96768500
F	-1.45968000	0.05428900	-3.84127400

### 3aa·HPF<sub>6</sub>

P	4.0281980	-0.8929340	0.2887020
F	5.2187750	-1.7847610	-0.3082550
F	4.8225650	-0.5886660	1.6434950
F	3.3291270	-2.2095260	0.9326370
F	2.7409120	0.0014170	0.8105350
F	4.6269980	0.4347840	-0.4234520
F	3.1333650	-1.1780010	-1.1106490
N	0.5198450	-0.3762360	-0.8094100
C	-1.1197860	0.7912570	3.3419150
C	-0.7773520	0.9358890	1.9981530
C	-1.7506270	0.8198870	1.0065670
C	-3.0866400	0.5455180	1.3545130
C	-3.4106940	0.3933330	2.7062210

C	-2.4386840	0.5214350	3.6945500
C	-4.1009360	0.3900780	0.2839700
C	-3.6764460	0.0505040	-1.0125000
C	-2.1984260	-0.1077800	-1.2770640
C	-4.6106010	-0.1380390	-2.0289950
C	-5.9727330	0.0138820	-1.7776780
C	-6.3991480	0.3732010	-0.5004420
C	-5.4699260	0.5636760	0.5183070
C	0.0445640	0.8326420	-0.7390550
C	0.9217510	1.9938940	-0.8537910
C	0.4866470	3.2330370	-0.3497870
C	2.2068360	1.8852800	-1.4100720
C	1.3293120	4.3351280	-0.3896570
C	3.0426760	2.9924610	-1.4479220
C	2.6065950	4.2156050	-0.9401080
C	-0.2596240	-1.5583670	-0.7009820
C	-1.6393780	-1.4725780	-0.9150350
C	0.3807870	-2.7553230	-0.3934390
C	-2.3913290	-2.6362390	-0.8112330
C	-0.3941810	-3.9085470	-0.2950660
C	-1.7707700	-3.8494330	-0.5024110
C	-1.4334140	0.9638330	-0.4819700
H	-4.2657470	-0.4045860	-3.0258360
H	-0.3504730	0.8727270	4.1030700
H	0.2630700	1.1195850	1.7384140
H	-4.4277550	0.1394320	2.9894950
H	-2.7097870	0.3903960	4.7376450
H	-2.0168890	0.0615480	-2.3491340
H	-6.6934160	-0.1333110	-2.5761570
H	-7.4564570	0.5152180	-0.2982950
H	-5.8139470	0.8702160	1.5016050
H	-0.4925970	3.3281530	0.1103470
H	2.5716210	0.9443670	-1.8095790
H	0.9947470	5.2841780	0.0165920
H	4.0416180	2.8869180	-1.8569340
H	3.2663620	5.0777160	-0.9658280
H	1.4530300	-2.7728640	-0.2144830
H	-3.4663260	-2.5921710	-0.9628930
H	0.0832110	-4.8509920	-0.0480060
H	-2.3702770	-4.7506080	-0.4181080
H	-1.7686480	1.9443710	-0.8369540
H	1.5402710	-0.5252760	-0.8603650

### 4aa·HPF<sub>6</sub>

P	-4.4577730	-0.3649560	-0.1404380
F	-5.6101110	-0.2631460	0.9679310
F	-5.5088940	-0.5219140	-1.3383630
F	-4.4398880	1.2484130	-0.3120440
F	-3.1937700	-0.4655250	-1.2013730
F	-3.2975350	-0.2178500	1.0603960
F	-4.3824090	-1.9797050	0.0511260
N	-0.6769160	-0.5194940	0.2156750
C	2.9303680	3.4298570	-1.6539450
C	2.0332780	2.5099480	-1.1464460
C	2.4783820	1.3090040	-0.5525240
C	3.8652510	1.0378420	-0.5261510
C	4.7599860	1.9883000	-1.0543420
C	4.3061560	3.1730980	-1.6001390

C	4.3381490	-0.2226720	0.0453060
C	3.4182500	-1.2722710	0.2799350
C	2.0017820	-1.0583150	0.0040570
C	3.8665020	-2.4416540	0.9345740
C	5.1945080	-2.6044110	1.2768050
C	6.1157090	-1.5897660	0.9868030
C	5.6871140	-0.4148040	0.3981090
C	0.1607530	0.5064190	0.1444380
C	-0.4171970	1.8208660	0.4972100
C	0.2405000	2.6489380	1.4177300
C	-1.6560180	2.1944180	-0.0301010
C	-0.3446650	3.8484050	1.7999540
C	-2.2358420	3.4000840	0.3582960
C	-1.5808420	4.2265350	1.2671380
C	-0.3238220	-1.8271330	-0.0206380
C	1.0503180	-2.1356050	-0.1211990
C	-1.3288630	-2.8064860	-0.1261770
C	1.3854150	-3.4721670	-0.4590370
C	-0.9549320	-4.1013870	-0.4032990
C	0.4034520	-4.4268650	-0.6005910
C	1.5434180	0.2612230	-0.1285910
H	3.1502110	-3.1980570	1.2318960
H	2.5604080	4.3397960	-2.1157800
H	0.9733820	2.7098110	-1.2421780
H	5.8236250	1.7792320	-1.0675440
H	5.0132510	3.8873490	-2.0104600
H	5.5133950	-3.5030410	1.7952170
H	7.1600810	-1.7067930	1.2595380
H	6.4036210	0.3839060	0.2450830
H	1.1978770	2.3467330	1.8339580
H	-2.1720090	1.5539660	-0.7397360
H	0.1567950	4.4863060	2.5211990
H	-3.2072980	3.6695370	-0.0426690
H	-2.0367970	5.1628820	1.5746740
H	-2.3727150	-2.5237920	-0.0232790
H	2.4170190	-3.7285570	-0.6680330
H	-1.7175740	-4.8665090	-0.5052680
H	0.6781520	-5.4375950	-0.8855180
H	-1.6656080	-0.3352350	0.4636600

**6aa**

N	-0.5881130	2.4498540	0.1501930
C	0.7320060	2.6976080	-0.0247230
C	1.1313590	4.0577620	-0.1192610
C	2.4275050	4.3909410	-0.4214450
C	3.3729250	3.3703720	-0.6662990
C	3.0247810	2.0458410	-0.5334600
C	1.7094660	1.6596300	-0.1536160
C	1.2602590	0.3046990	0.0200570
C	2.1475040	-0.8406530	0.2043540
C	3.4696810	-0.6999120	0.6856580
C	4.3027450	-1.7893110	0.8495380
C	3.8354730	-3.0729000	0.5429750
C	2.5241710	-3.2458910	0.1454070
C	1.6439840	-2.1533330	-0.0044990
C	0.2212300	-2.3547230	-0.2693080
C	-0.3084150	-3.6124690	-0.5950860
C	-1.6755690	-3.7930750	-0.7264100

C	-2.5492620	-2.7321760	-0.5114890
C	-2.0740470	-1.4555020	-0.1985230
C	-2.9848420	-0.3280120	0.0394680
C	-4.3809770	-0.4991580	0.1348880
C	-5.2247650	0.5750290	0.3556330
C	-4.6985420	1.8661110	0.4888730
C	-3.3323610	2.0588120	0.4054270
C	-2.4624290	0.9748530	0.1879800
C	-1.0152470	1.2027850	0.1077740
C	-0.1275040	0.0774140	0.0177420
C	-0.6658730	-1.2540520	-0.1210050
H	0.3648270	4.8103970	0.0203350
H	2.7192790	5.4313490	-0.5098600
H	3.7554170	1.2886600	-0.7774490
H	3.8254120	0.2758800	0.9803280
H	5.3066450	-1.6490820	1.2336160
H	-3.6114300	-2.9076350	-0.6134880
H	4.3778310	3.6310000	-0.9788080
H	4.4834190	-3.9341140	0.6600060
H	2.1619130	-4.2525460	-0.0125490
H	0.3472300	-4.4573590	-0.7555610
H	-2.0684250	-4.7681660	-0.9911320
H	-4.8140870	-1.4868040	0.0500220
H	-6.2941910	0.4118570	0.4294440
H	-5.3578960	2.7090270	0.6622280
H	-2.8986860	3.0444310	0.5076210

**6as**

N	-0.2329370	2.2016110	0.1232890
C	-1.4667390	2.6230380	0.4881040
C	-1.6028740	3.9912120	0.8483720
C	-2.7900560	4.4750910	1.3368080
C	-3.8851970	3.5993440	1.5076300
C	-3.7950440	2.2810760	1.1234380
C	-2.6031410	1.7559990	0.5520830
C	-2.4120710	0.3965910	0.1254680
C	-3.4929260	-0.5317850	-0.1950860
C	-4.7992600	-0.0826260	-0.5027450
C	-5.8167460	-0.9615860	-0.8156860
C	-5.5614400	-2.3379430	-0.8417000
C	-4.2782360	-2.7978570	-0.6235150
C	-3.2128310	-1.9199400	-0.3291860
C	-1.8361840	-2.3988120	-0.2351020
C	-1.5066450	-3.7591760	-0.3375880
C	-0.1824630	-4.1633180	-0.3800620
C	0.8461120	-3.2357170	-0.2526160
C	0.5742770	-1.8742220	-0.0600350
C	1.6449310	-0.8809500	0.0602620
C	2.9982780	-1.2383650	0.4757750
C	3.2571850	-2.3634580	1.2957950
C	4.5287630	-2.6534340	1.7495820
C	5.6000520	-1.8191390	1.4047170
C	5.3659320	-0.6835540	0.6549380
C	4.0739680	-0.3555650	0.1923500
C	3.8031670	0.8856330	-0.5177660
C	4.8415380	1.6645180	-1.0689460
C	4.5839200	2.8604390	-1.7083270
C	3.2626540	3.3116010	-1.8209370

C	2.2255390	2.5671110	-1.2947340
C	2.4589110	1.3365450	-0.6338440
C	1.3698590	0.4535660	-0.2238120
C	-0.0162940	0.9100240	-0.0554720
C	-1.0861310	-0.0530790	-0.0073880
C	-0.7857280	-1.4507710	-0.1158580
H	-0.7239640	4.6179430	0.7576030
H	-2.8791850	5.5158330	1.6271570
H	-4.6295750	1.6239200	1.3196820
H	-4.9995910	0.9768700	-0.5451950
H	-6.8027590	-0.5822870	-1.0583690
H	1.8678160	-3.5757860	-0.3317880
H	2.4352160	-2.9839370	1.6219970
H	4.6888330	-3.5116570	2.3923470
H	6.6010640	-2.0390650	1.7581600
H	6.1906790	-0.0122110	0.4561420
H	5.8628720	1.3114110	-1.0132530
H	5.3989880	3.4366740	-2.1317250
H	3.0465710	4.2415690	-2.3349790
H	1.2134090	2.9219370	-1.3926090
H	-4.7990300	3.9624860	1.9641600
H	-6.3556570	-3.0386870	-1.0727230
H	-4.0911440	-3.8590410	-0.7119820
H	-2.2815100	-4.5088650	-0.4169460
H	0.0570440	-5.2113400	-0.5202140

**SI**

C	0.9582640	2.7123640	-0.0714530
C	1.4931870	4.0201650	-0.2288850
C	2.8148700	4.2115970	-0.5419890
C	3.6493230	3.0896840	-0.7431890
C	3.1677480	1.8144180	-0.5575870
C	1.8208990	1.5752050	-0.1623200
C	1.2570080	0.2660340	0.0412150
C	2.0743670	-0.9265240	0.2599350
C	3.3774170	-0.8561580	0.8055140
C	4.1425010	-1.9882990	1.0105140
C	3.6241820	-3.2474810	0.6851010
C	2.3263070	-3.3503510	0.2234050
C	1.5179500	-2.2111670	0.0269490
C	0.1028420	-2.3304960	-0.3083830
C	-0.4666300	-3.5446310	-0.7191470
C	-1.8325420	-3.6546330	-0.9214240
C	-2.6653780	-2.5670950	-0.6820800
C	-2.1464000	-1.3329640	-0.2784620
C	-3.0196300	-0.1906600	0.0180460
C	-4.4171190	-0.3400470	0.1266840
C	-5.2404920	0.7291920	0.4279450
C	-4.6813920	1.9929730	0.6435460
C	-3.3120030	2.1602640	0.5502280
C	-2.4549050	1.0875090	0.2323370
C	-1.0010160	1.2697780	0.1267240
C	-0.1465540	0.1163140	0.0361740
C	-0.7352600	-1.1927660	-0.1474770
C	-0.4253590	2.5237770	0.1197200
H	0.8239260	4.8677640	-0.1236890
H	3.2098290	5.2127650	-0.6717760
H	3.8180940	0.9782620	-0.7681270

H	3.7706430	0.1007120	1.1161800
H	5.1321810	-1.8993440	1.4441080
H	-3.7289310	-2.6857330	-0.8373300
H	4.6747100	3.2328070	-1.0652680
H	4.2177960	-4.1414880	0.8386440
H	1.9136870	-4.3358690	0.0536040
H	0.1611210	-4.4074550	-0.8965780
H	-2.2561200	-4.5937610	-1.2589700
H	-4.8663070	-1.3150840	-0.0053980
H	-6.3112500	0.5818340	0.5110140
H	-5.3138030	2.8364340	0.8961720
H	-2.8988460	3.1405540	0.7462770
H	-1.0398640	3.4115850	0.1912560

**S2**

C	-1.5709240	2.6522230	0.6180330
C	-1.7904240	3.9811730	1.0749840
H	-0.9574990	4.6762720	1.0574780
C	-3.0131700	4.3715970	1.5579960
H	-3.1660870	5.3841840	1.9135880
C	-4.0620860	3.4282750	1.6343780
C	-3.8888220	2.1460810	1.1667030
H	-4.6924090	1.4357290	1.2930640
C	-2.6564680	1.7192750	0.5952360
C	-2.4045250	0.3842380	0.1175630
C	-3.4603350	-0.5552290	-0.2568740
C	-4.7536400	-0.1167590	-0.6297000
H	-4.9630630	0.9415740	-0.6704020
C	-5.7436620	-1.0016920	-1.0090640
H	-6.7185600	-0.6275550	-1.3005980
C	-5.4734060	-2.3748290	-1.0441170
C	-4.1983530	-2.8232600	-0.7617350
C	-3.1630330	-1.9386030	-0.3914730
C	-1.7894550	-2.4041320	-0.2221520
C	-1.4536330	-3.7664920	-0.2475580
C	-0.1286460	-4.1681730	-0.2221630
C	0.8921930	-3.2310610	-0.1068540
H	1.9163990	-3.5706560	-0.1405760
C	0.6114650	-1.8626600	0.0128010
C	1.6793800	-0.8631110	0.0978860
C	3.0421190	-1.1711580	0.5249440
C	3.3280770	-2.2559430	1.3890480
H	2.5230760	-2.8910190	1.7285450
C	4.6020980	-2.4851160	1.8710830
H	4.7799820	-3.3140810	2.5468150
C	5.6511420	-1.6287390	1.5132090
H	6.6528100	-1.8015880	1.8899430
C	5.3912530	-0.5320760	0.7151060
H	6.1967830	0.1573580	0.4985190
C	4.0977410	-0.2680890	0.2193790
C	3.8045510	0.9195090	-0.5693570
C	4.8197160	1.6918280	-1.1702260
H	5.8540170	1.3918610	-1.0632870
C	4.5256370	2.8078260	-1.9291640
H	5.3252520	3.3782060	-2.3879830
C	3.1885230	3.1726340	-2.1348360
H	2.9444890	4.0172520	-2.7692370
C	2.1749190	2.4347340	-1.5555070

H	1.1489680	2.6945110	-1.7738280	H	-6.2447060	-3.0794170	-1.3336380
C	2.4484810	1.3092390	-0.7411580	H	-3.9903050	-3.8795840	-0.8637660
C	1.3819120	0.4523240	-0.2377570	H	-2.2261320	-4.5203810	-0.3107970
C	0.0064490	0.9146390	-0.0535890	H	0.1179350	-5.2211610	-0.2995580
C	-1.0664970	-0.0416390	-0.0197920	C	-0.2798860	2.2378710	0.2334950
C	-0.7501670	-1.4432760	-0.1004530	H	0.5147420	2.9702700	0.2698720
H	-5.0068300	3.7096480	2.0859520				

#### 4-6. Measurements of Photophysical Properties of **4aa**, **6aa**, **4as** and **6as**

UV/Vis absorption spectra of **4aa**, **6aa**, **4as**, **6as** in CH<sub>2</sub>Cl<sub>2</sub> were recorded on a SHIMADZU UV-3600 spectrophotometer with a resolution of 0.5 nm. Emission spectrum and fluorescence quantum yield of **4aa** in CH<sub>2</sub>Cl<sub>2</sub> was measured with a SHIMADZU RF-6000 spectro fluorophotometer with a resolution of 1.0 nm upon excitation at 284 nm. Emission spectrum and fluorescence quantum yield of **6aa** in CH<sub>2</sub>Cl<sub>2</sub> was measured with a SHIMADZU RF-6000 spectro fluorophotometer with a resolution of 1.0 nm upon excitation at 287 nm. Emission spectrum and fluorescence quantum yield of **4as** in CH<sub>2</sub>Cl<sub>2</sub> was measured with a SHIMADZU RF-6000 spectro fluorophotometer with a resolution of 1.0 nm upon excitation at 260 nm. Emission spectrum and fluorescence quantum yield of **6as** in CH<sub>2</sub>Cl<sub>2</sub> was measured with a SHIMADZU RF-6000 spectro fluorophotometer with a resolution of 1.0 nm upon excitation at 260 nm. Dilute solution in degassed spectral grade CH<sub>2</sub>Cl<sub>2</sub> in a 1 cm square quartz cell was used for measurements.

#### 4-7. References

- [1] (a) Xiao, L.; Lan, H.; Kido, J. *Chem. Lett.* **2007**, *36*, 802. (b) Li, Y.-J.; Sasabe, H.; Su, S.-J.; Tanaka, D.; Takeda, T.; Pu, Y.-J.; Kido, J. *Chem. Lett.* **2009**, *38*, 712. (c) Bazzini, C.; Brovelli, S.; Caronna, T.; Gambarotti, C.; Giannone, M.; Macchi, P.; Meinardi, F.; Mele, A.; Panzeri, W.; Recupero, F.; Sironi, A.; Tubino, R. *Eur. J. Org. Chem.* **2005**, *2005*, 1247. (d) Nakayama, K.; Hashimoto, Y.; Sasabe, H.; Pu, Y.-J.; Yokoyama, M.; Kido, J. *Jpn. J. Appl. Phys.* **2010**, *49*, 01AB11. (e) Hiroto, S. *Chem. Asian J.* **2019**, *14*, 2514.
- [2] (a) Wang, X.-Y.; Yao, X.; Narita, A.; Müllen, K. *Acc. Chem. Res.* **2019**, *52*, 2491. (b) Su, S.-J.; Caib, C.; Kido, J. *J. Mater. Chem.* **2012**, *22*, 3447. (c) Yokoyama, D.; Sasabe, H.; Furukawa, Y.; Adachi, C.; Kido, J. *Adv. Funct. Mater.* **2011**, *21*, 1375. (d) Terrones, H.; Terrones, R. Lv, M.; Dresselhaus, M. S. *Rep. Prog. Phys.* **2012**, *75*, 062501. (e) Data, P.; Okazaki, M.; Takeda, Y.; Minakata, S. *J. Mater. Chem. C* **2019**, *7*, 6616. (f) Wu, Y.; Yin, Z.; Xiao, J.; Liu, Y.; Wei, F.; Tan, K. J.; Kloc, C.; Huang, L.; Yan, Q.; Hu, F.; Zhang, H.; Zhang, Q. *ACS Appl. Mater. Interfaces* **2012**, *44*, 1883. (g) Stępień, M.; Gońka, E.; Żyła, M.; Sprutta, N. *Chem. Rev.* **2017**, *117*, 3479.
- [3] (a) Durr, R. A.; Haberer, D.; Lee, Y.-L.; Blackwell, R.; Kalayjian, A. M.; Marangoni, T.; Ihm, J.; Louie, S. G.; Fischer, F. R. *J. Am. Chem. Soc.* **2018**, *140*, 807. (b) Sarau, G.; Heilmann, M.; Bashouti, M.; Latzel, M.; Tessarek, C.; Christiansen, S. *ACS Appl. Mater. Interfaces* **2017**, *9*, 10003. (c) Bronner, C.; Stremlau, S.; Gille, M.; Brauße, F.; Haase, A.; Hecht, S.; Tegeder, P. *Angew. Chem., Int. Ed.* **2013**, *52*, 4422. (d) Oki, K.; Takase, M.; Mori, S.; Shiotari, A.; Sugimoto, Y.; Ohara, K.; Okujima,



- T.; Uno, H. *J. Am. Chem. Soc.* **2018**, *140*, 10430. (e) Uno, H.; Ishiwata, M.; Muramatsu, K.; Takase, M.; Mori, S.; Okujima, T. *Bull. Chem. Soc. Jpn.* **2019**, *92*, 1001. (f) Yokoi, H.; Hiraoka, Y.; Hiroto, S.; Sakamaki, D.; Seki, S.; Shinokubo, H. *Nature Commun.* **2015**, *6*, 8215. (g) Yokoi, H.; Hiroto, S.; Shinokubo, H. *J. Am. Chem. Soc.* **2018**, *140*, 4649.
- [4] Jeong, E.-J.; Kim, Y.-K.; Park, J.-H.; Lee, E.-Y.; Hwang, S.-H. Condensed Cyclic Compounds and Organic Light-emitting Devices Including the Same. U. S. Patent US 2015/0349275 A1. 2015-12-03.
- [5] Selected recent reviews: (a) Hill, M. D. *Chem. Eur. J.* **2010**, *16*, 12052. (b) Varela, J. A.; Saa, C. *Chem. Rev.* **2003**, *103*, 3787. (c) Zhylitskaya, H.; Stepień, M. *Org. Chem. Front.* **2018**, *5*, 2395.
- [6] Selected recent examples for stepwise synthesis of N-PACs: (a) Vuong, H.; Dash, B. P.; Lill, S. O. N.; Klumpp, D. A. *Org. Lett.* **2018**, *20*, 1849. (b) Kouznetsov, V. V. *Tetrahedron* **2009**, *65*, 2721. (c) Pomeranz, C. *Monatsh* **1893**, *14*, 116. (d) Fritsch, P. *Ber.* **1893**, *26*, 419. (e) Marco-Contelles, J.; Pérez-Mayoral, E.; Samadi, A.; Carreiras, M. d. C.; Soriano, E. *Chem. Rev.* **2009**, *109*, 2652. (f) Colak, B.; Büyükkoyuncu, A.; Baycan, Koyuncu, F. B.; Koyuncu, S. *Polymer* **2017**, *123*, 366. (g) Hernandez-Perez, A. C.; Collins, S. K. *Angew. Chem., Int. Ed.* **2013**, *52*, 12696. (h) Wagaw, S.; Yang, B. H.; Buchwald, S. L. *J. Am. Chem. Soc.* **1999**, *121*, 10251. (i) Yum, E. K.; Refvik, M. D.; Larock, R. C. *J. Org. Chem.* **1998**, *63*, 7652. (j) Yum, E. K.; Larock, R. C. *J. Am. Chem. Soc.* **1991**, *113*, 6689. (k) Liu, X.; Wu, C.; Zhang, J.; Shi, Y.; Zhang, S.; Geng, Y.; Tunga, C.-H.; Wang, W. *Org. Chem. Front.* **2018**, *5*, 2997. (l) Leir, C. M. *J. Org. Chem.* **1977**, *42*, 911. (m) Hill, M. D.; Movassagh, M. *Org. Lett.* **2008**, *10*, 3485. (n) Jiang, T.-S.; Zhou, Y.; Dai, L.; Liu, X.; Zhang, X. *Tetrahedron Lett.* **2019**, *60*, 2078. (o) Blanchot, M.; Candito, D. A.; Larnaud, F.; Lautens, M. *Org. Lett.* **2011**, *13*, 1486. (p) Saha, M.; Bao, Y.-H.; Zhou, C. *Chem. Lett.* **2018**, *47*, 1383. (q) Wang, M.; Fan, Q.; Jiang, X. *Org. Lett.* **2018**, *20*, 216. (r) Uredi, D.; Motati, D. R.; Watkins, E. B. *Org. Lett.* **2018**, *20*, 6336. (s) Hewlins, M. J. E.; Salter, R. *Synthesis* **2007**, *14*, 2164. (t) Tobisu, M.; Koh, K.; Furukawa, T.; Chatani, N. *Angew. Chem., Int. Ed.* **2012**, *124*, 11525. (u) Tasiór, M.; Chotkowski, M.; Gryko, D. T. *Org. Lett.* **2015**, *17*, 6106. (v) Mishra, S.; Krzeszewski, M.; Pignedoli, C. A.; Ruffieux, P.; Fasel, R.; Gryko, D. T. *Nature Commun.* **2018**, *9*, 1714. (w) Navakouski, M.; Zhylitskaya, H.; Chmielewski, P. J.; Lis, T.; Cybińska, J.; Stepień, M. *Angew. Chem., Int. Ed.* **2019**, *58*, 4929. (x) Żyła-Karwowska, M.; Zhylitskaya, H.; Cybińska, J.; Lis, T.; Chmielewski, P. J.; Stepień, M. *Angew. Chem., Int. Ed.* **2016**, *55*, 14658. (y) Żyła, M.; Gońka, E.; Chmielewski, P. J.; Cybińska, J.; Stepień, M. *Chem. Sci.* **2016**, *7*, 286.
- [7] For reviews on APEX reactions, see: (a) Ito, H.; Ozaki, K.; Itami, K. *Angew. Chem., Int. Ed.* **2017**, *56*, 11144. (b) Ito, H.; Segawa, Y.; Murakami, K.; Itami, K. *J. Am. Chem. Soc.* **2019**, *141*, 3.
- [8] For contributions of Itami and Ito to APEX chemistry, see: (a) Ozaki, K.; Kawasumi, K.; Shibata, M.; Ito, H.; Itami, K. *Nature Commun.* **2015**, *6*, 6251. (b) Shibata, M.; Ito, H.; Itami, K. *J. Am. Chem. Soc.* **2018**, *140*, 2196. (c) Yano, Y.; Ito, H.; Segawa, Y.; Itami, K. *Synlett* **2016**, *27*, 2081. (d) Kato,

- K.; Segawa, Y.; Itami, K. *Can. J. Chem.* **2017**, *95*, 329. (e) Ozaki, K.; Zhang, H.; Ito, H.; Lei, A.; Itami, K. *Chem. Sci.* **2013**, *4*, 3416. (f) Ozaki, K.; Matsuoka, W.; Ito, H.; Itami, K. *Org. Lett.* **2017**, *19*, 1930. (g) Ozaki, K.; Murai, K.; Matsuoka, W.; Kawasumi, K.; Ito, H.; Itami, K. *Angew. Chem., Int. Ed.* **2017**, *56*, 1361. (h) Matsuoka, W.; Ito, H.; Itami, K. *Angew. Chem., Int. Ed.* **2017**, *56*, 12224. (i) Kitano, H.; Matsuoka, W.; Ito, H.; Itami, K. *Chem. Sci.* **2018**, *9*, 7556. (j) Nakamuro, T.; Kumazawa, K.; Ito, H.; Itami, K. *Synlett* **2019**, *30*, 423.
- [9] Examples of one-pot construction of nitrogen-containing aromatics using alkenes, alkynes, or unfunctionalized arenes: (a) Hiruta, K.; Kitahara, K.; Nishi, H.; Tokita, S. *Synthesis* **1982**, *1982*, 229. (b) Aksenov, A. V.; Aksenov, N. A.; Lyakhovnenko, A. S.; Aksenova, I. V. *Synthesis* **2009**, No.20, 3439. (c) Maiti, S.; Achar, T. K.; Mal, P. *Org. Lett.* **2017**, *19*, 2006. (d) Wu, X.-L.; Dong, L. *Org. Lett.* **2018**, *20*, 6990. (e) Obata, A.; Sasagawa, A.; Yamazaki, K.; Ano, Y.; Chatani, N. *Chem. Sci.* **2019**, *10*, 3242. (f) Ji, X.; Huang, H.; Li, Y.; Chen, H.; Jiang, H. *Angew. Chem., Int. Ed.* **2012**, *124*, 7404. (g) Krainova, G. F.; Chudinova, Y. O.; Gorbunov, A. A.; Mayorova, O. A.; Glushkov, V. A. *Mendeleev Commun.* **2012**, *22*, 201. (h) Schendera, E.; Unkel, L.-N.; Quyen, P. P. H.; Salkewitz, G.; Hoffmann, F.; Villinger, A.; Brasholz, M. *Chem. Eur. J.* **2020**, *26*, 269. (i) Tokimaru, Y.; Ito, S.; Nozaki, K. *Angew. Chem., Int. Ed.* **2018**, *57*, 9818. (j) Tokimaru, Y.; Ito, S.; Nozaki, K. *Angew. Chem., Int. Ed.* **2017**, *56*, 15560.
- [10] Tsuchida, N.; Yamazaki, S.; Yamabe, S. *J. Org. Chem.* **2005**, *70*, 10638.
- [11] Darbeau, R. W.; Pease, R. S.; Perez, E. V.; Gibble, R. E.; Ayo, F. A.; Sweeney, A. W. *J. Chem. Soc. Perkin Trans. 2* **2002**, 2146.
- [12] (a) Wang, Y.; Chen, C.; Peng, J.; Li, M. *Angew. Chem., Int. Ed.* **2013**, *52*, 5323. (b) Sheng, J.; Wang, Y.; Su, X.; He, R.; Chen, C. *Angew. Chem., Int. Ed.* **2017**, *56*, 4824. (c) Su, X.; Chen, C.; Wang, Y.; Chen, J.; Louac, Z.; Li, M. *Chem. Commun.* **2013**, *49*, 6752.
- [13] (a) Kawahara, K. P. (2018). 含窒素多環芳香族化合物の一段階構築反応の開発 (Development of the One-step Reaction for Synthesis of Nitrogen-containing Polycyclic Aromatic Compounds) (unpublished bachelor dissertation). Nagoya University, Japan. (b) Kawahara, K. P. (2020). Development of Aza-APEX Reaction toward Efficient Synthesis of Nitrogen-containing Polycyclic Aromatic Compounds (unpublished master thesis). Nagoya University, Japan.
- [14] Dijk, T. v.; Burck, S.; Rong, M. K.; Rosenthal, A. J.; Nieger, M.; Slootweg, J. C.; Lammertsma, K. *Angew. Chem., Int. Ed.* **2014**, *53*, 9068.
- [15] E.-J. Jeong, Y.-K. Kim, J.-H. Park, E.-Y. Lee, S.-H. Hwang, CONDENSED CYCLIC COMPOUNDS AND ORGANIC LIGHT-EMITTING DEVICES INCLUDING THE SAME. US 2015/0349275 A1, Dec. 3, 2015.
- [16] (a) Grzybowski, M.; Skonieczny, K.; Butenschön, H.; Gryko, D. T. *Angew. Chem., Int. Ed.* **2013**, *52*, 9900. (b) Avlasevich, Y.; Kohl, C.; Müllen, K. *J. Mater. Chem.* **2006**, *16*, 1053.
- [17] Examples of radical anion coupling reactions: (a) Piechowska, J.; Gałęzowski, M.; Gryko, D. T. *J.*

- Org. Chem.* **2010**, *75*, 1297. (b) Rickhaus, M.; Belanger, A. P.; Wegner, H. A.; Scott, L. T. *J. Org. Chem.* **2010**, *75*, 7358. (c) Schlichting, P.; Rohr, U.; Müllen, K. *J. Mater. Chem.* **1998**, *8*, 2651. (d) Solodovnikov, S. P.; Ioffe, S. T.; Zaks, Yu. B.; Kabacnik, M. I. *Russ. Chem. Bull.* **1968**, *17*, 442.
- [18] The commonly known range of interplanar distances by  $\pi$ - $\pi$  stacking is 3.3–3.8 Å according to a reference: Janiak, C. *J. Chem. Soc., Dalton Trans.* **2000**, 3885.
- [19] Alecu, I. M.; Zheng, J.; Zhao, Y.; Truhlar, D. G. *J. Chem. Theory Comput.* **2010**, *6*, 2872.
- [20] Gu, P.-Y.; Wang, Z.; Liu, G.; Yao, H.; Wang, Z.; Li, Y.; Zhu, J.; Li, S.; Zhang, Q. *Chem. Mater.* **2017**, *29*, 4172.
- [21] Schneider, T. L.; Halloran, K. T.; Hillner, J. A.; Conry, R. R.; Linton, B. R. *Chem. Eur. J.* **2013**, *19*, 15101.
- [22] Indu, S.; Subramanian, P.; Kaliappan, K. P. *Eur. J. Org. Chem.* **2014**, 7193.
- [23] David, E.; Pellet-Rostaing, S.; Lemaire, M. *Tetrahedron* **2007**, *63*, 8999.
- [24] Altomare, A.; Burla, M. C.; Camalli, M.; Cascarano, G. L.; Giacovazzo, C.; Guagliardi, A.; Moliterni, A. G. G.; Polidori, G.; Spagna, R. *J. Appl. Crystallogr.* **1999**, *32*, 115.
- [25] Sheldrick, G. M. *Acta Crystallogr. A.* **2008**, *64*, 112.
- [26] (a) Wakita, K. Yadokari-XG, Software for crystal structure analyses, 2001. (b) Kabuto, C.; Akine, S.; Nemoto, T.; Kwon, E. *J. Cryst. Soc. Jpn.* **2009**, *51*, 218.
- [27] Dolomanov, O. V.; Bourhis, L. J.; Gildea, R. J.; Howard, J. A. K.; Puschmann, H. OLEX2: a complete structure solution, refinement and analysis program. *J. Appl. Cryst.* **2009**, *42*, 229.
- [28] Zhao, Y.; Truhlar, D. G. *Theor. Chem. Acc.* **2008**, *120*, 215.
- [29] Levandowski, B. J.; Herath, D.; Gallup, N. M.; Houk, K. N. *J. Org. Chem.* **2018**, *83*, 2611.
- [30] Mennucci, B.; Cancès, E.; Tomasi, J. *J. Phys. Chem. B* **1997**, *101*, 10506.
- [31] Zhao, Y.; Truhlar, D. G. *Phys. Chem. Chem. Phys.* **2008**, *10*, 2813.
- [32] For calculation of Truhlar's quasi-harmonic corrections, an open free program GoodVibes v2.0.2 was used: J. Rodríguez-Guerra, J. Chen, IFunes, GoodVibes, v2.0.2, Pantan Lab, May 15, 2018. URL: <http://doi.org/10.5281/zenodo.1247565>.
- [33] (a) Becke, A. D. *J. Chem. Phys.* **1993**, *98*, 5648. (b) Lee, C.; Yang, W.; Parr, R. G. *Phys. Rev. B* **1988**, *37*, 785
- [34] GaussView, Version 6.1, R. Dennington, T. A. Keith, and J. M. Millam, Semichem Inc., Shawnee Mission, KS, 2016.
- [35] C. Y. Legault, CYLview, 1.0b, Université de Sherbrooke: Sherbrooke, QC, Canada, 2009: <http://www.cylview.org>.

## **Rapid Access to Polycyclic Thiopyrylium Compounds from Unfunctionalized Aromatics by Thia-APEX Reaction**

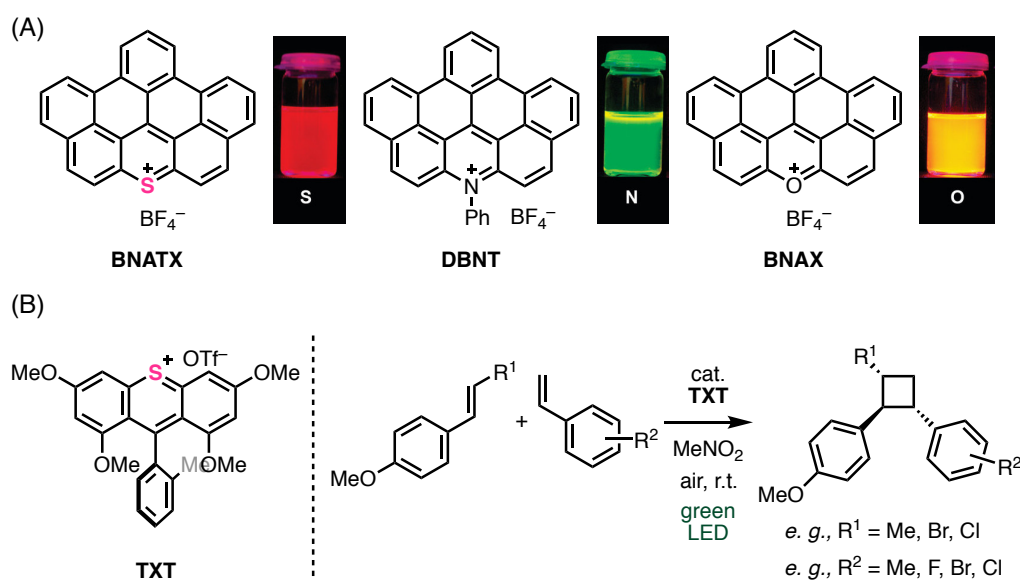
### **Abstract**

In this chapter, the development of a sulfur-embedding annulative  $\pi$ -extension (thia-APEX) reaction that can construct a sulfur-containing cationic hexagonal aromatic ring, thiopyrylium, onto unfunctionalized aromatic compounds in one step is described. The key to thia-APEX is the use of *S*-imidated *ortho*-arenoyl arenethiol derivatives as  $\pi$ -extending agents, and a variety of  $\pi$ -extended thiopyrylium compounds can be easily synthesized from unfunctionalized aromatics. Through measurement and analysis of the electronic and photophysical properties, the synthesized thiopyrylium compounds manifest diverse absorption and emission properties over the visible light to near-infrared region, depending on minor structural differences.

## 1. Introduction

### 1-1. $\pi$ -Extended thiopyrylium compounds

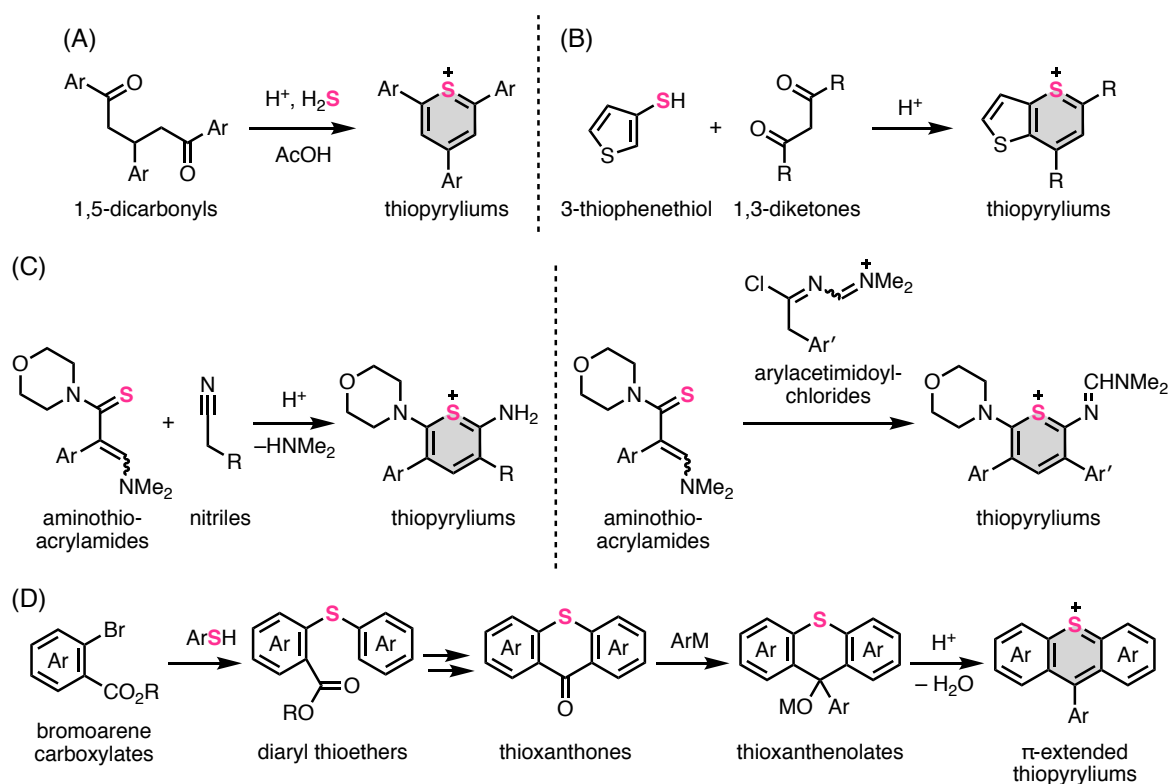
Thiopyrylium is a cationic organic skeleton which consists of sulfur-containing six-membered aromatic ring.<sup>[1]</sup> In recent years, polycyclic aromatic compounds containing thiopyrylium rings as well as other pyrylium rings<sup>[1h,1i]</sup> have gained attention and have been studied as candidate compounds for various functional materials because of their unique properties, such as long-wavelength absorption and emission, photoredox catalysis, and anion-sensing capability.<sup>[2]</sup> Figure 1 describes two representative examples of  $\pi$ -extended thiopyrylium compounds. In 2009, Feng and Müllen reported thiopyrylium salt **BNATX** (Figure 1A).<sup>[2c]</sup> **BNATX** emits red fluorescence in  $\text{CH}_2\text{Cl}_2$  by photoirradiation, whose emission properties are much different from those of the heteroatom-changed analogues **DBNT** (green fluorescence) and **BNAX** (yellow fluorescence). It means that thiopyrylium structure is favorable to longer wavelength absorption and emission. In 2020, Tanaka, Hoshino, and Honda reported thiopyrylium **TXT** which works as a photoredox catalyst (Figure 1B).<sup>[2h]</sup> Under aerobic and green light-irradiation conditions at room temperature, thiopyrylium **TXT** oxidatively activates  $\beta$ -substituted-(*E*)-styrene derivatives, which stereoselectively affords diarylcyclobutane derivatives through a formal [2+2] cycloaddition with another styrene derivatives. Different from similar photoredox reactions using transition metal complexes as a photoredox catalyst, the use of **TXT** is considered favorable to the [2+2] cycloaddition reaction using  $\beta$ -halogenated-(*E*)-styrene derivatives. As mentioned above,  $\pi$ -extended thiopyrylium compounds are recognized as useful heteroaromatics for various fields of science such as optoelectronics and organic reactions, which have increased high demands of novel  $\pi$ -extended thiopyrylium compounds having various structures and functions.



**Figure 1.** Representative  $\pi$ -extended thiopyrylium compounds.

## 1-2. Synthesis of thiopyrylium compounds

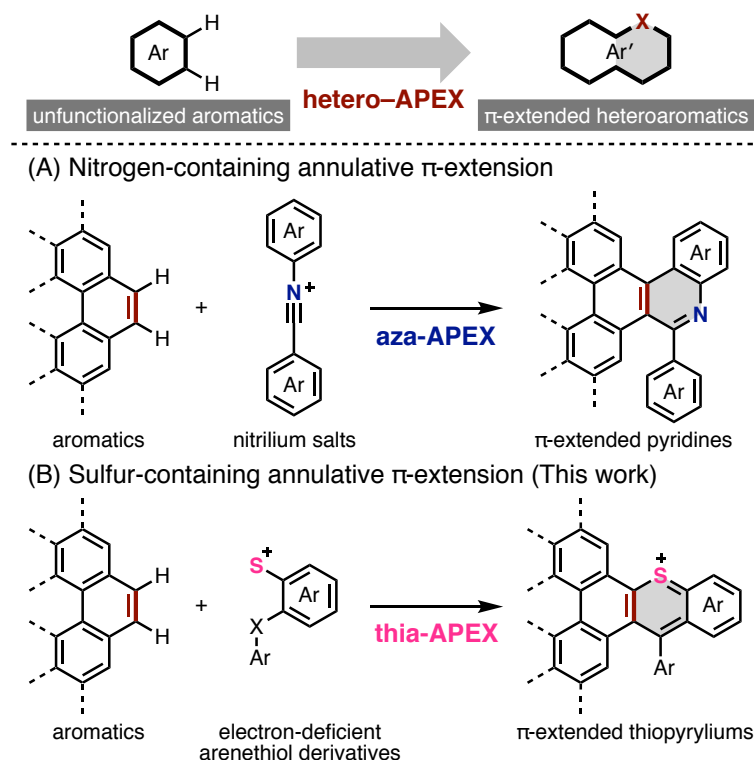
One of the classical methods for synthesizing thiopyryliums is the annulative condensation reaction of 1,5-dicarbonyls with  $\text{H}_2\text{S}$  and acetic acid in the form of Paal–Knorr synthesis (Figure 2A).<sup>[1c,3]</sup> Besides, thiopyrylium compounds can also be synthesized by reactions using arenethiols such as 3-thiophenethiol and 1,3-diketones with strong acids such as perchloric acid (Figure 2B). Moreover, aminothioacrylamide derivatives are chosen for thiopyrylium synthesis, which constructs a thiopyrylium structure by reacting with acid and nitriles or aryacetimidoylchlorides (Figure 2C).<sup>[4]</sup> These methods are useful for constructing small  $\pi$ -conjugation systems such as thiopyrylium and benzothiopyrylium compounds. On the other hand, largely  $\pi$ -extended thiopyrylium compounds are accessible through thioxanone/thioxanthenolate intermediates. In particular, after formation of thioxanone intermediates from bromoarene carboxylates and diaryl thioethers, 1,2-addition of arylmetal species ( $\text{ArM}$ ) toward thioxanones affords thioxanthenolates, after which Brønsted acid-mediated aromatization affords  $\pi$ -extended thiopyrylium compounds (Figure 2D).<sup>[1b,2d]</sup> Moreover, representative  $\pi$ -extended thiopyrylium compounds introduced in Figure 1 are synthesized via formation of similar diaryl thioether/thioxanthenolate/thioxanthenol intermediates.<sup>[2c,2h]</sup> These methods were chosen for synthesis of diverse small/large thiopyrylium compounds. However, each method requires prefunctionalization of the starting aromatics and multistep component-assembling reactions.



**Figure 2.** Conventional synthetic methods for small thiopyryliums and  $\pi$ -extended thiopyryliums.

### 1-3. This work

As part of our ongoing efforts to achieve streamlined and diversity-oriented synthesis of large  $\pi$ -conjugated systems, we have developed a series of one-step annulative  $\pi$ -extension reactions (APEX)<sup>[5]</sup> of polycyclic aromatic hydrocarbons (PAHs) and heteroaromatics. Region-selective APEX reactions allow access to unprecedented nanographenes that are difficult to synthesize using conventional coupling reactions.<sup>[6]</sup> In addition, we have developed the APEX reaction for constructing heteroaromatics (hetero-APEX reaction)<sup>[7]</sup> (Figure 3). For example, the nitrogen-embedding APEX (aza-APEX) reaction of unfunctionalized aromatics using highly electrophilic diaryl nitrilium salts rapidly constructed a new pyridine ring on unfunctionalized aromatics (Figure 3A).<sup>[7a]</sup> The author developed a novel sulfur-embedding APEX (thia-APEX) reaction that furnishes  $\pi$ -extended thiopyrylium compounds from unfunctionalized aromatics using electron-deficient arenethiol derivatives as  $\pi$ -extending agents (Figure 3B).



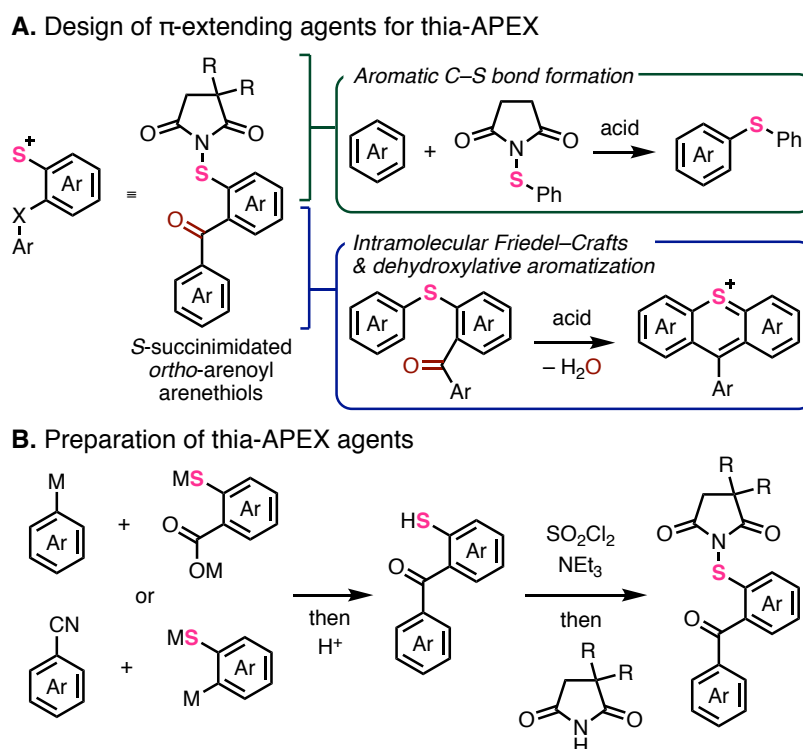
**Figure 3.** Heteroatom-embedding annulative  $\pi$ -extension (hetero-APEX) reactions: (A) Aza-APEX with nitrilium salts.<sup>[7a]</sup> (B) Thia-APEX with electron-deficient arenethiol derivatives.

## 2. Result and discussion

### 2-1. Preparation of sulfur-embedding $\pi$ -extending agent

To achieve the thia-APEX reaction, the author designed and adopted *S*-succinimidated *ortho*-arenoyl arenethiols as novel  $\pi$ -extending agents (Figure 4A). These thiols include two electrophilic reaction sites: the *S*-succinimide moiety for C–S bond formation and carbonyl group for C–C bond formation.

Succinimide groups act as leaving groups in the presence of Brønsted/Lewis acids to electrophilic sulfur atoms.<sup>[8]</sup> This electrophilic sulfur atom can form diaryl thioethers or benzothiophenes by reacting with other benzene derivatives or alkynes. We envisioned that an adjacent *ortho*-arenyl unit on the arenethiol would promote a sequence of C–S bond formation, intramolecular Friedel–Crafts addition, and dehydroxylative aromatization using acids.<sup>[9]</sup> With this concept, various new sulfur-embedding APEX agents were prepared utilizing the synthesis of benzophenonethiols from arylmetals and thiosalicylic acid or arylonitriles and arenethiols (Figure 4B, see Experimental Section for details).<sup>[10]</sup> Subsequently, the succinimide groups were introduced through *S*-chlorination reaction with SO<sub>2</sub>Cl<sub>2</sub> followed by reaction of succinimides with NEt<sub>3</sub>.<sup>[8b]</sup>



**Figure 4.** Design and preparation of sulfur-embedding  $\pi$ -extending agents for thia-APEX reaction. (A) Proposed reactivities of each unit. (B) Preparation methods for sulfur-embedding APEX agents that are described in this chapter.

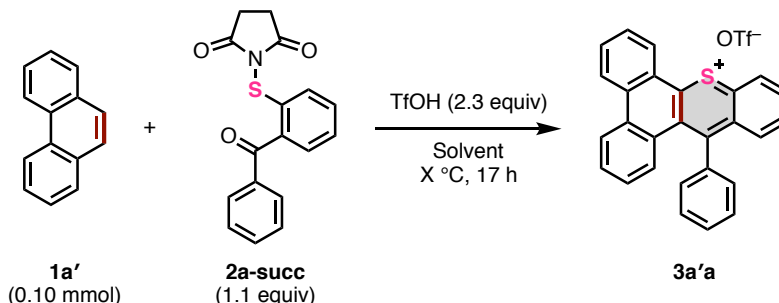
## 2-2. Optimization of thia-APEX reaction condition

The author optimized the conditions for the thia-APEX reaction of phenanthrene with the newly prepared sulfur-embedding APEX agents. First, the effect of solvents was examined (Table 1). Addition of even small volume of 1,1,1,3,3,3-hexafluoroisopropyl alcohol (HFIP) (0.10–0.50 mL) was found to promote thia-APEX reaction (entries 1 and 3). However, the reaction conditions using a large volume of HFIP (1.0 mL, 0.5 M of **1a'** to HFIP, entry 2) was adopted in terms of the efficiency on stirring and the reproducibility on product yields. Thia-APEX of **1a'** in other solvents afforded thiopyrylium compounds **3a'a** at room temperature but in lower yields (entries 5, 6 and 9). In addition, the use of 1,2-dichloroethane



as the solvent tended to decrease the product yields (entries 6–10). Although the maximum yields of thiopyrylium **3a'a** in a mixed solvent of 1,2-dichloroethane and HFIP were identical to that in HFIP (entries 2, 9 and 10), albeit in low reproducibility. The author decided to use the HFIP-only conditions because of the high reproducibility.

**Table 1.** Solvent effect in thia-APEX reaction.

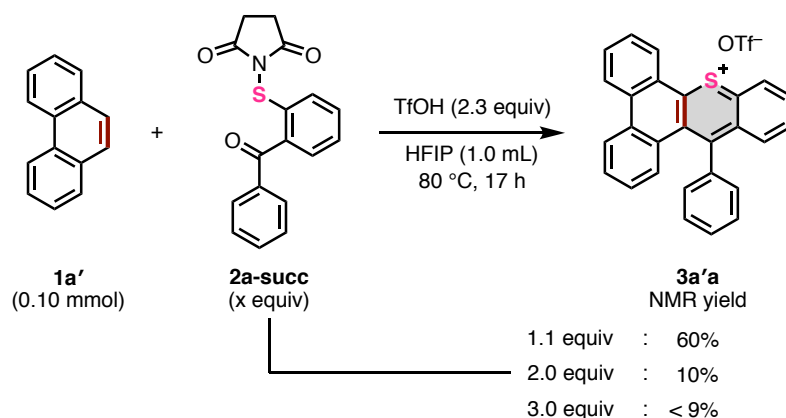


Entry	Solvent	Volume	Temp.	NMR yield <sup>a</sup>
1	HFIP	0.50 mL	80 °C	70%
2	HFIP	1.0 mL	80 °C	60%
3	HFIP	0.10 mL	80 °C	69%
4	none	–	80 °C	73%
5	HFIP	1.0 mL	r.t.	30%
6	ClCH <sub>2</sub> CH <sub>2</sub> Cl	1.0 mL	r.t.	20%
7	ClCH <sub>2</sub> CH <sub>2</sub> Cl	1.0 mL	100 °C	30%
8 <sup>b</sup>	ClCH <sub>2</sub> CH <sub>2</sub> Cl	1.0 mL	100 °C	0%
9	ClCH <sub>2</sub> CH <sub>2</sub> Cl/HFIP (1:1 v/v)	1.0 mL	r.t.	10–60%
10	ClCH <sub>2</sub> CH <sub>2</sub> Cl/HFIP (1:1 v/v)	1.0 mL	100 °C	26–60%

<sup>a</sup> Determined by <sup>1</sup>H NMR (internal standard: 0.10 mmol of CH<sub>2</sub>Br<sub>2</sub>).

<sup>b</sup> Sc(OTf)<sub>3</sub> (1.0 equiv) was used instead of TfOH.

When thia-APEX reactions of pristine phenanthrene (**1a'**) were conducted with 2.0 or 3.0 equiv of  $\pi$ -extending agent **2a-succ**, the yields of thiopyrylium salts dramatically decreased (Figure 5). In addition, when **2a-succ** (0.11 mmol, 1.0 equiv), TfOH (2.1 equiv), HFIP (1.0 mL), and excess amount of **1a'** (1.8 equiv) were used, thiopyrylium **3a'a** was formed in 73% NMR yield. Therefore, the use of excess amount of  $\pi$ -extending agent **2a-succ** was considered to be unsuitable for the thia-APEX probably due to the overreaction and/or the oligomerization caused by excess amount of **2a-succ**.

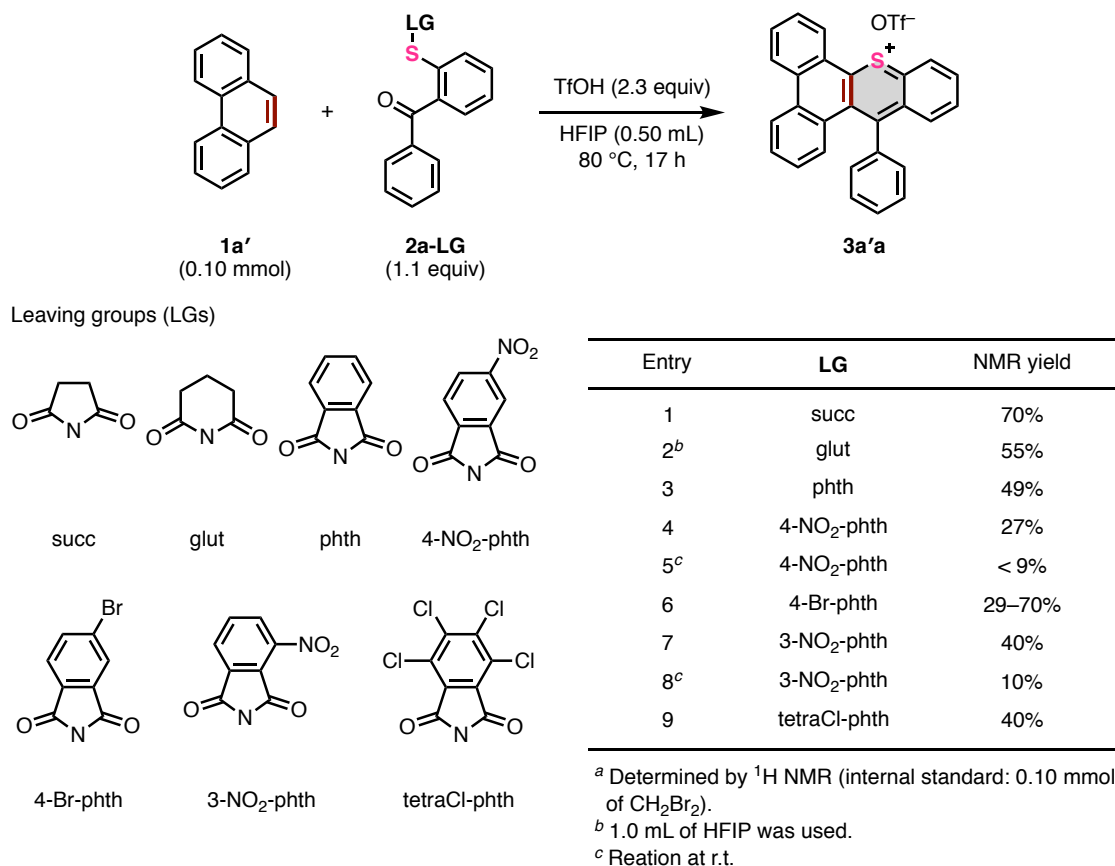


<sup>a</sup> Determined by <sup>1</sup>H NMR (internal standard: 0.10 mmol of CH<sub>2</sub>Br<sub>2</sub>).

<sup>b</sup> **1a'** (1.8 equiv), **2a-succ** (1.0 equiv), TfOH (2.1 equiv), HFIP (1.0 mL) → 73% NMR yield of **3a'a** formed.

**Figure 5.** Effect of amounts of **2a-succ** in thia-APEX reaction.

Besides, effects of succinimide-leaving groups attached on a sulfur atom were investigated (Figure 6). With **1a'** (0.10 mmol), TfOH (2.3 equiv), HFIP (0.5 mL), and **2a-succ** (1.1 equiv), thiopyrylium **3a'a** was formed in 70% NMR yield (entry 1). Using **2a-glut** containing glutarimide group instead of **2a-succ**, **3a'a** was formed in 55% NMR yield (entry 2). Furthermore, when using **2a-X-phth** (X = 4-NO<sub>2</sub>, 4-Br, 3-NO<sub>2</sub>, tetraCl), the yield of **3a'a** further decreased to 10–49% (entries 3–9). Although the use of **2a-4-Br-phth** afforded **3a'a** in 70% NMR yield as the most, this result could not be reproduced again and the yields were not constant (entry 6). As a result, the simple succinimide group (LG = succ) was considered to be most suitable in terms of both product yield and reproducibility (entry 1).



**Figure 6.** Effect of leaving groups in thia-APEX reaction. Each **2a-LG** was prepared according to a literature.<sup>[8a]</sup>

After screening the reaction parameters such as solvents, temperature, amounts of  $\pi$ -extending agents, and succinimide-moieties, the author found that the  $\pi$ -extending agent **2** (1.1 equiv) was efficiently activated by TfOH (2.3 equiv) in HFIP (0.2 M of aromatic substrate **1** to HFIP) to react with unfunctionalized aromatics **1** (Figure 7). After heating at 80 °C for 17 h, various fused thiopyrylium salts **3** were obtained. Because the obtained thiopyrylium salts were sensitive to excess amounts of water, working with water or purification by preparative thin-layer chromatography (PTLC) on silica gel resulted in the formation of thioxanthenol **3a'a-OH** (see Experimental Section for details). Therefore, the author chose a purification method involving precipitation, filtration, and washing with diethyl ether, followed by recrystallization to remove succinimides and other impurities, which allowed obtaining high-quality products. In some thia-APEX reactions, superior isolated yields were obtained using ethosuximide derivatives (**2-etho**) instead of succinimide derivatives (**2-succ**). This could be due to the higher solubility of **2-etho** than that of **2-succ**, which facilitated easy separation from the crude mixture by simple filtration and washing.

In the reactions of 1,2-dimethoxybenzene (**1a**) with *S*-succinimides having simple benzophenone structures (**2a-succ** and **2a-etho**) and phenyl substituents (**2b-succ**), thiopyrylium salts **3aa** and **3ab** were

obtained in 86–91% isolated yields. Thiopyrylium **3ba** and **3ca** were also obtained from 1,3-dimethoxybenzene (**1b**) and 1,4-dimethoxybenzene (**1c**) in 64–66% and 81% yields, respectively. The author considers that the electron-rich dimethoxy benzenes **1a–1b** possess comparably high reactivities, and the difference in yield is derived from the ease/difficulty of solidification of the products; thiopyrylium **3aa** and **3ca** are more easily solidified than **3ba**. Interestingly, no other regioisomers were obtained or isolated in the case of **3aa**, **3ab**, and **3ba**. 1,2,3,4-Tetramethylbenzene (**1d**) afforded thiopyrylium **3da** in a 67% yield. In addition, the use of ethosuximide **2a-etho** afforded thiopyrylium **3da** with better yield and reproducibility. The PAH-type substrates 2,7-di-*tert*-butylphenanthrene (**1e**), 2,7-di-*tert*-butylpyrene (**1f**), and pristine pyrene (**1g**) were used. From substrate **1e**, thiopyryliums **3ea–3ec** were obtained in 57–86% yields. The use of **2a-etho** increased the yield of thiopyrylium **3ea** from 58% (with **2a-succ**) to 75%. Thiopyrylium **3ec** was more difficult to solidify in crude oil, which seemed to cause a decrease in the yield. Substrate **1f** afforded not only the desired product **3fa** but also a small amount of double thia-APEX product that was not isolated, but detected by ESI-MS analysis. However, multiple recrystallizations of crude **3fa** afforded pure **3fa** in 59% yield. Interestingly, pyrene was regioselectively transformed into thiopyrylium **3ga** in up to 58% yield, whereas pyrene possessed multiple reaction sites. Furthermore, the reaction monitoring by <sup>1</sup>H NMR spectra indicates that the C–S bond formation proceeded at the C1 position on pyrene, which is a general reactive site for electrophilic aromatic substitutions, such as bromination and acylation.<sup>[11]</sup> However, when pristine phenanthrene was employed under the standard thia-APEX conditions, the first C–S bond formation seemed to proceed preferentially at the C9 position (*K*-region), but the reaction gave a complex mixture including regioisomeric mixtures which were difficult to be isolated (see Experimental Section for details).

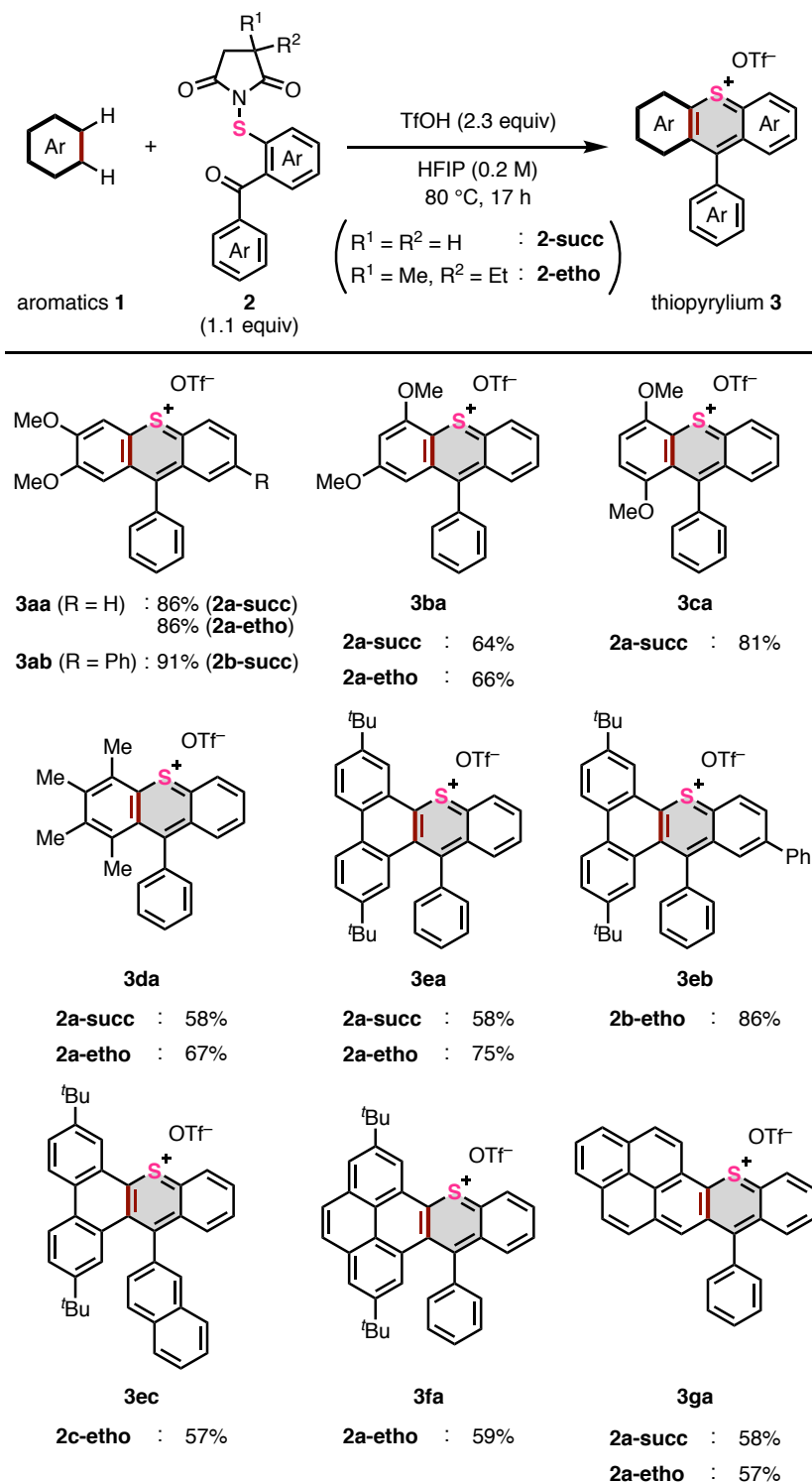
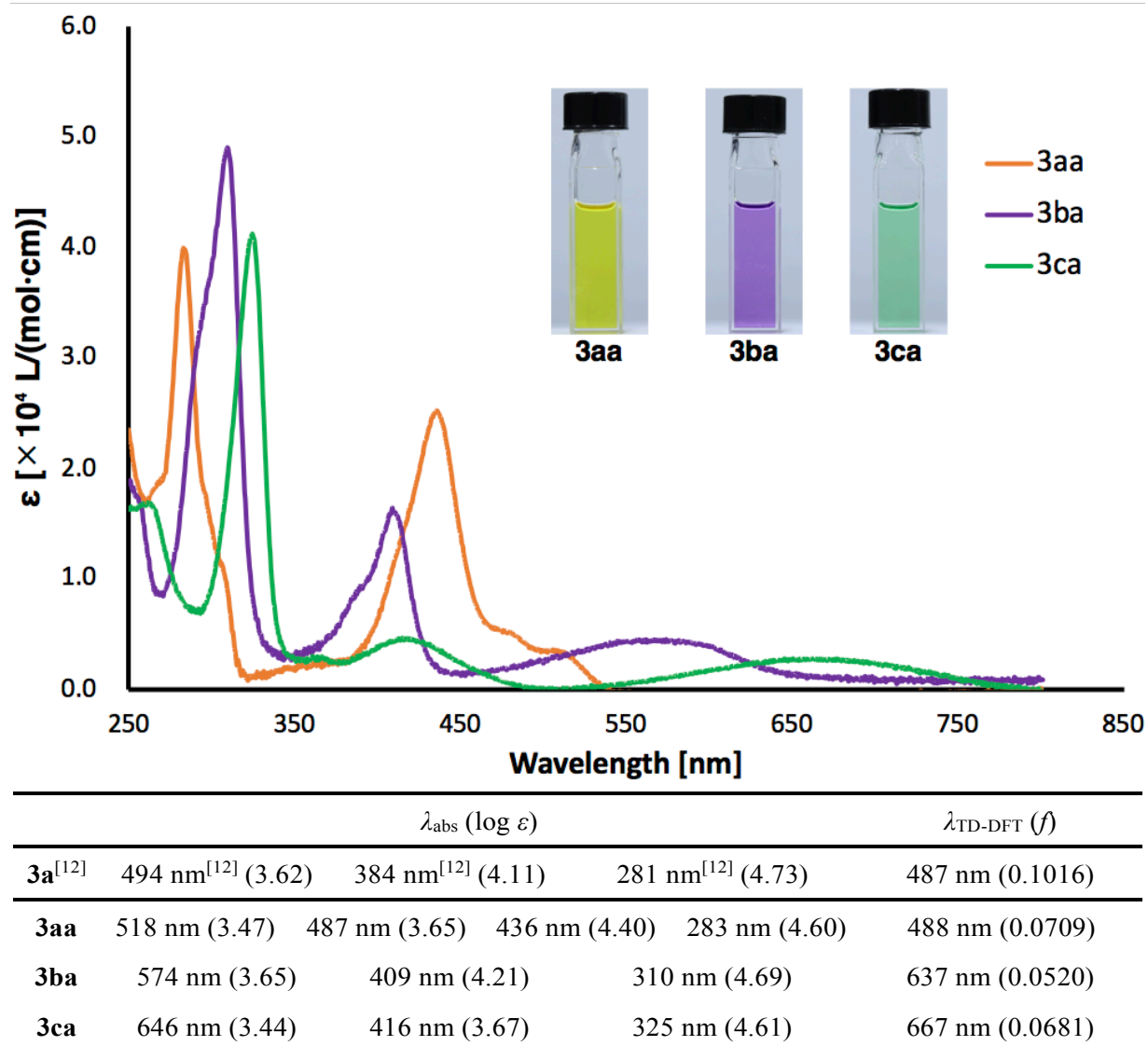


Figure 7. Optimized reaction conditions and substrate scope of thia-APEX reaction.

## 2-4. Absorption properties and DFT calculations

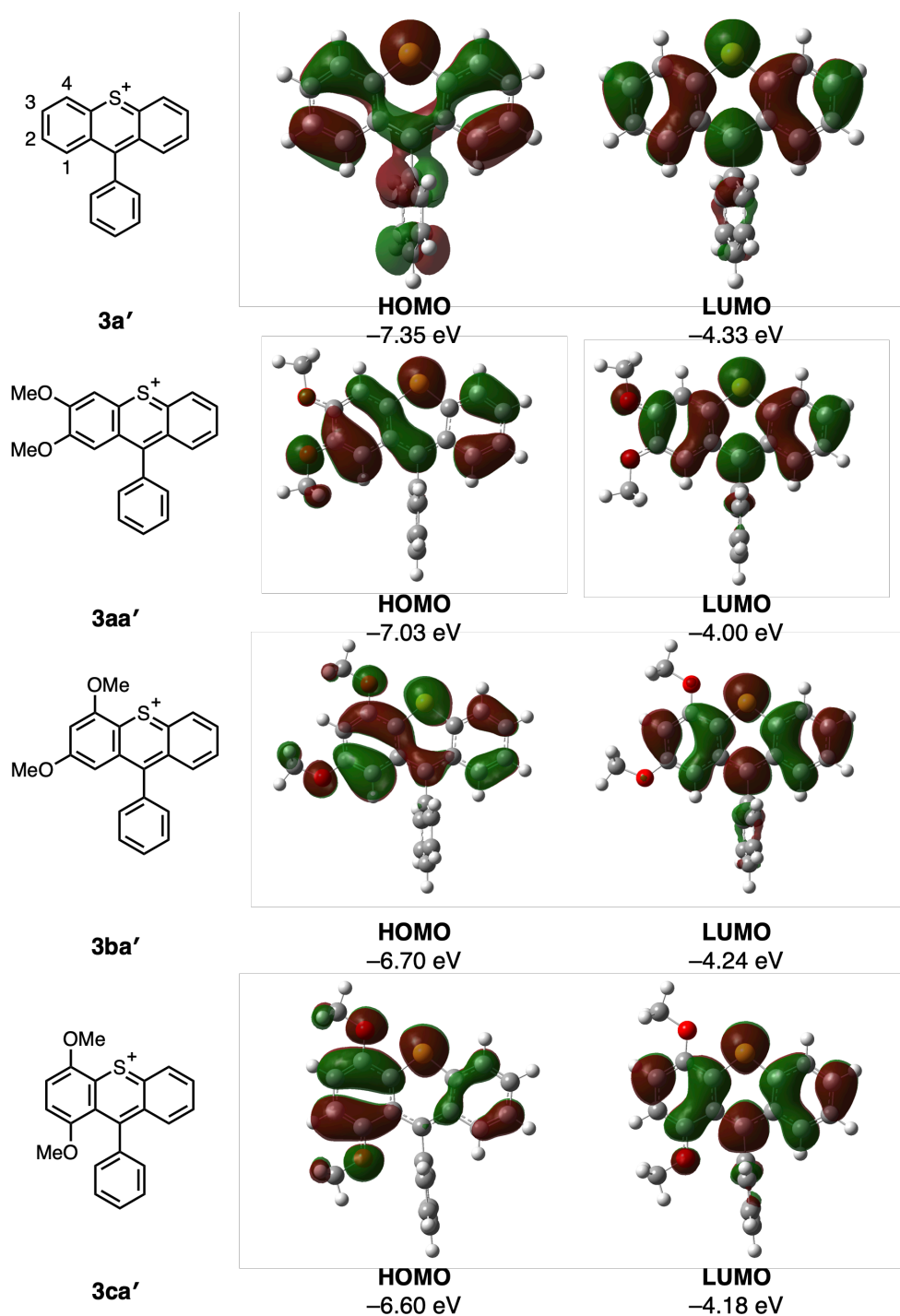
The synthesized  $\pi$ -extended thiopyrylium salts displayed diverse colors in CH<sub>2</sub>Cl<sub>2</sub>, indicating their interesting photophysical properties. Thus, the author first measured the UV-Vis-NIR absorption spectra of the  $\pi$ -extended thiopyrylium salts **3aa–3ca** (Figure 8). The reported spectroscopic data for 9-

phenylthioxanthylum triflate (**3a**)<sup>[12]</sup> are also described for comparison. The dimethoxy-substituted thiopyryliums **3aa–3ca** showed weak longest wavelength absorption maxima in the visible light region, and their wavelengths at each peak were dramatically red-shifted in the order **3aa** (518 nm,  $\log \epsilon = 3.47$ ) < **3ba** (574 nm,  $\log \epsilon = 3.65$ ) < **3ca** (646 nm,  $\log \epsilon = 3.44$ ). Interestingly, the subtle difference in substitution patterns dramatically altered the photophysical properties.



**Figure 8.** UV-Vis-NIR absorption spectra of  $\pi$ -extended thiopyryliums **3aa–3ca** in  $\text{CH}_2\text{Cl}_2$ , summary table of observed representative absorption peaks **3a**<sup>[12]</sup> and **3aa–3ca**, and estimated excitation wavelengths ( $\lambda_{\text{TD-DFT}}$ ) and oscillator strengths ( $f$ ) of corresponding cations **3a'** and **3aa'–3ca'** calculated via TD-DFT with the B3LYP/6-311++G(2d,p)//B3LYP/6-311+G(2d,p) level of theory. The concentrations of each compound: **3aa** =  $6.0 \times 10^{-6}$  M, **3ba** =  $4.6 \times 10^{-6}$  M, **3ca** =  $7.6 \times 10^{-6}$  M. The pictures were taken using the concentrated solutions of each compound. Absorption data of **3a** in MeCN at 298 K was referred from ref. [12], and the TD-DFT calculation of its cation **3a'** was performed at the same level of theory as other compounds.

According to the calculations of the corresponding cations **3a'** and **3aa'**–**3ca'** using time-dependent density functional theory (TD-DFT) with the B3LYP/6-311++G(2d,p)//B3LYP/6-311+G(2d,p) level of theory, the longest absorption peaks are attributed to the excitation from HOMO to LUMO, and the excitation wavelengths ( $\lambda_{\text{TD-DFT}}$ ) and oscillator strengths ( $f$ ) were calculated for **3aa'** (488 nm,  $f=0.0709$ ), **3ba'** (637 nm,  $f=0.0520$ ), and **3ca'** (667 nm,  $f=0.0681$ ), which correspond well to the observed spectra (Figures 8 and 9). Comparing the HOMO and LUMO orbitals in the ground state of **3aa'**–**3ca'** and **3a'**, HOMOs and LUMOs were mainly delocalized on a thioxanthylum core and electron push–pull structures from methoxy groups in **3aa'**–**3ca'** to thiopyrylium centers, resulting in large changes in HOMOs rather than LUMOs (Figure 9). In HOMOs, the 3-methoxy group in **3aa'** has less contribution to HOMOs, whereas the 1-methoxy, 2-methoxy, and 4-methoxy groups have larger contributions. As a result, slightly biased orbital localization was found in the dimethoxy-substituted benzene rings in the order of **3aa'** > **3ba'** > **3ca'** > **3a'**, which explains the increase in the HOMO energy levels in this order. In the LUMO of **3a'**, the molecular orbital tended to be localized on the C1 and C3 atoms, rather than on the C2 and C4 atoms. Therefore, it is theoretically reasonable that 2,4-dimethoxy group in **3ba'** has nearly no effect on the LUMO and its energy levels compared with **3a'** (**3ba'**:  $-4.24$  eV vs **3a'**:  $-4.33$  eV). In the other LUMOs in **3aa'** and **3ca'**, there seems to be a slight  $\pi$ -extension effect in the 1-methoxy and 3-methoxy groups, resulting in a slight decrease in the LUMO energy levels compared with **3a'**.

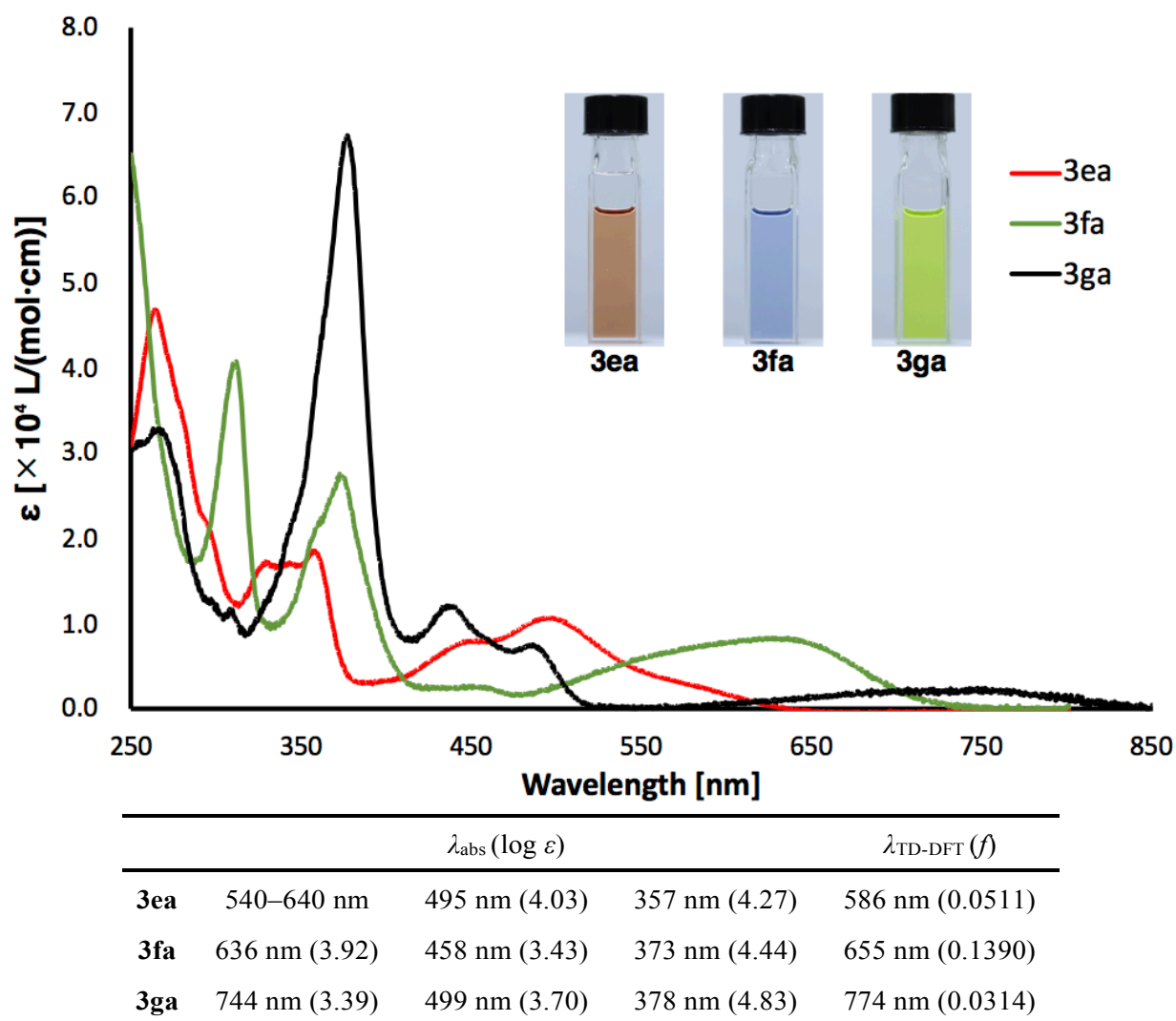


**Figure 9.** Illustrations on the distributions of HOMO and LUMO (isovalue = 0.02) of **3aa'**–**3ca'** and **3a'** in the grand state calculated by B3LYP/6-311++G(2d,p)//B3LYP/6-311+G(2d,p).

Next, the absorption spectra of the thiopyryliums **3ea**, **3fa**, and **3ga** were measured (Figure 10). Red shifts of the absorption maxima in the longest wavelength region were found as their  $\pi$ -conjugation lengths were extended, and the absorptions were observed at 540–640 nm (**3ea** as a shoulder peak), 636 nm (**3fa**,  $\log \epsilon = 3.92$ ), and 744 nm (**3fa**,  $\log \epsilon = 3.39$ ) (Figure 10). By comparing the TD-DFT calculation results for the corresponding cations **3ea'**, **3fa'**, and **3ga'**, the lowest excitations were estimated to

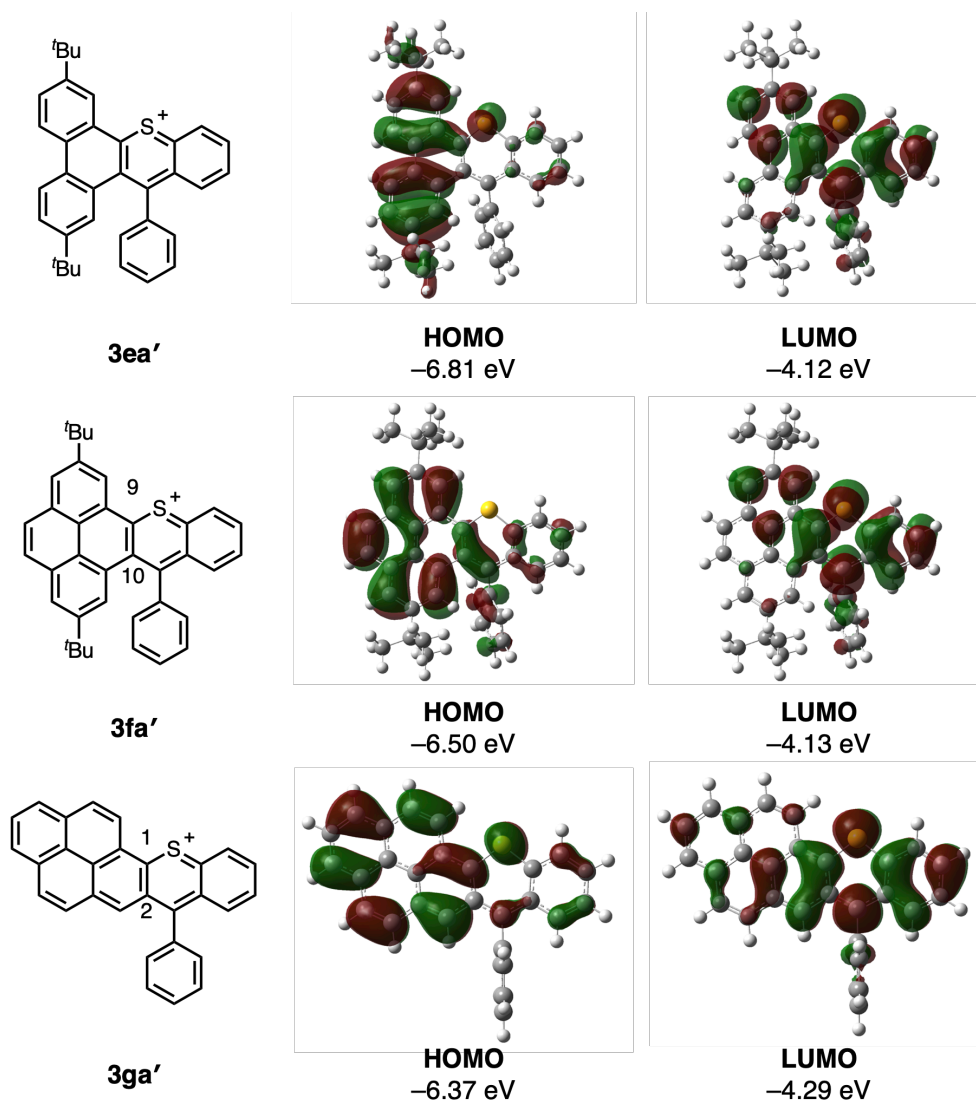


originate from HOMO to LUMO excitations. The calculated excitation wavelengths and  $f$  values (**3ea'**:586 nm/0.0511, **3fa'**:655 nm/0.1390, and **3ga'**:774 nm/0.0314) corresponded well with the observed absorptions of **3fa–3ga**. In the illustration of the HOMO and LUMO of **3ea'–3ga'**, the HOMOs are delocalized on the original PAH cores, whereas the LUMOs are biased toward the benzothiopyrylium cores, resulting in intramolecular charge transfer (CT) and long-wavelength absorption in the NIR region. In the  $\pi$ -extension from a phenanthrene core in **3ea'** to a pyrene core in **3fa'**, only the HOMO of **3fa'** was spatially extended and energetically increased ( $-6.81$  eV  $\rightarrow$   $-6.50$  eV) without changing the LUMO and its energy level ( $-4.12$  eV  $\rightarrow$   $-4.13$  eV) (Figure 11). In the comparison of **3fa'** and **3ga'**, the difference in pyrene ring fusion dramatically alters both the HOMO and LUMO energy levels, and it is expected that **3ga'** has a stronger thia-tetracene nature than **3fa'** because the acene nature of **3fa'** is weakened by peri-dibenzo-condensation. Thus, intramolecular CT in **3ga'** seems to be stronger than that in **3fa'**, resulting in longer wavelength absorption of **3ga** over the NIR region.



**Figure 10.** UV-Vis-NIR absorption spectra of  $\pi$ -extended thiopyryliums **3ea–3ga** in  $\text{CH}_2\text{Cl}_2$ , summary table of observed representative absorption peaks of **3ea–3ga**, and estimated excitation wavelengths ( $\lambda_{\text{TD-DFT}}$ ) and oscillator strengths ( $f$ ) of corresponding cations **3ea'–3ga'** calculated by TD-DFT with the

B3LYP/6-311++G(2d,p)//B3LYP/6-311+G(2d,p) level of theory. The concentrations of each compound: **3ea** =  $9.0 \times 10^{-6}$  M, **3fa** =  $4.9 \times 10^{-6}$  M, **3ga** =  $4.0 \times 10^{-6}$  M. The pictures were taken using the concentrated solutions of each compound.

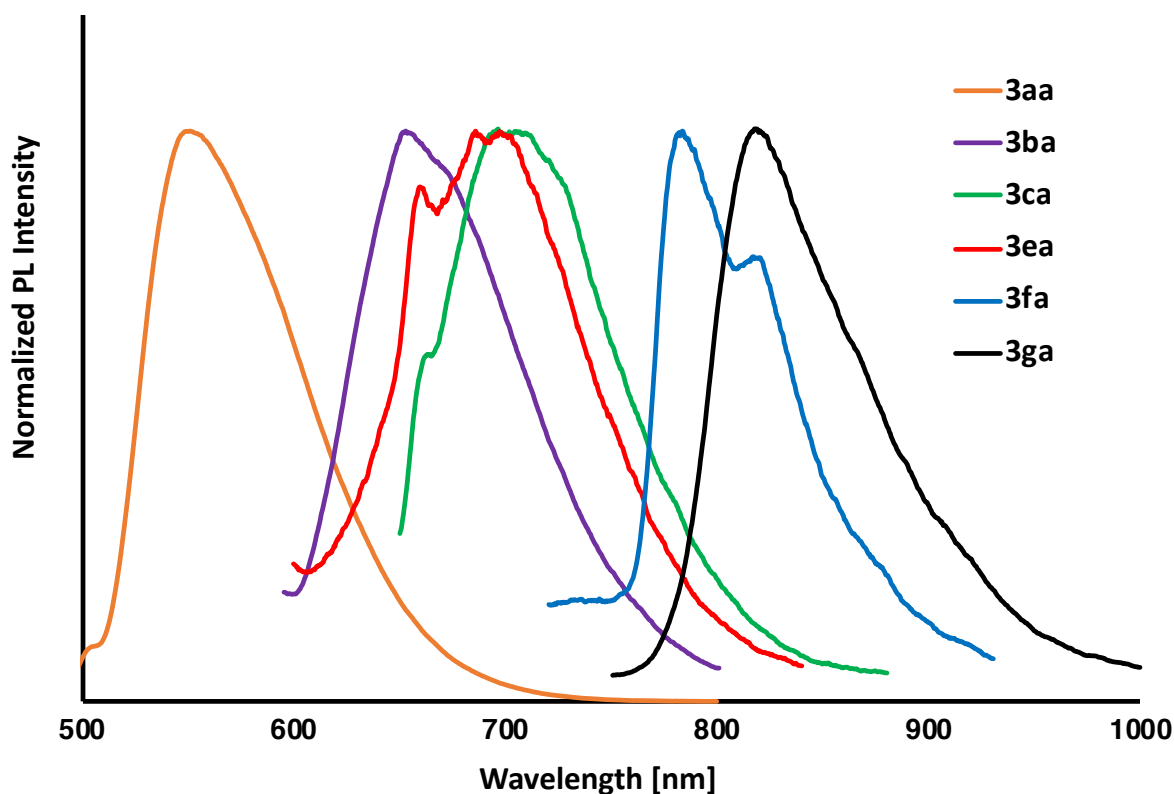


**Figure 11.** Illustrations of the distributions of HOMOs and LUMOs (isovalue = 0.02) of **3ea'**–**3ga'** calculated by B3LYP/6-311++G(2d,p)//B3LYP/6-311+G(2d,p).

## 2-5. Emission properties

In addition, thiopyryliums **3aa**–**3ca** and **3ea**–**3ga** exhibited weak emissions, as shown in Figure 12. The emission maxima of **3aa**, **3ba**, and **3ca** were found at 551 nm, 653 nm, and 696 nm, and the Stokes shifts were 33 nm (38 eV), 78 nm (16 eV), and 50 nm (25 eV), respectively. Similar to the absorption properties, the difference in the methoxylated sites induced a red shift in the emission wavelengths. The peak of **3ea** was observed at approximately 700 nm. Pyrene-fused thiopyryliums **3fa** and **3ga** exhibited NIR emission. The maximum peak tops of **3fa** and **3ga** were observed at 783 nm and 817 nm, respectively.

Larger Stokes shifts (147 and 73 nm, 8.4 and 17 eV) were observed in these compounds, which can be rationalized by the existence of structural relaxation owing to intramolecular CT in each excited state. Furthermore, only thiopyryliums **3aa** and **3ba** showed sufficient emission intensities for measurements of their quantum yields ( $\Phi_{\text{QY}}$ ) (1% and 0.8%, respectively) and fluorescence lifetimes ( $\tau$ ) (0.32 and 0.93 ns, respectively). According to these results, radiative decay rate constant ( $k_r$ ) of thiopyryliums **3aa** and **3ba** were calculated as  $3.1 \times 10^7 \text{ s}^{-1}$  and  $8.6 \times 10^6 \text{ s}^{-1}$ , respectively. Interestingly, the value of non-radiative decay constant ( $k_{\text{nr}}$ ) of **3ba** ( $1.1 \times 10^9 \text{ s}^{-1}$ ) was smaller than that of **3aa** ( $3.1 \times 10^9 \text{ s}^{-1}$ ), whereas thiopyrylium **3ba** has the narrower HOMO–LUMO gap than **3aa**. While the reason is unclear at this moment, it is of interest that the minor structural difference has a great impact on photophysical properties.



	$\lambda_{\text{em}}$ (nm)	$\Phi_{\text{QY}}$	$\tau$ (ns)	$k_r$ ( $\text{s}^{-1}$ )	$k_{\text{nr}}$ ( $\text{s}^{-1}$ )
<b>3aa</b>	551	0.010	0.32	$3.1 \times 10^7$	$3.1 \times 10^9$
<b>3ba</b>	653	0.008	0.93	$8.6 \times 10^6$	$1.1 \times 10^9$
<b>3ca</b>	696	–	–	–	–
<b>3ea</b>	700	–	–	–	–
<b>3fa</b>	783	–	–	–	–
<b>3ga</b>	817	–	–	–	–

**Figure 12.** Emission spectra of  $\pi$ -extended thiopyryliums **3aa–3ca** and **3ea–3ga** in  $\text{CH}_2\text{Cl}_2$ .  $\lambda_{\text{em}}$ : Wavelength at an emission maximum;  $\Phi_{\text{QY}}$ : Quantum yield of fluorescence;  $\tau$ : Fluorescence lifetime;  $k_r$ : Radiative decay rate constant;  $k_{\text{nr}}$ : Non-radiative decay rate constant. Excitation wavelengths for each

compound: **3aa** (436 nm), **3ba** (545 nm), **3ca** (600 nm), **3ea** (550 nm), **3fa** (636 nm), and **3ga** (564 nm).

### 3. Conclusion

The author developed a thia-APEX reaction, a new synthetic method for polycyclic thiopyrylium compounds from unfunctionalized aromatics. Using *S*-succinimide/*S*-ethosuximide-containing *ortho*-arenonylarenethiols as sulfur-embedding APEX agents, the thia-APEX reactions took place in one-pot through the sequence of C–S bond formation, intramolecular nucleophilic addition, and dehydrative aromatization under acidic conditions. This simple procedure afforded 12  $\pi$ -extended thiopyrylium compounds, ten of which were new compounds. Furthermore, each product exhibited characteristic photophysical properties and dramatic changes depending on the substitution pattern and core aromatic structures; some of them showed NIR absorption and emission. We expect that thia-APEX reactions, as well as the newly synthesized sulfur-containing polycyclic aromatics, will contribute to the rapid and efficient creation of novel functional aromatics.

## 4. Experimental section

### 4-1. General

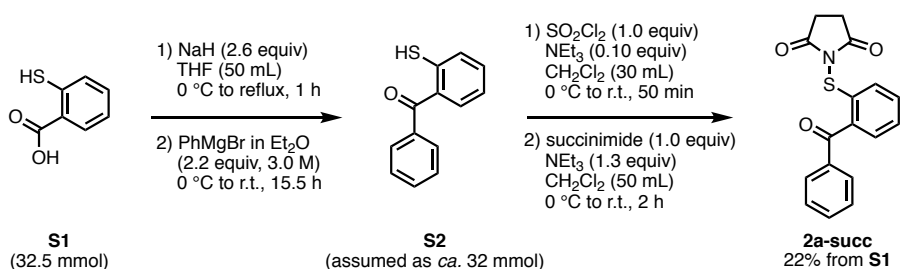
Unless otherwise noted, all materials including dry solvents were obtained from commercial suppliers and used without further purification. PhMgBr in Et<sub>2</sub>O, PhCN, *N,N,N',N'*-tetramethylethylenediamine (TMEDA), and pyrene (**1g**) were purchased from Aldrich. Tetrahydrofuran (THF), CH<sub>2</sub>Cl<sub>2</sub>, a reagent-grade of dimethylsulfoxide (DMSO), <sup>n</sup>BuLi in hexane, and NaH (dispersion in paraffin liquid) were purchased from KANTO. Thiosalicylic acid (**S1**), 2-naphthonitrile, 4-iodobiphenyl (**S4**), 1,2-ethanedithiol, trifluoromethanesulfonic acid (TfOH), a reagent-grade of 1,1,1,3,3,3-hexafluoro-2-propanol (HFIP), succinimide, ethosuximide, phthalimide, 3-nitrophthalimide, 4-nitrophthalimide, 4-bromophthalimide, 3,4,5,6-tetrachlorophthalimide, phenanthrene (**1a'**), *p*-dimethoxybenzene (**1c**), 1,2,3,4-tetramethylbenzene (**1d**) were purchased from TCI. CuSO<sub>4</sub>·5H<sub>2</sub>O was purchased from Nacalai Tesque. SO<sub>2</sub>Cl<sub>2</sub>, NEt<sub>3</sub>, PhLi in <sup>n</sup>Bu<sub>2</sub>O, NaOH, KOH, cyclohexane (CyH), PhSH (**S6**), mesitylene (**S10**), *o*-dimethoxybenzene (**1a**), *m*-dimethoxybenzene (**1b**), glutarimide, and phthalimide were purchased from Wako. 2,7-di-*tert*-butylphenanthrene (**1e**) and 2,7-di-*tert*-butylpyrene (**1f**) was synthesized by referring literatures.<sup>[13,14]</sup> Unless otherwise noted, all reactions were performed with dry solvents under an atmosphere of nitrogen in oven-dried glassware with standard vacuum-line techniques. All work-up and purification procedures were carried out with reagent-grade solvents in air.

Analytical thin-layer chromatography (TLC) was performed using E. Merck silica gel 60 F<sub>254</sub> precoated plates (0.25 mm). The developed chromatogram was analyzed by UV lamp (254 nm). Flash column chromatography was performed with KANTO Silica Gel 60N (spherical, neutral, 40-100 μm) or Biotage Isolera<sup>®</sup> equipped with a cartridge of Sfar DLV Empty 50–100 g Column with frit containing KANTO Silica Gel 60N (spherical, neutral, 40-100 μm). Preparative thin-layer chromatography (PTLC) was performed using Wako-gel<sup>®</sup> B5-F silica coated plates (0.75 mm) prepared in our laboratory. The developed chromatogram was analyzed by UV lamp (254 nm and 365 nm). High-resolution mass spectra (HRMS) were obtained from a Thermo Fisher Scientific Exactive Plus (ESI). Nuclear magnetic resonance (NMR) spectra were recorded on a JEOL Delta ECA-600 (<sup>1</sup>H 600 MHz, <sup>13</sup>C 150 MHz, <sup>19</sup>F 560 MHz) spectrometer and a JEOL Delta JNM-ECZ400S/L1 (<sup>1</sup>H 400 MHz, <sup>13</sup>C 100 MHz). Chemical shifts for <sup>1</sup>H NMR are expressed in parts per million (ppm) relative to tetramethylsilane (δ 0.00 ppm) or CD<sub>2</sub>Cl<sub>2</sub> (δ 5.32 ppm), or Cl<sub>2</sub>CDCDCl<sub>2</sub> (δ 6.00 ppm). Chemical shifts for <sup>13</sup>C NMR are expressed in ppm relative to CDCl<sub>3</sub> (δ 77.16 ppm) or CD<sub>2</sub>Cl<sub>2</sub> (δ 53.84 ppm) or Cl<sub>2</sub>CDCDCl<sub>2</sub> (δ 73.78 ppm). Chemical shifts for <sup>19</sup>F NMR are expressed in ppm relative to C<sub>6</sub>F<sub>6</sub> as an internal standard (δ -162.00 ppm). Data are reported as follows: chemical shift, multiplicity (s = singlet, d = doublet, dd = doublet of doublets, ddd = doublet of doublet of doublets, t = triplet, td = triplet of doublets, q = quartet, m = multiplet), coupling constant (Hz), and integration.

## 4-2. General procedures

### 4-2-1. Material preparation

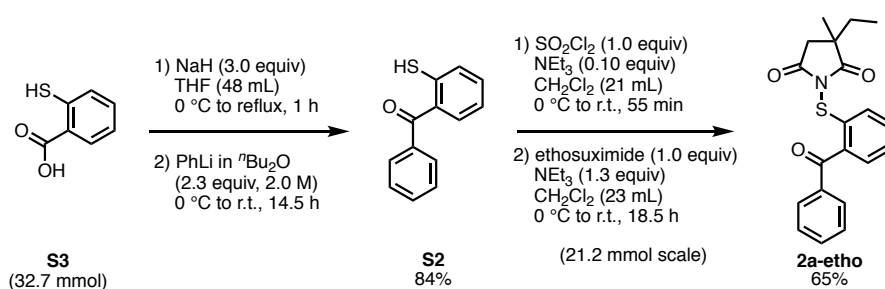
#### General Procedure A: preparation of **2a-succ**<sup>[8a,10]</sup>



**[First step]** To a pre-dried three-neck round-bottom flask (300 mL) containing a magnetic stirrer bar were added thiosalicylic acid (**S1**) (5.01 g, 32.5 mmol, 1.0 equiv) and dry THF (50 mL) under a stream of nitrogen. Then, the mixture was stirred and cooled to 0 °C using an ice-bath. After that, NaH (60% in paraffin liquid, 3.34 g, 83.5 mmol, 2.6 equiv) was added to the mixture at 0 °C. The resulting mixture was heated and stirred under reflux for an hour. After cooling the mixture to 0 °C again, 3.0 M PhMgBr in Et<sub>2</sub>O (24.0 mL, 72.0 mmol, 2.2 equiv) was added. After warming to and stirring at room temperature for 15.5 h, water was carefully added to quench, followed by addition of AcOEt. This mixture was acidified using 1 M HCl aq. until the pH became 1. The organic phase was extracted using AcOEt three times. The combined organic layers were dried over anhydrous Na<sub>2</sub>SO<sub>4</sub>, filtered, and concentrated *in vacuo*. The crude product of thiol **S2** (9.37 g, >100% crude yield) was used for the next step without further purifications.

**[Second step]** To a pre-dried round-bottom flask (100 mL) containing a magnetic stirring bar was added crude **S2** (assumed as *ca.* 32.5 mmol). After charge of nitrogen, NEt<sub>3</sub> (450 μL, 3.23 mmol, 0.10 equiv) and dry CH<sub>2</sub>Cl<sub>2</sub> (30 mL) were added under stream of nitrogen. To this mixture was added SO<sub>2</sub>Cl<sub>2</sub> (2.60 mL, 32.2 mmol, 1.0 equiv) at 0 °C. After stirring at 0 °C for 13 min., the mixture was warmed to room temperature and stirred for 37 min. After that, the resulting mixture was cooled to 0 °C again. This mixture was transferred via syringe to a pre-dried two-neck round-bottom flask (200 mL) containing a magnetic stirring bar, succinimide (3.19 g, 32.2 mmol, 1.0 equiv), dry CH<sub>2</sub>Cl<sub>2</sub> (50 mL), and NEt<sub>3</sub> (5.90 mL, 42.3 mmol, 1.3 equiv) at 0 °C. The resulting mixture was warmed and stirred at room temperature for 2 h. The resulting mixture was diluted with water. After that, the organic phase was extracted using CH<sub>2</sub>Cl<sub>2</sub> three times. The combined organic phase was dried over anhydrous Na<sub>2</sub>SO<sub>4</sub>, filtered, and concentrated *in vacuo*. The obtained crude product was purified by flash column chromatography on silica-gel (hexane/AcOEt = 4:1 → 3:2, then 3:2 → 0:100). The combined fractions containing **2a-succ** was concentrated and the solvent was evaporated to be solidified. The resulting solid was collected by suction filtration and was rinsed with cold (*ca.* 0 °C) AcOEt. After drying *in vacuo*, **2a-succ** was obtained as yellow solid (2.19 g, 7.03 mmol, 22% in two steps).

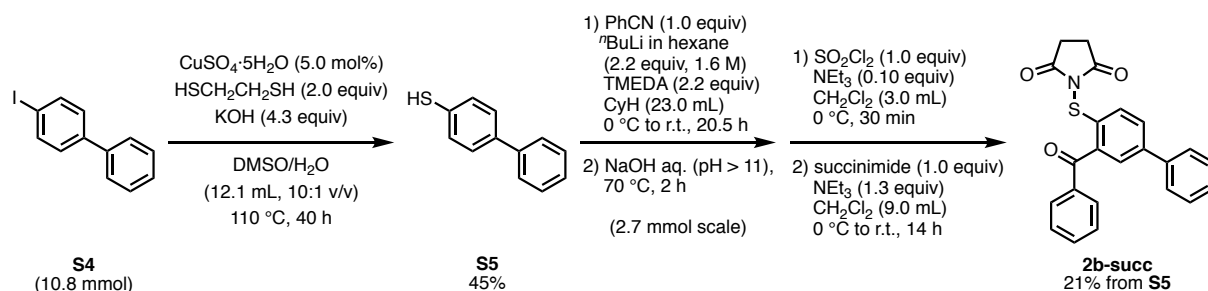
## General Procedure B: preparation of 2a-etho<sup>[8a,10]</sup>



**[First step]** To a pre-dried three-neck round-bottom flask (500 mL) containing a magnetic stirrer bar were added thiosalicylic acid (**S1**) (5.05 g, 32.7 mmol) and dry THF (48 mL) under a stream of nitrogen. Then, the mixture was stirred with cooling using an ice-bath, and NaH (60% in paraffin liquid, 3.88 g, 97.1 mmol, 3.0 equiv) was added to the mixture at 0 °C under stream of nitrogen. The resulting mixture was heated and stirred under reflux for an hour. After cooling the mixture to 0 °C again, 2.0 M PhLi in <sup>t</sup>Bu<sub>2</sub>O (38.0 mL, 75.0 mmol, 2.3 equiv) was added under stream of nitrogen. After warmed and stirring at room temperature for 15 h, water was carefully added to quench, followed by addition of AcOEt. This mixture was acidified using 12 M HCl aq. until the pH became *ca.* 3. The organic phase was extracted using AcOEt three times. The combined organic layers were dried over anhydrous Na<sub>2</sub>SO<sub>4</sub>, filtered, and concentrated *in vacuo*. The obtained crude product was purified by flash column chromatography on silica-gel (hexane/AcOEt = 8:1 → 4:1). As a result, thiol **S2**<sup>[10]</sup> was isolated (5.87 g, 27.4 mmol, 84%). <sup>1</sup>H NMR (400 MHz, CDCl<sub>3</sub>) δ 7.75–7.84 (m, 2H), 7.56–7.65 (m, 1H), 7.41–7.54 (m, 4H), 7.32–7.40 (m, 1H), 7.15–7.23 (m, 1H), 4.22 (s, 1H).

**[Second step]** To a pre-dried round-bottom flask (100 mL) containing a magnetic stirring bar was added isolated **S2** (4.55 g, 21.2 mmol). After charge of nitrogen, NEt<sub>3</sub> (300 μL, 2.15 mmol, 0.10 equiv) and dry CH<sub>2</sub>Cl<sub>2</sub> (21 mL) were added under stream of nitrogen. To this mixture was added SO<sub>2</sub>Cl<sub>2</sub> (1.75 mL, 21.7 mmol, 1.0 equiv) at 0 °C. After stirring at 0 °C for 20 min., the mixture was warmed to room temperature and stirred for 35 min. After that, the resulting mixture was cooled to 0 °C again. This mixture was transferred via syringe to a pre-dried two-neck round-bottom flask (100 mL) containing a magnetic stirring bar, ethosuximide (3.00 g, 21.2 mmol, 1.0 equiv), dry CH<sub>2</sub>Cl<sub>2</sub> (23 mL), and NEt<sub>3</sub> (3.80 mL, 27.3 mmol, 1.3 equiv) at 0 °C. The resulting mixture was warmed and stirred at room temperature for 19 hours. The resulting mixture was diluted with water. After that, the organic phase was extracted using CH<sub>2</sub>Cl<sub>2</sub> three times. The combined organic phase was dried over anhydrous Na<sub>2</sub>SO<sub>4</sub>, filtered, and concentrated *in vacuo*. The obtained crude product was purified by flash column chromatography on silica-gel using Isolera<sup>®</sup> (hexane/AcOEt = 100:0 → 4:1, then 4:1 → 0:100). The combined fractions containing **2a-etho** was concentrated and the solvent was evaporated to be solidified. The resulting solid was sonicated in minimum amount of AcOEt. After that, this solid was collected by suction filtration and was rinsed using AcOEt and hexane. After drying *in vacuo*, **2a-etho** was obtained as white solid (4.89 g, 13.8 mmol, 65%).

### General Procedure C: preparation of 2b-succ<sup>[8a,10b,15]</sup>



**[First step]** To a J-Young Schlenk tube containing a magnetic stirrer bar were added 4-iodobenzophenone (**S4**) (3.03 g, 10.8 mmol, 1.0 equiv), KOH (3.08 g, 85% purity, 46.7 mmol, 4.3 equiv), and  $\text{CuSO}_4\cdot 5\text{H}_2\text{O}$  (134.6 mg, 0.539 mmol, 5.0 mol%). The tube was connected to a manifold, and the contents were placed under nitrogen atmosphere using a general Schlenk technique. Then, water (1.1 mL), DMSO (11.1 mL), and 1,2-ethanedithiol (1.80 mL, 21.4 mmol, 2.0 equiv) were added to the mixture. The resulting mixture was stirred at 110 °C for 39 h. After cooling to room temperature, the resulting mixture was acidified at 0 °C with 1 M HCl aq. until the pH became *ca.* 1. After diluting with AcOEt, the reaction mixture was filtered using a pad of Celite<sup>®</sup>. The organic phase of filtrate was washed with water twice and brine in this order. Then, the organic phase was dried over anhydrous  $\text{Na}_2\text{SO}_4$ , filtered, and concentrated *in vacuo*. This crude product was purified by flash column chromatography on silica gel (eluent: hexane/AcOEt = 94:6  $\rightarrow$  0:100) using Isolera<sup>®</sup>. Finally, 4-phenylbenzenethiol (**S5**)<sup>[15]</sup> was obtained as an off-white solid (915 mg, 4.91 mmol, 45%).

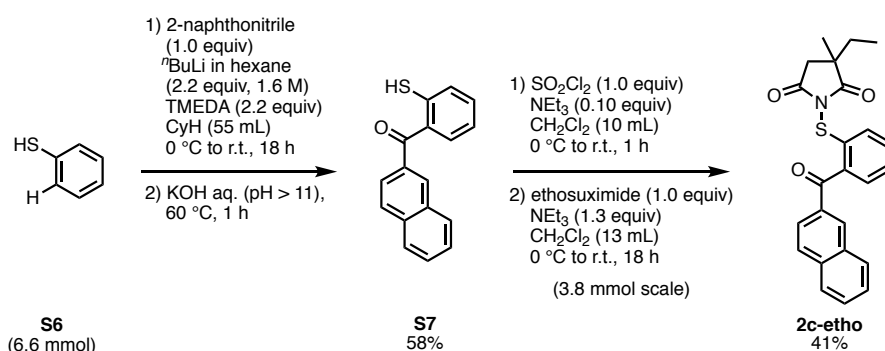
<sup>1</sup>H NMR (400 MHz,  $\text{CDCl}_3$ )  $\delta$  7.52–7.62 (m, 2H), 7.41–7.48 (m, 4H), 7.32–7.36 (m, 3H), 3.50 (s, 1H)

**[Second step]** To a pre-dried three-neck round-bottom flask (200 mL) containing a stirring bar were added dry cyclohexane (12 mL) and TMEDA (682.8 mg, 5.88 mmol, 2.2 equiv) under nitrogen atmosphere. This solution was cooled to 0 °C and 1.6 M <sup>t</sup>BuLi in hexane (3.80 mL, 5.93 mmol, 2.2 equiv) was added. To this solution, **S5** (494.2 mg, 2.65 mmol) in cyclohexane (8.0 mL) was added at 0 °C. Then, the resulting mixture was warmed and stirred at room temperature for 13 h. After that, benzonitrile (274.5 mg, 2.66 mmol, 1.0 equiv) in cyclohexane (3.0 mL) was added at room temperature to the reaction mixture and the resulting mixture was stirred at room temperature for 7 h. To this mixture was added water (5 mL), and the mixture was stirred at room temperature for 80 min. The aqueous phase was separated and pellets of NaOH were added to the aqueous phase including carboxylate ion at 0 °C until the pH became over 11. This basic water phase was stirred at 67 °C for two hours. After cooling to room temperature, the water phase was acidified at 0 °C by using 12 M HCl aq. until the pH became *ca.* 1. After diluting with AcOEt, the organic phase including carboxylic acid was extracted with AcOEt three times. The combined organic phase was dried over anhydrous  $\text{Na}_2\text{SO}_4$ , filtered, and concentrated *in vacuo*. The crude product was purified by flash column chromatography on silica gel (eluent: hexane/AcOEt = 100:0  $\rightarrow$  4:1, then 4:1  $\rightarrow$  0:100) using Isolera<sup>®</sup>. The resulting brown oil (460 mg, 60% crude yield) was used for the next step without further purifications.



**[Third step]** To a pre-dried round-bottom flask (50 mL) containing a magnetic stirring bar was added the crude product from the previous step (460 mg, assumed *ca.* 1.58 mmol). After replacing with nitrogen atmosphere, NEt<sub>3</sub> (20.6 mg, 0.20 mmol, 0.10 equiv) and dry CH<sub>2</sub>Cl<sub>2</sub> (3.0 mL) were added to the flask. To this mixture, SO<sub>2</sub>Cl<sub>2</sub> (130 μL, 1.61 mmol, 1.0 equiv) was added at 0 °C. After stirring at 0 °C for 26 min., the resulting mixture was transferred via a syringe to a pre-dried Schlenk tube containing a magnetic stirring bar, succinimide (157.1 mg, 1.59 mmol, 1.0 equiv), dry CH<sub>2</sub>Cl<sub>2</sub> (9.0 mL), and NEt<sub>3</sub> (214.1 mg, 290 μL, 2.12 mmol, 1.3 equiv) at 0 °C. The resulting mixture was warmed and stirred at room temperature (25 °C) for 14 h. The resulting mixture was diluted with water. After that, the organic phase was extracted with CH<sub>2</sub>Cl<sub>2</sub> (11 mL), dried over anhydrous Na<sub>2</sub>SO<sub>4</sub>, filtered, and concentrated *in vacuo*. The obtained crude product was purified by flash column chromatography on silica gel (eluent: hexane/AcOEt = 100:0 → 0:100) using Isolera<sup>®</sup>. As a result, **2b-succ** was obtained as an off-white solid (223 mg, 0.576 mmol, 1.6<sub>wt</sub>% of succinimide (<sup>1</sup>H NMR (600MHz, CD<sub>2</sub>Cl<sub>2</sub>) δ 2.72 (s, 0.26H)) was included. 21% yield from **S5**).

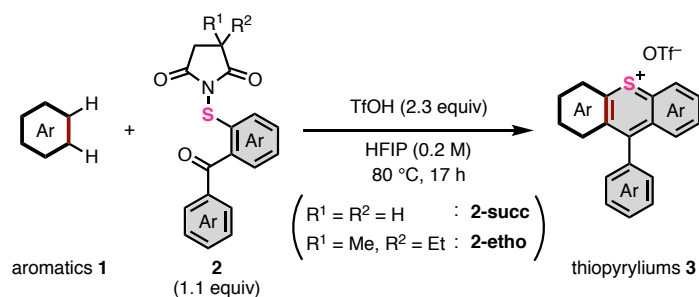
**General Procedure D: preparation of 2c-etho**<sup>[8a,10b]</sup>



**[First step]** To a pre-dried three-neck round-bottom flask (200 mL) were added dry cyclohexane (24 mL) and TMEDA (1.69 g, 14.6 mmol, 2.2 equiv) under nitrogen atmosphere. This solution was cooled to 0 °C and 1.6 M <sup>t</sup>BuLi in hexane (9.25 mL, 14.8 mmol, 2.2 equiv) was added. To this solution, benzenethiol (**S6**) (731.1 mg, 6.64 mmol, 1.0 equiv) in cyclohexane (10 mL) was added at 0 °C. Then, the resulting mixture was warmed and stirred at room temperature for 12 h. After that, 2-naphthonitrile (1.01 g, 6.60 mmol) in cyclohexane (21 mL) was added as a suspension at 0 °C. The resulting mixture was warmed and stirred at room temperature for 4.5 h. To this mixture was added water (10 mL) and stirred at room temperature for 76 min. After that, pellets of KOH were added to the bilayer mixture until the pH of the aqueous phase became over 11. This mixture was stirred at 60 °C for an hour. After cooling to room temperature, the resulting mixture was acidified at 0 °C by using 12 M HCl aq. until the pH became *ca.* 1. After dilution with AcOEt, the organic phase was extracted with AcOEt four times. The combined organic phases were dried over anhydrous Na<sub>2</sub>SO<sub>4</sub>, filtered, and concentrated *in vacuo*. The crude product was purified by flash column chromatography on silica gel (eluent: hexane/AcOEt = 100:0 → 9:1 → 7:3 → 0:100) using Isolera<sup>®</sup>. As a result, (2-mercaptophenyl)(naphthalen-2-yl)methanone (**S7**) was obtained as a yellow solid (1.01 g, 3.83 mmol, 58%).

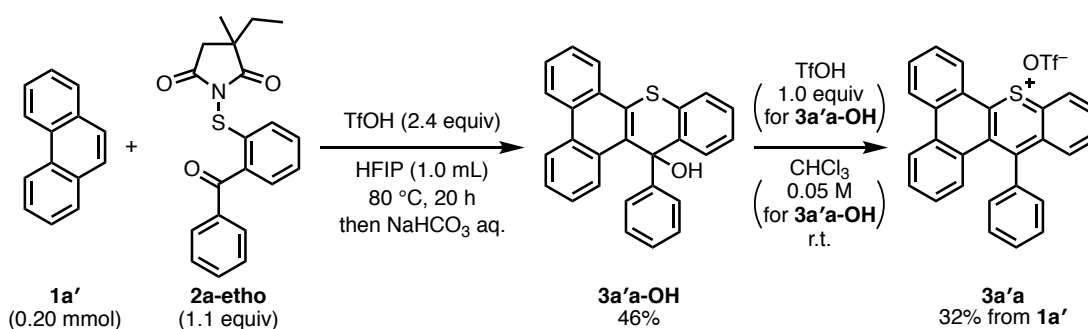
**[Second step]** To a pre-dried two-neck round-bottom flask (100 mL) containing a magnetic stirring bar was added isolated **S7** (1.01 g, 3.83 mmol). After charge of nitrogen, NEt<sub>3</sub> (60 μL, 0.43 mmol, 0.10 equiv) and dry CH<sub>2</sub>Cl<sub>2</sub> (10 mL) were added under stream of nitrogen. To this mixture was added SO<sub>2</sub>Cl<sub>2</sub> (310 μL, 3.84 mmol, 1.0 equiv) at 0 °C. After stirring at 0 °C for 20 min., the mixture was warmed to room temperature and stirred for 40 min. After that, the resulting mixture was cooled to 0 °C again. This mixture was transferred via syringe to a pre-dried two-neck round-bottom flask (100 mL) containing a magnetic stirring bar, ethosuximide (540.0 mg, 3.83 mmol, 1.0 equiv), dry CH<sub>2</sub>Cl<sub>2</sub> (13 mL), and NEt<sub>3</sub> (690 μL, 4.95 mmol, 1.3 equiv) at 0 °C. The resulting mixture was warmed and stirred at room temperature for 19 h. The resulting mixture was diluted with water. After that, the organic phase was extracted using CH<sub>2</sub>Cl<sub>2</sub> three times. The combined organic phases were dried over anhydrous Na<sub>2</sub>SO<sub>4</sub>, filtered, and concentrated *in vacuo*. The obtained crude product was purified by flash column chromatography on silica gel (eluent: hexane/AcOEt = 100:0 → 7:3, then 7:3 → 0:100) using Isolera<sup>®</sup>. As a result, crude **2c-etho** was obtained as a yellow amorphous product. This product was dissolved to hot AcOEt and recrystallized from hexane/AcOEt. The resulting crystal was collected by suction filtration and was rinsed using AcOEt. After drying *in vacuo*, **2c-etho** was obtained as a white solid (640.1 mg, 1.59 mmol, 41%).

#### 4-2-2. General Procedure of thia-APEX reaction



To an oven-dried screw-capped tube were added aromatic substrates **1** (0.10 mmol, 1.0 equiv),  $\pi$ -extending agents **2** (1.1 equiv), and HFIP (0.50 mL: 0.20 M for substrates **1**) under air. After that, TfOH (2.3 equiv) was added to the reaction mixture and the resulting mixture was stirred at 80 °C for 17 h. After cooling to room temperature, the reaction mixture was transferred to a vial using MeCN. Then, HFIP and MeCN were removed from the crude mixture by using a rotary evaporator in reduced pressure. Next, thioapyrylium salts **3** were precipitated by sonication in cold Et<sub>2</sub>O, collected by suction filtration and rinsed with cold Et<sub>2</sub>O. Drying this solid *in vacuo* afforded pure thioapyryliums **3**. Regarding thioapyrylium salts **3fa** and **3ga**, further purifications by recrystallization were required for obtaining pure products (see the descriptions of each compound).

#### 4-3. Stepwise synthesis of thiopyrylium salt **3a'a** from phenanthrene



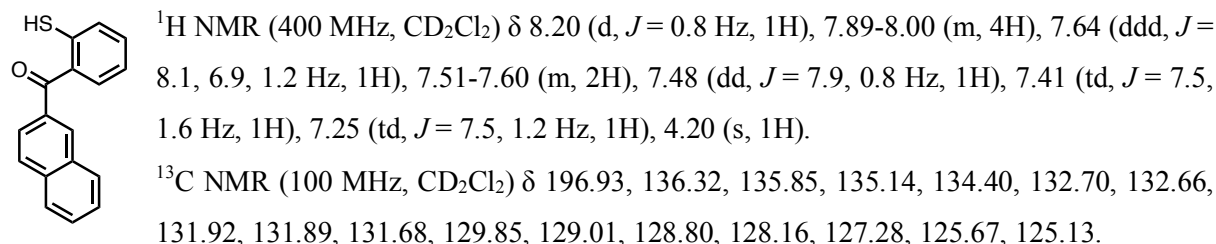
A single thiopyrylium product **3a'a** was able to be obtained through a stepwise synthesis of **3a'a** via aqueous work-up and isolation of OH-adduct **3a'a-OH** followed by dehydrative aromatization with TfOH. Although other regioisomers regarding ring fusions at C1, C2, C3 and C4 position of phenanthrene seemed to form to some extent, neutral **3a'ha-OH** was isolated as a major isomer by PTLC on silica-gel, and thus thiopyrylium salts **3a'a** was exclusively obtained.

**[First step]** A solution of crude thiopyrylium **3a'a** in HFIP was prepared from phenanthrene (**1a'**) (36.9 mg, 0.197 mmol), **2a-etho** (77.7 mg, 0.220 mmol, 1.1 equiv), TfOH (41 μL, 0.46 mmol, 2.4 equiv), and HFIP (1.0 mL) by following the general procedure of thia-APEX. Next, sat. NaHCO<sub>3</sub> aq. was added to the crude mixture, and the mixture was vigorously stirred at room temperature for 30 min. After diluting with CH<sub>2</sub>Cl<sub>2</sub>, the organic phase was extracted using CH<sub>2</sub>Cl<sub>2</sub> three times. Then, the solvent of combined organic phases was evaporated with a rotary evaporator *in vacuo*. After that, purification of the crude product was conducted by PTLC using hexane/CHCl<sub>3</sub> (9:1) as an eluent to give the intermediate **3a'a-OH** as a yellow solid (35.6 mg, 0.0912 mmol, 46%) with small amount of EtOAc. Intermediate **3a'a-OH** was instable toward heating and air, and used for the next step without further purifications.

**[Second step]** **3a'a-OH** (35.6 mg, 0.0912 mmol, 1.0 equiv) was dissolved in CHCl<sub>3</sub> (2.0 mL) in a screw-capped vial. Then, TfOH (8.0 μL, 0.091 mmol, 1.0 equiv) was added to this vial. After stirring at room temperature (24 °C) for 30 seconds, the resulting solution was concentrated using a rotary evaporator. After that, cold Et<sub>2</sub>O was added to the crude product, and sonication resulted in forming a precipitate of thiopyrylium salt **3a'a**, which was collected by suction filtration. Through rinsing with cold Et<sub>2</sub>O and drying *in vacuo*, pure **3a'a** was obtained as a dark-red solid (33.2 mg, 0.0635 mmol, 32% in 2 steps from **1h**). The regiochemistry of major isomer **3a'a** and **3a'a-OH** was determined by <sup>1</sup>H NMR spectroscopic and X-ray crystallographic analysis.

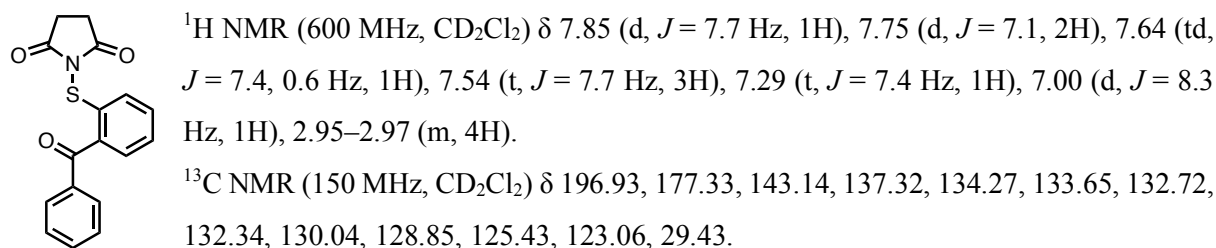
#### 4-4. Compound Data

##### (2-Mercaptophenyl)(naphthalen-2-yl)methanone (S7)



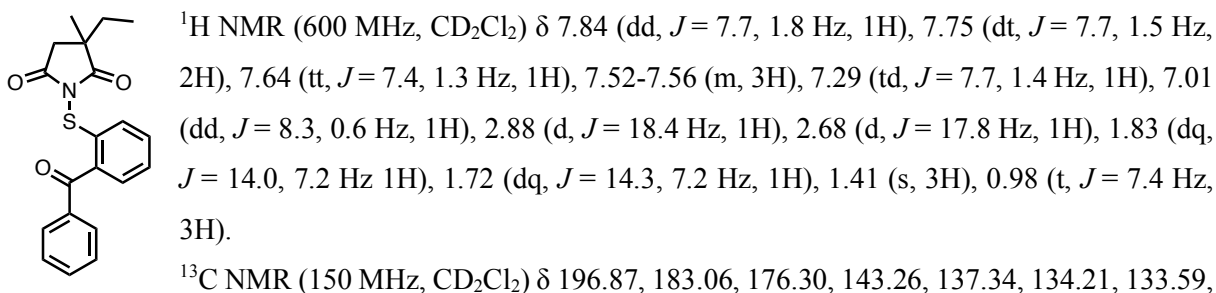
HRMS (ESI<sup>+</sup>)  $m/z$  calcd for  $\text{C}_{17}\text{H}_{12}\text{OS}$  [ $\text{M}+\text{Na}$ ]<sup>+</sup>: 287.0501, found: 287.0501.

##### 1-((2-Benzoylphenyl)thio)pyrrolidine-2,5-dione (2a-succ)



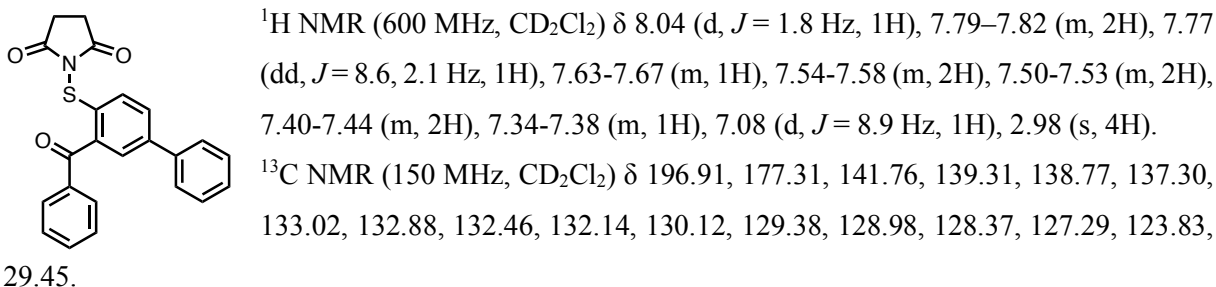
HRMS (ESI<sup>+</sup>)  $m/z$  calcd for  $\text{C}_{17}\text{H}_{13}\text{NO}_3\text{S}$  [ $\text{M}+\text{Na}$ ]<sup>+</sup>: 334.0508, found: 334.0507.

##### 1-((2-Benzoylphenyl)thio)-3-ethyl-3-methylpyrrolidine-2,5-dione (2a-etho)



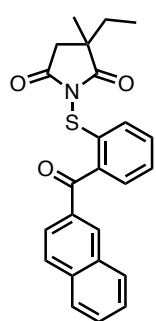
HRMS (ESI<sup>+</sup>)  $m/z$  calcd for  $\text{C}_{20}\text{H}_{19}\text{NO}_3\text{S}$  [ $\text{M}+\text{Na}$ ]<sup>+</sup>: 376.0978, found: 376.0978.

##### 1-((3-Benzoyl-[1,1'-biphenyl]-4-yl)thio)pyrrolidine-2,5-dione (2b-succ)



HRMS (ESI<sup>+</sup>)  $m/z$  calcd for  $\text{C}_{23}\text{H}_{17}\text{NO}_3\text{S}$  [ $\text{M}+\text{Na}$ ]<sup>+</sup>: 410.0821, found: 410.0820.

### 1-((2-(2-Naphthoyl)phenyl)thio)-3-ethyl-3-methylpyrrolidine-2,5-dione (**2c-etho**)



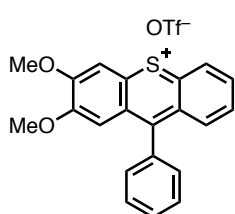
$^1\text{H}$  NMR (600 MHz,  $\text{CD}_2\text{Cl}_2$ )  $\delta$  8.27 (s, 1H), 7.94–8.05 (m, 3H), 7.92 (dd,  $J = 7.7, 1.2$  Hz, 1H), 7.86 (dd,  $J = 8.3, 1.8$  Hz, 1H), 7.65 (t,  $J = 7.1, 1.4$  Hz, 1H), 7.60 (t,  $J = 7.7$  Hz, 1H), 7.56 (td,  $J = 8.3, 1.2$  Hz, 1H), 7.32 (t,  $J = 7.4$  Hz, 1H), 7.05 (d,  $J = 8.3$  Hz, 1H), 2.89 (d,  $J = 18.4$  Hz, 1H), 2.68 (d,  $J = 18.4$  Hz, 1H), 1.80–1.89 (m, 1H), 1.69–1.77 (m, 1H), 1.42 (s, 3H), 0.97 (t,  $J = 7.7$  Hz, 3H).

$^{13}\text{C}$  NMR (150 MHz,  $\text{CD}_2\text{Cl}_2$ )  $\delta$  196.66, 183.04, 176.29, 143.14, 135.52, 134.57, 134.17, 133.53, 132.89, 132.66, 131.71, 129.70, 128.85 (2C), 128.20, 127.40, 125.93, 125.51,

123.19, 45.70, 41.40, 31.71, 24.50, 9.03.

HRMS (ESI<sup>+</sup>)  $m/z$  calcd for  $\text{C}_{24}\text{H}_{21}\text{NO}_3\text{S}$  [ $\text{M}+\text{Na}$ ]<sup>+</sup>: 426.1134, found: 426.1132.

### 2,3-Dimethoxy-9-phenylthioxanthylum trifluoromethanesulfonate (**3aa**)



According to the general procedure of thia-APEX reaction, **3aa** was obtained from 1,2-dimethoxybenzene (**1a**) (13.7 mg, 0.0992 mmol), **2a-succ** (33.5 mg, 0.108 mmol, 1.1 equiv), TfOH (20  $\mu\text{L}$ , 0.23 mmol, 2.3 equiv), and HFIP (0.50 mL) as an orange solid (41.2 mg, 0.854 mmol, 86%). When **2a-etho** was used instead of **2a-succ**, **3aa** was obtained in 86% yield.

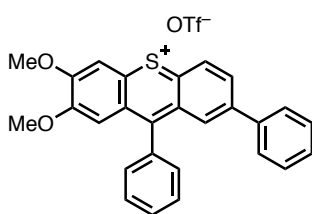
$^1\text{H}$  NMR (600 MHz,  $\text{CDCl}_3$ )  $\delta$  8.60 (s, 1H), 8.57 (d,  $J = 8.3$  Hz, 1H), 8.10 (t,  $J = 7.7$  Hz, 1H), 7.98 (d,  $J = 8.9$  Hz, 1H), 7.84 (t,  $J = 7.7$  Hz, 1H), 7.73–7.78 (m, 3H), 7.44–7.43 (m, 2H), 7.16 (s, 1H), 4.40 (s, 3H), 3.78 (s, 3H).

$^{13}\text{C}$  NMR (150 MHz,  $\text{CDCl}_3$ )  $\delta$  163.38, 160.54, 152.65, 149.57, 143.20, 135.18, 134.39, 133.95, 130.74, 130.02, 129.44, 129.11, 129.05, 127.44, 126.77, 121.00 ( $^1J_{\text{C-F}} = 321$  Hz), 111.01, 109.01, 59.28, 56.39.<sup>[16]</sup>

$^{19}\text{F}$  NMR (560 MHz,  $\text{CD}_2\text{Cl}_2$ )  $\delta$  -78.24.

HRMS (ESI<sup>+</sup>)  $m/z$  calcd for  $\text{C}_{21}\text{H}_{17}\text{O}_2\text{S}^+$  [ $\text{M}-\text{OTf}$ ]<sup>+</sup>: 333.0944, found: 333.0939.

### 2,3-Dimethoxy-7,9-diphenylthioxanthylum trifluoromethanesulfonate (**3ab**)



According to the general procedure of thia-APEX reaction, **3ab** was obtained from 1,2-dimethoxybenzene (**1a**) (20.6 mg, 0.149 mmol), **2b-succ** (63.6 mg, 0.164 mmol, 1.1 equiv), TfOH (30  $\mu\text{L}$ , 0.40 mmol, 2.3 equiv), and HFIP (0.75 mL) as a red solid (76.1 mg, 0.136 mmol, 91%).

$^1\text{H}$  NMR (600 MHz,  $\text{CDCl}_3$ )  $\delta$  8.66 (d,  $J = 8.9$  Hz, 1H), 8.63 (s, 1H), 8.33 (dd,  $J = 8.6, 2.1$  Hz, 1H), 8.08 (d,  $J = 2.4$  Hz, 1H), 7.74–7.80 (m, 3H), 7.42–7.54 (m, 7H), 7.15 (s, 1H), 4.41 (s, 3H), 3.78 (s, 3H).

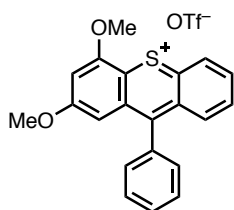
$^{13}\text{C}$  NMR (150 MHz,  $\text{CDCl}_3$ )  $\delta$  162.95, 160.42, 152.74, 149.32, 143.10, 142.18, 138.15, 135.29, 133.99, 130.82, 130.73, 129.61, 129.54, 129.32, 129.08, 128.01, 127.62, 127.02, 121.00 ( $^1J_{\text{C-F}} = 320$  Hz), 110.88,

109.15, 59.32, 56.40. One quaternary carbon peak was overlapped.

$^{19}\text{F}$  NMR (560 MHz,  $\text{CD}_2\text{Cl}_2$ )  $\delta$  -78.24.

HRMS (ESI<sup>+</sup>)  $m/z$  calcd for  $\text{C}_{27}\text{H}_{21}\text{O}_2\text{S}^+$  [M-OTf]<sup>+</sup>: 409.1257, found: 409.1253.

### 2,4-Dimethoxy-9-phenylthioxanthylum trifluoromethanesulfonate (**3ba**)



According to the general procedure of thia-APEX reaction, **3ba** was obtained from 1,3-dimethoxybenzene (**1b**) (11.9 mg, 0.0861 mmol), **2a-succ** (29.6 mg, 0.0951 mmol, 1.1 equiv), TfOH (17  $\mu\text{L}$ , 0.19 mmol, 2.2 equiv), and HFIP (0.45 mL) as a dark-purple solid (26.6 mg, 0.0551 mmol, 64%). When **2a-etho** was used instead of **2a-succ**, **3ba** was obtained in 66% yield.

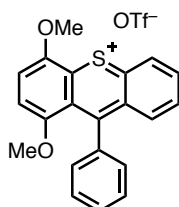
$^1\text{H}$  NMR (600 MHz,  $\text{Cl}_2\text{CDCDCl}_2$ )  $\delta$  8.80 (d,  $J$  = 8.3 Hz, 1H), 8.25 (ddd,  $J$  = 8.3, 6.8, 1.4 Hz, 1H), 8.13 (d,  $J$  = 8.9 Hz, 1H), 7.94 (ddd,  $J$  = 8.3, 7.0, 1.3 Hz, 1H), 7.71-7.79 (m, 3H), 7.53-7.57 (m, 2H), 7.35 (d,  $J$  = 1.8 Hz, 1H), 6.98 (d,  $J$  = 1.8 Hz, 1H), 4.32 (s, 3H), 3.81 (s, 3H).

$^{13}\text{C}$  NMR (150 MHz,  $\text{CDCl}_3$ )  $\delta$  167.54, 161.77, 155.67, 146.11, 136.19, 134.43, 134.25, 134.06, 132.68, 131.37, 131.09, 130.22, 129.24, 128.70, 127.90, 120.44 ( $^1J_{\text{C-F}}$  = 321 Hz) 108.79, 104.21, 57.91, 56.28.<sup>[16]</sup>

$^{19}\text{F}$  NMR (560 MHz,  $\text{CD}_2\text{Cl}_2$ )  $\delta$  -78.31.

HRMS (ESI<sup>+</sup>)  $m/z$  calcd for  $\text{C}_{21}\text{H}_{17}\text{O}_2\text{S}^+$  [M-OTf]<sup>+</sup>: 333.0944, found: 333.0948.

### 1,4-Dimethoxy-9-phenylthioxanthylum trifluoromethanesulfonate (**3ca**)



According to the general procedure of thia-APEX reaction, **3ca** was obtained from 1,4-dimethoxybenzene (**1c**) (15.2 mg, 0.110 mmol), **2a-succ** (37.6 mg, 0.121 mmol, 1.1 equiv), TfOH (22  $\mu\text{L}$ , 0.25 mmol, 2.3 equiv), and HFIP (0.55 mL) as a dark-green solid (43.0 mg, 0.0891 mmol, 81%).

$^1\text{H}$  NMR (600 MHz,  $\text{Cl}_2\text{CDCDCl}_2$ )  $\delta$  8.59 (d,  $J$  = 8.9 Hz, 1H), 8.27 (t,  $J$  = 7.7 Hz, 1H), 8.13 (d,  $J$  = 8.9 Hz, 1H), 7.93 (t,  $J$  = 7.7 Hz, 1H), 7.86 (d,  $J$  = 8.9 Hz, 1H), 7.63-7.69 (m, 3H), 7.25-7.31 (m, 3H), 4.29 (s, 3H), 3.54 (s, 3H).

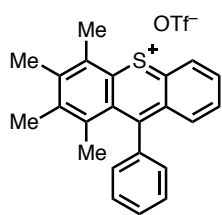
$^{13}\text{C}$  NMR (150 MHz,  $\text{Cl}_2\text{CDCDCl}_2$ )  $\delta$  170.70, 158.13, 147.92, 145.92, 138.16, 137.04, 136.09, 135.49, 130.66, 130.64, 129.26, 128.23, 127.34, 126.49, 122.24, 120.49 ( $^1J_{\text{C-F}}$  = 323 Hz), 120.22, 110.48, 57.82, 57.19.<sup>[16]</sup>

$^{19}\text{F}$  NMR (560 MHz,  $\text{CD}_2\text{Cl}_2$ )  $\delta$  -78.31.

HRMS (ESI<sup>+</sup>)  $m/z$  calcd for  $\text{C}_{21}\text{H}_{17}\text{O}_2\text{S}^+$  [M-OTf]<sup>+</sup>: 333.0944, found: 333.0938.

### 1,2,3,4-Tetramethyl-9-phenylthioxanthylum trifluoromethanesulfonate (**3da**)

According to the general procedure of thia-APEX reaction, **3da** was obtained from 1,2,3,4-



tetramethylbenzene (**1d**) (11.6 mg, 0.0864 mmol), **2a-etho** (33.9 mg, 0.0959 mmol, 1.1 equiv), TfOH (17  $\mu$ L, 0.19 mmol, 2.2 equiv), and HFIP (0.45 mL) as a dark-purple solid (27.7 mg, 0.0579 mmol, 67%). **3da** was obtained from **2a-succ** instead of **2a-etho** in 58%. Use of **2a-etho** was considered to be more suitable than use of **2a-succ** because the reproducibility of purification when using **2a-succ** was not

good. The author succeeded in the isolation of **3da** only once every three times when **2a-succ** was used.

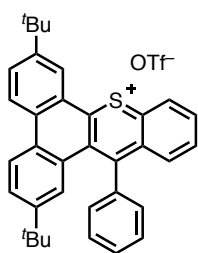
$^1\text{H}$  NMR (600 MHz,  $\text{CD}_2\text{Cl}_2$ )  $\delta$  8.65 (dd,  $J = 7.7, 0.6$  Hz, 1H), 8.42 (d,  $J = 9.5$  Hz, 1H), 8.25 (ddd,  $J = 8.3, 7.0, 1.3$  Hz, 1H), 7.98 (ddd,  $J = 8.6, 7.1, 1.5$  Hz, 1H), 7.75-7.79 (m, 1H), 7.70-7.73 (m, 2H), 7.44-7.47 (m, 2H), 2.96 (s, 3H), 2.72 (s, 3H), 2.47 (s, 3H), 1.88 (s, 3H).

$^{13}\text{C}$  NMR (150 MHz,  $\text{CD}_2\text{Cl}_2$ )  $\delta$  168.36, 151.29, 147.75, 144.15, 143.56, 143.29, 139.31, 136.26, 134.59, 131.63, 131.50, 131.38, 131.02, 130.88, 130.23, 129.57, 127.68, 23.06, 19.71, 18.02, 17.36.

$^{19}\text{F}$  NMR (560 MHz,  $\text{CD}_2\text{Cl}_2$ )  $\delta$  -78.31. Peaks of carbons on OTf anion were not found.

HRMS (ESI $^+$ )  $m/z$  calcd for  $\text{C}_{23}\text{H}_{21}\text{S}^+$  [M-OTf] $^+$ : 329.1358, found: 329.1356.

### 2,7-Di-*tert*-butyl-14-phenyldibenzo[*a,c*]thioxanthen-9-ium trifluoromethanesulfonate (**3ea**)



According to the general procedure of thia-APEX reaction, **3ea** was obtained from 2,7-di-*tert*-butylphenanthrene (**1e**) (28.8 mg, 0.0992 mmol), **2a-succ** (33.9 mg, 0.109 mmol, 1.1 equiv), TfOH (20  $\mu$ L, 0.23 mmol, 2.3 equiv), and HFIP (0.50 mL) as a dark-red solid (36.6 mg, 0.0577 mmol, 58%). **3ea** was also obtained from **1e** (289.9 mg, 0.998 mmol), **2a-etho** (388.4 mg, 1.10 mmol, 1.1 equiv), TfOH (205  $\mu$ L, 2.32 mmol, 2.3 equiv), and HFIP (5.0 mL) as a dark-red solid (477.8 mg, 0.753 mmol,

75%).

$^1\text{H}$  NMR (600 MHz,  $\text{CD}_2\text{Cl}_2$ )  $\delta$  8.82 (d,  $J = 8.3$  Hz, 1H), 8.79 (d,  $J = 1.8$  Hz, 1H), 8.64 (d,  $J = 8.9$  Hz, 1H), 8.53 (d,  $J = 8.9$  Hz, 1H), 8.44 (d,  $J = 8.3$  Hz, 1H), 8.29-8.33 (m, 1H), 8.21 (dd,  $J = 8.3, 1.8$  Hz, 1H), 8.08-8.13 (m, 1H), 7.85 (d,  $J = 1.8$  Hz, 1H), 7.74 (dd,  $J = 8.6, 1.5$  Hz, 1H), 7.67-7.72 (m, 3H), 7.52-7.57 (m, 2H), 1.56 (s, 9H), 1.04 (s, 9H).

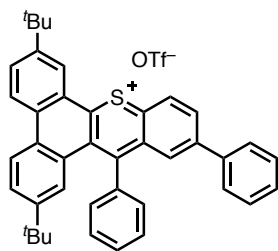
$^{13}\text{C}$  NMR (150 MHz,  $\text{CD}_2\text{Cl}_2$ )  $\delta$  163.54, 160.73, 153.92, 150.86, 140.41, 139.63, 135.98, 135.64, 134.14, 132.84, 132.75, 132.63, 131.83, 131.55, 131.41, 130.41, 129.53, 128.87, 128.85, 128.74, 128.08, 126.73, 124.74, 124.35, 123.86, 35.83, 35.28, 31.12, 31.10. Peaks of carbons on OTf anion were not found.

$^{19}\text{F}$  NMR (560 MHz,  $\text{CD}_2\text{Cl}_2$ )  $\delta$  -78.28.

HRMS (ESI $^+$ )  $m/z$  calcd for  $\text{C}_{35}\text{H}_{33}\text{S}^+$  [M-OTf] $^+$ : 485.2297, found: 485.2309.

### 2,7-Di-*tert*-butyl-12,14-diphenyldibenzo[*a,c*]thioxanthen-9-ium trifluoromethanesulfonate (**3eb**)

According to the general procedure of thia-APEX reaction, **3eb** was obtained from 2,7-di-*tert*-butylphenanthrene (**1e**) (58.1 mg, 0.200 mmol), **2b-succ** (85.6 mg, 0.221 mmol, 1.1 equiv), TfOH (41  $\mu$ L, 0.46 mmol, 2.3 equiv), and HFIP (1.0 mL) as a dark-red solid (121.7 mg, 0.171 mmol, 86%).



$^1\text{H}$  NMR of a concentrated **3eb** solution (600 MHz,  $\text{CD}_2\text{Cl}_2$ )  $\delta$  8.88 (d,  $J = 7.7$  Hz, 1H), 8.79 (d,  $J = 1.8$  Hz, 1H), 8.65 (d,  $J = 8.9$  Hz, 1H), 8.55–8.58 (m, 2H), 8.52 (d,  $J = 8.9$  Hz, 1H), 8.21 (dd,  $J = 8.3, 1.8$  Hz, 1H), 7.87 (d,  $J = 2.4$  Hz, 1H), 7.75 (dd,  $J = 8.3, 2.4$  Hz, 1H), 7.71–7.73 (m, 3H), 7.64–7.68 (m, 2H), 7.58–7.62 (m, 2H), 7.53–7.57 (m, 2H), 7.49–7.52 (m, 1H), 1.57 (s, 9H), 1.05 (s, 9H). Water peak was found around 5.9 ppm as a broad peak.

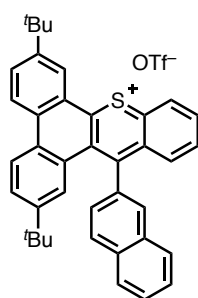
$^1\text{H}$  NMR of a diluted **3eb** solution (600 MHz,  $\text{CD}_2\text{Cl}_2$ )  $\delta$  8.81–8.84 (m, 1H), 8.77 (br s, 1H), 8.63 (d,  $J = 8.9$  Hz, 1H), 8.57–8.59 (m, 1H), 8.55 (dd,  $J = 8.3, 1.8$  Hz, 1H), 8.52 (d,  $J = 8.9$  Hz, 1H), 8.21 (dd,  $J = 8.6, 2.1$  Hz, 1H), 7.87 (d,  $J = 1.8$  Hz, 1H), 7.75 (dd,  $J = 8.6, 1.5$  Hz, 1H), 7.71–7.74 (m, 3H), 7.64–7.67 (m, 2H), 7.58–7.61 (m, 2H), 7.54–7.58 (m, 2H), 7.50–7.54 (m, 1H), 1.57 (s, 9H), 1.04 (s, 9H). Water peak was found 2.1–2.7 ppm as a broad peak.

$^{13}\text{C}$  NMR (150 MHz,  $\text{CD}_2\text{Cl}_2$ )  $\delta$  163.08, 160.27, 153.97, 150.89, 145.45, 139.72, 139.32, 138.26, 135.95, 135.02, 133.06, 132.69, 132.42, 131.56, 131.50, 131.02, 130.50, 129.97, 129.60, 128.90, 128.77, 128.53, 128.00, 126.83, 124.74, 124.38, 123.78, 35.84, 35.29, 31.11 (2C). One tertiary  $\text{sp}^2$ -carbon peak and one quaternary  $\text{sp}^2$ -carbon peak were overlapped. Peaks of carbons on OTf anion were not found.

$^{19}\text{F}$  NMR (560 MHz,  $\text{CD}_2\text{Cl}_2$ )  $\delta$  –78.36.

HRMS (ESI<sup>+</sup>)  $m/z$  calcd for  $\text{C}_{41}\text{H}_{37}\text{S}^+$  [M–OTf]<sup>+</sup>: 561.2610, found: 561.2606. The peak from methoxylated **3eb** was also found as  $m/z$  calcd for [M–OTf+OMe+Na]<sup>+</sup>: 615.2692, found: 615.2690. The OMe group was assumed to be attached from MeOH solvent which was used in the preparation of the HRMS sample.

### 2,7-Di-*tert*-butyl-14-(naphthalen-2-yl)dibenzo[*a,c*]thioxanthen-9-ium trifluoromethanesulfonate (**3ec**)



According to the general procedure of thia-APEX reaction, **3ec** was obtained from 2,7-di-*tert*-butylphenanthrene (**1e**) (58.3 mg, 0.201 mmol), **2a-etho** (88.4 mg, 0.219 mmol, 1.1 equiv), TfOH (41  $\mu\text{L}$ , 0.46 mmol, 2.3 equiv), and HFIP (1.0 mL) as a dark-red solid (77.8 mg, 0.114 mmol, 57%). Precipitation of **3ec** was more difficult than that of **3ea**, which repeating sonication in cold  $\text{Et}_2\text{O}$  and evaporation of the  $\text{Et}_2\text{O}$  were required until enough amounts of **3ec** were solidified.

$^1\text{H}$  NMR (600 MHz,  $\text{CD}_2\text{Cl}_2$ )  $\delta$  8.84 (d,  $J = 7.7$  Hz, 1H), 8.82 (d,  $J = 1.8$  Hz, 1H), 8.65 (d,  $J = 8.3$  Hz, 1H), 8.51 (d,  $J = 8.3$  Hz, 2H), 8.31 (ddd,  $J = 8.0, 7.1, 0.9$  Hz, 1H), 8.22 (dd,  $J = 8.3, 1.8$  Hz, 1H), 8.19 (d,  $J = 8.9$  Hz, 1H), 8.08 (ddd,  $J = 8.3, 7.1, 1.2$  Hz, 1H), 8.04 (d,  $J = 8.3$  Hz, 1H), 8.00 (d,  $J = 1.2$  Hz, 1H), 7.88 (d,  $J = 7.7$  Hz, 1H), 7.76 (d,  $J = 1.8$  Hz, 1H), 7.70–7.73 (m, 1H), 7.63–7.68 (m, 3H), 1.57 (s, 9H), 0.72 (s, 9H).

$^{13}\text{C}$  NMR (150 MHz,  $\text{CD}_2\text{Cl}_2$ )  $\delta$  163.65, 160.68, 153.94, 150.83, 140.46, 136.93, 136.01, 135.60, 134.36, 134.33, 133.73, 133.08, 132.76, 132.65, 131.96, 131.69, 130.34, 129.55, 129.13, 128.98, 128.95, 128.75,

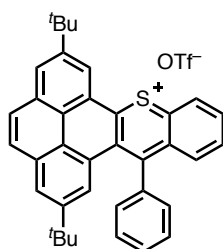


128.72, 128.36 (2C), 128.25, 128.12, 126.80, 124.75, 124.31, 123.87, 35.86, 34.96, 31.14, 30.63. Peaks of carbons on OTf anion were not found.

$^{19}\text{F}$  NMR (560 MHz,  $\text{CD}_2\text{Cl}_2$ )  $\delta$  -78.27.

HRMS (ESI<sup>+</sup>)  $m/z$  calcd for  $\text{C}_{39}\text{H}_{35}\text{S}^+$  [M-OTf]<sup>+</sup>: 535.2454, found: 535.2458.

### 2,7-Di-*tert*-butyl-14-phenylphenanthro[4,5-*abc*]thioxanthen-9-ium trifluoromethanesulfonate (**3fa**)



According to the general procedure of thia-APEX reaction, **3fa** was obtained from 2,7-di-*tert*-butylpyrene (**1f**) (61.7 mg, 0.196 mmol), **2a-etho** (76.7 mg, 0.217 mmol, 1.1 equiv), TfOH (39  $\mu\text{L}$ , 0.44 mmol, 2.3 equiv), and HFIP (0.98 mL). The operation by general thia-APEX procedure afforded crude **3fa** at first (107.7 mg, 0.163 mmol, 83% for **1f**). After recrystallization from hot  $\text{CHCl}_3$  and hexane overnight, pure **3fa** was obtained via collection by suction filtration, rinsing with

hexane, and following drying *in vacuo*, as a dark-blue solid (76.2 mg, 0.116 mmol, 59%).

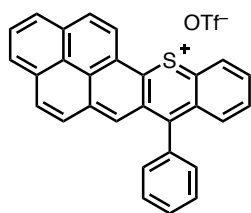
$^1\text{H}$  NMR (600 MHz,  $\text{CD}_2\text{Cl}_2$ )  $\delta$  9.22 (d,  $J$  = 1.2 Hz, 1H), 8.86 (d,  $J$  = 8.3 Hz, 1H), 8.70 (d,  $J$  = 1.2 Hz, 1H), 8.35 (d,  $J$  = 8.9 Hz, 1H), 8.27-8.33 (m, 2H), 8.22 (d,  $J$  = 1.8 Hz, 1H), 8.14 (d,  $J$  = 8.9 Hz, 1H), 8.07-8.12 (m, 2H), 7.71-7.76 (m, 3H), 7.55-7.60 (m, 2H), 1.68 (s, 9H), 1.15 (s, 9H).

$^{13}\text{C}$  NMR (150 MHz,  $\text{CD}_2\text{Cl}_2$ )  $\delta$  163.84, 162.11, 152.35, 149.90, 140.67, 139.96, 135.62, 134.32, 134.17, 133.23, 132.65, 132.44, 132.14, 131.86, 131.41, 131.00, 130.66, 129.69, 129.48, 128.03, 127.35, 127.16 (2C), 126.22, 124.65, 124.27, 123.96, 36.14, 35.55, 31.67, 31.48. Peaks of carbons on OTf anion were not found.

$^{19}\text{F}$  NMR (560 MHz,  $\text{CD}_2\text{Cl}_2$ )  $\delta$  -78.27.

HRMS (ESI<sup>+</sup>)  $m/z$  calcd for  $\text{C}_{37}\text{H}_{33}\text{S}^+$  [M-OTf]<sup>+</sup>: 509.2297 found: 509.2301.

### 7-Phenylphenaleno[1,9-*bc*]thioxanthen-12-ium trifluoromethanesulfonate (**3ga**)



According to the general procedure of thia-APEX reaction, **3ga** was obtained from pyrene (**1g**) (20.1 mg, 0.0994 mmol), **2a-succ** (34.5 mg, 0.111 mmol, 1.1 equiv), TfOH (20  $\mu\text{L}$ , 0.23 mmol, 2.3 equiv), and HFIP (0.50 mL) as a crude product (54.0 mg, 0.118 mmol, 99% for **1f**). After recrystallization from hot  $\text{CHCl}_3$  and hexane overnight, pure **3ga** was obtained via collection by suction

filtration, rinsing with hexane, and following drying *in vacuo*, as a dark-green solid (31.5 mg, 0.0576 mmol, 58%). **3ga** was obtained from the reaction with **2a-etho** instead of **2a-succ** in 57% yield.

$^1\text{H}$  NMR (600 MHz,  $\text{Cl}_2\text{CDCDCl}_2$ )  $\delta$  9.28 (d,  $J$  = 9.5 Hz, 1H), 8.96 (d,  $J$  = 8.3 Hz, 1H), 8.70-8.74 (m, 2H), 8.53 (d,  $J$  = 7.1 Hz, 1H), 8.47 (ddd,  $J$  = 8.0, 6.8, 1.2 Hz, 1H), 8.32-8.43 (m, 3H), 8.21 (d,  $J$  = 8.9 Hz, 1H), 8.13 (ddd,  $J$  = 8.3, 7.1, 1.2 Hz, 1H), 8.02 (d,  $J$  = 8.9 Hz, 1H), 7.95 (t,  $J$  = 7.4 Hz, 1H), 7.89 (t,  $J$  = 7.4 Hz, 2H), 7.66 (d,  $J$  = 7.1 Hz, 2H). The weak peak at 9.99 (s, 1H  $\times$  0.018) and 9.28 ppm (d,  $J$  = 9.5 Hz, 1H) were considered to be peaks from the regioisomer of **3ga**. According to peaks at 9.99 ppm

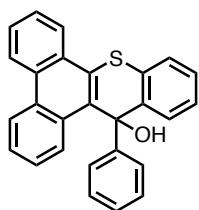
(s, 1H × 0.018), the purity of **3ga** was estimated as 98<sub>wt</sub>%.

<sup>13</sup>C NMR (150 MHz, Cl<sub>2</sub>CDCDCl<sub>2</sub>) δ 171.11, 144.94, 141.90, 137.28, 135.22, 134.72, 133.62, 133.43, 132.44, 132.11, 131.91, 131.23, 131.15, 130.98, 129.54, 129.16, 129.10, 128.62, 128.54, 128.43, 127.73, 127.45, 127.28, 126.93, 123.18, 120.44 (<sup>1</sup>J<sub>C-F</sub> = 321 Hz) 121.40.<sup>[16]</sup> One quaternary carbon peak was overlapped.

<sup>19</sup>F NMR (560 MHz, CD<sub>2</sub>Cl<sub>2</sub>) δ -78.27.

HRMS (ESI<sup>+</sup>) *m/z* calcd for C<sub>29</sub>H<sub>17</sub>S<sup>+</sup> [M-OTf]<sup>+</sup>: 397.1045 found: 397.1046.

#### 14-Phenyl-14H-dibenzo[*a,c*]thioxanthen-14-ol (**3a'a-OH**)



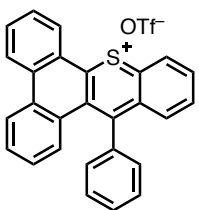
<sup>1</sup>H NMR (600 MHz, Cl<sub>2</sub>CDCDCl<sub>2</sub>) δ 8.74 (d, *J* = 8.4 Hz, 1H), 8.69 (d, *J* = 8.1 Hz, 1H), 8.62 (d, *J* = 7.8 Hz, 1H), 8.52 (d, *J* = 9.0 Hz, 1H), 7.96 (dd, *J* = 8.1, 1.5 Hz, 1H), 7.72–7.78 (m, 2H), 7.67 (d, *J* = 7.2 Hz, 2H), 7.48 (t, *J* = 7.5 Hz, 1H), 7.40 (dd, *J* = 7.5, 1.5 Hz, 1H), 7.36 (t, *J* = 7.8 Hz, 1H), 7.21–7.29 (m, 4H), 7.15 (t, *J* = 7.5 Hz, 1H), 3.18 (s, 1H).

<sup>13</sup>C NMR (150 MHz, Cl<sub>2</sub>CDCDCl<sub>2</sub>) δ 148.08, 138.74, 130.68, 130.12, 130.09, 130.05, 129.03, 128.68, 128.31, 127.81, 127.64, 127.22, 127.13, 126.77, 126.59, 125.95, 125.61, 125.50, 124.96, 124.88, 124.53, 122.74, 122.62, 76.34. Two quaternary carbon peaks were overlapped.

HRMS (ESI<sup>+</sup>) *m/z* calcd for C<sub>27</sub>H<sub>18</sub>SO<sup>+</sup> [M+Na]<sup>+</sup>: 413.0971 found: 413.0968.

From the MeOH solution of **3a'a-OH**, **3a'a** was also found as *m/z* calcd for [M-OH]<sup>+</sup>: 373.1045, found: 373.1042.

#### 14-Phenyldibenzo[*a,c*]thioxanthen-9-ium trifluoromethanesulfonate (**3a'a**)



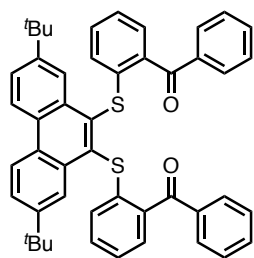
<sup>1</sup>H NMR (600 MHz, CD<sub>2</sub>Cl<sub>2</sub>) δ 8.99 (d, *J* = 8.3 Hz, 1H), 8.84 (d, *J* = 8.3 Hz, 1H), 8.73 (d, *J* = 8.3 Hz, 1H), 8.62 (d, *J* = 7.7 Hz, 1H), 8.52 (d, *J* = 8.9 Hz, 1H), 8.32 (ddd, *J* = 8.3, 7.0, 1.3 Hz, 1H), 8.16 (ddd, *J* = 8.3, 7.1, 1.2 Hz, 1H), 8.12 (ddd, *J* = 8.6, 7.3, 1.3 Hz, 1H), 7.97 (ddd, *J* = 8.0, 7.0, 1.0 Hz, 1H), 7.75 (tt, *J* = 7.4, 1.5 Hz, 1H), 7.66–7.71 (m, 3H), 7.63 (dd, *J* = 8.3, 0.6 Hz, 1H), 7.50–7.53 (m, 2H), 7.19 (ddd, *J* = 8.6, 7.1, 1.5 Hz, 1H).

<sup>13</sup>C NMR (150 MHz, Cl<sub>2</sub>CDCDCl<sub>2</sub>) δ 163.79, 159.73, 140.03, 138.18, 137.06, 135.48, 134.00, 133.77, 132.42, 131.73, 131.38, 131.14, 131.12, 130.73, 130.58, 130.42, 130.15, 129.93, 128.36, 127.54, 127.47, 127.31, 126.30, 124.55, 124.32, 120.54 (<sup>1</sup>J<sub>C-F</sub> = 321 Hz).<sup>[16]</sup>

<sup>19</sup>F NMR (560 MHz, Cl<sub>2</sub>CDCDCl<sub>2</sub>) δ -78.36.

HRMS (ESI<sup>+</sup>) *m/z* calcd for C<sub>27</sub>H<sub>17</sub>S<sup>+</sup> [M-OTf]<sup>+</sup>: 373.1045 found: 373.1046.

**[(2,7-Di-*tert*-butylphenanthrene-9,10-diyl)bis(sulfanediyl)]bis(2,1-phenylene) ]bis(phenylmethanone) (S9)**



The detail of synthesis was described on p27. Yellow solid. This product included some little impurities after PTLC.

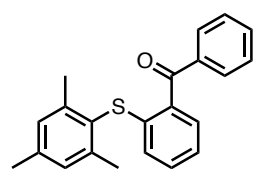
$^1\text{H NMR}$  (400 MHz,  $\text{CD}_2\text{Cl}_2$ )  $\delta$  8.62 (d,  $J = 8.7$  Hz, 2H), 8.51 (d,  $J = 2.0$  Hz, 2H), 7.74-7.82 (m, 6H), 7.57 (t,  $J = 7.3$  Hz, 2H), 7.40-7.47 (m, 6H), 7.02-7.11 (m, 4H), 6.73 (dd,  $J = 7.9, 1.6$  Hz, 2H), 1.28 (s, 18H).

$^{13}\text{C NMR}$  (100 MHz,  $\text{CD}_2\text{Cl}_2$ )  $\delta$  196.05, 150.52, 140.95, 139.09, 137.72, 136.06,

133.14, 131.95, 131.51, 131.27, 130.58, 129.88, 129.02, 128.69, 126.56, 125.38, 124.40, 122.97, 31.37.

HRMS (ESI<sup>+</sup>)  $m/z$  calcd for  $\text{C}_{48}\text{H}_{42}\text{S}_2\text{O}_2$  [ $\text{M}+\text{Na}$ ]<sup>+</sup>: 737.2518 found: 737.2511.

**(2-(Mesitylthio)phenyl)(phenyl)methanone (S11)**



The detail of synthesis was described on p27. Off-white solid.

$^1\text{H NMR}$  (400 MHz,  $\text{CD}_2\text{Cl}_2$ )  $\delta$  7.82 (d,  $J = 7.9$  Hz, 2H), 7.63 (t,  $J = 6.5$  Hz, 1H), 7.50 (t,  $J = 7.3$  Hz, 2H), 7.39 (d,  $J = 7.5$  Hz, 1H), 7.23 (td,  $J = 7.9, 1.7$  Hz, 1H), 7.13 (td,  $J = 7.3, 2.6$  Hz, 1H), 7.00 (s, 2H), 6.68 (dd,  $J = 7.9, 2.0$  Hz, 1H), 2.31

(s, 6H, and s, 3H).

$^{13}\text{C NMR}$  (100 MHz,  $\text{CD}_2\text{Cl}_2$ )  $\delta$  196.73, 143.91, 139.98, 139.89, 137.89, 136.62, 133.35, 131.42, 130.51, 130.44, 129.76, 128.79, 127.66, 126.54, 124.12, 21.73, 21.24.

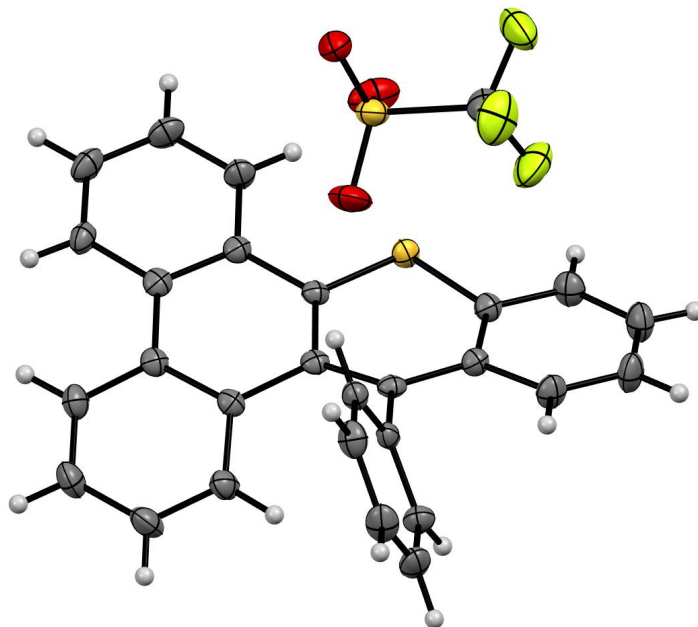
HRMS (ESI<sup>+</sup>)  $m/z$  calcd for  $\text{C}_{22}\text{H}_{20}\text{SO}$  [ $\text{M}+\text{Na}$ ]<sup>+</sup>: 355.1127 found: 355.1125.

**4-5. X-ray Crystal Structure Analysis<sup>[17,18,19]</sup>**

Details of the crystal data and a summary of the intensity data collection parameters for **3a'a** and **3a'a-OH** are listed in Table S1–S2. A single crystal of **3a'a** was prepared by vapor diffusion recrystallization using  $\text{Et}_2\text{O}$  and MeCN. A single crystal of **3a'a-OH** was prepared by vapor diffusion recrystallization using pentane and  $\text{CHCl}_3$ . A suitable crystal was mounted with mineral oil on a MiTeGen MicroMounts and transferred to the goniometer of the kappa goniometer of a RIGAKU XtaLAB Synergy-S system with 1.2 kW MicroMax-007HF microfocus rotating anode (Graphite-monochromated Mo  $K_\alpha$  radiation ( $\lambda = 0.71073$  Å)) and PILATUS200K hybrid photon-counting detector. Cell parameters were determined and refined, and raw frame data were integrated using CrysAlis<sup>Pro</sup> (Agilent Technologies, 2010). The structures were solved by direct methods with SHELXT<sup>[17]</sup> and refined by full-matrix least-squares techniques against  $F^2$  (SHELXL-2018/3)<sup>[18]</sup> by using Olex2 software package.<sup>[19]</sup> The intensities were corrected for Lorentz and polarization effects. The non-hydrogen atoms were refined anisotropically. Hydrogen atoms were placed using AFIX instructions. CCDC 2216401 and 2216402 contain the supplementary crystallographic data for this paper. These data can be obtained free of charge from The Cambridge Crystallographic Data Centre via [www.ccdc.cam.ac.uk/data\\_request/cif](http://www.ccdc.cam.ac.uk/data_request/cif).

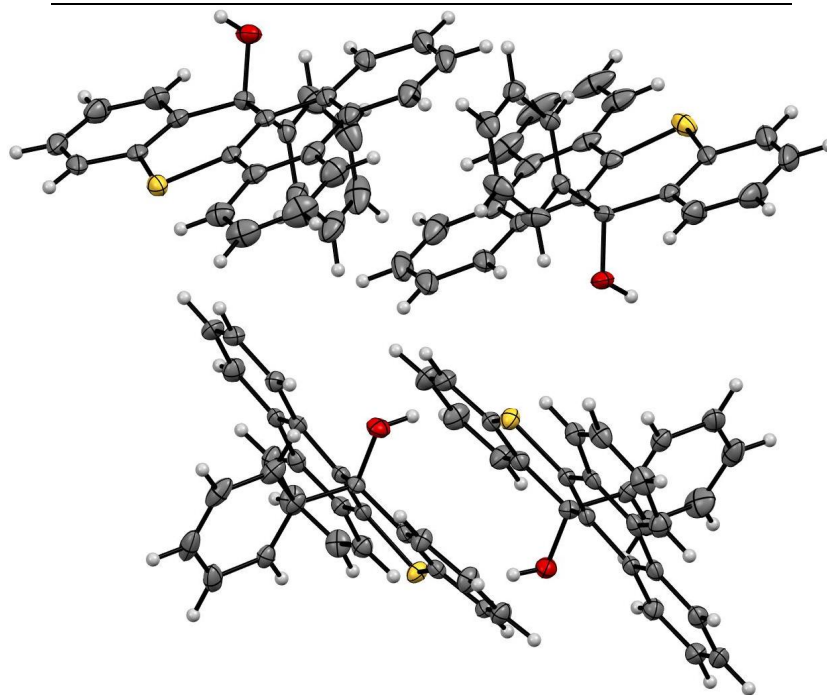
**Table S1.** Crystallographic data and structure refinement details for **3a'a**.

CCDC deposition No.	2216401
formula	C <sub>28</sub> H <sub>17</sub> F <sub>3</sub> O <sub>3</sub> S <sub>2</sub>
FW	522.53
<i>T</i> (K)	123(2) K
$\lambda$ (Å)	0.71073 Å
cryst syst	Monoclinic
space group	<i>P</i> 2 <sub>1</sub> / <i>c</i>
<i>a</i> (Å)	10.1260(7)
<i>b</i> (Å)	29.3015(15)
<i>c</i> (Å)	8.1823(5)
$\alpha$ (deg)	90
$\beta$ (deg)	112.755(8)
$\gamma$ (deg)	90
<i>V</i> (Å <sup>3</sup> )	2238.8(3)
<i>Z</i>	4
<i>D</i> <sub>calc</sub> (g / cm <sup>3</sup> )	1.550
$\mu$ (mm <sup>-1</sup> )	0.295
F(000)	1072.0
cryst size (mm)	0.15 × 0.1 × 0.15
$\theta$ range (deg)	4.362° to 56.292°
reflns collected	19945
indep reflns/ <i>R</i> <sub>int</sub>	4682/0.0896
params	325
GOF on <i>F</i> <sup>2</sup>	1.070
<i>R</i> <sub>1</sub> , <i>wR</i> <sub>2</sub> [ <i>I</i> > 2 $\sigma$ ( <i>I</i> )]	0.0503, 0.1220
<i>R</i> <sub>1</sub> , <i>wR</i> <sub>2</sub> (all data)	0.0746, 0.1317

**Figure S1.** Crystallographic structure of **3a'a** with the thermal ellipsoid at a 50% probability level.

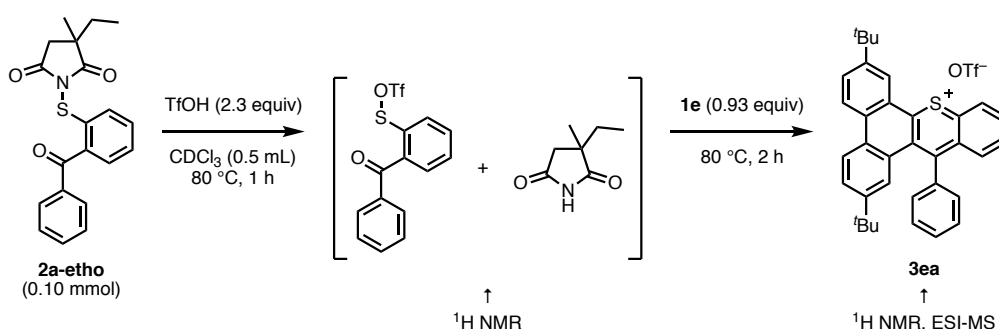
**Table S2.** Crystallographic data and structure refinement details for **3a'a -OH**.

CCDC deposition No.	2216402
formula	C <sub>108</sub> H <sub>72</sub> O <sub>4</sub> S <sub>4</sub>
FW	1561.89
<i>T</i> (K)	123(2) K
$\lambda$ (Å)	0.71073 Å
cryst syst	Triclinic
space group	<i>P</i> -1
<i>a</i> (Å)	12.4701(3)
<i>b</i> (Å)	13.9402(3)
<i>c</i> (Å)	22.0459(5)
$\alpha$ (deg)	86.3365(19)
$\beta$ (deg)	81.0292(18)
$\gamma$ (deg)	87.2974(17)
<i>V</i> (Å <sup>3</sup> )	3775.07(14)
<i>Z</i>	2
<i>D</i> <sub>calc</sub> (g / cm <sup>3</sup> )	1.374
$\mu$ (mm <sup>-1</sup> )	0.188
F(000)	1632.0
cryst size (mm)	0.1 × 0.1 × 0.1
$\theta$ range (deg)	3.308° to 56.496°
reflns collected	59446
indep reflns/ <i>R</i> <sub>int</sub>	15650/0.0764
params	1061
GOF on <i>F</i> <sup>2</sup>	1.014
<i>R</i> <sub>1</sub> , <i>wR</i> <sub>2</sub> [ <i>I</i> > 2 $\sigma$ ( <i>I</i> )]	0.0558, 0.1093
<i>R</i> <sub>1</sub> , <i>wR</i> <sub>2</sub> (all data)	0.1005, 0.1223

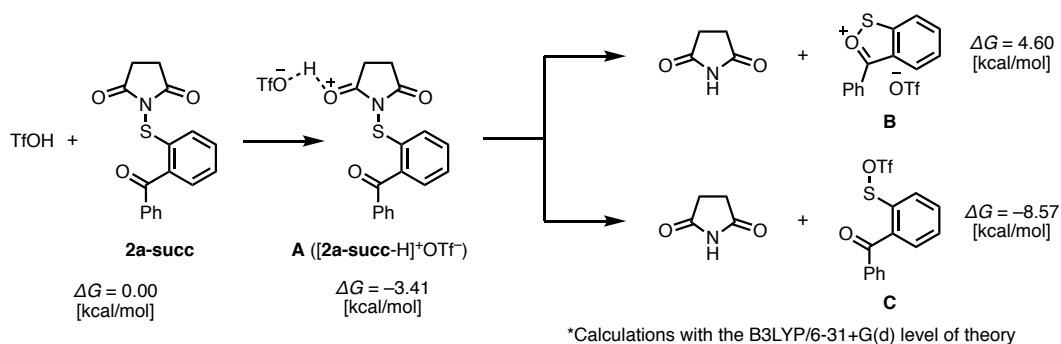
**Figure S2.** Crystallographic structure of **3a'a -OH** with the thermal ellipsoid at a 50% probability level.

#### 4-6. Reaction process

The reaction progress of thia-APEX was traced by  $^1\text{H}$  NMR (Figure S3). First, the mixture of **2a-etho** (37.7 mg, 0.107 mmol, 1.0 eq), TfOH (20  $\mu\text{L}$ , 0.23 mmol, 2.1 equiv) in  $\text{CDCl}_3$  (0.5 mL) was stirred in a screw-capped tube at 80  $^\circ\text{C}$  for an hour. Then, the resulting mixture was analyzed in an NMR tube by  $^1\text{H}$  NMR spectroscopy and a spectrum shown in Figure S6 was obtained. Observed peaks in this spectrum were considered to correspond to a mixture of sulfenyl trifluoromethanesulfonate and ethosuximide, which was rationalized by the overall downfield-shifted peaks in Figure S6 compared with a spectrum of **2a-etho** before the addition of TfOH (Figure S5). According to the DFT calculations on protonation of **2a-succ** with TfOH, the formation of intermediate **C** is thermodynamically the more feasible than those of intermediates **A** and **B** (Figure S4. Each detailed cartesian coordinate and Gibbs free energy was described in the section of DFT calculation. **2a-succ** was adopted instead of **2a-etho** for simplification of calculations.). Next, 2,7-di-*tert*-butylphenanthrene (**1e**) (28.9 mg, 0.0995 mmol, 0.93 equiv) was added to the mixture prepared from the reaction of **2a-etho** with TfOH, and the mixture was stirred at 80  $^\circ\text{C}$  for 2 h. The resulting mixture was analyzed by  $^1\text{H}$  NMR and HR-ESI-MS. The  $^1\text{H}$  NMR spectra showed characteristic peaks ( $\delta$  (ppm): 8.55 (d,  $J = 9.0$  Hz), 8.46 (d,  $J = 8.4$  Hz), 8.39 (d,  $J = 8.4$  Hz), 8.27 (t,  $J = 8.1$  Hz), 8.16 (dd,  $J = 8.4, 1.8$  Hz), 8.06 (ddd,  $J = 8.4, 7.0, 1.3$  Hz)) (Figure S7). HR-ESI-MS analysis showed the peak of  $m/z = 485.2298$  (calcd. for  $[\text{M}-\text{OTf}]^+$ : 485.2297). These spectral evidences support the formation of thiopyrylium **3ea**.



**Figure S3.** Tracing experiment in thia-APEX reaction by  $^1\text{H}$  NMR.



**Figure S4.** Possible intermediates and their thermodynamic stability in thia-APEX reaction.

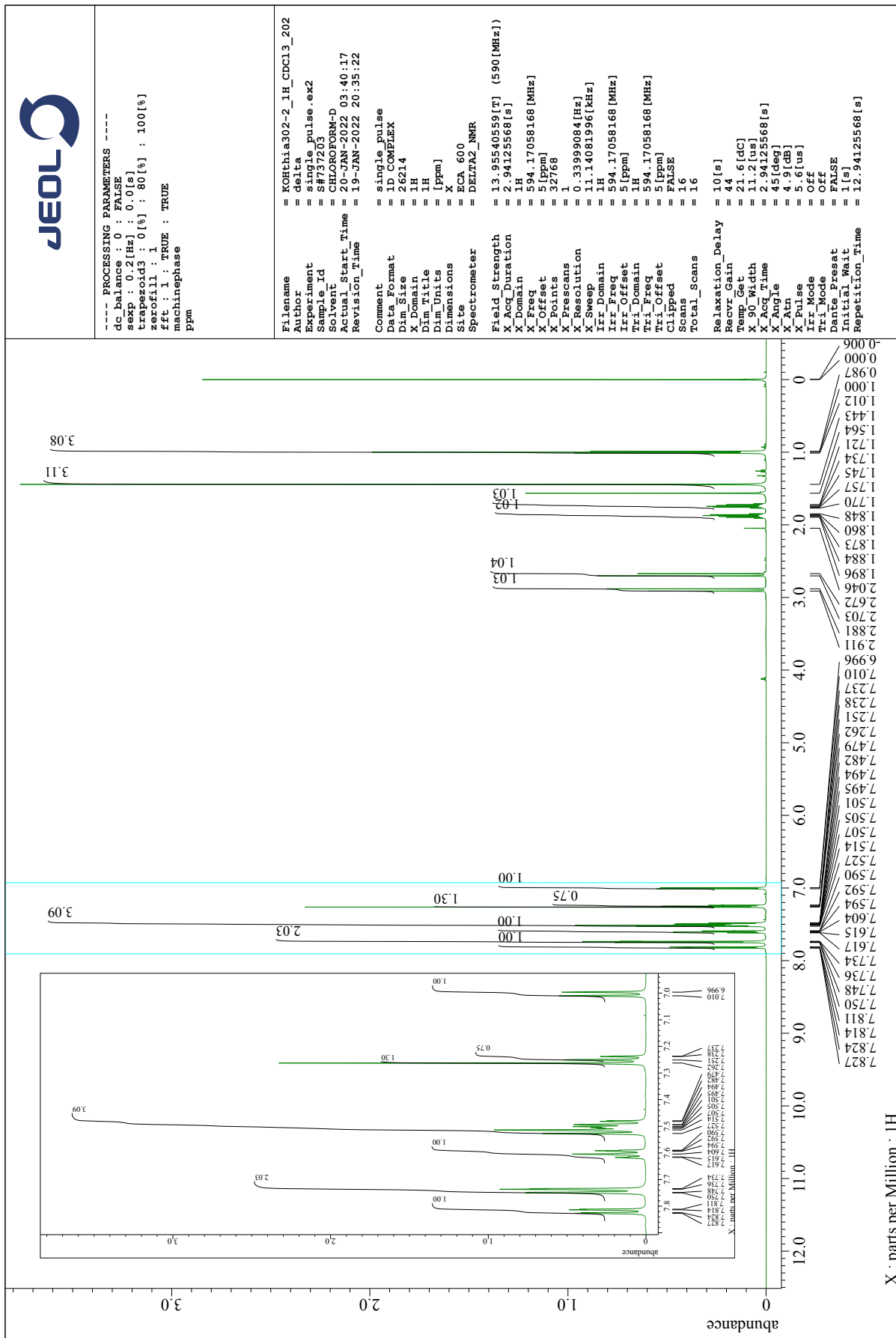
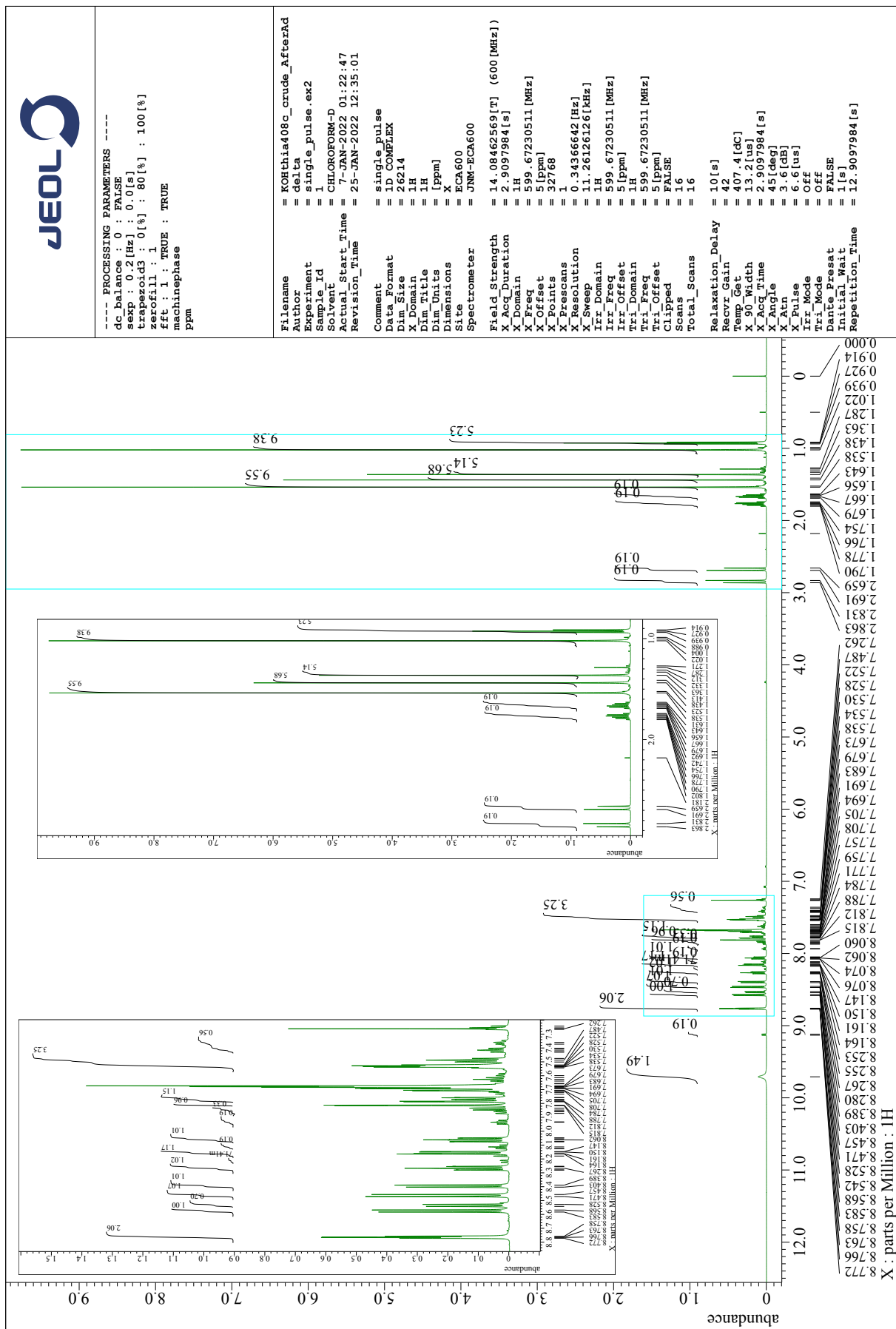
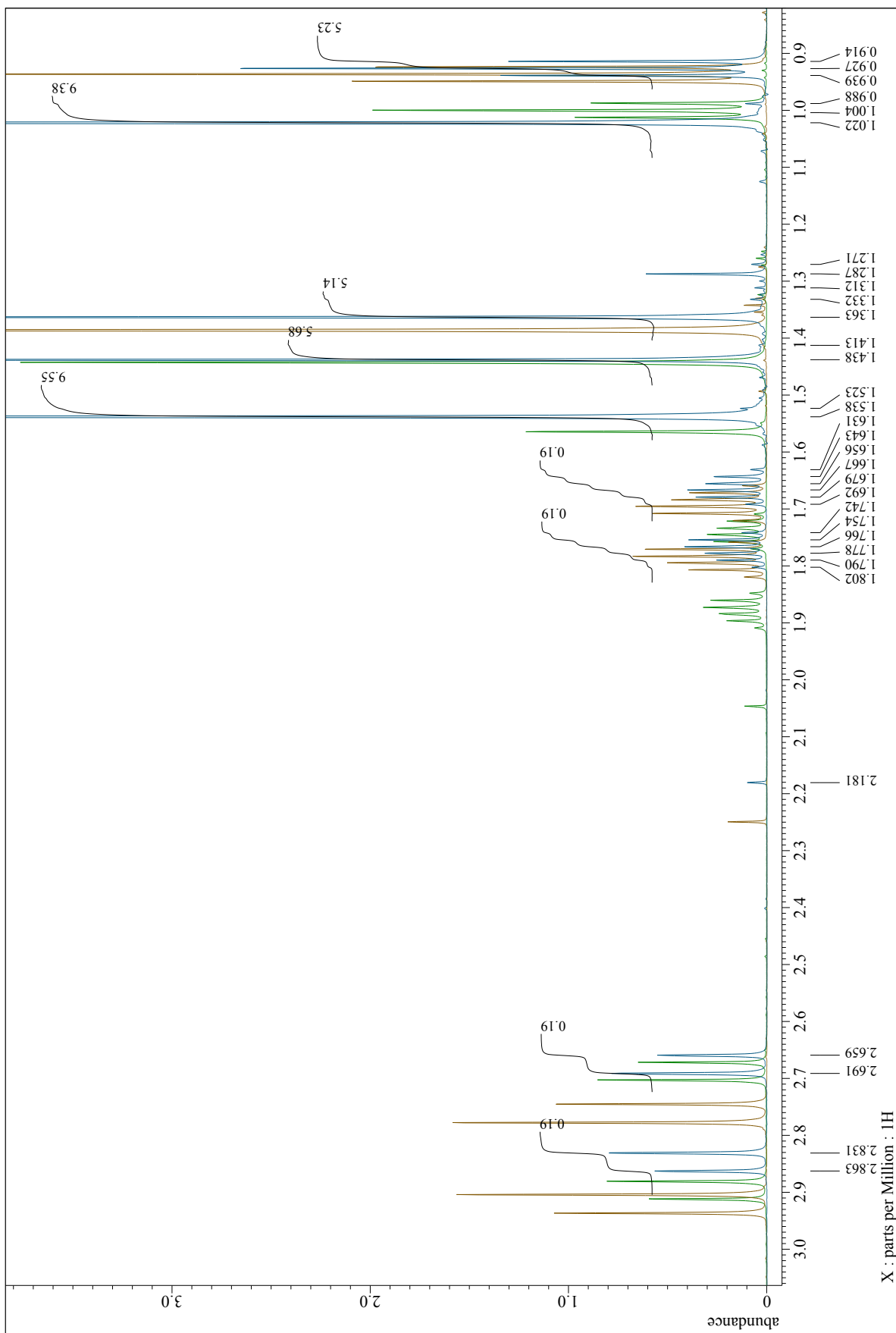


Figure S5. <sup>1</sup>H NMR spectra of **2a-etho** in CDCl<sub>3</sub>.

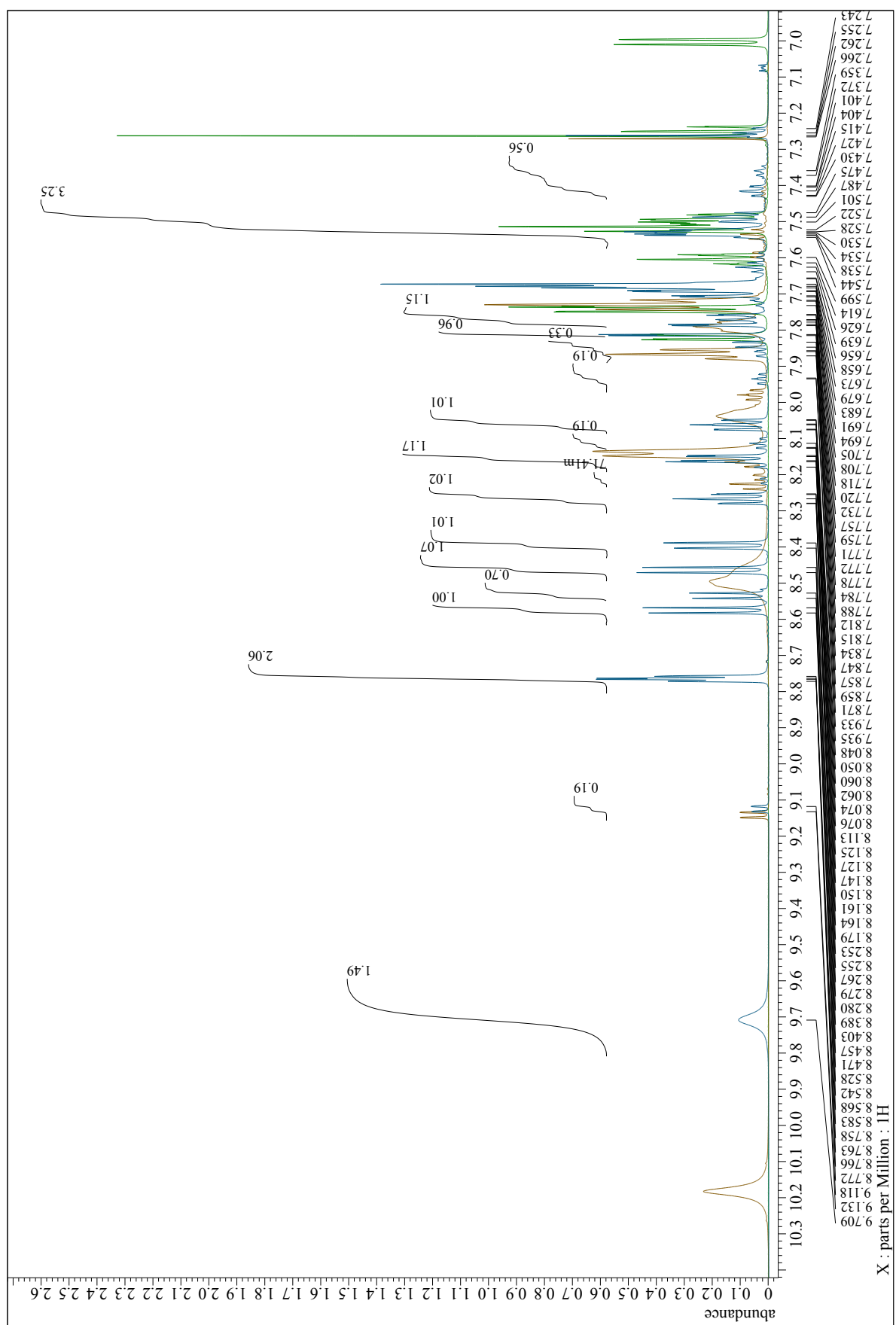






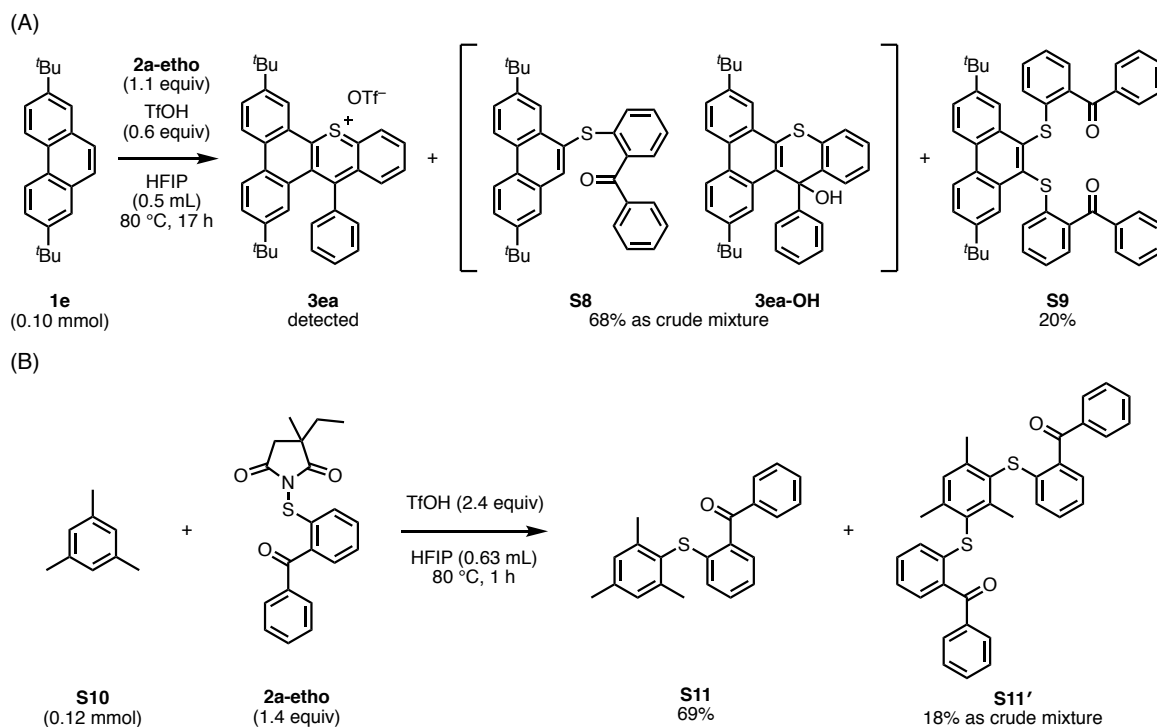


**Figure S8.** An overlay image of Figure S5–S7. Green line: Figure S5, **2a-etho**. Brown line: Figure S6, **2a-etho** + TfOH. Blue line: Figure S7, after addition of substrate **1e**.



**Figure S9.** An overlay image of Figure S5–S7. Green line: Figure S5, **2a-etho**. Brown line: Figure S6, **2a-etho** + TfOH. Blue line: Figure S7, after addition of substrate **1e**.

In addition, two experiments shown in Figure S10 supported a formation of thioether intermediate **S8**. When the thia-APEX reaction of **1e** (29.9 mg, 0.102 mmol) with 0.6 equiv of TfOH was examined, thioether **S8** and **S9** were afforded (Figure S10A). Although **S8** was obtained as a complex mixture with OH-adduct **3ea-OH** (HRMS (ESI<sup>+</sup>) *m/z* calcd for C<sub>35</sub>H<sub>34</sub>SO [M+Na]<sup>+</sup>: 525.2223 found: 525.2222.) and some impurities, **S9** was isolated in 20% yield (14.4 mg, 0.0201 mmol) by using PTLC (hexane/AcOEt = 10:1). Furthermore, thioether **S11** was obtained in 69% yield (28.0 mg, 0.0842 mmol) from mesitylene (**S10**) (15.2 mg, 97% purity, 0.123 mmol) under the general reaction conditions of thia-APEX (Figure S10B). These results show the first step of thia-APEX is a C–H/C–S bond formation.



**Figure S10.** Confirmation of C–H/C–S bond formation as the first step of thia-APEX.

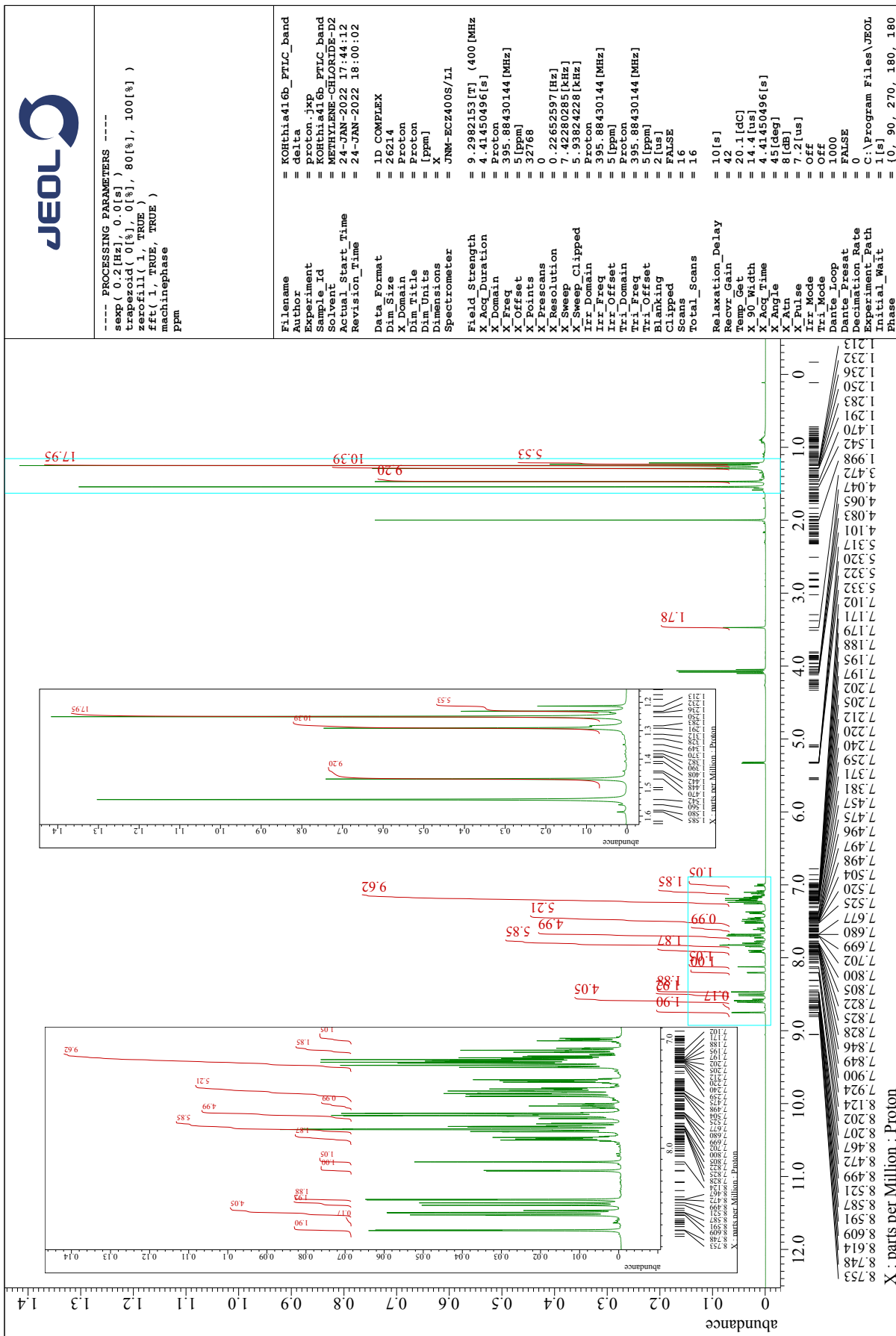
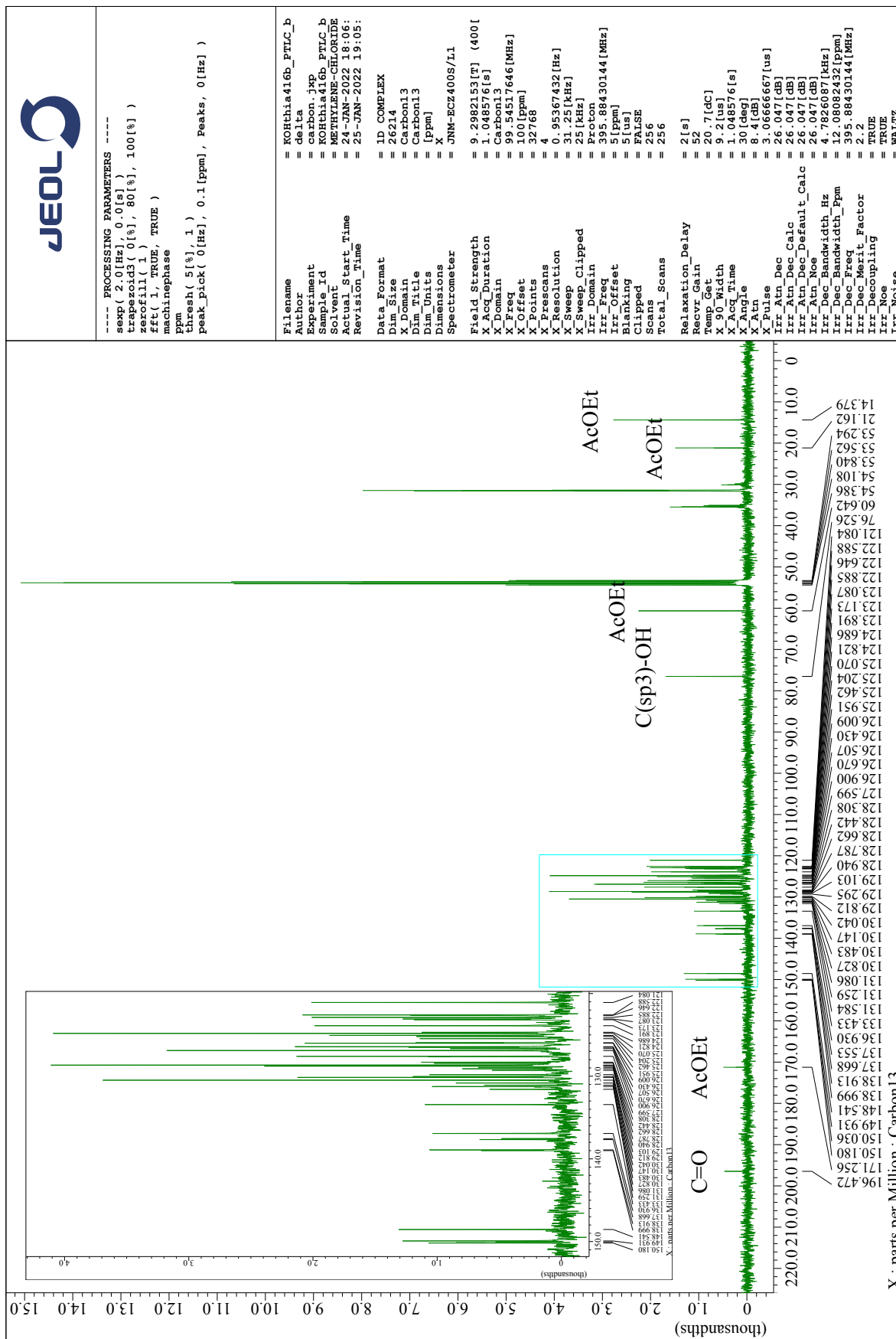


Figure S11. <sup>1</sup>H NMR spectra of mixture S8 + 3ea-OH.



**Figure S12.**  $^{13}\text{C}$  NMR spectra of mixture of **S8** and **3ea-OH**. The  $\text{sp}^3$ -carbon peak bonded with hydroxy group ( $\text{C}(\text{sp}^3)\text{-OH}$ ) was assigned at 76.53 ppm by referring to the  $^{13}\text{C}$  NMR of **3a'a-OH**.

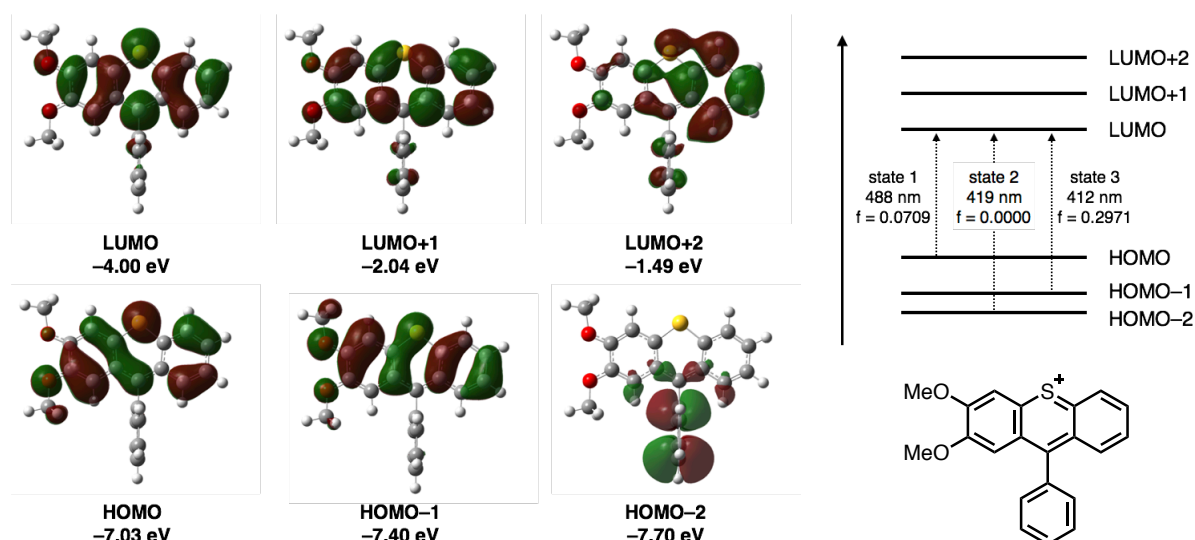
#### 4-7. DFT calculations

The Gaussian 16 program, revision C.01,<sup>[20]</sup> was used for all computational investigations. Following the literature,<sup>[21]</sup> geometry optimizations and harmonic vibration frequency calculations of the all local minima (with no imaginary frequency) were conducted using the B3LYP/6-31+G(d) or B3LYP/6-311+G(2d,p) level of theories in the gas phase at 298.15 K without any symmetry assumptions,<sup>[22]</sup> and those accurate energies were estimated by the single-point calculations of optimized geometries with the B3LYP/6-311++G(2d,p) level of theory in CH<sub>2</sub>Cl<sub>2</sub> (IEF-PCM<sup>[23]</sup>) as needed.<sup>[22]</sup> For investigations on photophysical properties, thiopyrylium salts **3aa–3ca**, **3ea–3ga** and their corresponding cations **3aa’–3ca’** and **3ea’–3ga’** were calculated by TD-DFT methods. Zero-point energy, enthalpy, and Gibbs free energy were estimated from the gas-phase unless otherwise noted. Harmonic vibration frequency calculations at the same level were performed to verify all stationary points as local minima with no imaginary frequency. Visualization of the results was performed by use of GaussView 6.1 software.<sup>[24]</sup>

**Table S3.** Uncorrected and thermal-corrected energies of optimized geometries (Hartree).<sup>a</sup>

Structure	<i>E</i>	<i>ZPE</i>	<i>H</i>	<i>G</i>	basis set
<b>3aa’ (M<sup>+</sup>)</b>	-1359.173577	0.324002	-1358.828325	-1358.899749	6-311+G(2d,p)
<b>3aa (M<sup>+</sup> + OTf)</b>	-2321.056727	0.351456	-2320.674646	-2320.770225	6-311+G(2d,p)
<b>3ba’ (M<sup>+</sup>)</b>	-1359.167933	0.323548	-1358.823068	-1358.894223	6-311+G(2d,p)
<b>3ba (M<sup>+</sup> + OTf)</b>	-2321.050912	0.350799	-2320.669306	-2320.765536	6-311+G(2d,p)
<b>3ca’ (M<sup>+</sup>)</b>	-1359.157507	0.323413	-1358.812794	-1358.884500	6-311+G(2d,p)
<b>3ca (M<sup>+</sup> + OTf)</b>	-2321.041160	0.350535	-2320.659752	-2320.757000	6-311+G(2d,p)
<b>3ea’ (M<sup>+</sup>)</b>	-1752.003206	0.575584	-1751.394973	-1751.490225	6-311+G(2d,p)
<b>3ea (M<sup>+</sup> + OTf)</b>	-2713.881969	0.603424	-2713.236703	-2713.356459	6-311+G(2d,p)
<b>3fa’ (M<sup>+</sup>)</b>	-1828.253218	0.588127	-1827.631716	-1827.728094	6-311+G(2d,p)
<b>3fa (M<sup>+</sup> + OTf)</b>	-2790.133400	0.615899	-2789.474911	-2789.595285	6-311+G(2d,p)
<b>3ga’ (M<sup>+</sup>)</b>	-1513.663533	0.364920	-1513.276538	-1513.350081	6-311+G(2d,p)
<b>3ga (M<sup>+</sup> + OTf)</b>	-2475.542387	0.392555	-2475.118452	-2475.217026	6-311+G(2d,p)
<b>3ga-isomer’ (M<sup>+</sup>)</b>	-1513.656375	0.365257	-1513.269285	-1513.340811	6-311+G(2d,p)
<b>3ga-isomer (M<sup>+</sup> + OTf)</b>	-2475.529945	0.392736	-2475.106021	-2475.203207	6-311+G(2d,p)
<b>9-phenylthioxanthylum’ (M<sup>+</sup>)</b>	-1130.042758	0.259179	-1129.767735	-1129.826584	6-311+G(2d,p)
<b>3aa-CH</b>	-999.905270	0.338333	-999.546309	-999.615832	6-311+G(2d,p)
<b>3aa-N</b>	-1015.953095	0.326574	-1015.606033	-1015.675934	6-311+G(2d,p)
<b>3aa-NH’ (M<sup>+</sup>)</b>	-1016.356826	0.340495	-1015.995662	-1016.064950	6-311+G(2d,p)
<b>3aa-O’ (M<sup>+</sup>)</b>	-1036.204036	0.327369	-1035.856163	-1035.924869	6-311+G(2d,p)
<b>3ea-CH</b>	-1392.740662	0.590575	-1392.118033	-1392.211828	6-311+G(2d,p)
<b>3ea-N</b>	-1408.793098	0.578641	-1408.182536	-1408.276224	6-311+G(2d,p)
<b>3ea-NH’ (M<sup>+</sup>)</b>	-1409.192488	0.592375	-1408.567917	-1408.662278	6-311+G(2d,p)
<b>3ea-O’ (M<sup>+</sup>)</b>	-1429.041580	0.579115	-1428.430392	-1428.524379	6-311+G(2d,p)
<b>TfOH</b>	-962.034489	0.038120	-961.987579	-962.029424	6-31+G(d)
<b>succinimide</b>	-360.685186	0.092192	-360.586136	-360.623202	6-31+G(d)
<b>2a-succ</b>	-1334.298058	0.263534	-1334.014565	-1334.085540	6-31+G(d)
<b>Intermediate A</b>	-2296.356201	0.303157	-2296.023745	-2296.120394	6-31+G(d)
<b>Intermediate B</b>	-1935.641934	0.210731	-1935.409697	-1935.484434	6-31+G(d)
<b>Intermediate C</b>	-1935.663611	0.211144	-1935.431196	-1935.505426	6-31+G(d)

a) *E*: electronic energy; *ZPE*: zero-point energy; *H* (enthalpy) = *E* + *TCE*: sum of electronic energy (*E*) and thermal correction to enthalpy; *G* (free energy) = *E* + *TCF*: sum of electronic energy (*E*) and thermal corrections to free energies.

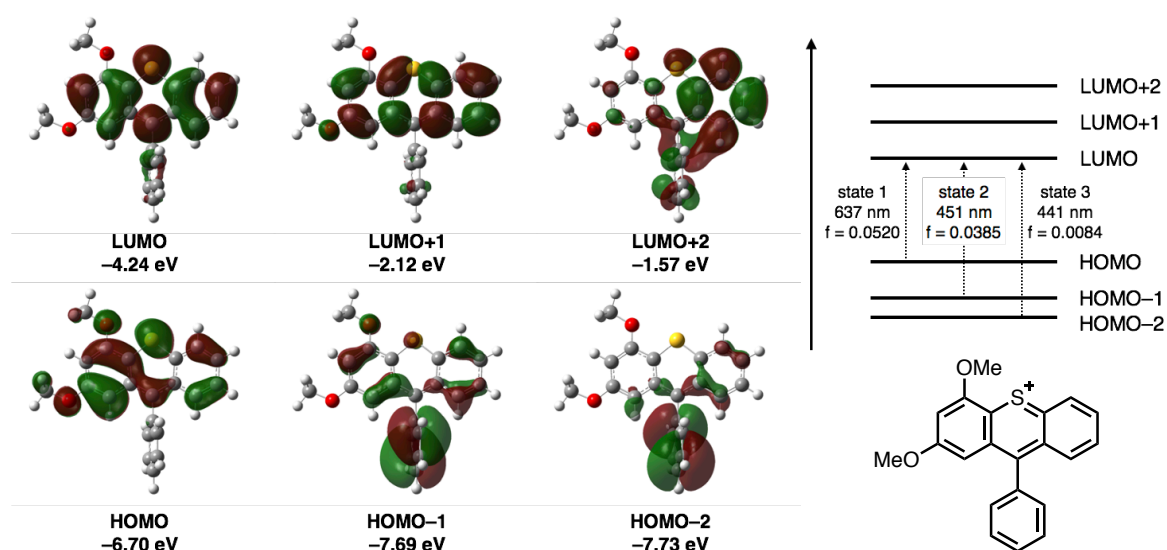


**Figure S13.** Representative frontier orbitals of **3aa'** ( $M^+$ ) (isovalue = 0.02). Geometry optimization was conducted with the B3LYP/6-311+G(2d,p) level of theory. The following single TD-DFT calculation was conducted with the B3LYP/6-311++G(2d,p) level of theory with consideration of IEF-PCM ( $CH_2Cl_2$ ).

**Table S4.** Results of TD-DFT calculations for **3aa'** ( $M^+$ ). Geometry optimization was conducted with the B3LYP/6-311+G(2d,p) level of theory. The following single point TD-DFT calculation was conducted with the B3LYP/6-311++G(2d,p) level of theory with consideration of IEF-PCM ( $CH_2Cl_2$ ).

Excited state	Energy gap [eV]	Wavelength [nm]	Oscillator strength ( <i>f</i> )	Electronic transition
1	2.5410	487.93	0.0709	HOMO -> LUMO (0.69244)
2	2.9571	419.28	0.0000	HOMO-2 -> LUMO (0.70529)
3	3.0079	412.2	0.2971	HOMO-3 -> LUMO (0.36430) HOMO-1 -> LUMO (0.58449)
4	3.0627	404.82	0.1094	HOMO-3 -> LUMO (0.60441) HOMO-1 -> LUMO (-0.35343)

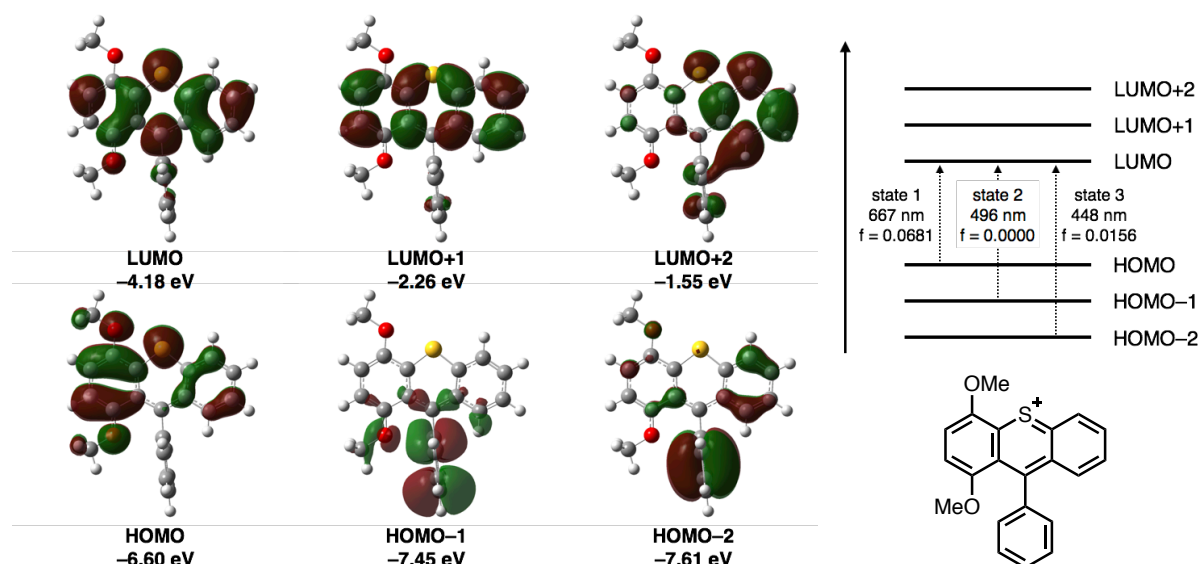




**Figure S14.** Representative frontier orbitals of **3ba'** ( $M^+$ ) (isovalue = 0.02). Geometry optimization was conducted with the B3LYP/6-311+G(2d,p) level of theory. The following single point TD-DFT calculation was conducted with the B3LYP/6-311++G(2d,p) level of theory with consideration of IEF-PCM ( $CH_2Cl_2$ ).

**Table S5.** Results of TD-DFT calculations for **3ba'** ( $M^+$ ). Geometry optimization was conducted with the B3LYP/6-311+G(2d,p) level of theory. The following single point TD-DFT calculation was conducted with the B3LYP/6-311++G(2d,p) level of theory with consideration of IEF-PCM ( $CH_2Cl_2$ ).

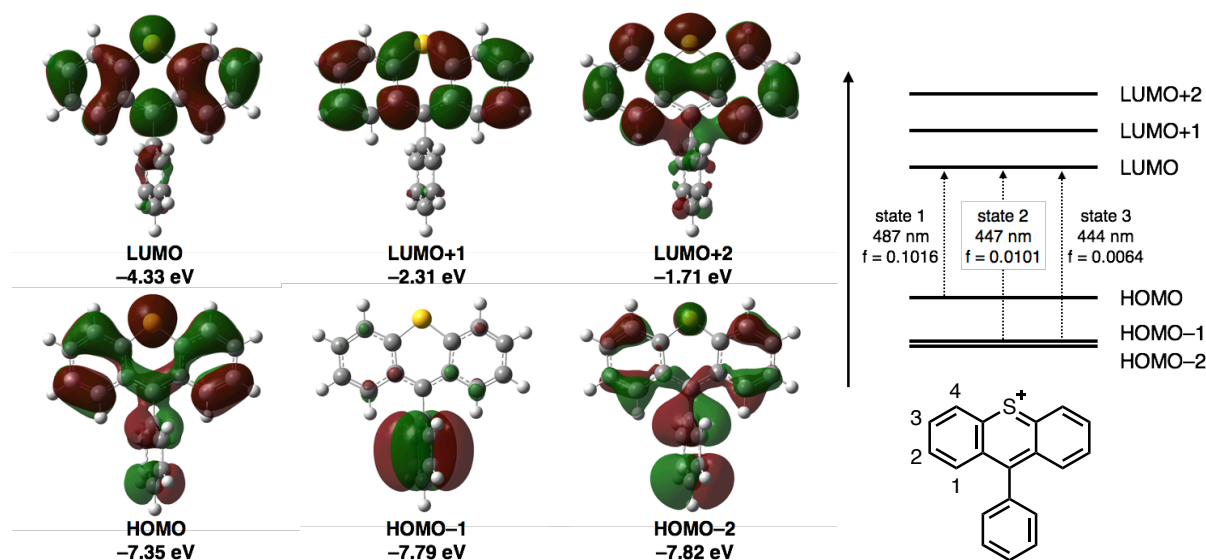
Excited state	Energy gap [eV]	wavelength [nm]	Oscillator strength ( <i>f</i> )	Electronic transition
1	1.9471	636.75	0.0520	HOMO -> LUMO (0.70356)
2	2.7494	450.95	0.0385	HOMO-2 -> LUMO (0.43630) HOMO-1 -> LUMO (0.55194)
3	2.8104	441.16	0.0084	HOMO-2 -> LUMO (0.55250) HOMO-1 -> LUMO (-0.43294)
4	3.1822	389.62	0.0472	HOMO-4 -> LUMO (0.66889) HOMO-3 -> LUMO (-0.19191)



**Figure S15.** Representative frontier orbitals of **3ca'** ( $M^+$ ) (isovalue = 0.02). Geometry optimization was conducted with the B3LYP/6-311+G(2d,p) level of theory. The following single TD-DFT calculation was conducted with the B3LYP/6-311++G(2d,p) level of theory with consideration of IEF-PCM ( $CH_2Cl_2$ ).

**Table S6.** Results of TD-DFT calculations for **3ca'** ( $M^+$ ). Geometry optimization was conducted with the B3LYP/6-311+G(2d,p) level of theory. The following single point TD-DFT calculation was conducted with the B3LYP/6-311++G(2d,p) level of theory with consideration of IEF-PCM ( $CH_2Cl_2$ ).

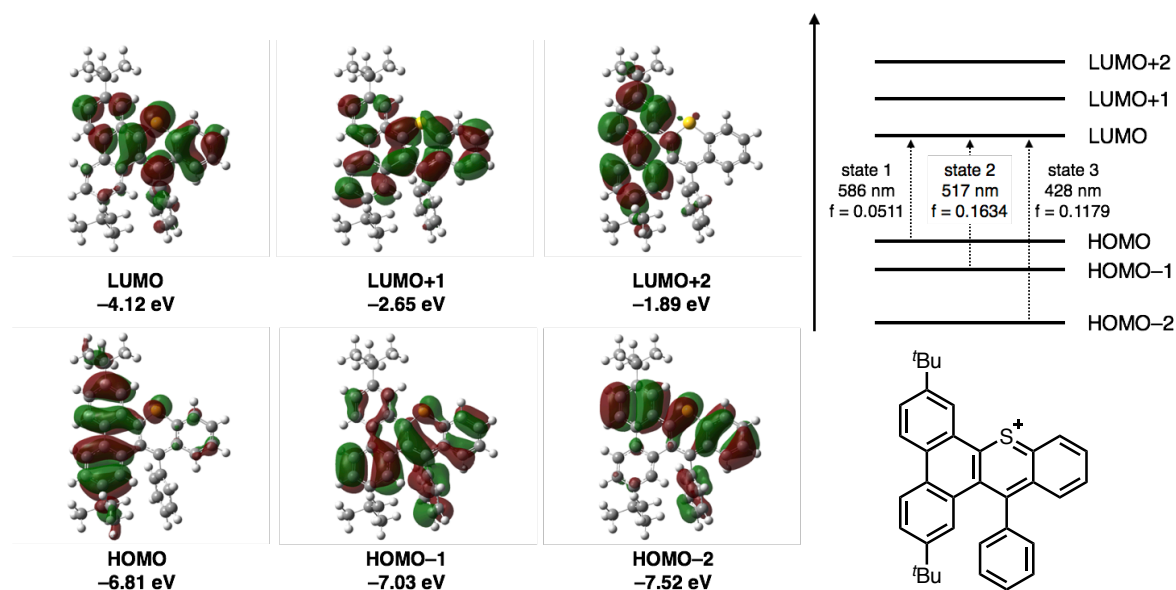
Excited state	Energy gap [eV]	wavelength [nm]	Oscillator strength ( <i>f</i> )	Electronic transition
1	1.8593	666.82	0.0681	HOMO -> LUMO (0.70525)
2	2.4982	496.30	0.0000	HOMO-1 -> LUMO (0.70518)
3	2.7669	448.10	0.0156	HOMO-2 -> LUMO (0.70347)
4	3.0794	402.63	0.0610	HOMO-3 -> LUMO (0.69453)



**Figure S16.** Representative frontier orbitals of 9-phenylthiopyrylium' ( $M^+$ ) (isovalue = 0.02). Geometry optimization was conducted with the B3LYP/6-311+G(2d,p) level of theory. The following single TD-DFT calculation was conducted with the B3LYP/6-311++G(2d,p) level of theory with consideration of IEF-PCM ( $CH_2Cl_2$ ).

**Table S7.** Results of TD-DFT calculations for 9-phenylthiopyrylium' ( $M^+$ ). Geometry optimization was conducted with the B3LYP/6-311+G(2d,p) level of theory. The following single point TD-DFT calculation was conducted with the B3LYP/6-311++G(2d,p) level of theory with consideration of IEF-PCM ( $CH_2Cl_2$ ).

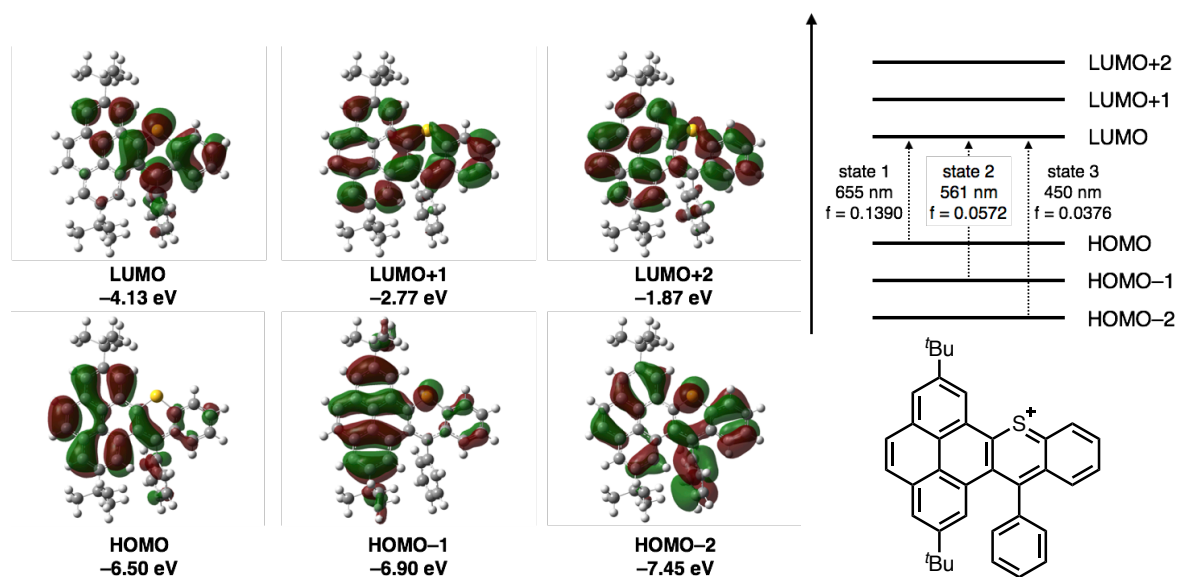
Excited state	Energy gap [eV]	Wavelength [nm]	Oscillator strength ( $f$ )	Electronic transition
1	2.5446	487.24	0.1016	HOMO -> LUMO (0.69734)
2	2.7723	447.23	0.0101	HOMO-2 -> LUMO (0.69923)
3	2.7934	443.84	0.0064	HOMO-1 -> LUMO (0.70558)
4	3.4641	357.91	0.1996	HOMO-4 -> LUMO (0.32263) HOMO-3 -> LUMO (0.60063) HOMO -> LUMO+1 (-0.17819)



**Figure S17.** Representative frontier orbitals of **3ea'** ( $M^+$ ) (isovalue = 0.02). Geometry optimization was conducted with the B3LYP/6-311+G(2d,p) level of theory. The following single TD-DFT calculation was conducted with the B3LYP/6-311++G(2d,p) level of theory with consideration of IEF-PCM ( $CH_2Cl_2$ ).

**Table S8.** Results of TD-DFT calculations for **3ea'** ( $M^+$ ). Geometry optimization was conducted with the B3LYP/6-311+G(2d,p) level of theory. The following single point TD-DFT calculation was conducted with the B3LYP/6-311++G(2d,p) level of theory with consideration of IEF-PCM ( $CH_2Cl_2$ ).

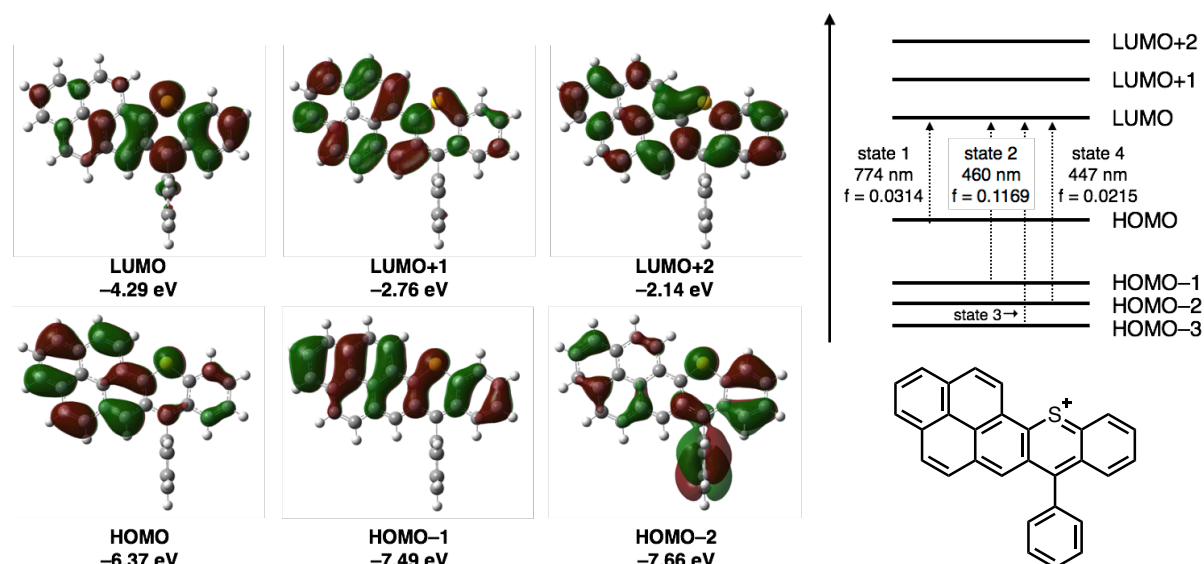
Excited state	Energy gap [eV]	wavelength [nm]	Oscillator strength ( <i>f</i> )	Electronic transition
1	2.1164	585.82	0.0511	HOMO -> LUMO (0.70314)
2	2.3904	518.68	0.1634	HOMO-1 -> LUMO (0.69873)
3	2.8986	427.74	0.1179	HOMO-3 -> LUMO (-0.23475) HOMO-2 -> LUMO (0.65402)
4	2.9754	416.69	0.0811	HOMO-3 -> LUMO (0.66295) HOMO-2 -> LUMO (0.22420)



**Figure S18.** Representative frontier orbitals of **3fa'** ( $M^+$ ) (isovalue = 0.02). Geometry optimization was conducted with the B3LYP/6-311+G(2d,p) level of theory. The following single TD-DFT calculation was conducted with the B3LYP/6-311++G(2d,p) level of theory with consideration of IEF-PCM ( $CH_2Cl_2$ ).

**Table S9.** Results of TD-DFT calculations for **3fa'** ( $M^+$ ). Geometry optimization was conducted with the B3LYP/6-311+G(2d,p) level of theory. The following single point TD-DFT calculation was conducted with the B3LYP/6-311++G(2d,p) level of theory with consideration of IEF-PCM ( $CH_2Cl_2$ ).

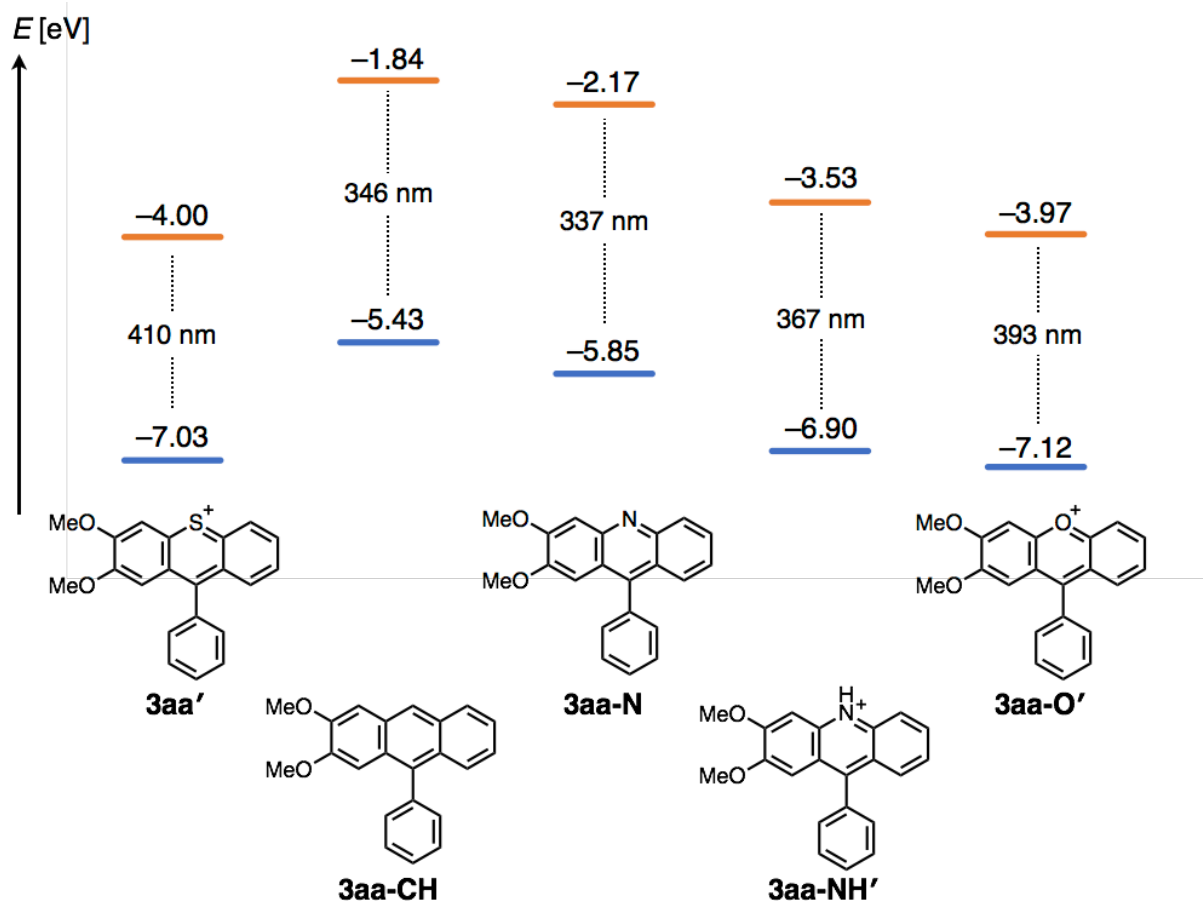
Excited state	Energy gap [eV]	wavelength [nm]	Oscillator strength ( <i>f</i> )	Electronic transition
1	1.8916	655.44	0.1390	HOMO -> LUMO (0.70296)
2	2.2106	560.87	0.0572	HOMO-1 -> LUMO (0.70071)
3	2.7534	450.30	0.0376	HOMO-2 -> LUMO (0.69428)
4	2.9676	417.79	0.0208	HOMO-3 -> LUMO (0.69667)



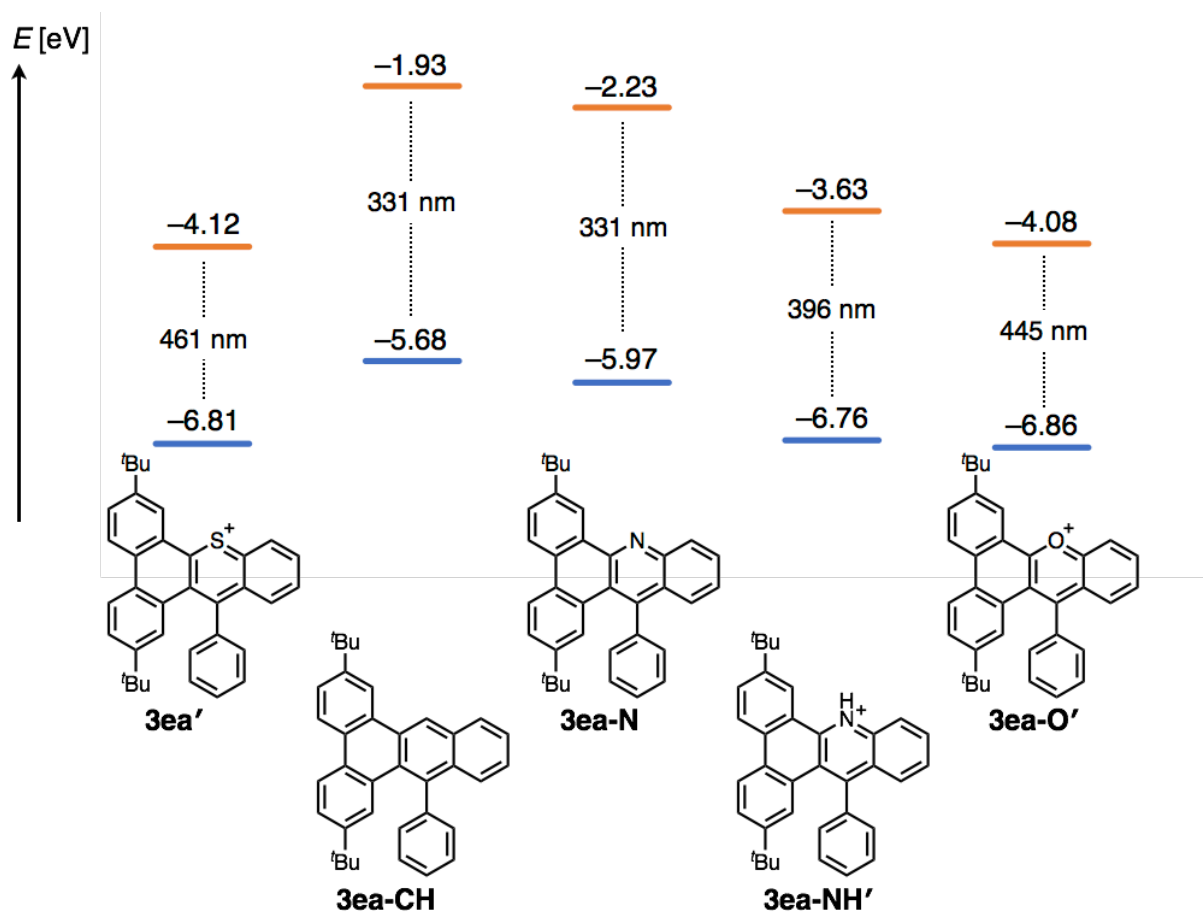
**Figure S19.** Representative frontier orbitals of **3ga'** ( $M^+$ ) (isovalue = 0.02). Geometry optimization was conducted with the B3LYP/6-311+G(2d,p) level of theory. The following single TD-DFT calculation was conducted with the B3LYP/6-311++G(2d,p) level of theory with consideration of IEF-PCM ( $CH_2Cl_2$ ).

**Table S10.** Results of TD-DFT calculations for **3ga'** ( $M^+$ ). Geometry optimization was conducted with the B3LYP/6-311+G(2d,p) level of theory. The following single point TD-DFT calculation was conducted with the B3LYP/6-311++G(2d,p) level of theory with consideration of IEF-PCM ( $CH_2Cl_2$ ).

Excited state	Energy gap [eV]	wavelength [nm]	Oscillator strength ( $f$ )	Electronic transition
1	1.6014	774.24	0.0314	HOMO $\rightarrow$ LUMO (0.70576)
2	2.6965	459.80	0.1169	HOMO-3 $\rightarrow$ LUMO (-0.20530) HOMO-2 $\rightarrow$ LUMO (0.10938) HOMO-1 $\rightarrow$ LUMO (0.61841) HOMO $\rightarrow$ LUMO+1 (0.21294)
3	2.7026	458.76	0.0149	HOMO-4 $\rightarrow$ LUMO (0.12327) HOMO-3 $\rightarrow$ LUMO (0.53010) HOMO-2 $\rightarrow$ LUMO (-0.37401) HOMO-1 $\rightarrow$ LUMO (0.23152)
4	2.7758	446.66	0.0215	HOMO-4 $\rightarrow$ LUMO (-0.20028) HOMO-3 $\rightarrow$ LUMO (0.41715) HOMO-2 $\rightarrow$ LUMO (0.53140)



**Figure S20.** Effects of heteroatom-substitutions on **3aa'** ( $M^+$ ). Geometry optimizations were conducted with the B3LYP/6-311+G(2d,p) level of theory. The following single point TD-DFT calculations were conducted with the B3LYP/6-311++G(2d,p) level of theory with consideration of IEF-PCM ( $CH_2Cl_2$ ). Each energy of orbitals was obtained by the TD-DFT calculations. The blue and orange lines are corresponding to HOMO and LUMO, respectively.



**Figure S21.** Effects of heteroatom-substitutions on **3ea'** ( $M^+$ ). Geometry optimization was conducted with the B3LYP/6-311+G(2d,p) level of theory. The following single point TD-DFT calculations were conducted with the B3LYP/6-311++G(2d,p) level of theory with consideration of IEF-PCM ( $CH_2Cl_2$ ). The blue and orange lines are corresponding to HOMO and LUMO, respectively.



**Table S11.** Cartesian coordinates of optimized **3aa'** (M<sup>+</sup>).

H	0.8765080	1.9756280	-0.0000480
H	-2.4023770	3.9594800	-2.1440080
H	-1.5602500	1.6410150	-2.1475110
H	-2.4015600	3.9597190	2.1441610
H	-2.8264140	5.1278020	0.0000920
H	-1.5594040	1.6412640	2.1476010
H	-5.3472720	-1.4215230	0.0001500
H	-3.6641640	0.3543100	0.0001400
H	4.9434050	-2.4046340	0.8978860
H	6.2596780	-1.6063870	-0.0000300
H	4.9434080	-2.4046610	-0.8979250
H	4.0197580	3.7651280	-0.0003730
H	2.5291900	3.3754420	0.8958160
H	2.5290910	3.3752040	-0.8962980
H	2.7789530	-2.6045710	-0.0000220
H	-4.6482640	-3.8077060	0.0000640
H	-2.2608870	-4.3974880	-0.0000080
C	3.2130410	-0.5089110	-0.0000390
C	2.3674760	-1.6050960	-0.0000210
C	2.6558350	0.8235800	-0.0000590
C	1.2980250	0.9838440	-0.0000370
C	0.9813500	-1.4347400	-0.0000070
C	0.3972390	-0.1274890	-0.0000020
C	-3.9008900	-3.0242100	0.0000590
C	-4.2950960	-1.6750320	0.0001040
C	-3.3522750	-0.6795570	0.0000970
C	-1.5004810	1.4873020	0.0000420
C	-1.7406950	2.1481690	-1.2068280
C	-1.7402170	2.1483100	1.2069300
C	-2.2154150	3.4558050	1.2037590
C	-2.4539160	4.1110410	0.0000780
C	-2.2158780	3.4556700	-1.2036210
C	-1.9586340	-0.9726120	0.0000390
C	5.1994890	-1.8396670	-0.0000280
C	3.1164120	3.1623040	-0.0002450
C	-1.5928250	-2.3474560	0.0000120
C	-0.9950850	0.0802890	0.0000250
C	-2.5654910	-3.3578440	0.0000170
O	3.5654500	1.8027180	-0.0000900
O	4.5337210	-0.5658380	-0.0000480
S	0.0490890	-2.8828290	-0.0000140

**Table S12.** Cartesian coordinates of optimized **3aa** (M<sup>+</sup> + OTf<sup>-</sup>).

H	0.2673660	-1.2549010	2.0811200
H	1.0230780	-4.4609640	-0.4252840
H	0.6114700	-2.0344190	-0.6845530
H	4.2192170	-3.6342140	2.3162770
H	2.8234770	-5.2679480	1.0798570
H	3.8374820	-1.2120620	2.0264460
H	5.6982970	0.2242200	-2.2381350
H	4.1081090	-0.9893450	-0.8328780
H	-2.9425740	3.9948090	2.2427670
H	-4.4585880	3.0673730	2.3483270
H	-3.4841950	2.9788390	0.8549180
H	-2.7971930	-2.2420670	3.7110080
H	-1.0190410	-2.1618160	3.7289910
H	-1.9035950	-2.2851240	2.1634850
H	-1.0857500	3.4007360	1.0751840
H	5.3978440	2.6609160	-2.6492030
H	3.4730580	3.8438130	-1.6726530
C	-1.6102330	1.5780240	2.0653820
C	-0.7730720	2.3975440	1.3258180
C	-1.1949170	0.2386600	2.3916140
C	-0.0123980	-0.2316230	1.8982420
C	0.4284090	1.9113610	0.8264370
C	0.8334440	0.5563980	1.0606130
C	4.6952540	2.1239030	-2.0240440
C	4.8660170	0.7504070	-1.7882490
C	3.9746850	0.0691770	-0.9976700
C	2.2091170	-1.4699060	0.6406330
C	1.4116570	-2.3912310	-0.0457390
C	3.2228600	-1.9245310	1.4880040
C	3.4379230	-3.2889350	1.6497430
C	2.6522120	-4.2051720	0.9569250
C	1.6435700	-3.7537590	0.1114410
C	2.8648590	0.7179110	-0.3894870
C	-3.4517890	3.0766720	1.9406630
C	-1.9211920	-1.8822770	3.1777340
C	2.7020390	2.0985080	-0.6723890
C	1.9601420	-0.0105610	0.4494160
C	3.6228250	2.7888850	-1.4760920
C	-3.0090430	-0.8975970	-2.6471950
O	-2.0687070	-0.4568730	3.1276750
O	-2.8075690	1.9243440	2.5039450
O	-0.7593910	-0.1279220	-1.5222410
O	-2.8809930	0.6525630	-0.5268100
O	-2.1851230	-1.7091780	-0.2821410
F	-3.0229150	0.1480250	-3.4907600
F	-4.2815940	-1.2473900	-2.4048110
F	-2.4127170	-1.9244350	-3.2771900
S	1.3589260	3.0223060	-0.1034090
S	-2.1097620	-0.4715730	-1.0606560

**Table S13.** Cartesian coordinates of optimized **3ba'** ( $M^+$ ).

H	1.4813880	1.7628400	2.0899670
H	2.8546320	3.8101460	2.0880840
H	3.7153770	3.2381440	-2.0738550
H	3.9677890	4.5620870	0.0057440
H	2.3778730	1.1671550	-2.0698650
H	4.8786890	-2.4215960	0.1074240
H	3.6759120	-0.2936880	0.1148140
H	3.6258980	-4.5684030	0.0189920
H	1.1695380	-4.5696230	-0.0271530
H	-5.1699500	-1.3632380	0.8977870
H	-5.1165000	-2.9125090	0.0220090
H	-5.1586030	-1.3878090	-0.8968110
H	-4.2815340	0.6114160	-0.0188440
H	-4.3519340	4.2166020	-0.1205990
H	-4.7234220	2.7499070	0.8128440
H	-4.7074050	2.7021370	-0.9812520
H	-0.3871350	2.3749640	-0.0643280
C	-3.2092800	0.4947320	-0.0138640
C	-2.6592170	-0.7702810	0.0058310
C	-2.3697410	1.6318170	-0.0387910
C	-0.9975250	1.4865840	-0.0337600
C	-1.2523480	-0.9362730	0.0094950
C	-0.3982640	0.2070020	0.0018810
C	3.0871490	-3.6290270	0.0220420
C	3.7971950	-2.4111690	0.0673980
C	3.1253930	-1.2210620	0.0690050
C	1.8399390	1.3249700	0.0107930
C	1.9727210	2.0819180	1.1784550
C	2.4796230	1.7452530	-1.1589560
C	3.2341750	2.9129430	-1.1598580
C	3.3730330	3.6572440	0.0070320
C	2.7459160	3.2371750	1.1756310
C	1.6968240	-1.1668880	0.0198360
C	1.0054800	-2.4188080	-0.0003780
C	1.0227460	0.0785930	0.0117490
C	1.7146320	-3.6336590	-0.0056340
C	-4.7942100	-1.8754290	0.0096710
C	-4.2461950	3.1359040	-0.0909400
O	-3.3614710	-1.9204990	0.0194920
O	-2.8359410	2.8928810	-0.0718730
S	-0.7049740	-2.5654260	-0.0003590

**Table S14.** Cartesian coordinates of optimized **3ba** ( $M^+$  + OTf<sup>-</sup>).

H	2.7162030	0.9994370	4.0434410
H	1.2556300	0.2648710	2.1839990
H	5.7573280	2.1191080	1.2318330
H	4.9635500	1.9370870	3.5733050
H	4.3247010	1.3426910	-0.6230700
H	4.4011020	-3.5136410	-0.8544210
H	3.8513490	-1.3707080	0.1817630
H	2.9844470	-4.4169840	-2.6910010
H	1.0009510	-3.1763050	-3.4442430
H	-3.9550960	0.8597210	-1.6043600
H	-4.2147040	0.3968820	-3.3096850
H	-3.9749690	2.1097390	-2.9050670
H	-2.5475620	3.1129140	-1.4467360
H	-1.9023720	5.7488860	0.9229820

H	-2.8397980	4.2717560	0.5989760
H	-2.2383440	5.2778300	-0.7576350
H	1.1962290	2.6872200	0.5688400
C	-1.6312360	2.5654160	-1.2910910
C	-1.4304080	1.3829620	-1.9660490
C	-0.6553280	3.0401970	-0.3900700
C	0.4896710	2.3150170	-0.1551420
C	-0.2544550	0.6327270	-1.7510210
C	0.7102160	1.0750670	-0.7979820
C	2.7415120	-3.4625570	-2.2403710
C	3.5460490	-2.9482960	-1.2025130
C	3.2405430	-1.7485220	-0.6238910
C	2.7050160	0.7446560	0.6642790
C	2.2481990	0.6565250	1.9836010
C	3.9732540	1.2675890	0.3996320
C	4.7798550	1.7033830	1.4451320
C	4.3320130	1.6033190	2.7586580
C	3.0708350	1.0781690	3.0229140
C	2.1162240	-0.9760390	-1.0481180
C	1.3028900	-1.5366600	-2.0772510
C	1.8246280	0.2698940	-0.4411580
C	1.6375950	-2.7711610	-2.6671010
C	-3.7027700	1.0846330	-2.6412450
C	-2.0216130	4.9052320	0.2476960
C	-2.6613270	-2.1242500	2.1965660
O	-2.3006150	0.8550930	-2.8563080
O	-0.7798250	4.2064070	0.2865350
O	-2.7239140	-0.3081920	0.2951840
O	-1.0223410	-0.0675790	2.0711080
O	-0.7882990	-1.8379670	0.3709690
F	-3.5509810	-1.4610000	2.9525460
F	-1.8478050	-2.8050890	3.0204260
F	-3.3375070	-3.0185280	1.4559660
S	-0.1488070	-0.8272490	-2.6373060
S	-1.6887080	-0.9486790	1.1109250

**Table S15.** Cartesian coordinates of optimized **3ca'** ( $M^+$ ).

H	-4.5283250	-1.1065690	2.1475700
H	-2.1952600	-0.3097990	2.1483160
H	-4.5350800	-1.0999230	-2.1406660
H	-5.7063450	-1.5136730	0.0046690
H	-2.2021290	-0.3028300	-2.1462830
H	-2.6082170	4.4443300	0.0002170
H	-2.7023330	2.0089120	0.0009870
H	-0.4129550	5.6154510	-0.0013420
H	1.6772520	4.3174750	-0.0015740
H	3.6550740	-2.9013310	0.0009330
H	1.4369250	-3.8890810	-0.0019930
H	-0.5722950	-4.4322290	-0.9011410
H	-2.0876790	-4.1513650	-0.0065710
H	-0.5745250	-4.4328960	0.8915590
H	5.4290900	-1.6024670	0.8984900
H	6.1598300	-0.2489420	0.0022930
H	5.4295280	-1.6018120	-0.8952790
C	2.7944970	-2.2469060	0.0003150
C	2.9587960	-0.8777390	0.0007220
C	1.5182810	-2.8132260	-0.0012380
C	0.3772230	-2.0365990	-0.0020830

C	1.8204000	-0.0504400	-0.0000380
C	0.4824730	-0.5805640	-0.0008450
C	-0.4504160	4.5331560	-0.0009760
C	-1.6905270	3.8706520	-0.0001440
C	-1.7430490	2.5015580	0.0002740
C	-2.0409630	-0.2679970	0.0008260
C	-2.7040540	-0.4877900	1.2081760
C	-2.7079330	-0.4838370	-1.2051070
C	-4.0229720	-0.9356420	-1.2005070
C	-4.6805730	-1.1666560	0.0035900
C	-4.0191630	-0.9394240	1.2063150
C	-0.5586680	1.7047580	-0.0002430
C	0.6786880	2.4077100	-0.0006850
C	-0.6465740	0.2755470	-0.0002910
C	0.7195830	3.8109700	-0.0011590
C	5.3590820	-0.9828810	0.0018150
C	-1.0135550	-3.9909560	-0.0051720
O	-0.8488200	-2.5674310	-0.0044440
O	4.1442540	-0.2240140	0.0017950
S	2.2119070	1.6297580	-0.0000160

**Table S16.** Cartesian coordinates of optimized **3ca** ( $M^+$  + OTf<sup>-</sup>).

H	-2.8989520	-3.6501980	1.0283620
H	-1.1989460	-1.8790760	0.7148650
H	-5.9011790	-1.0749380	-0.6338190
H	-5.2509310	-3.2615160	0.3401350
H	-4.2159540	0.7077460	-0.9049980
H	-3.3638290	2.2507360	3.7172170
H	-3.2785640	0.6515440	1.8810550
H	-1.7163120	4.1141020	3.8344580
H	0.0277480	4.3212500	2.1102560
H	2.2631790	0.4858130	-3.8868700
H	0.3879040	-1.0661070	-4.0551340
H	-1.6559260	-1.9037090	-4.3905760
H	-2.5731680	-2.7940480	-3.1503940
H	-0.7903170	-2.8476010	-3.1343860
H	3.9855750	1.0798840	-1.6599600
H	4.4565100	2.7953220	-1.8479950
H	4.0538290	1.8423080	-3.2907460
C	1.4527270	0.5581500	-3.1739450
C	1.4882350	1.5207830	-2.1912000
C	0.3834010	-0.3324590	-3.2641950
C	-0.6575090	-0.2988540	-2.3612390
C	0.4499890	1.5816150	-1.2523700
C	-0.6460790	0.6516120	-1.2601820
C	-1.6804840	3.4077060	3.0141450
C	-2.6120200	2.3573580	2.9457270
C	-2.5647610	1.4590500	1.9122760
C	-2.6041110	-0.4735920	-0.1055900
C	-2.2328110	-1.7032690	0.4412580
C	-3.9277410	-0.2485470	-0.4837590
C	-4.8760760	-1.2539860	-0.3316270
C	-4.5102090	-2.4808390	0.2136730
C	-3.1908730	-2.6988500	0.5998390
C	-1.5908930	1.5556420	0.8760740
C	-0.6468270	2.6098170	0.9900570
C	-1.5804880	0.6134070	-0.2026120
C	-0.7096260	3.5298070	2.0511150

C	3.8288470	1.9945740	-2.2323280
C	-1.6651710	-2.2302480	-3.3473640
C	2.7844880	-2.1513430	1.9145070
O	-1.7171000	-1.1126630	-2.4598830
O	2.4727530	2.4515710	-2.0599250
O	1.0714710	-2.0141590	-0.0795360
O	1.1092690	-0.1571310	1.5363710
O	2.9691750	-0.4293840	-0.0663050
F	1.9138490	-2.8170450	2.6934350
F	3.5779070	-1.4229790	2.7158280
F	3.5514800	-3.0583220	1.2890180
S	0.6703870	2.8260340	-0.0863250
S	1.8848390	-1.0633760	0.6841160

**Table S17.** Cartesian coordinates of optimized **3ea'** (M<sup>+</sup>).

H	0.4717030	-4.1429220	0.1840590
H	-1.8233680	-4.6865690	-0.2921430
H	-2.7421160	-0.5414050	-0.6917770
H	4.6285440	-3.1110020	0.9415600
H	2.2812390	-3.6345970	0.8975870
H	3.8211130	0.8904890	-0.2793010
H	-3.5265570	0.3002500	3.8561640
H	-1.4406700	0.5193020	2.5669690
H	-5.7501870	1.8451140	0.5310140
H	-5.6921150	0.9587700	2.8455740
H	-3.6642370	2.1045950	-0.7480850
H	1.6470500	4.7392250	-1.8367980
H	0.0211720	6.5445820	-1.4112950
H	-2.0251870	6.0727430	-0.0783570
H	-2.5110520	3.8124190	0.6794580
H	5.9458530	0.8777740	-1.1103120
H	7.3491870	0.8070370	-0.0525380
H	5.8199800	1.3967830	0.5829500
H	6.3125090	-1.6042240	-1.6679510
H	6.4913450	-2.7924570	-0.3734010
H	7.7303410	-1.5647650	-0.6133380
H	5.9599320	-0.3342200	2.4714140
H	7.5252110	-0.8166210	1.8074260
H	6.2856950	-2.0310960	2.1045200
H	-3.5613530	-2.6467110	-3.0944750
H	-4.1443060	-1.2002960	-2.2641320
H	-5.2571760	-2.5183050	-2.6153730
H	-3.5152650	-4.9162550	-1.8663980
H	-5.1958750	-4.6430720	-1.4191110
H	-4.0156750	-5.0075500	-0.1685550
H	-4.6959850	-2.8888340	1.0887080
H	-5.9201700	-2.6354730	-0.1606260
H	-4.7922370	-1.3403010	0.2461380
C	4.4262080	-1.0619720	0.2807140
C	3.9351760	-2.3394370	0.6317940
C	2.5927020	-2.6414740	0.6068230
C	1.6332760	-1.6908270	0.2227170
C	2.0970970	-0.3924650	-0.0971580
C	3.4872420	-0.1139460	-0.0644440
C	0.2234610	-2.0058720	0.0704310
C	-0.2268280	-3.3321300	0.0332490
C	-1.5392340	-3.6448220	-0.2554160
C	-2.4750990	-2.6436870	-0.5449970

C	-2.0393970	-1.3241380	-0.4597030
C	-0.7206690	-0.9703330	-0.1345740
C	1.1308550	0.6346800	-0.3749250
C	-0.2638190	0.4353480	-0.1482460
C	-3.9216940	-2.9598290	-0.9570440
C	5.9327390	-0.7803350	0.3265790
C	0.4574460	3.2339390	-0.8543840
C	-1.1070880	1.5404700	0.1112720
C	0.7206330	4.5314880	-1.3149810
C	-0.1823410	5.5395780	-1.0638700
C	-1.3417110	5.2691510	-0.3207950
C	-1.6162260	3.9924510	0.1058840
C	-2.4021520	1.3344560	0.8215830
C	-2.3823110	0.8118510	2.1188710
C	-3.6290660	1.7108190	0.2608380
C	-4.8067470	1.5632460	0.9820880
C	-4.7744620	1.0608850	2.2798300
C	-3.5599650	0.6881790	2.8456520
C	-0.7528750	2.9026910	-0.1948570
C	6.2685410	0.6606310	-0.0889470
C	6.6538910	-1.7467280	-0.6401870
C	6.4507570	-1.0072010	1.7646750
C	-4.1638920	-4.4711540	-1.1083800
C	-4.2336490	-2.2871210	-2.3122770
C	-4.8866920	-2.4196210	0.1208570
S	1.7548770	2.1079350	-0.9969740

**Table S18.** Cartesian coordinates of optimized **3ea** ( $M^+ + OTf^-$ ).

H	2.8345220	4.2840710	-0.2136000
H	5.0594090	3.7462110	-0.9633270
H	4.1044390	-0.4089000	-0.8390600
H	-1.1955110	5.2007670	1.1546740
H	1.1203810	4.6561020	0.7895520
H	-2.3355490	1.1627620	0.3762400
H	5.0963330	-1.1699640	3.6968640
H	2.9448190	-0.5712170	2.6564760
H	5.9868770	-3.7361060	0.3790080
H	6.6307310	-2.7544460	2.5636640
H	3.8227220	-3.1625920	-0.6461260
H	-2.2121670	-3.3232570	-0.8544690
H	-1.4601440	-5.6187460	-0.3021810
H	0.7578160	-5.9693300	0.7738280
H	2.2569450	-4.0918640	1.1507610
H	-3.9227050	1.6659270	1.9924270
H	-5.0150960	2.9901770	2.3735750
H	-3.3969460	2.9636060	3.0867360
H	-4.2096510	2.1241730	-0.4993270
H	-3.9007610	3.7450190	-1.1538160
H	-5.3115940	3.4429440	-0.1311860
H	-3.1584860	5.3687590	2.1938620
H	-4.7313360	5.2377050	1.4168560
H	-3.3260790	5.6891170	0.4570010
H	5.3987760	0.8864560	-3.5688840
H	5.4335030	-0.5771970	-2.5825210
H	6.9368820	0.0888700	-3.2143070
H	6.4617890	3.0655510	-2.6924600
H	7.9238010	2.1435040	-2.3493320
H	7.1825430	3.1034460	-1.0747390

H	7.0902530	1.0387110	0.4231210
H	7.9150960	0.1549800	-0.8681720
H	6.4161820	-0.4761760	-0.1792850
C	-1.9669810	3.2285470	0.7445770
C	-0.9486600	4.1863290	0.8742590
C	0.3825730	3.8756640	0.6635000
C	0.7831580	2.5864220	0.3054100
C	-0.2217930	1.5937500	0.2038960
C	-1.5747110	1.9353510	0.4216490
C	2.1607430	2.2490240	-0.0293780
C	3.1090470	3.2422830	-0.3033920
C	4.3791850	2.9342310	-0.7487030
C	4.7644840	1.6065130	-0.9674000
C	3.8347370	0.6182730	-0.6584100
C	2.5490020	0.8967840	-0.1679310
C	0.1815160	0.2225350	-0.0330820
C	1.5499110	-0.1723110	0.0536660
C	6.1411430	1.2268750	-1.5381700
C	-3.4484340	3.5583960	0.9802150
C	-0.3667370	-2.4198600	-0.2151920
C	1.8793160	-1.5034710	0.3794450
C	-1.2179060	-3.5110020	-0.4624550
C	-0.7986470	-4.7784310	-0.1324670
C	0.4556220	-4.9750030	0.4689790
C	1.3017220	-3.9156940	0.6827910
C	3.2308140	-1.8238830	0.9329360
C	3.6102610	-1.2637150	2.1557190
C	4.1004560	-2.7219130	0.3040580
C	5.3208520	-3.0463620	0.8832810
C	5.6836290	-2.4930470	2.1077950
C	4.8244150	-1.6025250	2.7417440
C	0.9468530	-2.5921700	0.2989410
C	-3.9690000	2.7379410	2.1824770
C	-4.2592910	3.1905510	-0.2823550
C	-3.6647900	5.0516620	1.2782350
C	6.9662950	2.4634890	-1.9331410
C	5.9611150	0.3531670	-2.7990210
C	6.9344000	0.4365640	-0.4750910
C	-6.1436900	-0.8569080	-1.0689800
O	-4.1014850	-0.2593080	0.4725530
O	-5.1502300	-2.4830190	0.7553160
O	-3.7825340	-1.9885990	-1.2455190
F	-7.0340610	-0.3228700	-0.2181450
F	-6.7503960	-1.8498780	-1.7344480
F	-5.8110280	0.0939970	-1.9624160
S	-1.0812570	-0.8623110	-0.4108830
S	-4.6305000	-1.4783920	-0.1557410

**Table S19.** Cartesian coordinates of optimized **3fa'** ( $M^+$ ).

H	-2.7950810	-0.5274100	-0.6969230
H	-1.6288030	-4.6003230	-0.2177940
H	4.7170790	-2.7977040	0.5610900
H	3.7089350	1.2890150	-0.1155760
H	6.5864300	-1.9610640	1.5224980
H	7.8398720	-1.1049800	0.6344590
H	6.7644460	-2.1989310	-0.2257930
H	5.7407650	0.2849130	2.4351460
H	5.4303740	1.6338830	1.3374200



H	7.0756530	1.0486020	1.5649320
H	6.1945900	-0.2842700	-1.8465370
H	7.3432840	0.7129770	-0.9474880
H	5.7041180	1.2940910	-1.2224960
H	-3.3139510	-4.9791260	-1.7620710
H	-5.0022350	-4.7792490	-1.3049290
H	-3.7930930	-5.0410870	-0.0564160
H	-4.5706920	-2.9218870	1.1389450
H	-5.8182150	-2.7745090	-0.1043310
H	-4.7597040	-1.4088260	0.2490150
H	-4.1344420	-1.3165780	-2.2738410
H	-3.4909420	-2.7606560	-3.0621910
H	-5.1859300	-2.6976210	-2.5672250
H	-1.6328920	0.6517010	2.5354180
H	-3.7509790	0.3357420	3.7508390
H	-5.9281780	1.7348370	0.3317600
H	-5.9091830	0.8733330	2.6564570
H	-3.8117740	2.0924500	-0.8734350
H	0.6561320	-5.1797830	0.3281910
H	3.0044680	-4.5242070	0.6186810
H	1.3768830	5.0767990	-1.6784130
H	-0.3541850	6.7818620	-1.2506160
H	-2.4143680	6.1605630	-0.0027790
H	-2.8038600	3.8556270	0.6685730
C	4.4005390	-0.7003060	0.2220100
C	3.9861270	-2.0214610	0.3788250
C	2.6385260	-2.4066490	0.3119610
C	1.6439490	-1.4223720	0.0893830
C	2.0500570	-0.0755420	-0.1074480
C	3.4114050	0.2531760	-0.0229600
C	2.2428820	-3.7770850	0.4302100
C	0.9457290	-4.1370300	0.2730640
C	-0.0727730	-3.1623140	0.0196540
C	0.2761070	-1.7882410	-0.0140300
C	-0.7406120	-0.8086730	-0.1903290
C	-0.3590530	0.6224540	-0.1748480
C	1.0301260	0.9071920	-0.3563120
C	-1.3985120	-3.5439860	-0.2308740
C	-2.3797960	-2.6134360	-0.5309630
C	-2.0290590	-1.2521350	-0.4789280
C	5.8727610	-0.2687330	0.3199760
C	6.8096580	-1.4601310	0.5777150
C	6.0327400	0.7348920	1.4836670
C	6.2974810	0.4037150	-1.0044490
C	-3.8132300	-3.0183760	-0.9112470
C	-3.9777100	-4.5440570	-1.0113970
C	-4.7952670	-2.4949750	0.1588470
C	-4.1716650	-2.4074890	-2.2843480
C	0.2383820	3.4822100	-0.7804330
C	-0.9714520	3.0664610	-0.1702740
C	-1.2637350	1.6787130	0.0858480
C	0.4472500	4.8053210	-1.1928010
C	-0.5148350	5.7570360	-0.9407110
C	-1.6810720	5.4023140	-0.2457530
C	-1.9010320	4.0998890	0.1325970
C	-2.5716730	1.3989510	0.7479460
C	-2.5715960	0.8903650	2.0504950
C	-3.7942640	1.7059660	0.1388510

C	-4.9887420	1.5046540	0.8191030
C	-4.9780720	1.0168520	2.1226040
C	-3.7673990	0.7120240	2.7354890
S	1.5914030	2.4247910	-0.9265890

**Table S20.** Cartesian coordinates of optimized **3fa** (M<sup>+</sup> + OTf<sup>-</sup>).

H	3.9707290	-0.9293920	-0.7152830
H	5.4800660	3.0391680	-0.3106460
H	-0.6631940	5.3796320	0.6467530
H	-2.3220180	1.4903150	0.0461000
H	-2.6115570	5.8519050	1.6469670
H	-4.1629240	5.8931210	0.8172200
H	-2.6806470	6.1103360	-0.1070600
H	-3.2204150	3.5460200	2.6307780
H	-3.8644220	2.2768680	1.5658740
H	-4.7882550	3.7480710	1.8368240
H	-3.4316070	4.1748200	-1.6598230
H	-4.9131200	4.1300280	-0.6947520
H	-4.0022420	2.6525940	-0.9459840
H	7.0136330	2.3146550	-1.8972640
H	8.2654800	1.1543920	-1.4581290
H	7.4828460	2.1053890	-0.2017830
H	6.8827690	-0.0369130	1.0432040
H	7.7601650	-0.9245280	-0.2102260
H	6.1047150	-1.3776770	0.2011170
H	5.4824100	-1.1226880	-2.3131550
H	5.8021650	0.4069380	-3.1342720
H	7.1421900	-0.6453680	-2.6602660
H	2.4285580	-1.2277640	2.5790310
H	4.3612740	-2.2433770	3.7213940
H	5.1870390	-4.5966650	0.2333440
H	5.7516120	-3.9337140	2.5557000
H	3.2364640	-3.6049100	-0.8975430
H	4.0078350	4.8699020	0.2622120
H	1.7389340	5.7425120	0.6181910
H	-2.7676540	-2.9014890	-1.4334230
H	-2.3869780	-5.3164250	-1.0111250
H	-0.3127810	-6.0523640	0.1523320
H	1.4102010	-4.4433520	0.7421470
C	-1.6689680	3.5062050	0.3538730
C	-0.5475130	4.3190190	0.4673220
C	0.7621180	3.8230440	0.3574960
C	0.9645790	2.4412770	0.1343390
C	-0.1693620	1.6024050	-0.0215460
C	-1.4565780	2.1423980	0.1053310
C	1.9006000	4.6869770	0.4323890
C	3.1526020	4.2042060	0.2395260
C	3.3816100	2.8127850	-0.0096790
C	2.2808230	1.9186120	-0.0038530
C	2.5077480	0.5252690	-0.1740010
C	1.3490480	-0.3985520	-0.1147700
C	0.0567500	0.1941040	-0.2703220
C	4.6666720	2.3265270	-0.2934880
C	4.8896830	0.9924210	-0.5867880
C	3.7972990	0.1108770	-0.4985750
C	-3.1012090	4.0415410	0.5010610
C	-3.1267670	5.5621880	0.7271990
C	-3.7770500	3.3538030	1.7093160

C	-3.9023720	3.7249010	-0.7816010
C	6.2717040	0.4562690	-0.9969940
C	7.3104540	1.5808770	-1.1443120
C	6.7803600	-0.5315390	0.0744520
C	6.1619530	-0.2699300	-2.3559540
C	-0.8541280	-2.3242690	-0.6421520
C	0.3852750	-2.7158360	-0.0696550
C	1.4559250	-1.7815010	0.1420400
C	-1.8368070	-3.2601840	-1.0082450
C	-1.6254350	-4.5932940	-0.7473410
C	-0.4514210	-5.0073650	-0.0960900
C	0.5218450	-4.0988680	0.2377770
C	2.6971600	-2.3426760	0.7608500
C	3.0330030	-1.9637790	2.0630590
C	3.4843900	-3.3003510	0.1124840
C	4.5830480	-3.8617660	0.7517940
C	4.9015340	-3.4878330	2.0540080
C	4.1233860	-2.5380620	2.7065470
C	-5.7541660	-1.8359630	0.3635130
O	-4.1983810	-1.3418530	-1.6896040
O	-6.0811850	0.2103590	-1.2676850
O	-4.1094040	0.1974370	0.2261040
F	-6.5723970	-2.6307950	-0.3422870
F	-6.4661060	-1.2812310	1.3537330
F	-4.8129980	-2.6243900	0.9293540
S	-1.3203530	-0.6733280	-0.7824750
S	-4.9604450	-0.5337630	-0.7262890

**Table S21.** Cartesian coordinates of optimized **3ga'** ( $M^{+}$ ).

H	-1.8170890	-3.3090800	0.0449770
H	3.6603640	3.9317380	2.1508790
H	2.5435960	1.7329640	2.1422750
H	4.1020740	3.7314490	-2.1098400
H	4.4392020	4.9421640	0.0261310
H	3.0046960	1.5230590	-2.1236090
H	2.7737360	-4.4424060	-0.0265100
H	5.2120360	-4.1334620	-0.0036740
H	6.1872920	-1.8468130	0.0448180
H	4.7237400	0.1148900	0.0537170
H	-4.1064500	3.5390100	-0.0671080
H	-1.6553070	3.5018970	-0.0715780
H	-6.2586310	2.3273460	-0.0393490
H	-6.3540790	-1.9569150	0.0336980
H	-7.5301370	0.2124440	0.0000640
H	-4.2314620	-3.2439170	0.0504350
H	0.4232980	2.2400760	-0.0475910
C	-3.6708190	-2.3168950	0.0330980
C	-4.3880310	-1.0831440	0.0152560
C	-3.6473170	0.1312850	-0.0056380
C	-2.2284750	0.1008130	-0.0069330
C	-1.5409430	-1.1412000	0.0088060
C	-2.3136420	-2.3476680	0.0293200
C	-1.4957770	1.3358490	-0.0296130
C	-2.2206880	2.5781120	-0.0529990
C	-0.1188670	1.3067760	-0.0279290
C	-0.1215840	-1.1359760	0.0028180
C	0.6192470	0.0938240	-0.0049850
C	2.3463890	-2.3284060	-0.0073930

C	2.0375540	0.1419580	0.0028150
C	3.1970580	-3.4454060	-0.0134490
C	4.5607030	-3.2683380	0.0003730
C	5.1126200	-1.9731050	0.0257940
C	4.2946550	-0.8755750	0.0297610
C	2.7000700	1.4811570	0.0085860
C	2.8854600	2.1682360	1.2105620
C	3.1455950	2.0496830	-1.1869690
C	3.7648510	3.2950960	-1.1778050
C	3.9524810	3.9749130	0.0211500
C	3.5143630	3.4087800	1.2138480
C	2.8734550	-1.0053580	0.0058210
C	-4.3362090	1.3789260	-0.0261980
C	-3.5718710	2.5965620	-0.0504720
C	-5.7895230	-1.0323990	0.0174320
C	-6.4475760	0.1860330	-0.0015790
C	-5.7301190	1.3815960	-0.0236040
S	0.6615480	-2.6750750	-0.0073110

**Table S22.** Cartesian coordinates of optimized **3ga** ( $M^+$  +  $OTf^-$ ).

H	1.7225480	1.6838120	-0.4663100
H	-5.9642560	-3.5856220	-1.7239030
H	-3.7142910	-2.6112810	-2.0040060
H	-5.4353040	-3.5859870	2.5315080
H	-6.8345850	-4.0770040	0.5448160
H	-3.1857950	-2.6102680	2.2525920
H	2.5645910	-2.9127310	-0.6540380
H	2.1288340	-5.3468980	-0.6042580
H	-0.1894320	-6.2027910	-0.3034240
H	-2.0552370	-4.6424240	-0.0546020
H	-4.9377120	4.3781400	0.3572000
H	-5.0496560	1.9296960	0.3472080
H	-3.6057880	6.4545810	0.2162200
H	0.6480080	6.2868740	-0.2978180
H	-1.4281800	7.5961050	-0.0350360
H	1.7958930	4.0823930	-0.4524440
H	-3.9271980	-0.2212140	0.1948710
C	0.8380350	3.5870660	-0.3459720
C	-0.3386740	4.3772370	-0.1985910
C	-1.5888500	3.7150930	-0.0548420
C	-1.6444790	2.2957260	-0.0629640
C	-0.4569400	1.5396120	-0.2152860
C	0.7895670	2.2281860	-0.3545630
C	-2.9126400	1.6369670	0.0847990
C	-4.0991910	2.4384500	0.2366280
C	-2.9685340	0.2623890	0.0801330
C	-0.5452770	0.1130590	-0.2233860
C	-1.8096600	-0.5466420	-0.0705680
C	0.4944140	-2.3917700	-0.3808320
C	-1.9339650	-1.9586300	-0.0642560
C	1.5610810	-3.3021780	-0.5230780
C	1.3064440	-4.6506380	-0.4948880
C	-0.0078940	-5.1354650	-0.3242900
C	-1.0520600	-4.2648510	-0.1852260
C	-3.3001010	-2.5451470	0.1056560
C	-4.0911340	-2.8239250	-1.0104470
C	-3.7941370	-2.8233720	1.3814560
C	-5.0624880	-3.3730520	1.5369870

C	-5.8473930	-3.6485820	0.4221480
C	-5.3592490	-3.3729770	-0.8508830
C	-0.8469770	-2.8506310	-0.2075980
C	-2.7822330	4.4799280	0.0970760
C	-4.0356750	3.7879400	0.2419790
C	-0.3048450	5.7827050	-0.1885850
C	-1.4692010	6.5136260	-0.0410360
C	-2.7003000	5.8700280	0.1010150
C	4.9507150	-0.2884820	1.1473180
O	3.8760820	-1.3712850	-0.9755180
O	3.6818540	1.0643090	-0.6996740
O	5.8669600	0.0628750	-1.2982120
F	3.8129030	-0.4703800	1.8592130
F	5.5603370	0.8001050	1.6370570
F	5.7412390	-1.3471480	1.3823770
S	0.9390490	-0.7328680	-0.4325900
S	4.5676970	-0.1056180	-0.6796970

**Table S23.** Cartesian coordinates of optimized **3ga-isomer'** ( $M^+$ ).

H	0.2339370	1.9546070	-1.1896300
H	-2.4566160	4.6334440	-1.3056730
H	-2.5482590	2.2039590	-1.7067130
H	-0.6811820	3.9368180	2.5355860
H	-1.5249640	5.5112660	0.8175550
H	-0.7257930	1.5078060	2.1188520
H	-4.6779450	-3.3378610	-0.4749580
H	-6.6257980	-1.8444890	-0.2630670
H	-6.2851360	0.5727080	0.2220440
H	-4.0380020	1.4895860	0.3755600
H	5.1350970	-2.8716840	0.9024920
H	2.9094920	-3.9056150	0.9105340
H	6.5723170	-0.9230950	0.4684110
H	4.8889720	2.7531890	-0.9437840
H	6.8562770	1.4180760	-0.2723430
H	2.4374470	2.8955730	-1.3592150
H	0.5316290	-3.7813100	0.3860370
C	2.3177300	1.8999660	-0.9480510
C	3.4687940	1.1821250	-0.5430780
C	3.2949640	-0.1544870	-0.1053790
C	1.9916960	-0.7224470	-0.0364180
C	0.8414610	0.0579590	-0.3307090
C	1.0636330	1.3648400	-0.8435940
C	1.8686330	-2.1090300	0.2999860
C	3.0287810	-2.8624950	0.6445270
C	0.6140120	-2.7125330	0.2265780
C	-0.4938780	-0.5337500	-0.1648790
C	-0.5237090	-1.9720240	-0.0329680
C	-3.2399480	-1.7584930	-0.2039800
C	-1.6843260	0.2126120	-0.0372210
C	-4.5372280	-2.2757780	-0.3141690
C	-5.6243420	-1.4401250	-0.1853060
C	-5.4311630	-0.0767540	0.0797660
C	-4.1610450	0.4395590	0.1645440
C	-1.6325870	1.6887540	0.1754190
C	-2.1351580	2.5813270	-0.7786210
C	-1.1059510	2.1903280	1.3683910
C	-1.0779910	3.5603810	1.6008830
C	-1.5556480	4.4437430	0.6383990

C	-2.0813240	3.9510420	-0.5530410
C	-3.0054340	-0.3705430	-0.0194640
C	4.4390050	-0.9250610	0.2465430
C	4.2610630	-2.2894960	0.6343660
C	4.7648490	1.7328040	-0.6006610
C	5.8654590	0.9841810	-0.2297220
C	5.7047990	-0.3368290	0.1887490
S	-1.9632720	-2.9194770	-0.2041890

**Table S24.** Cartesian coordinates of optimized **3ga-isomer** (M<sup>+</sup> + OTf<sup>-</sup>).

H	-3.6136170	1.0847160	1.1784640
H	-4.5710690	4.7068400	1.6343770
H	-2.4095440	3.5462290	1.8829780
H	-4.9675740	3.1171060	-2.3287600
H	-5.8614070	4.4971880	-0.4733130
H	-2.8231410	1.9275360	-2.0666050
H	3.4326530	2.7326310	0.1399750
H	3.1057660	5.1900140	0.0612050
H	0.8083740	6.1228970	-0.1666170
H	-1.1221240	4.6532030	-0.2206390
H	-1.7557990	-5.5212890	-0.9809780
H	0.2194700	-4.0567660	-1.0256740
H	-4.1426530	-5.8465480	-0.5008670
H	-6.5470280	-2.6132330	0.9577880
H	-6.3237910	-4.9785390	0.2772860
H	-5.4923560	-0.3933790	1.3628730
H	1.2621320	-1.9032360	-0.5419770
C	-4.5663380	-0.7641550	0.9383980
C	-4.4937720	-2.1187900	0.5291470
C	-3.2425880	-2.6035430	0.0697980
C	-2.1200680	-1.7287830	-0.0160330
C	-2.2472310	-0.3492210	0.2890560
C	-3.4978800	0.0772360	0.8229690
C	-0.8480330	-2.2863370	-0.3839810
C	-0.7510750	-3.6718080	-0.7375570
C	0.2790720	-1.4880310	-0.3426690
C	-1.0893990	0.5375890	0.1144030
C	0.1777890	-0.1221410	-0.0760030
C	1.3258870	2.3068020	0.0667240
C	-1.1571680	1.9492570	0.0479450
C	2.4407110	3.1692480	0.1061220
C	2.2503180	4.5261180	0.0434070
C	0.9496980	5.0526620	-0.0817840
C	-0.1398470	4.2224890	-0.1102810
C	-2.4744500	2.6473040	-0.0714930
C	-2.9716890	3.4481010	0.9616880
C	-3.2046410	2.5368680	-1.2562280
C	-4.4150370	3.2056590	-1.4012910
C	-4.9150870	3.9822260	-0.3615960
C	-4.1903760	4.1008210	0.8211160
C	-0.0060920	2.8056430	0.0007520
C	-3.1195420	-3.9772730	-0.2910170
C	-1.8392160	-4.4756300	-0.7076320
C	-5.5968790	-2.9927700	0.6000960
C	-5.4698410	-4.3145730	0.2236390
C	-4.2382590	-4.8048830	-0.2168500
C	5.3795290	-1.3333050	0.8939450
O	3.4821090	-1.5061650	-0.8981760

O	4.5622700	0.6837760	-0.5610120
O	5.7939630	-1.1371550	-1.7022230
F	4.4884600	-1.0440340	1.8691460
F	6.5357080	-0.7343630	1.2144660
F	5.5810570	-2.6597010	0.9145900
S	1.7161340	0.6433220	-0.0203200
S	4.7461780	-0.7599980	-0.7753540

**Table S25.** Cartesian coordinates of optimized 9-phenylthiopyrylium' ( $M^+$ ).

H	-4.3681980	-0.6107570	2.0555910
H	-1.9036570	-0.6340650	2.0538330
H	-4.3682250	0.6103070	-2.0555730
H	-5.6102720	-0.0002590	0.0000050
H	-1.9036850	0.6337920	-2.0537910
H	-0.2702350	4.5974440	0.1641750
H	-1.3886380	2.4231190	0.1430420
H	2.2108960	4.7285090	0.0753970
H	3.5600390	2.6761050	0.0035230
H	2.2115550	-4.7282370	-0.0754390
H	-0.2695700	-4.5975120	-0.1643260
H	-1.3882710	-2.4232970	-0.1432070
H	3.5604290	-2.6756430	-0.0034770
C	1.7206300	-3.7630190	-0.0651440
C	2.4789610	-2.6164320	-0.0225810
C	0.3155470	-3.6887150	-0.1103720
C	-0.3110310	-2.4719860	-0.0954930
C	1.8510860	-1.3613280	-0.0107450
C	0.4267000	-1.2515640	-0.0271020
C	1.7200910	3.7632300	0.0651120
C	0.3150280	3.6887370	0.1102790
C	-0.3114000	2.4719150	0.0953870
C	-1.7366530	-0.0001380	0.0000180
C	-2.4408410	-0.3594930	1.1536410
C	-2.4408560	0.3591840	-1.1536020
C	-3.8308420	0.3462380	-1.1533140
C	-4.5275050	-0.0002360	0.0000060
C	-3.8308250	-0.3466470	1.1533370
C	0.4264950	1.2515960	0.0271000
C	1.8508800	1.3615440	0.0107480
C	-0.2469850	-0.0000530	0.0000490
C	2.4785780	2.6167360	0.0225860
S	2.9053430	0.0001920	0.0000500

**Table S26.** Cartesian coordinates of optimized **3aa-CH**.

H	0.8173750	-1.9225310	0.0001770
H	-2.7322480	-3.7091890	2.1437610
H	-1.7138370	-1.4584020	2.1397130
H	-2.7296130	-3.7104790	-2.1436780
H	-3.2443810	-4.8459970	0.0000650
H	-1.7111570	-1.4597060	-2.1397300
H	-5.1285420	2.1660750	-0.0004990
H	-3.7452970	0.1519730	-0.0004960
H	4.9480050	2.3839640	-0.8933230
H	6.2706190	1.5913220	0.0002150
H	4.9476230	2.3842590	0.8931150
H	3.8886610	-3.7790970	-0.0001800
H	2.4109840	-3.3335510	-0.8924450
H	2.4113950	-3.3338910	0.8927470

H	2.8135050	2.6220570	-0.0000180
H	-4.0789160	4.4237560	-0.0000040
H	-1.6268010	4.6419140	0.0001560
H	0.5915210	3.6149210	0.0000000
C	3.1988060	0.5288860	0.0000490
C	2.3903530	1.6269820	-0.0000180
C	2.6106630	-0.7897910	0.0001140
C	1.2535750	-0.9356470	0.0000990
C	0.9664540	1.5058360	-0.0000330
C	0.3760090	0.1948430	0.0000030
C	-3.4512630	3.5404370	-0.0000840
C	-4.0483490	2.2534210	-0.0002970
C	-3.2749680	1.1263860	-0.0002990
C	-1.6394930	-1.3023610	-0.0000100
C	-1.9346840	-1.9533230	1.2009860
C	-1.9331850	-1.9540560	-1.2009780
C	-2.5069060	-3.2218600	-1.2021810
C	-2.7961740	-3.8594300	0.0000460
C	-2.5084010	-3.2211320	1.2022430
C	-1.8494200	1.2051600	-0.0000600
C	5.2043380	1.8062790	0.0000350
C	3.0118510	-3.1353730	0.0000600
C	-1.2486160	2.5128650	-0.0000200
C	-1.0228850	0.0600450	-0.0000130
C	-2.0914350	3.6618110	0.0000290
C	0.1435420	2.6263850	-0.0000100
O	3.5094660	-1.8048770	0.0001590
O	4.5545640	0.5441790	0.0001490

**Table S27.** Cartesian coordinates of optimized **3aa-N**.

H	0.7697930	-1.9770780	0.0000890
H	-2.9098600	-3.6229770	2.1437720
H	-1.7885860	-1.4218690	2.1408340
H	-2.9107170	-3.6225020	-2.1437530
H	-3.4752900	-4.7333100	0.0000030
H	-1.7894470	-1.4213950	-2.1407740
H	-4.9779430	2.4578250	0.0000210
H	-3.7524540	0.3361480	0.0000410
H	4.9492820	2.2831360	-0.8930500
H	6.2641620	1.4748660	-0.0002860
H	4.9495760	2.2833620	0.8926760
H	3.8279520	-3.8678520	-0.0005250
H	2.3553580	-3.4069110	-0.8932030
H	2.3553810	-3.4074440	0.8924670
H	2.8039200	2.5566630	0.0000330
H	-3.7533940	4.6221300	-0.0000150
H	-1.2728970	4.6426040	-0.0000160
C	3.1829180	0.4482080	0.0000690
C	2.3909230	1.5588340	0.0000540
C	2.5807660	-0.8667850	0.0000560
C	1.2225010	-0.9972520	0.0000610
C	0.9670950	1.4550540	0.0000390
C	0.3658100	0.1473620	0.0000520
C	-3.1954360	3.6930280	-0.0000080
C	-3.8943880	2.4583380	0.0000110
C	-3.2118860	1.2739000	0.0000210
C	-1.7097510	-1.2709490	0.0000300
C	-2.0327160	-1.9055520	1.2021330



C	-2.0332080	-1.9052800	-1.2020820
C	-2.6649000	-3.1450400	-1.2024490
C	-2.9820610	-3.7685700	0.0000080
C	-2.6644160	-3.1453060	1.2024760
C	-1.7866710	1.2498750	0.0000120
C	5.2010400	1.7039620	-0.0001570
C	2.9577520	-3.2154260	-0.0003180
C	-1.0807610	2.5024740	0.0000050
C	-1.0310020	0.0594370	0.0000330
C	-1.8298420	3.7139380	-0.0000090
N	0.2591460	2.5853660	0.0000140
O	3.4686380	-1.8896440	0.0000630
O	4.5351790	0.4473350	0.0001080

**Table S28.** Cartesian coordinates of optimized **3aa-NH'** (M<sup>+</sup>).

H	0.8018500	-1.9729580	-0.0491870
H	-2.3033370	-3.9289220	2.0817490
H	-1.2152130	-1.7153780	2.0780640
H	-3.3454420	-3.4299580	-2.0476320
H	-3.3656170	-4.7976220	0.0184750
H	-2.2826110	-1.2047940	-2.0508890
H	-5.0587150	2.2986950	0.0863680
H	-3.7535140	0.2182770	0.0777750
H	4.9525160	2.3499220	-0.8943250
H	6.2547830	1.5149830	-0.0105180
H	4.9558120	2.3254140	0.9011100
H	3.9295720	-3.8027040	-0.1260580
H	2.4357890	-3.3692350	-0.9969070
H	2.4530560	-3.4158670	0.7942420
H	2.7908290	2.5889270	0.0099060
H	-3.9107280	4.4980680	0.0401500
H	-1.4509990	4.6227120	0.0065580
H	0.5992140	3.4414540	0.0070700
C	3.1842740	0.4832090	-0.0145940
C	2.3671340	1.5943150	0.0032020
C	2.6033420	-0.8453270	-0.0367050
C	1.2446350	-0.9900110	-0.0266400
C	0.9733360	1.4375210	0.0086520
C	0.3733340	0.1397280	0.0055630
C	-3.3250370	3.5874180	0.0357690
C	-3.9775310	2.3363340	0.0586120
C	-3.2514820	1.1749220	0.0519650
C	-1.6730730	-1.3106560	0.0125550
C	-1.6782440	-2.0904710	1.1727890
C	-2.2835870	-1.8005970	-1.1456320
C	-2.8826200	-3.0554660	-1.1429600
C	-2.8913230	-3.8241160	0.0164390
C	-2.2921860	-3.3381490	1.1740880
C	-1.8307310	1.2020710	0.0179750
C	5.1985950	1.7665340	-0.0048750
C	3.0349130	-3.1874280	-0.1016380
C	-1.2001570	2.4771280	0.0115620
C	-1.0268560	0.0304160	0.0119500
C	-1.9544790	3.6627030	0.0159930
N	0.1640570	2.5271280	0.0090030
O	3.5023220	-1.8350360	-0.0709000
O	4.5090310	0.5086130	-0.0207730

**Table S29.** Cartesian coordinates of optimized **3aa-O'** (M<sup>+</sup>).

H	0.7865770	-2.0121710	-0.0692030
H	-2.1878890	-4.0199860	1.9886030
H	-1.0280490	-1.8447340	1.9827870
H	-3.6982090	-3.2338820	-1.9473120
H	-3.5176320	-4.7274880	0.0212640
H	-2.5748510	-1.0406150	-1.9458810
H	-4.9555120	2.4953850	0.1223890
H	-3.7646120	0.3455390	0.1124320
H	4.9348390	2.3121700	-0.8974930
H	6.2408860	1.4735640	-0.0204350
H	4.9431440	2.2809990	0.8975990
H	3.9131190	-3.8476290	-0.1774550
H	2.4171240	-3.4016890	-1.0375300
H	2.4410850	-3.4699260	0.7534210
H	2.7577440	2.5571960	0.0106730
H	-3.6908740	4.6269650	0.0598220
H	-1.2047230	4.6047130	0.0135550
C	3.1743210	0.4371420	-0.0189910
C	2.3553340	1.5554470	0.0048690
C	2.5922400	-0.8892550	-0.0485880
C	1.2320140	-1.0308930	-0.0344580
C	0.9778600	1.3877330	0.0139750
C	0.3664250	0.1030620	0.0112870
C	-3.1565880	3.6852430	0.0516990
C	-3.8742740	2.4752340	0.0826220
C	-3.2116630	1.2730160	0.0729090
C	-1.7195760	-1.2939850	0.0168560
C	-1.6070040	-2.1494210	1.1190490
C	-2.4880720	-1.6909180	-1.0836330
C	-3.1197540	-2.9285280	-1.0843160
C	-3.0140330	-3.7688660	0.0195220
C	-2.2629660	-3.3744060	1.1223760
C	-1.7940870	1.2275800	0.0236380
C	5.1855620	1.7275310	-0.0109560
C	3.0194910	-3.2315290	-0.1421650
C	-1.1109650	2.4651040	0.0162230
C	-1.0352300	0.0205380	0.0171380
C	-1.7777360	3.6870250	0.0241450
O	3.4889110	-1.8800640	-0.0967440
O	4.4940810	0.4664820	-0.0298160
O	0.2420140	2.5111420	0.0132540

**Table S30.** Cartesian coordinates of optimized **3ea-CH**.

H	0.6298500	-4.0590820	0.2030690
H	-1.6644480	-4.6748180	-0.1694660
H	-2.6986760	-0.5588830	-0.5752090
H	4.7673150	-2.9968310	0.8497500
H	2.4197910	-3.5362080	0.8473170
H	3.8658090	0.9975950	-0.3382630
H	-4.0660990	0.7811170	3.5172700
H	-1.8111890	0.8647730	2.5201300
H	-5.7643210	1.9602910	-0.2384130
H	-6.0570970	1.3313350	2.1437210
H	-3.5074280	2.0523720	-1.2263760
H	2.1247820	4.5595250	-1.4158360
H	0.6154820	6.5015450	-1.2064870
H	-1.6834200	6.1826210	-0.3053740

H	-2.4869170	3.9693930	0.2960630
H	5.9649320	1.0286030	-1.2114300
H	7.3983610	0.9808330	-0.1876080
H	5.8682920	1.5402370	0.4819770
H	6.3675020	-1.4403200	-1.7834030
H	6.6006210	-2.6269000	-0.4985190
H	7.8138090	-1.3739360	-0.7654880
H	6.0876070	-0.1874330	2.3592640
H	7.6505220	-0.6371130	1.6610390
H	6.4358020	-1.8757930	1.9827210
H	-3.6214180	-2.6790360	-2.8871210
H	-4.1862820	-1.2483920	-2.0204860
H	-5.2910830	-2.5912480	-2.3073960
H	-3.4391220	-4.9431690	-1.6682080
H	-5.1018630	-4.7131510	-1.1272150
H	-3.8398820	-5.0480640	0.0533710
H	-4.4950260	-2.9535190	1.3510850
H	-5.8014510	-2.7228120	0.1798320
H	-4.6754220	-1.4055480	0.5247810
H	2.5876570	2.2456730	-0.9608010
C	4.5110460	-0.9455210	0.2102500
C	4.0593210	-2.2293530	0.5616830
C	2.7175100	-2.5380430	0.5568020
C	1.7411200	-1.5913350	0.2002580
C	2.1646060	-0.2893560	-0.1159240
C	3.5455410	-0.0056740	-0.1097970
C	0.3235670	-1.9315820	0.0934450
C	-0.0962490	-3.2680510	0.0770260
C	-1.4104930	-3.6240890	-0.1530120
C	-2.3797500	-2.6487000	-0.4067560
C	-1.9689030	-1.3199350	-0.3606750
C	-0.6496580	-0.9182310	-0.0878960
C	1.1661710	0.7668180	-0.3474810
C	-0.2329240	0.5026860	-0.1153460
C	-3.8414820	-2.9988590	-0.7341280
C	6.0152100	-0.6326800	0.2188990
C	0.6731120	3.1278220	-0.7040580
C	-1.1095390	1.5927100	0.0269960
C	1.1084380	4.4325350	-1.0592770
C	0.2743460	5.5091540	-0.9368030
C	-1.0330230	5.3251670	-0.4322980
C	-1.4863080	4.0762900	-0.0956780
C	-2.4963580	1.4591970	0.5753470
C	-2.6775760	1.1015760	1.9141910
C	-3.6281660	1.7697760	-0.1868540
C	-4.9009480	1.7195870	0.3709660
C	-5.0662730	1.3657800	1.7067600
C	-3.9493680	1.0559020	2.4754900
C	-0.6653030	2.9221660	-0.2518950
C	6.3186870	0.8151650	-0.1999570
C	6.7395470	-1.5778410	-0.7654330
C	6.5779480	-0.8489830	1.6413030
C	-4.0574240	-4.5155020	-0.8752620
C	-4.2555660	-2.3360790	-2.0660970
C	-4.7562040	-2.4854790	0.3987920
C	1.5575140	2.0423530	-0.7032950

**Table S31.** Cartesian coordinates of optimized **3ea-N**.

H	0.5419410	-4.0823370	0.2890920
H	-1.7647460	-4.6653350	-0.0568480
H	-2.7354550	-0.5414010	-0.5298010
H	4.7316380	-3.0680800	0.7669150
H	2.3873930	-3.6056170	0.7984150
H	3.7862000	0.9688910	-0.3348760
H	-4.3241710	1.0395890	3.2969650
H	-1.9974360	0.9922350	2.4767260
H	-5.6769780	2.1543410	-0.6156550
H	-6.1772640	1.6200330	1.7544170
H	-3.3474370	2.1232780	-1.4268220
H	2.4457500	4.3047150	-1.1359430
H	1.0652500	6.3703010	-1.0383820
H	-1.3149000	6.2255860	-0.3326980
H	-2.3284490	4.0714600	0.1905520
H	5.8997810	0.9946560	-1.2279880
H	7.3620290	0.9175510	-0.2446700
H	5.8483400	1.4637920	0.4763310
H	6.2737290	-1.4610790	-1.8722650
H	6.5350500	-2.6812000	-0.6241020
H	7.7484100	-1.4290390	-0.8945400
H	6.1180890	-0.3099310	2.3056710
H	7.6575270	-0.7531290	1.5536870
H	6.4432100	-1.9913330	1.8785840
H	-3.7139240	-2.7012920	-2.7960550
H	-4.2446540	-1.2399940	-1.9592120
H	-5.3760550	-2.5690930	-2.2035630
H	-3.5610010	-4.9380540	-1.5245310
H	-5.2134420	-4.6654600	-0.9724610
H	-3.9451640	-4.9942290	0.2031160
H	-4.5515440	-2.8570100	1.4555690
H	-5.8649540	-2.6325800	0.2910650
H	-4.7139230	-1.3267700	0.5925270
C	4.4774860	-1.0002310	0.1832240
C	4.0212260	-2.2893960	0.5162390
C	2.6783980	-2.5985070	0.5331470
C	1.6994470	-1.6372740	0.2234440
C	2.1377180	-0.3375020	-0.0676100
C	3.5136150	-0.0469440	-0.0963720
C	0.2741330	-1.9535160	0.1325840
C	-0.1702860	-3.2816170	0.1469130
C	-1.4925590	-3.6191060	-0.0658040
C	-2.4482190	-2.6332720	-0.3295680
C	-2.0149380	-1.3106940	-0.3127720
C	-0.6861010	-0.9274430	-0.0617520
C	1.1612020	0.7412250	-0.2661360
C	-0.2481900	0.4852370	-0.0944050
C	-3.9191290	-2.9649690	-0.6340270
C	5.9835640	-0.7010450	0.1580490
C	0.8383730	3.0058770	-0.5534710
C	-1.0828370	1.6057630	0.0204920
C	1.3975350	4.2729130	-0.8663950
C	0.6325320	5.4049830	-0.8034930
C	-0.7225660	5.3214410	-0.4081210
C	-1.2927650	4.1103720	-0.1147500
C	-2.5090610	1.5475390	0.4669420
C	-2.8037490	1.2445290	1.7984890

C	-3.5610860	1.8799850	-0.3924370
C	-4.8739930	1.8993070	0.0659350
C	-5.1553700	1.5991490	1.3952340
C	-4.1155820	1.2722450	2.2594060
C	-0.5423920	2.9046740	-0.2113940
C	6.2816160	0.7554040	-0.2330690
C	6.6732140	-1.6264280	-0.8689580
C	6.5832490	-0.9571490	1.5584890
C	-4.1631430	-4.4804490	-0.7359290
C	-4.3339110	-2.3270740	-1.9779190
C	-4.8138120	-2.4081040	0.4943880
N	1.6550620	1.9381420	-0.5272530

**Table S32.** Cartesian coordinates of optimized **3ea-NH'** (M<sup>+</sup>).

H	0.5361560	-4.0951910	0.1906220
H	-1.7714450	-4.6675640	-0.1462390
H	-2.7621000	-0.5397150	-0.5089610
H	4.7050050	-3.0867240	0.7323180
H	2.3637060	-3.6172410	0.7282290
H	3.8694690	0.9575990	-0.2588490
H	-4.1789460	0.9278770	3.4023860
H	-1.8912260	0.8964750	2.4863720
H	-5.6961410	2.1660540	-0.4122850
H	-6.0916580	1.5581720	1.9580820
H	-3.4066460	2.1713660	-1.3239960
H	2.3801470	4.3706920	-1.2410910
H	0.9684420	6.3942100	-1.1239480
H	-1.3915210	6.2235130	-0.3745320
H	-2.3633970	4.0541150	0.1913560
H	5.9547450	1.0177450	-1.1325390
H	7.3815050	0.8963250	-0.1138500
H	5.8684720	1.4422590	0.5923750
H	6.3067060	-1.4268590	-1.8360780
H	6.5288370	-2.6827790	-0.6148940
H	7.7548530	-1.4361660	-0.8224100
H	6.0689000	-0.3904970	2.3764290
H	7.6163000	-0.8273130	1.6419470
H	6.3892680	-2.0620740	1.9059250
H	-3.7480800	-2.6457580	-2.8212820
H	-4.2832460	-1.2085570	-1.9429840
H	-5.4019300	-2.5413500	-2.2083710
H	-3.5726650	-4.9169700	-1.6038950
H	-5.2180930	-4.6649550	-1.0302400
H	-3.9423970	-5.0162400	0.1265860
H	-4.5409680	-2.9085010	1.4385140
H	-5.8649440	-2.6678760	0.2928040
H	-4.7236360	-1.3595170	0.6100930
H	2.5535780	2.0712470	-0.7530900
C	4.4746580	-1.0061880	0.1949870
C	4.0005270	-2.3019840	0.4881270
C	2.6595160	-2.6077780	0.4828310
C	1.6827190	-1.6432380	0.1783360
C	2.1328100	-0.3344520	-0.0871860
C	3.5183310	-0.0488550	-0.0775430
C	0.2635540	-1.9612230	0.0827880
C	-0.1756010	-3.2909160	0.0734680
C	-1.4991590	-3.6220380	-0.1338920
C	-2.4622640	-2.6338520	-0.3648300

C	-2.0347120	-1.3095250	-0.3204990
C	-0.7024660	-0.9354130	-0.0813060
C	1.1430030	0.6987420	-0.2855480
C	-0.2591480	0.4718510	-0.1111220
C	-3.9328440	-2.9665490	-0.6629980
C	5.9809630	-0.7172970	0.2115250
C	0.7836750	3.0589080	-0.6122410
C	-1.0866960	1.6056350	0.0228250
C	1.3393850	4.3047760	-0.9451130
C	0.5519490	5.4268880	-0.8732190
C	-0.7895590	5.3274840	-0.4532680
C	-1.3371050	4.1099720	-0.1372600
C	-2.4905680	1.5329280	0.5192270
C	-2.7224750	1.1758800	1.8503120
C	-3.5729350	1.8969160	-0.2887740
C	-4.8643990	1.8933650	0.2255590
C	-5.0864640	1.5493230	1.5554590
C	-4.0131810	1.1932260	2.3655970
C	-0.5728060	2.9165440	-0.2378100
C	6.3009760	0.7463740	-0.1315920
C	6.6789350	-1.6232000	-0.8280390
C	6.5416490	-1.0203060	1.6193510
C	-4.1676850	-4.4806120	-0.7982290
C	-4.3607660	-2.2962880	-1.9871740
C	-4.8147320	-2.4398570	0.4904010
N	1.5657760	1.9426780	-0.5804860

**Table S33.** Cartesian coordinates of optimized **3ea-O'** ( $M^+$ ).

H	0.4472530	-4.1106820	0.2977470
H	-1.8690570	-4.6494120	-0.0466000
H	-2.7842080	-0.5130570	-0.5154000
H	4.6599010	-3.1257410	0.7261490
H	2.3205490	-3.6570170	0.7547730
H	3.7912310	0.9289130	-0.3056120
H	-4.2887180	1.0315890	3.2785320
H	-1.9743150	0.9114180	2.4410240
H	-5.6215290	2.3684040	-0.5720460
H	-6.1225650	1.7529400	1.7759410
H	-3.3026310	2.2958960	-1.4035270
H	2.6017640	4.1589890	-1.0586550
H	1.3006600	6.2829470	-1.0193350
H	-1.1006520	6.2509880	-0.4023590
H	-2.2249830	4.1374210	0.1149250
H	5.8989020	0.9520410	-1.1894010
H	7.3499710	0.8260870	-0.2028740
H	5.8527470	1.3855260	0.5312050
H	6.2181990	-1.4992830	-1.8878140
H	6.4565100	-2.7514660	-0.6650250
H	7.6883350	-1.5170370	-0.9069250
H	6.0838470	-0.4375150	2.3223380
H	7.6100380	-0.8938770	1.5567060
H	6.3781730	-2.1154830	1.8554790
H	-3.7651280	-2.6856900	-2.7987570
H	-4.2826920	-1.2068600	-1.9813920
H	-5.4262020	-2.5241350	-2.2188290
H	-3.6598360	-4.9141610	-1.5006030
H	-5.3068140	-4.6095630	-0.9589090
H	-4.0537030	-4.9446390	0.2272520

H	-4.6352430	-2.7786270	1.4534340
H	-5.9341480	-2.5552700	0.2761550
H	-4.7742100	-1.2576470	0.5662330
C	4.4365030	-1.0460550	0.1802570
C	3.9546770	-2.3385340	0.4911440
C	2.6122570	-2.6467350	0.5073260
C	1.6364570	-1.6798820	0.2157250
C	2.1016750	-0.3729970	-0.0575780
C	3.4882010	-0.0818450	-0.0836340
C	0.2139480	-1.9761170	0.1302530
C	-0.2495080	-3.2978190	0.1521140
C	-1.5771570	-3.6092320	-0.0587270
C	-2.5208250	-2.6103060	-0.3240370
C	-2.0718240	-1.2919470	-0.3050390
C	-0.7357400	-0.9377850	-0.0622430
C	1.1354090	0.6549950	-0.2369030
C	-0.2675340	0.4610680	-0.1007510
C	-3.9928060	-2.9249430	-0.6337650
C	5.9454080	-0.7752030	0.1620400
C	0.8924160	2.9803300	-0.5272490
C	-1.0615670	1.6185110	0.0161840
C	1.5454160	4.1725150	-0.8253840
C	0.8152740	5.3418140	-0.7939240
C	-0.5474370	5.3219320	-0.4481260
C	-1.1812140	4.1369630	-0.1598210
C	-2.4793970	1.5986120	0.4629920
C	-2.7705610	1.2332770	1.7809020
C	-3.5159350	2.0172760	-0.3782580
C	-4.8238530	2.0569750	0.0909480
C	-5.1050850	1.7080320	1.4081620
C	-4.0760630	1.3002500	2.2512660
C	-0.4777900	2.9065430	-0.2218620
C	6.2681310	0.6838850	-0.1964390
C	6.6109050	-1.6940930	-0.8873100
C	6.5333770	-1.0766280	1.5589620
C	-4.2561050	-4.4378820	-0.7189050
C	-4.3837650	-2.2936080	-1.9883920
C	-4.8833880	-2.3398680	0.4842100
O	1.6491960.	1.8618770.	-0.4810850

**Table S34.** Cartesian coordinates of optimized TfOH.

H	1.4221640	1.8999630	-0.3191670
C	-1.0119930	0.0048360	-0.0031910
O	1.2324150	-1.3539900	-0.6335040
O	1.2597780	0.1489100	1.4451360
O	1.2631430	1.1135410	-0.8783380
F	-1.4368360	-0.1573870	-1.2548600
F	-1.3736910	1.2174140	0.4367690
F	-1.5497760	-0.9307640	0.7803550
S	0.8656140	-0.1475020	0.0757240

**Table S35.** Cartesian coordinates of optimized succinimide.

H	-1.2062330	1.7430110	0.8810170
H	-1.2072770	1.7439310	-0.8793380
H	1.2072410	1.7439170	0.8793460
H	1.2063480	1.7431480	-0.8809470
H	0.0001660	-1.9747720	-0.0001950
C	-1.1755710	-0.2130190	0.0000010
C	-0.7703710	1.2603880	0.0003140
C	0.7704050	1.2603690	-0.0003660
C	1.1755960	-0.2129360	-0.0000530
N	-0.0000160	-0.9601380	-0.0002230
O	2.2962190	-0.6779730	0.0003010
O	-2.2962800	-0.6779120	-0.0000130

**Table S36.** Cartesian coordinates of optimized **2a-succ**.

H	-1.9859260	2.7474560	1.6326160
H	-1.5119950	4.7811470	0.2784150
H	0.0535410	4.6355250	-1.6568500
H	1.1543810	2.4811150	-2.1992270
H	2.2617000	-2.1579150	-1.3677610
H	4.4975100	-2.7995270	-0.4668810
H	5.7282490	-1.2285200	1.0180660
H	4.7277780	0.9708200	1.6047070
H	2.5064510	1.5996670	0.7077760
H	-2.7324670	-3.8228240	-0.3487990
H	-1.9567590	-2.9911030	-1.6991860
H	-4.5335420	-2.2123820	-0.3836780
H	-3.7908540	-1.4433450	-1.7851920
C	-0.1420090	3.7601660	-1.0430570
C	0.4793330	2.5470460	-1.3494170
C	0.2514020	1.4097040	-0.5649640
C	-0.6401940	1.4941010	0.5200400
C	-1.2751160	2.7087240	0.8133330
C	-1.0158130	3.8435890	0.0431130
C	0.9154380	0.1077350	-0.9692630
C	2.2461140	-0.2394210	-0.3997330
C	2.8173350	-1.4819390	-0.7263290
C	4.0639630	-1.8346530	-0.2177140
C	4.7550100	-0.9508920	0.6209370
C	4.1936240	0.2855200	0.9519720
C	2.9419060	0.6398730	0.4464230
C	-1.3984700	-2.2382460	0.2092130
C	-2.4375490	-2.8392490	-0.7272420
C	-3.5893900	-1.8225900	-0.7783170
C	-3.1459440	-0.6563510	0.0962560
N	-1.8626030	-0.9587950	0.5916820
O	0.3501390	-0.6064410	-1.7903610
O	-3.7605820	0.3600310	0.3338660
O	-0.3684610	-2.7465030	0.5871870
S	-0.9541530	0.1060030	1.6204480

**Table S37.** Cartesian coordinates of optimized **Intermediate A**.

H	-4.9462210	2.0729960	-1.1471190
H	-6.7863650	1.2558020	0.3134570
H	-6.3475080	-0.5882880	1.9339520
H	-4.0940470	-1.6094890	2.0650130
H	0.3727650	-2.3516350	1.1120670
H	0.9281390	-4.6403030	0.2955210



H	-0.7290510	-5.9033340	-1.0632220
H	-2.9301770	-4.8831340	-1.6057950
H	-3.4778320	-2.6110170	-0.7888750
H	1.7928800	2.9705060	0.0579550
H	1.1808820	1.9551120	1.3584050
H	0.1170300	4.6457880	0.5720100
H	-0.3974950	3.6650680	1.9440530
H	2.1439420	0.0925070	-1.1553150
C	-5.5555010	-0.2318280	1.2808020
C	-4.2847190	-0.8079460	1.3555270
C	-3.2471680	-0.3667600	0.5249460
C	-3.4998460	0.6770440	-0.3869260
C	-4.7747120	1.2549980	-0.4548680
C	-5.8028820	0.7979550	0.3717630
C	-1.8672500	-0.9613380	0.7177570
C	-1.5865910	-2.3366360	0.2250790
C	-0.3410740	-2.9189930	0.5234900
C	-0.0363670	-4.1967390	0.0640040
C	-0.9698630	-4.9067510	-0.7020580
C	-2.2081610	-4.3348880	-1.0067590
C	-2.5174930	-3.0547260	-0.5447360
C	0.1862870	1.6599550	-0.4877220
C	0.8784300	2.5705820	0.5043580
C	-0.1689960	3.6329680	0.8743240
C	-1.4308340	3.2410350	0.1205850
C	4.4092870	-0.3678210	0.9816300
N	-1.1336380	2.0690090	-0.6224250
O	-1.0233860	-0.3001020	1.3150670
O	-2.5064340	3.7906400	0.1258890
O	0.6714820	0.7207630	-1.1070810
O	3.9471720	1.7899740	-0.5363240
O	5.4547820	-0.0477520	-1.4661370
O	3.0156310	-0.4173580	-1.2867610
F	5.4279100	0.2042300	1.6322090
F	4.6162580	-1.6855370	0.9103980
F	3.2742090	-0.1421320	1.6650510
S	-2.2953500	1.2235260	-1.6059290
S	4.2749680	0.3806820	-0.7396010

**Table S38.** Cartesian coordinates of optimized **Intermediate B**.

H	-2.5310650	-3.5252570	2.2817220
H	-2.2479540	-3.8451010	-0.1543060
H	0.7289880	-0.7212560	2.4020350
H	-1.0801520	-1.9686110	3.5484220
H	2.9410900	-1.1058740	1.7418370
H	2.0491120	1.0333060	-1.8965210
H	3.9755770	2.5483740	-1.4671150
H	5.3538500	2.2536310	0.5815060
H	4.8293690	0.4273930	2.1852400
C	-1.5713370	-3.2029930	0.3996130
C	-0.5398570	-2.5073540	-0.2378160
C	0.3326500	-1.6484100	0.4788430
C	0.1220110	-1.4379730	1.8609490
C	-0.8957690	-2.1266870	2.4906070
C	-1.7277670	-3.0080820	1.7647460
C	1.2690870	-1.0361000	-0.3923720
C	2.3748450	-0.1319890	-0.1117590
C	2.6847070	0.8898310	-1.0302500

C	3.7518250	1.7449320	-0.7714460
C	4.5219150	1.5824610	0.3856380
C	4.2239160	0.5607700	1.2932850
C	3.1504690	-0.2939310	1.0524830
C	-1.7069380	2.2690270	0.6141830
O	1.1699390	-1.4437170	-1.6516600
O	-0.3526910	0.8541500	-1.1536260
O	-2.4206390	-0.1460280	-0.2087540
O	-2.5823410	1.7620060	-1.8416950
F	-0.9688230	1.7566000	1.6336010
F	-2.9286320	2.5486780	1.1007050
F	-1.1291920	3.4266520	0.2426730
S	-0.1526070	-2.4791060	-1.9260940
S	-1.7993740	1.0530890	-0.8207810

**Table S39.** Cartesian coordinates of optimized **Intermediate C**.

H	0.0610280	4.4707060	0.0480870
H	1.3494530	2.4026600	-0.3029920
H	-3.5950270	2.2352090	0.3567490
H	-2.4020470	4.4069090	0.4015440
H	-4.5277330	0.9425510	-1.2400080
H	-3.2594870	-2.4234600	1.1345490
H	-5.6141500	-3.1997630	1.2824940
H	-7.4220800	-1.9028270	0.1687150
H	-6.8669590	0.1622970	-1.1002390
C	0.2770250	2.3582810	-0.1712210
C	-0.3862090	1.1184140	-0.1931310
C	-1.8025990	1.0836310	-0.0490060
C	-2.5256410	2.2771360	0.1830900
C	-1.8570050	3.4859380	0.2180070
C	-0.4608520	3.5177440	0.0260210
C	-2.3285760	-0.2507120	-0.1022270
C	-3.7399090	-0.6690710	-0.0250870
C	-4.0547850	-1.8571330	0.6601180
C	-5.3765090	-2.2899970	0.7383860
C	-6.3926010	-1.5593960	0.1128800
C	-6.0829500	-0.3934590	-0.5934480
C	-4.7642440	0.0566690	-0.6593820
C	4.3247130	-1.1471860	-0.2842750
O	-1.4416040	-1.1624220	-0.2178280
O	2.1600670	0.3397950	-0.6118430
O	2.7920810	-0.2989340	1.7434810
O	4.1219830	1.4262670	0.4362360
F	3.5784270	-2.2537390	-0.4354540
F	5.3546010	-1.4286770	0.5245650
F	4.7997670	-0.7818890	-1.4811990
S	0.3763220	-0.4610330	-0.3603810
S	3.2888340	0.2273880	0.4738290

## 9. Measurements of Photophysical Properties of **3aa–3ca** and **3ea–3ga**

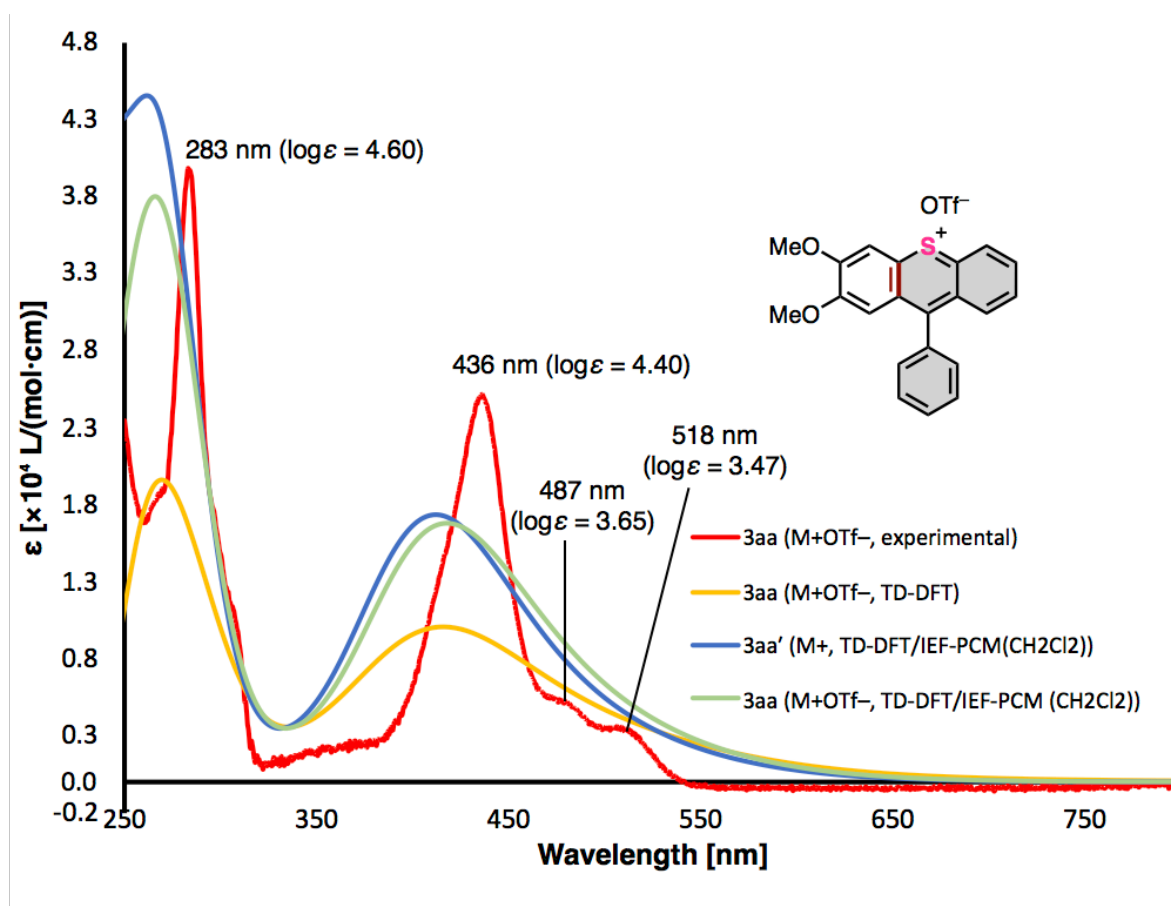
All photophysical measurements were conducted in the diluted solution of compounds in CH<sub>2</sub>Cl<sub>2</sub> (super dehydrated grade, KANTO) in a 1 × 1 cm square quartz cell.

UV-Vis-NIR absorption spectra of **3aa–3ca** and **3ea–3ga** in CH<sub>2</sub>Cl<sub>2</sub> were recorded on a SHIMADZU UV-3600 spectrophotometer with a resolution of 0.5 nm. Experimental absorption spectra were compared to the calculated ones with the B3LYP/6-311++G(2d,p)//B3LYP/6-311+G(2d,p) level of theories in CH<sub>2</sub>Cl<sub>2</sub> (IEF-PCM). Same calculations with CAM-B3LYP/6-311++G(2d,p)//CAM-B3LYP/6-311+G(2d,p) level of theories in CH<sub>2</sub>Cl<sub>2</sub> (IEF-PCM) and M06-2X/6-311++G(2d,p)//M06-2X/6-311+G(2d,p) level of theories in CH<sub>2</sub>Cl<sub>2</sub> (IEF-PCM) were conducted. As a result, simulated absorption spectra using the B3LYP level were more consistent with the experimental spectra than those using CAM-B3LYP and M06-2X levels.

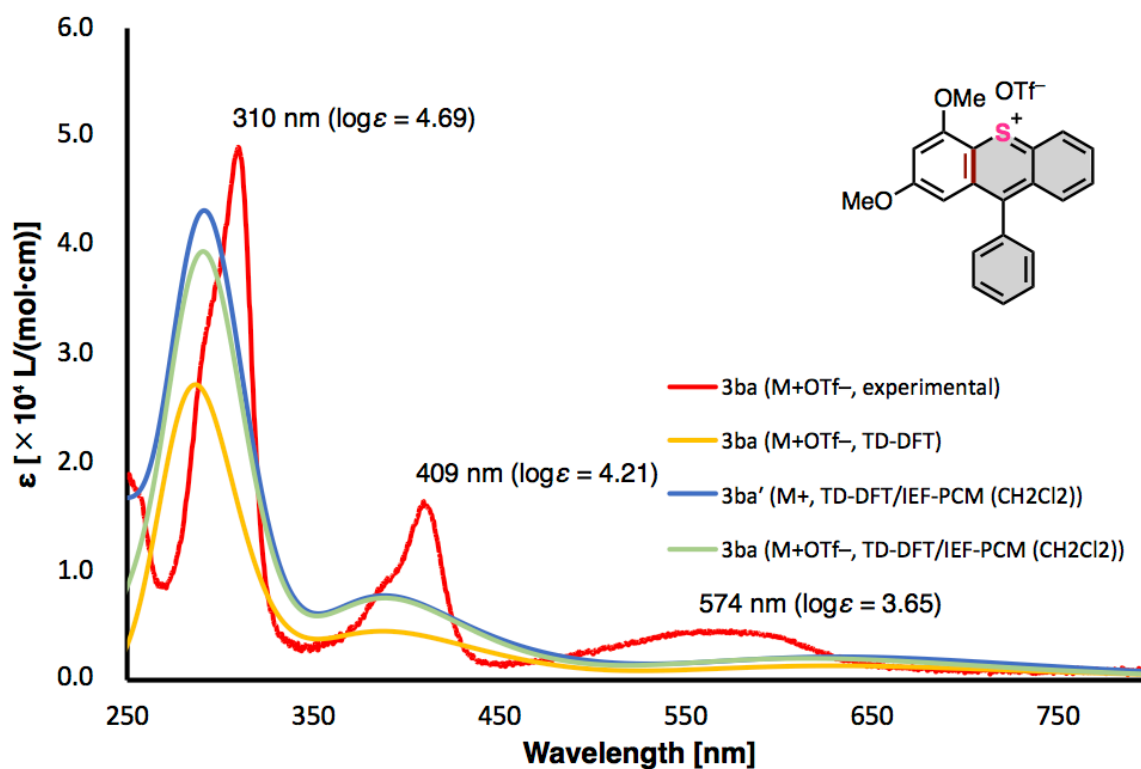
Emission spectra of degassed solution of **3aa–3ca** and **3ea–3ga** in CH<sub>2</sub>Cl<sub>2</sub> were recorded with a JASCO FP-6600 fluorescence spectrometer with a resolution of 0.4 nm upon excitation at 436 nm (**3aa**), 545 nm (**3ba**), 600 nm (**3ca**), 495 nm (**3ea**), 636 nm (**3fa**) and 564 (**3ga**). Besides, a UV-34 color filter glass was attached to the entrance side or detector side of excitation light for fluorescence spectroscopy of **3ea** and **3ga** to remove extra diffracted light outside the range of 400–2700 nm.<sup>[25]</sup>

Quantum yields were measured with a HAMAMATSU Quantaaurus-QY Plus UV-NIR absolute PL quantum yield spectrometer C13534.

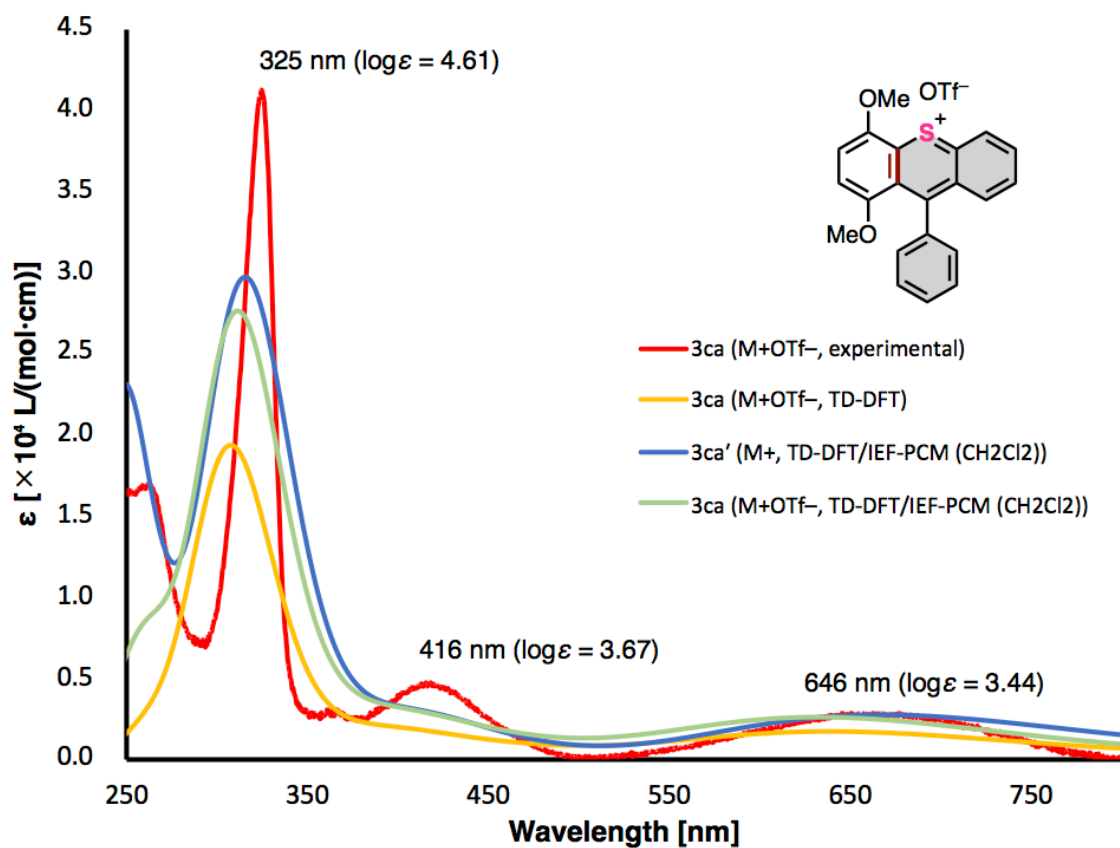
Fluorescent lifetime was measured with a HAMAMATSU near infrared compact fluorescence lifetime spectrometer C12132 equipped with a HAMAMATSU TDC unit M12977.



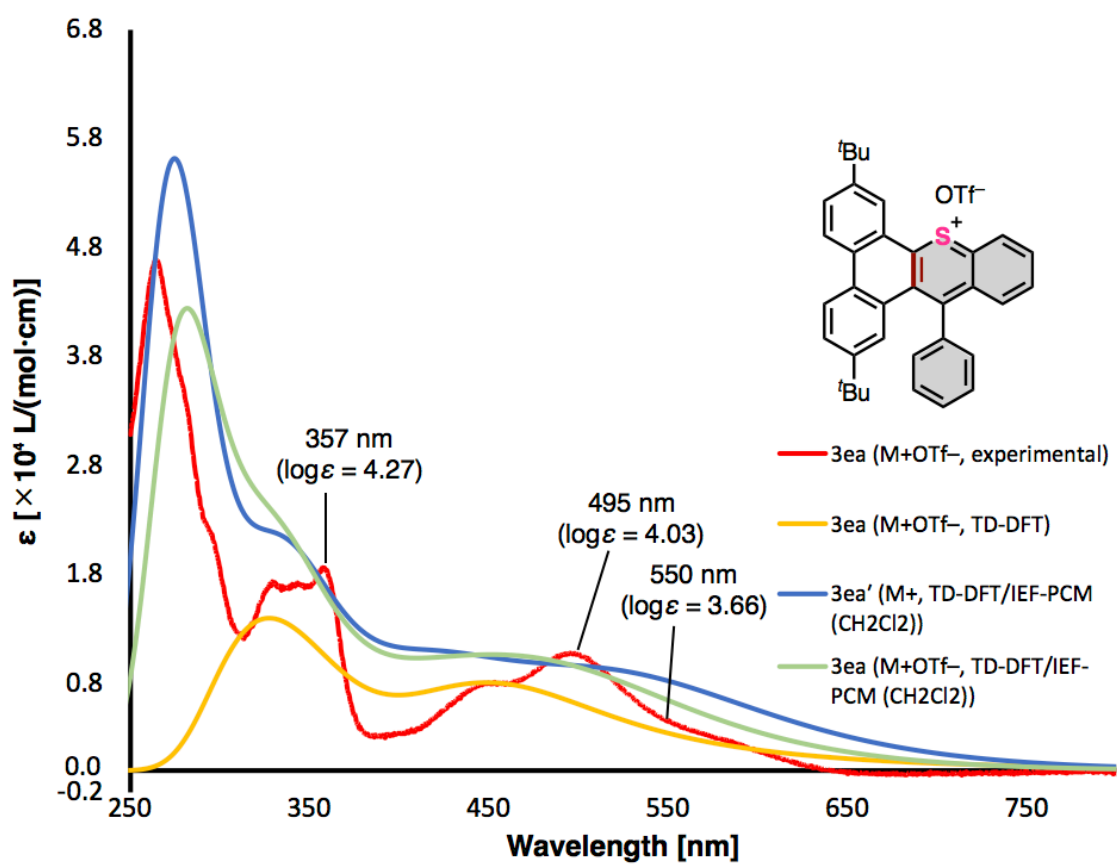
**Figure S22.** UV-Vis-NIR absorption spectra of **3aa** in  $\text{CH}_2\text{Cl}_2$  ( $c = 6.0 \times 10^{-6} \text{ M}$ ), and simulated absorption spectra of free cation **3aa'** and salt **3aa** calculated by TD-DFT/B3LYP/6-311++G(2d,p)//B3LYP/6-311+G(2d,p) with/without the consideration of IEF-PCM ( $\text{CH}_2\text{Cl}_2$ ).



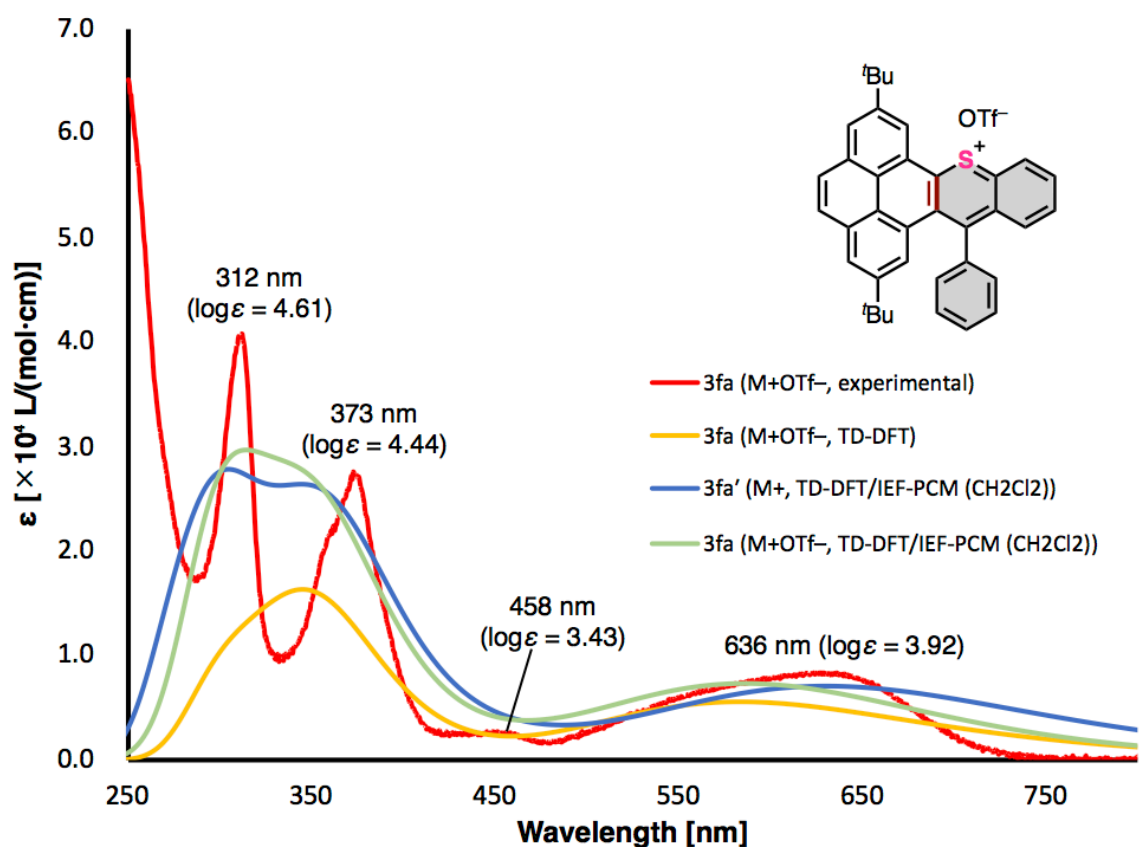
**Figure S23.** UV-Vis-NIR absorption spectra of **3ba** in  $\text{CH}_2\text{Cl}_2$  ( $c = 4.6 \times 10^{-6} \text{ M}$ ), and simulated absorption spectra of free cation **3ba'** and salt **3ba** calculated by TD-DFT/B3LYP/6-311++G(2d,p)//B3LYP/6-311+G(2d,p) with/without the consideration of IEF-PCM ( $\text{CH}_2\text{Cl}_2$ ).



**Figure S24.** UV-Vis-NIR absorption spectra of **3ca** in  $\text{CH}_2\text{Cl}_2$  ( $c = 7.6 \times 10^{-6}$  M), and simulated absorption spectra of free cation **3ca'** and salt **3ca** calculated by TD-DFT/B3LYP/6-311++G(2d,p)//B3LYP/6-311+G(2d,p) with/without the consideration of IEF-PCM ( $\text{CH}_2\text{Cl}_2$ ).

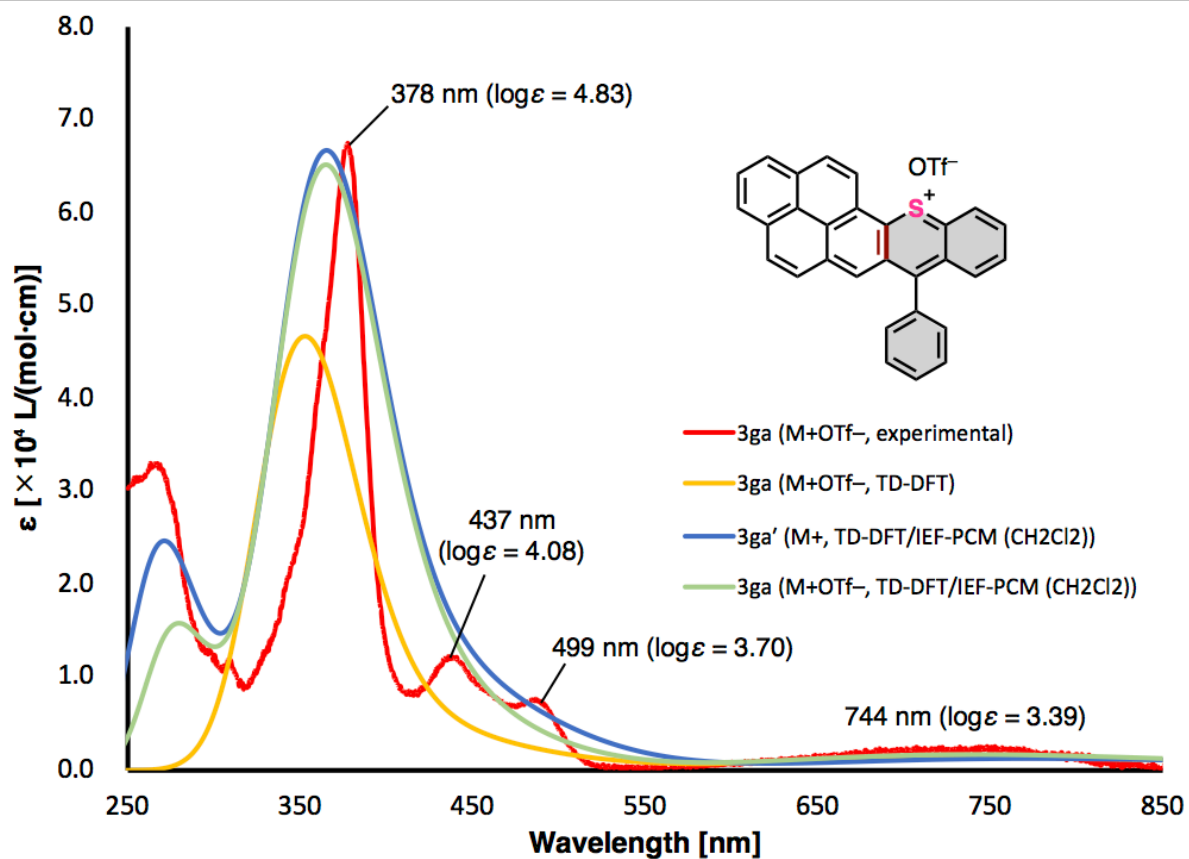


**Figure S25.** UV-Vis-NIR absorption spectra of **3ea** in  $\text{CH}_2\text{Cl}_2$  ( $c = 9.0 \times 10^{-6} \text{ M}$ ), and simulated absorption spectra of free cation **3ea'** and salt **3ea** calculated by TD-DFT/B3LYP/6-311++G(2d,p)//B3LYP/6-311+G(2d,p) with/without the consideration of IEF-PCM ( $\text{CH}_2\text{Cl}_2$ ).

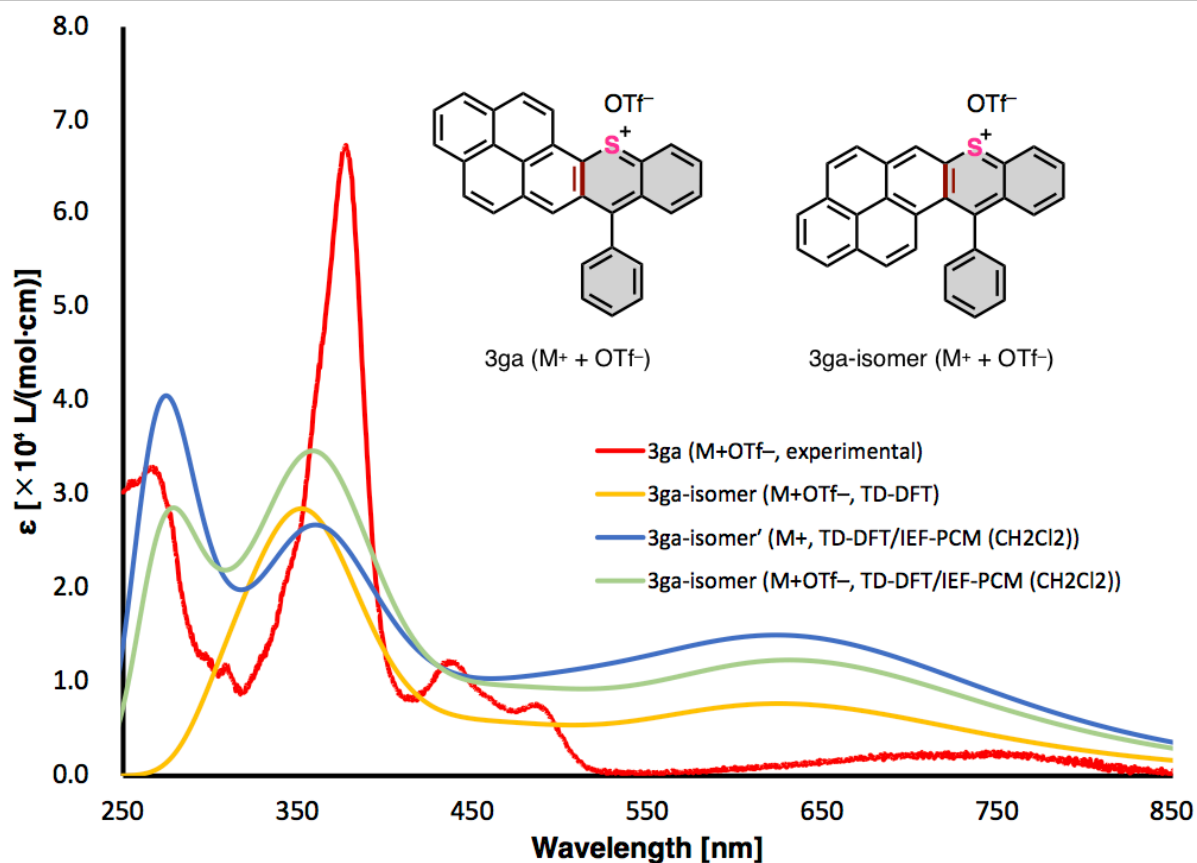


**Figure S26.** UV-Vis-NIR absorption spectra of **3fa** in  $\text{CH}_2\text{Cl}_2$  ( $c = 4.9 \times 10^{-6} \text{ M}$ ), and simulated absorption spectra of free cation **3fa'** and salt **3fa** calculated by TD-DFT/B3LYP/6-311++G(2d,p)//B3LYP/6-311+G(2d,p) with/without the consideration of IEF-PCM ( $\text{CH}_2\text{Cl}_2$ ).

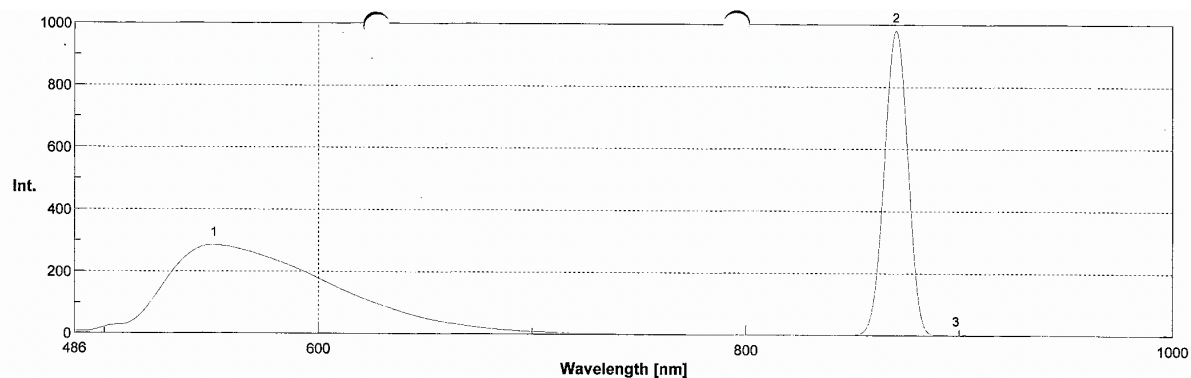




**Figure S27.** UV-Vis-NIR absorption spectra of **3ga** in  $\text{CH}_2\text{Cl}_2$  ( $c = 4.0 \times 10^{-6} \text{ M}$ ), and simulated absorption spectra of free cation **3ga'** and salt **3ga** calculated by TD-DFT/B3LYP/6-311++G(2d,p)//B3LYP/6-311+G(2d,p) with/without the consideration of IEF-PCM ( $\text{CH}_2\text{Cl}_2$ ). Note: This sample solution was prepared from **3ga** whose purity was estimated as 98<sub>wt</sub>% by  $^1\text{H}$  NMR.

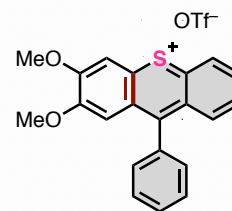


**Figure S28.** Comparison with experimental UV-Vis-NIR absorption spectra of **3ga** in  $\text{CH}_2\text{Cl}_2$  and simulated absorption spectra of free cation **3ga-isomer'** and salt **3ga-isomer** calculated by TD-DFT/B3LYP/6-311++G(2d,p)//B3LYP/6-311+G(2d,p) with/without the consideration of IEF-PCM ( $\text{CH}_2\text{Cl}_2$ ).



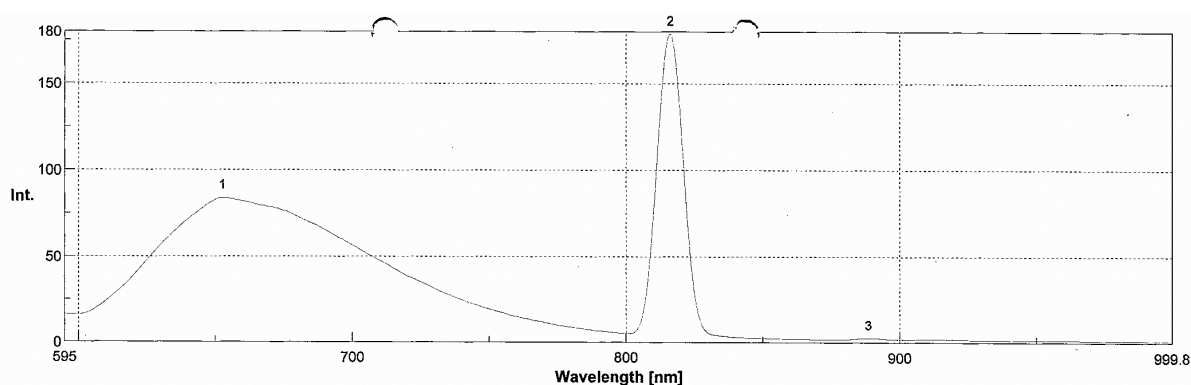
日時 2021/12/13 21:18  
 機種名 FP-6600  
 シリアル番号 D092860822  
 測定モード 蛍光スペクトル  
 励起側バンド幅 5 nm  
 蛍光側バンド幅 10 nm  
 レスポンス 2 sec  
 感度 High  
 測定範囲 486 - 1000 nm  
 データ取込間隔 0.4nm  
 励起波長 436.0 nm  
 走査速度 200 nm/min  
 試料番号 113  
 繰返し回数 1

ファイル名 KOHthia303e\_Ex436\_CH2Cl2.jws



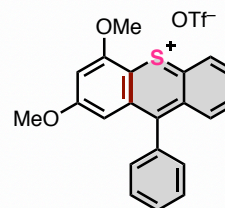
No.	nm	Int.	No.	nm	Int.	No.	nm	Int.
1	551.2	284.58	2	870.4	982.162	3	982.4	4.04412

**Figure S29.** Emission spectra of **3aa** in  $\text{CH}_2\text{Cl}_2$ . The peak at 870 nm was derived from the secondary diffracted light of the excitation light at 436 nm.



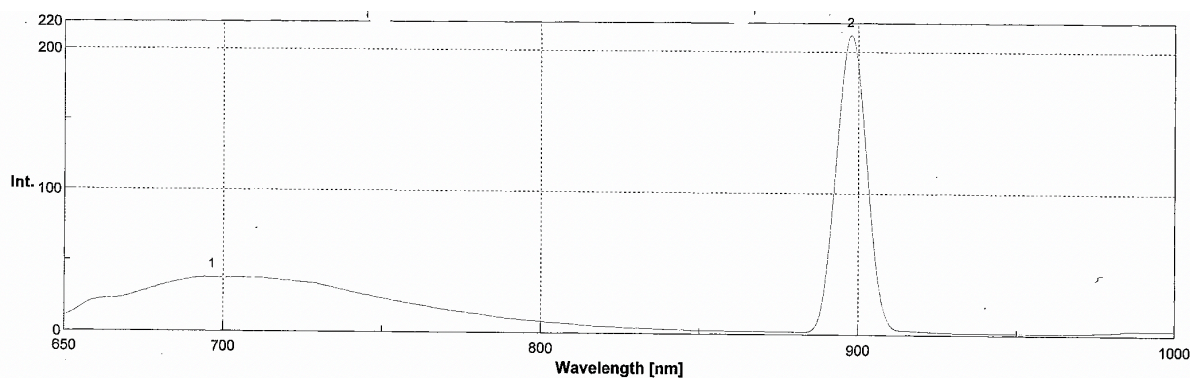
日時 2021/12/13 21:29  
 機種名 FP-6600  
 シリアル番号 D092860822  
 測定モード 蛍光スペクトル  
 励起側バンド幅 5 nm  
 蛍光側バンド幅 10 nm  
 レスポンス 2 sec  
 感度 High  
 測定範囲 595 - 999.8 nm  
 データ取込間隔 0.4nm  
 励起波長 545.0 nm  
 走査速度 200 nm/min  
 試料番号 116  
 繰返し回数 1

ファイル名 KOHthia388e\_Ex545\_CH2Cl2.jws



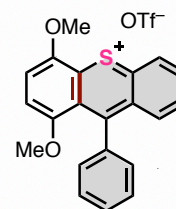
No.	nm	Int.	No.	nm	Int.	No.	nm	Int.
1	652.6	83.8001	2	816.2	178.741	3	886.6	2.51644

**Figure S30.** Emission spectra of **3ba** in  $\text{CH}_2\text{Cl}_2$ . The peak at 816 nm was derived from the tertiary diffracted light of the secondary diffracted light of excitation light at 545 nm.



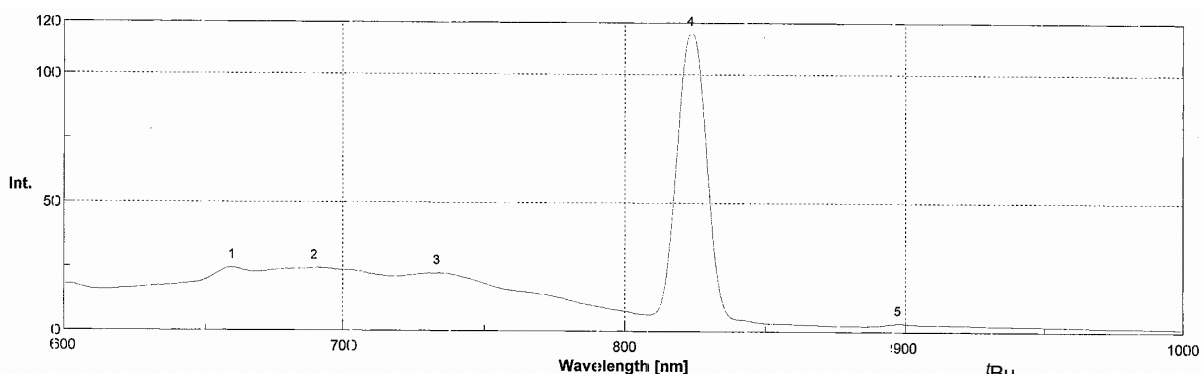
日時 2021/12/13 21:44  
 機種名 FP-6600  
 シリアル番号 D092860822  
 測定モード 蛍光スペクトル  
 励起側バンド幅 5 nm  
 蛍光側バンド幅 10 nm  
 レスポンス 2 sec  
 感度 High  
 測定範囲 650 - 1000 nm  
 データ取込間隔 0.4nm  
 励起波長 600.0 nm  
 走査速度 200 nm/min  
 試料番号 119  
 繰返し回数 1

ファイル名 KOHthia294c\_Ex600\_CH2Cl2.jws



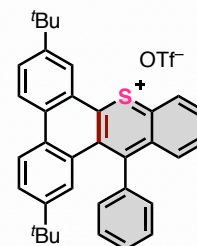
No.	nm	Int.	No.	nm	Int.
1	696.4	38.3352	2	897.6	211.762

**Figure S31.** Emission spectra of **3ca** in CH<sub>2</sub>Cl<sub>2</sub>. The peak at 898 nm was derived from the tertiary diffracted light of the secondary diffracted light of excitation light at 600 nm.



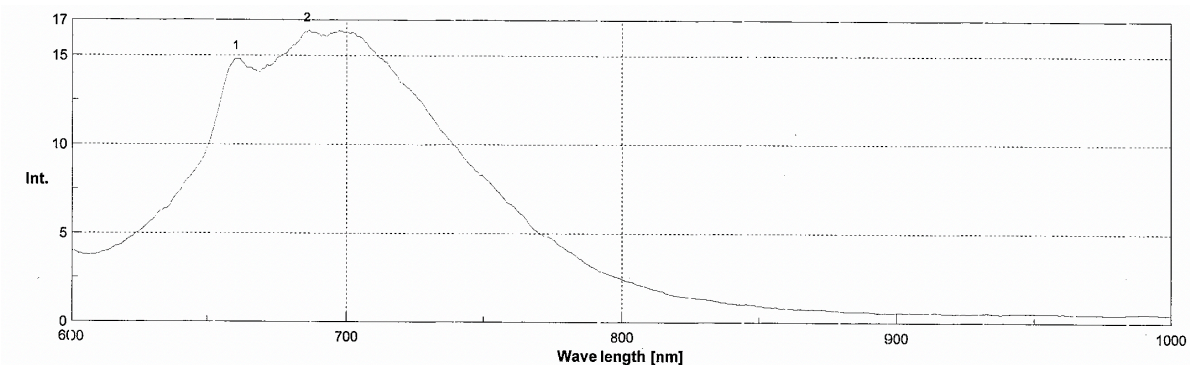
日時 2022/03/08 21:29  
 機種名 FP-6600  
 シリアル番号 D092860822  
 測定モード 蛍光スペクトル  
 励起側バンド幅 5 nm  
 蛍光側バンド幅 10 nm  
 レスポンス 2 sec  
 感度 High  
 測定範囲 600 - 1000 nm  
 データ取込間隔 0.4nm  
 励起波長 550.0 nm  
 走査速度 200 nm/min  
 試料番号 35  
 繰返し回数: 1

ファイル名 KOHthia370-2g\_Ex550\_20220308\_DCM.jws



No.	nm	Int.	No.	nm	Int.	No.	nm	Int.	No.	nm	Int.	No.	nm	Int.
1	659.6	24.6369	2	689.6	24.5532	3	733.2	22.6496	4	823.6	115.714	5	897.2	3.39619

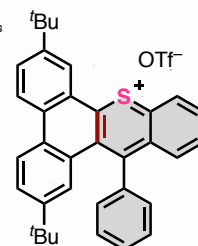
**Figure S32.** Emission spectra of **3ea** in CH<sub>2</sub>Cl<sub>2</sub>. The peak at 824 nm was derived from the tertiary diffracted light of the secondary diffracted light of excitation light at 550 nm.



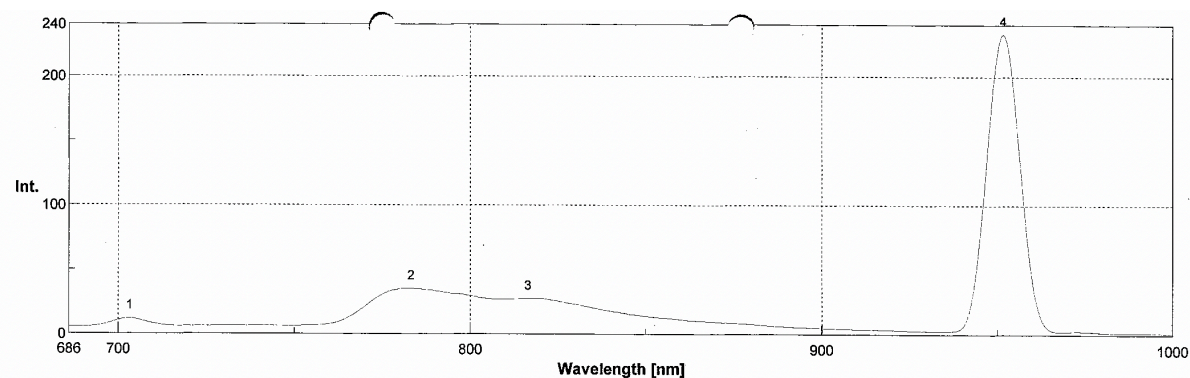
日時 2022/03/08 21:21  
 機種名 FP-6600  
 シリアル番号 D092890822  
 測定モード 蛍光スペクトル  
 励起側バンド幅 5 nm  
 蛍光側バンド幅 10 nm  
 レスポンス 2 sec  
 感度 High  
 測定範囲 600 - 1000 nm  
 データ取込間隔 0.4nm  
 励起波長 550.0 nm  
 走査速度 200 nm/min  
 試料番号 32  
 繰返し回数 1  
 試料名  
 測定者  
 コメント

ファイル名

KOHthia370-2d\_Ex550\_20220308\_DCM\_CutByUV-34\_jws



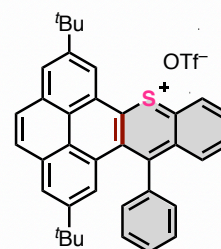
**Figure S33.** Emission spectra of **3ea** in  $\text{CH}_2\text{Cl}_2$  when a color filter glass (UV-34) was used. Wavelength of the excitation light at 550 nm.



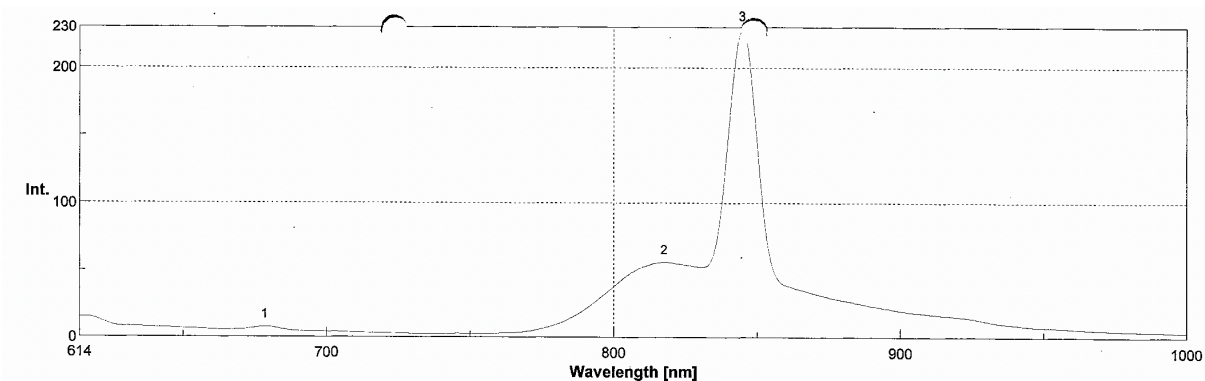
日時 2021/12/15 13:32  
 機種名 FP-6600  
 シリアル番号 D092860822  
 測定モード 蛍光スペクトル  
 励起側バンド幅 5 nm  
 蛍光側バンド幅 10 nm  
 レスポンス 2 sec  
 感度 High  
 測定範囲 686 - 1000 nm  
 データ取込間隔 0.4nm  
 励起波長 636.0 nm  
 走査速度 200 nm/min  
 試料番号 125  
 繰返し回数 1  
 試料名  
 測定者  
 コメント

ファイル名

KOHthia309-2a\_Ex636\_OH2012\_jws

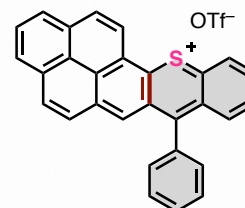


**Figure S34.** Emission spectra of **3fa** in  $\text{CH}_2\text{Cl}_2$ . The peak at 952 nm was derived from the tertiary diffracted light of the secondary diffracted light of excitation light at 636 nm.



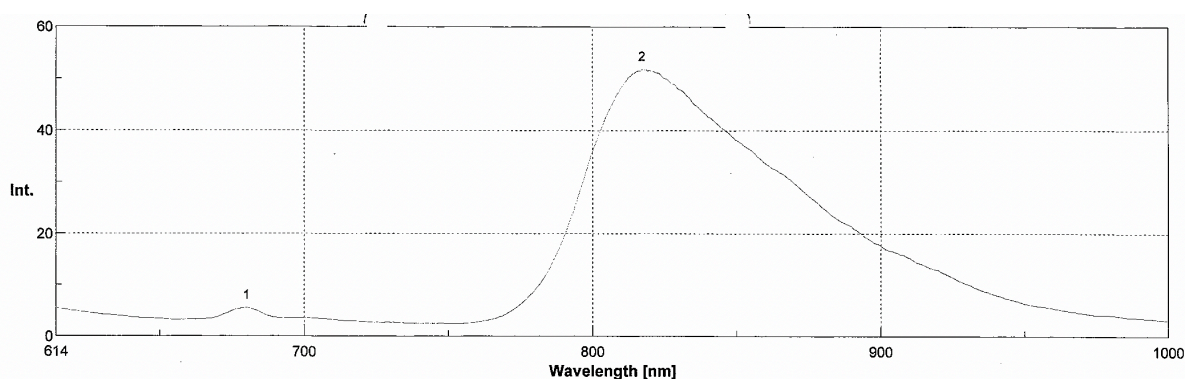
日時 2021/12/15 13:45  
 機種名 FF-6600  
 シリアル番号 D092860822  
 測定モード 蛍光スペクトル  
 励起側バンド幅 5 nm  
 蛍光側バンド幅 10 nm  
 レスポンス 2 sec  
 感度 High  
 測定範囲 614 - 1000 nm  
 テータ取込間隔 0.4nm  
 励起波長 564.0 nm  
 走査速度 200 nm/min  
 試料番号 129  
 繰返し回数 1

ファイル名 KOHthia326-2a\_Ex564\_CH2Cl2.jws



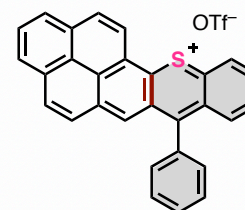
No.	nm	Int.	No.	nm	Int.	No.	nm	Int.
1	678.4	7.51772	2	817.6	56.0132	3	844.8	228.764

**Figure S35.** Emission spectra of **3ga** in  $\text{CH}_2\text{Cl}_2$ . The peak at 845 nm was derived from the tertiary diffracted light of the secondary diffracted light of excitation light at 564 nm. Note: This sample solution was prepared from **3ga** whose purity was estimated as 98<sub>wt</sub>% by  $^1\text{H}$  NMR.



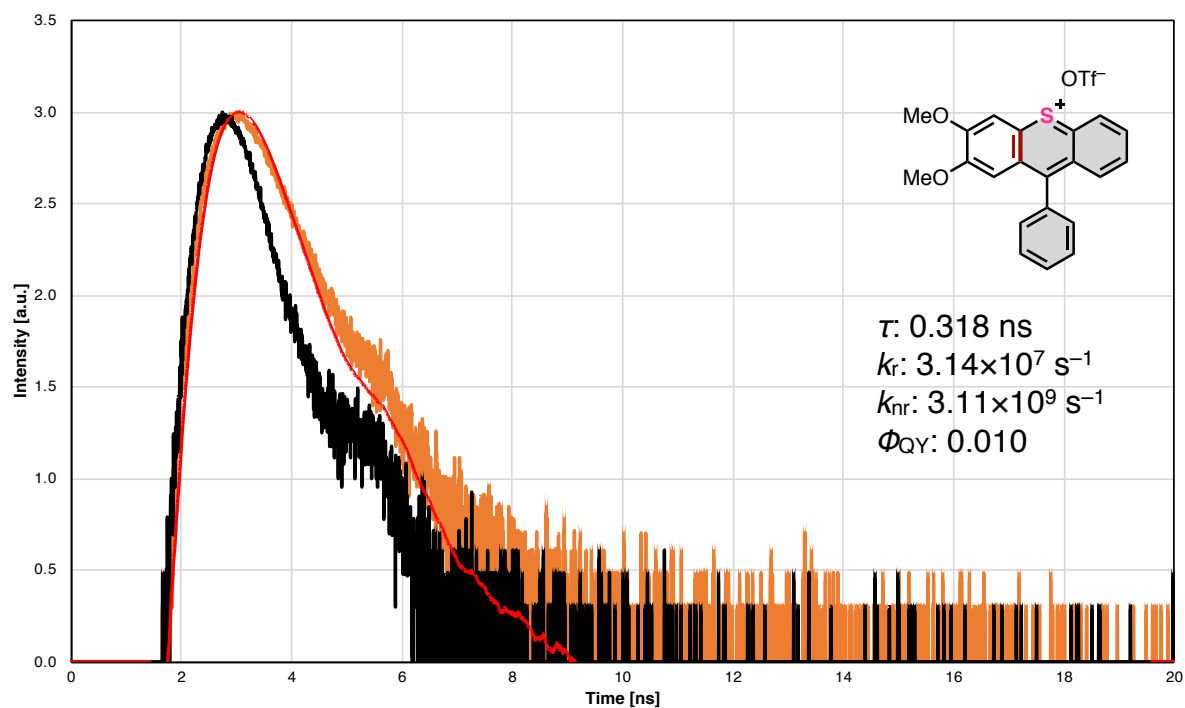
日時 2021/12/15 13:57  
 機種名 FF-6600  
 シリアル番号 D092860822  
 測定モード 蛍光スペクトル  
 励起側バンド幅 5 nm  
 蛍光側バンド幅 10 nm  
 レスポンス 2 sec  
 感度 High  
 測定範囲 614 - 1000 nm  
 テータ取込間隔 0.4nm  
 励起波長 564.0 nm  
 走査速度 200 nm/min  
 試料番号 132  
 繰返し回数 1

ファイル名 KOHthia326-2d\_Ex564\_OutByUV-34\_detector\_CH2Cl2.jws

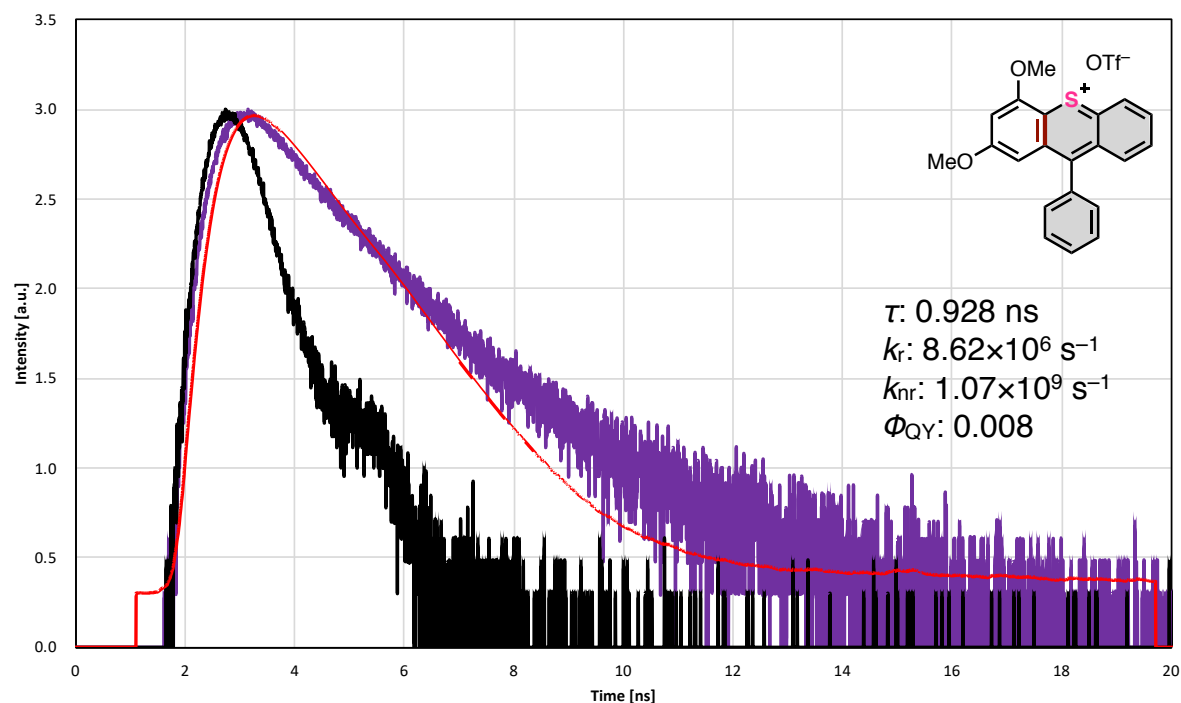


No.	nm	Int.	No.	nm	Int.
1	680	5.53499	2	817.2	51.8267

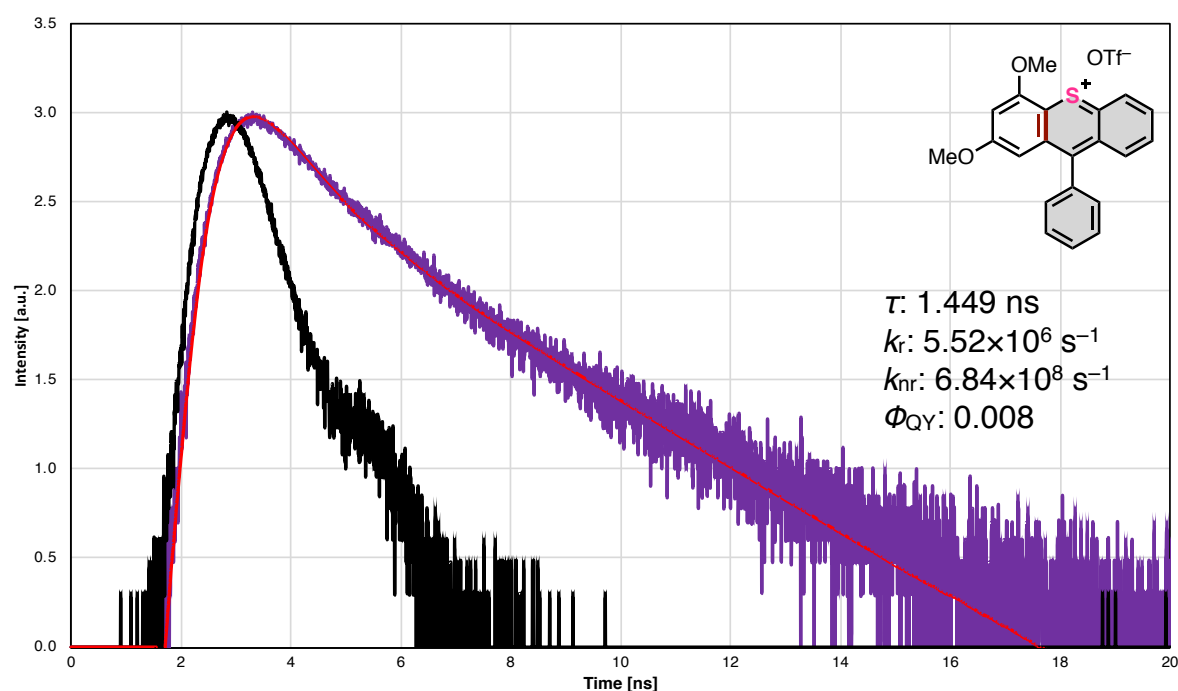
**Figure S36.** Emission spectra of **3ga** in  $\text{CH}_2\text{Cl}_2$  when a color filter glass (UV-34) was used. Wavelength of the excitation light at 564 nm. Note: This sample solution was prepared from **3ga** whose purity was estimated as 98<sub>wt</sub>% by  $^1\text{H}$  NMR.



**Figure S37.** The profile of fluorescence decay on thiopyrylium **3aa** in  $\text{CH}_2\text{Cl}_2$ . Excitation wavelength: 355 nm. Emission wavelength: 550 nm. Fluorescence intensity was described as common logarithm. Orange line: experimental fluorescence decay of **3aa**. Black line: curve of IRF. Red line: Fitting plot.



**Figure S38.** The profile of fluorescence decay on thiopyrylium **3ba** in  $\text{CH}_2\text{Cl}_2$ . Excitation wavelength: 355 nm. Emission wavelength: 650 nm. Fluorescence intensity was described as common logarithm. Purple line: experimental fluorescence decay of **3ba**. Black line: curve of IRF. Red line: Fitting plot.



**Figure S39.** The profile of fluorescence decay on thiopyrylium **3ba** in  $\text{CH}_2\text{Cl}_2$ . Excitation wavelength: 532 nm. Emission wavelength: 650 nm. Fluorescence intensity was described as common logarithm. Purple line: experimental fluorescence decay of **3ba**. Black line: curve of IRF. Red line: Fitting plot.

## 5. References

- [1] (a) Mckinnon, D. M. *Can. J. Chem.* **1970**, *48*, 3388. (b) Berényi, S.; Tóth, M.; Gyulai, S.; Szilágyi, L. *Heterocycles* **2002**, *57*, 135. (c) Rudorf, W. D. *Sci. Synth.* **2003**, *14*, 649. (d) Kassae, M. Z.; Jalalimanesh, N.; Musavi, S. M. *J. Mol. Struct.: THEOCHEM* **2007**, *816*, 153. (e) Seller, R. V.; Reshetov, P. V.; Kriven'ko, A. P. *Chem. Heterocycl. Compd.* **2001**, *37*, 797. (f) Kharchenko, V. G.; Chalaya, S. N.; Konovalova, T. M. *Chem. Heterocycl. Compd* **1975**, *11*, 125. (g) Doddi, G.; Ercolani, G. *Adv. Heterocycl. Chem.* **1994**, *60*, 65. (h) Stępień, M.; Gońka, E.; Żyła, M.; Sprutta, N. *Chem. Rev.* **2017**, *117*, 3479. (i) Borissov, A.; Maurya, Y. K.; Moshniaha, L.; Wong, W.-S.; Żyła-Karwowska, M.; Stępień, M. *Chem. Rev.* **2022**, *122*, 565.
- [2] (a) Scarpaci, A.; Nantalaksakul, A.; Hales, J. M.; Matichak, J. D.; Barlow, S.; Rumi, M.; Perry, J. W. Marder, S. R. *Chem. Mater.* **2012**, *24*, 1606. (b) Wagner, S. J.; Skripchenko, A.; Cincotta, L.; Thompson-Montgomery, D.; Awatefe, H. *Transfusion* **2005**, *45*, 752. (c) Wu, D.; Pisula, W.; Haberecht, M. C.; Feng, X.; Müllen, K. *Org. Lett.* **2009**, *11*, 5686. (d) Nagahora, N.; Kushida, T.; Shioji, K.; Okuma, K. *Organometallics* **2019**, *38*, 1800. (e) Nagahora, N.; Kitahara, K.; Mizuhata, Y.; Tokitoh, N.; Shioji, K.; Okuma, K. *J. Org. Chem.* **2020**, *85*, 7748. (f) Nagahora, N.; Tanaka, R.; Tada, T.; Yasuda, A.; Yamada, Y.; Shioji, K.; Okuma, K. *Org. Lett.* **2020**, *22*, 6192. (g) Tanaka, K.; Kishimoto, M.; Sukekawa, M.; Hoshino, Y.; Honda, K. *Tetrahedron Lett.* **2018**, *59*, 3361. (h) Tanaka,



- K.; Iwama, Y.; Kishimoto, M.; Ohtsuka, N.; Hoshino, Y.; Honda, K. *Org. Lett.* **2020**, *22*, 5207. (i) Zhou, H.; Zeng, X.; Li, A.; Zhou, W.; Tang, L.; Hu, W.; Fan, Q.; Meng, X.; Deng, H.; Duan, L.; Li, Y.; Deng, Z.; Hong, X.; Xiao, Y. *Nat. Commun.* **2020**, *11*, 6183. (j) Browne, W. R.; Pollard, M. M.; Lange, B. d.; Meetsma, A.; Feringa, B. L. *J. Am. Chem. Soc.* **2006**, *128*, 12412. (k) Kearns, H.; Sengupta, S.; Sasselli, I. R.; Bromley III, L.; Faulds, K.; Tuttle, T.; Bedics, M. A.; Detty, M. R.; Velarde, L.; Graham, D.; Smith, W. E. *Chem. Sci.* **2016**, *7*, 5160.
- [3] Kharchenko, V. G.; Kleimenova, V. I.; Yakoreva, A. R. *Chem. Heterocycl. Compd.* **1970**, *6*, 834.
- [4] (a) Liebscher, J.; Abegaz, B.; Knoll, A. *Phosphorus Sulfur Silicon Relat. Elem.* **1988**, *35*, 5. (b) Fabian, J.; Hartmann, H. *Tetrahedron Lett.* **1969**, *10*, 239.
- [5] Reviews on APEX reaction: (a) Ito, H.; Ozaki, K.; Itami, K. *Angew. Chem., Int. Ed.* **2017**, *56*, 11144. (b) Ito, H.; Segawa, Y.; Murakami, K.; Itami, K. *J. Am. Chem. Soc.* **2019**, *141*, 3.
- [6] Our representative examples of APEX reaction of PAH and heteroaromatics: (a) Ozaki, K.; Kawasumi, K.; Shibata, M.; Ito, H.; Itami, K. *Nat. Commun.* **2015**, *6*, 6251. (b) Matsuoka, W.; Ito, H.; Itami, K. *Angew. Chem., Int. Ed.* **2017**, *56*, 12224. (c) Matsuoka, W.; Ito, H.; Sarlah, D.; Itami, K. *Nat. Commun.* **2021**, *12*, 3940.
- [7] Hetero-APEX reactions: (a) Kawahara, K. P.; Matsuoka, W.; Ito, H.; Itami, K. *Angew. Chem., Int. Ed.* **2020**, *59*, 6383. (b) Yan, J.; Pulis, A. P.; Perry, G. J. P.; Procter, D. J. *Angew. Chem., Int. Ed.* **2019**, *58*, 15675. (c) Schendera, E.; Unkel, L.-N.; Quyen, P. P. H.; Salkewitz, G.; Hoffmann, F.; Villinger, A.; Brasholz, M. *Chem. Eur. J.* **2020**, *26*, 269. (d) Yu, Z.; Zhang, Y.; Tang, J.; Zhang, L.; Liu, Q.; Li, Q.; Gao, G.; You, J. *ACS Catal.* **2020**, *10*, 203. (e) Tokita, S.; Hiruta, K.; Kitahara, K.; Nishi, H. *Synthesis* **1982**, *3*, 229. (f) Maiti, S.; Achar, T. K.; Mal, P. *Org. Lett.* **2017**, *19*, 2006. (g) Regar, R.; Mishra, R.; Mondal, P. K.; Sankar, J. *J. Org. Chem.* **2018**, *83*, 9547. (h) Tokimaru, Y.; Ito, S.; Nozaki, K. *Angew. Chem., Int. Ed.* **2017**, *56*, 15560. (i) Qarah, A.; Gasonoo, M.; Do, D.; Klumpp, D. A. *Tetrahedron Lett.* **2016**, *57*, 3711. (j) Chen, C.; Wang, Y.; Shi, X.; Sun, W.; Zhao, J.; Zhu, Y.-P.; Liu, L.; Zhu, B. *Org. Lett.* **2020**, *22*, 4097. (k) Wang, M.; Kong, L.; Wang, F.; Lia, X. *Adv. Synth. Catal.* **2017**, *359*, 4411.
- [8] (a) Ramesh, E.; Shankar, M.; Dana, S.; Sahoo, A. K. *Org. Chem. Front.* **2016**, *3*, 1126. (b) Wang, X.; Gensch, T.; Glorius, F. *Org. Chem. Front.* **2016**, *3*, 1619. (c) Ramesh, E.; Guntreddi, T.; Sahoo, A. K.; *Eur. J. Org. Chem.* **2017**, 4405. (d) Saravanan, P.; Anbarasan, P. *Org. Lett.* **2014**, *16*, 848. (e) Hostier, T.; Ferey, V.; Ricci, G.; Pardo, D. G.; Cossy, J. *Org. Lett.* **2015**, *17*, 3898.
- [9] (a) Ye, X.; Xu, B.; Sun, J.; Dai, L.; Shao, Y.; Zhang, Y.; Chen, J. *J. Org. Chem.* **2020**, *85*, 13004. (b) Pang, X.; Lou, Z.; Li, M.; Wen, L.; Chen, C. *Eur. J. Org. Chem.* **2015**, 3361.
- [10] (a) Souza, L. W.; Squitieri, R. A.; Dimirjian, C. A.; Hodur, B. M.; Nickerson, L. A.; Penrod, C. N.; Cordova, J.; Fettinger, J. C.; Shaw, J. T. *Angew. Chem., Int. Ed.* **2018**, *57*, 15213. (b) Katritzky, A. R.; Kirichenko, K.; Ji, Y.; Prakash, I. *Chem. Heterocycl. Compd.* **2002**, *38*, 156.

- [11] Representative reports on C1-selective S<sub>E</sub>Ar reactions of pristine pyrene: (a) Liu, M.; Gong, X.; Zheng, C.; Gao, D. *Asian J. Org. Chem.* **2017**, *6*, 1903. (b) Gumprecht, W. H. *Org. Synth.* **1968**, *48*, 30. (c) Zych, D. *Molecules* **2019**, *24*, 2551.
- [12] Hogan, D. T.; Sutherland, T. C. *J. Phys. Chem. Lett.* **2018**, *9*, 2825.
- [13] P.-Y. Gu, Z. Wang, G. Liu, H. Yao, Z. Wang, Y. Li, J. Zhu, S. Li, and Q. Zhang, *Chem. Mater.* **2017**, *29*, 4172.
- [14] (a) V. Mamane, and A. Fürstner, *J. Org. Chem.* **2002**, *67*, 6264. (b) K. Ozaki, K. Kawasumi, M. Shibata, H. Ito, and K. Itami, *Nat. Commun.* **2015**, *6*, 6251.
- [15] Liu, Y.; Kim, J.; Seo, H.; Park, S.; Chae, J. *Adv. Synth. Catal.* **2015**, *357*, 2205.
- [16] [https://sdb.sdb.aist.go.jp/sdb/cgi-bin/cre\\_index.cgi](https://sdb.sdb.aist.go.jp/sdb/cgi-bin/cre_index.cgi), SDBS No.: 13687, Compound name: silver(I) teifluoromethanesulfonate, Spectral Code: <sup>13</sup>C NMR in D<sub>2</sub>O.
- [17] Sheldrick, G. M. *Acta Crystallogr.* **2015**, *A71*, 3.
- [18] Sheldrick, G. M. *Acta Crystallogr.* **2015**, *C71*, 3.
- [19] Dolomanov, O. V.; Bourhis, L. J.; Gildea, R. J.; Howard, J. A. K.; Puschmann, H. *J. Appl. Crystallogr.* **2009**, *42*, 339.
- [20] Gaussian 16, Revision C.01, M. J. Frisch, G. W. Trucks, H. B. Schlegel, G. E. Scuseria, M. A. Robb, J. R. Cheeseman, G. Scalmani, V. Barone, G. A. Petersson, H. Nakatsuji, X. Li, M. Caricato, A. V. Marenich, J. Bloino, B. G. Janesko, R. Gomperts, B. Mennucci, H. P. Hratchian, J. V. Ortiz, A. F. Izmaylov, J. L. Sonnenberg, D. Williams-Young, F. Ding, F. Lipparini, F. Egidi, J. Goings, B. Peng, A. Petrone, T. Henderson, D. Ranasinghe, V. G. Zakrzewski, J. Gao, N. Rega, G. Zheng, W. Liang, M. Hada, M. Ehara, K. Toyota, R. Fukuda, J. Hasegawa, M. Ishida, T. Nakajima, Y. Honda, O. Kitao, H. Nakai, T. Vreven, K. Throssell, J. A. Montgomery, Jr., J. E. Peralta, F. Ogliaro, M. J. Bearpark, J. J. Heyd, E. N. Brothers, K. N. Kudin, V. N. Staroverov, T. A. Keith, R. Kobayashi, J. Normand, K. Raghavachari, A. P. Rendell, J. C. Burant, S. S. Iyengar, J. Tomasi, M. Cossi, J. M. Millam, M. Klene, C. Adamo, R. Cammi, J. W. Ochterski, R. L. Martin, K. Morokuma, O. Farkas, J. B. Foresman, D. J. Fox, Gaussian, Inc., Wallingford CT, **2016**.
- [21] Levandowski, B. J.; Herath, D.; Gallup, N. M.; Houk, K. N. *J. Org. Chem.* **2018**, *83*, 2611.
- [22] (a) Becke, A. D. *J. Chem. Phys.* **1993**, *98*, 5648. (b) Lee, C.; Yang, W.; Parr, R. G. *Phys. Rev. B* **1988**, *37*, 785.
- [23] Mennucci, B.; Cancès, E.; Tomasi, J. *J. Phys. Chem. B* **1997**, *101*, 10506.
- [24] GaussView, Version 6.1, R. Dennington, T. A. Keith, and J. M. Millam, Semichem Inc., Shawnee Mission, KS, 2016.
- [25] Optical data on UV-34 filter: <https://hoyaoptics.com/colored-glass-filters/uv-filters-uv-series/>



## Rapid Access to Polycyclic Thianthrenes from Unfunctionalized Aromatics by Thia-APEX Reaction

### Abstract

In this chapter, thia-APEX reactions affording  $\pi$ -extended thianthrene derivatives from unfunctionalized aromatics including polycyclic aromatic hydrocarbons (PAHs) are described. By utilizing *S*-diimidated 1,2-areneedithiol as a 1,2-disulfonium synthon, a new benzodithiine arm was fused to the aromatic substrates in one step, affording the thia-APEX products ( $\pi$ -extended thianthrenes) in 21–87% yield. The present thia-APEX reaction occurs with equimolar amounts of aromatic substrates and *S*-diimidated 1,2-areneedithiol and a catalytic amount of TfOH, which is advantageous in the efficient creation of novel  $\pi$ -extended thianthrenes. In addition, a novel  $\pi$ -extended thianthrene showing a unique packing structure in the solid state was discovered via thia-APEX reaction.

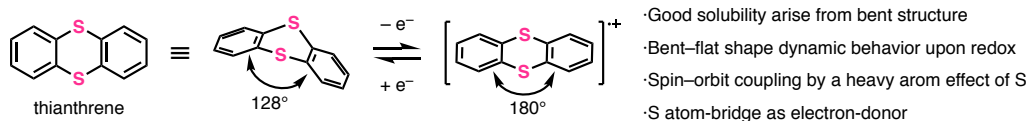
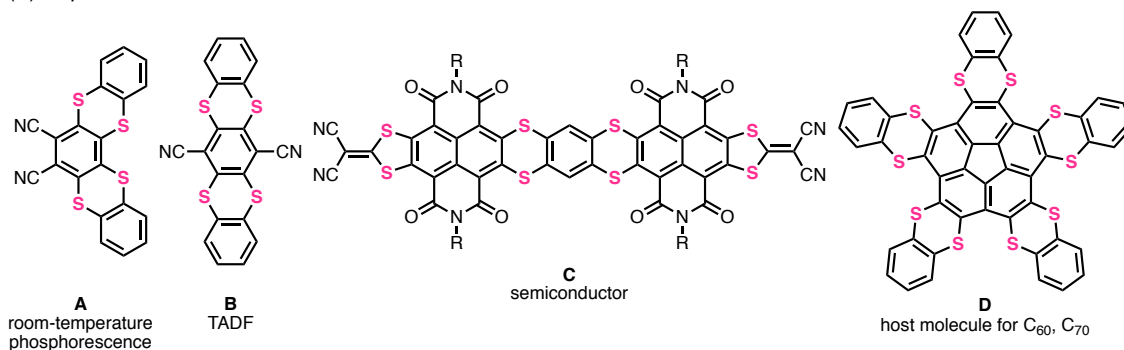
## 1. Introduction

### 1-1. $\pi$ -Extended Thianthrenes

Thianthrene is a six-membered sulfur-containing heterocyclic compound consisting of dibenzo-fused 1,4-dithiine ring, in which two sulfur atoms are embedded diagonally (Figure 1A).<sup>[1]</sup> Thianthrene shows unique and variety of properties and functions originated from diagonally-aliened two sulfur atoms. For example, neutral thianthrene adopts a bent structure whose C–S–C angle is *ca.* 128 degrees, whereas it transforms to a planar structure in the state of radical cation.<sup>[1c,2]</sup> This bent–planar dynamic behavior is known to be reversible upon oxidation and reduction. Utilizing this dynamic redox behavior, some of thianthrenes are applied to supramolecular chemistry and cathode materials for Li-ion batteries and so on.<sup>[2a,3,4]</sup> Besides, the flexible structure of thianthrene is also useful to improve the solubility.<sup>[5]</sup> Moreover, a strong electron-donating effect of sulfur atoms in thianthrene structure is useful for developing novel electroluminescent materials, and the dithiine core is favorable to localize the HOMOs on sulfur atoms. Furthermore, spin–orbit coupling caused by heavy atom effect of sulfur atom accelerates both intersystem crossing and reverse intersystem crossing between excited singlet and triplet states, thus enhancing phosphorescence<sup>[6a,6b,6c]</sup> and favorable to thermally activated delayed fluorescence (TADF).<sup>[6d,6e,6f]</sup>

To utilize these attractive features of thianthrenes, conjugations of thianthrene structures and aromatic systems have been examined in recent years.<sup>[2b,2c,3,5,6,7]</sup> For example, various  $\pi$ -extended thianthrenes shown in Figure 1B have been discovered and developed so far. In 2022, Su and coworkers reported benzo[5,6][1,4]dithiino[2,3-*a*]thianthrene-6,7-dicarbonitrile (**A**, bTEoCN) as a room temperature-phosphorescent (RTP) dye having an ability of efficient singlet-to-triplet intersystem crossing induced by a heavy atom effect and an electron-donor–acceptor structure between thianthrene moieties and cyano groups.<sup>[6d]</sup> In addition, a pentacene-like thianthrene **B** which is a regioisomer of thianthrene **A** was also reported as a TADF molecule.  $\pi$ -Extended thianthrene **C** is a naphthalene diimide analogue having a bisthianthrene moiety.<sup>[5]</sup> This compound works as an organic semiconductor, and shows a good solubility in CH<sub>2</sub>Cl<sub>2</sub>, CHCl<sub>3</sub>, and THF unlike general planar polycyclic aromatics. Pentakisthianthrene having a corannulene core **D** was synthesized by Georghiou, Scott and coworkers from decachlorocorannulene and benzendithiol.<sup>[3]</sup> The three of five thianthrene arms on corannulene core form a flytrap-like conformation, which allows a formation of inclusion complex of benzene molecules in compound **D** in the crystalline state. Although general corannulene does not make any complexes with C<sub>60</sub> and C<sub>70</sub>, compound **D** can form 1:1 complexes with them.

## (A) Structural features of thianthrenes

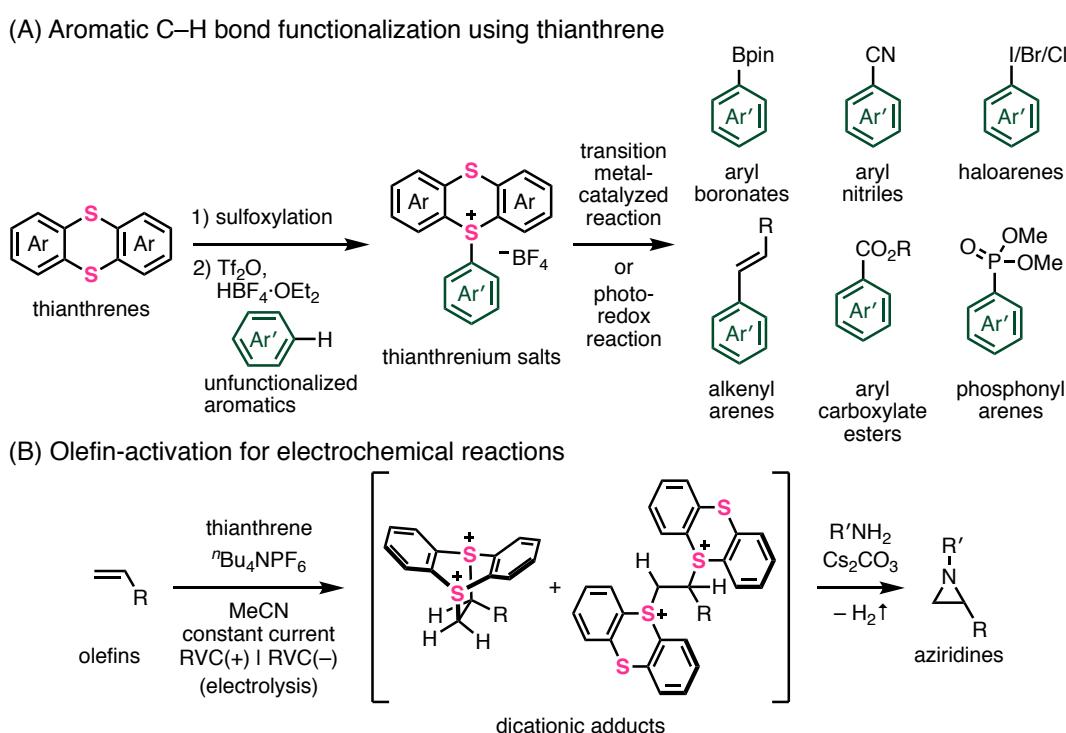
(B) Representative  $\pi$ -extended thianthrenes and their functions

**Figure 1.**  $\pi$ -Extended thianthrenes: structures, properties, and applications.

Thianthrenes can contribute to not only materials science and supramolecular chemistry but also organic synthesis. Recently, Ritter and coworkers developed an indirect aromatic C–H bond functionalization method using thianthrenium salts (Figure 2A).<sup>[8,9a–f]</sup> Upon monosulfoxylation of thianthrene, aryl thianthrenium salts are prepared from unfunctionalized aromatics in the presence of  $\text{Ti}_2\text{O}_3$ ,  $\text{HBF}_4$  through  $\text{S}_{\text{N}}\text{Ar}$  reaction. Then aryl thianthrenium salts can participate in various transformations such as borylation, nitrilation, halogenation, alkenylation, esterification, phosphorylation and so on by transition metal-catalyzed cross-coupling reactions and photochemical reactions. In other words, diverse aromatic compounds can be easily prepared from thianthrenes. In addition, Wickens and coworkers developed an electrochemical synthetic method of aziridines from unfunctionalized olefins and primary amines using thianthrene (Figure 2B).<sup>[9g,9h]</sup> In this protocol, an olefin affords a dicationic adduct with thianthrene under constant current derived from reticulated vitreous carbon (RVC) electrode. Thereafter, the dicationic adduct is attacked by a primary amine under basic condition using  $\text{Cs}_2\text{CO}_3$ , resulting in the formation of an aziridine accompanied by the generation of hydrogen gas. In general, the direct aziridination of olefin with primary amine along with the generation of hydrogen gas is thermodynamically difficult because the Gibbs energy of reaction system increases by over 30 kcal/mol. Therefore, thianthrene in electrochemical synthesis enables a thermodynamically disfavored reaction by passing through active intermediates, which will contribute to future development and design of new reactions.

As mentioned above, thianthrene derivatives are useful not only as PACs themselves but also as stoichiometric mediators for recently emerging methodologies in organic synthesis. In the researches on thianthrenes, symmetric thianthrenes consisting of two non-substituted or

substituted benzene units are preferably utilized. Regarding  $\pi$ -extended thianthrenes such as naphthalene-, PAHs-conjugated ones and bithianthrenes, only limited examples were reported.<sup>[2b,2c,2e,3,4a,5,6,7]</sup> These can be due to the lack of efficient synthetic methods for larger  $\pi$ -extended thianthrenes. The relationships between thianthrene structures and properties/reactivities in terms of the ring-fusion style, kind, and number of larger polycyclic aromatic rings are highly interesting. Therefore, such an investigation can lead to the development of further improved reaction using thianthrenes and the creation of novel  $\pi$ -extended thianthrenes having attractive properties. In this regard, easy preparation and modification of thianthrene structure are considered to be important.



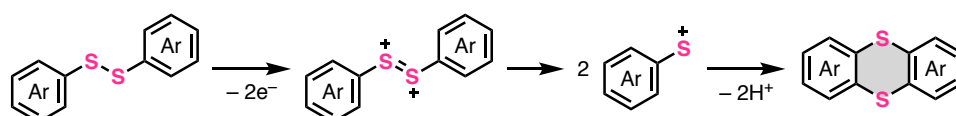
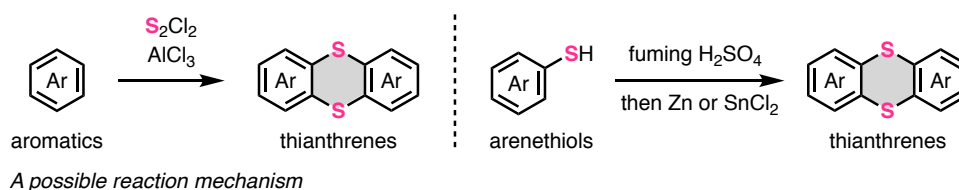
**Figure 2.** Thianthrene-utilized organic synthesis.

## 1-2. Conventional synthetic methods

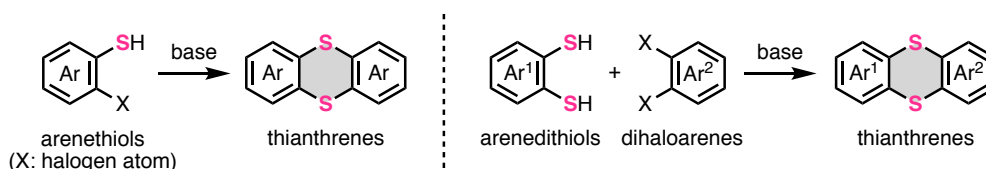
Symmetric thianthrene structures can be directly constructed from aromatic substrates with  $S_2Cl_2$  and Lewis acids such as  $AlCl_3$  (Figure 3A, left).<sup>[9a,10]</sup> This reaction is considered to be a Friedel–Crafts-type reaction, which includes the formation of a diaryldisulfide intermediate. Although the accurate reaction mechanism is still ambiguous, the additional oxidations of diaryldisulfide intermediate and the following cleavage of disulfide bond are considered to be possible elementary reactions according to a literature.<sup>[10c]</sup> Besides, similar syntheses of symmetric thianthrenes are possible by utilizing arenethiols as starting materials with fuming  $H_2SO_4$  and reductants such as zinc and  $SnCl_2$  (Figure 3A, right).<sup>[11]</sup> As another synthetic method,

$S_NAr$ -type homoannulation reactions using *ortho*-halogenated arylthiols and base are also useful for the preparation of symmetric thianthrenes.<sup>[12]</sup> Furthermore, cross-annulation reactions using arylthiols and 1,2-dihaloarenes are frequently employed to construct unsymmetrically substituted thianthrene structures and large organic frameworks consisting of multiple thianthrene bridges (Figure 3B).<sup>[2c,4a,7c,7e,7h-k,13]</sup> Indeed, all the representative  $\pi$ -extended thianthrenes described in Figure 1 are prepared by  $S_NAr$  reactions using 1,2-benzenedithiol or benzene-1,2,4,5-tetrathiol, and 1,2-difluoro/dichloro/dibromoarenes.<sup>[3,5,6d]</sup> To date, these synthetic methods have been established as conventional ones for symmetric/unsymmetric thianthrenes and other  $\pi$ -extended S-heterocycles. However, the characteristics of multistep transformations counting from the starting unfunctionalized aromatics diminish the synthetic utility and the efficiency in the whole synthetic scheme to thianthrenes. In particular, the preparation of both oligo-halogenated and oligo-sulfurated arenes would cause a synthetic difficulty when arenes are larger than benzene. Furthermore, there are some one-step synthetic methods for thianthrenes using unfunctionalized simple arenes such as benzene,  $S_2Cl_2$  and  $AlCl_3$ , whereas these one-step protocols are difficult to be applied to the preparation of unsymmetric thianthrenes and largely  $\pi$ -extended thianthrenes. Therefore, a novel one-step reaction such as hetero-APEX reactions would be desired to realize more efficient creation of  $\pi$ -extended thianthrenes.

(A) Synthesis by oxidative homoannulation



(B)  $S_NAr$ -type synthesis of thianthrenes



● stepwise protocol    ● lack of direct synthesis of asymmetric thianthrenes


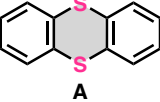
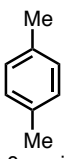
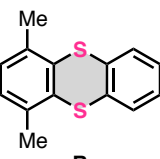
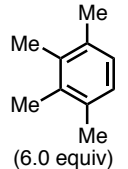
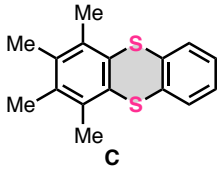
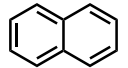
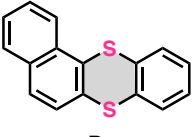
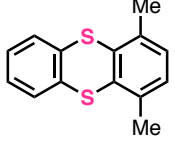
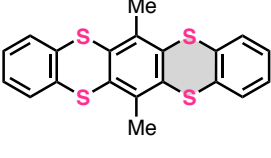
Figure 3. Conventional synthetic methods for thianthrenes.



### 1-3. Pioneering one-step synthesis of S-PACs

As a pioneering work on one-step synthesis of unsymmetrically  $\pi$ -extended thianthrenes from unfunctionalized arenes, a Friedel–Crafts-type annulation reaction using benzopentathiepin (BPT) and  $\text{AlCl}_3$  was reported by Sato and coworkers in 1988 (Table 1).<sup>[14]</sup> In the presence of  $\text{AlCl}_3$  as a Lewis acid, BPT is electrophilically activated and functions as 1,2-phenylenedisulfonium ion, achieving the one-step synthesis of various thianthrenes **A**, **B** and **C**, benzothianthrene **D** and bisthianthrene **E** from benzene, *p*-xylene, 1,2,3,4-tetramethylbenzene, naphthalene and thianthrene, respectively (entries 1–5). Not only symmetric  $\pi$ -extended thianthrenes but also unsymmetric ones are obtained from unfunctionalized aromatics by this method. However, this reaction requires excess amounts (or sometimes employed as a solvent) of unfunctionalized aromatics to ensure high yield. Besides, over 1 equiv of  $\text{AlCl}_3$  and relatively harsh reaction conditions are needed. As long as the result in entry 5, 2:1 reaction of thianthrene and BPT gave the product in only 20% yield. Consequently, the development of a further efficient and mild one-step reaction, and extension of scope of starting material and product are still needed for synthetic chemistry of thianthrenes.

**Table 1.** A pioneering one-step synthesis of  $\pi$ -extended thianthrene using benzopentathiepine as a disulfonium synthon.

Entry <sup>a</sup>	Aromatics (equiv for BPT)	AlCl <sub>3</sub> (equiv for BPT)	Temperature	Time	Products	Yield <sup>c</sup>
1	 (112 equiv)	1.0 equiv	80 °C	16 h	 <b>A</b>	44%
2 <sup>b</sup>	 (2.0 equiv)	2.0 equiv	r.t.	32 h	 <b>B</b>	65%
3 <sup>b</sup>	 (6.0 equiv)	2.0 equiv	r.t.	24 h	 <b>C</b>	83%
4	 (78 equiv)	1.0 equiv	100 °C	5 h	 <b>D</b>	93%
5 <sup>b</sup>	 <b>B</b> (0.94 equiv)	2.0 equiv	r.t.	33 h	 <b>E</b>	20% <sup>d</sup>

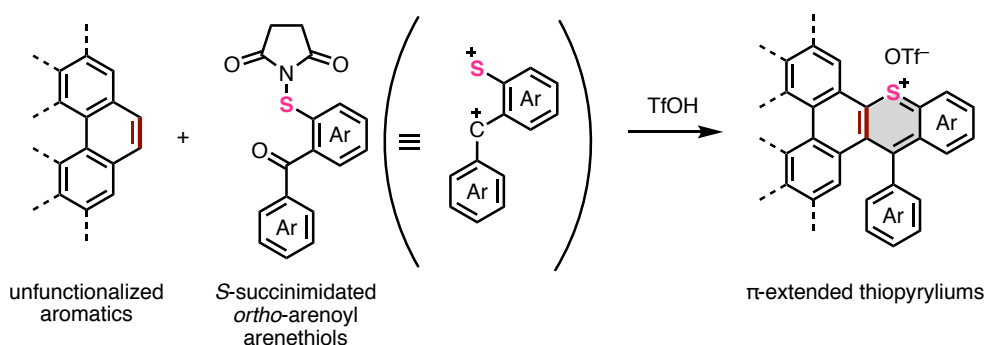
<sup>a</sup> BPT: 0.5 mmol. Unless otherwise noted, reaction was conducted under neat condition. <sup>b</sup> CH<sub>2</sub>Cl<sub>2</sub> was used as a solvent (5 mL). <sup>c</sup> Unless otherwise noted, isolated yield based on BPT. <sup>d</sup> Isolated yield based on starting material **B**.

#### 1-4. This work

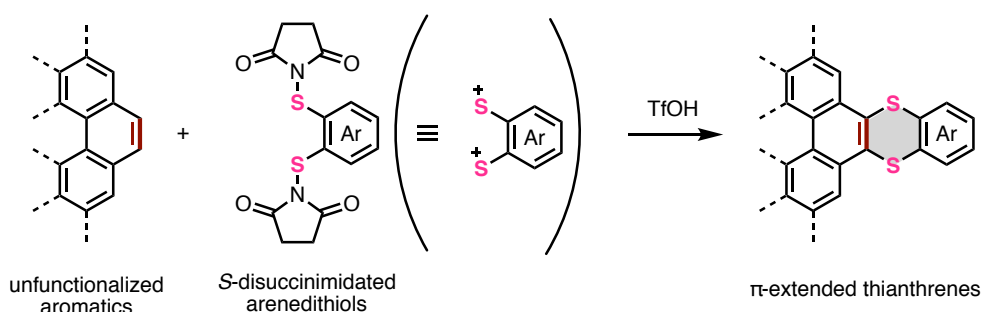
With these backgrounds and synthetic issues in mind, the author conceived a new one-step reaction for synthesis of  $\pi$ -extended thianthrenes. Then, the author interpreted again a concept of annulative  $\pi$ -extension (APEX) and heteroatom-embedding APEX (hetero-APEX): one-step synthesis of thianthrene from unfunctionalized aromatics through double C–H bond functionalizations can also be defined as quasi-hetero-APEX (quasi-thia-APEX) reaction,

whereas the newly constructed ring is a nonaromatic heterocycle. As one of the author's campaigns toward the development of hetero-APEX chemistry, in this chapter, the development of new  $\pi$ -extending agents working as a 1,2-arylenedisulfonium synthon in the thia-APEX reaction of unfunctionalized aromatics is described. Inspired by the previously-developed thia-APEX reaction (in Chapter 2) using *S*-succinimidated *ortho*-arenyl arenethiols that implements the C–S/C–C bond formation onto unfunctionalized aromatics by the protonation-assisted activation of carbonyl/succinimide groups as a synthon of 1,4-dication,<sup>[15]</sup> the author conceived that 1,2-arylenedithiols having two succinimide groups will work as a synthon of 1,2-arylenedisulfonium cation. In this context, preparations of various *S*-diimidated 1,2-arenedithiols were conducted according to the similar synthetic procedure of *S*-succinimidated *ortho*-arenyl arenethiols. Compared to the previous method by Sato, newly developed *S*-succinimidated 1,2-arylenedithiols showed higher reactivities toward one-step construction of benzodithiine structure from unfunctionalized aromatics, resulting in stoichiometrically economical equimolar thia-APEX reactions under mild reaction conditions. Furthermore, some characteristic photophysical properties and structural future of  $\pi$ -extended thianthrene obtained by the thia-APEX reaction are discussed in detail by experimental measurements and DFT calculations.

(A) Previous thia-APEX reaction affording  $\pi$ -extended thiopyryliums



(B) This work: thia-APEX reaction affording  $\pi$ -extended thianthrenes

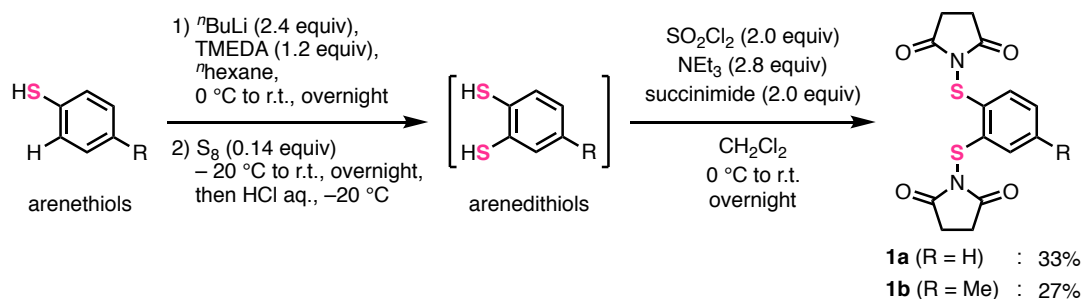


**Figure 4.** Previous and current synthetic strategies for sulfur-containing PACs by thia-APEX reaction.

## 2. Results and Discussion

### 2-1. Preparation of $\pi$ -extending agents

To obtain *S*-succinimidated *ortho*-arenoyl arenethiols, benzenethiol and 4-methylbenzenethiol were *ortho*-thiolated using octasulfur through *ortho*-lithiation with *n*-butyllithium and 1,1,2,2-tetramethylethylenediamine (TMEDA). The resulting arenedithiols were protected using succinimide via *S*-chlorination with  $\text{SO}_2\text{Cl}_2$ , which afforded *S*-diimidated benzenedithiol **1a** in 33% yield from benzenethiol and *S*-diimidated 4-methylbenzenedithiol **1b** in 27% yield from 4-methylbenzenethiol (Figure 5).



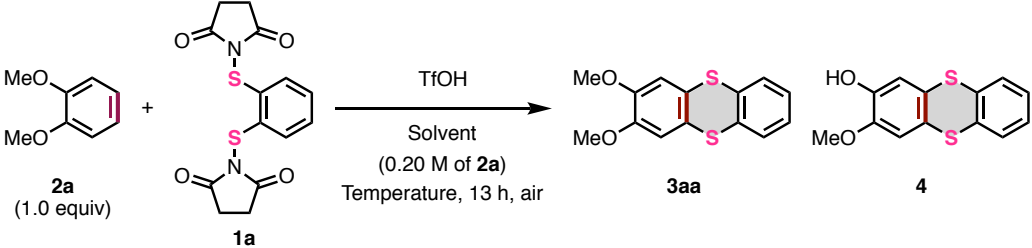
**Figure 5.** Preparation of *S*-diimidated benzenedithiol derivatives **1a** and **1b**.

### 2-3. Optimization of thia-APEX reaction conditions

Using 1,2-dimethoxybenzene (**2a**) as a functionalized aromatic and thioamide **1a** as a  $\pi$ -extending agent, the optimized conditions of thia-APEX reaction were examined for efficient one-step formation of 2,3-dimethoxythianthrene (**3aa**) (Table 2). When a mixture containing 0.20 mmol of **2a**, 1.1 equiv of **1a**, and *ca.* 2.3 equiv of TfOH in HFIP (1.0 mL), which is the best solvent in the previous thia-APEX reaction,<sup>[15]</sup> was stirred at 80 °C under air for 13 hours, the desired thia-APEX reaction proceeded to afford thianthrene **3aa** in 38% along with a formation of demethylated by-product **4** in 25% isolated yield. The use of excess amount of **1a** or a mixed solvent of dry  $\text{ClCH}_2\text{CH}_2\text{Cl}$  and HFIP increased the yields of **3aa** with decreasing the formation of **4**. Using dry  $\text{ClCH}_2\text{CH}_2\text{Cl}$  alone as the solvent tended to show higher yield than the use of HFIP solvent. (entries 4–6). In this regard, HFIP molecule or  $\text{H}_2\text{O}$  in HFIP are considered to attack to a protonated OMe group to form the deprotection by-product **4**. To my delight, even less amount of TfOH (*ca.* 0.6 equiv) was suitable for increasing the yield of product **3aa** (99% NMR yield, entry 7). The use of trifluoroacetic acid (TFA) instead of TfOH dramatically decreased the yield of product **3aa** (entries 4 and 8). The thia-APEX reaction at 100 °C decreased the yield of product **3aa** and increased the formation of **4** compared to the reaction at 80 °C (entries 4 and 9). Finally, an equimolar reaction of **1a** and **2a** in the presence of 0.6 equiv of TfOH in  $\text{ClCH}_2\text{CH}_2\text{Cl}$  at room temperature (23 °C) was found to be the best reaction conditions for the thia-APEX reaction with maximizing the yield of **3aa** and minimalizing the formation of **4**, exclusively

affording **3aa** in 83% isolated yield (entry 10). Compared to the pioneering report on one-step thianthrene synthesis (Table 1),<sup>[14]</sup> the present thia-APEX reaction realizes a 1:1 annulation between the unfunctionalized arene and the  $\pi$ -extending agent with catalytic amounts of acid even at room temperature, which would be a huge benefit for the reactions and late-stage functionalizations of not only simple aromatics but also other complicated larger aromatics.

**Table 2.** Optimization of reaction conditions for thia-APEX reaction of **2a** with **1a**.



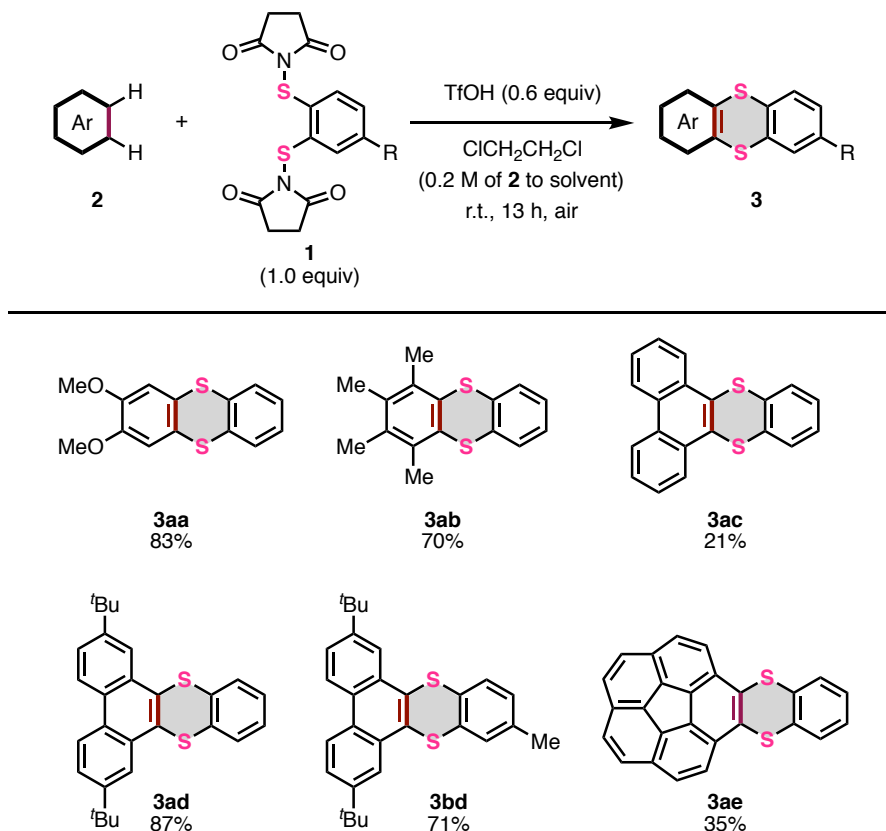
Entry	<b>1a</b> [equiv]	TfOH [equiv]	Solvent	Temperature	NMR yield ( <b>3aa</b> ) <sup>b</sup>	NMR yield ( <b>4</b> ) <sup>b</sup>
1	1.1	2.3	HFIP	80 °C	38% (38% <sup>c</sup> )	16% (25% <sup>c</sup> )
2	2.0	2.5	HFIP	80 °C	57%	0%
3	1.0	2.4	CICH <sub>2</sub> CH <sub>2</sub> Cl/HFIP (1:1 v/v)	80 °C	65%	17%
4	1.0	2.3	CICH <sub>2</sub> CH <sub>2</sub> Cl <sup>a</sup>	80 °C	71%	19%
5	1.0	1.1	CICH <sub>2</sub> CH <sub>2</sub> Cl <sup>a</sup>	80 °C	50%	26%
6	2.0	2.3	CICH <sub>2</sub> CH <sub>2</sub> Cl <sup>a</sup>	80 °C	65%	0%
7	1.0	0.64	CICH <sub>2</sub> CH <sub>2</sub> Cl <sup>a</sup>	80 °C	99% (78% <sup>c</sup> )	0% (0% <sup>c</sup> )
8	1.1	0.52 (TFA)	CICH <sub>2</sub> CH <sub>2</sub> Cl <sup>a</sup>	80 °C	3%	0%
9	1.0	2.2	CICH <sub>2</sub> CH <sub>2</sub> Cl <sup>a</sup>	100 °C	34%	25%
10	1.0	0.62	CICH <sub>2</sub> CH <sub>2</sub> Cl <sup>a</sup>	r.t. (23 °C)	> 99% (83% <sup>c</sup> )	0% (0% <sup>c</sup> )

<sup>a</sup> Dry CICH<sub>2</sub>CH<sub>2</sub>Cl was used. <sup>b</sup> Determined by <sup>1</sup>H NMR spectroscopy using CH<sub>2</sub>Br<sub>2</sub> as an internal standard. <sup>c</sup> Isolated yield.

#### 2-4. Scope of substrates

With the optimized conditions in hand, a scope of thia-APEX reactions using other aromatic substrates was examined (Figure 6). 1,2,3,4-Tetramethylbenzene (**2b**) was transformed to the corresponding thianthrene **3ab** in 70% yield. Thianthrene **3ac** was obtained in 21% yield from phenanthrene (**2c**) and the reaction mainly occurred at a *K*-region (C9, C10-positions of phenanthrene: concave armchair edges in PAH). The reason of low yield seems to be a low conversion of **2c** and a preferential overreaction of mono-thia-APEX product **3ac** to oligomeric products. Notably, the observed *K*-region preference was similar to that in the previous thia-APEX reaction.<sup>[15]</sup> In contrast, thia-APEX reaction using 2,7-di-*tert*-butylphenanthrene (**2d**) efficiently proceeded to afford dibenzothianthrene **3ad** in 87% yield. Besides, by employing methylated  $\pi$ -extending agent **1b** instead of compound **1a**, di-*tert*-butylphenanthrene **2d** was transformed to the corresponding dibenzothianthrene **3bd** in 71% yield. Thanks to bulky *tert*-

butyl groups, the  $\pi$ -extensions on other regions such as C1–C2, C2–C3 and C3–C4 positions are considered to be prevented, which contributes to selective thia-APEX reaction. Moreover, corannulene (**2e**) was transformed to benzodithiine-fused corannulene **3ae** in 35% yield, while multi-thia-APEX products were also observed in the reaction mixture.

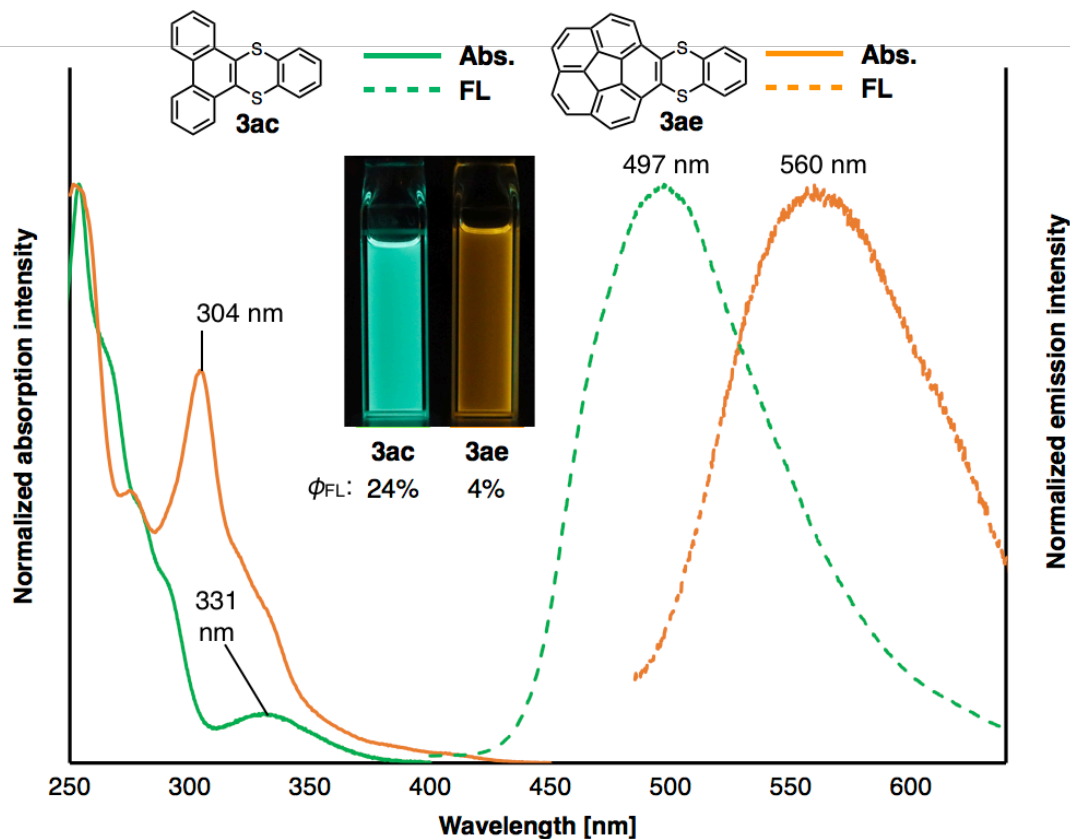


**Figure 6.** Scope of substrates in thia-APEX reaction.

## 2-5. Photophysical properties of $\pi$ -extended thianthrenes

Because  $\pi$ -extended thianthrenes **3ac** and **3ae** showed remarkable green and yellow fluorescence by UV light irradiation respectively, photophysical properties of **3ac** and **3ae** were investigated. First, thianthrene **3ac** showed the longest wavelength absorption maxima at 331 nm in CH<sub>2</sub>Cl<sub>2</sub> (Figure 7, green line). When thianthrene **3ac** was excited with 330 nm light, the fluorescence maximum was observed at 497 nm in CH<sub>2</sub>Cl<sub>2</sub> (Figure 7, green dashed line). In the case of thianthrene **3ae**, remarkable absorption maximum was observed at 304 nm in CH<sub>2</sub>Cl<sub>2</sub>. Moreover, thianthrene **3ae** showed weak absorption around 350–450 nm, which was considered to be the longest wavelength absorption of thianthrene **3ae** (Figure 7, orange line). Moreover, by irradiation of 405 nm light, thianthrene **3ae** emitted fluorescence with the peak top at 560 nm (Figure 7, orange dashed line). In addition, both thianthrene **3ac** and **3ae** showed *ca.* 160 nm of Stokes shifts, whose large values were considered to be derived from their dynamic thianthrene

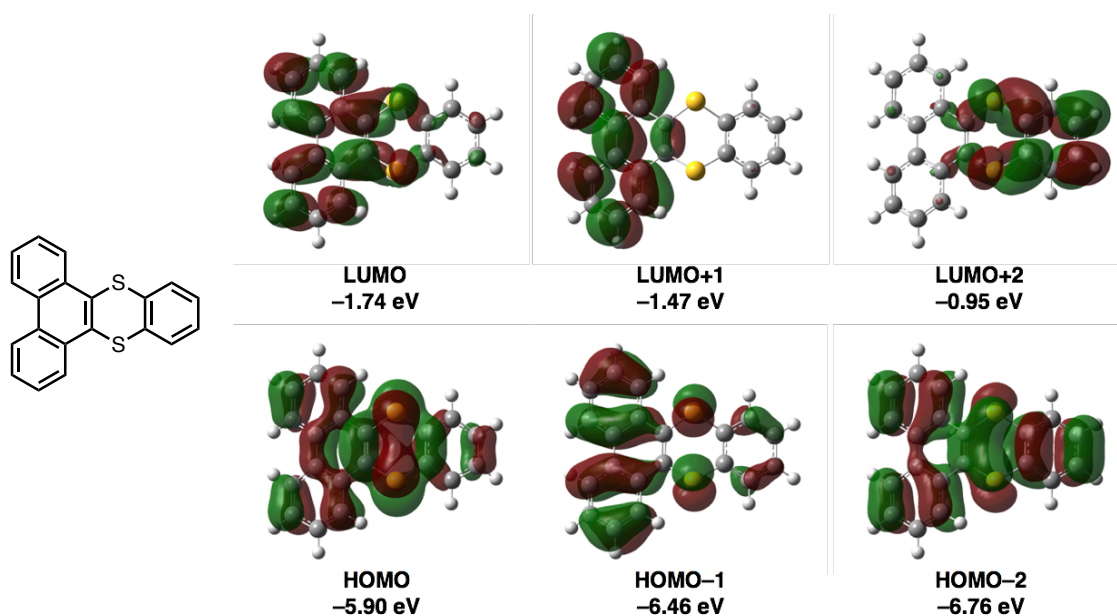
skeletons.<sup>[1,7]</sup> Furthermore, fluorescence quantum yields of thianthrene **3ac** and **3ae** were measured as 24% and 4%, respectively. Notably, the 24% quantum yield of **3ac** was larger than that of pristine phenanthrene and triphenylene (*ca.* 10%),<sup>[16]</sup> which can be rationalized by the heavy atom effect of sulfur atoms and prevention of quenching fluorescence by its bent structure.<sup>[17]</sup>



**Figure 7.** Absorption and emission spectra of  $\pi$ -extended thianthrenes **3ac** and **3ae** in  $\text{CH}_2\text{Cl}_2$ . Excitation wavelength for fluorescence (FL): 330 nm (**3ac**), 405 nm (**3ae**). The pictures of emission color were taken using the concentrated solutions of each compound under 365 nm of UV light irradiation.

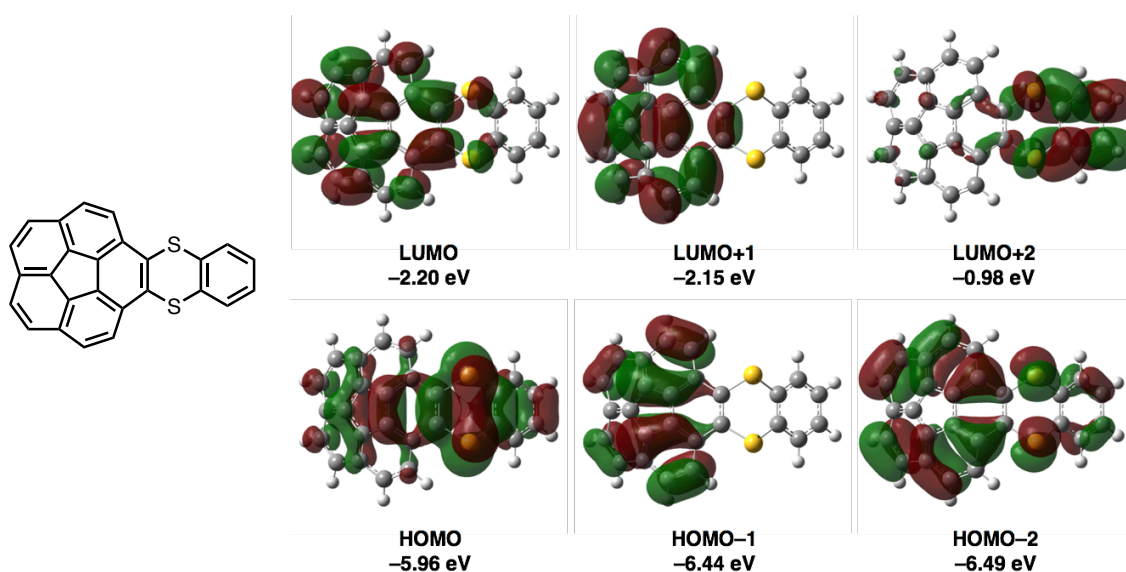
Next, absorption properties and electronic structures of  $\pi$ -extended thianthrenes **3ac** and **3ae** were evaluated by the density functional theory (DFT) and time-dependent DFT (TD-DFT) calculations using a Gaussian 16 program with the B3LYP/6-31+G(d,p) level of theory<sup>[18]</sup> and consideration of solvent effect by integral equation formalism-polarizable continuum model (IEF-PCM)<sup>[19]</sup> in  $\text{CH}_2\text{Cl}_2$ . As described in Figure 8, energy levels of HOMO and LUMO of **3ac** were calculated as  $-5.90$  eV and  $-1.74$  eV, respectively. While HOMO of **3ac** was localized on a roughly entire molecule, it was mainly localized on the 1,4-dithiine moiety. On the other hand, LUMO of **3ac** was slightly localized onto the phenanthrene moiety. A similar HOMO and LUMO

localization tendency was also found in **3ae**, and the energy levels of HOMO and LUMO of **3ae** were calculated as  $-5.96$  eV and  $-2.20$  eV, respectively. Compared with HOMO and LUMO energy levels of pristine phenanthrene (HOMO:  $-6.12$  eV; LUMO:  $-1.43$  eV) and corannulene (HOMO:  $-6.35$  eV; LUMO:  $-2.01$  eV), the effect of benzodithiine-fusion is slightly more predominant in increasing the energy levels of HOMO ( $\Delta = +0.22$  and  $+0.39$  eV) rather than in decreasing those of LUMO ( $\Delta = -0.31$  and  $-0.19$  eV) (Figures 8 and 9). As a result, the HOMO–LUMO energy gaps of **3ac** and **3ae** are reduced by  $0.53$ – $0.58$  eV compared with phenanthrene and corannulene. As summarized in Table 3, the calculated excitation wavelength ( $\lambda_{\text{TD-DFT}}$ ) of HOMO→LUMO transition of thianthrene **3ac** was  $347.21$  nm ( $f = 0.0993$ ), which is consistent with the experimental longest wavelength absorption of **3ac** as a weak peak ( $\lambda_{\text{abs}} = 331$  nm). Besides, second and third excitations attributed to HOMO→LUMO+1 and HOMO–1→LUMO transitions were calculated as  $334.84$  nm ( $f = 0.0023$ ) and  $299.47$  nm ( $f = 0.2015$ ), respectively. The latter allowed excitation is considered to be the shoulder absorption peak around  $290$  nm. Regarding **3ae**, the electron transitions in three lowest energies were also estimated as  $395.93$  nm ( $f = 0.0162$ , HOMO→LUMO),  $388.71$  nm ( $f = 0.0229$ , HOMO→LUMO+1) and  $356.73$  nm ( $f = 0.0000$ , HOMO–1→LUMO+1), whose small or zero values of  $f$  show a good agreement with weak shoulder absorptions between  $350$  to  $450$  nm. Moreover,  $\lambda_{\text{TD-DFT}}$  of HOMO–1→LUMO+1 transition of **3ae** was determined as a forbidden transition.



**Figure 8.** Representative frontier orbitals of **3ac** (isovalue = 0.02). Geometry optimization and energy calculation were conducted with the B3LYP/6-31+G(d,p) level of theory.





**Figure 9.** Representative frontier orbitals of **3ae** (isovalue = 0.02). Geometry optimization and energy calculation were conducted with the B3LYP/6-31+G(d,p) level of theory.

**Table 3.** Results of TD-DFT calculations using the B3LYP/6-31+G(d,p) level of theory in CH<sub>2</sub>Cl<sub>2</sub> (IEF-PCM).  $\lambda_{\text{TD-DFT}}$ : estimated excitation wavelength;  $f$ : oscillator strength;  $\lambda_{\text{abs}}$ : the experimental observed longest wavelength absorption in CH<sub>2</sub>Cl<sub>2</sub>.

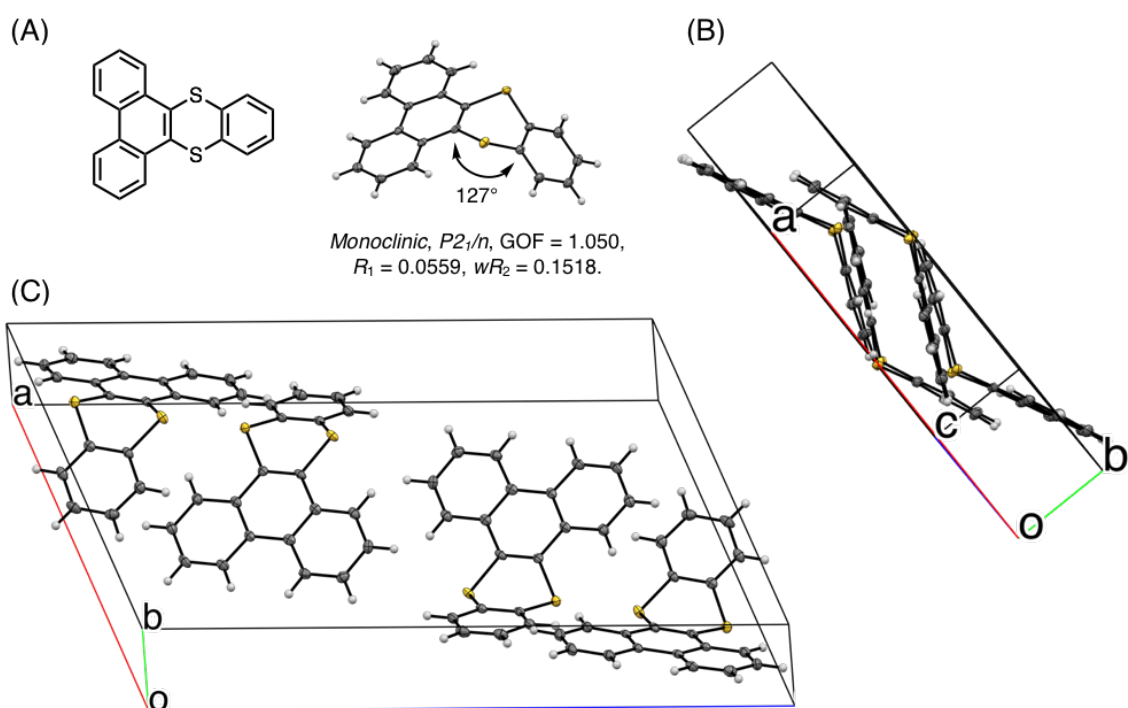
	$\lambda_{\text{TD-DFT}}$	$f$	Electronic transition (coefficient)	$\lambda_{\text{abs}}$
<b>3ac</b>	347.21 nm	0.0993	HOMO $\rightarrow$ LUMO (0.67256)	331 nm
	334.84 nm	0.0023	HOMO $\rightarrow$ LUMO+1 (0.61319)	
	299.47 nm	0.2015	HOMO-1 $\rightarrow$ LUMO (0.56362)	
<b>3ae</b>	395.93 nm	0.0162	HOMO $\rightarrow$ LUMO (0.68456)	350–450 nm
	388.71 nm	0.0229	HOMO $\rightarrow$ LUMO+1 (0.65994)	
	356.73 nm	0.0000	HOMO-1 $\rightarrow$ LUMO+1 (0.61773)	

## 2-6. Solid state structure of $\pi$ -extended thianthrene **3ac** and **3ae**

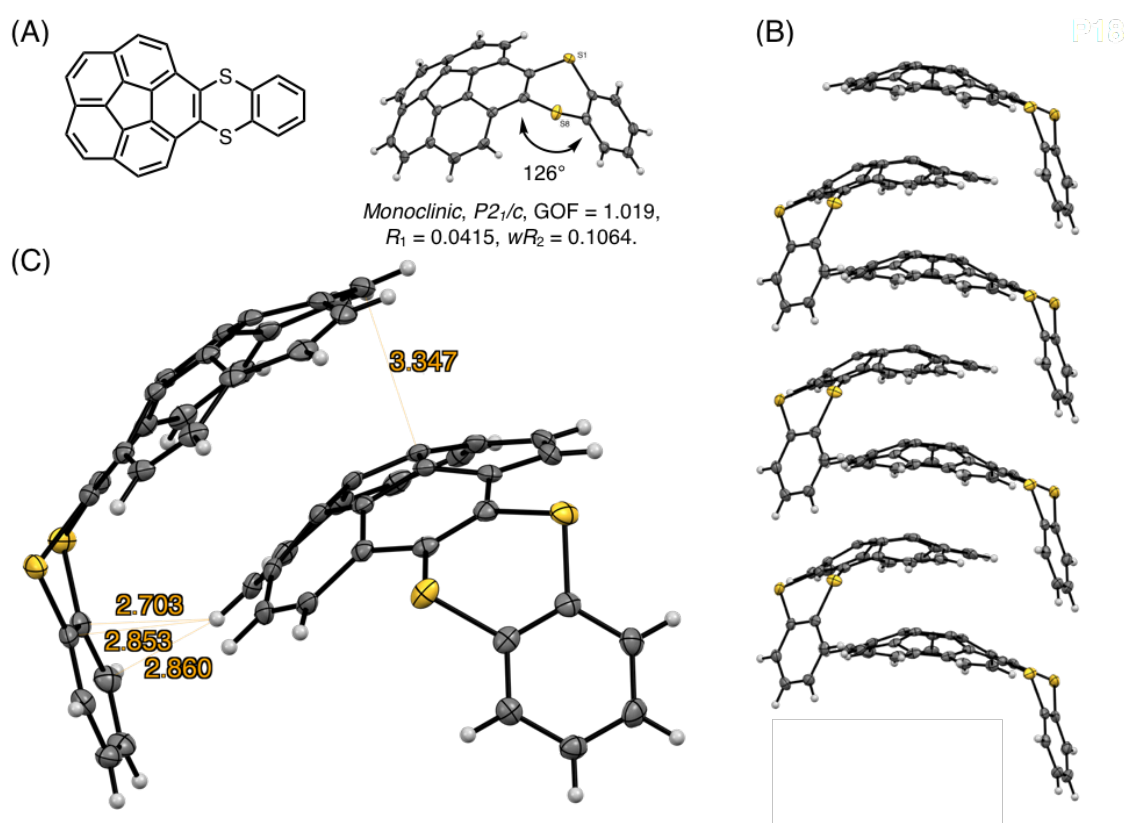
Single crystals of **3ac** and **3ae** were obtained by recrystallization from chloroform/pentane. In X-ray crystallographic analysis of **3ac**, two pairs of two molecules were observed in a unit cell, and both pairs consist of two molecules arranging in pseudo- $C_2$  symmetry whose dithiine cores are directing in a same axis with *ca.* 127 degrees of bent angles. Each pair is directing in an opposite direction and positioned in  $C_i$  symmetry, forming the two pseudo-enantiomeric pair of two racemic molecules (Figures 10A–10C). Furthermore, each molecule is aligned in the direction of *b* axis, forming columnar stacking with keeping *ca.* 3.6 Å of intermolecular distance which indicates weak  $\pi$ - $\pi$  interactions of **3ac** molecules.<sup>[20]</sup> This characteristic columnar packing is identical to that of unsubstituted thianthrene.<sup>[21]</sup> In the X-ray crystallographic analysis of **3ae**,

the bent angle of thianthrene moiety in **3ae** was found to be 126 degrees, which is also well identical to that of **3ac** and unsubstituted thianthrene (Figure 11A).<sup>[1,21]</sup> Besides, the dangling benzodithiine arm is bent toward the concave face of corannulene core, which forms like a ladle shape. The one-dimensional columnar packings of **3ae** are aligned in an antiparallel to neighboring molecular columns, counteracting the dipole moments of each column (Figure 11B). Focusing on the distances between two neighboring molecules, each corannulene core is longitudinally aligned at 3.3 Å intervals, which are smaller than the sum of van der Waals radii of two carbon atoms and indicated the existence of the  $\pi$ - $\pi$  interaction.<sup>[20]</sup> Furthermore, the distances between peripheral C–H bond in corannulene core and the carbon atoms in dangling benzene ring are close, and ranged from 2.7 to 2.9 Å. These values are within the sum of van der Waals radii of one hydrogen and one carbon atom, showing the existence of CH/ $\pi$  interactions (Figure 11C).<sup>[22]</sup>

Depicting isosurfaces by non-covalent interaction (NCI) plot analysis by a NCIPLOT 4.0 program<sup>[23]</sup>, green isosurfaces, which indicate the weak non-covalent interactions, are visually and clearly confirmed between the corannulene cores ( $\pi$ - $\pi$ ) and between the corannulene core and the benzene ring (CH/ $\pi$ ) (Figure 12). Because unsubstituted corannulene in the solid state forms a disordered arrangement derived from CH/ $\pi$  interactions, thianthrene arms are considered to contribute to the formation of columnar packing structure. In addition, the columnar packing structure of thianthrene **3ae** is the first example as mono-benzodithiine-fused corannulene,<sup>[3,7e]</sup> whereas there are a lot of other *rim*-region-fused or *rim*-region-substituted corannulene derivatives showing a similar columnar stacking ability.<sup>[24]</sup> The author hopes that the columnar stacking achieved by the simple structural motif of benzodithiinocorannulene can provide a fruitful insight for application of corannulene-based functional materials to organic electronics<sup>[25]</sup> and supramolecular chemistry<sup>[26]</sup> as well as host-guest chemistry.<sup>[3]</sup>

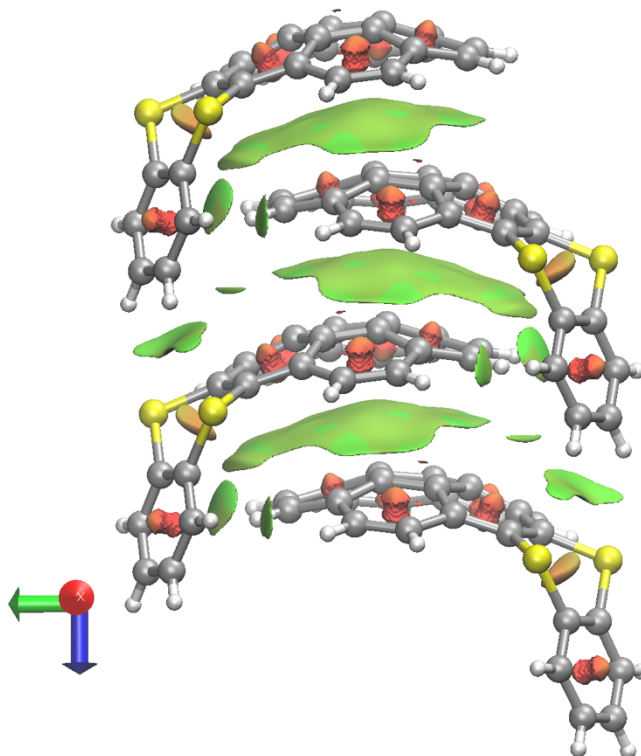


**Figure 10.** Structures of  $\pi$ -extended thianthrene **3ac**: (A) structure and ORTEP drawing of **3ac** with 50% probability, (B) side view of unit cell, (C) top view of unit cell.



**Figure 11.** Structures of  $\pi$ -extended thianthrene **3ae**: (A) structure and ORTEP drawing of **3ae**

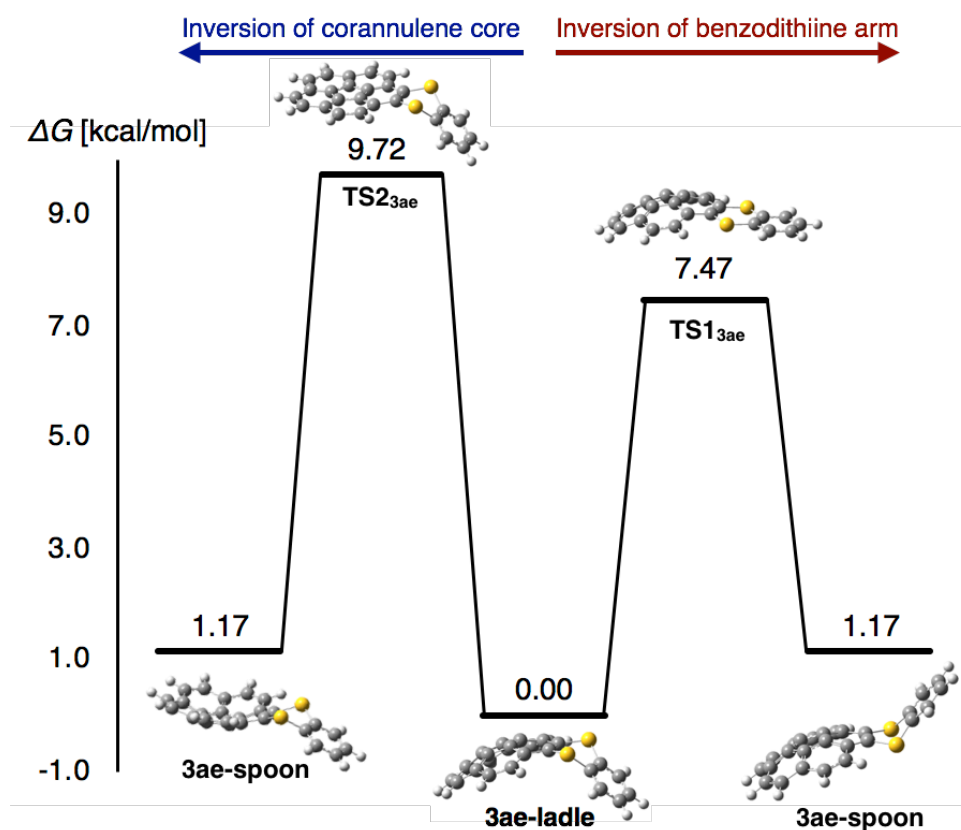
with 50% probability, (B) ORTEP drawing of columnar packing structure of **3ae**, (C) an extracted dimer structure with distances of  $\pi$ - $\pi$  and CH/ $\pi$  interaction in units of Å.



**Figure 12.** NCI analysis and RDG isosurface (isosurface value = 0.3) by a NCIPLOT4 program for  $\pi$ -extended thianthrene **3ae**. A color code based of sign ( $\lambda_2$ )  $\rho$  was uses:  $-0.07$  a.u. (blue)  $<$   $0.00$  a.u. (green)  $<$   $0.07$  a.u. (red). Blue and red isosurfaces show regions having attractive and repulsive interactions, respectively, and green isosurfaces show week van der Waals interactions such as  $\pi$ - $\pi$  interaction. Structure of **3ae** was extracted from the data of X-ray crystallographic analysis.

To obtain insights about bent structures of thianthrenes **3ac** and **3ae** in crystalline and solution states, their inversion barriers were examined using DFT calculations. Structures of thianthrenes **3ac** and **3ae** in ground and transition states were optimized using the B3LYP/6-31+G(d,p) level of theory. **3ac** has only one stable bent structure (see Experimental Section), whereas **3ae** has two stable structures, a ladle-shape one (**3ae-ladle**) and a spoon-shape one (**3ae-spoon**), which are resulting from the inversion of the corannulene core and the benzodithiine arm (Figure 13). **3ae-ladle** was a most stable conformer in **3ae**, whose structure was also observed in the X-ray crystallographic analysis (Figures 11 and 13). Each transition state (**TS1<sub>3ac</sub>** and **TS1<sub>3ae</sub>**) and inversion barrier regarding the inversion of benzodithiine arms was calculated as 7.31 kcal/mol for **TS1<sub>3ac</sub>** and 7.47 kcal/mol for **TS1<sub>3ae</sub>**, respectively. The values of **TS1<sub>3ac</sub>** and **TS1<sub>3ae</sub>** is larger

than that of pristine thianthrene (5.1 kcal/mol, with B3LYP/6-31+G(d,p)),<sup>[27]</sup> indicating that PAH structures of phenanthrene and corannulene make inversion barriers of benzodithiine arms higher. Furthermore, the transition state of corannulene core flipping in **3ae** (TS2<sub>3ae</sub>) was optimized and its barrier was calculated as 9.72 kcal/mol. This value is also well identical to that of pristine corannulene.<sup>[28]</sup> In conclusion, newly synthesized **3ac** and **3ae** were found to be hybrid molecules of thianthrene and PAHs. Those bent structures and conformational changes well reflect the nature of both thianthrene and PAH cores.



**Figure 13.** Two possible pathways of structural inversion of thianthrene **3ae** and their calculated barrier using the B3LYP/6-31+G(d,p) level of theory.

### 3. Conclusion

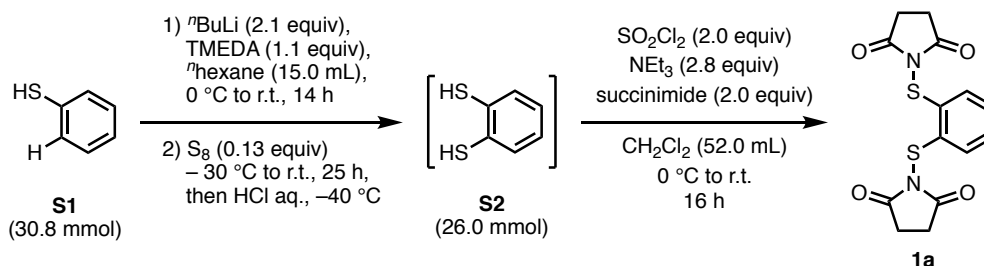
Using *S*-diimidated 1,2-benzenedithiol derivatives as new  $\pi$ -extending agents, thianthrenes and  $\pi$ -extended thianthrenes were efficiently obtained by the thia-APEX reaction of unfunctionalized aromatic substrates in one step. Although one similar reaction system has already been found over 30 years ago, the present thia-APEX reaction has a potential to realize equimolar reactions of substrates and  $\pi$ -extending agents with less amounts of TfOH. In addition, characteristic photophysical and electronical properties and structural features of thia-APEX products were elucidated by UV-vis absorption and emission spectroscopy, DFT calculations and X-ray crystallographic analysis. In particular, the  $\pi$ -extended thianthrenes having phenanthrene and corannulene cores (**3ac** and **3ae**) showed emission properties with the larger Stokes shift. **3ac** showed larger fluorescence quantum yields than that of pristine phenanthrene and triphenylene. Regarding corannulene-fused thianthrene **3ae**, the 1D-columnar packing in the solid state was observed, which is in stark contrast to the pristine corannulene. The newly developed thia-APEX is expected to contribute to a rapid and efficient creation of unique  $\pi$ -extended thianthrenes having various aromatics cores.

## 4. Experimental section

### 4-1. General

Unless otherwise noted, all materials including dry solvents were obtained from commercial suppliers and used without further purification. *N,N,N',N'*-tetramethylethylenediamine (TMEDA), octasulfur, 4-methylbenzenethiol (**S3**), and 1,2-dimethoxybenzene (**2a**) were purchased from Aldrich. CH<sub>2</sub>Cl<sub>2</sub>, 1,2-dichloroethane, and corannulene (**2e**) were purchased from KANTO. Trifluoromethanesulfonic acid (TfOH), a reagent-grade of 1,1,1,3,3,3-hexafluoro-2-propanol (HFIP), succinimide, 1,2,3,4-tetramethylbenzene (**2b**) phenanthrene (**2c**), were purchased from TCI. <sup>n</sup>BuLi in hexane, SO<sub>2</sub>Cl<sub>2</sub>, NEt<sub>3</sub>, hexane, benzenethiol (**S1**), trifluoroacetic acid (TFA) were purchased from Wako. 2,7-di-*tert*-butylphenanthrene (**2d**) was synthesized by referring literatures.<sup>[29]</sup> Fresh bottles of commercially available benzenethiol (**S1**) from TCI and 4-methylbenzenethiol (**S3**) from Aldrich were used. NEt<sub>3</sub> was degassed with argon bubbling before use. Unless otherwise noted, all reactions were performed with dry solvents under an atmosphere of nitrogen in oven-dried glassware with standard vacuum-line techniques. All work-up and purification procedures were carried out with reagent-grade solvents in air. Analytical thin-layer chromatography (TLC) was performed using E. Merck silica gel 60 F254 precoated plates (0.25 mm). The developed chromatogram was analyzed by UV lamp (254 nm and 365 nm). Flash column chromatography was performed with KANTO Silica Gel 60N (spherical, neutral, 40-100 μm) or Biotage Isolera<sup>®</sup> equipped with a cartridge of Sfar DLV Empty 50-100 g Column with frit containing KANTO Silica Gel 60N (spherical, neutral, 40–100 μm). Preparative thin-layer chromatography (PTLC) was performed using Wako-gel<sup>®</sup> B5-F silica coated plates (0.75 mm) prepared in our laboratory. The developed chromatogram was analyzed by UV lamp (254 nm and 365 nm). Gel Permeation Chromatography (GPC) was performed with a LaboACE LC-5060 Series instrument equipped with JAIGEL-2HR columns using chloroform as an eluent. High-resolution mass spectra (HRMS) were obtained from a Thermo Fisher Scientific Exactive Plus (ESI) or JEOL JMS-T100TD (DART). Nuclear magnetic resonance (NMR) spectra were recorded on a JEOL Delta ECA-600 (<sup>1</sup>H 600 MHz, <sup>13</sup>C 150 MHz) spectrometer and a JEOL Delta JNM-ECZ400S/L1 (<sup>1</sup>H 400 MHz, <sup>13</sup>C 100 MHz) and JEOL ECA 600II with Ultra COOL<sup>™</sup> probe (<sup>1</sup>H 600 MHz, <sup>13</sup>C 150 MHz). Chemical shifts for <sup>1</sup>H NMR are expressed in parts per million (ppm) relative to tetramethylsilane (δ 0.00 ppm) or CD<sub>2</sub>Cl<sub>2</sub> (δ 5.32 ppm), or Cl<sub>2</sub>CDCDCl<sub>2</sub> (δ 6.00 ppm). Chemical shifts for <sup>13</sup>C NMR are expressed in ppm relative to CDCl<sub>3</sub> (δ 77.16 ppm) or CD<sub>2</sub>Cl<sub>2</sub> (δ 53.84 ppm) or Cl<sub>2</sub>CDCDCl<sub>2</sub> (δ 73.78 ppm). Data are reported as follows: chemical shift, multiplicity (s = singlet, d = doublet, dd = doublet of doublets, ddd = doublet of doublet of doublets, t = triplet, td = triplet of doublets, q = quartet, m = multiplet), coupling constant (Hz), and integration.

## 4-2. Material preparation

4-2-1. Preparation of *S*-diimidated benzenedithiol **1a**<sup>[30,31]</sup>

**[First step]** To a pre-dried three-neck round-bottom flask (300 mL) were added dry hexane (15.0 mL) and TMEDA (3.94 g, 99% purity, 35.6 mmol, 1.09 equiv) under argon atmosphere. This solution was cooled to  $0\text{ }^\circ\text{C}$  with an ice bath, and 1.6 M  $n\text{BuLi}$  in hexane (41.2 mL, 65.9 mmol, 2.14 equiv) was added. To this solution, benzenedithiol (**S1**) (3.57 g, 95.0% purity, 30.8 mmol) was added at  $0\text{ }^\circ\text{C}$ . After 1 h, the ice bath was removed and the stirring continued at room temperature ( $23\text{ }^\circ\text{C}$ ) for 14 h. The resulting mixture was cooled to  $-30\text{ }^\circ\text{C}$  with a dry ice/ice/MeOH bath, after which sulfur (1.03 g, 4.00 mmol, 0.130 equiv as  $\text{S}_8$  molecule) was slowly added under argon flow. The resulting mixture was stirred at  $-30\text{ }^\circ\text{C}$  for 1 h, and the stirring continued at room temperature ( $24\text{ }^\circ\text{C}$ ) for 24 h. After that, the resulting mixture was acidified at  $-40\text{ }^\circ\text{C}$  (dry ice/ice/MeOH bath) using 12 M HCl aq. until the pH became *ca.* 1, under argon flow. After addition of  $\text{Et}_2\text{O}$  and water under argon flow, the organic layers was separated. The aqueous layer was extracted with  $\text{Et}_2\text{O}$  three times. After that, all organic layers were combined, washed with brine. The separated organic layer was dried over anhydrous  $\text{Na}_2\text{SO}_4$ , filtered, and concentrated *in vacuo* at room temperature to afford 1,2-benzenedithiol (**S2**) as brown oil (3.69 g, 84% crude yield). This product was used for next step without further purifications.

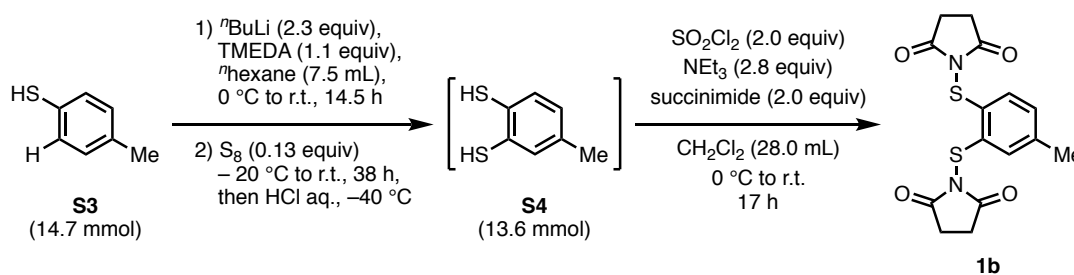
**Note:** The use of a flesh bottle of commercially available **S1** afforded **2a** in the indicated high yield, otherwise the yield was decreased along with the formation of disulfide and other impurities.

**[Second step]** To a pre-dried round-bottom flask (100 mL) containing a magnetic stirring bar was added the crude **S2** (3.69 g, assumed *ca.* 26.0 mmol), and the flask was placed *in vacuo*. After replacing with argon atmosphere,  $\text{NEt}_3$  (523.3 mg, 5.17 mmol, 0.199 equiv) and dry  $\text{CH}_2\text{Cl}_2$  (16.0 mL) were added to the flask. To this mixture,  $\text{SO}_2\text{Cl}_2$  (7.08 g, 52.6 mmol, 2.02 equiv) was added at  $0\text{ }^\circ\text{C}$ . After stirring at  $0\text{ }^\circ\text{C}$  for 15 min., the mixture was warmed to room temperature and stirred for 31 min. After that, the resulting mixture was cooled to  $0\text{ }^\circ\text{C}$  again. This mixture was transferred via a syringe to a pre-dried two-neck round-bottom flask (300 mL) containing a magnetic stirring bar, succinimide (5.14 g, 51.8 mmol, 2.00 equiv), dry  $\text{CH}_2\text{Cl}_2$  (46.0 mL), and  $\text{NEt}_3$  (6.87 g, 67.9 mmol, 2.61 equiv) at  $0\text{ }^\circ\text{C}$ . The resulting mixture was warmed and stirred at room temperature ( $24\text{ }^\circ\text{C}$ ) for 15 h. After adding water to the mixture, the organic layer was extracted with  $\text{CH}_2\text{Cl}_2$  three times, and the combined organic layers were dried over anhydrous  $\text{Na}_2\text{SO}_4$ , filtered, and



concentrated *in vacuo*. The obtained crude product was purified by flash column chromatography on silica gel (eluent: hexane/AcOEt = 100:0 → 15:85) using Isolera<sup>®</sup>. The combined fractions containing **2a** was concentrated using a rotary evaporator, and **2a** was solidified. The resulting yellow precipitate was dissolved in a small amount of AcOEt with sonicating. After adding excess amount of hexane and sonicating again, the resulting solid was collected by suction filtration and rinsed with hexane. After drying *in vacuo* at 60 °C, **2a** was obtained as a yellow solid (3.45 g, 9.57 mmol, 93<sub>wt</sub>% purity, 6.8<sub>wt</sub>% of **2a'** was contained according to <sup>1</sup>H NMR and MS analysis (see compound data of **2a** and **2a'** in Section 4.) in three steps overall 31% yield from **S1**. In the multiple repetition experiments, compound **2a** could be prepared with 88<sub>wt</sub>%–96<sub>wt</sub>% purities, and in these purity range, the quality of **2a** did not affect the thia-APEX reaction in terms of yield and reproducibility.

#### 4-2-2. Preparation of S-diimidated toluenedithiol **1b**<sup>[30,31]</sup>

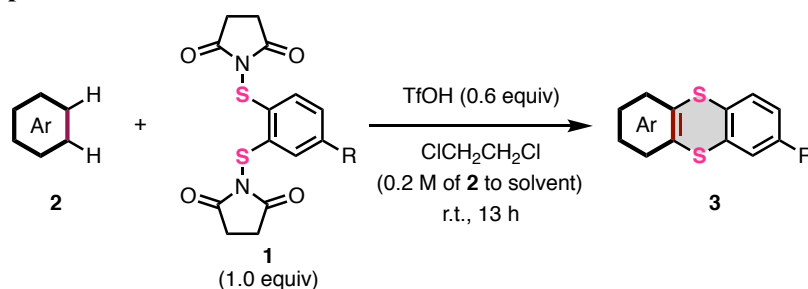


**[First step]** To a pre-dried three-necked round-bottom flask (300 mL) were added dry hexane (7.5 mL) and TMEDA (1.93 g, 99% purity, 16.5 mmol, 1.12 equiv) under argon atmosphere. This solution was cooled to 0 °C with ice bath and 1.6 M <sup>n</sup>BuLi in hexane (21.0 mL, 33.6 mmol, 2.28 equiv) was added. To this solution, 4-methylbenzenethiol (**S3**) (1.86 g, 98% purity, 14.7 mmol) was added at 0 °C. After 1 h, the ice bath was removed and the stirring continued at room temperature (24 °C) for 14 h. The resulting mixture was cooled to -36 °C with dry ice/ice/MeOH bath, after which sulfur (500.7 mg, 1.95 mmol, 0.13 equiv as S<sub>8</sub> molecule) was slowly added under argon flow. The resulting mixture was stirred at -36 to -5 °C for 3 h, and the stirring continued at room temperature (23 °C) for 35 h. After that, the resulting mixture was acidified at -40 °C (dry ice/ice/MeOH bath) using 12 M HCl aq. until the pH became ca. 1, under argon flow. After addition of Et<sub>2</sub>O and water under argon flow, the organic layer was separated. The aqueous layer was extracted with Et<sub>2</sub>O two times. After that, all organic layers were combined, washed with brine. The separated organic layer was dried over anhydrous Na<sub>2</sub>SO<sub>4</sub>, filtered, and concentrated *in vacuo* at room temperature to afford 1,2-toluenedithiol (**S4**) as a brown oil (2.09 g, 91% crude yield). This product was used for next step without further purifications.

**[Second step]** To a pre-dried round-bottom flask (100 mL) containing a magnetic stirring bar was added the crude product **S4** (2.09 g, assumed ca. 13.4 mmol), and the flask was placed *in vacuo*.

After replacing with argon atmosphere,  $\text{NEt}_3$  (266.4 mg, 2.63 mmol, 0.197 equiv) and dry  $\text{CH}_2\text{Cl}_2$  (8.0 mL) was added to the flask. To this mixture,  $\text{SO}_2\text{Cl}_2$  (3.62 g, 26.8 mmol, 2.01 equiv) was added at 0 °C. After stirring at 0 °C for 17 min., the mixture was warmed to room temperature (23 °C) and stirred for 28 min. After that, the resulting mixture was cooled to 0 °C again. This mixture was transferred via a syringe to a pre-dried round-bottomed flask (300 mL) containing a magnetic stirring bar, succinimide (2.65 g, 26.7 mmol, 2.00 equiv), dry  $\text{CH}_2\text{Cl}_2$  (20.0 mL), and  $\text{NEt}_3$  (3.52 g, 34.8 mmol, 2.61 equiv) at 0 °C. The resulting mixture was warmed and stirred at room temperature (24 °C) for 17 h. The resulting mixture was quenched with water (75 mL), and the organic layer was extracted with  $\text{CH}_2\text{Cl}_2$  (10 mL) two times. The combined organic layers were washed with brine (100 mL), dried over anhydrous  $\text{Na}_2\text{SO}_4$ , filtered, and concentrated *in vacuo*. The obtained crude product was purified by flash column chromatography on silica gel (eluent: hexane/AcOEt = 80:20  $\rightarrow$  50:50  $\rightarrow$  20:80  $\rightarrow$  0:100) using Isolera<sup>®</sup>. The combined fractions containing **1b** was concentrated using a rotary evaporator, and viscous crude of **1b** was solidified. The resulting viscous crude product was dissolved in AcOEt with sonicating. Removal of AcOEt by evaporation using a rotary evaporator resulted in the formation of powder, which was dissolved again in a small amount of AcOEt with sonicating. After adding excess amount of hexane and sonicating again with vigorous mixing using a spatula, thus formed solid was collected by suction filtration and rinsed with hexane. After drying *in vacuo* at 60 °C, **1b** was obtained as a yellow solid (1.42 g, 4.04 mmol, 27% from **S3**).

#### 4-3. General procedure of thia-APEX reaction



To an oven-dried screw-capped tube were added *S*-diimidated arenethiols **1** (1.0 equiv), aromatic substrates **2** (0.20 mmol, 1.0 equiv), and dry 1,2-dichloroethane (1.0 mL: 0.20 M for **2**) under air. After that, TfOH (0.6 equiv) was added to the reaction mixture and the resulting mixture was stirred at room temperature (ca. 23 °C) for 13 h. After that, the reaction mixture was diluted with  $\text{CH}_2\text{Cl}_2$  (4 mL), after which sat.  $\text{NaHCO}_3$  aq. (4 mL) was added. the organic layer was extracted with  $\text{CH}_2\text{Cl}_2$  (2 mL) three times. The combined organic layers were dried over anhydrous  $\text{Na}_2\text{SO}_4$ , filtered, and concentrated *in vacuo*. The obtained crude product was purified by flash column chromatography on silica gel using Isolera<sup>®</sup>, or PTLC (eluent: hexane/AcOEt) to afford  $\pi$ -extended thianthrene **3**.

## 4-4. Compound data

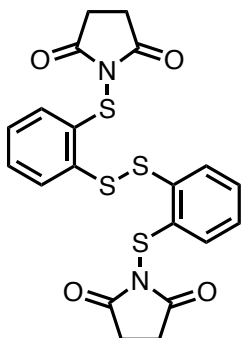
**1,1'-(1,2-Phenylenebis(sulfanediyl))-bis(pyrrolidine-2,5-dione) (1a)**

$^1\text{H}$  NMR (400 MHz,  $\text{CD}_2\text{Cl}_2$ )  $\delta$  7.23–7.32 (m, 4H), 2.86 (s, 8H).

$^{13}\text{C}$  NMR (100 MHz,  $\text{CD}_2\text{Cl}_2$ )  $\delta$  176.57, 134.82, 131.19, 129.88, 29.19.

HRMS (ESI<sup>+</sup>)  $m/z$  calcd for  $\text{C}_{14}\text{H}_{12}\text{N}_2\text{O}_4\text{S}_2\text{Na}^+$   $[\text{M}+\text{Na}]^+$ : 359.0131, found: 359.0130.

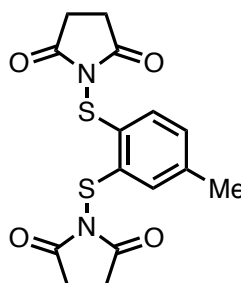
Note: A collected solid of **1a** included an inseparable byproduct showing  $m/z$  = 498.9886 for  $\text{C}_{20}\text{H}_{16}\text{N}_2\text{O}_4\text{S}_4\text{Na}^+$  in ESI analysis, which was considered to correspond to disulfide **1a'** (calcd.: 498.9885  $[\text{M}+\text{Na}]^+$ ). In addition, a weak singlet peak (0.26 H against to 8.0 H of ethylene protons of succinimide) was observed at 2.90 ppm in  $^1\text{H}$  NMR spectra of **1a**. This peak was considered to be derived from succinimide moieties of **1a'**. The purity (wt%) of resulting **1a** was estimated by accounting the  $^1\text{H}$  NMR integral ratio of **1a** and **1a'**.

**1,1'-((Disulfanediylbis(2,1-phenylene))-bis(sulfanediyl))bis(pyrrolidine-2,5-dione) (1a')**

Byproduct **1a'** including a small amount of **1a** and unknown impurities was separated from compound **1a** by GPC using  $\text{CHCl}_3$  as an eluent.

$^1\text{H}$  NMR (400 MHz,  $\text{CD}_2\text{Cl}_2$ )  $\delta$  7.52 (dd,  $J$  = 7.5, 1.6 Hz, 1.78H), 7.20–7.30 (m, 4.45H), 7.09 (dd,  $J$  = 7.7, 1.4 Hz, 1.77H), 2.90 (s, 8H).

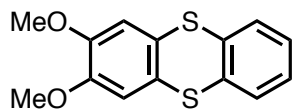
HRMS (ESI<sup>+</sup>)  $m/z$  calcd for  $\text{C}_{20}\text{H}_{16}\text{N}_2\text{O}_4\text{S}_4\text{Na}^+$   $[\text{M}+\text{Na}]^+$ : 498.9885, found: 498.9884. While enough quality of  $^{13}\text{C}$  NMR spectrum was not obtained due to the presence of other impurities, the structure of **1a'** was assigned by the results of  $^1\text{H}$  NMR and HRMS.

**1,1'-((4-Methyl-1,2-phenylene)bis-(sulfanediyl))bis(pyrrolidine-2,5-dione) (1b)**

$^1\text{H}$  NMR (600 MHz,  $\text{CDCl}_3$ )  $\delta$  7.42 (d,  $J$  = 7.7 Hz, 1H), 7.04 (d,  $J$  = 8.3 Hz, 1H), 7.01 (d,  $J$  = 0.6 Hz, 1H), 2.91 (s, 4H), 2.85 (s, 4H), 2.29 (s, 3H).

$^{13}\text{C}$  NMR (150 MHz,  $\text{CDCl}_3$ )  $\delta$  176.35, 176.33, 141.30, 136.30, 133.94, 130.22, 130.18, 129.52, 28.94, 28.89, 21.43.

HRMS (ESI<sup>+</sup>)  $m/z$  calcd for  $\text{C}_{14}\text{H}_{12}\text{N}_2\text{O}_4\text{S}_2\text{Na}^+$   $[\text{M}+\text{Na}]^+$ : 373.0285, found: 373.0287.

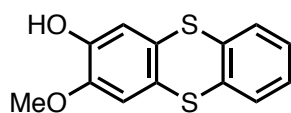
**2,3-Dimethoxythianthrene (3aa)**

According to the general procedure of thia-APEX reaction, **3aa** was obtained as a white solid (46.5 mg, 0.168 mmol, 83%) from **1a** (78.2 mg, 88<sub>wt</sub>%, 0.205 mmol, 1.01 equiv), 1,2-dimethoxybenzene (**2a**) (28.2 mg, 99% purity, 0.202 mmol), TfOH (11  $\mu$ L, 0.125 mmol, 0.62 equiv), and 1,2-dichloroethane (1.0 mL). Eluents of PTLC: hexane/AcOEt = 99:1  $\rightarrow$  97:3.

$^1\text{H}$  NMR (400 MHz,  $\text{CD}_2\text{Cl}_2$ )  $\delta$  7.47–7.51 (m, 2H), 7.22–7.27 (m, 2H), 7.01 (s, 2H), 3.82 (s, 6H).

$^{13}\text{C}$  NMR (100 MHz,  $\text{CD}_2\text{Cl}_2$ )  $\delta$  149.58, 136.69, 128.96, 127.95, 126.91, 112.27, 56.44.

HRMS (DART<sup>+</sup>)  $m/z$  calcd for  $\text{C}_{14}\text{H}_{13}\text{O}_2\text{S}_2$  [ $\text{M}+\text{H}$ ]<sup>+</sup>: 277.0357, found: 277.0340.

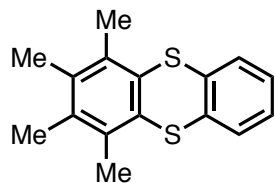
**3-Methoxythianthren-2-ol (4)**

When thia-APEX reaction to obtain **3aa** was conducted, **4** was also isolated from the crude mixture by column chromatography on silica gel (eluents: hexane/AcOEt = 99:1  $\rightarrow$  4:1) and following GPC (eluent:  $\text{CHCl}_3$ ).

$^1\text{H}$  NMR (400 MHz,  $\text{Cl}_2\text{CDCDCl}_2$ )  $\delta$  7.48–7.53 (m, 2H), 7.24–7.30 (m, 2H), 7.09 (s, 1H), 7.01 (s, 1H), 5.64 (s, 1H), 3.89 (s, 3H).

$^{13}\text{C}$  NMR (150 MHz,  $\text{Cl}_2\text{CDCDCl}_2$ )  $\delta$  146.39, 145.37, 136.04, 135.97, 128.72, 128.63, 127.60, 127.56, 127.31, 125.75, 114.75, 111.14, 56.25.

HRMS (ESI<sup>+</sup>)  $m/z$  calcd for  $\text{C}_{13}\text{H}_9\text{O}_2\text{S}_2\text{Na}$  [ $\text{M}-\text{H}+\text{Na}$ ]: 283.9936, found: 283.9938.

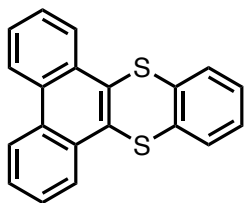
**1,2,3,4-Tetramethylthianthrene (3ab)**

According to the general procedure of thia-APEX reaction, **3ab** was obtained as a white solid (44.4 mg, 0.163 mmol, 70%) from **1a** (85.6 mg, 93<sub>wt</sub>%, 0.237 mmol, 1.01 equiv), 1,2,3,4-tetramethylbenzene (**2b**) (31.4 mg, 0.234 mmol), TfOH (12  $\mu$ L, 0.136 mmol, 0.58 equiv), and 1,2-dichloroethane (1.2 mL). Eluents of column chromatography on silica gel: hexane/AcOEt = 100:0  $\rightarrow$  99:1.

$^1\text{H}$  NMR (400 MHz,  $\text{CDCl}_3$ )  $\delta$  7.52–7.58 (m, 2H), 7.20–7.27 (m, 2H), 2.52 (s, 6H), 2.23 (s, 6H).

$^{13}\text{C}$  NMR (100 MHz,  $\text{CD}_2\text{Cl}_2$ )  $\delta$  137.60, 135.33, 133.60, 132.74, 129.07, 127.85, 18.57, 17.16

HRMS (DART<sup>+</sup>)  $m/z$  calcd for  $\text{C}_{16}\text{H}_{16}\text{S}_2$  [ $\text{M}$ ]<sup>+</sup>: 272.0693, found: 272.0694.

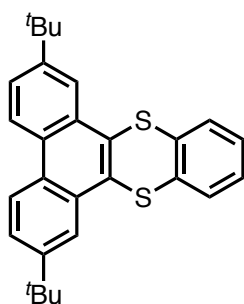
**Dibenzo[*a,c*]thianthrene (3ac)**

According to the general procedure of thia-APEX reaction, crude **3ac** was obtained from **1a** (73.6 mg, 93<sub>wt</sub>%, 0.203 mmol, 1.00 equiv), phenanthrene (**2c**) (36.3 mg, 0.204 mmol), TfOH (10  $\mu$ L, 0.113 mmol, 0.56 equiv), and 1,2-dichloroethane (1.0 mL). This crude mixture contained **3ac** and other regioisomers as well as oligomeric thia-APEX products. The purification by column chromatography on silica gel (eluents: hexane/AcOEt = 99:1  $\rightarrow$  97:3) followed by GPC using CHCl<sub>3</sub> as eluent afforded **3ac** as a semi-pure product. Finally, recrystallization from chloroform/pentane by vapor diffusion afforded pure **3ac** as a white solid (13.7 mg, 0.0433 mmol, 21%). The structure was determined by X-ray crystallographic analysis using a single crystal obtained by the same method.

<sup>1</sup>H NMR (400 MHz, Cl<sub>2</sub>CDCDCl<sub>2</sub>)  $\delta$  8.61-8.73 (m, 4H), 7.67-7.77 (m, 6H), 7.32-7.38 (m, 2H).

<sup>13</sup>C NMR (150 MHz, Cl<sub>2</sub>CDCDCl<sub>2</sub>)  $\delta$  136.42, 132.50, 130.17, 129.62, 128.89, 127.95, 127.41, 127.24, 125.17, 123.01.

HRMS (DART<sup>+</sup>) *m/z* calcd for C<sub>20</sub>H<sub>13</sub>S<sub>2</sub> [M+H]<sup>+</sup>: 317.0459, found: 317.0460.

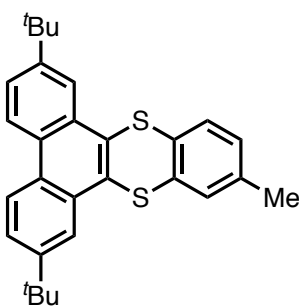
**2,7-Di-*tert*-butyldibenzo[*a,c*]thianthrene (3ad)**

According to the general procedure of thia-APEX reaction, **3ad** was obtained as a white solid (74.2 mg, 0.173 mmol, 87%) from **1a** (76.8 mg, 88<sub>wt</sub>%, 0.201 mmol, 1.00 equiv), 2,7-di-*tert*-butylphenanthrene (**2d**) (58.1 mg, 0.200 mmol), TfOH (10  $\mu$ L, 0.113 mmol, 0.57 equiv), and 1,2-dichloroethane (1.0 mL). Eluents of PTLC: hexane/AcOEt = 99:1.

<sup>1</sup>H NMR (400 MHz, CD<sub>2</sub>Cl<sub>2</sub>)  $\delta$  8.57-8.62 (m, 4H), 7.77 (dd, *J* = 8.7, 2.4 Hz, 2H), 7.69-7.73 (m, 2H), 7.31-7.36 (m, 2H), 1.50 (s, 18H)

<sup>13</sup>C NMR (150 MHz, CDCl<sub>3</sub>)  $\delta$  149.96, 137.11, 132.69, 130.18, 129.04, 127.88, 127.82, 125.49, 122.85, 121.15, 35.30, 31.57.

HRMS (DART<sup>+</sup>) *m/z* calcd for C<sub>28</sub>H<sub>29</sub>S<sub>2</sub> [M+H]<sup>+</sup>: 429.1711, found: 429.1713.

**2,7-Di-*tert*-butyl-11-methyl- dibenzo[*a,c*]thianthrene (3bd)**

According to the general procedure of thia-APEX reaction, **3bd** was obtained as a white solid (63.0 mg, 0.142 mmol, 71%) from **1b** (70.1 mg, 0.200 mmol, 1.00 equiv), 2,7-di-*tert*-butylphenanthrene (**2d**) (58.1 mg, 0.200 mmol), TfOH (10  $\mu$ L, 0.113 mmol, 0.57 equiv), and 1,2-dichloroethane (1.0 mL). Eluents of column chromatography on silica gel: hexane/AcOEt = 100:0  $\rightarrow$  99:1.

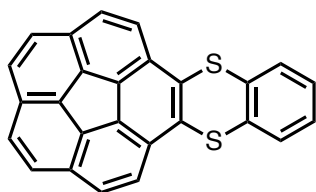
<sup>1</sup>H NMR (600 MHz, CDCl<sub>3</sub>)  $\delta$  8.58-8.60 (m, 2H), 8.55 (d, *J* = 8.3

Hz, 2H), 7.71 (dd,  $J = 8.9, 1.2$  Hz, 2H), 7.55 (d,  $J = 8.3$  Hz, 1H), 7.52 (s, 1H), 7.09 (d,  $J = 8.3$  Hz, 1H), 2.35 (s, 3H), 1.50 (s, 18H).

$^{13}\text{C}$  NMR (150 MHz,  $\text{CDCl}_3$ )  $\delta$  149.91, 138.05, 137.04, 133.59, 133.22, 132.75, 130.24, 130.20, 129.61, 128.79, 128.74, 127.78, 125.43, 125.40, 122.83, 121.18, 121.14, 35.29, 31.58, 21.07. Three  $\text{sp}^2$ -quaternary carbon peaks were overlapped.

HRMS (DART $^+$ )  $m/z$  calcd for  $\text{C}_{29}\text{H}_{31}\text{S}_2$   $[\text{M}+\text{H}]^+$ : 443.1867, found: 443.1863.

### Benzo[6,7]fluorantheno[1,10-*abc*]thianthrene (3ae)



According to the general procedure of thia-APEX reaction, **3ae** was obtained as a yellow solid (27.4 mg, 0.0705 mmol, 35%) from **1a** (76.8 mg, 88 $_{\text{wt}}\%$ , 0.201 mmol, 1.00 equiv), corannulene (**2e**) (50.2 mg, 0.201 mmol), TfOH (10  $\mu\text{L}$ , 0.113 mmol, 0.56 equiv), and 1,2-dichloroethane (1.0 mL). Purification was performed by PTLC

(eluent: hexane/AcOEt = 99:1) followed by GPC using  $\text{CHCl}_3$  as eluent.

$^1\text{H}$  NMR (400 MHz,  $\text{CD}_2\text{Cl}_2$ )  $\delta$  8.14 (d,  $J = 8.7$  Hz, 2H), 7.84 (d,  $J = 9.1$  Hz, 2H), 7.76 (s, 4H), 7.52-7.57 (m, 2H), 7.18-7.23 (m, 2H). According to a DFT calculation in section 4-6, Figure S3, the singlet peaks were considered to be characterized to four protons of *rim*-regions opposite to the benzodithiine arm. The structure was determined by X-ray crystallographic analysis using a single crystal obtained by recrystallization from chloroform/pentane by vapor diffusion.

$^{13}\text{C}$  NMR (150 MHz,  $\text{CD}_2\text{Cl}_2$ )  $\delta$  136.39, 135.94, 135.72, 135.70, 134.01, 131.43, 131.28, 131.16, 129.02, 128.55, 128.29, 127.92, 127.40, 125.82.

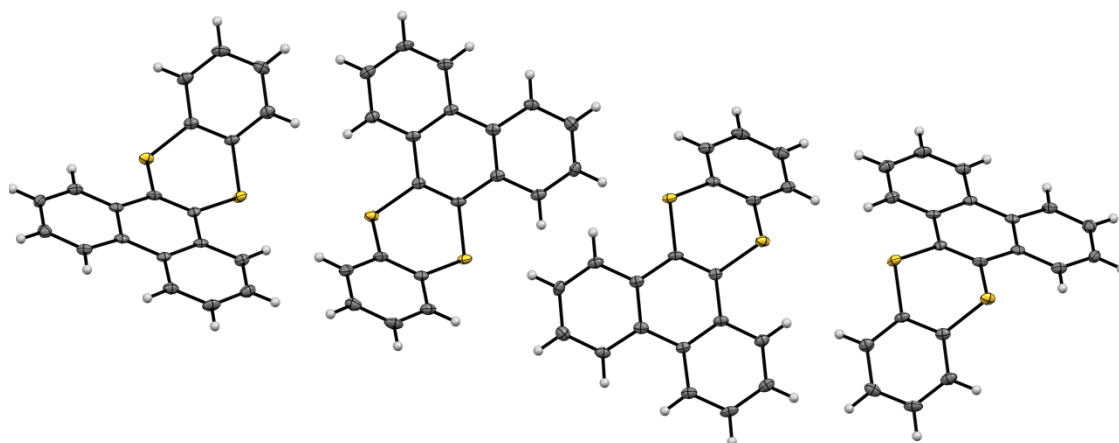
HRMS (DART $^+$ )  $m/z$  calcd for  $\text{C}_{26}\text{H}_{13}\text{S}_2$   $[\text{M}+\text{H}]^+$ : 389.0459, found: 389.0467.

**4-5. X-ray Crystal Structure Analysis**<sup>[32,33,34]</sup>

Details of the crystal data and a summary of the intensity data collection parameters for **3ac** and **3ae** are listed in Table S1–S2. A single crystal of **3ac** was prepared by vapor diffusion recrystallization using CHCl<sub>3</sub> and pentane. A single crystal of **3ae** was prepared by vapor diffusion recrystallization from CHCl<sub>3</sub> and pentane. A suitable crystal was mounted with mineral oil on a MiTeGen MicroMounts and transferred to the goniometer of the kappa goniometer of a RIGAKU XtaLAB Synergy-S system with 1.2 kW MicroMax-007HF microfocus rotating anode (Graphite-monochromated Mo K<sub>α</sub> radiation ( $\lambda = 0.71073 \text{ \AA}$ )) and PILATUS200K hybrid photon-counting detector. Cell parameters were determined and refined, and raw frame data were integrated using CrysAlis<sup>Pro</sup> (Agilent Technologies, 2010). The structures were solved by direct methods with SHELXT<sup>[32]</sup> and refined by full-matrix least-squares techniques against F<sup>2</sup> (SHELXL-2018/3)<sup>[33]</sup> by using Olex2 software package.<sup>[34]</sup> The intensities were corrected for Lorentz and polarization effects. The non-hydrogen atoms were refined anisotropically. Hydrogen atoms were placed using AFIX instructions. CCDC 2223786 and 2223785 contain the supplementary crystallographic data for this paper. These data can be obtained free of charge from The Cambridge Crystallographic Data Centre via [www.ccdc.cam.ac.uk/data\\_request/cif](http://www.ccdc.cam.ac.uk/data_request/cif).

**Table S1.** Crystallographic data and structure refinement details for **3ac**.

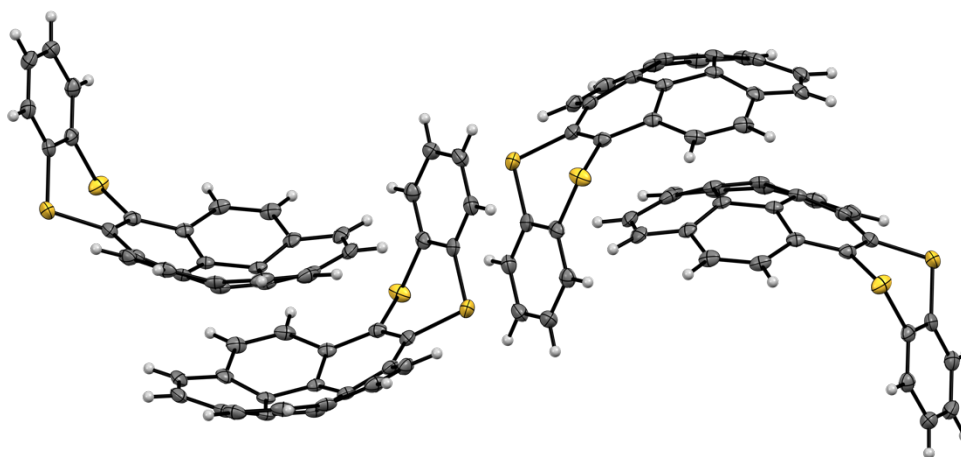
CCDC deposition No.	2223786
formula	C <sub>20</sub> H <sub>12</sub> S <sub>2</sub>
FW	316.42
<i>T</i> (K)	123(2) K
$\lambda$ (Å)	0.71073 Å
cryst syst	Monoclinic
space group	<i>P2<sub>1</sub>/n</i>
<i>a</i> (Å)	16.7176(12)
<i>b</i> (Å)	3.9059(2)
<i>c</i> (Å)	22.6639(19)
$\alpha$ (deg)	90
$\beta$ (deg)	109.384(9)
$\gamma$ (deg)	90
<i>V</i> (Å <sup>3</sup> )	1396.00(18)
<i>Z</i>	4
<i>D</i> <sub>calc</sub> (g / cm <sup>3</sup> )	1.505
$\mu$ (mm <sup>-1</sup> )	0.373
F(000)	656.0
cryst size (mm)	0.2 × 0.1 × 0.03
$\theta$ range (deg)	5.166° to 59.656°
reflns collected	12465
indep reflns/ <i>R</i> <sub>int</sub>	3295/0.1229
params	199
GOF on <i>F</i> <sup>2</sup>	1.050
<i>R</i> <sub>1</sub> , <i>wR</i> <sub>2</sub> [ <i>I</i> > 2 $\sigma$ ( <i>I</i> )]	0.0559, 0.1410
<i>R</i> <sub>1</sub> , <i>wR</i> <sub>2</sub> (all data)	0.0768, 0.1518

**Figure S1.** Crystallographic structure of **3ac** with the thermal ellipsoid at a 50% probability level.



**Table S2.** Crystallographic data and structure refinement details for **3ae**.

CCDC deposition No.	2223785
formula	C <sub>26</sub> H <sub>12</sub> S <sub>2</sub>
FW	388.48
<i>T</i> (K)	123(2) K
$\lambda$ (Å)	0.71073 Å
cryst syst	Monoclinic
space group	<i>P2<sub>1</sub>/c</i>
<i>a</i> (Å)	9.7599(7)
<i>b</i> (Å)	24.6462(18)
<i>c</i> (Å)	7.4158(5)
$\alpha$ (deg)	90
$\beta$ (deg)	103.413(7)
$\gamma$ (deg)	90
<i>V</i> (Å <sup>3</sup> )	1735.2(2)
<i>Z</i>	4
<i>D</i> <sub>calc</sub> (g / cm <sup>3</sup> )	1.487
$\mu$ (mm <sup>-1</sup> )	0.316
F(000)	800.0
cryst size (mm)	0.1 × 0.05 × 0.05
$\theta$ range (deg)	4.29° to 59.514°
reflns collected	18455
indep reflns/ <i>R</i> <sub>int</sub>	4146/ 0.0645
params	253
GOF on <i>F</i> <sup>2</sup>	1.019
<i>R</i> <sub>1</sub> , <i>wR</i> <sub>2</sub> [ <i>I</i> > 2 $\sigma$ ( <i>I</i> )]	0.0415, 0.0969
<i>R</i> <sub>1</sub> , <i>wR</i> <sub>2</sub> (all data)	0.0652, 0.1064

**Figure S2.** Crystallographic structure of **3ae** with the thermal ellipsoid at a 50% probability level.

#### 4-6. DFT calculations

The Gaussian 16 program, revision C.01,<sup>[35]</sup> was used for all computational investigations. Following the literature,<sup>[36]</sup> geometry optimizations and harmonic vibration frequency calculations of the all local minima (with no imaginary frequency), and transition states (with one imaginary frequency) were conducted using the B3LYP/6-31+G(d,p) level of theories in the gas phase at 298.15 K without any symmetry assumptions,<sup>[18]</sup> and those accurate energies were estimated by the single-point calculations of optimized geometries with the B3LYP/6-31+G(d,p) level of theory in CH<sub>2</sub>Cl<sub>2</sub> (IEF-PCM<sup>[19]</sup>) as needed.<sup>[18]</sup> For investigations on photophysical properties,  $\pi$ -extended thianthrenes **3ac** and **3ae** were calculated by TD-DFT methods. Zero-point energy, enthalpy, and Gibbs free energy were estimated from the gas-phase unless otherwise noted. Harmonic vibration frequency calculations at the same level were performed to verify all stationary points as local minima with no imaginary frequency. <sup>1</sup>H NMR spectra of **3ae** was estimated using the GIAO-B3LYP/6-31+G(d,p) level of theory in CH<sub>2</sub>Cl<sub>2</sub> (IEF-PCM).<sup>[37]</sup> Visualization of the results was performed by use of GaussView 6.1 software.<sup>[38]</sup>

**Table S3.** Uncorrected and thermal-corrected energies of optimized geometries (Hartree), with the B3LYP/6-31+G(d,p) level of theory.<sup>a</sup>

Structure	<i>E</i>	<i>ZPE</i>	<i>H</i>	<i>G</i>
<b>3ac</b>	-1565.802942	0.255801	-1565.530027	-1565.591065
<b>3ae-ladle</b>	-1794.424410	0.292961	-1794.112175	-1794.177032
<b>3ae-spoon</b>	-1794.422306	0.292826	-1794.110148	-1794.175168
<b>TS1<sub>3ac</sub></b>	-1565.791948	0.255148	-1565.520177	-1565.579422
<b>TS1<sub>3ae</sub></b>	-1794.412840	0.292349	-1794.101747	-1794.165130
<b>TS2<sub>3ae</sub></b>	-1794.409079	0.292379	-1794.097993	-1794.161540
<b>phenanthrene</b>	-539.572509	0.194287	-539.367825	-539.413067
<b>corannulene</b>	-768.188342	0.231458	-767.944404	-767.993636
<b>tetramethylsilane</b>	-449.218326	0.147168	-449.060762	-449.103927

a) *E*: electronic energy; *ZPE*: zero-point energy; *H* (enthalpy) = *E* + *TCE*: sum of electronic energy (*E*) and thermal correction to enthalpy (*TCE*); *G* (free energy) = *E* + *TCF*: sum of electronic energy (*E*) and thermal corrections to free energies (*TCF*).

**Table S4.** Cartesian coordinates of optimized **3ac**.

H	0.3245260	-3.3888480	0.2995270
H	2.3738850	-4.6440170	-0.2223020
H	4.4967650	-3.4133300	-0.7061090
H	4.5326280	-0.9754860	-0.6795030
H	4.5326180	0.9755000	-0.6795290
H	4.4967460	3.4133440	-0.7061320
H	2.3738660	4.6440230	-0.2223020
H	0.3245150	3.3888460	0.2995390
H	-5.5756020	-1.2456690	-1.6006190
H	-3.7054030	-2.4848130	-0.5331880
H	-5.5756050	1.2456710	-1.6006080
H	-3.7054090	2.4848100	-0.5331670
C	2.3952720	-3.5585890	-0.1984190
C	3.5879030	-2.8664690	-0.4732700
C	3.6024240	-1.4832600	-0.4551660
C	2.4420660	-0.7285920	-0.1574140
C	1.2367490	-1.4356750	0.1360670
C	1.2444540	-2.8528730	0.0984990
C	2.4420630	0.7285980	-0.1574160
C	3.6024150	1.4832710	-0.4551800
C	3.5878880	2.8664790	-0.4732830
C	2.3952580	3.5585950	-0.1984210
C	1.2444440	2.8528750	0.0985050
C	1.2367440	1.4356760	0.1360710
C	0.0481400	-0.6863100	0.4911170
C	0.0481380	0.6863060	0.4911220
C	-2.6937710	-0.7008340	0.1259800
C	-2.6937730	0.7008280	0.1259870
C	-3.7240630	-1.3994690	-0.5159690
C	-4.7701890	-0.6991390	-1.1194280
C	-3.7240660	1.3994660	-0.5159560
C	-4.7701910	0.6991390	-1.1194220
S	-1.4162780	-1.5944530	0.9906300
S	-1.4162820	1.5944420	0.9906430

**Table S5.** Cartesian coordinates of optimized **3ae-ladle**.

H	-0.4601630	3.5013670	-0.2710690
H	1.7183930	4.2490490	0.4740510
H	1.7183930	-4.2490500	0.4740510
H	-0.4601630	-3.5013670	-0.2710690
H	-6.0169110	1.2459770	2.5071460
H	-4.4677450	2.4840290	1.0119570
H	-6.0169110	-1.2459770	2.5071460
H	-4.4677440	-2.4840290	1.0119580
H	5.6260300	1.4179090	1.7870870
H	4.2774070	3.3784540	1.3296900
H	5.6260300	-1.4179090	1.7870870
H	4.2774070	-3.3784540	1.3296900
C	1.6326520	3.2479200	0.0587430
C	2.7803630	2.3667920	0.0783280
C	2.5711410	1.1465830	-0.5441440
C	1.2965770	0.7090870	-0.9830860
C	0.1474590	1.4668040	-0.8277230
C	0.3794790	2.8207080	-0.3685200
C	1.2965770	-0.7090870	-0.9830860
C	2.5711420	-1.1465830	-0.5441440
C	2.7803630	-2.3667920	0.0783280
C	1.6326520	-3.2479200	0.0587430
C	0.3794790	-2.8207080	-0.3685200
C	0.1474590	-1.4668040	-0.8277230
C	-1.0859420	0.7008990	-0.9376880
C	-1.0859410	-0.7008990	-0.9376880
C	-3.6493300	0.7010920	0.1226720
C	-3.6493300	-0.7010920	0.1226720
C	-4.4895920	1.3986020	0.9996620
C	-5.3548480	0.6989900	1.8428180
C	-4.4895920	-1.3986020	0.9996620
C	-5.3548480	-0.6989900	1.8428180
C	3.3598530	0.0000000	-0.2758140
C	4.4076560	0.0000000	0.6308090

C	4.7729240	-1.3135090	1.1211600
C	3.9989320	-2.4390270	0.8585270
C	4.7729240	1.3135090	1.1211590
C	3.9989320	2.4390270	0.8585270
S	-2.6236520	1.6062080	-1.0267710
S	-2.6236520	-1.6062080	-1.0267710

**Table S6.** Cartesian coordinates of optimized **3ae-spoon**.

C	-1.8054470	3.2578380	0.1704210
C	-2.8904990	2.3703330	-0.1920410
C	-2.4768000	1.1464040	-0.6913860
C	-1.1299460	0.7080980	-0.6516170
C	-0.1068180	1.4686740	-0.1143400
C	-0.4812370	2.8314320	0.2051020
C	-1.1299470	-0.7080980	-0.6516170
C	-2.4767990	-1.1464040	-0.6913860
C	-2.8904990	-2.3703330	-0.1920410
C	-1.8054470	-3.2578380	0.1704200
C	-0.4812360	-2.8314320	0.2051020
C	-0.1068170	-1.4686740	-0.1143400
C	1.0686940	0.7012580	0.2713920
C	1.0686930	-0.7012570	0.2713920
H	0.2752060	3.5264330	0.5575990
H	-2.0270220	4.2680970	0.5055290
H	-2.0270210	-4.2680980	0.5055270
H	0.2752060	-3.5264330	0.5575980
S	2.4814770	1.6019690	0.9012930
S	2.4814770	-1.6019680	0.9012960
C	3.8282800	0.7011460	0.1525310
C	3.8282800	-0.7011460	0.1525310
C	4.9093660	1.3990990	-0.4002500
C	6.0033270	0.6990450	-0.9123500
C	4.9093660	-1.3990990	-0.4002490
C	6.0033260	-0.6990450	-0.9123500
H	6.8463420	1.2459000	-1.3235430
H	4.8915950	2.4843750	-0.4205590

H	6.8463420	-1.2459010	-1.3235430
H	4.8915950	-2.4843760	-0.4205570
C	-3.3089140	0.0000000	-0.7152640
C	-4.6086740	0.0000000	-0.2362120
C	-5.1218220	-1.3151760	0.0917120
C	-4.3054010	-2.4418810	0.1120480
C	-5.1218230	1.3151760	0.0917120
C	-4.3054010	2.4418800	0.1120490
H	-6.1540250	1.4211370	0.4164110
H	-4.7331470	3.3822190	0.4509470
H	-6.1540250	-1.4211380	0.4164120
H	-4.7331470	-3.3822190	0.4509460

**Table S7.** Cartesian coordinates of optimized TS1<sub>3ac</sub>.

C	0.0000000	3.5530050	-2.5388680
C	-0.0000010	2.8622870	-3.7618330
C	-0.0000010	1.4791950	-3.7663880
C	0.0000000	0.7274670	-2.5675330
C	0.0000010	1.4278220	-1.3262330
C	0.0000000	2.8471170	-1.3500920
C	0.0000000	-0.7274670	-2.5675330
C	0.0000010	-1.4791950	-3.7663880
C	0.0000010	-2.8622870	-3.7618330
C	0.0000000	-3.5530050	-2.5388680
C	0.0000000	-2.8471170	-1.3500920
C	-0.0000010	-1.4278220	-1.3262330
C	0.0000010	0.6855520	-0.0743560
C	-0.0000010	-0.6855520	-0.0743560
H	0.0000000	3.4044990	-0.4213510
H	0.0000000	4.6386790	-2.5214320
H	-0.0000010	3.4078090	-4.7006840
H	-0.0000020	0.9682250	-4.7212590
H	0.0000020	-0.9682250	-4.7212590
H	0.0000010	-3.4078090	-4.7006840
H	0.0000000	-4.6386790	-2.5214320
H	0.0000000	-3.4044990	-0.4213510

S	0.0000040	1.7426960	1.3716480
S	-0.0000040	-1.7426960	1.3716480
C	0.0000010	0.6983340	2.8098390
C	-0.0000010	-0.6983340	2.8098390
C	0.0000030	1.3870370	4.0331060
C	0.0000010	0.6984980	5.2443010
C	-0.0000030	-1.3870370	4.0331060
C	-0.0000010	-0.6984980	5.2443010
H	0.0000020	1.2516210	6.1782420
H	0.0000050	2.4737180	4.0284520
H	-0.0000020	-1.2516210	6.1782420
H	-0.0000050	-2.4737180	4.0284520

**Table S8.** Cartesian coordinates of optimized TS1<sub>3ae</sub>.

C	-0.1442260	-1.8245890	3.2466250
C	0.0440860	-2.9570210	2.3674860
C	0.6138740	-2.6348530	1.1464630
C	0.8086240	-1.3020510	0.7082310
C	0.4438230	-0.2006630	1.4590110
C	0.0443140	-0.5141420	2.8167830
C	0.8086240	-1.3020510	-0.7082310
C	0.6138740	-2.6348530	-1.1464630
C	0.0440860	-2.9570210	-2.3674860
C	-0.1442260	-1.8245890	-3.2466250
C	0.0443140	-0.5141420	-2.8167830
C	0.4438230	-0.2006630	-1.4590110
C	0.3074910	1.0410990	0.6987670
C	0.3074910	1.0410990	-0.6987670
H	-0.2003540	0.2855410	3.5089210
H	-0.5288560	-1.9822670	4.2512370
H	-0.5288560	-1.9822670	-4.2512370
H	-0.2003540	0.2855410	-3.5089210
S	0.0581890	2.4615170	1.7492140
S	0.0581890	2.4615170	-1.7492140
C	-0.1062110	3.8919210	0.6995440
C	-0.1062110	3.8919210	-0.6995440

C	-0.2446710	5.1077140	1.3864750
C	-0.3880000	6.3110920	0.6981780
C	-0.2446710	5.1077140	-1.3864750
C	-0.3880000	6.3110920	-0.6981780
H	-0.4959400	7.2384900	1.2517370
H	-0.2396430	5.1041630	2.4731890
H	-0.4959400	7.2384900	-1.2517370
H	-0.2396430	5.1041630	-2.4731890
C	0.4973480	-3.4599650	0.0000000
C	-0.1970790	-4.6584010	0.0000000
C	-0.6099730	-5.1088390	-1.3143130
C	-0.4953410	-4.2999730	-2.4398830
C	-0.6099730	-5.1088390	1.3143130
C	-0.4953410	-4.2999730	2.4398830
H	-1.1047430	-6.0713690	1.4187560
H	-0.9050320	-4.6618960	3.3797130
H	-1.1047430	-6.0713690	-1.4187560
H	-0.9050320	-4.6618960	-3.3797130

**Table S9.** Cartesian coordinates of optimized **TS2<sub>3ac</sub>**.

C	-1.7759660	-3.3496030	-0.0678040
C	-2.8964730	-2.4322500	0.1323620
C	-2.4773870	-1.1312760	0.0685560
C	-1.1695820	-0.6985640	-0.1678920
C	-0.0850520	-1.5056360	-0.3689820
C	-0.4585320	-2.9170270	-0.2998280
C	-1.1695820	0.6985640	-0.1678910
C	-2.4773860	1.1312760	0.0685570
C	-2.8964730	2.4322500	0.1323620
C	-1.7759650	3.3496030	-0.0678040
C	-0.4585310	2.9170260	-0.2998280
C	-0.0850520	1.5056360	-0.3689820
C	1.1224850	-0.7095550	-0.6162810
C	1.1224850	0.7095540	-0.6162820
H	0.3012080	-3.6820240	-0.4303930
H	-1.9423150	-4.4235240	-0.0384620



H	-1.9423130	4.4235240	-0.0384620
H	0.3012090	3.6820230	-0.4303930
S	2.6287660	-1.6003240	-0.9795180
S	2.6287660	1.6003230	-0.9795190
C	3.8267080	-0.7009900	-0.0065960
C	3.8267080	0.7009890	-0.0065970
C	4.7947350	-1.3991170	0.7259610
C	5.7827250	-0.6990040	1.4210140
C	4.7947360	1.3991170	0.7259600
C	5.7827260	0.6990040	1.4210130
H	6.5416140	-1.2458070	1.9723810
H	4.7743090	-2.4844850	0.7420430
H	6.5416140	1.2458080	1.9723800
H	4.7743090	2.4844860	0.7420410
C	-3.2860100	0.0000000	0.2126670
C	-4.6353070	0.0000000	0.4384830
C	-5.1500670	1.3669670	0.5209100
C	-4.3365780	2.5046560	0.3782900
C	-5.1500680	-1.3669670	0.5209100
C	-4.3365790	-2.5046560	0.3782900
H	-6.2091310	-1.5366000	0.6985710
H	-4.8240900	-3.4732260	0.4564540
H	-6.2091310	1.5366010	0.6985710
H	-4.8240890	3.4732270	0.4564530

**Table S10.** Cartesian coordinates of optimized phenanthrene.

H	-3.3513050	1.8390410	-0.0001800
H	1.2322580	3.0325450	0.0001050
H	4.6505970	-0.2728770	0.0000860
H	3.3513050	1.8390410	0.0002160
H	1.0079510	-2.5337680	-0.0003040
H	3.4480050	-2.4599410	-0.0002420
H	-1.2322570	3.0325450	-0.0001370
H	-4.6505960	-0.2728810	-0.0000330
H	-3.4480100	-2.4599390	0.0002350
H	-1.0079430	-2.5337650	0.0002710

C	3.5648860	-0.2970400	0.0000410
C	2.8399160	0.8797460	0.0001230
C	1.4238510	0.8667420	0.0000670
C	0.7294190	-0.3803870	-0.0000170
C	1.5007180	-1.5681010	-0.0001410
C	2.8848470	-1.5311900	-0.0001170
C	0.6806030	2.0960640	0.0000450
C	-0.7294200	-0.3803850	0.0000040
C	-1.4238500	0.8667420	-0.0000730
C	-0.6806040	2.0960640	-0.0000650
C	-2.8399180	0.8797460	-0.0001000
C	-3.5648850	-0.2970390	-0.0000160
C	-2.8848450	-1.5311920	0.0001190
C	-1.5007190	-1.5681030	0.0001270

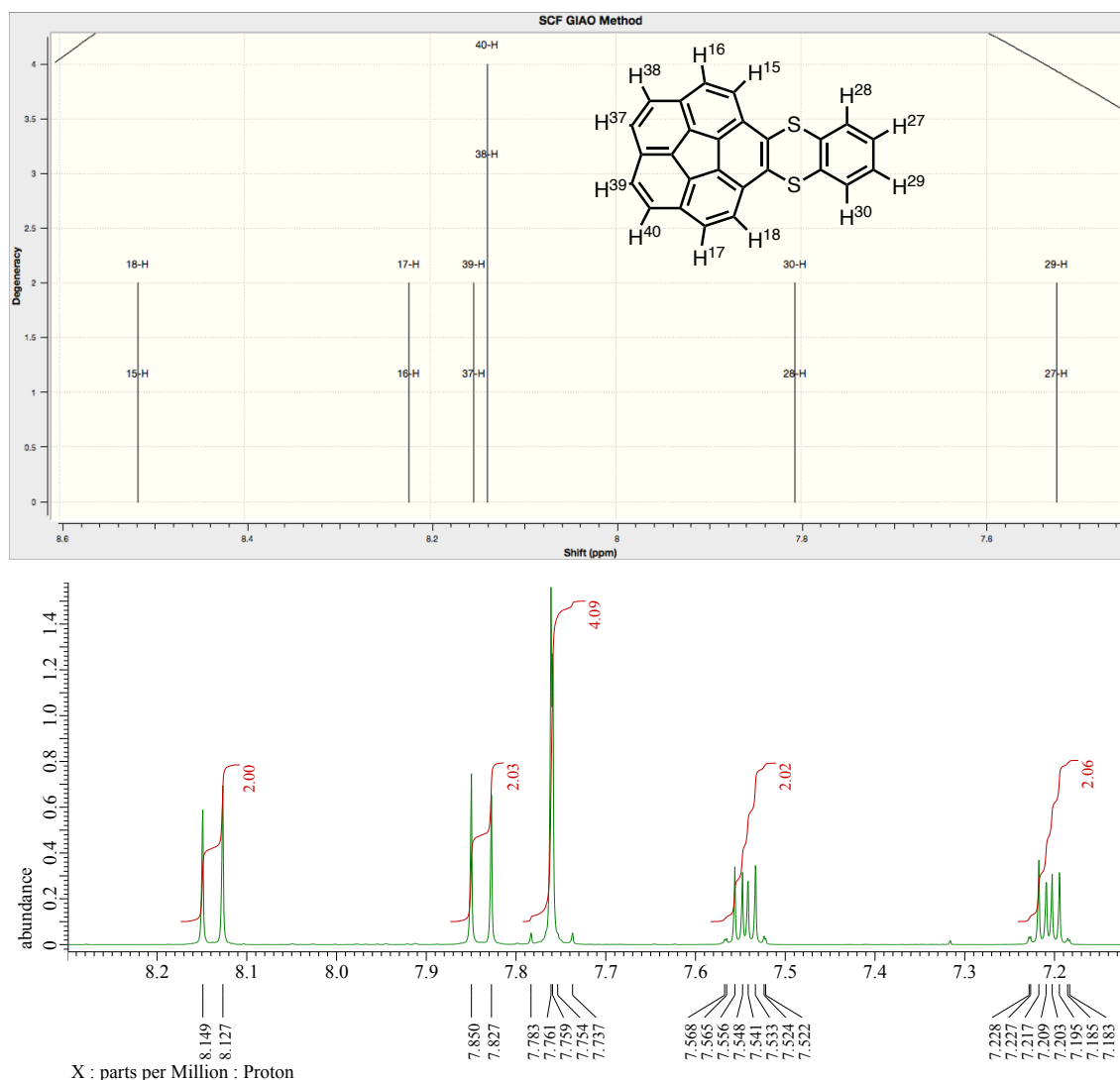
**Table S11.** Cartesian coordinates of optimized corannulene.

H	2.6792670	-3.3058070	-0.6136340
H	0.4395930	-4.2323820	-0.6137980
H	-2.3161550	-3.5696780	-0.6135420
H	-3.8895460	-1.7259990	-0.6134450
H	-4.1107180	1.0997010	-0.6134990
H	-2.8434610	3.1658070	-0.6134380
H	2.1321710	3.6825030	-0.6135850
H	-0.2243950	4.2492880	-0.6135940
H	4.1612340	-0.8898140	-0.6134030
H	3.9720070	1.5265240	-0.6135220
C	-0.2820430	-1.1726600	0.6192460
C	1.0281280	-0.6306030	0.6193200
C	0.9174540	0.7829270	0.6192580
C	-0.4611080	1.1144590	0.6192140
C	-1.2024440	-0.0941490	0.6192670
C	-0.5819950	-2.4197710	0.0947290
C	-1.9765100	-2.6010470	-0.2547300
C	-2.8795420	-1.5428870	-0.2546870
C	-2.4812330	-0.1942330	0.0948070
C	-0.9514640	2.2997060	0.0947010

C	-2.3571980	2.2618050	-0.2547190
C	-3.0845380	1.0759970	-0.2546990
C	1.8931740	1.6155520	0.0947760
C	1.4226900	2.9407090	-0.2548040
C	0.0701640	3.2659700	-0.2548940
C	2.1215460	-1.3012780	0.0948690
C	3.2364910	-0.4443100	-0.2546170
C	3.1278810	0.9425340	-0.2547050
C	1.8629930	-2.6834830	-0.2548080
C	0.5775550	-3.2152620	-0.2549450

**Table S12.** Cartesian coordinates of optimized tetramethylsilane.

H	1.4310380	-2.0164390	-0.4336960
H	1.4050180	-0.9536230	-1.8489790
H	0.0240980	-2.0069630	-1.5077620
H	2.0163140	0.4672590	1.4204990
H	0.9377160	1.8703500	1.3873510
H	1.9901060	1.5300950	0.0052690
H	-0.4446770	-1.4100800	2.0289530
H	-1.8515970	-1.4006040	0.9548570
H	-1.5231620	-0.0069610	1.9953690
H	-1.5698850	1.8868940	-0.5265180
H	-1.8980190	0.4931560	-1.5672220
H	-0.5171580	1.5466720	-1.9083520
C	0.7885130	-1.3720230	-1.0448920
C	1.3629780	1.0663060	0.7755160
C	-1.0528070	-0.7768050	1.3725830
C	-1.0986240	1.0825720	-1.1032590
Si	-0.0000110	-0.0000040	0.0000390



**Figure S3.** Comparison with calculated proton peaks in  $^1\text{H}$  NMR (above, GIAO-B3LYP/6-31+G(d,p), in  $\text{CH}_2\text{Cl}_2$  (IEF-PCM), reference: tetramethylsilane (magnetic shielding tensor = 31.6495 ppm, GIAO-B3LYP/6-31+G(d,p), in  $\text{CH}_2\text{Cl}_2$  (IEF-PCM)) and experimental  $^1\text{H}$  NMR spectra of **3ae** in  $\text{CD}_2\text{Cl}_2$  with 400 MHz of resonant frequency (below).

#### 4-7. Measurements of Photophysical Properties of **3ac** and **3ae**

All photophysical measurements were conducted in the diluted solution of compounds in  $\text{CH}_2\text{Cl}_2$  (super dehydrated grade, KANTO) in a  $1 \times 1$  cm square quartz cell. UV/Vis absorption spectra of **3ac** and **3ae** in  $\text{CH}_2\text{Cl}_2$  were recorded on a SHIMADZU UV-3600 spectrophotometer with a resolution of 0.5 nm. Emission spectra and fluorescence quantum yield of **3ac** in  $\text{CH}_2\text{Cl}_2$  was measured with a SHIMADZU RF-6000 spectrofluorophotometer with a resolution of 1.0 nm upon excitation at 330 nm. Emission spectra and fluorescence quantum yield of **3ae** in  $\text{CH}_2\text{Cl}_2$  was measured with a SHIMADZU RF-6000 spectrofluorophotometer with a resolution of 1.0 nm

upon excitation at 350 nm. Fluorescence quantum yield of phenanthrene in CH<sub>2</sub>Cl<sub>2</sub> was measured with a SHIMADZU RF-6000 spectrofluorophotometer with a resolution of 1.0 nm upon excitation at 295 nm. Fluorescence quantum yield of corannulene in CH<sub>2</sub>Cl<sub>2</sub> was measured with a SHIMADZU RF-6000 spectrofluorophotometer with a resolution of 1.0 nm upon excitation at 324 nm. All quantum yield was measured using an integral sphere.

## 5. References

- [1] (a) Kobayashi, K.; Gajurel, C. L. *J. Sulphur Chem.* **1986**, *7*, 123. (b) Etkind, S. I.; Swager, T. M. *Synthesis* **2022**, *54*, 4843. (c) Gallaher, K. L.; Bauer, S. H. *J. Chem. Soc., Faraday Trans. 2* **1975**, *71*, 1173. (d) Kobayashi, K. *J. Synth. Org. Chem. Jpn.* **1982**, *40*, 642. (e) Ito, A.; Ino, H.; Ichiki, H.; Tanaka, K. *J. Phys. Chem. A* **2002**, *106*, 8716.
- [2] (a) Yuan, J.; Lv, W.; Li, A.; Zhu, K. *Chem. Commun.* **2021**, *57*, 12848. (b) Yamashita, M.; Hayashi, H.; Suzuki, M.; Kuzuhara, D.; Yuasa, J.; Kawai, T.; Aratani, N.; Yamada, H. *RSC Adv.* **2016**, *6*, 70700. (c) Tang, S.; Zhang, L.; Ruan, H.; Zhao, Y.; Wang, X. *J. Am. Chem. Soc.* **2020**, *142*, 7340. (d) Casarini, D.; Coluccini, C.; Lunazzi, L.; Mazzanti, A. *J. Org. Chem.* **2006**, *71*, 6248. (e) Ong, W. J.; Bertani, F.; Dalcanale, E.; Swager, T. M. *Synthesis* **2017**, *49*, 358.
- [3] (a) Bancu, M.; Rai, A. K.; Cheng, P.; Gilardi, R. D.; Scott, L. T. *Synlett* **2004**, No. 1, 173. (b) Georghiou, P. E.; Tran, A. H.; Mizyed, S.; Bancu, M.; Scott, L. T. *J. Org. Chem.* **2005**, *70*, 6158.
- [4] (a) Haldar, S.; Wang, M.; Bhauriyal, P.; Hazra, A.; Khan, A. H.; Bon, V.; Isaacs, M. A.; De, A.; Shupletsov, L.; Boenke, T.; Grothe, J.; Heine, T.; Brunner, E.; Feng, X.; Dong, R.; Schneemann, A.; Kaskel, S. *J. Am. Chem. Soc.* **2022**, *144*, 9101. (b) Fu, M.; Zhang, C.; Chen, Y.; Fan, K.; Zhang, G.; Zou, J.; Gao, Y.; Dai, H.; Wang, X.; Wang, C. *Chem. Commun.* **2022**, *58*, 11993. (c) Yao, M.; Taguchi, N.; Ando, H.; Takeichi, N.; Kiyobayashi, T. *Commun. Mater.* **2020**, *1*, 70.
- [5] Luo, H.; He, D.; Zhang, Y.; Wang, S.; Gao, H.; Yan, J.; Cao, Y.; Cai, Z.; Tan, L.; Wu, S.; Wang, L.; Liu, Z. *Org. Lett.* **2019**, *21*, 9734.
- [6] (a) Pander, P.; Swist, A.; Turczyn, R.; Pouget, S.; Djurado, D.; Lazauskas, A.; Pashazadeh, R.; Grazulevicius, J. V.; Motyka, R.; Klimash, A.; Skabara, P. J.; Data, P.; Soloduchko, J.; Dias, F. B. *J. Phys. Chem. C* **2018**, *122*, 24958. (b) Wen, Y.; Liu, H.; Zhang, S.-T.; Pan, G.; Yang, Z.; Lu, T.; Li, B.; Cao, J.; Yang, B. *CCS Chem.* **2020**, *2*, 1940. (c) Yang, Z.; Zhao, S.; Zhang, X.; Liu, M.; Liu, H.; Yang, B. *Front. Chem.* **2022**, *9*, 810304. (d) Li, M.; Xie, W.; Cai, X.; Peng, X.; Liu, K.; Gu, Q.; Zhou, J.; Qiu, W.; Chen, Z.; Gan, Y.; Su, S.-J. *Angew. Chem., Int. Ed.* **2022**, *61*, e202209343. (e) Chen, J.; Tian, H.; Yang, Z.; Zhao, J.; Yang, Z.; Zhang, Y.; Aldred, M. P.; Chi, Z. *Adv. Optical Mater.* **2021**, *9*, 2001550. (f) Tomkeviciene, A.; Matulaitis, T.; Guzauskas, M.; Andruleviciene, V.; Volyniuk, D.; Grazulevicius, J. V. *Org. Electron.* **2019**, *70*, 227.
- [7] (a) Bartl, A.; Fröhner, J. *Synth. Met.* **1992**, *51*, 115. (b) Fiedler, B.; Rojo-Wiechel, E.; Klassen,

- J.; Simon, J.; Beck, J.; Sokolowski, M. *Surf. Sci.* **2012**, *606*, 1855. (c) Liu, Z.; Wang, W.; Xu, W.; Chen, H.; Zhang, X.; Ren, T.; Wang, X.; Zhao, J.; Xiao, J. *Dyes Pigm.* **2015**, *115*, 143. (d) Denis, P. A. *RSC Adv.* **2013**, *3*, 25296. (e) Barát, V.; Budanović, M.; Halilovic, D.; Huh, J.; Webster, R. D.; Mahadevegowda, S. H.; Stuparu, M. C. *Chem. Commun.* **2019**, *55*, 3113. (f) Ren, T.; Xiao, J.; Wang, W.; Xu, W.; Wang, S.; Zhang, X.; Wang, X.; Chen, H.; Zhao, J.; Jiang, L. *Chem. Asian J.* **2014**, *9*, 1943. (g) Riebe, S.; Adam, S.; Roy, B.; Maisuls, I.; Daniliuc, C. G.; Dubbert, J.; Strassert, C. A.; Schapiro, I.; Voskuhl, J. *Chem Asian J.* **2021**, *16*, 2307. (h) Etkind, S. I.; Lopez, J.; Zhu, Y. G.; Fang, J.-H.; Ong, W. J.; Shao-Horn, Y.; Swager, T. M. *ACS Sustainable Chem. Eng.* **2022**, *10*, 11739. (i) Nelson, Z.; Delage-Laurin, L.; Peeks, M. D.; Swager, T. M. *J. Am. Chem. Soc.* **2021**, *143*, 7096. (j) Ong, W. J.; Swager, T. M. *Nat. Chem.* **2018**, *10*, 1023. (k) Jin, T.; Kunze, L.; Breimaier, S.; Bolte, M.; Lerner, H.-W.; Jäkle, F.; Winter, R. F.; Braun, M.; Mewes, J.-M.; Wagner, M. *J. Am. Chem. Soc.* **2022**, *144*, 13704.
- [8] Meng, H.; Liu, M.-S.; Shu, W. *Chem. Sci.* **2022**, Advance Article (DOI: 10.1039/d2sc04507a).
- [9] (a) Berger, F.; Plutschack, M. B.; Riegger, J.; Yu, W.; Speicher, S.; Ho, M.; Frank, N.; Ritter, T. *Nature* **2019**, *567*, 223. (b) Chen, J.; Li, J.; Plutschack, M. B.; Berger, F.; Ritter, T. *Angew. Chem., Int. Ed.* **2020**, *59*, 5616. (c) Jia, H.; Ritter, T. *Angew. Chem., Int. Ed.* **2022**, *61*, e202208978. (d) Jia, H.; Häring, A. P.; Berger, F.; Zhang, L.; Ritter, T. *J. Am. Chem. Soc.* **2021**, *143*, 7623. (e) Juliá, F.; Shao, Q.; Duan, M.; Plutschack, M. B.; Berger, F.; Mateos, J.; Lu, C.; Xue, X.-S.; Houk, K. N.; Ritter, T. *J. Am. Chem. Soc.* **2021**, *143*, 16041. (f) Juliá, F.; Yan, J.; Paulus, F.; Ritter, T. *J. Am. Chem. Soc.* **2021**, *143*, 12992. (g) Holst, D. E.; Wang, D. J.; Kim, M. J.; Guzei, I. A.; Wickens, Z. K. *Nature* **2021**, *596*, 74. (h) Wang, D. J.; Targos, K.; Wickens, Z. K. *J. Am. Chem. Soc.* **2021**, *143*, 21503. (i) Xiong, Y.; Zhang, X.; Guo, H.-M.; Wu, X. *Org. Chem. Front.* **2022**, *9*, 3532.
- [10] (a) Rakitin, O.A.; Konstantinova, L.S. *Adv. Heterocycl. Chem.* **2008**, *96*, 175. (b) Link, T.; Oberjat, M.; Klar, G. *J. Chem. Res. (S)* **1997**, 435. (c) Mostaghimi, F.; Lork, E.; Hong, I.; Roemmele, T. L.; Boere, R. T.; Mebs, S.; Beckmann, J. *New J. Chem.* **2019**, *43*, 12754. (d) Spurg, A.; Schnakenburg, G.; Waldvogel, S. R. *Chem. Eur. J.* **2009**, *15*, 13313. (e) Ariyan, Z.S.; Martin, R. L. *J. Chem. Soc., Perkin Trans. 1* **1972**, 1687. (f) Wang, S.; Yuan, J.; Xie, J.; Lu, Z.; Jiang, L.; Mu, Y.; Huo, Y.; Tsuchido, Y.; Zhu, K. *Angew. Chem., Int. Ed.* **2021**, *60*, 18443.
- [11] (a) Edson, J. B.; Knauss, D. M. *Polym. Chem.* **2004**, *42*, 6353. (b) Fries, K.; Koch, H.; Slukenbrock, H. *Justus Liebigs Ann. Chem.* **1929**, *468*, 162.
- [12] Still, I. W. J.; Sayeed, V. A. *Synth. Commun.* **1983**, *13*, 1181.
- [13] (a) Preedasuriyachai, P.; Charoonniyomporn, P.; Karoonnirun, O.; Thongpanchang, T.; Thebtaranonth, Y. *Tetrahedron Lett.* **2004**, *45*, 1343. (b) Marti, C.; Irurre, J.; Alvarez-Larena, A.; Piniella, J. F.; Brillas, E.; Fajari, L.; Alemán, C.; Juliá, L. *J. Org. Chem.* **1994**, *59*, 6200.
- [14] Sato, R.; Onodera, A.; Goto, T.; Saito, M. *Heterocycles* **1988**, *27*, 2563.
- [15] Kawahara, K. P.; Ito, H.; Itami, K. *Chem. Commun.* **2022**, *accepted*.

- [16] (a) Masetti, F.; Mazzucato, U. *J. Lumin.* **1971**, *4*, 8. (b) Parker, C. A.; Hatchard, C. G. *Analyst* **1962**, *87*, 664. (c) Kyushin, S.; Fujii, H.; Negishi, K.; Matsumoto, H. *Mendeleev Commun.* **2022**, *32*, 87.
- [17] The fluorescent quantum yield of commercially available pristine phenanthrene and corannulene in CH<sub>2</sub>Cl<sub>2</sub> were measured by a spectrofluorophotometer in the author's laboratory (see section 4-7), and determined as 3% and 1%, respectively. These values were lower than those reported in the literatures (ref. 16 and Mack, J.; Vogel, P.; Jones, D.; Kavala, N.; Suttona, A. *Org. Biomol. Chem.* **2007**, *5*, 2448.).
- [18] (a) Becke, A. D. *J. Chem. Phys.* **1993**, *98*, 5648. (b) Lee, C.; Yang, W.; Parr, R. G. *Phys. Rev. B* **1988**, *37*, 785.
- [19] Mennucci, B.; Cancès, E.; Tomasi, J. *J. Phys. Chem. B* **1997**, *101*, 10506.
- [20] The commonly known range of interplanar distances by  $\pi$ - $\pi$  stacking is 3.3–3.8 Å according to a reference: Janiak, C. *J. Chem. Soc., Dalton Trans.* **2000**, 3885.
- [21] (a) Rowe, I.; Post, B. *Acta. Cryst.* **1958**, *11*, 372. (b) Lynton, H.; Cox, E. G. *J. Chem. Soc.* **1956**, 4886.
- [22] (a) Nishio, M. *CrystEngComm.* **2004**, *6*, 130. (b) Aragay, G.; Hernández, D.; Verdejo, B.; Escudero-Adán, E. C.; Martínez, M.; Ballester, P. *Molecules* **2015**, *20*, 16672.
- [23] (a) Johnson, E. R.; Keinan, S.; Mori-Sánchez, P.; Contreras-García, J.; Cohen, A. J.; Yang, W. *J. Am. Chem. Soc.* **2010**, *132*, 6498. (b) Contreras-García, J.; Johnson, E. R.; Keinan, S.; Chaudret, R.; Piquemal, J.-P.; Beratan, D. N.; Yang, W. *J. Chem. Theory Comput.* **2011**, *7*, 625. (c) Boto, R. A.; Peccati, F.; Laplaza, R.; Quan, C.; Carbone, A.; Piquemal, J.-P.; Maday, Y.; Contreras-García, J. *J. Chem. Theory Comput.* **2020**, *16*, 4150.
- [24] (a) Sanyal, S.; Manna, A. K.; Pati, S. K. *ChemPhysChem* **2014**, *15*, 885. (b) Guo, T.; Li, A.; Xu, J.; Baldrige, K. K.; Siegel, J. *Angew. Chem., Int. Ed.* **2021**, *60*, 25809. (c) Schmidt, B. M.; Topolinski, B.; Roesch, P.; Lentz, D. *Chem. Commun.* **2012**, *48*, 6520. (d) Steinauer, A.; Butterfield, A. M.; Linden, A.; Molina-Ontario, A.; Buck, D. C.; Cotta, R. W.; Echegoyen, L.; Baldrige, K. K.; Siegel, J. S. *J. Braz. Chem. Soc.* **2016**, *27*, 1866. (e) Non-substituted corannulene is favor to form a disordered close-packed structure according to this paper.: Parc, R. L.; Hermet, P.; Rols, S.; Maurin, D.; Alvarez, L.; Ivanov, A.; Quimby, J. M.; Hanley, C. G.; Scott, L. T.; Bantignies, J.-L. *J. Phys. Chem. C* **2012**, *116*, 25089.
- [25] (a) Chen, R.; Lu, R.-Q.; Shi, P.-C.; Cao, X.-Y. *Chin. Chem. Lett.* **2016**, *27*, 1175. (b) Chena, X.; Wanga, H.; Wanga, B.; Wanga, Y.; Jinb, X.; Bai, F.-Q. *Org. Electron.* **2019**, *68*, 35. (c) Menekse, K.; Renner, R.; Mahlmeistera, B.; Stoltea, M.; Würthner, F. *Org. Mater.* **2020**, *2*, 229.
- [26] (a) Kang, J.; Miyajima, D.; Mori, T.; Inoue, Y.; Itoh, Y.; Aida, T. *Science* **2015**, *347*, 646. (b) Miyajima, D.; Tashiro, K.; Araoka, F.; Takezoe, H.; Kim, J.; Kato, K.; Takata, M.; Aida, T. *J. Am. Chem. Soc.* **2009**, *131*, 44.

- [27] (a) Kim, S.; Kwon, Y.; Lee, J.-P.; Choi, S.-Y.; Choo, J. *J. Mol. Struct.* **2003**, *655*, 451. (b) Chickos, J.; Mislow, K. *J. Am. Chem. Soc.* **1967**, *89*, 4815.
- [28] Biedermann, P. U.; Pogodin, S.; Agranat, I. *J. Org. Chem.* **1999**, *64*, 3655.
- [29] (a) Mamane, V.; Fürstner, A. *J. Org. Chem.* **2002**, *67*, 6264. (b) Ozaki, K.; Kawasumi, K.; Shibata, M.; Ito, H.; Itami, K. *Nat. Commun.* **2015**, *6*, 6251.
- [30] Giolando, D. M.; Kirschbaum, K. *Synthesis* **1992**, 451.
- [31] Wang, X.; Gensch, T.; Glorius, F. *Org. Chem. Front.* **2016**, *3*, 1619.
- [32] Sheldrick, G. M. *Acta Crystallogr.* **2015**, *A71*, 3.
- [33] Sheldrick, G. M. *Acta Crystallogr.* **2015**, *C71*, 3.
- [34] Dolomanov, O. V.; Bourhis, L. J.; Gildea, R. J.; Howard, J. A. K.; Puschmann, H. *J. Appl. Crystallogr.* **2009**, *42*, 339.
- [35] Gaussian 16, Revision C.01, M. J. Frisch, G. W. Trucks, H. B. Schlegel, G. E. Scuseria, M. A. Robb, J. R. Cheeseman, G. Scalmani, V. Barone, G. A. Petersson, H. Nakatsuji, X. Li, M. Caricato, A. V. Marenich, J. Bloino, B. G. Janesko, R. Gomperts, B. Mennucci, H. P. Hratchian, J. V. Ortiz, A. F. Izmaylov, J. L. Sonnenberg, D. Williams-Young, F. Ding, F. Lipparini, F. Egidi, J. Goings, B. Peng, A. Petrone, T. Henderson, D. Ranasinghe, V. G. Zakrzewski, J. Gao, N. Rega, G. Zheng, W. Liang, M. Hada, M. Ehara, K. Toyota, R. Fukuda, J. Hasegawa, M. Ishida, T. Nakajima, Y. Honda, O. Kitao, H. Nakai, T. Vreven, K. Throssell, J. A. Montgomery, Jr., J. E. Peralta, F. Ogliaro, M. J. Bearpark, J. J. Heyd, E. N. Brothers, K. N. Kudin, V. N. Staroverov, T. A. Keith, R. Kobayashi, J. Normand, K. Raghavachari, A. P. Rendell, J. C. Burant, S. S. Iyengar, J. Tomasi, M. Cossi, J. M. Millam, M. Klene, C. Adamo, R. Cammi, J. W. Ochterski, R. L. Martin, K. Morokuma, O. Farkas, J. B. Foresman, D. J. Fox, Gaussian, Inc., Wallingford CT, **2016**.
- [36] Levandowski, B. J.; Herath, D.; Gallup, N. M.; Houk, K. N. *J. Org. Chem.* **2018**, *83*, 2611.
- [37] Bohmann, J. A.; Weinhold, F.; Farrar, T. C. *J. Chem. Phys.* **1997**, *107*, 1173.
- [38] GaussView, Version 6.1, R. Dennington, T. A. Keith, and J. M. Millam, Semichem Inc., Shawnee Mission, KS, 2016.





## Conclusion of this thesis

In this Ph.D. research, the author has developed several heteroatom-embedding annulative  $\pi$ -extension (hetero-APEX) reactions realizing rapid synthesis of heteroatom-embedded polycyclic aromatic compounds (hetero-PACs) from unfunctionalized aromatic compounds. In Chapter 1, a new aza-annulative  $\pi$ -extension (aza-APEX) reaction that allows rapid access to a range of nitrogen-embedded polycyclic aromatic compounds (N-PACs) from readily available unfunctionalized aromatics and diarylarylnitrilium intermediates was developed. In addition, the synthesis of a novel nitrogen-embedded nanographene through a sequence of aza-APEX reaction and potassium-mediated cyclodehydrogenation has been achieved. In Chapter 2, a sulfur-embedding annulative  $\pi$ -extension (thia-APEX) reaction that can construct a sulfur-containing cationic hexagonal aromatic ring, thiopyrylium, onto unfunctionalized aromatic compounds has been established. The key to the thia-APEX is the use of *S*-imidated *ortho*-arenoyl arenethiol derivatives with TfOH. The synthesis of a variety of  $\pi$ -extended thiopyrylium compounds having characteristic longer wavelength absorption and emission has been achieved. In Chapter 3, another thia-APEX reaction affording  $\pi$ -extended thianthrene derivatives from unfunctionalized aromatic substrates has been developed. *S*-Diimidated 1,2-arenedithiol was newly designed and synthesized as a disulfonium synthon, which works in concert with catalytic amounts of TfOH to achieve one-step synthesis of  $\pi$ -extended thianthrenes. Furthermore, a novel  $\pi$ -extended thianthrenes having characteristic solid-state structures and photophysical properties were discovered.

Novel and useful hetero-PAC molecules and their effective synthetic methods play a key role in the development of future functional materials. In this regard, the author's new concept of hetero-APEX would contribute to synthetic chemistry of hetero-PACs, physical organic chemistry as well as materials science. Furthermore, through the actual development of several hetero-APEX reactions such as aza-APEX and thia-APEX reactions, the author succeeded to demonstrate (1) rapid accessibility to hetero-PACs by direct functionalizations of aromatics, (2) late-stage tunability of hetero-APEX reaction, and (3) diverse and unique photophysical and structural properties of hetero-PACs. These new findings can potentially stimulate and accelerate further applications of hetero-PACs in various research fields. While this initial foray of hetero-APEX chemistry opened new doors, there are a huge room for further developments and improvements. For example, development of phospho-APEX, boro-APEX and oxa-APEX as well as alternant versions of aza-APEX and thia-APEX are highly demanded. In the future, the author expects that hetero-APEX reactions will be recognized as the most powerful and reliable synthetic tool enabling easy introduction of various heteroaromatics and will open a new avenue for heteroaromatic chemistry.



## List of Publications

(副論文)

1. Synthesis of Nitrogen-Containing Polyaromatics by Aza-Annulative  $\pi$ -Extension of Unfunctionalized Aromatics  
Kou P. Kawahara, Wataru Matsuoka, Hideto Ito, Kenichiro Itami  
*Angew. Chem., Int. Ed.* **2020**, *59*, 6383-6388.
2. Rapid access to polycyclic thiopyrylium compounds from unfunctionalized aromatics by thia-APEX reaction  
Kou P. Kawahara, Hideto Ito, Kenichiro Itami  
*Chem. Commun.* **2023**, *59*, 1157.

(参考論文)

1.  $\pi$ -Extended Rubrenes via Dearomative Annulative  $\pi$ -Extension Reaction  
Wataru Matsuoka, Kou P. Kawahara, Hideto Ito, David Sarlah, Kenichiro Itami  
*J. Am. Chem. Soc.* **2023**, *145*, 658.



(副論文)

## Polycycles

Synthesis of Nitrogen-Containing Polyaromatics by Aza-Annulative  $\pi$ -Extension of Unfunctionalized Aromatics

Kou P. Kawahara, Wataru Matsuoka, Hideto Ito,\* and Kenichiro Itami\*

**Abstract:** Nitrogen-containing polycyclic aromatic compounds (N-PACs) are an important class of compounds in materials science. Reported here is a new aza-annulative  $\pi$ -extension (aza-APEX) reaction that allows rapid access to a range of N-PACs in 11–84% yields from readily available unfunctionalized aromatics and imidoyl chlorides. In the presence of silver hexafluorophosphate, arenes and imidoyl chlorides couple in a regioselective fashion. The follow-up oxidative treatment with *p*-chloranil affords structurally diverse N-PACs, which are very difficult to synthesize. DFT calculations reveal that the aza-APEX reaction proceeds through the formal [4+2] cycloaddition of an arene and an in situ generated diarylnitrilium salt, with sequential aromatizations having relatively low activation energies. Transformation of N-PACs into nitrogen-doped nanographenes and their photophysical properties are also described.

## Introduction

Nitrogen-containing polycyclic aromatic compounds (N-PACs) have recently received considerable attention in synthetic chemistry and materials science.<sup>[1]</sup> The structures of N-PACs greatly affect their electronic structures and properties such as HOMO–LUMO gaps, absorption and emission properties, redox potentials, basicity, metallic coordination, biological activity, and supramolecular behavior.<sup>[2]</sup> Furthermore, upon appropriate  $\pi$ -extension, N-PACs can enter the realm of nitrogen-doped nanographenes, which are an emerging class of materials in molecular electronics and devices.<sup>[3]</sup> Owing to these beneficial uses, there is substantial demand for efficient and precise synthetic methods for N-PACs. Typical synthetic strategies for N-PACs rely, however, on multistep reactions.<sup>[4,5]</sup> For example, aromatic aldehyde–amine condensations and subsequent cyclization are versatile means of obtaining N-PACs having pyrrole, pyridine, pyrazine, and quinoline substructures. Transition-metal-catalyzed

cross-coupling reactions such as the Suzuki–Miyaura coupling and Buchwald–Hartwig amination provide alternative synthetic routes for N-PACs. Nevertheless, development of functionalized starting materials is necessary, thus resulting in stepwise protocols for producing N-PACs.

One-step  $\pi$ -extension of unfunctionalized (hetero)arenes is considered an efficient approach in achieving rapid access to fused aromatics such as N-PACs and nitrogen-doped nanographenes. Recently, we formulated APEX (annulative  $\pi$ -extension) as a step/atom-economical strategy for a range of fused  $\pi$ -conjugated systems, and developed several new catalytic carbon-based APEX reactions for the rapid synthesis of polycyclic aromatic hydrocarbons (PAHs), nanographenes, and graphene nanoribbons.<sup>[6,7]</sup> If one could develop an APEX reaction to construct new fused heteroaromatic rings, that is, hetero-APEX,<sup>[8]</sup> the accessibility and utilization of emerging N-PACs and nitrogen-doped nanographenes will be significantly enhanced. Recently, the groups of Mal,<sup>[8a]</sup> and Nozaki and Ito<sup>[9]</sup> reported one-step and two-step aza-APEX reactions that construct new pyrrole rings onto benzene, naphthalene, and corannulene (Figures 1a and b). We have also reported APEX reactions producing pyrrole-fused N-PACs by utilizing pyrroles and indoles as template aromatics,<sup>[7d,e,g,h]</sup> but aza-APEX reactions constructing pyridine skeletons have yet to be achieved.<sup>[10]</sup> Herein we report a new aza-APEX reaction that, by an one-step operation (Figure 1c), realizes efficient  $\pi$ -extension of a pyridine ring onto unfunctionalized PAHs and heteroaromatics. The use of imidoyl chlorides, which are readily prepared from the corresponding amides, enabled a regioselective formal [4+2] cycloaddition to afford structurally and electronically diverse N-PACs and nitrogen-doped nanographenes.

## Results and Discussion

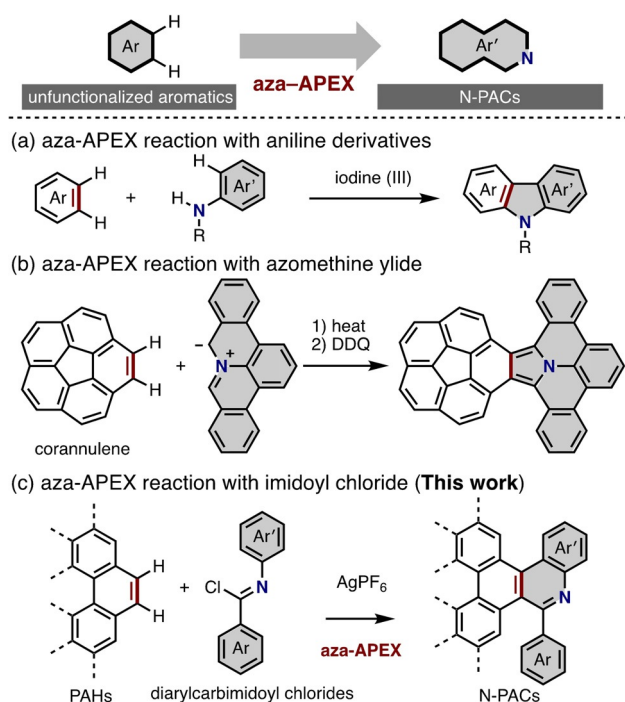
Through extensive investigation of new  $\pi$ -extending agents capable of achieving aza-APEX reactions with pyridine-core construction, we found that *N*-phenylbenzimidoyl chloride (**2a**), which is easily derived from benzanilide with SOCl<sub>2</sub>, had potential. When **2a** was treated with phenanthrene (**1a**) in the presence of AgPF<sub>6</sub> in 1,2-dichloroethane at 80 °C, 5-phenyldihydrodibenzophenanthridine (**3aa**) was obtained (68% yield) along with the desired aza-APEX product **4aa** (14% yield; Scheme 1). Interestingly, **3aa** was slowly and spontaneously converted into **4aa** in the crude reaction mixture under an aerobic atmosphere. Addition of *p*-chloranil was quite effective for the complete conversion of products into **4aa**, resulting in the formation of **4aa** in 80% yield upon isolation (see the Supporting Information for the optimiza-

[\*] K. P. Kawahara, W. Matsuoka, Dr. H. Ito, Prof. Dr. K. Itami  
Graduate School of Science, Nagoya University  
Chikusa, Nagoya 464-8602 (Japan)  
E-mail: ito.hideto@g.mbox.nagoya-u.ac.jp  
itami@chem.nagoya-u.ac.jp

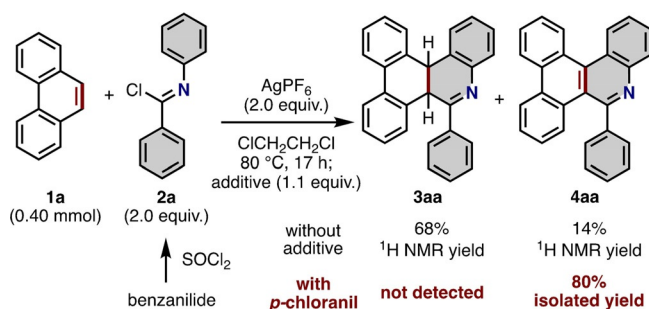
Dr. H. Ito, Prof. Dr. K. Itami  
JST-ERATO, Itami Molecular Nanocarbon Project, Nagoya University  
Chikusa, Nagoya 464-8602 (Japan)

Prof. Dr. K. Itami  
Institute of Transformative Bio-Molecules (WPI-ITbM), Nagoya  
University, Chikusa, Nagoya 464-8601 (Japan)

Supporting information and the ORCID identification number(s) for the author(s) of this article can be found under:  
<https://doi.org/10.1002/anie.201913394>.



**Figure 1.** Schematic illustration of aza-annulative  $\pi$ -extension (aza-APEX) of unfunctionalized aromatic compounds. a) Aza-APEX reactions of benzene and naphthalene with aniline derivatives and hypervalent iodine reagents. b) Two-step aza-APEX reaction of corannulene with azomethine ylides. c) Aza-APEX reactions of PAHs and heteroaromatics with diarylcarbamidoyl chlorides (this work).



tion of the reaction conditions). In this reaction, perfect regioselectivity on the *K*-region (red-colored position in **1a**) was observed, and the structure of 5-phenyldibenzo- $[i,k]$ phenanthridine (**4aa**) was confirmed by X-ray crystallographic analysis (see the Supporting Information for details).

To assess the generality and the applicability of the present aza-APEX reaction, we explored the substrate scope of unfunctionalized PAHs/heteroarenes (**1**) and diarylcarbamidoyl chlorides (**2**; Scheme 2). The present reaction conditions showed high generality toward the aza-APEX of **1a** with **2a**, even for a gram-scale reaction, and **4aa** was isolated in 78 % yield (1.11 g). When structural analogues of phenanthrene, such as the methylene-bridged phenanthrene **1b**, 2,9-di-*tert*-butylpyrene (**1c**), and corannulene (**1d**), were used,

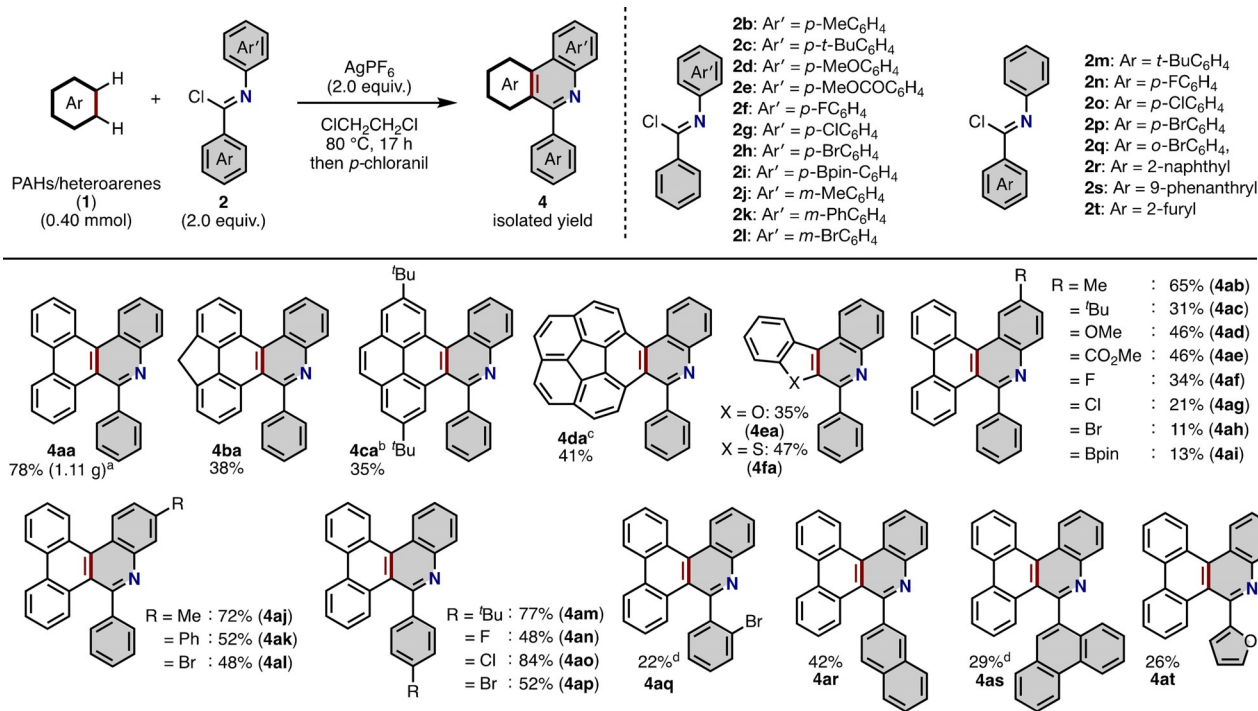
they afforded the corresponding N-PACs **4ba**, **4ca**, and **4da** in yields of 35–41 %. Furthermore, benzo[*b*]furan (**1e**) and benzo[*b*]thiophene (**1f**) also reacted with **2a** to give the benzofuroisoquinoline **4ea** and benzothienoisoquinoline **4fa**, respectively, in 35–47 % yields. It is noted that the reaction using other aromatic compounds such as anisole and naphthalene neither gave corresponding cyclized products **3** nor **4** at all.

For the scope of  $\pi$ -extending agents, we tested aza-APEX reactions of **1a** with various imidoyl chlorides (**2**) derived from corresponding amides (Scheme 2). The *para*-substituents (R) on *N*-aryl groups (Ar) in **2** were tolerated when R was Me, <sup>*t*</sup>Bu, OMe, and CO<sub>2</sub>Me, producing **4ab**, **4ac**, **4ad**, and **4ae**, respectively, in 31–65 % yields. The *para*-fluoro, *para*-chloro, *para*-bromo, and *para*-Bpin groups on the *N*-phenyl moieties showed lower tolerances to afford **4af**, **4ag**, **4ah**, and **4ai**, respectively, probably a result of electronic effects (11–34 % yields). However, even though further modifications are required to synthesize N-PACs containing transformable substituents, these reactions represent rare examples achieving direct  $\pi$ -extension of functionalized PAHs. In the reactions with **2j** and **2k**, having *meta*-methyl and *meta*-phenyl groups, respectively, only the corresponding single products **4aj** and **4ak** were obtained in 52–72 % yields as single regioisomers. These products were probably formed by avoiding steric repulsion in the cyclization step. The use of **2l**, having an *N*-*meta*-bromophenyl group, did not markedly drop the reactivity and produced the bromodibenzo- $[i,k]$ phenanthridine **4al** in 48 % yield. Regarding the variability of *N*-aryl groups (Ar') on the benzimide moiety, *para*-<sup>*t*</sup>Bu, fluoro, chloro, bromo, 2-naphthyl, 9-phenanthryl, and 2-furyl groups afforded the corresponding 5-aryldibenzo- $[i,k]$ phenanthridines (**4am**–**4ap** and **4ar**–**4at**) in 26–84 % yields, whilst an *ortho*-bromophenyl group decreased the yield of the product **4aq** (22 % yield).

To further emphasize the utility of present aza-APEX reaction, we compared it with representative examples of synthesizing the benzophenanthrene skeleton.<sup>[11]</sup> In an early example by Kesavan et al., benzophenanthridine was synthesized from 1-cyclohexylnaphthalene in five steps including nitration, reduction to amino group, formylation, cyclization, and aromatization.<sup>[11a]</sup> Zhang and Yu reported photoredox reaction between biphenyl-1-ylisocyanides with *sym*-bromoesters for efficient synthesis of 6-alkylated phenanthridine.<sup>[11b]</sup> Samsung Display Co., Ltd. also showed in a patent that the same phenanthridine derivatives, including **4al** and **4ap**, can be synthesized from phenanthrene by stepwise protocols performing borylation, coupling reaction, reduction, condensation, and cyclization, thus resulting in the low reaction efficiency and total yield. Compared with these reports, the present aza-APEX reaction can provide an alternative or an efficient one-step synthetic strategy for N-PACs starting from simple and readily available unfunctionalized PAHs.

Following this work, computational investigations were carried out on the reaction mechanism of the current aza-APEX reaction of **1a** with **2a** and AgPF<sub>6</sub>. Based on the literature<sup>[12]</sup> and our hypothesis that *N*-phenyl benzonitrilium hexafluorophosphate (**5**) or its equivalent imidoyl fluoride-PF<sub>5</sub> complex **5'** would be initially formed by the reaction of **2a**





<sup>a</sup> The reaction was carried out in the 4.0 mmol scale of **1a**. <sup>b</sup> The reaction was carried out for 12 hours. <sup>c</sup> The reaction was carried out in the 0.20 mmol scale of **1a**. <sup>d</sup> The reaction was carried out in 1,2-dichlorobenzene at 150 °C.

**Scheme 2.** a) The substrate scope with respect to the PAHs/heteroarenes **1** and imidoyl chloride **2** in the aza-APEX reaction.

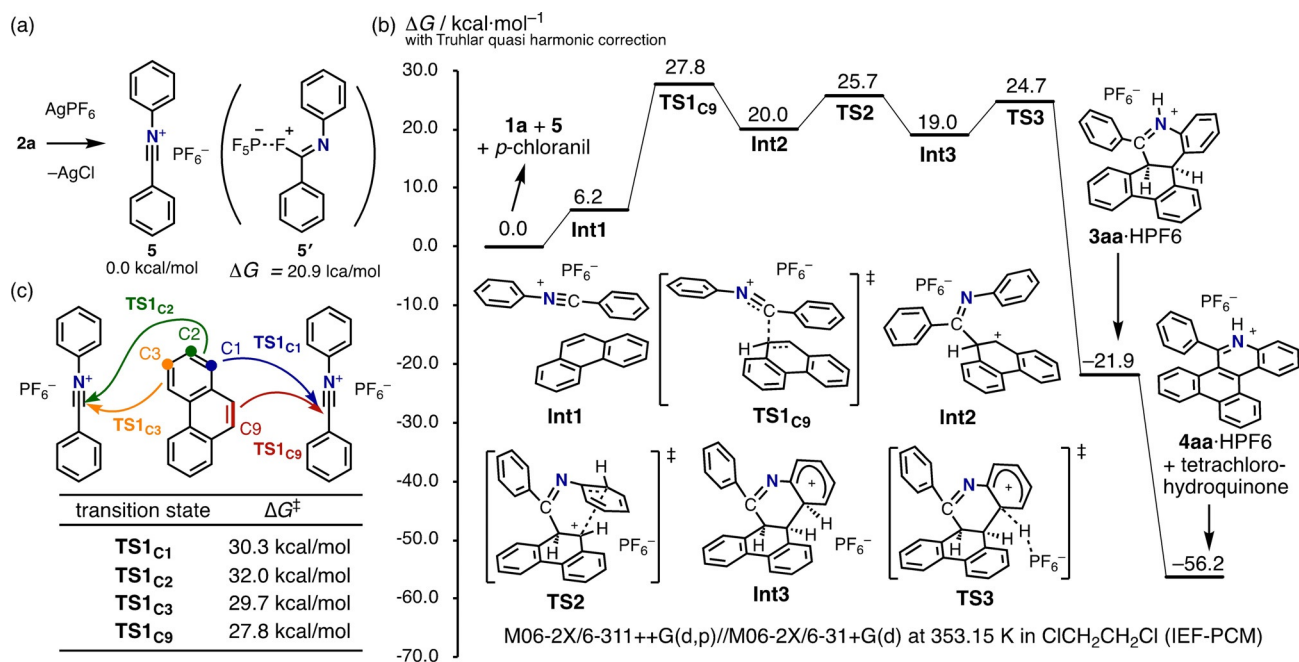
with AgPF<sub>6</sub> (Figure 2a), computations were performed using Gaussian16, revision C.01,<sup>[13]</sup> with the M06-2X<sup>[14]</sup> density function. According to the literature,<sup>[15]</sup> geometry optimizations and frequency calculations of the all minima and transition states using the 6-31+G(d) level of theory, in the gas phase at 353.15 K, were calculated by single-point calculations of optimized geometries with the 6-311++G-(d,p) level of theory at 353.15 K in 1,2-dichloroethane (IEF-PCM<sup>[16]</sup>). All calculated Gibbs energies were corrected with Truhlar's quasi-harmonic correction<sup>[17-19]</sup> by setting all positive frequencies below 100 cm<sup>-1</sup> to a value of 100 cm<sup>-1</sup> using 0.967 as a scaling factor<sup>[18]</sup> to zero-point energy.

Through extensive calculations of possible intermediates and transition states, we found that the reaction likely proceeds through a formal [4+2] cycloaddition of **1a** with the nitrilium salt **5** rather than the imidoyl fluoride **5'** (Figure 2b). At the start of the reaction, **1a** and **5** give the semi-stable cation- $\pi$  stacking complex of **5** and **1a** (**Int1**; less stable by 6.18 kcal mol<sup>-1</sup>). Thereafter, the electrophilic addition of an electron-deficient sp-hybridized carbon in nitrilium salt to C9 (*K*-region) of phenanthrene occurs, forming the dihydrophenanthrenium intermediate **Int2** via the transition state **TS1<sub>C9</sub>** with a relatively higher activation energy ( $\Delta G^\ddagger$ ) of 27.8 kcal mol<sup>-1</sup>. The intramolecular aromatic electrophilic substitution (S<sub>E</sub>Ar) between a benzylic cation and an *ortho*-carbon atom on the N-phenyl group then takes place rather than rearomatization by deprotonation. Through the transition-state **TS2** with a 25.7 kcal mol<sup>-1</sup> activation barrier, the arenium ion intermediate **Int3**, having *cis*-dihydrophenanthrene structure is formed. Subsequent abstraction of a proton

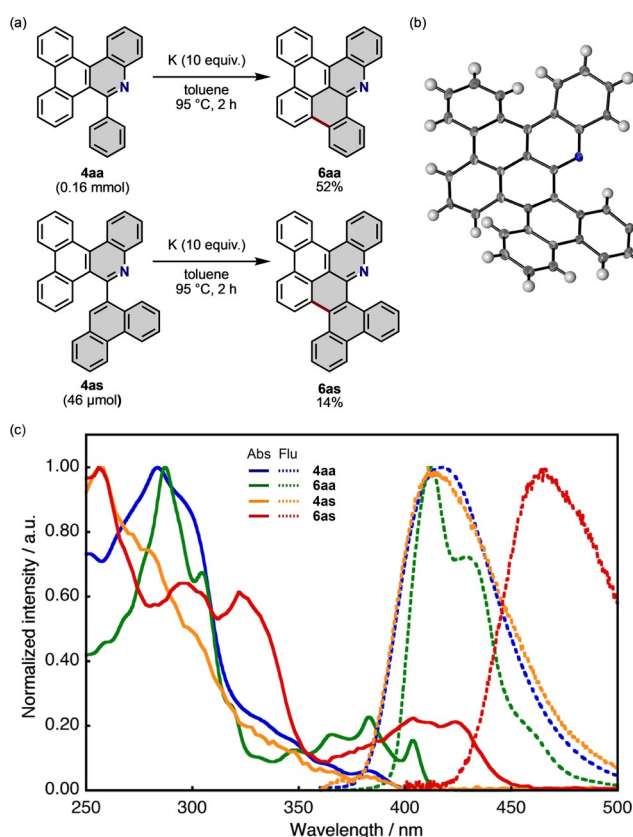
assisted by a PF<sub>6</sub><sup>-</sup> ion along with rearomatization are shown to be kinetically and thermodynamically favorable, affording **3aa**-HPF<sub>6</sub> via **TS3** ( $\Delta G^\ddagger = 24.7$  kcal mol<sup>-1</sup> from **1a** + **5**). Finally, oxidation of **3aa**-HPF<sub>6</sub> with *p*-chloranil gives the much more stable product **4aa**-HPF<sub>6</sub> along with tetrachloro-hydroquinone as a side product.

We further estimated the predominant selectivity within the *K*-region (C9,C10-position in **1a**) in the present aza-APEX reaction (Figure 2c). In the electrophilic addition step, activation energies of additions to C1, C2, and C3 on **1a** were calculated as 30.3, 32.0 and 29.7 kcal mol<sup>-1</sup>, respectively, and they are higher (by more than 1.9 kcal mol<sup>-1</sup>) than that in the addition to *K*-region. In the case of the C2-addition pathway, relative free energies of the resulting adduct and subsequent transition state for cyclization were estimated to be 29.9 and 45.8 kcal mol<sup>-1</sup>, respectively. These energies can result from the less aromatic resonance stabilization on the phenanthrene rings in the transition-states **TS1<sub>C1</sub>**, **TS1<sub>C2</sub>**, and **TS1<sub>C3</sub>**, other adducts, and subsequent transition states while two aromatic sextets are retained in the phenanthrene part in the more stable **TS1<sub>C9</sub>**.

The structural characteristics of the 5-aryl pendants in aza-APEX products were utilized in the synthesis of further  $\pi$ -extensions. Radical-anion coupling reactions (by potassium in toluene)<sup>[20]</sup> of **4aa** and **4as** were used to synthesize the nitrogen-doped nanographenes **6aa** (52%) and **6as** (14%), respectively (Figure 3a). Their planarized structures were confirmed by X-ray crystallographic analyses (Figure 3b; see Figures S2–S4).<sup>[21]</sup> After the radical-anion coupling, new, longer absorption peaks appeared at 350–420 nm for **6aa**,



**Figure 2.** a) Formation of **5** and **5'** by the reaction of **2a** with  $\text{AgPF}_6$ . b) Energy diagram of calculated reaction pathway in the aza-APEX reaction of **1a** with **5**. *p*-Chloranil molecules were omitted in the structures of each intermediate and transition state for clarity. c) Comparison of activation energies in the transition states of electrophilic addition (**TS1**) at each carbon atom on phenanthrene.



**Figure 3.** a) Transformation of **4aa** and **4as** into the nitrogen-doped nanographenes **6aa** and **6as**, respectively, by radical-anion coupling reactions. b) X-ray crystallographic structure of **6as** with 50% thermal ellipsoids at the 50% probability. c) UV-vis absorption and emission spectra of **4aa**, **4as**, **6aa**, and **6as** in  $\text{CH}_2\text{Cl}_2$ . Excitation wavelengths: 280 nm for **4aa** and **6aa**, and 260 nm for **4as** and **6as**.

and 360–460 nm for **6as**, which correspond well with the calculated allowed HOMO–LUMO excitation ( $\lambda_{\text{ex}} = 388$  nm for **6aa** and 447 nm for **6as**). While **4aa** and **4as** show only very weak emission around 420 nm with a negligible emission quantum yield ( $\Phi_{\text{FL}}(\mathbf{4aa}) < 0.01$ ,  $\Phi_{\text{FL}}(\mathbf{4as}) < 0.01$ ), the planarized aza-nanographene **6aa** showed narrower and strengthened emission with a maximum emission peak at 412 nm ( $\Phi_{\text{FL}} = 0.23$ ). Similar patterns were also observed in the absorption and emission spectra of **4as** and **6as** where **6as** showed strengthened and redshifted emission at 464 nm with  $\Phi_{\text{FL}} = 0.05$ . Compared to the hydrocarbon analogues **S1** and **S2** (see Figure S7 in the Supporting Information), **6aa** and **6as** possess lower lying (by ca. 0.3 eV) HOMOs and LUMOs than those of **S1** and **S2** without significant changes in the HOMO–LUMO gap energy (**S1**: 3.55 eV, **6aa**: 3.60 eV, **S2**: 3.14 eV, **6as**: 3.17 eV; see Figure S7). These results imply that the construction of one pyridine structure into nanographene represents an effective strategy for increasing its electro-accepting ability without changing a HOMO–LUMO gap, which will provide an opportunity for applications in easily available electron transporting materials by using aza-APEX.

## Conclusion

In summary, we have established a new synthetic method for N-PACs: the aza-APEX reaction of unfunctionalized aromatics with imidoyl chlorides as  $\pi$ -extending agents with  $\text{AgPF}_6$  as an activating additive. Given the abundance of diarylcarbimidoyl chlorides which are easily prepared from commercially available benzanilide analogues, a broad range of 5-aryldibenzo[*i,k*]phenanthridines were successfully syn-

thesized. From the DFT calculations, the reaction seems to proceed through the sequence of *K*-region selective electrophilic addition of nitrilium salts, intramolecular S<sub>E</sub>Ar reaction, and aromatization. Furthermore, we showed that synthesized N-PACs can be applied to the transformation into nitrogen-doped nanographenes that have potential applications in organic electronic devices. We believe that the present aza-APEX reaction offers a new opportunity for the synthesis of a series of nitrogen-containing polycyclic aromatic systems. Development of other potential hetero-APEX reactions that can produce oxygen-, sulfur-, and phosphine-containing PACs are now underway.

## Acknowledgements

This work was supported by the ERATO program of the JST (JPMJER1302 to K.I.), the CREST program of JST (JPMJCR19R1 to H.I.), JSPS KAKENHI (Grant Nos. 19H05463 to K.I., JP26810057, JP16H00907, JP17K1955 and JP18H02019 to H.I.), the Sumitomo Foundation (141495 to H.I.), the DAIKO Foundation (H.I.), and the JSPS research fellowship for young scientist (18J23379 to W.M). We thank Dr. Yasutomo Segawa and Mr. Ryo Okude for helping with X-ray diffraction analyses. Computations were performed using the Research Center for Computational Science, Okazaki, Japan. ITbM is supported by the World Premier International Research Center Initiative (WPI), Japan.

## Conflict of interest

The authors declare no conflict of interest.

**Keywords:** cyclizations · heteroarenes · nanographene · polycycles · synthetic methods

**How to cite:** *Angew. Chem. Int. Ed.* **2020**, *59*, 6383–6388  
*Angew. Chem.* **2020**, *132*, 6445–6450

- [1] a) L. Xiao, H. Lan, J. Kido, *Chem. Lett.* **2007**, *36*, 802; b) Y.-J. Li, H. Sasabe, S.-J. Su, D. Tanaka, T. Takeda, Y.-J. Pu, J. Kido, *Chem. Lett.* **2009**, *38*, 712; c) C. Bazzini, S. Brovelli, T. Caronna, C. Gambarotti, M. Giannone, P. Macchi, F. Meinardi, A. Mele, W. Panzeri, F. Recupero, A. Sironi, R. Tubino, *Eur. J. Org. Chem.* **2005**, 1247; d) K. Nakayama, Y. Hashimoto, H. Sasabe, Y.-J. Pu, M. Yokoyama, J. Kido, *Jpn. J. Appl. Phys.* **2010**, *49*, 01AB11; e) S. Hiroto, *Chem. Asian J.* **2019**, *14*, 2514.
- [2] a) X.-Y. Wang, X. Yao, A. Narita, K. Müllen, *Acc. Chem. Res.* **2019**, *52*, 2491; b) S.-J. Su, C. Caib, J. Kido, *J. Mater. Chem.* **2012**, *22*, 3447; c) D. Yokoyama, H. Sasabe, Y. Furukawa, C. Adachi, J. Kido, *Adv. Funct. Mater.* **2011**, *21*, 1375; d) H. Terrones, R. Lv, M. Terrones, M. S. Dresselhaus, *Rep. Prog. Phys.* **2012**, *75*, 062501; e) P. Data, M. Okazaki, S. Minakata, Y. Takeda, *J. Mater. Chem. C* **2019**, *7*, 6616; f) Y. Wu, Z. Yin, J. Xiao, Y. Liu, F. Wei, K. J. Tan, C. Kloc, L. Huang, Q. Yan, F. Hu, H. Zhang, Q. Zhang, *ACS Appl. Mater. Interfaces* **2012**, *4*, 1883.
- [3] a) R. A. Durr, D. Haberer, Y.-L. Lee, R. Blackwell, A. M. Kalayjian, T. Marangoni, J. Ihm, S. G. Louie, F. R. Fischer, *J. Am. Chem. Soc.* **2018**, *140*, 807; b) G. Sarau, M. Heilmann, M. Bashouti, M. Latzel, C. Tessarek, S. Christiansen, *ACS Appl. Mater. Interfaces* **2017**, *9*, 10003; c) C. Bronner, S. Stremmlau, M. Gille, F. Brauße, A. Haase, S. Hecht, P. Tegeeder, *Angew. Chem. Int. Ed.* **2013**, *52*, 4422; *Angew. Chem.* **2013**, *125*, 4518; d) K. Oki, M. Takase, S. Mori, A. Shiotari, Y. Sugimoto, K. Ohara, T. Okujima, H. Uno, *J. Am. Chem. Soc.* **2018**, *140*, 10430; e) H. Uno, M. Ishiwata, K. Muramatsu, M. Takase, S. Mori, T. Okujima, *Bull. Chem. Soc. Jpn.* **2019**, *92*, 1001; f) H. Yokoi, Y. Hiraoka, S. Hiroto, D. Sakamaki, S. Seki, H. Shinokubo, *Nat. Commun.* **2015**, *6*, 8215; g) H. Yokoi, S. Hiroto, H. Shinokubo, *J. Am. Chem. Soc.* **2018**, *140*, 4649.
- [4] Selected recent reviews: a) M. Stępień, E. Gońka, M. Żyła, N. Sprutta, *Chem. Rev.* **2017**, *117*, 3479; b) M. D. Hill, *Chem. Eur. J.* **2010**, *16*, 12052; c) J. A. Varela, C. Saa, *Chem. Rev.* **2003**, *103*, 3787; d) H. Zhylitskaya, M. Stępień, *Org. Chem. Front.* **2018**, *5*, 2395.
- [5] Selected recent examples for stepwise synthesis of N-PACs: a) X. Liu, C. Wu, J. Zhang, Y. Shi, S. Zhang, Y. Geng, C.-H. Tunga, W. Wang, *Org. Chem. Front.* **2018**, *5*, 2997; b) C. M. Leir, *J. Org. Chem.* **1977**, *42*, 911; c) M. D. Hill, M. Movassagh, *Org. Lett.* **2008**, *10*, 3485; d) T.-S. Jiang, Y. Zhou, L. Dai, X. Liu, X. Zhang, *Tetrahedron Lett.* **2019**, *60*, 2078; e) M. Blanchot, D. A. Candito, F. Larnaud, M. Lautens, *Org. Lett.* **2011**, *13*, 1486; f) M. Saha, Y.-H. Bao, C. Zhou, *Chem. Lett.* **2018**, *47*, 1383; g) M. Wang, Q. Fan, X. Jiang, *Org. Lett.* **2018**, *20*, 216; h) D. Uredi, D. R. Motati, E. B. Watkins, *Org. Lett.* **2018**, *20*, 6336; i) M. J. E. Hewlins, R. Salter, *Synthesis* **2007**, *14*, 2164; j) M. Tobisu, K. Koh, T. Furukawa, N. Chatani, *Angew. Chem. Int. Ed.* **2012**, *51*, 11363; *Angew. Chem.* **2012**, *124*, 11525; k) M. Tasiar, M. Chotkowski, D. T. Gryko, *Org. Lett.* **2015**, *17*, 6106; l) S. Mishra, M. Krzeszewski, C. A. Pignedoli, P. Ruffieux, R. Fasel, D. T. Gryko, *Nat. Commun.* **2018**, *9*, 1714; m) M. Navakouski, H. Zhylitskaya, P. J. Chmielewski, T. Lis, J. Cybińska, M. Stępień, *Angew. Chem. Int. Ed.* **2019**, *58*, 4929; *Angew. Chem.* **2019**, *131*, 4983; n) M. Żyła-Karwowska, H. Zhylitskaya, J. Cybińska, T. Lis, P. J. Chmielewski, M. Stępień, *Angew. Chem. Int. Ed.* **2016**, *55*, 14658; *Angew. Chem.* **2016**, *128*, 14878; o) M. Żyła, E. Gońka, P. J. Chmielewski, J. Cybińska, M. Stępień, *Chem. Sci.* **2016**, *7*, 286.
- [6] For reviews on APEX reactions, see: a) H. Ito, K. Ozaki, K. Itami, *Angew. Chem. Int. Ed.* **2017**, *56*, 11144; *Angew. Chem.* **2017**, *129*, 11296; b) H. Ito, Y. Segawa, K. Murakami, K. Itami, *J. Am. Chem. Soc.* **2019**, *141*, 3.
- [7] For our contributions to APEX chemistry, see: a) K. Ozaki, K. Kawasumi, M. Shibata, H. Ito, K. Itami, *Nat. Commun.* **2015**, *6*, 6251; b) Y. Yano, H. Ito, Y. Segawa, K. Itami, *Synlett* **2016**, 27, 2081; c) K. Kato, Y. Segawa, K. Itami, *Can. J. Chem.* **2017**, *95*, 329; d) K. Ozaki, H. Zhang, H. Ito, A. Lei, K. Itami, *Chem. Sci.* **2013**, *4*, 3416; e) K. Ozaki, W. Matsuoka, H. Ito, K. Itami, *Org. Lett.* **2017**, *19*, 1930; f) K. Ozaki, K. Murai, W. Matsuoka, K. Kawasumi, H. Ito, K. Itami, *Angew. Chem. Int. Ed.* **2017**, *56*, 1361; *Angew. Chem.* **2017**, *129*, 1381; g) W. Matsuoka, H. Ito, K. Itami, *Angew. Chem. Int. Ed.* **2017**, *56*, 12224; *Angew. Chem.* **2017**, *129*, 12392; h) H. Kitano, W. Matsuoka, H. Ito, K. Itami, *Chem. Sci.* **2018**, *9*, 7556; i) T. Nakamuro, K. Kumazawa, H. Ito, K. Itami, *Synlett* **2019**, *30*, 423; j) Y. Yano, N. Mitoma, K. Matsushima, F. Wang, K. Matsui, A. Takakura, Y. Miyauchi, H. Ito, K. Itami, *Nature* **2019**, *571*, 387; k) N. Mitoma, Y. Yano, Y. Miyauchi, H. Ito, K. Itami, *ACS Appl. Nano Mater.* **2019**, *2*, 4825.
- [8] Examples of one-pot construction of heteroatom-containing aromatics using alkenes, alkynes, or unfunctionalized arenes: a) S. Maiti, T. K. Achar, P. Mal, *Org. Lett.* **2017**, *19*, 2006; b) H. Vuong, B. P. Dash, S. O. N. Lill, D. A. Klumpp, *Org. Lett.* **2018**, *20*, 1849; c) X.-L. Wu, L. Dong, *Org. Lett.* **2018**, *20*, 6990; d) A. Obata, A. Sasagawa, K. Yamazaki, Y. Ano, N. Chatani, *Chem. Sci.* **2019**, *10*, 3242; e) E. K. Yum, R. C. Larock, *J. Am. Chem. Soc.* **1991**, *113*, 6689; f) X. Ji, H. Huang, Y. Li, H. Chen, H. Jiang,

- Angew. Chem. Int. Ed.* **2012**, *51*, 7292; *Angew. Chem.* **2012**, *124*, 7404; g) G. F. Krainova, Y. O. Chudinova, A. A. Gorbunov, O. A. Mayorova, V. A. Glushkov, *Mendeleev Commun.* **2012**, *22*, 201; h) V. V. Kouznetsov, *Tetrahedron* **2009**, *65*, 2721; i) J. Sheng, Y. Wang, X. Su, R. He, C. Chen, *Angew. Chem. Int. Ed.* **2017**, *56*, 4824; *Angew. Chem.* **2017**, *129*, 4902; j) Y. Wang, C. Chen, J. Peng, M. Li, *Angew. Chem. Int. Ed.* **2013**, *52*, 5323; *Angew. Chem.* **2013**, *125*, 5431; k) J. Yan, A. P. Pulis, G. J. P. Perry, D. J. Procter, *Angew. Chem. Int. Ed.* **2019**, *58*, 15675; *Angew. Chem.* **2019**, *131*, 15822; l) E. Schendera, L.-N. Unkel, P. P. H. Quyen, G. Salkewitz, F. Hoffmann, A. Villinger, M. Brasholz, *Chem. Eur. J.* **2020**, *26*, 269.
- [9] a) Y. Tokimaru, S. Ito, K. Nozaki, *Angew. Chem. Int. Ed.* **2018**, *57*, 9818; *Angew. Chem.* **2018**, *130*, 9966; b) Y. Tokimaru, S. Ito, K. Nozaki, *Angew. Chem. Int. Ed.* **2017**, *56*, 15560; *Angew. Chem.* **2017**, *129*, 15766; c) S. Ito, Y. Tokimaru, K. Nozaki, *Chem. Commun.* **2015**, *51*, 221; d) S. Ito, Y. Tokimaru, K. Nozaki, *Angew. Chem. Int. Ed.* **2015**, *54*, 7256; *Angew. Chem.* **2015**, *127*, 7364; e) Z. Zhou, Z. Wei, Y. Tokimaru, S. Ito, K. Nozaki, M. A. Petrukhina, *Angew. Chem. Int. Ed.* **2019**, *58*, 12107; *Angew. Chem.* **2019**, *131*, 12235.
- [10] S. Tokita, K. Hiruta, K. Kitahara, H. Nishi, *Synthesis* **1982**, 229.
- [11] a) V. Kesavan, V. C. Devanathan, N. Arumugam, *Bull. Chem. Soc. Jpn.* **1968**, *41*, 3008; b) H. Jiang, Y. Cheng, R. Wang, M. Zheng, Y. Zhang, S. Yu, *Angew. Chem. Int. Ed.* **2013**, *52*, 13289; *Angew. Chem.* **2013**, *125*, 13531; c) "Condensed cyclic compounds and organic light-emitting devices including the same": E.-J. Jeong, Y.-K. Kim, J.-H. Park, E.-Y. Lee, S.-H. Hwang, US 2015/0349275 A1, Dec. 3, **2015**.
- [12] T. van Dijk, S. Burck, M. K. Rong, A. J. Rosenthal, M. Nieger, J. C. Slootweg, K. Lammertsma, *Angew. Chem. Int. Ed.* **2014**, *53*, 9068; *Angew. Chem.* **2014**, *126*, 9214.
- [13] Gaussian 16, Revision C.01, M. J. Frisch, G. W. Trucks, H. B. Schlegel, G. E. Scuseria, M. A. Robb, J. R. Cheeseman, G. Scalmani, V. Barone, G. A. Petersson, H. Nakatsuji, X. Li, M. Caricato, A. V. Marenich, J. Bloino, B. G. Janesko, R. Gomperts, B. Mennucci, H. P. Hratchian, J. V. Ortiz, A. F. Izmaylov, J. L. Sonnenberg, D. Williams-Young, F. Ding, F. Lipparini, F. Egidi, J. Goings, B. Peng, A. Petrone, T. Henderson, D. Ranasinghe, V. G. Zakrzewski, J. Gao, N. Rega, G. Zheng, W. Liang, M. Hada, M. Ehara, K. Toyota, R. Fukuda, J. Hasegawa, M. Ishida, T. Nakajima, Y. Honda, O. Kitao, H. Nakai, T. Vreven, K. Throssell, J. A. Montgomery, Jr., J. E. Peralta, F. Ogliaro, M. J. Bearpark, J. J. Heyd, E. N. Brothers, K. N. Kudin, V. N. Staroverov, T. A. Keith, R. Kobayashi, J. Normand, K. Raghavachari, A. P. Rendell, J. C. Burant, S. S. Iyengar, J. Tomasi, M. Cossi, J. M. Millam, M. Klene, C. Adamo, R. Cammi, J. W. Ochterski, R. L. Martin, K. Morokuma, O. Farkas, J. B. Foresman, D. J. Fox, Gaussian, Inc., Wallingford CT, **2016**.
- [14] Y. Zhao, D. G. Truhlar, *Theor. Chem. Acc.* **2008**, *120*, 215.
- [15] B. J. Levandowski, D. Herath, N. M. Gallup, K. N. Houk, *J. Org. Chem.* **2018**, *83*, 2611.
- [16] B. Mennucci, E. Cancès, J. Tomasi, *J. Phys. Chem. B* **1997**, *101*, 10506–10517.
- [17] Y. Zhao, D. G. Truhlar, *Phys. Chem. Chem. Phys.* **2008**, *10*, 2813.
- [18] I. M. Alecu, J. Zheng, Y. Zhao, D. G. Truhlar, *J. Chem. Theory Comput.* **2010**, *6*, 2872–2887.
- [19] For calculation of Truhlar's quasi-harmonic corrections, an open free program GoodVibes v2.0.2 was used: J. Rodríguez-Guerra, J. Chen, IFunes, GoodVibes, v2.0.2, Panton Lab, May 15, **2018**. URL: <http://doi.org/10.5281/zenodo.1247565>.
- [20] Conventional oxidative cyclodehydrogenations such as Scholl reactions with either FeCl<sub>3</sub> or MoCl<sub>5</sub> did not give a desired cyclized product **6aa** (see Figure S1). For examples of radical-anion coupling reactions, see: a) J. Piechowska, M. Gałżowski, D. T. Gryko, *J. Org. Chem.* **2010**, *75*, 1297; b) M. Rickhaus, A. P. Belanger, H. A. Wegner, L. T. Scott, *J. Org. Chem.* **2010**, *75*, 7358; c) P. Schlichting, U. Rohr, K. Müllen, *J. Mater. Chem.* **1998**, *8*, 2651; d) S. P. Solodovnikov, S. T. Ioffe, Yu. B. Zaks, M. I. Kabacnik, *Russ. Chem. Bull.* **1968**, *17*, 442. See our attempt to obtain **6aa** under oxidative cyclodehydrogenation conditions (see Figure S1).
- [21] CCDC 1960273, 1960274 and 1960275 (**4aa**, **4da**, **6as**) contain the supplementary crystallographic data for this paper. These data can be obtained free of charge from The Cambridge Crystallographic Data Centre.

Manuscript received: October 20, 2019

Revised manuscript received: January 13, 2020

Accepted manuscript online: February 3, 2020

Version of record online: March 2, 2020



Cite this: *Chem. Commun.*, 2023, 59, 1157

Received 2nd November 2022,  
Accepted 20th December 2022

DOI: 10.1039/d2cc06706d

rsc.li/chemcomm

# Rapid access to polycyclic thiopyrylium compounds from unfunctionalized aromatics by thia-APEX reaction†

Kou P. Kawahara,<sup>a</sup> Hideto Ito<sup>ib</sup>\*<sup>a</sup> and Kenichiro Itami<sup>ib</sup>\*<sup>ab</sup>

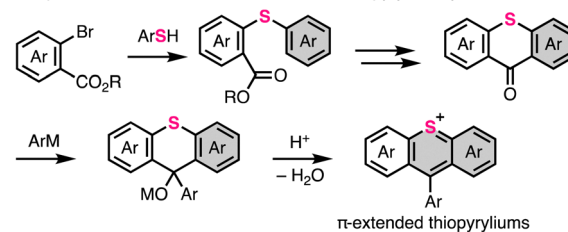
We developed a sulfur-embedding annulative  $\pi$ -extension (thia-APEX) reaction that could construct a sulfur-embedding cationic hexagonal aromatic ring, thiopyrylium, onto unfunctionalized aromatics in one step. The key of thia-APEX is the use of *S*-imidated *ortho*-arenoyl arenethiols, and a variety of  $\pi$ -extended thiopyryliums can easily be synthesized. The synthesized thiopyryliums showed diverse absorption and emission properties over the visible light to NIR region, depending on minor structural differences.

Thiopyrylium is a cationic organic skeleton which consists of a sulfur-containing six-membered aromatic ring.<sup>1</sup> In recent years, polycyclic aromatic compounds containing thiopyrylium rings as well as other pyrylium rings<sup>1*h,i*</sup> have gained attention and have been studied as candidate compounds for various functional materials because of their unique properties, such as long-wavelength absorption and emission, photoredox catalysis, and anion-sensing capability.<sup>2</sup> One of the classical methods for synthesizing thiopyryliums is the annulative condensation reaction of 1,5-dicarbonyl with H<sub>2</sub>S in the form of Paal-Knorr synthesis.<sup>1*c,3*</sup> Thiopyrylium compounds can also be synthesized by reactions of arenethiols and 1,3-diketones or aminothioacrylamide derivatives with acids.<sup>4</sup> These methods are useful for constructing small  $\pi$ -conjugation systems such as thiopyrylium and benzothiopyrylium compounds. On the other hand, largely  $\pi$ -extended thiopyrylium compounds are accessible through inter/intramolecular Friedel-Crafts reactions of aromatic thioethers bearing an *ortho*-alkoxycarbonyl group followed by 1,2-addition using aryl metal reagents and acid-mediated aromatization (Fig. 1A).<sup>1*b,2d*</sup> Although this method is useful, it

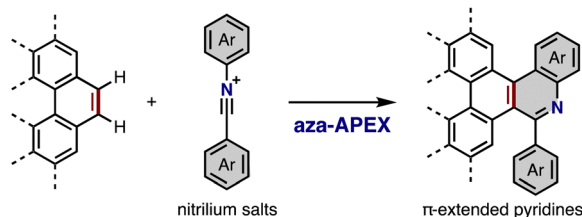
requires prefunctionalization of the starting aromatics and multistep component-assembling reactions.

As part of our ongoing efforts to achieve streamlined and diversity-oriented synthesis of large  $\pi$ -conjugated systems, we have developed a series of one-step annulative  $\pi$ -extension reactions (APEX)<sup>5</sup> of polycyclic aromatic hydrocarbons (PAHs) and heteroaromatics. Region-selective APEX reactions allow access to unprecedented nanographenes that are difficult to synthesize using conventional coupling reactions.<sup>6</sup> In addition,

### A. Representative conventional methods for thiopyrylium synthesis



### B. Nitrogen-embedding APEX (previous work)



### C. Sulfur-embedding APEX (this work)

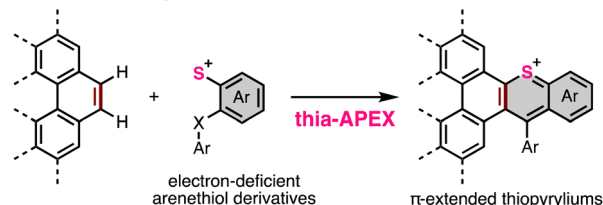


Fig. 1 (A) Representative conventional methods for thiopyrylium synthesis. (B and C) Heteroatom-embedding annulative  $\pi$ -extension (hetero-APEX) reactions: (B) Aza-APEX with nitrilium salts.<sup>7*a*</sup> (C) Thia-APEX with electron-deficient arenethiol derivatives.

<sup>a</sup> Graduate School of Science, Nagoya University, Chikusa, Nagoya 464-8602, Japan. E-mail: Itamiito.hideto.p4@f.mail.nagoya-u.ac.jp, itami@chem.nagoya-u.ac.jp

<sup>b</sup> Institute of Transformative Bio-Molecules (WPI-ITbM), Nagoya University, Chikusa, Nagoya 464-8602, Japan

† Electronic supplementary information (ESI) available: Syntheses, NMR, UV-vis absorption, emission, DFT calculations and crystallographic table. CCDC 2216401 (3ha) and 2216402 (3ha-OH). For ESI and crystallographic data in CIF or other electronic format see DOI: <https://doi.org/10.1039/d2cc06706d>

we have developed the APEX reaction for constructing heteroaromatics (hetero-APEX reaction)<sup>7</sup> (Fig. 1B and C). For example, the nitrogen-embedding APEX (aza-APEX) reaction of unfunctionalized aromatics using highly electrophilic diaryl nitrilium salts rapidly constructed a new pyridine ring on unfunctionalized aromatics (Fig. 1B).<sup>7a</sup> Herein, we report a novel sulfur-embedding APEX (thia-APEX) reaction that furnishes  $\pi$ -extended thiopyrylium compounds from unfunctionalized aromatics using electron-deficient arenethiol derivatives as  $\pi$ -extending agents (Fig. 1C).

To achieve the thia-APEX reaction, we designed and adopted *S*-succinimidated *ortho*-arenoyl arenethiols as novel  $\pi$ -extending agents (Fig. 2). These thiols include two electrophilic reaction sites: the *S*-succinimide moiety for C–S bond formation and carbonyl group for C–C bond formation. Succinimide groups act as leaving groups in the presence of Brønsted/Lewis acids to electrophilic sulfur atoms.<sup>8</sup> This electrophilic sulfur atom can form diaryl thioethers or benzothiophenes by reacting with other benzene derivatives or alkynes. We envisioned that an adjacent *ortho*-arenoyl unit on the arenethiol would promote a sequence of C–S bond formation, intramolecular Friedel–Crafts addition, and dehydroxylative aromatization using acids.<sup>9</sup> With this concept, various new sulfur-embedding APEX agents were prepared utilizing the synthesis of benzophenonethiols from arylmetals and thiosalicylic acid or arylonitriles and arenethiols.<sup>10</sup> Subsequently, the succinimide groups were introduced through *S*-chlorination reaction with SO<sub>2</sub>Cl<sub>2</sub> followed by reaction of succinimides with NEt<sub>3</sub> (see ESI† for details).<sup>8b</sup>

First, we optimized the conditions for the thia-APEX reaction of phenanthrene with the newly prepared sulfur-embedding APEX agents (see ESI† for details). After screening the reaction parameters such as solvents, temperature, amounts of  $\pi$ -extending agents, and succinimide-moieties, we found that the  $\pi$ -extending agent **2** (1.1 equiv.) was efficiently activated by TfOH (2.3 equiv.) in 1,1,1,3,3,3-hexafluoroisopropyl alcohol (HFIP) (0.2 M of aromatic substrate **1** to HFIP) to react with unfunctionalized aromatics **1** (Fig. 3). After heating at 80 °C for 17 h, various fused thiopyrylium salts **3** were obtained. Because the obtained thiopyrylium salts were sensitive to excess amounts of water, working with water or purification by preparative thin-layer chromatography (PTLC) on silica gel resulted in the formation of thioxanthenol **3ha-OH** (see ESI† for details). Therefore, we chose a purification method involving precipitation, filtration, and washing

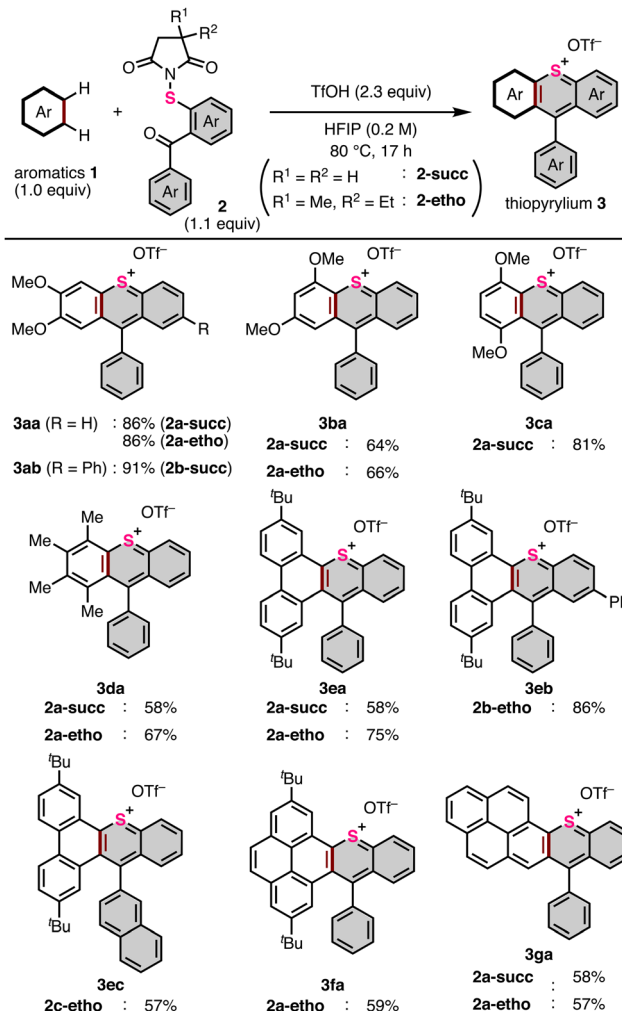


Fig. 3 Optimized reaction conditions and substrate scope of thia-APEX reaction.

with diethyl ether, followed by recrystallization to remove succinimides and other impurities, which allowed us to obtain high-quality products. In some thia-APEX reactions, superior isolated yields were obtained using ethosuximide derivatives (**2-etho**) instead of succinimide derivatives (**2-succ**). This could be due to the higher solubility of **2-etho** than that of **2-succ**, which facilitated easy separation from the crude mixture by simple filtration and washing.

In the reactions of 1,2-dimethoxybenzene (**1a**) with *S*-succinimides having simple benzophenone structures (**2a-succ** and **2a-etho**) and phenyl substituents (**2b-succ**), thiopyrylium salts **3aa** and **3ab** were obtained in 86–91% isolated yields. Compounds **3ba** and **3ca** were also obtained from 1,3-dimethoxybenzene (**1b**) and 1,4-dimethoxybenzene (**1c**) in 64–66% and 81% yields, respectively. We consider that the electron-rich dimethoxy benzenes **1a–1b** possess comparably high reactivities, and the difference in yield is derived from the ease/difficulty of solidification of the products; thiopyrylium **3aa** and **3ca** are more easily solidified than **3ba**. Interestingly, no other regioisomers were obtained or isolated in the case of **3aa**, **3ab**, and **3ba**. 1,2,3,4-Tetramethylbenzene (**1d**) afforded

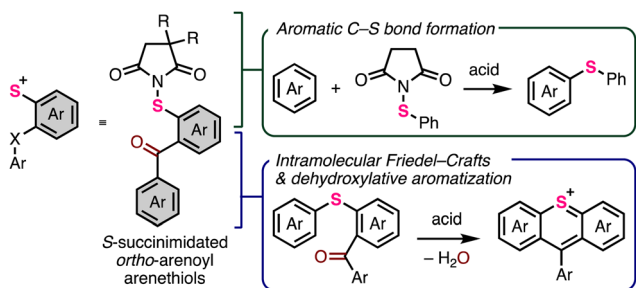
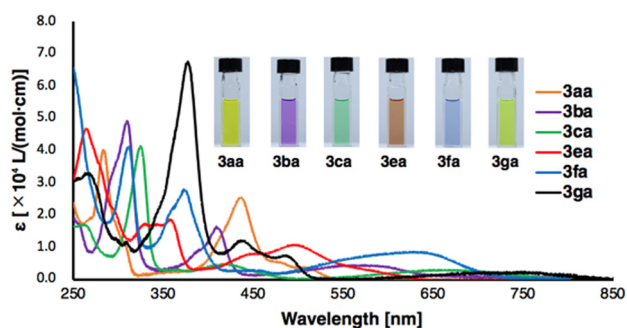


Fig. 2 Design of sulfur-embedding  $\pi$ -extending agents for thia-APEX reaction.

thiopyrylium **3da** in a 67% yield. In addition, the use of ethosuximide **2a-etho** afforded thiopyrylium **3da** with better yield and reproducibility. The PAH-type substrates 2,7-di-*tert*-butylphenanthrene (**1e**), 2,7-di-*tert*-butylpyrene (**1f**), and pristine pyrene (**1g**) were used. From substrate **1e**, thiopyryliums **3ea–3ec** were obtained in 57–86% yields. The use of **2a-etho** increased the yield of thiopyrylium **3ea** from 58% (with **2a-succ**) to 75%. Thiopyrylium **3ec** was more difficult to solidify in crude oil, which seemed to cause a decrease in the yield. Substrate **1f** afforded not only the desired product **3fa** but also a small amount of double thia-APEX that was not isolated, but detected by ESI-MS analysis. However, multiple recrystallizations of crude **3fa** afforded pure **3fa** in 59% yield. Interestingly, pyrene was regioselectively transformed into thiopyrylium **3ga** in up to 58% yield, whereas pyrene possessed multiple reaction sites. Furthermore, the reaction monitoring by <sup>1</sup>H NMR spectra indicates that the C–S bond formation proceeded at the C1 position on pyrene, which is a general reactive site for electrophilic aromatic substitutions, such as bromination and acylation.<sup>11</sup> However, when pristine phenanthrene was employed under the standard thia-APEX conditions, the first C–S bond formation seemed to proceed preferentially at the C9 position (*K*-region), but the reaction gave a complex mixture including regioisomeric mixtures which were difficult to be isolated (see ESI† for details).

Because synthesized  $\pi$ -extended thiopyrylium salts displayed diverse colors in CH<sub>2</sub>Cl<sub>2</sub>, we first measured the UV-Vis-NIR absorption spectra of the  $\pi$ -extended thiopyrylium salts **3aa–3ca** (Fig. 4). The reported spectroscopic data for 9-phenylthioxanthylum triflate (**3a**)<sup>12</sup> are also described for comparison. The dimethoxy-substituted thiopyryliums **3aa–3ca** showed weak longest wavelength absorption maxima in



	$\lambda_{\text{abs}}$ [nm] (log $\epsilon$ )				$\lambda_{\text{TD-DFT}}$ (f)
	<b>3a</b> <sup>12</sup>	<b>3aa</b>	<b>3ba</b>	<b>3ca</b>	
<b>3aa</b>	494 <sup>12</sup> (3.62)	384 <sup>12</sup> (4.11)	281 <sup>12</sup> (4.73)	487 (0.1016)	
<b>3ba</b>	518 (3.47)	487 (3.65)	436 (4.40)	283 (4.60)	
<b>3ca</b>	574 (3.65)	409 (4.21)	310 (4.69)	637 (0.0520)	
<b>3ea</b>	646 (3.44)	416 (3.67)	325 (4.61)	667 (0.0681)	
<b>3fa</b>	540–640	495 (4.03)	357 (4.27)	586 (0.0511)	
<b>3ga</b>	636 (3.92)	458 (3.43)	373 (4.44)	655 (0.1390)	
	744 (3.39)	499 (3.70)	378 (4.83)	774 (0.0314)	

Fig. 4 UV-Vis-NIR absorption spectra of **3aa–3ca** and **3ea–3ga** in CH<sub>2</sub>Cl<sub>2</sub>, summary table of observed representative absorption peaks **3a**,<sup>12</sup> **3aa–3ca** and **3ea–3ga**, and calculated excitation wavelengths ( $\lambda_{\text{TD-DFT}}$ ) and oscillator strengths (f) of corresponding cations **3a'**, **3aa'**, **3ba'** and **3ea'–3ga'** (B3LYP/6-311++G(2d,p)//B3LYP/6-311+G(2d,p)). Concentrations: **3aa** =  $6.0 \times 10^{-6}$  M, **3ba** =  $4.6 \times 10^{-6}$  M, **3ca** =  $7.6 \times 10^{-6}$  M, **3ea** =  $9.0 \times 10^{-6}$  M, **3fa** =  $4.9 \times 10^{-6}$  M, **3ga** =  $4.0 \times 10^{-6}$  M. The pictures were taken using the concentrated solutions of each compound.

the visible light region, and their wavelengths at each peak were dramatically red-shifted in the order **3aa** < **3ba** < **3ca**.

Interestingly, the subtle difference in substitution patterns dramatically altered the photophysical properties (see ESI† for detailed discussions). Next, we measured the absorption spectra of the thiopyryliums **3ea**, **3fa**, and **3ga** (Fig. 4). Red shifts of the absorption maxima in the longest wavelength region were found as their  $\pi$ -conjugation lengths were extended, and the absorptions were observed at 540–640 nm (**3ea**), 636 nm (**3fa**), and 744 nm (**3ga**) (Fig. 4). By comparing the TD-DFT calculation results for the corresponding cations **3ea'**, **3fa'**, and **3ga'**, the lowest excitations were estimated to be originated from HOMO to LUMO excitations (see ESI† for details).

In addition, thiopyryliums **3aa–3ca** and **3ea–3ga** exhibited weak emissions, as shown in Fig. 5. The emission maxima of **3aa**, **3ba**, and **3ca** were found at 551, 653, and 696 nm, and the Stokes shifts were 33, 79, and 50 nm, respectively. Similar to the absorption properties, the difference in the methoxylated sites induced a red shift in the emission wavelengths. The peak of **3ea** was observed at approximately 700 nm. Pyrene-fused thiopyryliums **3fa** and **3ga** exhibited NIR emission. The maximum peak tops of **3fa** and **3ga** were observed at 783 and 817 nm, respectively. Larger Stokes shifts (147 and 73 nm) were observed in these compounds, which can be rationalized by the existence of structural relaxation owing to intramolecular CT in each excited state. Furthermore, only thiopyryliums **3aa** and **3ba** showed sufficient emission intensities for measurements of their quantum yields (1% and 0.8%, respectively) and fluorescence lifetimes (0.32 and 0.93 ns, respectively) (see ESI†).

In summary, we developed a thia-APEX reaction, a new synthetic method for polycyclic thiopyrylium compounds from unfunctionalized aromatics. Using *S*-succinimide/*S*-ethosuximide-containing *ortho*-arenonylarene thiols and TFOH, thia-APEX reactions took place to afford 12  $\pi$ -extended thiopyrylium salts in one-step. Furthermore, each product exhibited characteristic photophysical properties and dramatic changes depending on the substitution pattern and core aromatic structures; some of them showed NIR absorption and emission. We expect that thia-APEX reactions will contribute to the rapid and efficient creation of functional aromatics.

This work was supported by the JST-CREST program and JSPS KAKENHI (JP19H05463 to K. I., JPMJCR19R1, JP20K21192,

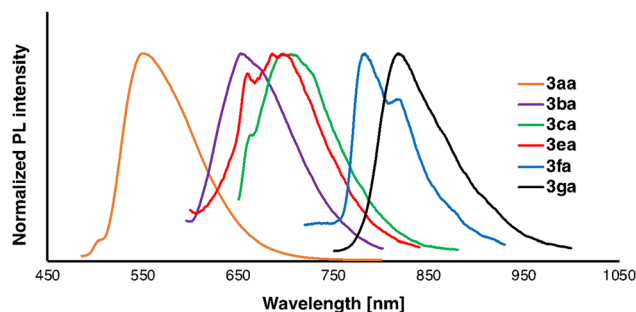


Fig. 5 Emission spectra of  $\pi$ -extended thiopyryliums **3aa–3ca** and **3ea–3ga** in CH<sub>2</sub>Cl<sub>2</sub>. Excitation wavelengths for each compound: **3aa** (436 nm), **3ba** (545 nm), **3ca** (600 nm), **3ea** (550 nm), **3fa** (636 nm), and **3ga** (564 nm).

JP21H01931 to H. I.), and Noguchi Research Foundation and Foundation of Public Interest of Tatematsu (to H. I.), JSPS Research Fellowship for Young Scientists (to K. P. K.). We thank Hiroki Shudo and Dr Wataru Matsuoka for helping with the X-ray crystallographic analysis, Ms Haruka Fujimori (Nagoya University) for assistance with ESI-MS measurements, Dr Kinichi Oyama (Nagoya University) for helping with the emission spectroscopy, and Mr Yu Kusakabe, Prof. Tomoya Nakamura, and Prof. Atsushi Wakamiya (Kyoto University) for helping with the measurement of quantum yields and fluorescence lifetimes. Emission spectroscopy was conducted using resources from the Chemical Instrumentation Facility (CIF), Research Center for Materials Science (RCMS), Nagoya University. The quantum yield and fluorescence lifetime were measured at the Institute for Chemical Research (ICR), Kyoto University. Calculations were performed using the resources of the Research Center for Computational Science, Okazaki, Japan (Projects: 20-IMS-C072, 21-IMS-C070 and 22-IMS-C069), and the SuperComputer System, Institute for Chemical Research, Kyoto University.

*Note added after first publication:* This article replaces the version published on 3<sup>rd</sup> January 2023 which contained errors in Fig. 4.

## Conflicts of interest

There are no conflicts to declare.

## Notes and references

- (a) D. M. Mckinnon, *Can. J. Chem.*, 1970, **48**, 3388; (b) S. Berényi, M. Tóth, S. Gyulai and L. Szilágyi, *Heterocycles*, 2002, **57**, 135; (c) W. D. Rudolf, *Sci. Synth.*, 2003, **14**, 649; (d) M. Z. Kassae, N. Jalalimanesh and S. M. Musavi, *THEOCHEM*, 2007, **816**, 153; (e) R. V. Seller, P. V. Reshetov and A. P. Kriven'ko, *Chem. Heterocycl. Compd.*, 2001, **37**, 797; (f) V. G. Kharchenko, S. N. Chalaya and T. M. Konovalova, *Chem. Heterocycl. Compd.*, 1975, **11**, 125; (g) G. Doddi and G. Ercolani, *Adv. Heterocycl. Chem.*, 1994, **60**, 65; (h) M. Stępień, E. Gońka, M. Żyła and N. Sprutta, *Chem. Rev.*, 2017, **117**, 3479; (i) A. Borisso, Y. K. Maurya, L. Moshniaha, W.-S. Wong, M. Żyła-Karowska and M. Stępień, *Chem. Rev.*, 2022, **122**, 565.
- (a) A. Scarpaci, A. Nantalaksakul, J. M. Hales, J. D. Matichak, S. Barlow, M. Rumi, J. W. Perry and S. R. Marder, *Chem. Mater.*, 2012, **24**, 1606; (b) S. J. Wagner, A. Skripchenko, L. Cincotta, D. Thompson-Montgomery and H. Awatefe, *Transfusion*, 2005, **45**, 752; (c) D. Wu, W. Pisula, M. C. Haberecht, X. Feng and K. Müllen, *Org. Lett.*, 2009, **11**, 5686; (d) N. Nagahora, T. Kushida, K. Shioji and K. Okuma, *Organometallics*, 2019, **38**, 1800; (e) N. Nagahora, K. Kitahara, Y. Mizuhata, N. Tokitoh, K. Shioji and K. Okuma, *J. Org. Chem.*, 2020, **85**, 7748; (f) N. Nagahora, R. Tanaka, T. Tada, A. Yasuda, Y. Yamada, K. Shioji and K. Okuma, *Org. Lett.*, 2020, **22**, 6192; (g) K. Tanaka, M. Kishimoto, M. Sukekawa, Y. Hoshino and K. Honda, *Tetrahedron Lett.*, 2018, **59**, 3361; (h) K. Tanaka, Y. Iwama, M. Kishimoto, N. Ohtsuka, Y. Hoshino and K. Honda, *Org. Lett.*, 2020, **22**, 5207; (i) H. Zhou, X. Zeng, A. Li, W. Zhou, L. Tang, W. Hu, Q. Fan, X. Meng, H. Deng, L. Duan, Y. Li, Z. Deng, X. Hong and Y. Xiao, *Nat. Commun.*, 2020, **11**, 6183; (j) W. R. Browne, M. M. Pollard, B. d Lange, A. Meetsma and B. L. Feringa, *J. Am. Chem. Soc.*, 2006, **128**, 12412; (k) H. Kearns, S. Sengupta, I. R. Sasselli, L. Bromley III, K. Faulds, T. Tuttle, M. A. Bedics, M. R. Detty, L. Velarde, D. Graham and W. E. Smith, *Chem. Sci.*, 2016, **7**, 5160.
- V. G. Kharchenko, V. I. Kleimenova and A. R. Yakoreva, *Chem. Heterocycl. Compd.*, 1970, **6**, 834.
- (a) J. Liebscher, B. Abegaz and A. Knoll, *Phosphorus, Sulfur Silicon Relat. Elem.*, 1988, **35**, 5; (b) J. Fabian and H. Hartmann, *Tetrahedron Lett.*, 1969, **10**, 239.
- Reviews on APEX reaction: (a) H. Ito, K. Ozaki and K. Itami, *Angew. Chem., Int. Ed.*, 2017, **56**, 11144; (b) H. Ito, Y. Segawa, K. Murakami and K. Itami, *J. Am. Chem. Soc.*, 2019, **141**, 3.
- (a) K. Ozaki, K. Kawasumi, M. Shibata, H. Ito and K. Itami, *Nat. Commun.*, 2015, **6**, 6251; (b) W. Matsuoka, H. Ito and K. Itami, *Angew. Chem., Int. Ed.*, 2017, **56**, 12224; (c) W. Matsuoka, H. Ito, D. Sarlah and K. Itami, *Nat. Commun.*, 2021, **12**, 3940.
- Hetero-APEX reactions: (a) K. P. Kawahara, W. Matsuoka, H. Ito and K. Itami, *Angew. Chem., Int. Ed.*, 2020, **59**, 6383; (b) J. Yan, A. P. Pulis, G. J. P. Perry and D. J. Procter, *Angew. Chem., Int. Ed.*, 2019, **58**, 15675; (c) E. Schendera, L.-N. Unkel, P. P. H. Quyen, G. Salkewitz, F. Hoffmann, A. Villinger and M. Brasholz, *Chem. – Eur. J.*, 2020, **26**, 269; (d) Z. Yu, Y. Zhang, J. Tang, L. Zhang, Q. Liu, Q. Li, G. Gao and J. You, *ACS Catal.*, 2020, **10**, 203; (e) S. Tokita, K. Hiruta, K. Kitahara and H. Nishi, *Synthesis*, 1982, 229; (f) S. Maiti, T. K. Achar and P. Mal, *Org. Lett.*, 2017, **19**, 2006; (g) R. Regar, R. Mishra, P. K. Mondal and J. Sankar, *J. Org. Chem.*, 2018, **83**, 9547; (h) Y. Tokimaru, S. Ito and K. Nozaki, *Angew. Chem., Int. Ed.*, 2017, **56**, 15560; (i) A. Qarah, M. Gasonoo, D. Do and D. A. Klumpp, *Tetrahedron Lett.*, 2016, **57**, 3711; (j) C. Chen, Y. Wang, X. Shi, W. Sun, J. Zhao, Y.-P. Zhu, L. Liu and B. Zhu, *Org. Lett.*, 2020, **22**, 4097; (k) M. Wang, L. Kong, F. Wang and X. Lia, *Adv. Synth. Catal.*, 2017, **359**, 4411.
- (a) E. Ramesh, M. Shankar, S. Dana and A. K. Sahoo, *Org. Chem. Front.*, 2016, **3**, 1126; (b) X. Wang, T. Gensch and F. Glorius, *Org. Chem. Front.*, 2016, **3**, 1619; (c) E. Ramesh, T. Guntreddi and A. K. Sahoo, *Eur. J. Org. Chem.*, 2017, 4405; (d) P. Saravanan and P. Anbarasan, *Org. Lett.*, 2014, **16**, 848; (e) T. Hostier, V. Ferey, G. Ricci, D. G. Pardo and J. Cossy, *Org. Lett.*, 2015, **17**, 3898.
- (a) X. Ye, B. Xu, J. Sun, L. Dai, Y. Shao, Y. Zhang and J. Chen, *J. Org. Chem.*, 2020, **85**, 13004; (b) X. Pang, Z. Lou, M. Li, L. Wen and C. Chen, *Eur. J. Org. Chem.*, 2015, 3361.
- (a) L. W. Souza, R. A. Squitieri, C. A. Dimirjian, B. M. Hodur, L. A. Nickerson, C. N. Penrod, J. Cordova, J. C. Fettinger and J. T. Shaw, *Angew. Chem., Int. Ed.*, 2018, **57**, 15213; (b) A. R. Katritzky, K. Kirichenko, Y. Ji and I. Prakash, *Chem. Heterocycl. Compd.*, 2002, **38**, 156.
- Representative reports on C1-selective S<sub>E</sub>Ar reactions of pristine pyrene: (a) M. Liu, X. Gong, C. Zheng and D. Gao, *Asian J. Org. Chem.*, 2017, **6**, 1903; (b) W. H. Gumprecht, *Org. Synth.*, 1968, **48**, 30; (c) D. Zych, *Molecules*, 2019, **24**, 2551.
- D. T. Hogan and T. C. Sutherland, *J. Phys. Chem. Lett.*, 2018, **9**, 2825.





(参考論文)

# $\pi$ -Extended Rubrenes via Dearomative Annulative $\pi$ -Extension Reaction

Wataru Matsuoka, Kou P. Kawahara, Hideto Ito,\* David Sarlah, and Kenichiro Itami\*



Cite This: *J. Am. Chem. Soc.* 2023, 145, 658–666



Read Online

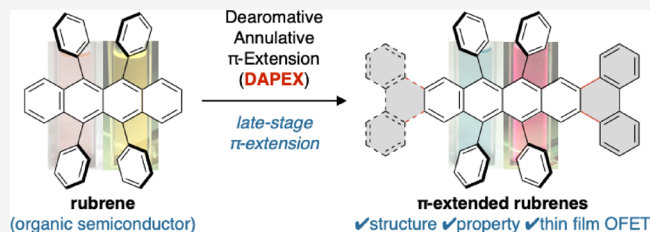
ACCESS |

Metrics & More

Article Recommendations

Supporting Information

**ABSTRACT:** Among a large variety of organic semiconducting materials, rubrene (5,6,11,12-tetraphenyltetracene) represents one of the most prominent molecular entities mainly because of its unusually high carrier mobility. Toward finding superior rubrene-based organic semiconductors, several synthetic strategies for related molecules have been established. However, despite its outstanding properties and significant attention in the field of materials science, late-stage functionalizations of rubrene remains undeveloped, thereby limiting the accessible chemical space of rubrene-based materials. Herein, we report on a late-stage  $\pi$ -extension of rubrene by dearomative annulative  $\pi$ -extension (DAPEX), leading to the generation of rubrene derivatives having an extended acene core. The Diels–Alder reaction of rubrene with 4-methyl-1,2,4-triazoline-3,5-dione occurred to give 1:1 and 1:2 cycloadducts which further underwent iron-catalyzed annulative diarylation. The thus-formed 1:1 and 1:2 adducts were subjected to radical-mediated oxidation and thermal cycloreversion to furnish one-side and two-side  $\pi$ -extended rubrenes, respectively. These  $\pi$ -extended rubrenes displayed a marked red shift in absorption and emission spectra, clearly showing that the acene  $\pi$ -system of rubrene was extended not only structurally but also electronically. The X-ray crystallographic analysis uncovered interesting packing modes of these  $\pi$ -extended rubrenes. Particularly, two-side  $\pi$ -extended rubrene adopts a brick-wall packing structure with largely overlapping two-dimensional face-to-face  $\pi$ – $\pi$  interactions. Finally, organic field-effect transistor devices using two-side  $\pi$ -extended rubrene were fabricated, and their carrier mobilities were measured. The observed maximum hole mobility of  $1.49 \times 10^{-3} \text{ cm}^2 \text{ V}^{-1} \text{ s}^{-1}$ , which is a comparable value to that of the thin-film transistor using rubrene, clearly shows the potential utility of two-side  $\pi$ -extended rubrene in organic electronics.



## INTRODUCTION

Over the past several decades,  $\pi$ -conjugated compounds such as polycyclic aromatic hydrocarbons have gathered great attention as organic semiconductors (OSCs).<sup>1</sup> OSC-based devices such as organic field-effect transistors (OFETs) and organic light-emitting diodes are generally more flexible, lightweight, and potentially less expensive than their inorganic counterparts.<sup>2</sup> Motivated by such potential applications, the development of efficient synthetic methods for  $\pi$ -conjugated molecules has been intensively investigated.<sup>3</sup> Considering the necessity for evaluating an enormous number of molecules to find an appropriate molecular entity for device applications, late-stage functionalization of existing OSCs can be regarded as one of the most important strategies. Because it would enable chemists to directly install functional groups which perturb the physical properties of a parent molecule, fine-tuning of OSCs can be rapidly carried out without starting their synthesis from scratch.

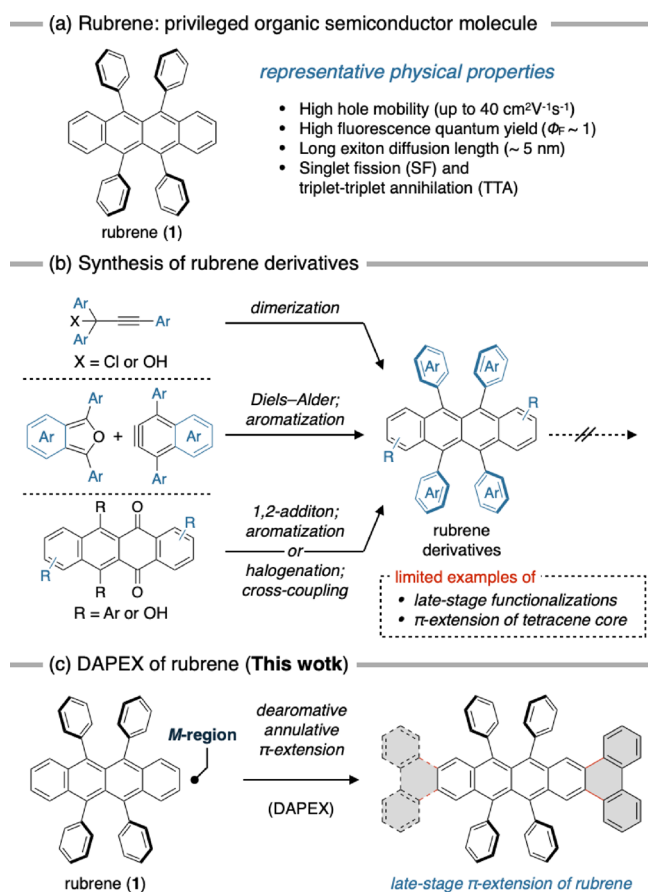
Among a large variety of OSCs, rubrene (**1**) stands out as a promising molecular entity because of its high carrier mobility in single crystals (Figure 1a).<sup>4</sup> Since a transistor using a single crystal of rubrene was reported to exhibit unusually high carrier mobility (15–40  $\text{cm}^2/\text{Vs}$ ), rubrene has been recognized as the benchmark in this field and has become one of the most

frequently studied molecules.<sup>5</sup> During these studies, hundreds of rubrene derivatives have been synthesized and characterized to discover postrubrene materials having enhanced physical properties.<sup>6</sup> As shown in Figure 1b, these derivatives are typically synthesized through an assembly of molecular components by dimerization of propargyl chlorides/alcohols, Diels–Alder reaction of isobenzofuran and aryne, 1,2-addition of organometallic reagents to naphthacenequinone, and cross-coupling reaction of 5,6,11,12-tetrachlorotetracene.<sup>6</sup> However, despite their compelling properties and potential applications to a wide variety of organic electronic materials, late-stage functionalizations of rubrene and its derivatives have been rarely reported,<sup>7</sup> forcing chemists to install functional groups of interest in the early stage of lengthy synthetic protocols. This constraint, which stems from the inertness of C–H bonds and the inherent instability of rubrene toward light and molecular

Received: October 26, 2022

Published: December 23, 2022





**Figure 1.** Rubrene (1) as a prominent molecular entity for OSCs. (a) Molecular structure of rubrene and representative physical properties. (b) Conventional synthetic strategies for rubrene derivatives. (c)  $\pi$ -Extension of rubrene by DAPEX strategy.

oxygen,<sup>8</sup> often limits the synthetic accessibility of rubrene-based electronic materials. Therefore, strategies for the late-stage functionalizations of rubrene have been highly sought after.

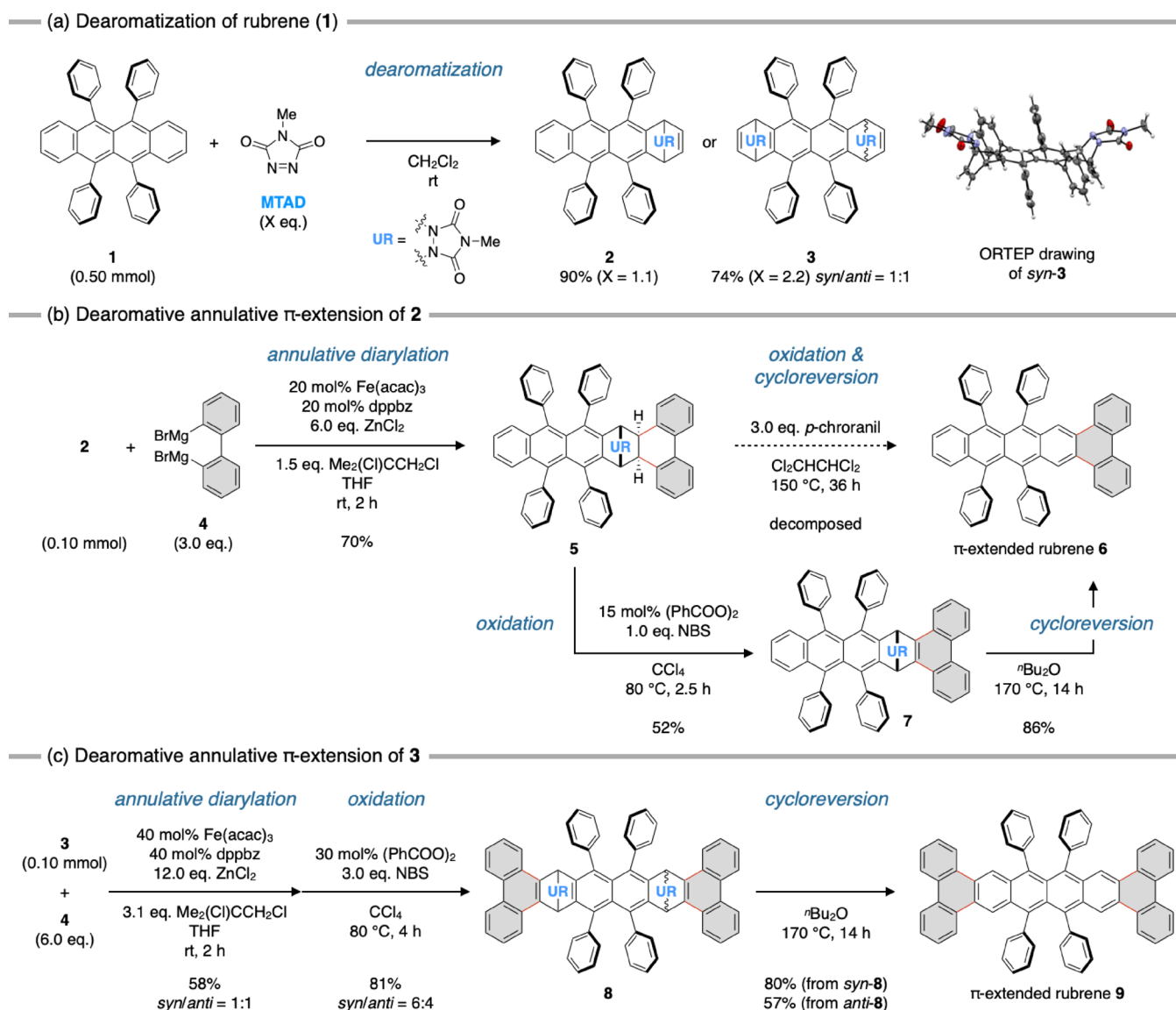
Recently, during our campaign to develop efficient synthetic methods for nanographenes,<sup>9,10</sup> we have reported a unique  $\pi$ -extension method termed as dearomatative annulative  $\pi$ -extension (DAPEX).<sup>10</sup> In this method, terminal regions in the longitudinal direction of the acene substructure (*M*-region) of unfunctionalized fused aromatic compounds are selectively  $\pi$ -extended through formal C–H functionalizations. We anticipated that the DAPEX would be a suitable synthetic strategy for the late-stage  $\pi$ -extension of rubrene because (i) rubrene has two *M*-regions at the edge of tetracene core and (ii) the unstable tetracene moiety, which inherently prevents late-stage functionalizations,<sup>8</sup> can be masked by tentative dearomatization<sup>10</sup> (Figure 1c).

In this study, we applied DAPEX to rubrene, and successfully obtained novel rubrene derivatives having pentacene and hexacene cores. Although a major part of rubrene's unique physical properties is provided by its tetracene core, rubrene derivatives having a larger acene core have rarely been synthesized.<sup>11,12</sup> Exceptionally, the family of twistacenes has been synthesized,<sup>12</sup> but these compounds would no longer preserve the unique physical properties of rubrene due to their high distortion of the acene core. Therefore, the present synthetic protocol, which is potentially

applicable to the late-stage  $\pi$ -extension of reported rubrene derivatives, would allow chemists to easily explore a new chemical space of  $\pi$ -extended rubrene-based materials. Fundamental properties including photophysical, structural, and semiconducting properties of  $\pi$ -extended rubrenes were investigated, and it was confirmed that one of these compounds (two-side  $\pi$ -extended rubrene) showed semiconducting behavior comparable to rubrene in thin films.

## RESULTS AND DISCUSSION

**Synthesis of  $\pi$ -Extended Rubrenes.** The DAPEX method consists of three fundamental steps: (i) a dearomatative [4 + 2] cycloaddition of 4-methyl-1,2,4-triazoline-3,5-dione (MTAD) with aromatic compound;<sup>13</sup> (ii) an iron-catalyzed annulative diarylation, which was originally developed by Nakamura and co-workers;<sup>14</sup> (iii) aromatization by the removal of MTAD.<sup>10</sup> Hence, the DAPEX of rubrene was initiated by the dearomatization of the tetracene core (Figure 2a). As previously reported,<sup>13a</sup> the Diels–Alder reaction of rubrene (1) with 1.1 equivalents of MTAD selectively occurred at the terminal benzene ring of the tetracene core to give 1:1 cycloadduct 2 in 90% yield. In addition, the use of an excess amount of MTAD (2.2 equivalents) resulted in the formation of 1:2 cycloadduct 3 as a mixture of *syn*- and *anti*-diastereomers. The relative configuration of *syn*-3 was determined by X-ray crystallographic analysis. Then, the iron-catalyzed annulative diarylation of 2 and the subsequent rearomatization were examined (Figure 2b). Treatment of 2 with biphenyl bis-Grignard reagent 4 in the presence of  $\text{Fe}(\text{acac})_3$  (acac = acetylacetonato), 1,2-bis(diphenylphosphino)benzene (dppbz),  $\text{ZnCl}_2$ , and 1,2-dichloroisobutane successfully afforded the desired diarylated compound 5 in 70% yield with preferential *exoselectivity*. However, the subsequent rearomatization of 5 under previously reported conditions,<sup>10</sup> where both oxidation and retro-Diels–Alder reactions take place in one-pot by heating with *p*-chloranil, only gave a trace amount of the desired product 6, probably due to the overoxidation of the product.<sup>15</sup> Therefore, the rearomatization of 5 was redesigned to prevent the overoxidation of 6 as shown in Figure 2b. The oxidation of a diarylated compound 5 without loss of the MTAD moiety would give another precursor 7. Because this oxidized precursor can be hypothetically rearomatized simply by heating, the  $\pi$ -extended product 6 would be generated in the absence of the oxidant, preventing 6 from the overoxidation. Indeed, similar approaches using a thermally reactive precursor are well investigated in the synthesis of unstable acenes and related compounds,<sup>16</sup> and beneficial for the fabrication of electronic devices. Reaction conditions were investigated, and the oxidation of diarylated compound 5 was successfully achieved by heating with benzoyl peroxide (15 mol %) and *N*-bromosuccinimide (NBS, 1.0 equivalents) at 80 °C to give the oxidized precursor 7 in 52% yield. As expected, the rearomatization of 7 proceeded simply by heating in dibutyl ether (*n*-Bu<sub>2</sub>O) at 170 °C to afford the one-side  $\pi$ -extended rubrene 6 in 86% yield. The two-side  $\pi$ -extended rubrene 9 was also obtained using the same reaction protocol (Figure 2c). Iron-catalyzed annulative diarylation at both activated olefins of 1:2 cycloadduct 3 (1:1 diastereomixture) successfully gave the tetraarylated product in 58% yield. The subsequent oxidation with benzoyl peroxide and NBS afforded the oxidized precursors 8 in 81% total yield. The diastereoisomers of 8 could be easily separated by preparative thin-layer chromatography, giving *syn*-8 and *anti*-8 in a 6:4

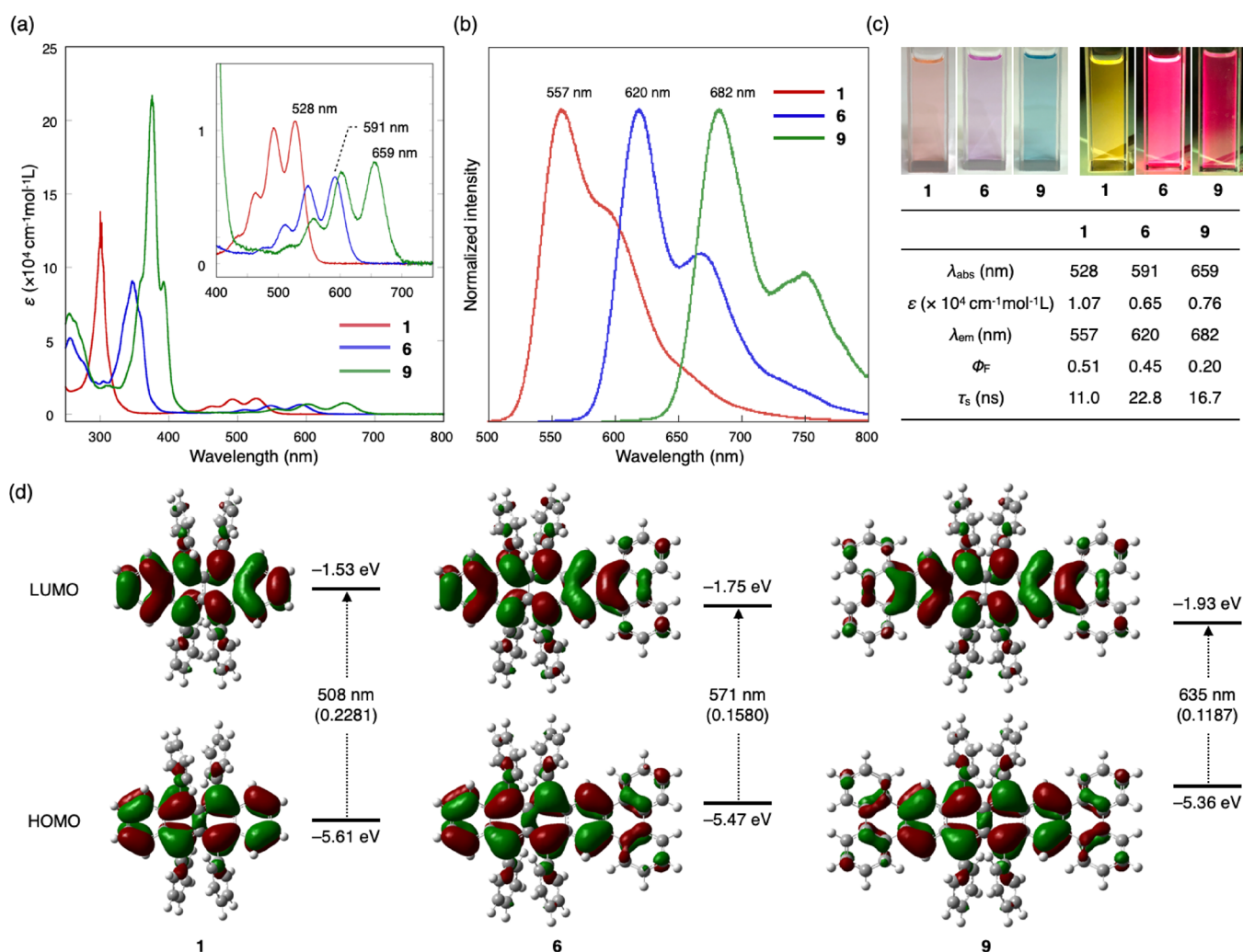


**Figure 2.** DAPEX of rubrene (1). (a) Regioselective dearomative [4 + 2] cycloaddition of MTAD. (b) Annulative diarylation and subsequent rearomatization of cycloadduct 2 to give one-side  $\pi$ -extended rubrene 6. (c) Annulative diarylation and subsequent rearomatization of cycloadduct 3 to give two-side  $\pi$ -extended rubrene 9.

diastereomeric ratio, and the relative configuration of *syn*-8 was determined by X-ray crystallographic analysis (see [Supporting Information](#) for details). Finally, the thermal cycloreversion of 8 was performed, and two-side  $\pi$ -extended rubrene 9 was successfully obtained. While the cycloreversion of *syn*-8 proceeded in good yield (80%), *anti*-8 only gave the product in 57% yield, probably due to the low reactivity of *anti*-8 caused by its poor solubility in *n*-Bu<sub>2</sub>O.

**Photophysical Properties.** With the  $\pi$ -extended rubrenes in hand, UV–vis absorption and fluorescence spectra of rubrene (1) and  $\pi$ -extended rubrenes 6 and 9 in dichloromethane were measured to elucidate the effect of the  $\pi$ -extension on the electronic properties (Figure 3). While the longest absorption maximum of 1 was observed at 528 nm ( $\epsilon = 1.07 \times 10^4 \text{ cm}^{-1}\text{mol}^{-1}\text{L}$ ),  $\pi$ -extended rubrenes 6 and 9 have red-shifted absorption maxima at 591 nm ( $\epsilon = 6.5 \times 10^3 \text{ cm}^{-1}\text{mol}^{-1}\text{L}$ ) and 659 nm ( $\epsilon = 7.6 \times 10^3 \text{ cm}^{-1}\text{mol}^{-1}\text{L}$ ), respectively (Figure 3a,c). Similar marked red shifts were also observed in the fluorescence spectra of 6 ( $\lambda_{\text{em}} = 620 \text{ nm}$ ,  $\Phi_{\text{F}} =$

0.45) and 9 ( $\lambda_{\text{em}} = 682 \text{ nm}$ ,  $\Phi_{\text{F}} = 0.20$ ) compared to that of 1 ( $\lambda_{\text{em}} = 557 \text{ nm}$ ,  $\Phi_{\text{F}} = 0.51$ ) (Figure 3b,c and see [SI](#) for further discussions about fluorescence quantum yields ( $\Phi_{\text{F}}$ ) and photostability of the compounds). The fluorescence lifetime ( $\tau_{\text{s}}$ ) of 6 (22.8 ns) was twice as long as that of 1 (11.0 ns), while symmetrically  $\pi$ -extended rubrene 9 showed a slightly shorter lifetime (16.7 ns). To understand the electronic structures, density functional theory (DFT) calculations were performed at the BHandHLYP/TZVP//B3LYP/6-31G(d,p) level of theory.<sup>17</sup> As shown in Figure 3d, both the HOMO and LUMO of 1 are localized on the tetracene core. Similarly, the frontier molecular orbitals of 6 and 9 are localized on the tetracene moieties with small, but nonnegligible contributions from newly constructed benzene rings. The observed longest absorption maxima of these molecules were assigned to the HOMO→LUMO transitions ( $\lambda = 508 \text{ nm}$ ,  $f$  (oscillator strength) = 0.2281 for 1;  $\lambda = 571 \text{ nm}$ ,  $f = 0.1580$  for 6;  $\lambda = 635 \text{ nm}$ ,  $f = 0.1187$  for 9) by time-dependent DFT (TD-DFT) calculations. These results, along with the observed marked red



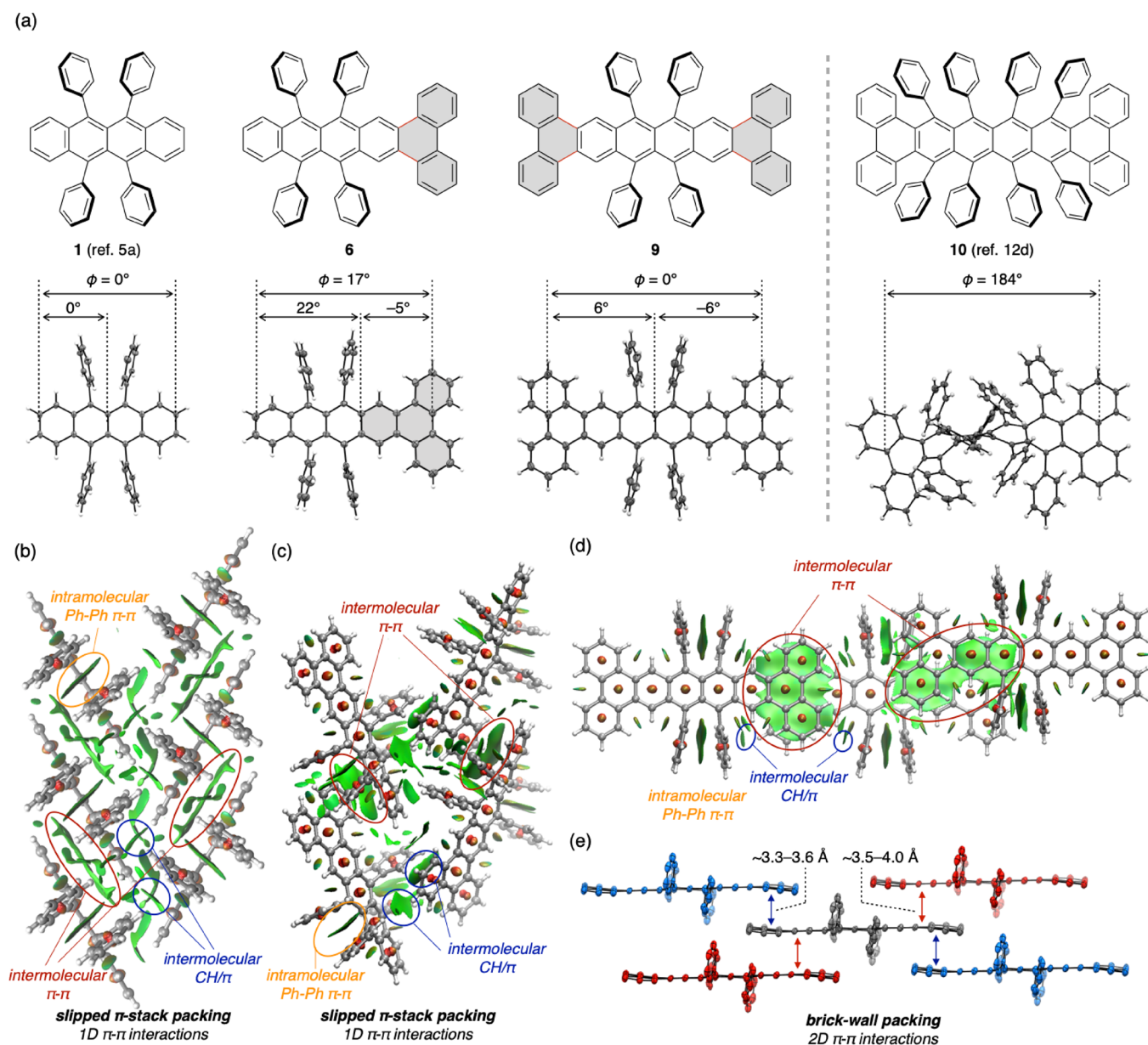
**Figure 3.** Photophysical properties of rubrene (**1**) and  $\pi$ -extended rubrenes **6** and **9**. (a) UV-vis absorption spectra of **1**, **6**, and **9** in  $\text{CH}_2\text{Cl}_2$ . (b) Normalized emission spectra of **1**, **6**, and **9** in  $\text{CH}_2\text{Cl}_2$  in the region between  $\lambda = 500$  and  $800$  nm. (c) Solution/emission colors of **1**, **6**, and **9** in  $\text{CH}_2\text{Cl}_2$  and summary of optoelectronic properties. (d) Pictorial frontier molecular orbitals and possible transitions calculated by TD-DFT at the BHandHLYP/TZVP//B3LYP/6-31G(d,p) level of theory.

shift in absorption and emission spectra, indicate that the acene  $\pi$ -system of **1** was successfully extended not only structurally but also electronically.

**X-ray Crystallographic Analysis.** To disclose the effect of tetracene core  $\pi$ -extension on the molecular and packing structures of rubrene, single crystals of **6** and **9** were grown from diethyl ether and diphenyl ether solution, respectively, and analyzed by X-ray crystallography. The results are shown in Figure 4, along with the reported crystal structure of the parent rubrene (**1**)<sup>5a</sup> and compound **10**, which possesses the common core framework (tetrabenzo[*a,c,n,p*]hexacene moiety) with **9**.<sup>12d</sup> Whereas the tetracene core of **1** is completely planar in the single crystal ( $\phi = 0^\circ$ , where  $\phi$  is an end-to-end dihedral angle defined by four carbon atoms at the edge of an acene moiety), and this nature is believed to contribute largely to its unusually high carrier mobility,<sup>4</sup> the one-side  $\pi$ -extended rubrene **6** has a slightly twisted structure (Figure 4a,  $\phi = 17^\circ$ ). The gray-filled triphenylene moiety of **6** is almost planar ( $\phi = -5^\circ$ ), and the remaining anthracene moiety is twisted ( $\phi = 22^\circ$ ), most likely due to the steric repulsion between the four dangling phenyl groups. On the other hand, the two-side  $\pi$ -extended rubrene **9** was found to have a planar acene core ( $\phi = 0^\circ$ ). A structurally similar molecule **10**, reported by Kilway and

coworkers, is known as a family of “twistacene” having a largely twisted acene substructure ( $\phi = 184^\circ$ ).<sup>12d</sup> With the removal of four phenyl groups at peri positions of **10**, newly synthesized **9** seemed to decrease intramolecular steric repulsions to result in the planar structure, thereby greatly increasing the chance for intermolecular  $\pi$ - $\pi$  interactions like rubrene.

To analyze the packing structures of these rubrene compounds, we performed the noncovalent interaction plot (NCIPLOT)<sup>18</sup> analysis for **1**, **6**, and **9** which were extracted from the X-ray crystallographic analysis (Figure 4b–d). Regarding the packing structure, **1** is known to adopt the so-called slipped  $\pi$ -stack packing structure,<sup>5a</sup> where largely overlapping intermolecular face-to-face  $\pi$ - $\pi$  interactions and face-to-edge CH/ $\pi$  interactions exist (Figure 4b).<sup>19</sup> Compound **6** also adopted a similar packing structure as **1**, while both  $\pi$ - $\pi$  and CH/ $\pi$  interactions of **6** look smaller than those of **1**, resulting in weakened intermolecular interactions in **6** (Figure 4c). On the other hand, two-side  $\pi$ -extended rubrene **9** adopted a brick-wall packing structure with largely overlapping two-dimensional (2D) face-to-face  $\pi$ - $\pi$  interactions, which is known as one of the most suitable packing structures for the applications in electronic devices (Figure 4d,e).<sup>20</sup> One of the  $\pi$ - $\pi$  stacking modes is the interaction between blue- and gray-



**Figure 4.** X-ray crystallographic structure of **1**, **6**, **9**, and **10**. (a) Oak Ridge thermal-ellipsoid plot program drawing of the top view.  $\phi$  is an end-to-end dihedral angle of acene cores. NCI analysis and reduced density gradient isosurface (isosurface value = 0.3) by a NCIPlot4 program for (b) **1**, (c) **6**, and (d) **9**. Color code based on sign  $(\lambda_2)\rho$  was  $-0.7$  a.u. (blue)  $< 0.0$  a.u. (green)  $< 0.7$  a.u. (red). Blue and red isosurfaces show regions having attractive and repulsive interactions, respectively, and green isosurfaces show weak van der Waals interactions such as  $\pi$ - $\pi$  interaction. Each structure was extracted from the data of X-ray crystallographic analyses. (e) Crystal packing structure of **9** and solvent molecules in the NCI plot of **6** are omitted for clarity.

colored molecules in which the terminal phenanthrene moieties are overlapped with each other. The other mode is the stacking between red- and gray-colored molecules, where terminal benzene rings interact with naphthalene moieties in the middle of the hexacene core (Figure 4e). The distances between the closest pair of carbon atoms in each stacking mode were estimated to be 3.32 and 3.45 Å, respectively, indicating the existence of moderate to strong  $\pi$ - $\pi$  interactions. Through these  $\pi$ - $\pi$  interactions, one molecule of **9** can interact with four neighboring molecules (Figure 4e), forming a 2D network of  $\pi$ - $\pi$  interactions. It should be noted that, among a large variety of rubrene derivatives reported to date,<sup>6</sup> only a few molecules are found to adopt this packing structure,<sup>21</sup> and that compound **9** is, to the best of our

knowledge, the first example of an electronically unbiased rubrene derivative having 2D  $\pi$ - $\pi$  interactions in the crystal structure. The observed change in packing structures from **1** to **9** might be understandable by analogy of a well-known crystal engineering strategy for 6,13-bis((trialkylsilyl)ethynyl)pentacenes (TAS-pentacenes).<sup>22</sup> Anthony and coworkers revealed that the packing structure of TAS-pentacene is determined by the ratio of the diameter of trialkylsilyl groups ( $r$ ) at peri positions to the length of the acene core ( $L$ ), and the brick-wall packing structure would be observed when this ratio ( $r/L$ ) becomes close to 0.5.<sup>22</sup> Considering the similarity in molecular structures of rubrene and TAS-pentacene, DAPEX of **1** caused the increase of the length of the acene core ( $L$ ), while keeping the size of substituent at peri positions

(phenyl groups) unchanged, resulting in an appropriate ratio of  $r$  to  $L$ .

**Evaluation of Hole Mobility.** Because the observed brick-wall packing structure of two-side  $\pi$ -extended rubrene **9** is believed to contribute to the high carrier mobility in thin-film OFET using prominent OSCs such as TIPS-pentacene, oxo(phthalocyaninato)titanium (TiOPc), and  $N,N'$ -bis-(cyclohexyl) naphthalene-1,4,5,8-bis(dicarboximide),<sup>20,22,23</sup> OFET devices using **9** were fabricated, and their carrier mobilities were measured. The  $p$ -type OFET devices were fabricated in the top-contact/bottom-gate (TC/BG) configurations, and a thin film of **9** was formed by vapor deposition on the SiO<sub>2</sub> substrate treated with octadecyltrimethoxysilane (see SI for detailed procedure). To our delight, the thin-film layer of compound **9** showed semiconducting behavior, and the average hole mobility for 16 independent devices was estimated to be  $7.11 \times 10^{-4} \text{ cm}^2\text{V}^{-1} \text{ s}^{-1}$  with a threshold voltage of  $-4.7 \text{ V}$  and on/off current ratio of  $1.8 \times 10^4$  (Table 1, entry 1). Although the device performance was only

**Table 1. OFET Performance of Compound **9** and Rubrene (**1**)**

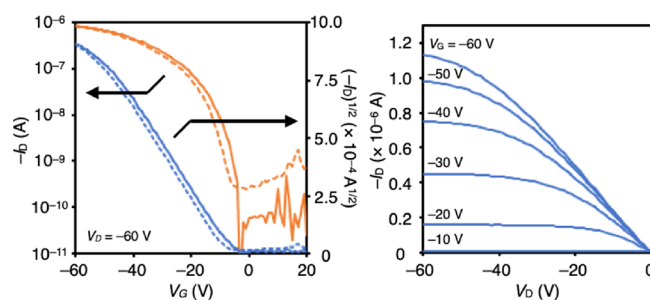
entry	$T^a$ (°C)	$\mu_{\text{ave}}^b$ (cm <sup>2</sup> /VS)	$\mu_{\text{max}}^c$ (cm <sup>2</sup> /VS)	$V_{\text{th}}^d$ (V)	on/off ratio <sup>e</sup>
1		$7.11 \times 10^{-4}$	$7.69 \times 10^{-4}$	-4.7	$1.8 \times 10^4$
2	100	$6.26 \times 10^{-4}$	$6.98 \times 10^{-4}$	-5.7	$1.6 \times 10^4$
3	120	$7.76 \times 10^{-4}$	$1.12 \times 10^{-3}$	-7.4	$1.7 \times 10^4$
4	140	$7.28 \times 10^{-4}$	$1.49 \times 10^{-3}$	-7.1	$4.0 \times 10^3$
5	160	$6.72 \times 10^{-4}$	$8.42 \times 10^{-4}$	-7.9	$6.3 \times 10^3$
6 <sup>f</sup>		$2.62 \times 10^{-3}$	$2.71 \times 10^{-3}$	-3.3	$2.1 \times 10^5$

<sup>a</sup>Annealing temperature. <sup>b</sup>Average hole mobility over five independent devices. <sup>c</sup>Maximum hole mobility over five independent devices. <sup>d</sup>Average threshold voltage over five independent devices. <sup>e</sup>Average on/off current ratio over five independent devices. <sup>f</sup>Rubrene (**1**) was used instead of compound **9**.

moderately good, the hole mobility could be improved by thermal annealing (entries 2–5). The maximum hole mobility of  $1.49 \times 10^{-3} \text{ cm}^2\text{V}^{-1} \text{ s}^{-1}$ , which is a comparable value to the thin-film transistor using rubrene ( $2.71 \times 10^{-3} \text{ cm}^2\text{V}^{-1} \text{ s}^{-1}$ , entry 6), was observed when the thin film was annealed at 140 °C for 15 min (entry 4). The thermal stability of compound **9** was confirmed by thermogravimetry-differential thermal analysis (TG-DTA, see SI), where no decomposition and no enthalpy change of compound **9** occurred below 400 °C, indicating that the observed change in hole mobilities could be accounted by a subtle change in aggregation morphology around the substrate surface. The transfer and output characteristics of this device are shown in Figure 5. Although a comparison of hole mobilities in the single crystal could not be carried out due to the difficulty in preparing devices, the results described above could imply the possibility of two-side  $\pi$ -extended rubrene **9** as a novel class of rubrene-based OSCs with comparable mobility to rubrene.

## CONCLUSIONS

In conclusion, we have applied our DAPEX method to one of the promising OSCs, rubrene, and successfully obtained  $\pi$ -extended rubrene derivatives **6** and **9**. The Diels–Alder reaction of rubrene with MTAD occurred selectively at the terminal benzene ring of the tetracene core to give 1:1 and 1:2 cycloadducts which further underwent iron-catalyzed annula-



**Figure 5.** Transfer (left) and output (right) characteristics of the TC/BG device for the thin-film layer of compound **9** prepared by vapor deposition followed by thermal annealing at 140 °C for 15 min.

tive diarylation with the biphenyl bis-Grignard reagent. The thus-formed 1:1 and 1:2 adducts were subjected to radical-mediated oxidation and thermal cycloreversion to furnish one-side and two-side  $\pi$ -extended rubrenes **6** and **9**, respectively. These  $\pi$ -extended rubrenes **6** and **9** displayed a marked red shift in absorption and emission spectra, clearly showing that the acene  $\pi$ -system of rubrene was extended not only structurally but also electronically. The X-ray crystallographic analysis uncovered interesting packing modes of these  $\pi$ -extended rubrenes. Particularly, two-side  $\pi$ -extended rubrene **9** adopts a brick-wall packing structure with largely overlapping 2D face-to-face  $\pi$ – $\pi$  interactions, which is known as one of the most suitable packing structures for applications in electronic devices. Finally, the OFET devices using two-side  $\pi$ -extended rubrene **9** were fabricated, and their carrier mobilities were measured. The observed maximum hole mobility of  $1.49 \times 10^{-3} \text{ cm}^2\text{V}^{-1} \text{ s}^{-1}$ , which is a comparable value to a thin-film transistor using rubrene, clearly shows the potential utility of two-side  $\pi$ -extended rubrene in organic electronics. The established synthetic method not only represents one of the limited examples of late-stage functionalization of rubrene, but also enables access to a previously untapped chemical space of rubrene derivatives having a larger acene core.

## ASSOCIATED CONTENT

### Supporting Information

The Supporting Information is available free of charge at <https://pubs.acs.org/doi/10.1021/jacs.2c11338>.

Experimental procedures, preparation of Grignard reagents, synthesis of  $\pi$ -extended rubrenes **6** and **9**, X-ray crystallographic analysis, computational detail, photophysical properties, fabrication and evaluation of OFETs, TG-DTA of rubrene **9**, <sup>1</sup>H and <sup>13</sup>C NMR spectra (PDF)

### Accession Codes

CCDC 2040996–2040999 contain the supplementary crystallographic data for this paper. These data can be obtained free of charge via [www.ccdc.cam.ac.uk/data\\_request/cif](http://www.ccdc.cam.ac.uk/data_request/cif), or by emailing [data\\_request@ccdc.cam.ac.uk](mailto:data_request@ccdc.cam.ac.uk), or by contacting The Cambridge Crystallographic Data Centre, 12 Union Road, Cambridge CB2 1EZ, UK; fax: +44 1223 336033.

CCDC 2040996–2040999 contain the supplementary crystallographic data for this paper. These data can be obtained free of charge via [www.ccdc.cam.ac.uk/data\\_request/cif](http://www.ccdc.cam.ac.uk/data_request/cif).



## AUTHOR INFORMATION

### Corresponding Authors

**Hideto Ito** – Department of Chemistry, Graduate School of Science, Nagoya University, Nagoya 464-8602, Japan; Email: [ito.hideto.p4@f.mail.nagoya-u.ac.jp](mailto:ito.hideto.p4@f.mail.nagoya-u.ac.jp)

**Kenichiro Itami** – Department of Chemistry, Graduate School of Science and Institute of Transformative Bio-Molecules (WPI-ITbM), Nagoya University, Nagoya 464-8602, Japan; [orcid.org/0000-0001-5227-7894](https://orcid.org/0000-0001-5227-7894); Email: [itami@chem.nagoya-u.ac.jp](mailto:itami@chem.nagoya-u.ac.jp)

### Authors

**Wataru Matsuoka** – Department of Chemistry, Graduate School of Science, Nagoya University, Nagoya 464-8602, Japan; Present Address: Department of Chemistry, Faculty of Science, Hokkaido University, Sapporo 060-0810, Japan; [orcid.org/0000-0002-8342-249X](https://orcid.org/0000-0002-8342-249X)

**Kou P. Kawahara** – Department of Chemistry, Graduate School of Science, Nagoya University, Nagoya 464-8602, Japan

**David Sarlah** – Department of Chemistry, University of Illinois, Urbana, Illinois 61801, United States; [orcid.org/0000-0002-8736-8953](https://orcid.org/0000-0002-8736-8953)

Complete contact information is available at:

<https://pubs.acs.org/10.1021/jacs.2c11338>

### Notes

The authors declare no competing financial interest.

## ACKNOWLEDGMENTS

This work was supported by the ERATO program from JST (JPMJER1302 to K.I.), JST-CREST program (JPMJCR19R1 to H.I.), the JSPS KAKENHI (Grant No. JP21H01931), the Noguchi Research Foundation, and the Yazaki Memorial Foundation for Science and Technology, and the Foundation of public interest of Tatematsu (to H.I.). We thank Dr. Yasutomo Segawa for helping with the X-ray diffraction analysis. MS measurements were conducted using the resources of the Chemical Instrumentation Facility (CIF), Research Center for Materials Science (RCMS), Nagoya University. The computation was performed using Research Center for Computational Science, Okazaki, Japan (Project Nos.: 21-IMS-C070, 22-IMS-C069). ITbM is supported by the World Premier International Research Center Initiative (WPI), Japan. Fabrication of OFET devices and those evaluation were conducted using Custom Evaluation Service of OFET performance by Tokyo Chemical Industry, Co. Ltd. (TCI) in Japan.

## REFERENCES

- (1) For selected reviews, see: (a) Forrest, S. The path to ubiquitous and low-cost organic electronic appliances on plastic. *Nature* **2004**, *428*, 911–918. (b) Wang, C.; Dong, H.; Jiang, L.; Hu, W. Organic semiconductor crystals. *Chem. Soc. Rev.* **2018**, *47*, 422–500. (c) Klauk, H. Organic thin-film transistors. *Chem. Soc. Rev.* **2010**, *39*, 2643–2666.
- (2) For selected reviews, see: (a) Someya, T.; Sekitani, T.; Iba, S.; Kato, Y.; Kawaguchi, H.; Sakurai, T. A large-area, flexible pressure sensor matrix with organic field-effect transistors for artificial skin applications. *Proc. Natl. Acad. Sci. U. S. A.* **2004**, *101*, 9966–9970. (b) Arias, A. C.; MacKenzie, J. D.; McCulloch, I.; Rivnay, J.; Salleo, A. Materials and applications for large area electronics: solution-based approaches. *Chem. Rev.* **2010**, *110*, 3–24. (c) Root, S. E.; Savagatrup, S.; Printz, A. D.; Rodriguez, D.; Lipomi, D. J. Mechanical properties

of organic semiconductors for stretchable, highly flexible, and mechanically robust electronics. *Chem. Rev.* **2017**, *117*, 6467–6499.

- (3) For selected reviews, see: (a) Wu, J.; Pisula, W.; Müllen, K. Graphenes as potential material for electronics. *Chem. Rev.* **2007**, *107*, 718–747. (b) Grzybowski, M.; Sadowski, B.; Butenschön, H.; Gryko, D. T. Synthetic applications of oxidative aromatic coupling—from biphenols to nanographenes. *Angew. Chem., Int. Ed.* **2020**, *59*, 2998–3027. (c) Sun, Z.; Ye, Q.; Chi, C.; Wu, J. Low band gap polycyclic hydrocarbons: from closed-shell near infrared dyes and semiconductors to open-shell radicals. *Chem. Soc. Rev.* **2012**, *41*, 7857–7889.

- (4) For selected examples, see: (a) Podzorov, V.; Pudalov, V. M.; Gershenson, M. E. Field-effect transistors on rubrene single crystals with parylene gate insulator. *Appl. Phys. Lett.* **2003**, *82*, 1739–1741. (b) Sundar, V. C.; Zaumseil, J.; Podzorov, V.; Menard, E.; Willett, R. L.; Someya, T.; Gershenson, M. E.; Rogers, J. A. Elastomeric transistor stamps: Reversible probing of charge transport in organic crystals. *Science* **2004**, *303*, 1644–1646. (c) Podzorov, V.; Menard, E.; Borissov, A.; Kiryukhin, V.; Rogers, J. A.; Gershenson, M. E. Intrinsic charge transport on the surface of organic semiconductors. *Phys. Rev. Lett.* **2004**, *93*, No. 086602. (d) Takeya, J.; Yamagishi, M.; Tominari, Y.; Hirahara, R.; Nakazawa, Y.; Nishikawa, T.; Kawase, T.; Shimoda, T.; Ogawa, S. Very high-mobility organic single-crystal transistors with in-crystal conduction channels. *Appl. Phys. Lett.* **2007**, *90*, No. 102120.

- (5) For selected examples, see: (a) Jurchescu, O. D.; Meetsma, A.; Palstra, T. T. M. Low-temperature structure of rubrene single crystals grown by vapor transport. *Acta Cryst. B* **2006**, *62*, 330–334. (b) Huang, L.; Liao, Q.; Shi, Q.; Fu, H.; Ma, J.; Yao, J. Rubrene micro-crystals from solution routes: their crystallography, morphology and optical properties. *J. Mater. Chem.* **2010**, *20*, 159–166. (c) Irkhin, P.; Biaggio, I. Direct imaging of anisotropic exciton diffusion and triplet diffusion length in rubrene single crystals. *Phys. Rev. Lett.* **2011**, *107*, No. 017402. (d) Najafov, H.; Lee, B.; Zhou, Q.; Feldman, L. C.; Podzorov, V. Observation of long-range exciton diffusion in highly ordered organic semiconductors. *Nat. Mater.* **2010**, *9*, 938–943. (e) Ma, L.; Zhang, K.; Kloc, C.; Sun, H.; Michel-Beyerle, M. E.; Gurzadyan, G. G. Singlet fission in rubrene single crystal: direct observation by femtosecond pump-probe spectroscopy. *Phys. Chem. Chem. Phys.* **2012**, *14*, 8307–8312. (f) Miyata, K.; Kurashige, Y.; Watanabe, K.; Sugimoto, T.; Takahashi, S.; Tanaka, S.; Takeya, J.; Yanai, T.; Matsumoto, Y. Coherent singlet fission activated by symmetry breaking. *Nat. Chem.* **2017**, *9*, 983–989. (g) Singh-Rachford, T. N.; Castellano, F. N. J. Pd(II) phthalocyanine-sensitized triplet–triplet annihilation from rubrene. *Phys. Chem. A* **2008**, *112*, 3550–3556. (h) Gray, V.; Dzebo, D.; Abrahamsson, M.; Albinsson, B.; Moth-Poulsen, K. Triplet–triplet annihilation photon-upconversion: towards solar energy applications. *Phys. Chem. Chem. Phys.* **2014**, *16*, 10345–10352. (i) Huang, Z.; Xu, Z.; Mahboub, M.; Liang, Z.; Jaimes, P.; Xia, P.; Graham, K. R.; Tang, M. L.; Lian, T. Enhanced near-infrared-to-visible upconversion by synthetic control of PbS nanocrystal triplet photosensitizers. *J. Am. Chem. Soc.* **2019**, *141*, 9769–9772. (j) Podzorov, V.; Menard, E.; Rogers, J. A.; Gershenson, M. E. Hall effect in the accumulation layers on the surface of organic semiconductors. *Phys. Rev. Lett.* **2005**, *95*, No. 226601. (k) Lee, B.; Chen, Y.; Fu, D.; Yi, H. T.; Czelen, K.; Najafov, H.; Podzorov, V. Trap healing and ultralow-noise Hall effect at the surface of organic semiconductors. *Nat. Mater.* **2013**, *12*, 1125–1129.

- (6) For review, see: (a) Clapham, M. L.; Murphy, E. C.; Douglas, C. J. Synthesis and crystal engineering of rubrene and its derivatives. *Synthesis* **2021**, *53*, 461–474. For selected examples, see: (b) Braga, D.; Jaafari, A.; Miozzo, L.; Moret, M.; Rizzato, S.; Papagni, A.; Yassar, A. The rubrenic synthesis: the delicate equilibrium between tetracene and cyclobutene. *Eur. J. Org. Chem.* **2011**, *2011*, 4160–4169. (c) Uttiya, S.; Miozzo, L.; Fumagalli, E. M.; Bergantin, S.; Ruffo, R.; Parravicini, M.; Papagni, A.; Moret, M.; Sassella, A. Connecting molecule oxidation to single crystal structural and charge transport properties in rubrene derivatives. *J. Mater. Chem. C* **2014**, *2*, 4147–4155. (d) Dodge, J. A.; Bain, J. D.; Chamberlin, A. R. Regioselective

synthesis of substituted rubrenes. *J. Org. Chem.* **1990**, *55*, 4190–4198. (e) Allen, C. F. H.; Gilman, L. A. Synthesis of rubrene. *J. Am. Chem. Soc.* **1936**, *58*, 937–940. (f) Zhang, Z.; Ogden, W. A.; Young, V. G., Jr.; Douglas, C. J. Synthesis, electrochemical properties, and crystal packing of perfluororubrene. *Chem. Commun.* **2016**, *52*, 8127–8130. (g) McGarry, K. A.; Xie, W.; Sutton, C.; Risko, C.; Wu, Y.; Young, V. G., Jr.; Brédas, J.-L.; Frisbie, C. D.; Douglas, C. J. Rubrene-based single-crystal organic semiconductors: synthesis, electronic structure, and charge-transport properties. *Chem. Mater.* **2013**, *25*, 2254–2263. (h) Mamada, M.; Katagiri, H.; Sakanoue, T.; Tokito, S. Characterization of new rubrene analogues with heteroaryl substituents. *Cryst. Growth Des.* **2015**, *15*, 442–448. (i) Xie, G.; Hahn, S.; Rominger, F.; Freudenberger, J.; Bunz, U. F. H. Synthesis and characterization of two different azarubrenes. *Chem. Commun.* **2018**, *54*, 7593–7596. Also see, ref 20

(7) For reported late-stage functionalizations of rubrene, see (a) Aubry, J. M.; Rigaudy, J.; Cuong, N. K. A water-soluble rubrene derivative: Synthesis, properties and trapping of  $^1\text{O}_2$  in aqueous solution. *Photochem. Photobiol.* **1981**, *33*, 149–153. (b) Fagan, P. J.; Ward, M. D.; Caspar, J. V.; Calabrese, J. C.; Krusic, P. J. Synthesis and unusual properties of a helically twisted multiply metalated rubrene derivative. *J. Am. Chem. Soc.* **1988**, *110*, 2982–2983. (c) Freedman, D. A.; Matachek, J. R.; Mann, K. R. Ion pairing effects in the photochemistry of the cyclopentadienyl( $\eta^6$ -benzene)osmium(II) cation. Synthesis and reactions of a synthetically useful intermediate: the cyclopentadienyltris(acetonitrile)osmium(II) cation. *Inorg. Chem.* **1993**, *32*, 1078–1080.

(8) (a) Ly, J.; Martin, K.; Thomas, S.; Yamashita, M.; Yu, B.; Pointer, C. A.; Yamada, H.; Carter, K. R.; Parkin, S.; Zhang, L.; Brédas, J.-L.; Young, E. R.; Briseno, A. L. Short excited-state lifetimes enable photo-oxidatively stable rubrene derivatives. *J. Phys. Chem. A* **2019**, *123*, 7558–7566. (b) Aubry, J.-M.; Pierlot, C.; Rigaudy, J.; Schmidt, R. Reversible binding of oxygen to aromatic compounds. *Acc. Chem. Res.* **2003**, *36*, 668–675.

(9) (a) Ito, H.; Ozaki, K.; Itami, K. Annulative  $\pi$ -extension (APEX): Rapid access to fused arenes, heteroarenes, and nanographenes. *Angew. Chem., Int. Ed.* **2017**, *56*, 11144–11164. (b) Ozaki, K.; Kawasumi, K.; Shibata, M.; Ito, H.; Itami, K. One-shot *K*-region-selective annulative  $\pi$ -extension for nanographene synthesis and functionalization. *Nat. Commun.* **2015**, *6*, 6251. (c) Matsuoka, W.; Ito, H.; Itami, K. Rapid access to nanographenes and fused heteroarenes by palladium-catalyzed annulative  $\pi$ -extension reaction of unfunctionalized aromatics with diiodobiaryls. *Angew. Chem., Int. Ed.* **2017**, *56*, 12224–12228. (d) Kitano, H.; Matsuoka, W.; Ito, H.; Itami, K. Annulative  $\pi$ -extension of indoles and pyrroles with diiodobiaryls by Pd catalysis: Rapid synthesis of nitrogen-containing polycyclic aromatic compounds. *Chem. Sci.* **2018**, *9*, 7556.

(10) Matsuoka, W.; Ito, H.; Sarlah, D.; Itami, K. Diversity-oriented synthesis of nanographenes enabled by dearomative annulative  $\pi$ -extension. *Nat. Commun.* **2021**, *12*, 3940.

(11) (a) Jang, B.-B.; Lee, S. H.; Kafafi, Z. H. Asymmetric pentacene derivatives for organic light-emitting diodes. *Chem. Mater.* **2006**, *18*, 449–457. (b) Ebisawa, A.; Kitagawa, S.; Inoue, T. Compound for organic EL element and organic EL element. JP5101055B2, December 19, 2021.

(12) (a) Smyth, N.; Engen, D. V.; Pascal, R. A., Jr. Synthesis of longitudinally twisted polycyclic aromatic hydrocarbons via a highly substituted aryne. *J. Org. Chem.* **1990**, *55*, 1937–1940. (b) Rodríguez-Lojo, D.; Pérez, D.; Peña, D.; Guitián, E. One-pot synthesis of sterically congested large aromatic hydrocarbons via 1,4-diphenyl-2,3-triphenylacetylene. *Chem. Commun.* **2013**, *49*, 6274–6276. (c) Clevenger, R. G.; Kumar, B.; Menuey, E. M.; Lee, G.-H.; Patterson, D.; Kilway, K. V. A superior synthesis of longitudinally twisted acenes. *Chem. – Eur. J.* **2018**, *24*, 243–250. (d) Clevenger, R. G.; Kumar, B.; Menuey, E. M.; Kilway, K. V. Synthesis and structure of a longitudinally twisted hexacene. *Chem. – Eur. J.* **2018**, *24*, 3113–3116. (e) Xiao, Y.; Mague, J. T.; Schmehl, R. H.; Haque, F. M.; Pascal, R. A., Jr. Dodecaphenyltetracene. *Angew. Chem., Int. Ed.* **2019**, *58*, 2831–2833.

(13) (a) Qualizza, B. A.; Ciszek, J. W. Experimental survey of the kinetics of acene Diels–Alder reactions. *J. Phys. Org. Chem.* **2015**, *28*, 629–634. (b) Kjell, D. P.; Sheridan, R. S. Photochemical cycloaddition of *N*-methyltriazolinedione to naphthalene. *J. Am. Chem. Soc.* **1984**, *106*, 5368–5370. (c) Southgate, E. H.; Pospech, J.; Fu, J.; Holycoss, D. R.; Sarlah, D. Dearomative dihydroxylation with arenophiles. *Nat. Chem.* **2016**, *8*, 922–928. (d) Hernandez, L. W.; Klöckner, U.; Pospech, J.; Hauss, L.; Sarlah, D. Nickel-catalyzed dearomative trans-1,2-carboamination. *J. Am. Chem. Soc.* **2018**, *140*, 4503–4507. (e) Tang, C.; Okumura, M.; Zhu, Y.; Hooper, A. R.; Zhou, Y.; Lee, Y.-H.; Sarlah, D. Palladium-catalyzed dearomative syn-1,4-carboamination with Grignard reagents. *Angew. Chem., Int. Ed.* **2019**, *58*, 10245–10249. (f) Piacentini, P.; Bingham, T. W.; Sarlah, D. Dearomative ring expansion of polycyclic arenes. *Angew. Chem., Int. Ed.* **2022**, *61*, No. e202208014.

(14) (a) Ito, S.; Itoh, T.; Nakamura, M. Diastereoselective carbometalation of oxa- and azabicyclic alkenes under iron catalysis. *Angew. Chem., Int. Ed.* **2011**, *50*, 454–457. (b) Matsumoto, A.; Ilies, L.; Nakamura, E. Phenanthrene synthesis by iron-catalyzed [4+2] benzannulation between alkyne and biaryl or 2-alkenylphenyl Grignard reagent. *J. Am. Chem. Soc.* **2011**, *133*, 6557–6559.

(15) Mishima, D.; Nakanishi, H.; Tsuboi, Y.; Kishimoto, Y.; Yamanaka, Y.; Harada, A.; Togo, M.; Yamada, Y.; Muraoka, M.; Murata, M. Domino cross-Scholl reaction of tetracene with molecular benzene: Synthesis, structure, and mechanism. *Org. Lett.* **2021**, *23*, 7921–7926.

(16) For selected reviews, see: (a) Watanabe, M.; Chen, K.-Y.; Chang, Y. J.; Chow, T. J. Acenes generated from precursors and their semiconducting properties. *Acc. Chem. Res.* **2013**, *46*, 1606–1615. (b) Dorel, R.; Echavarren, A. M. Strategies for the Synthesis of Higher Acenes. *Eur. J. Org. Chem.* **2017**, *2017*, 14–24. (c) Yamada, H.; Hayashi, H. Synthesis of oligoacenes using precursors for evaluation of their electronic structures. *Photochem. Photobiol. Sci.* **2022**, *21*, 1511–1532. (d) Yamada, H.; Kuzuhara, D.; Suzuki, M.; Hayashi, H.; Aratani, N. Synthesis and morphological control of organic semiconducting materials using the precursor approach. *Bull. Chem. Soc. Jpn.* **2020**, *93*, 1234–1267.

(17) Ma, L.; Galstyan, G.; Zhang, K.; Kloc, C.; Sun, H.; Soci, C.; Michel-Beyerle, M. E.; Gurzadyan, G. G. Two-photon-induced singlet fission in rubrene single crystal. *J. Chem. Phys.* **2013**, *138*, No. 184508.

(18) NCIPLLOT: (a) Johnson, E. R.; Keinan, S.; Mori-Sánchez, P.; Contreras-García, J.; Cohen, A. J.; Yang, W. Revealing Noncovalent Interactions. *J. Am. Chem. Soc.* **2010**, *132*, 6498. (b) Contreras-García, J.; Johnson, E. R.; Keinan, S.; Chaudret, R.; Piquemal, J.-P.; Beratan, D. N.; Yang, W. NCIPLLOT: A Program for Plotting Noncovalent Interaction Regions. *J. Chem. Theory Comput.* **2011**, *7*, 625. (c) Boto, R. A.; Peccati, F.; Laplaza, R.; Quan, C.; Carbone, A.; Piquemal, J.-P.; Maday, Y.; Contreras-García, J. NCIPLLOT4: Fast, Robust, and Quantitative Analysis of Noncovalent Interactions. *J. Chem. Theory Comput.* **2020**, *16*, 4150.

(19) (a) Troisi, A. Prediction of the absolute charge mobility of molecular semiconductors: The case of rubrene. *Adv. Mater.* **2007**, *19*, 2000–2004. (b) Nakayama, Y.; Uragami, Y.; Machida, S.; Koswattage, K. R.; Yoshimura, D.; Setoyama, H.; Okajima, T.; Mase, K.; Ishii, H. Full picture of valence band structure of rubrene single crystals probed by angle-resolved and excitation-energy-dependent photoelectron spectroscopy. *Appl. Phys. Express* **2012**, *5*, No. 111601.

(20) (a) Fratini, S.; Nikolka, M.; Salleo, A.; Schweicher, G.; Sirringhaus, H. Charge transport in high-mobility conjugated polymers and molecular semiconductors. *Nat. Mater.* **2020**, *19*, 491–502. (b) Dong, H.; Wang, C.; Hu, W. High performance organic semiconductors for field-effect transistors. *Chem. Commun.* **2010**, *46*, 5212–5222. (c) Wang, C.; Dong, H.; Hu, W.; Liu, Y.; Zhu, D. Semiconducting  $\pi$ -conjugated systems in field-effect transistors: A material odyssey of organic electronics. *Chem. Rev.* **2012**, *112*, 2208–2267. (d) Wang, C.; Dong, H.; Li, H.; Zhao, H.; Meng, Q.; Hu, W. Dibenzothiophene derivatives: From herringbone to lamellar packing motif. *Cryst. Growth Des.* **2010**, *10*, 4155–4160.

(21) (a) Ogden, W. A.; Ghosh, S.; Bruzek, M. J.; McGarry, K. A.; Balhorn, L.; Young, V.; Purvis, L. J.; Wegwerth, S. E.; Zhang, Z.; Serratore, N. A.; Cramer, C. J.; Gagliardi, L.; Douglas, C. J. Partial fluorination as a strategy for crystal engineering of rubrene derivatives. *Cryst. Growth Des.* **2017**, *17*, 643–658. (b) Sakamoto, Y.; Suzuki, T. Perfluorinated and half-fluorinated rubrenes: Synthesis and crystal packing arrangements. *J. Org. Chem.* **2017**, *82*, 8111–8116. (c) Li, J.; Ni, Z.; Zhang, X.; Li, R.; Dong, H.; Hu, W. Enhanced stability of a rubrene analogue with a brickwork packing motif. *J. Mater. Chem. C* **2017**, *5*, 8376–8379.

(22) (a) Anthony, J. E. Functionalized Acenes and Heteroacenes for Organic Electronics. *Chem. Rev.* **2006**, *106*, 5028–5048. (b) Anthony, J. E.; Eaton, D. L.; Parkin, S. R. A road map to stable, soluble, easily crystallized pentacene derivatives. *Org. Lett.* **2002**, *4*, 15–18. (c) Sheraw, C. D.; Jackson, T. N.; Eaton, D. L.; Anthony, J. E. Functionalized pentacene active layer organic thin-film transistors. *Adv. Mater.* **2003**, *15*, 2009–2011.

(23) (a) Li, L.; Tang, Q.; Li, H.; Yang, X.; Hu, W.; Song, Y.; Shuai, Z.; Xu, W.; Liu, Y.; Zhu, D. An ultra closely  $\pi$ -stacked organic semiconductor for high performance field-effect transistors. *Adv. Mater.* **2007**, *19*, 2613–2617. (b) Shukla, D.; Nelson, S. F.; Freeman, D. C.; Rajeswaran, M.; Ahearn, W. G.; Meyer, D. M.; Carey, J. T. Thin-film morphology control in naphthalene-diimide-based semiconductors: High mobility *n*-type semiconductor for organic thin-film transistors. *Chem. Mater.* **2008**, *20*, 7486–7491. (c) Ando, S.; Murakami, R.; Nishida, J.; Tada, H.; Inoue, Y.; Tokito, S.; Yamashita, Y. *n*-Type organic field-effect transistors with very high electron mobility based on thiazole oligomers with trifluoromethylphenyl groups. *J. Am. Chem. Soc.* **2005**, *127*, 14996–14997.

## Recommended by ACS

### Dibenzotropylium-Capped Orthogonal Geometry Enabling Isolation and Examination of a Series of Hydrocarbons with Multiple $14\pi$ -Aromatic Units

Yuki Hayashi, Yusuke Ishigaki, *et al.*

JANUARY 06, 2023  
JOURNAL OF THE AMERICAN CHEMICAL SOCIETY

READ 

### Photochemical Organocatalytic Functionalization of Pyridines via Pyridinyl Radicals

Emilien Le Saux, Paolo Melchiorre, *et al.*

DECEMBER 27, 2022  
JOURNAL OF THE AMERICAN CHEMICAL SOCIETY

READ 

### Photoinduced Halogen-Atom Transfer by *N*-Heterocyclic Carbene-Ligated Boryl Radicals for $C(sp^3)$ - $C(sp^3)$ Bond Formation

Ting Wan, Timothy Noël, *et al.*

DECEMBER 30, 2022  
JOURNAL OF THE AMERICAN CHEMICAL SOCIETY

READ 

### Intermolecular Organophotocatalytic Cyclopropanation of Unactivated Olefins

David M. Fischer, Erick M. Carreira, *et al.*

JANUARY 06, 2023  
JOURNAL OF THE AMERICAN CHEMICAL SOCIETY

READ 

Get More Suggestions >